UNIVERSITY OF CAMBRIDGE

Understanding the Structure-Property Relationship in Diketopyrrolopyrroles for Organic Electronics

by

Lisa Sharma

Supervisor: Dr Hugo Bronstein

This thesis is submitted for the degree of

Doctor of Philosophy

in the subject of

Chemistry

at

St Catharine's College

University of Cambridge

September 2020

Declaration

I, Lisa Sharma, confirm that this thesis is the result of my own work and includes nothing which is the outcome of work done in collaboration except as declared in the Preface and specified in the text.

It is not substantially the same as any that I have submitted, or, is being concurrently submitted for a degree or diploma or other qualification at the University of Cambridge or any other University or similar institution except as declared in the Preface and specified in the text.

I further state that no substantial part of my thesis has already been submitted, or, is being concurrently submitted for any such degree, diploma or other qualification at the University of Cambridge or any other University or similar institution except as declared in the Preface and specified in the text. It does not exceed the prescribed word limit for the Degree Committee of Physics and Chemistry.

Lisa Sharma

Abstract

Understanding the Structure-Property Relationship in Diketopyrrolopyrroles for Organic Electronics

Lisa Sharma

The effects of chain length, encapsulation and asymmetry of conjugated DPP-based polymers and small molecules were investigated.

The first part of this thesis explored how chain length can affect the optical properties of conjugated DPP-based materials. Previously in our group, a series of thienyl-DPP oligomers (n = 1-5) and their polymeric counterpart were synthesised *via* a series of Suzuki-Miyaura cross-couplings. However, the tetramer was found to be impure. Thus, in *this* work the tetramer was re-synthesised *via* alternative reaction conditions. In addition, the DPP monomer, dimer and polymer were also re-synthesised for this study. The optical properties of the DPP oligomers were studied and it was observed that as the chain length increased from monomer to dimer, the extinction coefficient did also, at which it reached a maximum. Then, as the chain length increased from the dimer to the pentamer, the value largely decreased, suggesting that a saturation limit had been reached. On the other hand, this was challenged by the polymer's largely red-shifted absorption compared to any other compound in the study. However, as the expected size of the red shift should decrease with extending conjugation length, this result was unexpected. It is possible that this may have been due to aggregation of the polymer chains, thus suggesting that the absorption of the DPP compounds does not rely solely on the ECL alone.

The second part of this thesis explores the effect of encapsulation of the DPP core, on the performance of OPV devices. Two series of DPP-based polymers doped with an increasing amount of an encapsulated DPP monomer were synthesised, and the corresponding OPV devices were fabricated. In general, the encapsulated devices achieved higher V_{oc} values than the reference, however the optimum amount of encapsulation was found to vary in different polymer systems. It is possible that through the introduction of the encapsulated dopant, this alters the donor-acceptor interface by either increasing the difference in the static dipole moment, reducing the ratio of the CT-state density or reducing the reorganization energy, thus resulting in an increase of the V_{oc}. However, these results may have been affected by differences in polymer molecular weight. Three additional ring sizes of the encapsulated monomer were also investigated, followed by the synthesis of a series of encapsulated DPP-BDT based polymers. It was observed that the ring size of the encapsulated monomer had an influence over the optical properties and performance of the corresponding polymers, thus highlighting the importance of choosing the optimum ring size. The synthesis of an encapsulated and linear chained DPP-bi-thiophene

co-polymer consisting of ethylene glycol side chains was also attempted, for application in bioelectronics.

The final part of this thesis explores the different synthetic attempts towards a novel DPP polymer consisting of a higher DPP to thiophene ratio than previously reported. Based upon previous electronic calculations, this polymer is theorised to show increased tolerance towards energetic/torsional disorder, due to secondary overlap contribution between the thiophene/DPP units. Several synthetic building blocks were synthesised, among them alkylated thienyl pyrrolinone esters. These were used to develop a novel synthetic methodology towards fully asymmetric DPP derivatives. Four fully asymmetric DPP derivatives were synthesised, including a pair of structural isomers. It was observed that their optical and theoretical properties were found to lie in-between that of their symmetrical counterparts. Thus, it is possible to fine tune properties such as absorption and optical band gap *via* such asymmetric design strategies.

Contributions

The content of this thesis would have not been made possible without the generous help and collaboration of several people and research groups.

- The DPP trimer and pentamer of *Chapter II* used in the optical study were synthesised in our research group by Dr Anastasia Leventis, University of Cambridge. The project was a continuation of her previous work and thus, I thank her for her guidance with this work.
- The UV-vis absorption spectra and extinction coefficients in *Chapter II* were obtained at the Centre for Plastic Electronics and Department of Physics, Imperial College London, in Prof. Jenny Nelson's group by Dr Elham Rezasolatani.
- Compounds **11** and **12** in *Chapter III*, were synthesised in our research group by Dr Anastasia Leventis, University of Cambridge.
- All X-ray crystallographic analysis was performed by Dr Andrew Bond at the Department of Chemistry, University of Cambridge.
- Molecular weights of the polymers within the *Ph-series* in *Chapter III*, were determined at the Department of Chemistry, University of Warwick in Prof. Dave Haddleton's group by Dr Samuel Lawton.
- Molecular weight of **PDPP-T2** in *Chapter III* was determined at the Department of Chemistry, University of Oxford in Prof. Charlotte Williams's group by Dr Patrick de Jongh.
- All OPV devices reported in *Chapter III* were fabricated and tested at the KAUST Solar Centre, King Abdullah University of Science and Technology, Saudi Arabia, in Dr Derya Baran's group by Anirudh Sharma and Jules Bertrandie.
- Computational density functional theory calculations (DFT) discussed in this thesis were performed by Lisa Sharma with the guidance of Dr Anastasia Leventis.
- Compound **28** (**P-DPP**) in *Chapter IV* was synthesised in our research group by Hayden Francis.
- NMR spectra data were obtained at the Department of Chemistry, UCL with the help of Dr Abil Aliev, and at the Department of Chemistry, University of Cambridge with the help of Duncan Howe and Andrew Mason.
- Mass spectrometry data was obtained at the Department of Chemistry, UCL with the help of Dr Kersti Karu and at the Department of Chemistry, University of Cambridge with the help of Dr Dijana Matak-Vinkovic, Asha Boodhun, Dr Roberto Canales and Dr Maria Ciaccia.

Acknowledgments

First and foremost, I would like to thank my supervisor, Dr Hugo Bronstein, for giving me the opportunity to work in his research group. I'm incredibly grateful to have had such an understanding, kind and supportive supervisor throughout my PhD, from whom I've learnt so much. Again, I thank him for his patience and guidance throughout the years.

Secondly, I would like to thank all current and past members of the Bronstein group, who have made my PhD experience more enjoyable and have countlessly brightened my day including- Anastasia L, Dave, Kealan, Alex, Niall, Jerry, Dan, Anastasia K, Wei, Hayden and Michael. In particular, I would like to thank Anastasia Leventis once more for her friendship, guidance and company over the years. She has been a great mentor and my time here would not have been the same without her. To Alex- thank you for being so caring and loving, I'm so glad to have met you.

I would also like to thank all the staff and students at Cambridge, UCL and other institutions who have helped me carry out my research. Their work and efforts are truly appreciated and whom without, this work would not be possible.

Additionally, I would like to thank the ERC for funding my PhD.

Thank you to my close friends, who have supported and encouraged me throughout the years. To my best friend Alice, who I consider family and whose friendship I will treasure always. To the lovely Mollie, whose friendship made my time at Cambridge so wonderful. Thank you for your encouragement, support and always lending me an ear. To my long-time friends Stefanie and Hafsah, for their continued support and friendship over the last 14 years. To my good friends Zainab and Kate. To my good friend Peter, whose friendship I truly cherish. I will always miss our 'Tuesday night drinks' during that first year, thank you for all the good times.

Finally, I dedicate this thesis to my family, whose love and strength I'm forever grateful for. To my parents, my brother and my grandparents, I thank them for their encouragement and support which without, this work would not be possible. To my uncle and aunt, Prof. Bagshawe and Dr Sharma, I thank them for their inspiration, kindness and continued support. Thank you for always believing in me.

Again, I sincerely thank you all,

Table of Contents

List of Abbreviations

α	Polarizability constant
ε	Extinction coefficient
λ	Wavelength
λ_{max}^{film}	Film absorption maximum
λ_{max}^{soln}	Solution absorption maximum
λ_0	Low-frequency reorganization energy
λ_i	High-frequency reorganization energy
μg	Microgram
$\vec{\mu}_{ij}$	Transitional dipole moment from state *i* to *j*
$\lvert\Delta\vec{\mu}\rvert$	Difference in the static dipole moment between the CT state and GS respectively
μ_{ind}	Induced dipole moment
ΦF	Fluorescence quantum yield
°	Degrees
2D	Two dimensional
A	Acceptor
A	Absorbance
Å	Angstrom
AM	Air mass coefficient
Aq	Aqueous

ASAP	Atmospheric Solids Analysis Probe
BDT	Benzodithiophene
BHJ	Bulk heterojunction
BLA	Bond length alternation
BT_z	Benzothiadiazole
c	Concentration
CB	Chlorobenzene
CB	Conduction band
C-C	Carbon-Carbon
CS	Charge separated state
CT	Charge transfer state
D	Debye
D	Donor
DCM	Dichloromethane
DMF	Dimethylformamide
DMSO	Dimethyl sulfoxide
DPE	Diphenyl ether
DPO	(2-(1,10-phenanthrolin-3-yl)naphth-6-yl)diphenylphosphine oxide
DPP	Diketopyrrolopyrrole
E	Strength of the electric field
EA	Electron affinity

E_{abs}	Energy of the optical absorption gap
ECL	Effective conjugation length
E_{CT}	Energy of the charge transfer state
EDG	Electron withdrawing group
E_g	Optical band gap energy
EI	Electron ionisation
EL	Electroluminescence
E_{photon}	Photon energy
EQE	External quantum efficiency
ESD	Electrospray deposition
ESI	Electrospray ionisation
ESP	Electrostatic potential
eV	Electron volt
EWG	Electron withdrawing group
f	Oscillator strength
FA	Fullerene acceptor
FF	Fill factor
FREAs	Fused rings electron acceptors
G	Global solar spectrum
GIWAX	Grazing incidence wide-angle X-ray scattering
GPC	Gel permeation chromatography

GS	Ground state
h	Hours
HOMO	Highest occupied molecular orbital
IEF	Intermolecular electric field
IMW	Insulated molecular wire
IR	Infrared
ITIC	3,9-bis(2-methylene-(3-(1,1-dicyanomethylene)-indanone))-5,5,11,11-tetrakis(4-hexylphenyl)-dithieno[2,3-d:2’,3’-d’]-s-indaceno[1,2-b:5,6-b’]dithiophene
ITO	Indium tin oxide
I-V	Current-voltage
J_m	Current maximum
J_{sc}	Short current density
kDa	Kilodalton
l	Path length
LD	Laser desorption
LUMO	Lowest unoccupied molecular orbital
M	Mass
M	Transition dipole moment
m/z	Mass/charge
MALDI	Matrix-assisted laser desorption/ionization
MALDI-TOF	Matrix-assisted laser desorption/ionization-time-of- flight

mg	Milligram
mL	Millilitre
M_n	Number average molecular weigh
mV	Millivolt
M_w	Weight average molecular weight
n	Number of monomer units
NBS	N-Bromosuccinimide
n-BuLi	n-Butyllithium
NDIs	Naphthalene diimides
NFA	Non-fullerene acceptor
nm	Nanometre
NMR	Nuclear magnetic resonance
n-type	Negative charge carrier
NT_z	Naphthobisthiadiazole
N_π	Number of π-electrons
o	Ortho
OECT	Organic electrochemical transistors
OEG	Oligio(ethylene glycol)
OFET	Organic field-effect transistors
OLED	Organic light emitting diodes
OPV	Organic photovoltaic

P(*o*-tol)$_3$	Tri(*o*-tolyl)phosphine ligands
P3HT	Poly(3-hexylthiophene)
PA	Polyacetylene
pA	Picoampere
PCE (*η)*	Power conversion efficiency
PDI	Polydispersity index
PEDOT	Poly(3,4-ethylenedioxythiophene)
PEG	Polyethylene glycol
Ph	Phenyl
P_{in}	Power of the incident light energy
PITN	Polyisothianaphthene
P_{out}	Maximum electrical power output
PPh_3	Triphenylphosphine
ppm	Parts per million
PPV	Poly(phenylenevinylene)
PS	Polystyrene
PSS	Poly(styrene sulfonate)
p-type	Positive charge carrier
q	Elementary charge
Q_{LED}	External quantum efficiency of the electroluminescence emission
RT	Room temperature

RID	Refractive index detector
S_0-S_1	First electronic transition
Sat	Saturated
SDPP	Thioether DPP derivatives
SEC	Size exclusion chromatography
S-O	Sulfur-Oxygen
STM	Scanning tunnelling microscopy
TAA	*Tert*-amyl alcohol/ 2-methyl-2-butanol
TD-DFT	Time-dependent density functional theory
TEA	Triethylamine
TEEG	Tetraethylene glycol
THF	Tetrahydrofuran
TLC	Thin-layer chromatography
TT	Thienothiophene
UHV	Ultra-high vacuum
UV-vis	Ultraviolet-visible
VB	Valence band
V_{bias}	Bias voltage
V_m	Voltage maximum
V_{oc}	Open circuit voltage
W	Weight

I

Introduction

1.1 An Introduction to Conjugated Organic Materials

1.1.1 A Brief History

At the beginning of the 19th century, the first observation of photoconductivity in an organic compound (anthracene) was reported, thus marking the start of the organic electronics field.[1] In the 1960s, interest in the field intensified following the discovery of electroluminescence in conductive polymers. Up until then, polymers were considered insulators possessing no conductive or optical properties. In 1963, McNeill *et al*[2] reported the first example of doping in a polypyrrole polymer, in which modest levels of conductivity were observed.

Undoubtedly, the major breakthrough of the field arrived in 1977, following the study on polyacetylene (**PA**) (Figure 1.1a) and the discovery of its high electrical conductivity upon doping, reported by H. Shirakawa, A. Heeger and A. MacDiarmid.[3] For their '*discovery and development of conductive polymers',* they were jointly awarded the Nobel Prize in 2000. Their work led the way to major advances within the field and forever changed the way polymers were viewed.

Since then, a significant amount of progress has been made and a large library of conjugated polymers (of which are either conductors or semiconductors) consisting of various motifs have been developed for application in optoelectronics. Among them are poly(3-hexylthiophene) (**P3HT**) and poly(phenylenevinylene) (**PPV**) (Figure 1.1b), which compared to **PA** show a greater solubility in organic solvents, stability in air and are readily processable.[4]

*Figure 1.1- Chemical structure of conjugated polymers: a) polyacetylene (**PA**); b) poly(3-hexylthiophene) (**P3HT**), poly(phenylenevinylene) (**PPV**).*

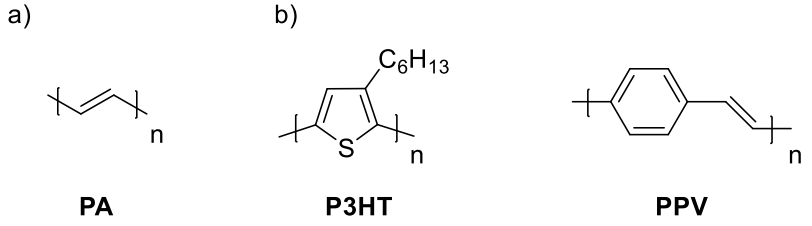

1.1.2 Conjugation

Organic semiconducting materials all consist of conjugated double bonds. The polymer backbone is built up by sp^2 hybridized carbons while perpendicular to this, the remaining p_z orbitals form a series of conjugated alternating double (π) and single bonds. The conjugation length can therefore be defined as the number of double bonds between the terminal carbon atoms.[5] As neighbouring p_z (π)- orbitals can overlap with each other, this subsequently leads to delocalized electron bonding along the backbone of the polymer. This extended overlap across the entirety of the backbone allows charge-carrier mobility, therefore giving rise to semi-conductive behaviour.

The energy levels in organic semiconductors are organised in bands rather than discrete levels, similar to their inorganic counterpart. Ethene has discrete frontier MOs: a highest occupied (HOMO) and a lowest occupied (LUMO) molecular orbital (Figure 1.2). As the conjugation length is increased from ethene to butadiene, there is hybridization between the MOs, which in turn both increases the level of the HOMO and lowers the level of the LUMO. As there is addition of each new monomer unit and the conjugation length further extends, hybridization continues until differences between the energy levels becomes so small, that the system then adopts a band-like structure consisting of a valence band (VB) for occupied states and a conduction band (CB) for unfilled states. Thus, this leads to narrowing of the band gap and enables organic conjugated material to possess semi-conductive properties. [6,7,8]

Figure 1.2- An energy diagram depicting the formation of the band structure in organic conjugated polymers as conjugation length increases (i.e. from ethene to polyacetylene). Figure amended from Fallon.[7]

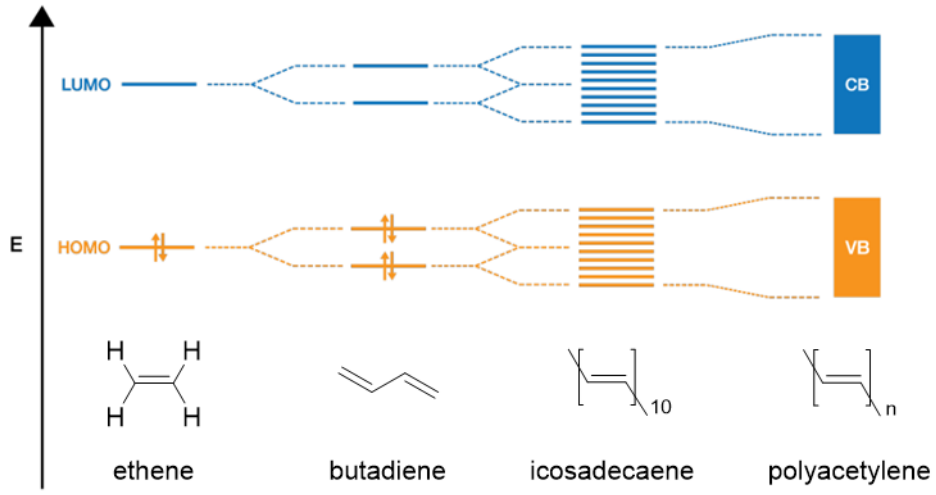

The frontier orbitals of the VB and CB of the conjugated polymer remain to be known as the HOMO and LUMO respectively. In general, almost all the thermodynamic and optical properties of the polymer are dependent on the absolute energetic values of the VB and CB. The difference between these two

levels is known as the fundamental band gap. The fundamental band gap energy is related to the optical band gap energy (E_g), however the two values are not identical.[7,8] While the fundamental band gap refers to the minimum energy required to generate a charge carrier (an electron-hole pair which are not bound together), the optical band gap is the energy of the lowest optical transition accessible upon absorption of a single photon. The optical band gap energy is usually lower in value, as in the excited state (in contrast to the ionized state), the electron-hole pair remain electrostatically bound together. Thus, the difference in energy between the fundamental and optical band gap is a measure of the electron-hole pair binding energy.[9]

Following the absorption of a photon, provided that the $E_{photon} \geq E_g$, an electron can be excited from the HOMO to the LUMO (photoexcitation) generating a bound electron-hole pair (exciton).[10,11] As organic semiconductors generally exhibit a E_g ranging from 1.0-3.0 eV, they are able to absorb photons in the UV-vis and near-IR regions of the electromagnetic spectrum (400-1200 nm) (Figure 1.3).[7,11,12]

Figure 1.3- Irradiance of solar spectrum against photon wavelength (nm). Figure provided by K. Fitch and C. Kemke, Fondriest Environmental Inc.[13]

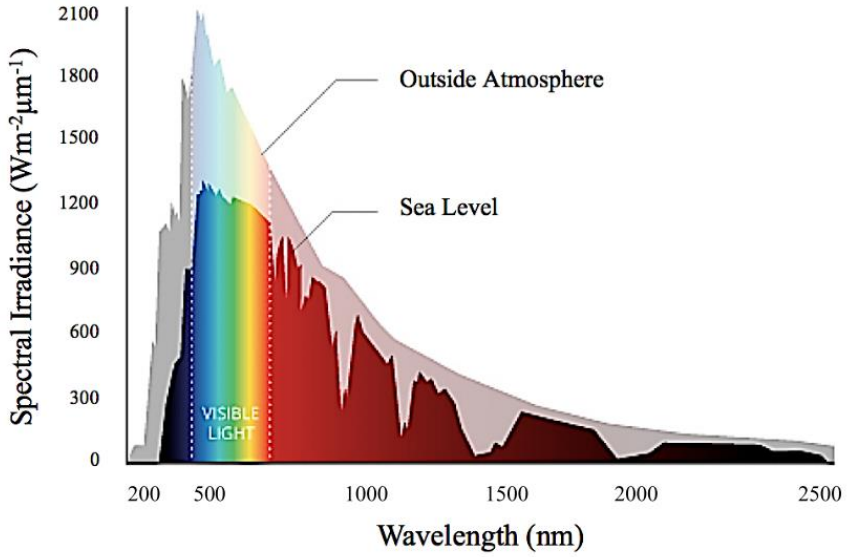

1.2 Applications of Conjugated Materials

Conjugated polymers have demonstrated large potential in a variety of applications due to their semiconducting and optical properties, particularly in plastic electronic devices. When synthesising such devices, the aim is not necessarily to compete with the performance levels of commercially available silicon technology, but rather to enable new functionalities, such as mechanical flexibility, optical transparency and impact resistance.[14]

Organic light emitting diodes (OLED)s are an example of such application. In the late 1980s, a research group led by Prof. Richard Friend in Cambridge discovered that conjugated polymers were able to act as electroluminescent devices, as shown with poly(phenylenevinylene) (PPV).[15] Since then, many advancements have been made and as of 2009 Nokia, Google and Samsung have released various electronic devices containing OLED touch screens.[16] Other applications include organic field-effect transistors (OFET)s and organic photovoltaic cells (OPV)s (the latter shall be discussed in further detail in the following section), which have become increasingly important with the growing need for cheap and renewable energy sources.[14]

1.2.1 Organic Photovoltaics (OPVs)

As organic semiconducting materials can absorb photons in the UV-vis and near-IR regions of the electromagnetic spectrum, they are able to act as light-harvesting active layers in organic photovoltaic cells (OPV).[7,11,12]

1.2.1.1 Device Architecture

Originally, organic solar cell devices consisted of one active layer between two electrodes with different work functions, and the performance of the cell was highly dependent on the nature of the electrodes. This led to poorly performing devices with low PCEs (0.5%) as a result of poor charge carrier generation and unbalanced charge transport.[11,17]

In 1986, Tang[18] reported a bilayer heterojunction device consisting of a donor layer and an acceptor layer, sandwiched between an indium tin oxide conducting layer and a Ag layer. This improved the photocurrent and therefore the PCE to 1%.[11] He discovered that the PCE of the solar cell was dependant on the interfacial region between the two organic layers.

The problem remained however, that excitons have limited lifetimes and consequently can only travel short distances (5-14 nm), therefore donor excitons that are generated further away from the heterojunction interface often decay to the ground state, before getting a chance to reach the acceptor. Unfortunately, the performance of bilayer heterojunction devices are therefore limited, as there is only a small area of interface between the donor and acceptor in which charge generation can occur.[11] Another issue is that the exciton diffusion length then also limits the maximum thickness of the active layer. In turn, this then limits the maximum fraction of incident light that the device can absorb and generate electricity from.[19,20]

This problem was overcome by Yu *et al*[21] through the introduction of bulk heterojunction (BHJ) devices (Figure 1.4),[22] which consists of a blend of donor and acceptor materials in a bulk volume, to give an interpenetrating network. As a result, each interface within the device is a distance less than the

diffusion length of the exciton from the adsorption site. Therefore, BHJs have largely increased the interfacial area, thus leading to a substantial increase in the efficiency of solar cells.[11]

Figure 1.4- The structure of a) a bilayer heterojunction and b) bulk heterojunction organic photovoltaic device. Republished with permission of Royal Society of Chemistry, from Y. Lin, Y. Li and X. Zhan, Chem. Soc. Rev., ***41****, 2012, copyright 2021 RSC; permission conveyed through Copyright Clearance Center Inc.*[22]

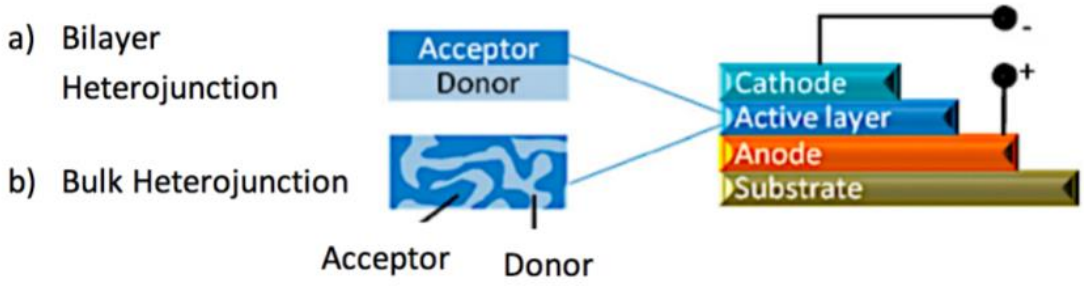

In the past decade, a remarkable amount of progress has been made, with performance levels of BHJ devices improving steadily. Historically, fullerenes have been widely used as acceptors in BHJs due to their strong electron accepting properties, high conductivity and high electron mobility.[22] Previously, the most common type of acceptor used across all BHJs was [6,6]-phenyl-C61-butyric acid methyl ester (**$PC_{61}BM$**) (Figure 1.5a). One of the shortcomings of **$PC_{61}BM$**, is its limited absorption in the visible spectrum due to its high degree of structural symmetry, which forbids low energy transitions. In order to increase the efficiency, **$PC_{71}BM$** can be used as an alternative, as it possesses a lower structural symmetry than **$PC_{61}BM$** and thus, can undergo more transitions. As a result, this increases its absorption from 400 nm to 700 nm, and thereby enhances the performance within a BHJ device.[11,22]

More recently, in order to further enhance performance levels, large amounts of research have gone into the use of non-fullerene acceptors (NFAs), that aim to retain the advantageous properties of fullerene acceptors (FAs) discussed earlier but to also overcome their insufficiencies. Compared to FAs, their optical and electronic properties can be readily tuned, and other advantages include greater thermal stability, greater photochemical stability and longer device lifetimes. FAs also often require time-consuming purification particularly **$PC_{71}BM$**, which results in higher costs. While the performance of NFAs have previously lagged behind fullerene-based devices, recent rapid development has led to efficiencies of over 13% in NFA organic solar cells, demonstrating its potential to overtake FAs in next-generation high performing OPV devices.[23,24]

Currently, one of the most promising types of NFAs are based upon rylene diimides, including perylene diimides (PDIs) and naphthalene diimides (NDIs), due to their high electron mobilities and electron affinities comparable to that of FAs, while also exhibiting strong optical absorption and photostability.

In order to control aggregation, dimeric PDIs are often implemented consisting of an aromatic linker between the units (Figure 1.5b) in order to introduce a twist into the structure. These PDI based small molecules can often achieve high efficiencies, for example it was reported by Liu *et al*[25] that a PDI dimer linked by an unsubstituted spirofluorene (**SF-PDI$_2$**) achieved a PCE of 9.5% when used as an acceptor in a solar cell device. As well as rylene diimides, other popular NFAs include those based upon fused rings electron acceptors (FREAs) and in particular, those based upon a high performing material with the abbreviated name ITIC. These compounds contain a push-pull type structure which is achieved by combining electron-rich and electron-poor units. This results in a narrowed optical band gap, extended absorption as well as control and tunability of the HOMO and LUMO energy levels.[23,24,26] Some of the best performing NFAs are based upon ITIC derivatives, with an impressive PCE of 13.1% reported for **IT-4F**.[27]

On the other hand, a wide library of electron rich donor materials (Figure 1.5c) have been employed, examples including high performing polymers based upon diketopyrrolopyrrole (**DPP**)[28], poly(3-hexylthiophene) (**P3HT**)[29] and benzodithiophene (**BDT**)[30] to name only but a few. The optical band gap E_g of the donor material often dictates the performance of the polymers, for example while a band gap of 1.1 eV is capable of harvesting 77% of the solar radiation, a band gap above 2.0 eV can only harvest 30% of solar photons. Thus, in order to fully exploit the source of solar energy, designing conjugated polymers with a low narrow band gap is desirable.[7,11,12]

Figure 1.5- a) Structures of FAs ***PC$_{61}$BM*** *and* ***PC$_{71}$BM****; b) Structures of high performing NFAs; c) Examples of high performing organic semiconductor donor material.*

a)

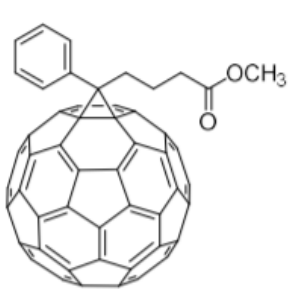

PC$_{61}$BM

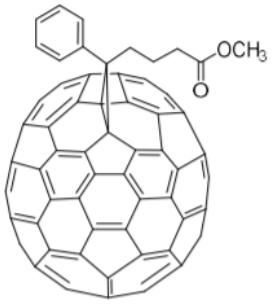

PC$_{71}$BM

b)

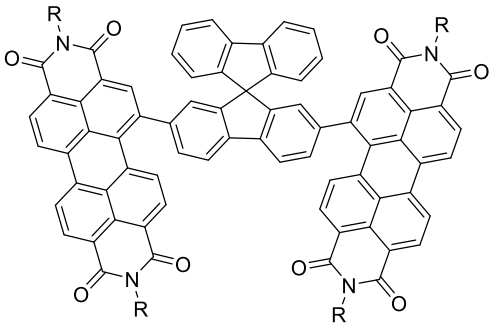

SF-PDI$_2$
PCE 9.5 %

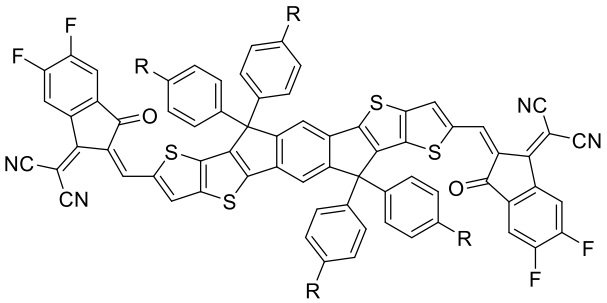

IT-4F
PCE 13.1 %

c)

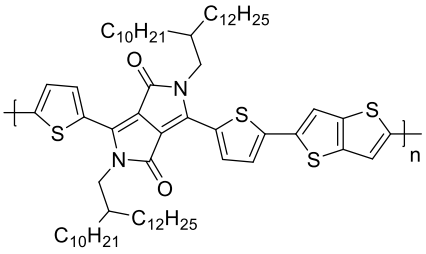

P2
PCE 9.4 %

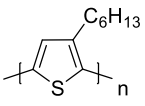

P3HT
PCE 7.3 %

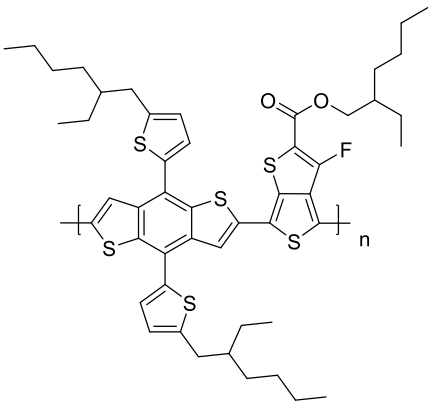

PTB7-Th
PCE 9.35 %

1.2.1.2 Operational Principles

Organic photovoltaic cells are made up of organic semiconductors generally consisting of both donor and acceptor type material (as seen in Figure 1.5), which convert solar energy into electrical power. The general mechanical picture of an organic solar cell comprises of three key steps (Figure 1.6). The process begins with the absorption of a photon, which allows the formation of an exciton (a neutral electron-hole pair). The exciton then diffuses to a region where it can undergo charge separation (through an electron-transfer process) at the donor-acceptor interface. Finally charge dissociation takes place and the separated free charge carriers (electrons and holes) transport to their respective electrodes (cathode and anode), aided by an internal electric field. As a result, photocurrent and photovoltage is generated.[11]

*Figure 1.6- Schematic diagram depicting the internal processes in an organic photovoltaic device. Republished with permission of Royal Society of Chemistry, from S. B. Darling and F. You, RSC Adv., **3**, 2013, copyright 2021 RSC; permission conveyed through Copyright Clearance Center Inc.*[31]

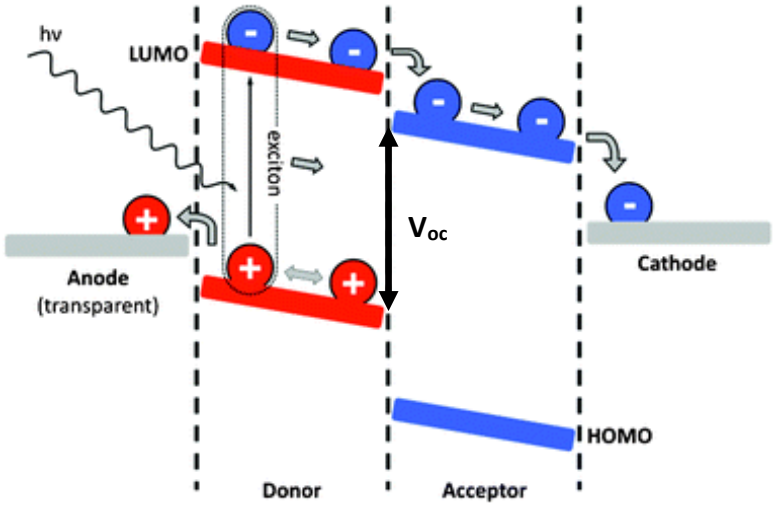

For exciton dissociation to successfully take place, the active layer in an OPV generally consists of an electron donor and an electron acceptor. The donor-acceptor interface has a high ionization potential and a high electron affinity, respectively. An electron excited from the HOMO to the LUMO of the donor, will transfer to the LUMO of the acceptor, providing that the LUMO of the acceptor is lower than the LUMO of the donor. For any OPV device, effective charge transfer with a low energy offset between the donor/acceptor molecular states and a high photoluminescent yield of the semiconducting material, is desirable. Provided that these conditions are met, this then reduces non-radiative recombination allowing the separated free charges to migrate to their respective electrodes.[31,32]

1.2.1.3 OPV Performance Parameters

The power conversion efficiency (PCE) is the ratio of maximum electrical power output (P_{out}) to the power of the incident light energy (P_{in}) and is one of the most important parameters in evaluating the performance of OPVs.[33] Currently, inorganic silicon solar cells dominate the commercial market with efficiencies reaching ~ 24% in crystalline Si cells.[31] In comparison organic solar cells are less efficient, but over the years significant progress has been made with record PCEs achieving above 15%.[34–36] As well as this, organic semiconductors are able to be processed by techniques not available to inorganic semiconductors. This, among other attractive properties of conjugated organic polymers (plastics), make them a promising candidate for use in solar cell devices.[1]

The PCE (η) can be extracted from a current-voltage (I-V) curve (Figure 1.7) of a solar cell measured under a simulated solar light and is determined by the following formulas.

Equation 1.1:

$$PCE(\eta) = \frac{P_{out}}{P_{in}} = \frac{J_{sc}V_{oc}FF}{P_{in}}$$

Equation 1.2:

$$FF = \frac{J_m V_m}{J_{sc}V_{oc}}$$

The simulated light intensity (P_{in}) used to measure the PCE is standardised at 1000 W/m^2 and is known as the AM 1.5 spectrum. This has the same spectral intensity distribution matching that of the sun on the earth's surface. The maximum electrical power output (P_{out}) and therefore the PCE, is dependent upon three important parameters; the open circuit voltage (V_{oc}), the short-circuit current density (J_{sc}) and the fill factor (FF) (Equation 1.2).[20]

The energy difference between the donors HOMO and the acceptors LUMO, is related to the maximum open circuit voltage (V_{oc}) output possible from an OPV. This voltage is the potential difference across the two electrodes (the cell) when the system is in a quasi-equilibrium state and the net current is at zero.[37] The V_{oc} is always lower in value than the E_g, thus the energetic loss of a solar cell can be measured by the difference between the two parameters. The V_{oc} in general, has a relationship with many influencing parameters within an OPV including the donor-acceptor interface, charge transfer states, energetic disorder and density of states, many of which will be discussed in further detail in future chapters.[37]

The short-circuit current density (J_{sc}) is defined as the maximum current produced by the OPV under illumination without applying any external potential. The fill factor (*FF*) is expressed in *Equation 1.2*, where V_m and J_m are the voltage and current at the maximum power point in the I-V curve, respectively. The *FF* itself is defined as the ratio of the maximum power (J_mV_m) to the external short and open circuit values ($J_{sc}V_{oc}$), representing the "squareness" of the I-V curve under illumination. Therefore, an ideal OPV device would have a rectangular shaped I-V curve and an *FF* approaching 1.[14,33,38]

Figure 1.7- Current-voltage (I-V) curve in the dark and under illumination of an OPV cell. Figure reproduced from T. Xu and L. Yu.[12]

A current-voltage (I-V) curve diagram removed for copyright reasons. Copyright holder is Elsevier Ltd.

1.3 The Fundamental Properties of Conjugated Polymers

1.3.1 Engineering the Band gap

The energy positions of the HOMO and LUMO levels as well as the size of the band gap E_g, are highly important factors in determining the optical and electrical properties in conjugated polymers and in turn, the performance of photovoltaic devices. Therefore, a fundamental understanding of molecular design and finetuning of the band gap through structural engineering, is crucial.

1.3.1.1 Aromatic and Quinoid Resonance Forms

Conjugated polymers have two possible resonance structures for the ground state with non-degenerate energy. The first, is the aromatic form in which each aryl unit has confined π-electrons therefore maintaining its aromaticity. The second, is the quinoidal form which instead consists of delocalized π-electrons along the backbone of the polymer, resulting in the conversion of double bonds into single bonds and *vice versa.* The quinoid resonance structure is less stable than the aromatic structure as in order to adopt the quinoid form, it requires the destruction of aromaticity and a loss in the stabilization energy. This then results in a smaller band gap and can be considered the first strategy in engineering the band gap. In general, the more stable the quinoid form of a conjugated polymer, the smaller the band gap.[11,39] Aromatic structures may be converted in to the quinoidal structure through oxidation. Oxidising agents such as potassium ferricyanide[40] or aerial oxidation[41] have been previously reported to obtain the quinoidal structure.

The bond length alternation (BLA) is a geometric parameter in which the ratio of aromatic to quinoid presence in a conjugated system can be represented. It is defined as the average of the difference in length between the adjacent carbon–carbon bonds, in a polyene chain. The more predominant the aromatic character in the ground state, the larger the BLA value. In contrast, when the quinoidal structure prevails, there is an increase in the presence of double bonds between two aromatic units, thereby lowering the BLA. The value of the BLA is highly reliant upon the aromaticity of the conjugated system and in general, the lower the BLA, the lower the band gap.[11,39]

In the examples below (Figure 1.8), polyphenylene (a) is observed to have a high band gap of 3.2 eV, due to the highly aromatic nature of the benzene ring. This effect can be diluted as seen with poly(phenylenevinylene) (**PPV**) (b), by adding a double bond spacer in between the phenyl rings, thereby reducing the aromaticity. As a result, the band gap is then lowered to 2.5 eV. Thienyl units are less aromatic than phenyl units, therefore it is more favourable for polythiophene (c) to adopt the quinoid form, demonstrated by its lower band gap of 2.0 eV. A creative way to lower the band gap further still, is presented with polyisothianaphthene (**PITN**) (d), relating back again to the fact that

benzene (1.56 eV) is more aromatic than thiophene (1.26 eV) units. In order to maintain the benzene aromaticity within the polymers structure, the conjugated backbone then favours the quinoidal form.[11] Thus, this lowers the band gap down to 1.0 eV, being one of the first polymers reported to do so.[42]

*Figure 1.8- The aromatic and quinoidal structures and E_g of a) polyphenylene, b) poly(phenylenevinylene) (**PPV**), c) polythiophene and d) polyisothianaphthene (**PITN**).*

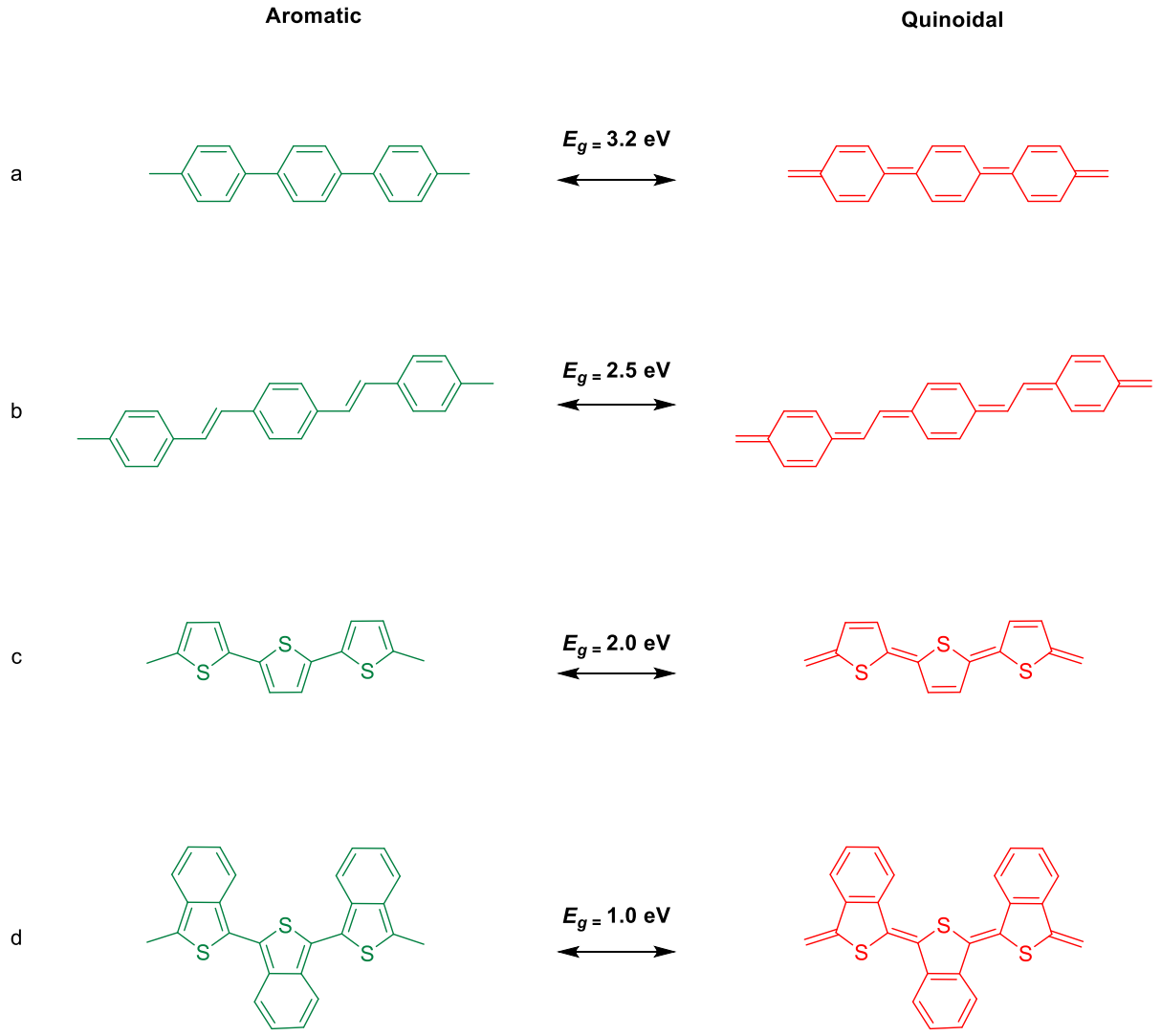

1.3.1.2 Fused Rings

Planarization of the conjugated polymer backbone is highly important in achieving a lower band gap. Bond twisting and rotation arising from steric hindrance, often leads to a distribution of the torsional angles between the conjugated rings along the chain of the polymer. Consequently, this causes localization of the orbitals which in turn decreases the π-orbital overlap, reduces the conjugation length and as a result, increases the optical band gap.[43]

A second strategy of band gap engineering used to overcome rotational disorder, is by implementing aromatic units that are fused together by covalent bonding, thereby rigidifying the system and greatly enhancing the planarity of the chain. Examples of fused units commonly used in conjugated polymers include benzodithiophene (**BDT**), fluorene, thienothiophene (**TT**) and carbazole (Figure 1.9).[11,12]

*Figure 1.9- Structures of fused ring systems **BDT**, fluorene, **TT** and carbazole.*[11,12]

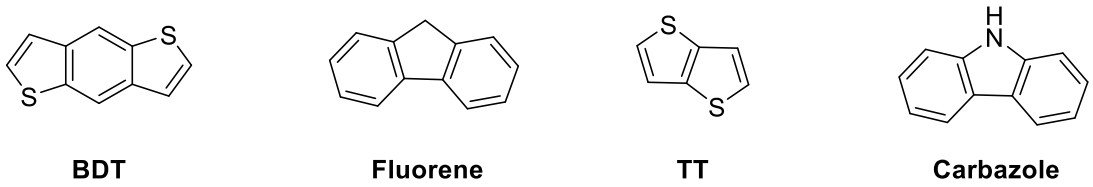

The use of fused rings as building blocks in conjugated polymers, has proven to be an effective strategy in lowering the band gap. One example involved the synthesis of a polymer (**PNTz4T**) (Figure 1.10a) consisting of a naphthobisthiadiazole (**NTz**) unit, the structure of which resembles two benzothiadiazole (**BTz**) units fused together, as reported by Osaka *et al.*[44] As a result of the **NTz** unit's strong electron affinity and highly π-extended structure, a small band gap of 1.54 eV and a PCE of 6.3% was achieved. In comparison, the polymer based on **BTz** (**PBTz4T**) had a wider band gap of 1.65 eV and a lower PCE of 2.6%. Another example demonstrating the effectiveness of this technique was reported by Brisset *et al*,[45] through the synthesis of **Poly(1)** (Figure 1.10b) containing a bi-thiophene unit that had been rigidified and fused together *via* bridging at the sp^3 carbon atom of the ketal group. This gave the polymer an impressively low band gap of 1.2 eV.

Figure 1.10- Structures of a) ***PNTz4T*** *and* ***PNTz4T****; b)* ***Poly(1)****.*[44,45]

a)

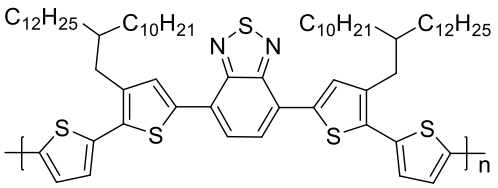

PBTz4T

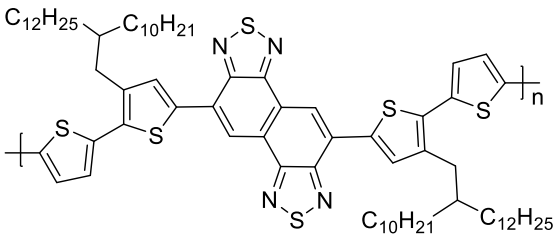

PNTz4T

b)

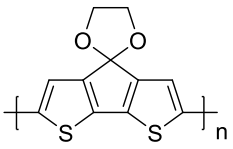

Poly(1)

1.3.1.3 Donor and Acceptor Co-polymers

One of the most powerful and widely employed strategies of band gap engineering, is the alternation of electron rich donor (D) units and electron deficient acceptor (A) units along the backbone of the polymer. As there are intrinsic push-pull driving forces between the D-A units, this then facilitates π-electron delocalization, thereby inducing quinoidal mesomeric structure and reducing the BLA.[11] More crucially, this then leads to interaction between the D and A, resulting in hybridization of their molecular orbitals (Figure 1.11a) to generate two new HOMO and LUMO levels for the D-A co-polymer. Ultimately, this results in a higher lying HOMO and a lower lying LUMO, which in turn lowers the optical band gap E_g.[39]

The HOMO and LUMO levels are largely localized on the D and A respectively, meaning individual tuning of the energy levels and the E_g can be achieved by selecting the appropriate units.[46] The extent of effect this has on the E_g, is largely reliant on the strength of the electron donating and electron accepting properties of the D and A units.[39] Since the introduction of this strategy in 1993 by Havinga *et al*,[47] a wide range of D and A units (Figure 1.11b) have been utilized in order to synthesise high performing, low band gap polymers.

Figure 1.11- a) Molecular orbital hybridization diagram of an electron rich donor (D) and electron deficient acceptor (A) unit; b) Examples of commonly used D/A building blocks found in organic semiconductors.

a)

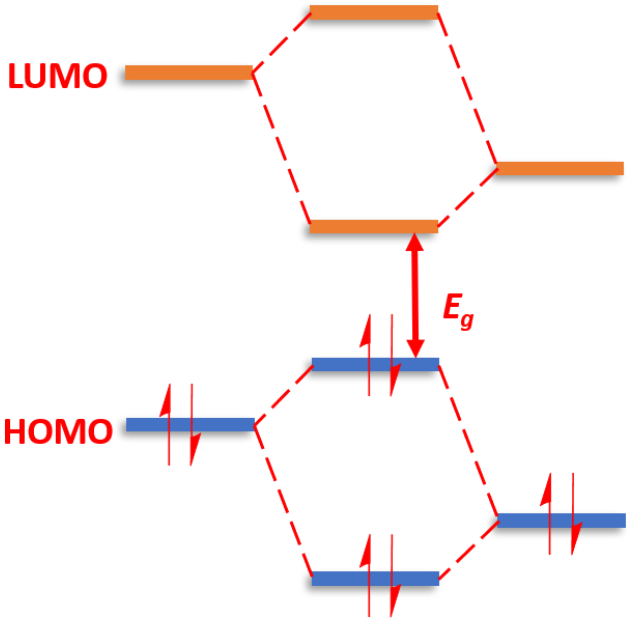

b)

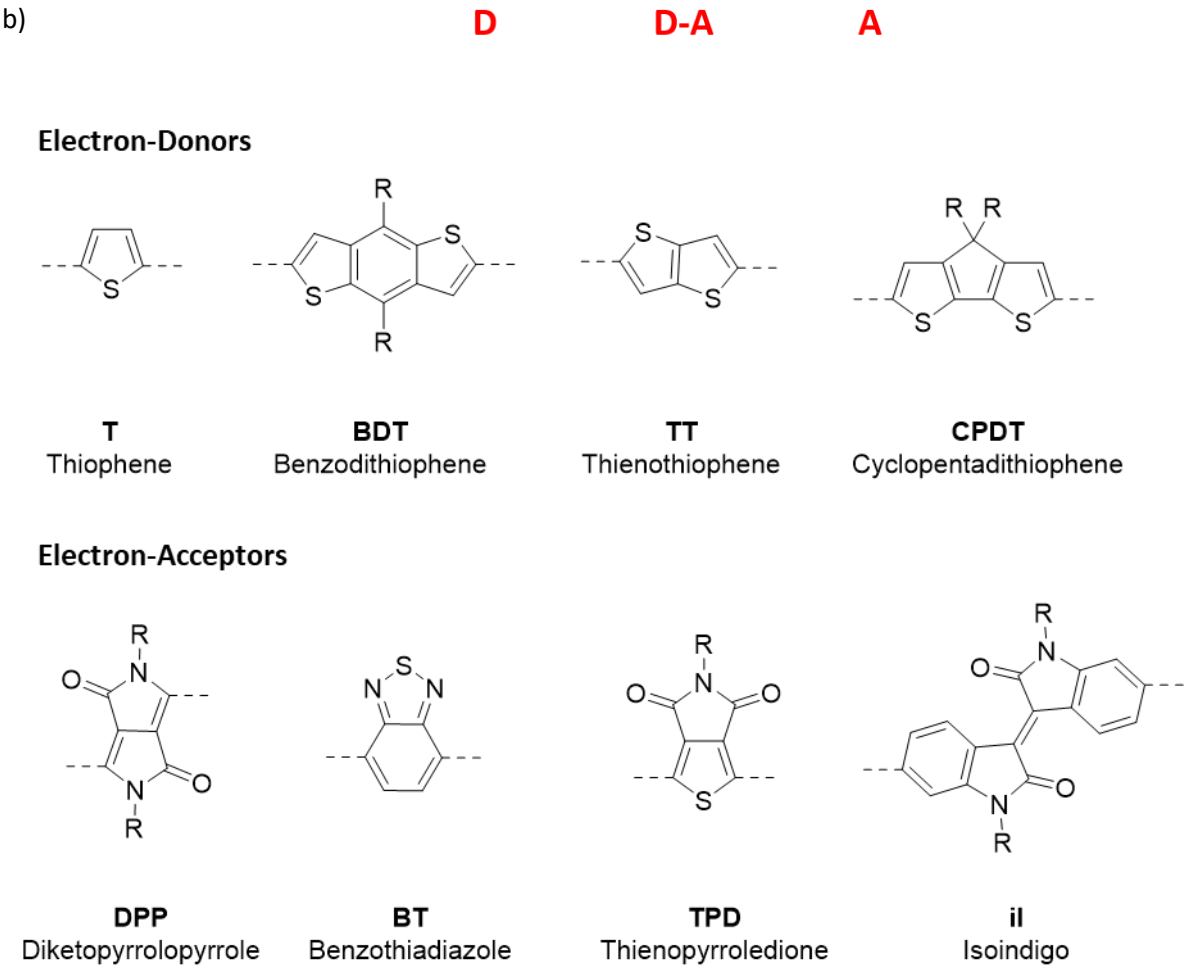

1.3.1.4 Electron Withdrawing and Donating Groups

Another straightforward strategy involves the incorporation of electron withdrawing groups (**EWG**) and/or electron donating groups (**EDG**) on to the monomer units along the polymer chain, in order to finetune the band gap *via* inductive or mesomeric effects.[11] In general, EDGs have the effect of raising the HOMO level of the polymer while EWGs lower the LUMO, resulting in a narrowed band gap.[39] Investigation of these effects were first reported in 1994 by Bredas and Heeger,[48] on their studies on the influence of substituents on the energy levels of PPV. Electron withdrawing cyano groups were found to lower the LUMO, while electron donating alkoxy groups raised the HOMO. In both these cases, a lower E_g was observed than that of PPV alone.

The addition of halogens into the polymer chain can also be an effective way in lowering the HOMO and LUMO levels. For example, fluorine which exhibits a high electronegativity of 4.0, can replace a hydrogen atom as an inductively EWG. Due to its similar size to hydrogen, fluorine can be used to fine tune energy levels within a polymer, without generating steric hindrance.[12] The effectiveness of this strategy was demonstrated in a series of polymers consisting of thieno[3,4-*b*]thiophene and benzodithiophene units (Figure 1.12), reported by Liang *et al.*[49] It was discovered that through the introduction of the EW fluorine atom on the backbone of the polymer (**PTB4**), the levels of the HOMO and LUMO were lowered compared to that of the non-fluorinated reference polymer (**PTB5**). As a result, this led to an increase in the V_{oc} of **PTB4** compared to that of **PTB5**, and a PCE of 6.1%.

*Figure 1.12- Structures and HOMO/LUMO levels of **PTB4** and **PTB5**.*[49]

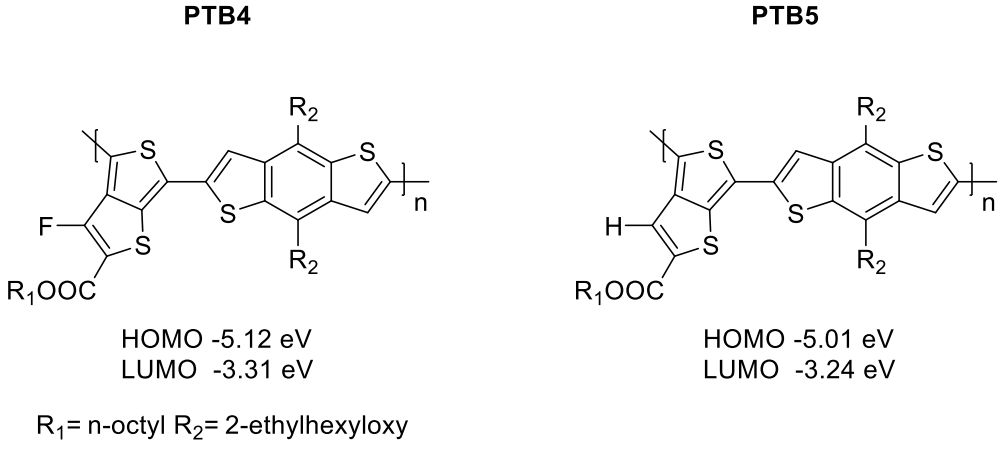

1.3.1.5 Conformational Locks

More recently, another strategy in rigidifying the polymer backbone and increasing planarity, involves the use of non-covalent intramolecular interactions known as conformational locks. Various examples of long-range interactions particularly between heteroatoms have been reported, such as O···S, N···S,

X···S (X= halide) and hydrogen bonding.[50–52] Many polymers (Figure 1.13) have been designed and synthesised to utilize their interactions through space, resulting in reduced rotational disorder.[53]

Figure 1.13- Examples of long-range interactions to form conformational locks and reduce rotational disorder found in polymers between heteroatoms.[50–52]

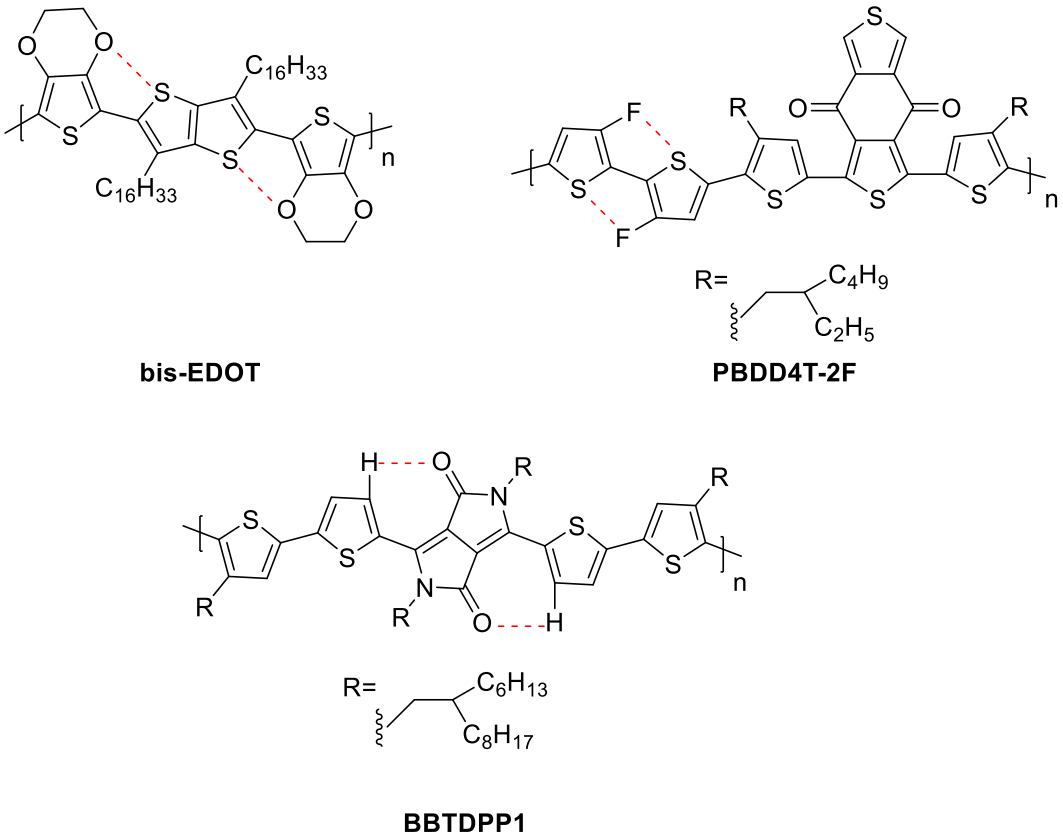

An example of this strategy was effectively demonstrated in polymer **PPTz** (Figure 1.14) reported by Bronstein *et al.*[54] The structure of **PPTz** is isostructural to poly(3-hexylthiophene) (**P3HT**) but instead, consisting of alternating thiophene and thiazole units. Due to the presence of non-covalent N···S interactions, enhancement of the backbone planarity was observed compared to that of **P3HT**. As a result, **PPTz** achieved deeper HOMO and LUMO energy levels.

*Figure 1.14- Structure of **P3HT** and **PPTz** (showing non-covalent N···S interaction).*[54]

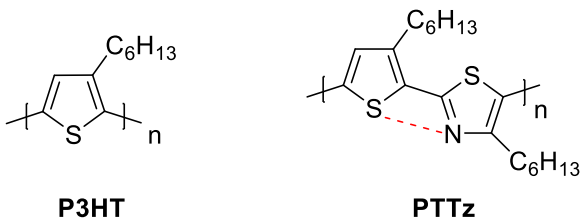

1.3.2 Microstructure of Conjugated Polymers

The microstructural morphology of the semiconducting thin-film largely influences the charge-carrier mobility of the polymer, and in turn the performance of the device.

There are two main directions in which charge-carriers can transport along. The first, is the intermolecular pathway in the π-π stacking direction, in which charge-carriers can transport *via* hopping to neighbouring π-orbitals. Factors that affect transport through this pathway include conjugation length and π-π stacking distances.[55] The second, is the intramolecular pathway along the π-conjugated backbone of the polymer, as observed in polythiophene (Figure 1.15a).[56] Thus, in order to promote high charge-carrier mobility, the polymer backbone should be of high planarity and high purity, with minimum torsional disorder and chain defects. Thus overall, charge transport *via* both the intra-chain and inter-chain transport channels are determined by a balance of various factors. While it is often possible to control alkyl stacking distances *via* incorporation of alkyl chains of different lengths, it is often more challenging to control distances in the π-π stacking direction.

As conjugated polymer chains have various degrees of conformational freedom and interact weakly with each other, this results in complex microstructures in the solid state, ranging from completely amorphous to crystalline. It was generally observed that polycrystalline inorganic semiconductors have superior charge transport efficiency compared to that of their amorphous analogues.[57] Thus, based on these results, many organic conjugated polymers were designed with regioregularity and crystallinity in mind such as **P3HT**, in order to achieve efficient charge transport.[11,14,57,58] However in recent years, this idea has been challenged by several seemingly amorphous polymers also displaying high-charge carrier mobility.[59,60] It was later discovered that energetic disorder within conjugated polymers led to electron localization, giving rise to charge traps and thus, limiting charge-transport. As a result, in order to achieve high charge-carrier mobility in conjugated polymers, a planar torsion-free backbone is critical.[57,61] This is discussed in further detail in *Chapter IV*. Overall, the relationship between microstructure and charge transport in conjugated polymers is still not fully understood and ongoing investigation continues. This is particularly the case for materials with a microstructure that lies between (poly)crystalline and amorphous.[57]

A semi-crystalline high molecular weight polymer such as **P3HT**, displays a continuous variation in order within its microstructure, in which both amorphous and semi-crystalline regions co-exist. In general, **P3HT** is one of the most widely studied and well understood polymers within the field, and current understanding of its charge transport is as follows.

The semi-ordered regions consist of large domains with 3D long-range order, known as crystallites (Figure 1.15b).[57] These regions can also comprise of smaller domains that instead possess short-range

order of a few molecular units, known as aggregates (Figure 1.15c). On the other hand, amorphous regions possess no local or long-range order and take on a 'spaghetti' like structure (Figure 1.15d).[57]

*Figure 1.15- a) A schematic illustration of the charge transport in a semi-crystalline polymer film such as **P3HT**. Figure reproduced from A. Salleo[56]; b) microstructure of a semi-crystalline polymer film (**P3HT**) c) disordered aggregates, d) amorphous film. Shadowed areas represent ordered regions that are connected via long polymer chains highlighted in red. Figure amended from R. Noriega et al.*[57]

A picture of a) a schematic illustration of the charge transport in a semi-crystalline polymer film such as P3HT and; b) microstructure of a semi-crystalline polymer film (P3HT) c) disordered aggregates, d) amorphous film removed for copyright reasons. Copyright holders are Elsevier Ltd. and Nature Publishing Group respectively.

In general, charge transport mainly occurs in the semi-ordered areas, as an energy barrier must be overcome for charges to be transported from ordered to amorphous regions. It was observed that the amorphous regions in the **P3HT** film had a wider band gap compared to the aggregates, due to a shorter conjugation length. As a result, no energetic overlap of electronic states between amorphous and ordered regions were observed, thus amorphous regions do not contribute to charge transport. Providing that the molecular weight of the polymer is high enough, with a sufficient amount of density of ordered material, efficient charge transport can occur through a network of ordered regions connected *via* long polymer chains acting as tie molecules.[57]

1.4 Synthesis of Conjugated Materials

1.4.1 Palladium Catalysed Cross-Coupling

Since their discovery, chemists have explored many different methods in order to prepare organic semiconducting materials including chemical oxidation polymerisation, electrochemical polymerisation and organometallic polycondensation.[62] Ultimately, the synthesis of conjugated polymers relies upon single carbon-carbon bond formation between aromatic units and as mentioned, while there are various routes one could use, in this thesis we will only be discussing palladium mediated cross-couplings.[11]

In general, transition-metal-catalysed reactions provide a powerful strategy for generating new sp^2-sp^2 C-C bonds. Examples of such couplings include the Heck reaction (organohalide/triflate with an alkene), Sonagashira cross-coupling (terminal alkynes with an organocopper reagent), Negishi reaction (organohalides with an organozinc) and Kumada reaction (organohalides with a Grignard reagent). A further two methods widely exploited in the synthesis of conjugated polymers are the Stille cross-coupling and the Suzuki cross-coupling. These are palladium catalysed reactions between organohalides with either organostannanes or boronic acids, respectively. It is these two couplings only, that are utilized and discussed in this thesis.

Reaction conditions for Stille and Suzuki couplings are generally mild, which is highly important when considering compatibility with a variety of functional groups which may be present on the monomers/polymer. They are widely considered the most robust and efficient methods of preparing alternating co-polymers.[11] As a general rule, Stille couplings are more suited to thiophene-containing polymers, while Suzuki couplings are usually used to prepare phenyl-containing polymers due to the poor reactivity of benzene stannnanes under Stille conditions.[63]

1.4.1.1 Stille Cross-Coupling

The Stille cross-coupling is the palladium ($Pd^{(0)}$) catalysed reaction between an organic electrophile (i.e. organic halide) and an organostannane (organotin) to generate new C-C bonds.[64]

The catalytic cycle is shown below (Scheme 1.1). To begin, the active 14-electron $Pd^{(0)}L_2$ species (L=PPh_3 or P(*o*-tol)$_3$) is generated from a 16-electron $Pd^{(II)}$ precursor *via* reduction by the organotin compound, before entering the catalytic cycle.

Scheme 1.1- Catalytic cycle of Stille cross-coupling.

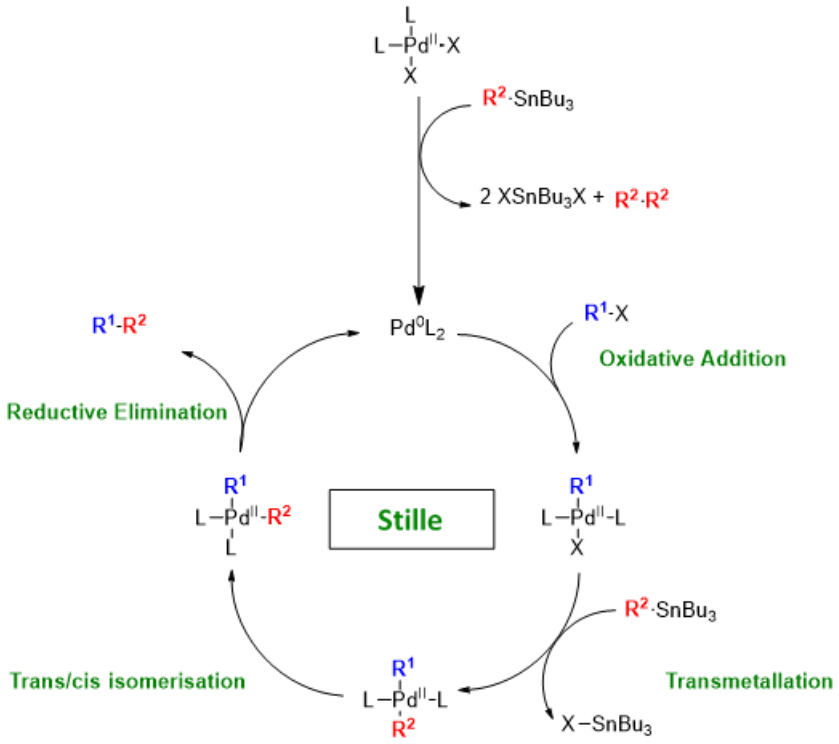

After formation of the coordinatively unsaturated $Pd^{(0)}L_2$ species, it readily undergoes oxidative addition with an organic electrophile (R^1-X), occurring *via* a concerted reaction to form a stable 16-electron $Pd^{(II)}$ species. Initially, a *cis*-tetravalent species is produced however this rapidly isomerises to the *trans* product, which is more thermodynamically stable. The *trans*-isomer (R^1PdL_2X) then undergoes a slow transmetallation step with an organotin nucleophile (often R^2-$SnBu_3$) to form $R^1PdL_2R^2$. For the final step to take place, *trans* to *cis* isomerisation must occur so that the two coupling R groups are in a *cis*-position to each other, to allow reductive elimination. This then produces the R^1-R^2 elimination product as well as regenerating the $Pd^{(0)}L_2$ catalyst, allowing the cycle to continue.[64]

There are many advantages of employing Stille cross-coupling when making conjugated materials. Many organostannane reagents are commercially available, making the reaction an easily accessible method. These reagents are often relatively insensitive to moisture and oxygen compared to their other organometallic counterparts, allowing harsher reaction conditions if needed. The robust nature of the reaction allows for microwave-assisted couplings to take place, greatly improving the efficiency of the reaction and in general are often high yielding, largely tolerant to functional groups and provide good monomer solubility. For these reasons, Stille is considered one of the most versatile methods in the arsenal of organometallic chemistry.[65,66]

There are however some drawbacks, for example organotins are highly toxic compounds, resulting in the production of toxic by-products that have a low solubility in water making disposal an issue. This also makes separation of product from impurities highly challenging.[67]

1.4.1.2 Suzuki Cross Coupling

The Suzuki-Miyaura cross-coupling (or simply Suzuki cross-coupling) is the palladium ($Pd^{(0)}$) catalysed reaction between an organic electrophile (i.e. organic halide) and an organoboron compound in the presence of base, to form new C-C bonds.[68] The catalytic cycle of Suzuki (Scheme 1.2) is very similar to that of the Stille cycle discussed previously, however the main difference being before transmetallation can occur, the organoboron species must be activated using a base.

Scheme 1.2- Catalytic cycle of Suzuki cross-coupling.

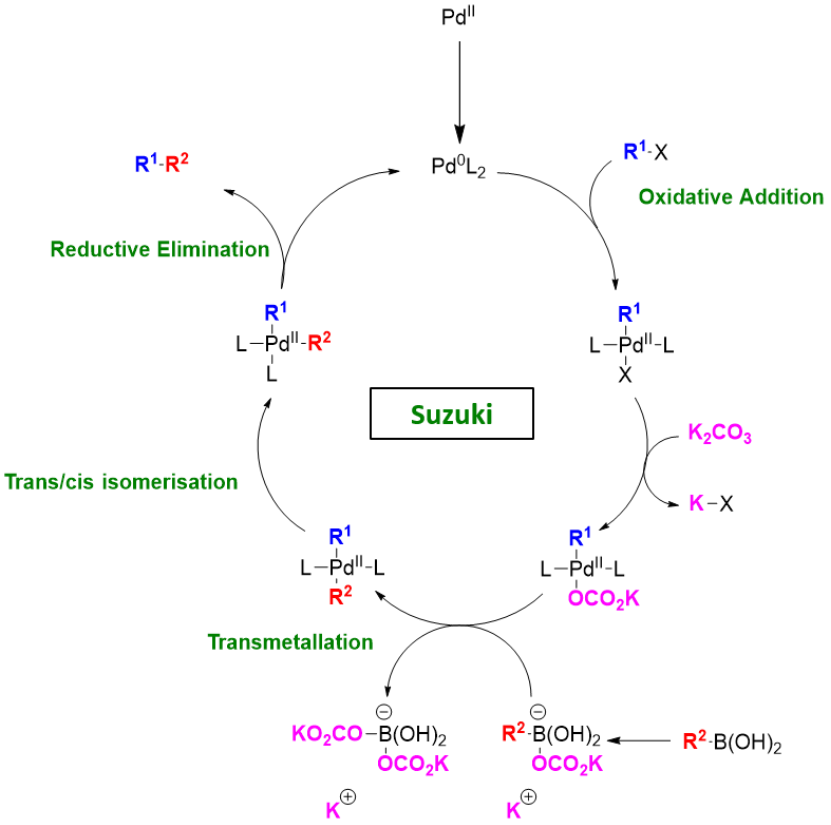

As with the Stille coupling, the cycle begins with oxidative addition to form a *cis*-tetravalent species which rapidly isomerises to the *trans* product ($Pd^{(II)}$ species). The halide on the $Pd^{(II)}$ species is then replaced with a base (such as hydroxide, alkoxide, phosphate or in this case carbonate as shown in Scheme 1.2) forming a *trans*-R^1PdL_2OR species. Organoborane species do not readily undergo transmetallation due to the weak carbanion character of the organic groups, therefore the base also reacts with the organoborane species to form a more nucleophilic borate complex, thereby activating it. This polarisation of the organic ligand (R^2) then accelerates the following transmetallation step, generating

the *trans*-$R^1PdL_2R^2$ species. This then undergoes a *trans* to *cis* isomerisation followed by reductive elimination (similarly to the Stille), forming the R^1-R^2 product and once again regenerating the $Pd^{(0)}L_2$ catalyst, so that the cycle may continue.[69]

The advantages of the Suzuki cross-coupling over Stille include the wide range of boronic acids that are commercially available, often cheaper than organotin reagents. Additionally, organoboranes are often more stable and are much less toxic, allowing for easier preparation and purification. The reaction itself is also insensitive to moisture. Another positive aspect of Suzuki coupling is that they are often far more environmentally friendly than Stille, regarding the solvents and reagents that are used. For example, due to the polar nature of the by-products in Suzuki couplings (i.e. inorganic impurities), they are often highly soluble in water/methanol, allowing for easier and safer disposal. While the solvents used in Stille couplings are often chlorinated (i.e. chlorobenzene), Suzuki couplings instead are generally carried out in a toluene-water system, which is far less damaging to the environment.

On the other hand, Suzuki couplings do face some limitations. While Stille reactions are highly tolerant to most functional groups, due to the reaction conditions required in Suzuki couplings, precursors containing base-labile functionalities cannot be used. Stille in general is a more robust reaction, and can tolerate microwave-assisted methods, while Suzuki couplings are less so and tend to require 3-day reaction times, making them less efficient. The purity of boronic acids can also be an issue as they have a tendency to undergo dimerization or cyclic trimerization, generating boronic acid anhydrides or boroxines.[70]

1.4.1.3 Palladium Catalysts

A variety of palladium catalysts have been employed in cross-coupling reactions. One of the most frequently used $Pd^{(0)}$ catalysts is tetrakis(triphenylphosphine)palladium(0) [$Pd(PPh_3)_4$] and can be simply referred to as *tetrakis*. An issue, however, is its poor stability in air as the phosphine ligands are readily oxidized, therefore deactivating the catalyst.[71]

Another widely used palladium catalyst is tris(dibenzylideneacetone)dipalladium(0), [$Pd_2(dba)_3$], which has a higher air-stability than tetrakis. However, as this pallidum species does not contain any phosphine ligands these must be added in combination, usually in the form of triphenylphosphine (PPh_3) or tri(*o*-tolyl)phosphine ligands (P(*o*-tol)$_3$). These ligands are used due to their bulky nature, therefore giving them a large bite angle which forces the R^1 and R^2 groups closer together in the *cis*-$R^1R^2Pd^{(II)}L_2$ complex. As a result, this increases the rate of the reductive elimination step.[71]

As well as $Pd^{(0)}$ sources, $Pd^{(II)}$ sources such as palladium (II) acetate [$Pd(OAc)_2$] and palladium (II) chloride [$PdCl_2$], can also be used. In general $Pd^{(II)}$ catalysts are more stable and can generate the activated $Pd^{(0)}$ species *in situ.* It is to be noted that $Pd^{(II)}$ species are often more expensive than their $Pd^{(0)}$ counterparts, however very little is needed in the catalytic reaction.[71]

1.5 Polymer Definitions and Parameters

By definition, a polymer is a large molecule made up of repeat units of the same chemical structure called monomers. A homopolymer consists of only one type of monomer, while co-polymers are made up of two or more different types of monomers. In this thesis, specifically co-polymers are prepared and discussed.

An important value used to understand various physical properties of polymers including mechanical strength, solubility and thermal behaviour, is its molecular weight. A polymers molecular weight is defined as a distribution rather than a single value, as polymer growth occurs randomly resulting in a series of chains of unequal length with different molecular weights. Such systems are said to be polydisperse and thus, the molecular weight of a polymer represents the average molecular weight calculated from the molecular weights of all the chains in the sample.[72,73]

1.5.1 Number Average Molecular Weight

There are two different ways to characterise the molecular weight of a polymer, with the most important being the number average molecular weight M_n. This is an average based on the number of polymer chains in a sample, and is defined by the following equation:

Equation 1.3:

$$M_n = \frac{\sum N_i M_i}{\sum N_i}$$

Where the N_i is the number of moles of chains composed of i monomer units, while the M_i is the molecular weight of that chain composed of i monomer units.

1.5.2 Weight Average Molecular Weight

The second distribution used is the weight average molecular weight M_w, this time including the mass of the individual chains as a contributing factor. It takes into account, that bigger chains contain more mass than smaller chains (i.e. oligomers), therefore have a larger contribution to the overall molecular weight average.

The weight of a molecule W_i, with a molecular mass of M_i is given by the following formula:

Equation 1.4:

$$W_i = N_i M_i$$

Thus, the M_w is then given by:

Equation 1.5:

$$M_w = \frac{\sum W_i M_i}{\sum W_i} = \frac{\sum N_i M_i^2}{\sum N_i M_i}$$

1.5.3 Polydispersity Index

Once the M_n and M_w are determined for any given polymer, it is then possible to calculate its polydispersity index (PDI). The PDI is used to measure the broadness of the molecular weight distribution of a polymer and is given by:

Equation 1.6:

$$PDI = \frac{M_w}{M_n}$$

The larger the value of the PDI, the broader the molecular weight of the polymer. A monodisperse polymer in which all the chains are of equal length would have a PDI of 1. Polymers with a PDI between 1.02-1.10 are typically used for calibration.[73]

1.5.4 Gel Permeation Chromatography

Gel permeation chromatography (GPC) is a type of size exclusion chromatography (SEC), which allows the M_n and M_w to be measured at the same time, by measuring the entire distribution of the polymer. It is one of the most common and convenient methods used by chemists to obtain such measurements. First a dilute solution of the polymer is prepared in a suitable solvent, which is then injected into a column packed with a gel (stationary phase) and a continuing stream of solvent (mobile phase). For majority of the polymers discussed in this thesis, the solvent system used within the GPC was chlorobenzene. The stationary phase consists of a distribution of controlled pore sizes that separate the polymer chains by size. Thus, lower molecular weight material is retained for longer in the column, while higher molecular weight material larger than the pores diameter, elute from the column first. As

the size separated chains exit the column, they are 'counted' using a refractive index detector (RID) according to their elution time. A GPC trace is then generated in which the molecular weight is plotted as a function of elution time (Figure 1.16).[74–76]

Figure 1.16- A GPC trace displaying the spectrum of polystyrene (PS) which is used as the calibration standard (red) and a polydisperse sample (blue). Figure reproduced from I. Yudhipratama.[74]

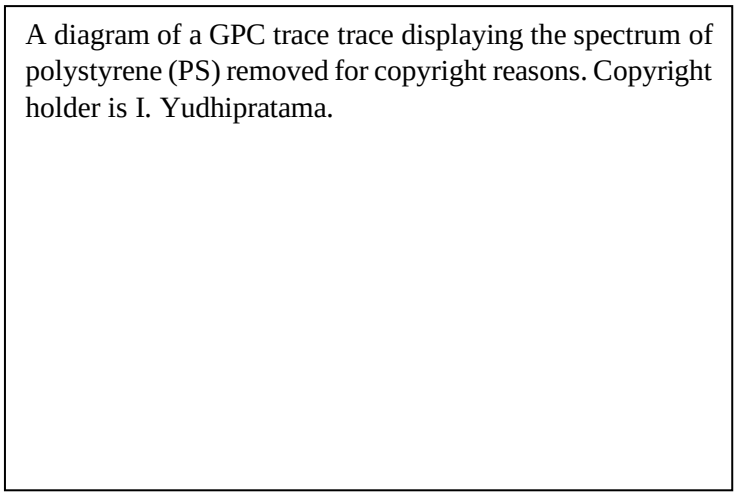

The GPC must be calibrated so it is possible to assign a molecular weight to each retention time slice for the eluted polymer. The most common method is to use a relative calibration that is based on a set of well characterised polymer standards, with very narrow dispersity such as polystyrene. For a polymer to be considered acceptable for use as a GPC standard, its PDI must be below 1.10. It is to be noted that the molecular weights obtained from a GPC are relative to that of the calibrant. While the values given may not be absolute is not so important, but rather that they lie within the acceptable range.[75]

1.6 Types of Organic Semiconducting Materials

In general, organic semiconducting materials are classified as either conjugated polymers (long length), small molecules (short length) or oligomers (intermediate length). The synthesis of conjugated polymers often involves stepwise transition-metal catalysed polymerisation techniques such as Stille and Suzuki cross-couplings, between bi-functional monomers. However as mentioned previously, polymer growth occurs randomly producing a series of chain lengths of different sizes. Shorter lengths (i.e. dimers, trimers, tetramers, pentamers etc.) are considered oligomers and can exist at any point during the polymerisation. As the reaction time continues, the distribution increases and moves towards higher molecular weights (polymers). The conjugation length at which an oligomer is considered a polymer, is still often debatable.

During polymerisation as the conjugation length increases, the E_g decreases as previously discussed. Eventually, once the number of monomer units exceed a certain value, the reduction of the E_g, reaches a plateau. At this point, the optical and electronic properties of the polymer reach a saturation limit and is said to be at the effective conjugation length (ECL). Any further extension beyond this length results in limited reduction of the optical band gap, and it is at this point the molecule is generally considered a polymer.[11] The number of monomer units itself needed for the E_g to reach its saturation limit, is dependent on the chemical structure of the monomer. For example, polymers based on poly(*p*-phenylene) (PPP) derivatives often have wide optical band gaps as a result of twisting between the aromatic rings, due to steric hinderance. This then limits the effective conjugation length of the polymer.[77]

Regardless of whether an organic semiconducting material is categorised as a polymer, small molecule or an oligomer, in order to perform well in optoelectronic devices both are ruled by the same key factors, including absorption/emission ability and charge-carrier mobility. Thus, a fundamental understanding of controlling these factors are crucial when designing high performing materials.

1.6.1 Conjugated Polymers

The most extensively studied organic semiconductors in organic photovoltaics are conjugated polymers, possessing a variety of favourable properties (i.e. low production costs, mechanical flexibility, solution processability and high charge-carrier mobility). For these reasons, they have demonstrated to be highly promising materials for a range of applications including OPVs, OFETs, OLEDs, photodetectors and sensors.[78] Currently, both academic researchers and industrial research groups are pushing these devices towards commercialization, with some already having done so. More recently, due to the high luminescent yields found in various conjugated polymers, these materials are also being considered for use in solid state lasers.[79]

Over the years, considerable progress has led the way to highly impressive PCEs being achieved in OPVs, with an increasing number of devices obtaining PCEs above 10%. In 2019, Yuan *et al* reported a single junction organic solar cell consisting of an NFA acceptor **Y6**, matched with a benzodithiophene polymer donor **PM6** to yield a remarkable PCE of 15.6% (Figure 1.17).[80]

*Figure 1.17- Chemical structure of NFA **Y6** (acceptor) which achieved a PCE of 15.6% when mixed with conjugated polymer **PM6** (donor).*[80]

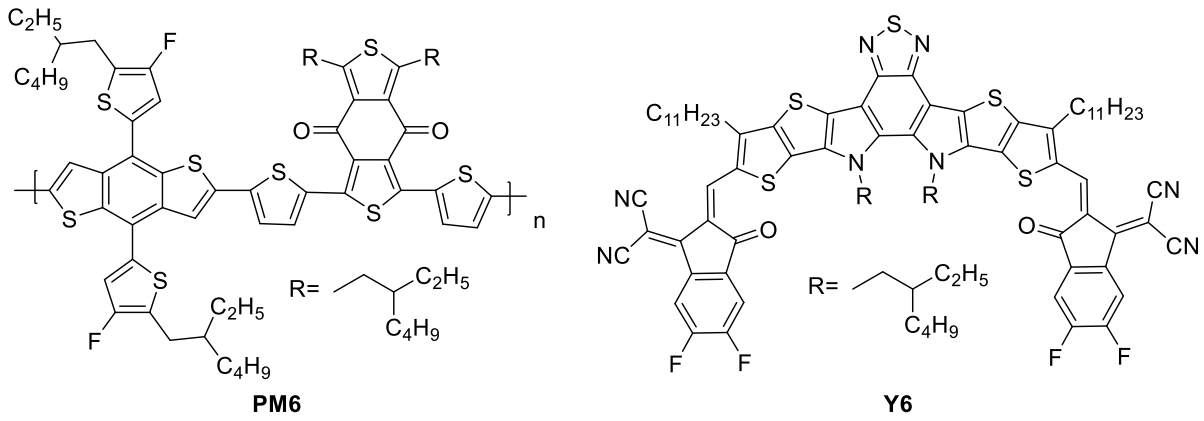

Compared to small molecules, conjugated polymers tend to perform better in devices, generally achieving higher PCEs. Additionally, thin films of polymeric material are smooth and uniform, which allows control over large-scale film characteristics such as structure and morphology.[14] Issues however, lie within batch to batch variations for a given polymer. These variations can include solubility, molecular weight, polydispersity and purity, which as a result lead to differences in properties and performance.[81] In particular, polydispersity is often found within conjugated polymers leading to charge traps in segments of longer conjugation lengths, therefore decreasing charge-carrier mobility. As a result, this decreases the performance of the polymer. This was observed by fractioning polymers based on PPV with a high polydispersity. When small amounts of low band gap material were introduced to a fraction of large band gap material, device performance significantly decreased below that of either individual component.[82]

1.6.2 Conjugated Small Molecules and Oligomers

In contrast, conjugated small molecules that are of an intermediate length, are a way of overcoming many of the batch to batch variations associated with conjugated polymers. Thus, in comparison small molecules tend to have more reproducible fabrication protocols. As small molecules and oligomeric materials are synthesised in a stepwise manner, this results in well-defined structures that allow a better understanding of structure-property relationships, within conjugated systems. In turn, these materials can also be used as model compounds for rationalizing the properties of well-known high molecular weight polymers, as well as allowing prediction of those yet unrealized.[81,83]

However, it has been shown that conjugation length can directly influence several fundamental properties of conjugated systems including the E_g, conductivity, the ECL and the extinction coefficient (ε) (the latter is discussed in further detail in *Chapter II)*. Over the years, efforts have been made to raise the efficiencies of small molecule-based devices, due to their various advantages over conjugated polymers. In 2018, Yang *et al*[84] reported the synthesis of **H22**, a small molecule donor based on a central benzodithiophene core containing alkyl silyl-thienyl conjugated side chains (Figure 1.18). It was observed that the incorporation of terminal cyanoacetic esters, led to higher charge-carrier mobility and better 3D charge pathway in blend films. When paired with an NFA acceptor (**IDIC**) in an organic solar cell device, a PCE of 10.29% was achieved. Thus, demonstrating the great potential of organic conjugated small molecules, in competing with conjugated polymers.

*Figure 1.18- Structure of small molecule donor **H22** which achieved a PCE of 10.29% when mixed with NFA **IDIC** acceptor.*[84]

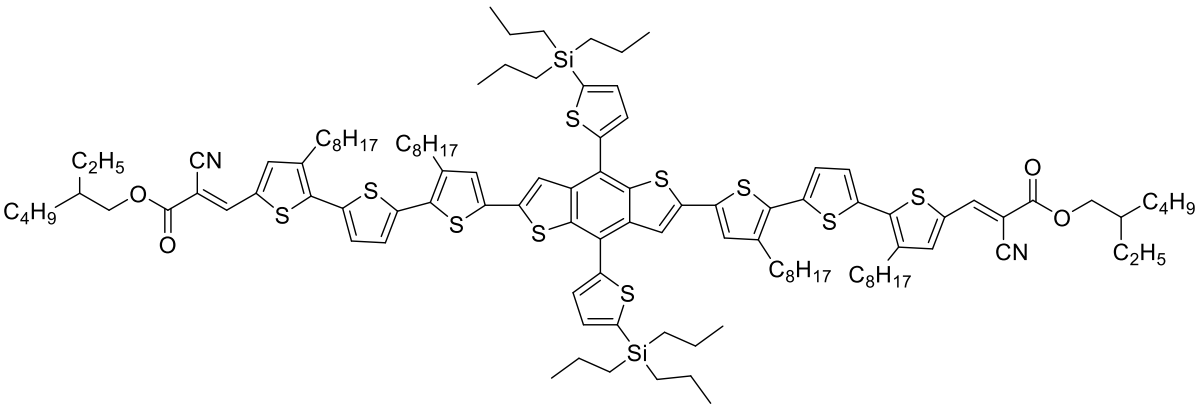

H22
PCE 10.29 %

In addition to conjugated small molecules, there has also been much research on conjugated oligomeric systems based on compounds such as thiophene,[85] *para*-phenylene,[86] fluorene,[77] and phenylenevinylene.[87] Such studies are often used in order to estimate the effective conjugation length, in a series of homologous oligomers. This enables the possibility of substituting polymers of high molecular weight for shorter oligomers, that have reached convergence of their physical properties.[83]

1.7 Diketopyrrolopyrrole (DPP)

Diketopyrrolopyrrole (DPP) was first reported in 1974 by Farnum *et al*,[88] while attempting to synthesise an unsaturated *β*-lactam. The reaction was carried out under modified Reformatsky conditions (the reaction between an aldehyde or ketone, with an α-halo carbonyl compound in the presence of zinc, to give a β-hydroxyester),[89,90] using ethyl acetate, benzonitrile and zinc. While the intended product was not obtained, a brilliantly red, highly insoluble and crystalline pigment (DPP) was isolated, in yields ranging between 5-20%.

Due to poor yields, the discovery of DPP was largely left aside until 1988, when Iqbal *et al*[91] reported the synthesis of DPP *via* a new one-step route, using benzonitrile and diethylsuccinate in the presence of base. This revised synthesis largely increased the yield up to 60-70%, encouraging the commercialization of DPP for use as a pigment in inks, varnishes and paints.[90] While in 1993 the first conjugated polymer based on DPP was reported by Chan *et al*,[92] it was not until much later in 2008 when DPP based materials were utilized in solution processed OPVs[93,94] and OFETs.[52]

Currently, DPP which has been observed to possess high fluorescence and exceptional electrochemical stability,[95] is one of the most widely used motifs for application in optoelectronics including chemosensors,[96] solid-state dye lasers,[97] photocathodes,[98] OLEDS, OPVs and OFETs.[99–102]

All DPP compounds are structurally based on 2,5-dihydropyrrolo[4,3-c]pyrrolo-1,4-dione (Figure 1.19).

*Figure 1.19- Structure of diketopyrrolopyrrole (**DPP**) where Ar represents aryl groups.*

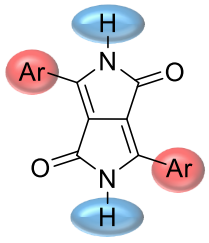

DPP

It is this π- conjugated bicyclic dilactam structure, that is responsible for the unusual properties of DPP derivatives.[90] The structure of the DPP core gives the compound its electron deficient nature, which allows synthesis of extremely narrow band gap donor-acceptor materials.[60] As a result, DPP possesses excellent light-harvesting properties allowing DPP-based materials to deliver exceptional performance in OPVs. Additionally, DPP's skeleton is highly planar, encouraging strong intermolecular π-π interactions that facilitate efficient charge-carrier mobility in OFET devices.[100] The DPP core is electron deficient due to the two amide groups present in the ring. This allows incorporation of electron rich

moieties such as thiophene or benzene, as flanking groups on either side of the DPP core. By doing so, it is possible to fine tune properties such as the HOMO and LUMO energy levels, and therefore the E_g. Over the years, these properties have been exploited to produce a variety of high-performing optoelectronic devices containing DPP-based materials.[95,100]

1.7.1 Modifications of DPP

DPP is generally considered a useful building block in donor-acceptor synthetic strategy, due to the various modifications that are possible on the DPP core. DPP polymers consist of four main components that include: a) the DPP core, b) alkyl-side chains, c) aryl substituents and d) an adjacent π-conjugated segment (Figure 1.20).[103]

Figure 1.20- Basic structure of DPP polymers consisting of a) the DPP core (black), b) alkyl-side chains (blue), c) aryl substituents (red) and d) adjacent π-conjugated segment (orange).

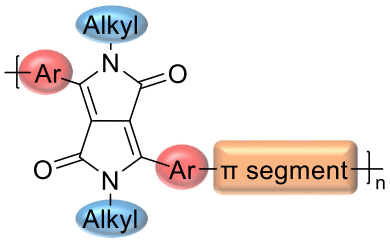

DPP

1.7.1.1 Modification of the Aryl Substituents

The aromatic flanking groups present on either side of the DPP core, are introduced during synthesis *via* an aromatic nitrile precursor and have a strong influence on the properties of the DPP polymer. The synthesis of the DPP core generally occurs *via* a condensation reaction between one equivalent of diethyl succinate and two equivalents of an aromatic nitrile, under basic conditions (Scheme 1.3). Optimisation has shown that the reaction is best performed using a tertiary alkoxide as the base.[90]

Scheme 1.3- General synthesis of the DPP core via condensation between diethyl succinate and an aromatic nitrile.

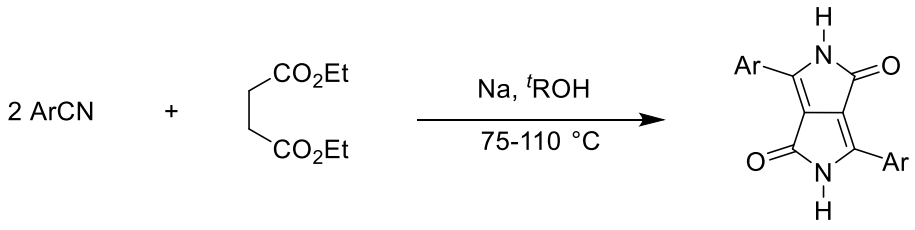

DPP

The most common aromatic substituents found within the literature are either that of phenyl or thienyl groups. Phenyl-DPP was the very first to be synthesised and has since been co-polymerised with a variety of different π-conjugated segments. However, in general phenyl-DPP based-polymers show poor performance in OPV devices, with PCEs usually remaining below 2%, as well as demonstrating low charge carrier mobility in OFETs. This is due to the large dihedral angle (30°) observed between the phenyl moieties and the DPP core, as a result of steric hindrance. Thus, this leads to a reduction in conjugation, widening of the band gap and reduction in charge-carrier mobility.[104]

On the other hand, thienyl-DPP based-polymers show far more favourable characteristics, including co-planarity between the thiophene units and the DPP core. Additionally, as thiophene is a strong electron donating substituent, this enables a 'push-pull' donor-acceptor strategy, leading to efficient orbital overlap and a highly narrow optical band gap (near IR region). Compared to phenyl-DPP based-polymers, electron and hole mobilities are much improved and figures of >1 cm^2/Vs have been achieved.[103,105] While this thesis will mainly discuss thienyl-DPP based-polymers, various other aryl flanking groups have been reported including pyridine,[106] thienothiophene,[60] furan,[107] naphthalene,[108] thiazole[109] and selenophene[110] to name a few (Figure 1.21).

Figure 1.21- Examples of different flanking aryl substituents of DPP.

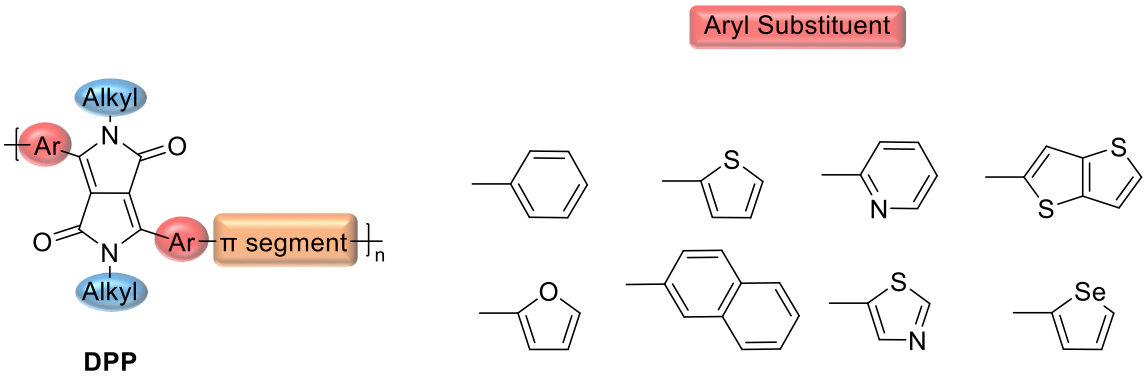

1.7.1.2 Modification of the Side Chain

The amide groups present on unsubstituted DPP units, result in the formation of intermolecular hydrogen bonds between the nitrogen and oxygen atoms in the solid state. As a result, DPP is a highly insoluble material. In order to improve solubility and enable solution processable fabrication of electronic devices using DPP polymers, it is necessary to incorporate alkyl chains at the lactam N-H positions.

Generally, linear alkyl chains are inadequate at solubilising DPP based polymers. Rather, branched chains are widely used on DPP polymers to provide sufficient solubility. However, the length of such chains has been found to have a critical influence on the performance of the polymer.[103] In a study

reported by Janssen *et al,*[111] the effects of different length branched alkyl chains were investigated by increasing side chain length from 2-hexyldecyl (**HD**) to 2-octyldodecyl (**OD**) to 2-decyltetradecyl (**DT**), on DPP polymer **PDPPTPT** (Figure 1.22). It was observed that as the alkyl chain length increased, the PCE values decreased from 7.4% to 5.8% to 3.2% respectively, as a result of the different phase separations between the acceptor (**PCBM**) and the donor (**PDPPTPT**). The polymers formed an extended semi-crystalline fibrillar network, in which the width of the fibrils increase with the length of the alkyl chain. For **DT-PDPPTPT** the fibril width was 30 nm, while in contrast **HD-PDPPTPT** was found to have a narrower width of only 8 nm. As the typical exciton diffusion length is only around 10 nm long, smaller fibril distances as found with **HD-PDPPTPT**, allow a larger number of excitons to reach the donor-acceptor interface for charge generation, thus resulting in a higher device efficiency. However, it is to be noted that in order to access a larger range of comonomer units, increased solubility is required, thus (**DT**) chains are still implemented alongside shorter branched alkyl chains within DPP polymers.[112]

*Figure 1.22- Structure of polymer **PDPPTPT** and the increasing alkyl chain lengths; 2-hexyldecyl (**HD**), 2-octyldodecyl (**OD**), 2-decyltetradecyl (**DT**).*[111]

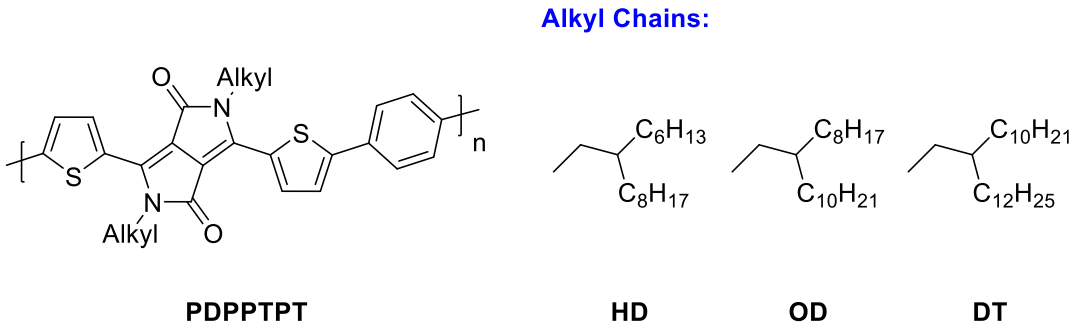

As well as length, the branching point of alkyl chains can also significantly affect the performance of DPP polymers. McCulloch *et al,*[113] reported a systematic study on a thienothiophene DPP polymer (**DPPT-TT**), in which the effect of increasing branching points (**C1**, **C2** and **C3**) from the polymer backbone was investigated (Figure 1.23). As the branching point moved further away from the polymer backbone, a small decrease in π-π stacking distances and general increase in the degree of crystallinity and hole mobility were observed, however the branching point at **C2** resulted in the highest PCE of 7.3%. Overall, these studies demonstrate the importance in selecting the optimum alkyl side chain when designing high performing DPP-based polymers.

*Figure 1.23- Structure of **DPPTT-T** and alkyl chains of different branching points (number of atoms between the lactam nitrogen on the DPP core and branching point i.e. 1 carbon (**C1**), 2 carbons (**C2**) and 3 carbons (**C3**)).*[113]

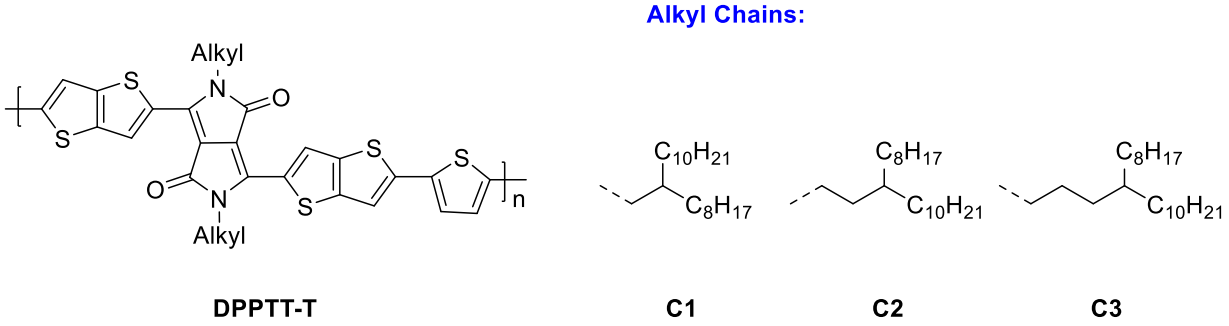

While *alkyl* chains are the most commonly used side chains in DPP polymers, *oligio(ethylene glycol)* side chains (OEGs) have also been investigated in recent years. For example, Kanimozhi *et al*[114] reported a DPP-DPP co-polymer (**N-CS2DPP-OD-TEG**) (Figure 1.24), consisting of DPP units with branched alkyl chains and linear OEG chains in an alternating fashion. **N-CS2DPP-OD-TEG** was observed to possess an extended absorption of up to ~ 1100 nm, and when used in a field-effect transistor the device demonstrated electron mobilities of up to 3 $cm^2\ V^{-1}\ s^{-1}$. In 2016, Wang *et al*[115] reported the use of branched OEG chains on thiophene-DPP polymer **PDPP3T-O20**. Compared to its alkyl chain counterpart **PDPP3T-C20**, smaller π-π stacking distances were observed due to the increased flexibility of the OEG side chains. Additionally, a higher dielectric constant, higher hole mobility, a red-shifted absorption spectrum and a larger surface area was observed. This resulted in a higher PCE of 5.37%, as supposed to 3.0% for the alkylated variant. Thus, in certain DPP polymers, OEG side chains can offer advantageous properties that can be utilized in various optoelectronic devices, including sensors.[116]

*Figure 1.24- Structure of DPP polymers **N-CS2DPP-OD-TEG** and **PDPP3T-O20** containing OEG side chains.*[114,115]

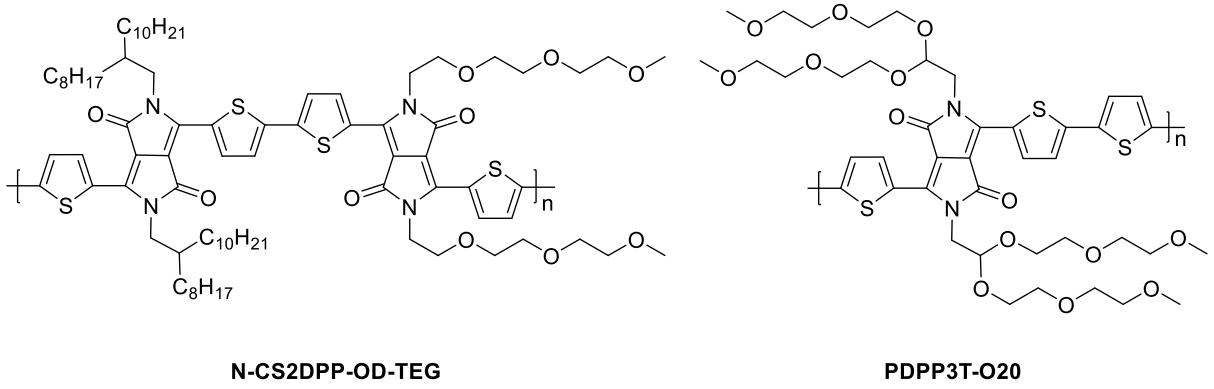

1.7.1.3 Modification of the π-conjugated segments

The choice of adjacent π-conjugated segment is also a key factor in determining the optical properties of DPP polymers. Generally, through the introduction of stronger electron donating π-conjugated segments, the optical band gap can be reduced (Figure 1.25). Starting with a simple aromatic such as benzene and moving towards more electron donating groups such as benzodithiophene, bithiophene, thienothiophene and pyrrole, results in narrowing of the band gap from 1.56 eV to 1.34 eV. To lower the band gap further still, highly electron donating groups such as dithienopyrrole can be employed (E_g =1.23 eV).[103]

In some cases, electron accepting/deficient groups such as thienopyrroledione (1.42 eV) or benzothiadiazole (1.19 eV) have been introduced, also resulting in low band gaps. However, while employing benzothiadiazole afforded an impressively low band gap, the polymer only achieved a low PCE of 1.2%. This was attributed to the small LUMO offset which led to ineffective photoinduced electron transfer.[103] Thus, through careful selection of aryl substituents and π-conjugated segments, it is possible to effectively tune the energy levels and optical band gap of DPP polymers.

Figure 1.25- Examples of different π-conjugated segments found in thienyl-DPP polymers and their optical band gap.[103]

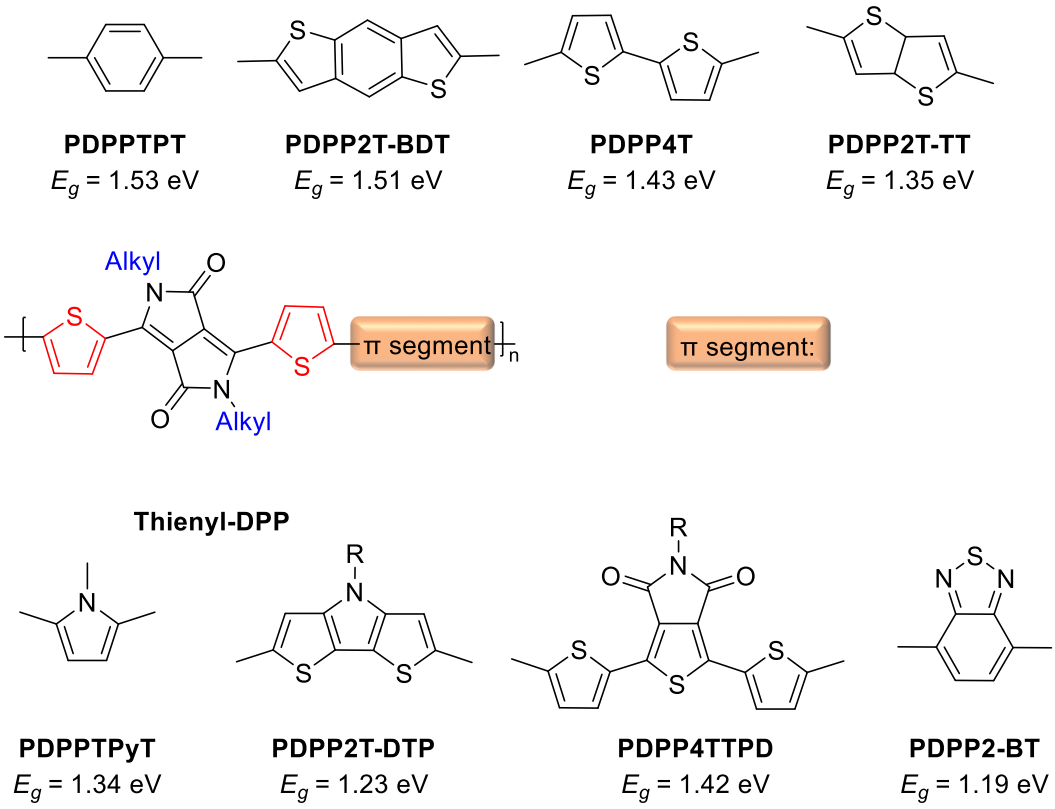

1.7.2 High Performing DPP Polymers

Thienyl-DPP based-polymers have demonstrated great potential for application in various optoelectronic devices due to their high charge-carrier mobilities, high fluorescence and excellent stability.

One of the most highest performing thienyl-DPP polymers for OPV devices include **P2**, reported by Heeger *et al* (Figure 1.26).[28] This thienyl-DPP-thienothiophene co-polymer achieved an impressive PCE of 9.4%, due to a high J_{sc} of 20.07 mA cm^{-2} and a *FF* of 0.7. Another high performing DPP polymer **(PDPPTPT**) consisting of a phenyl co-monomer, was first reported as having a reasonable PCE of 5.5%. However, Janssen *et al*[117] later reported an improved PCE of 7.4% as a result of a higher molecular weight polymer, highlighting the importance of molecular weight on the performance of conjugated polymers. In 2017, Hou *et al*[118] reported a novel DPP-BDD (1,3-bis(thiophen-2-yl)-5,7-bis(2-ethylhexyl)benzo-[1,2-c:4,5-c′]dithiophene-4,8-dione) based polymer, **P266**. As the polymer displayed strong aggregation, the donor and acceptor materials were dissolved in different solvents and mixed for film casting. This alternative method of preparation allowed the polymer to form aggregates under mild conditions, that induced the formation of robust polymer fibril bundles. This led to distinct phase separation, that helped reduced charge recombination and improved charge transport. As a result, **P266** achieved a PCE of 9.18%.

As well as OPVs, DPP polymers have demonstrated high performance as semiconducting p-type, n-type, or ambipolar materials in OFETs, due to the highly ordered packing and excellent charge-transport properties found in thienyl-DPP polymers.[100] Ong *et al*,[119] reported the synthesis of a p-type DPP polymer **P1**, that demonstrated a remarkably high mobility of up to 10.5 $cm^2\ V^{-1}\ s^{-1}$. While mobilities of n-type materials are usually lower, Yun *et al*[120] reported an n-type DPP polymer (**PDPP-CNTVT**) exhibiting high electron mobility of up to 7.0 $cm^2\ V^{-1}\ s^{-1}$ *via* careful selection of the incorporation point of the nitrile group, along the polymer backbone.

Figure 1.26- Examples of high performing DPP polymers used in OPVs and OFETs.

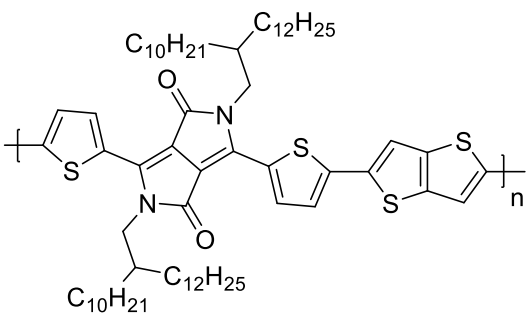

P2
PCE 9.4 %

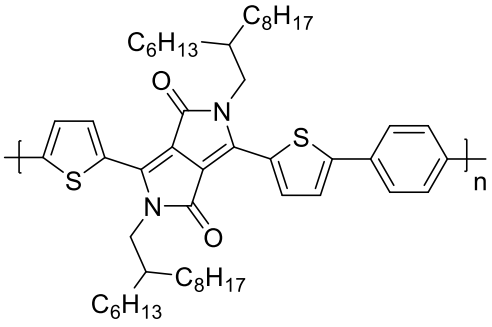

PDPPTPT
PCE 7.4 %

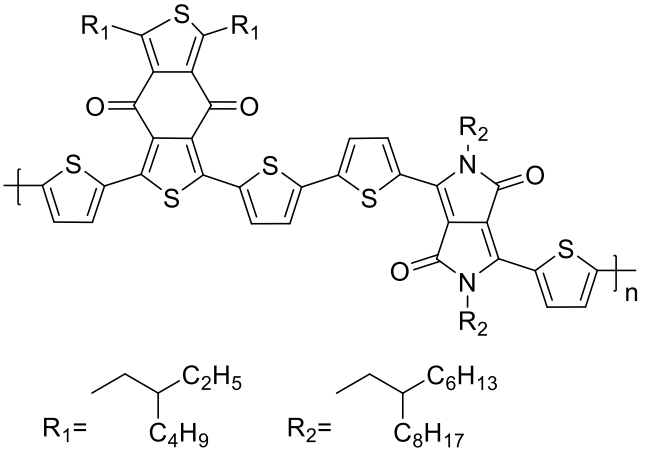

P266
PCE 9.18 %

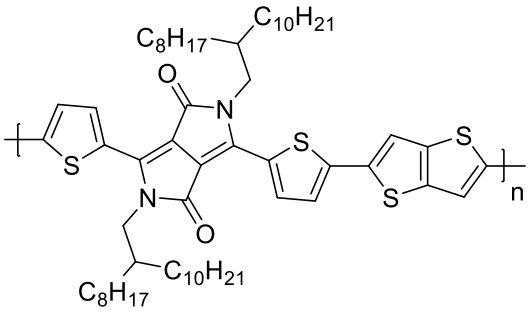

P1
μ_h = 10.5 cm^2 V^{-1} s^{-1}

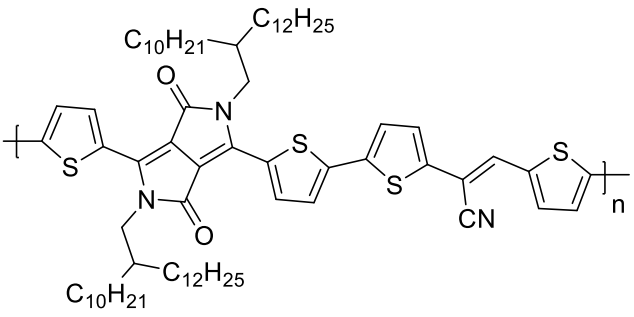

PDPP-CNTVT
μ_e = 7.0 cm^2 V^{-1} s^{-1}

1.8 Thesis Scope and Aims

The performance of conjugated polymers is often limited by batch to batch variation and a lack of reproducibility during organic synthesis, as well as structural defects and energetic (torsional) disorder within the polymer chain. In addition, low V_{oc} values in organic solar cells are often observed, resulting in poor device performance. To allow these materials to reach their full potential for application in a wide variety of optoelectronic devices, further investigation of their structure-property relationship is required.

When studying these complex structure-property relationships, it is useful to base these studies on a widely investigated and well characterised conjugated motif, such as DPP. As previously discussed, DPP shows high fluorescence and possesses exceptional electrochemical stability. Its electron deficient core allows the synthesis of extremely narrow band gap donor-acceptor materials. Therefore, these materials show great potential for use in optoelectronic devices, demonstrated by several high performing DPP-based polymers, reported previously in literature.

Thus, this thesis broadly investigates chain length, encapsulation and asymmetry of conjugated DPP-based polymers and small molecules. In this work, we investigate how these different variables affect the materials absorptive properties and performance, including strength of absorption (extinction coefficient), optical band gap and the $V_{oc.}$ Therefore, the general aim of this thesis is to gain a better understanding of the structure-property relationships within DPP-based materials, so we can begin to overcome the general limitations faced by conjugated polymers in this field.

The first part of this thesis is a continuation on the previous work by another member of our research group, Dr Anastasia Leventis, who sought to answer how chain length, polydispersity and defects can affect the wavelength and strength of absorption, of conjugated materials. Thus, Leventis synthesised a series of thienyl-DPP oligomers (n = 1-5) and their polymeric counterpart (**PDPPTPT**), a well-studied polymer previously reported in literature.[117] However, among the oligomers, the tetramer was found to be impure (Figure 1.27). Thus, in *this* work the tetramer was re-synthesised *via* alternative reaction conditions, in an attempt to achieve a higher purity. In addition, new samples of the monomer, dimer and reference polymer **PDPPTPT** to be used in *this* study, were also prepared. Samples of the trimer and pentamer previously prepared by Leventis were are also used in this study. As the polymer was based upon the same monomer unit as the oligomers, this allowed direct comparison of their optical properties.

Figure 1.27- Structure of the DPP tetramer.

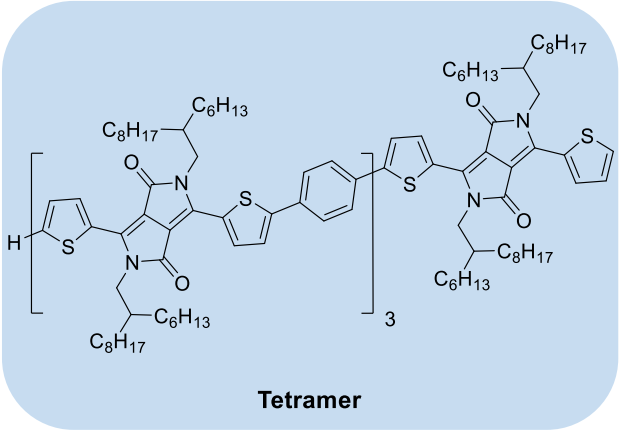

The second part of this thesis investigates the effect of partial encapsulation of the DPP core, on the performance of organic solar cell devices. By doing so, we aimed to alter the donor-acceptor interface and thus, better understand how we can improve the V_{oc}. In the first study, the synthesis of a novel encapsulated DPP monomer (**EC10DPPT**) is discussed, followed by the synthesis of two series (Ph- and TT-) of novel DPP based polymers, doped with an increasing amount of **EC10DPPT** (Figure 1.28). This is followed by discussion of the polymer's absorptive properties and device performance, specifically focusing on the $V_{oc.}$

*Figure 1.28- Structures of -Ph and -TT DPP polymer series, and novel encapsulated thienyl-DPP monomer **EC10DPPT**.*

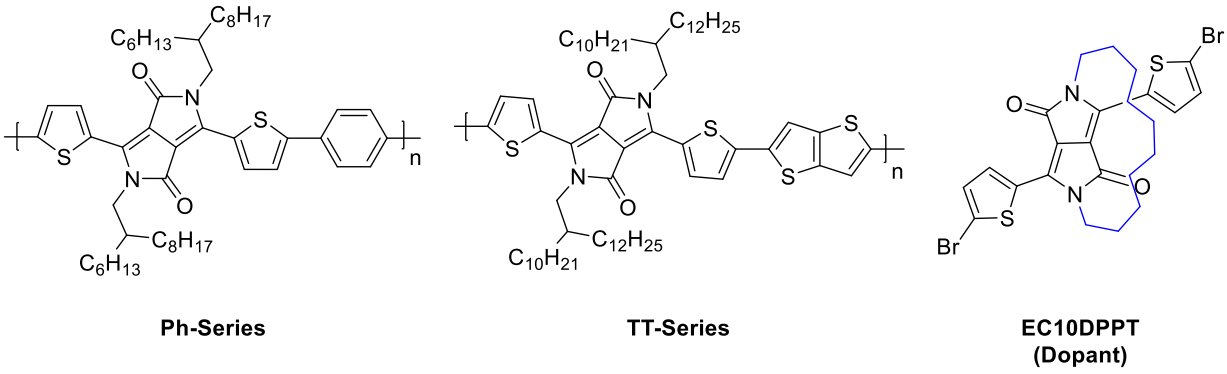

The second part of this study investigates the effect of ring size, on the properties of encapsulated DPP polymers. The synthesis of three additional encapsulated DPP monomers of different ring size are discussed (including one with an ethylene glycol-based ring), followed by the synthesis of a novel series of encapsulated DPP-BDT based polymers (Figure 1.29). This is followed by discussion of the polymer's absorptive properties and device performance. In addition, the performance of fullerene and non-fullerene devices, are compared.

Figure 1.29- Structures of the encapsulated DPP-BDT polymers.

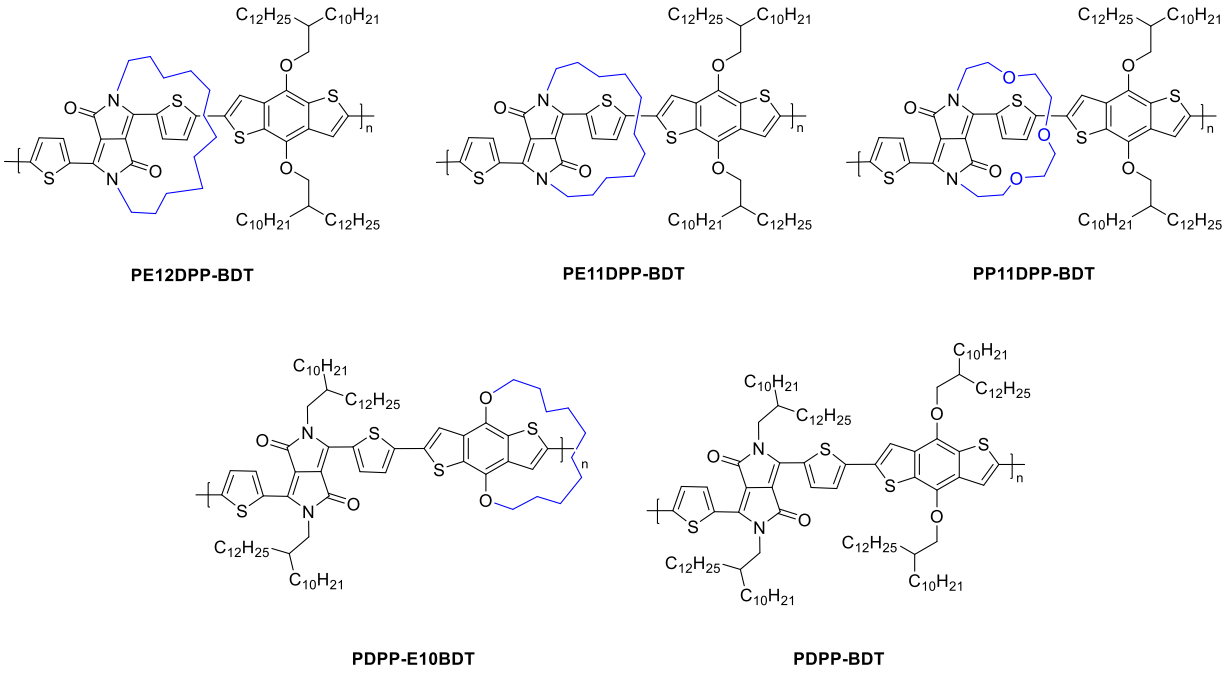

Finally in the third study, building upon McCulloch *et al's* research,[121] we intend to investigate the effect of encapsulation on the properties of ethylene glycol chained DPP-based polymers, for potential application in organic electrochemical transistors (OECTs). Here we discuss the synthesis of an encapsulated and linear chained DPP monomer, as well as a bi-thiophene co-monomer, all of which consist of ethylene glycol chains. We then attempt to synthesise polymers **PE14DPP-T2** and **PDPP-T2** (Figure 1.30).

*Figure 1.30- Structures of the encapsulated **PE14DPP-T2** and the linear chained **PDPP-T2**.*

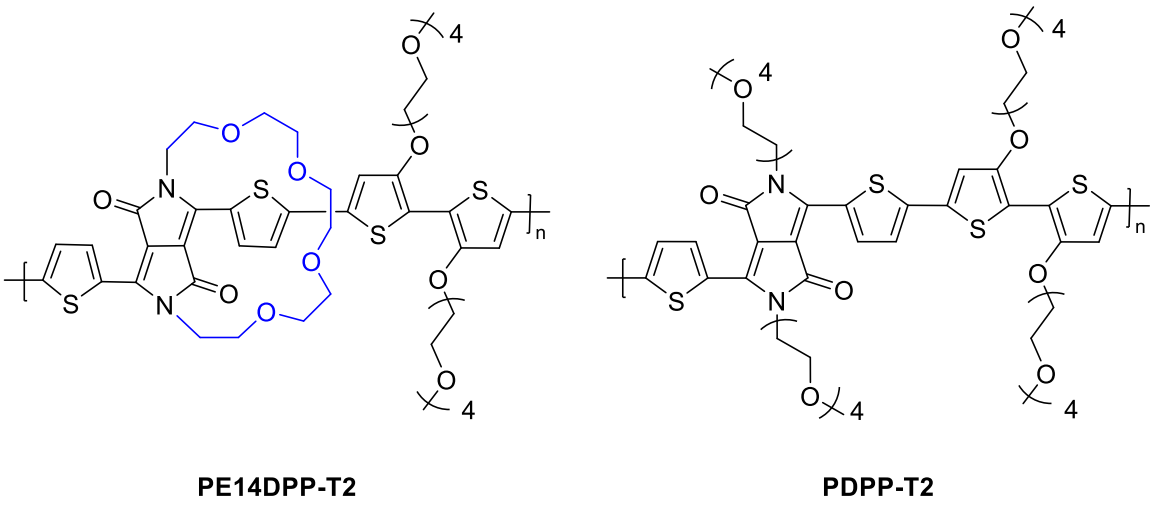

The third part of this thesis aims to investigate the effect of energetic/torsional disorder on charge transport within DPP polymers, and how we can begin to overcome this problem. Based upon previous electronic structure calculations by Troisi,[43] here we attempt to synthesise a novel DPP polymer, consisting of a higher DPP to thiophene ratio than previously reported in literature (Figure 1.31). Based on Troisi's results, it is theorised that due to secondary overlap contribution between the thiophene/DPP units, this novel polymer will show a higher tolerance to energetic/torsional disorder, than previously reported for DPP polymers.

*Figure 1.31- Structure of Target Polymer (**a**).*

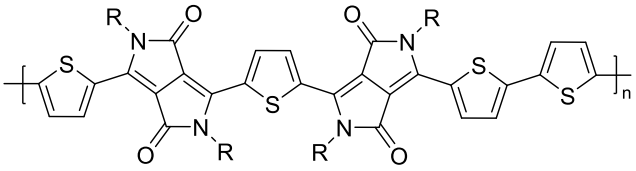

P(a)

R= Alkyl Chain

The synthesis of several novel coupling precursors towards the target monomer are discussed, among them a series of alkylated thienyl pyrrolinone esters. These compounds were also used to develop a novel synthetic strategy towards fully asymmetric DPP derivatives. Within this sub-chapter we discuss the synthesis of four novel fully asymmetric DPP derivatives, of which two are structural isomers. We then compare their electronic and absorptive properties to their symmetrical counterparts, to better understand how asymmetry effects the properties of conjugated small molecules based on DPP (Figure 1.32).

Figure 1.32- Fully asymmetric DPP.

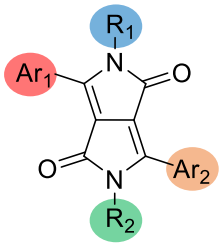

II

The Effect of Chain Length on the Optical Properties of Conjugated Materials Based on DPP

2.1 Introduction

2.1.1 Conjugated Oligomers

As previously mentioned in *Chapter I*, conjugated polymers have been widely studied, with significant efforts devoted towards investigating their electronic and optical properties. However, such studies can be challenging as conjugated polymers do not have well defined structures, with many suffering poor solubility and large polydispersity. Thus, small conjugated molecules and oligomers which are often made *via* a stepwise synthesis, can be utilized as model compounds for rationalizing the properties of well-known high molecular weight polymers. Additionally, conjugated oligomers can develop our understanding on how chain length affects the optical properties of conjugated systems, which is crucial in enabling rational design of new materials with tailored properties.[81,83,122]

Previously, there have been several studies on wider band gap oligomeric material based on well-known conjugated systems, however, there have been fewer studies on narrow band gap D-A oligomers. As these materials show differences in effective conjugation length (ECL), chain flexibility and intra/inter-molecular interactions, it is expected that these different materials may also possess different optical properties and such studies are currently ongoing.[11] An example includes Yuan *et al*,[123] who reported a comparison study between an oligomer (**O-BDTdFBT**) and polymer (**P-BDTdFBT)**, based upon the same repeating benzodithiophene unit (Figure 2.1). As expected, the shorter conjugation length of the oligomer resulted in a wider band gap, however it also achieved a higher PCE of 8.10% when applied in a BHJ solar cell, compared to its polymeric counterpart (7.10%). The high performance of the oligomer was the result of its high degree molecular ordering and well-defined structure. Additionally, **O-BDTdFBT** showed excellent intrinsic phase separation with $PC_{71}BM$. In contrast, the performance of the polymer was limited by chain entanglement and low crystallinity. Thus, the study demonstrated the ability of oligomers to compete with their polymeric counterparts, for application in OPV devices.[123]

*Figure 2.1- Structures of **O-BDTdFBT** and **P-BDTdFBT**.*[123]

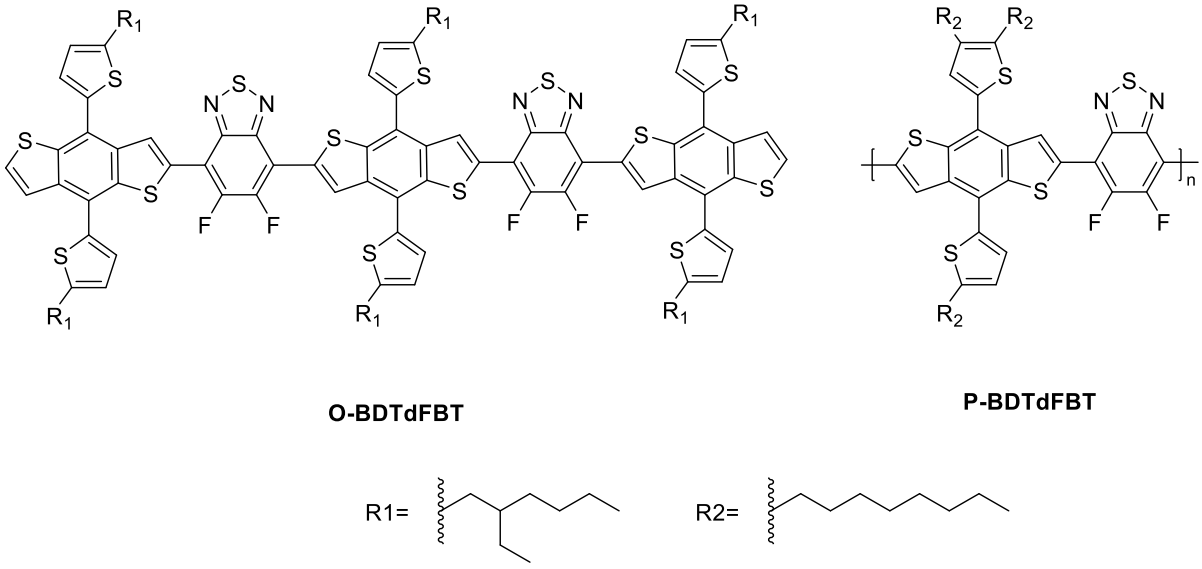

An interesting example includes a series of oligo(phenylene vinylene) compounds reported by Maddux *et al,*[87] in which chain lengths 1-5 were synthesised. When tripling the conjugation length from monomer to trimer, as expected a red shift of 32 nm was observed in the absorption spectra. However, it was noted that little to no red shift was observed beyond the chain length of the trimer, thus the saturation in λ_{max} and the effective conjugation length (ECL) had been reached. This was due to limited electron delocalization in the longer oligomers, as a result of a decrease in planarity.[87]

Poly- and oligo(α-thiophene)s are one of the most carefully studied class of conjugated systems and have been largely investigated by multiple research groups. Meier *et al,*[124] reported the UV-vis related ECL of non-substituted oligo(α-thiophene)s to be around 17 monomer units long. Some of the longest monodisperse and fully characterised oligo(α-thiophene)s bearing an octyl chain are the icosamer (20-mer) and heptacosamer (27-mer), as reported by Otsubo *et al*.[125] The study revealed that as the chain length increased up to the 20-mer, the π–π* transitions were progressively shifted to longer wavelengths in the electronic absorption spectra. However, no further shift was observed from the 20-mer to the 27-mer, suggesting that the ECL of the system had been reached. In contrast, a progressive increase in conductivity was observed from the 6-mer to the 27-mer, suggesting that extension of the conjugated system is beneficial towards charge hopping between adjacent oligomeric chains.[83,125] Longer even still, are the oligo(3-hexylthiophene)s based on **P3HT**, as reported by Heeney *et al,*[126] synthesised *via* "Fibonacci's route" up to a length of 21 repeating units. Following the introduction of a protecting group, an oligo(3-hexylthiophene) with an impressive length of 36 repeating units was also synthesised.

While the effect of chain length on the band gap, conductivity and the ECL, has been investigated in several conjugated systems, its dependence on the magnitude of optical absorption (i.e. the extinction coefficient (ε)) has gone largely undiscussed in literature.

2.1.2 The Extinction Coefficient

For efficient performance in OPV devices, conjugated materials must meet certain criteria including a low optical band gap for a broad absorption range that covers the solar spectrum and a high extinction coefficient (ε), for capturing more solar energy.[19] The extinction coefficient is a measure of how strongly a molecule can absorb light at a given wavelength. The Beer Lambert Law (Equation 2.1) relates the absorbance of a material (A) to the extinction coefficient (ε), as seen in the following equation.

Equation 2.1:

$$A = \varepsilon c l$$

The concentration of the sample (c) is given in mol-L^{-1}, the path length of the sample (l) is given in cm and the extinction coefficient (ε) is given in L-mol^{-1} cm^{-1}. Absorbance is a dimensionless quantity and is therefore unitless.

When ε is at 0, light passes straight through the material thus making it appear transparent. However, when $\varepsilon > 0$ absorption can occur. The higher the value of ε, the better the molecule is at absorbing solar energy. Thus, the extinction coefficient is an important parameter that should be evaluated when designing next generation materials for OPV devices, however it has been largely ignored in previous literature.[127] One of the ways in which the extinction coefficient can be controlled is through film thickness. However, this is often dependant on the structure of the material, for example it was reported than an increase in film thickness led to small increases in the extinction coefficient for DPP-based polymers,[128] while in another study, the opposite trend was observed for poly(alkyl-thiophenes).[129]

The probability of a photon being absorbed in transitions between energy levels of an atom or molecule, is known as the oscillator strength (f). This value is proportional to the integral of the extinction coefficient and corresponds to the area under the absorption curve, on a plot of molar absorptivity against wavelength (ε vs. λ). The oscillator strength can be calculated using time-dependent density functional theory (TD-DFT).

For an electronic transition to take place, an oscillating dipole must be induced *via* interaction of the molecule's electric field (internal dipole moment) with electromagnetic radiation (light absorption). Following excitation, the electron density within the molecule is redistributed, thus undergoing a transitional dipole moment.[127] The magnitude of the transitional dipole moment is proportional to the oscillator strength as shown in Equation 2.2:

Equation 2.2:

$$f \propto \left|\vec{\mu}_{ij}\right|^2$$

In which $\vec{\mu}_{ij}$ is the transitional dipole moment from state *i* to *j*.[128]

In general, increased co-planarization of the donor/acceptor units within a conjugated system, results in an increase of the conjugation length. Therefore, this leads to a reduction of the band gap and an increase in the oscillator strength. This was observed in a study by Zhokhavets *et al*[130] on P3HT molecules, in which upon annealing, an increase in the mean conjugation length was observed. This was attributed to a lack of structural defects (such as chain kinks) and increased co-planarization in the annealed P3HT crystallites. As a result, a red shift in the absorption spectra was observed, as well as an increase in the oscillator strength and the absorption coefficient.[130]

A rare example of investigation on the extinction coefficient and its dependence on chain length, was reported by Vezie *et al*,[128] whose work explored this relationship by measuring different molecular weight fractions, of a thienothiophene DPP-based polymer (**DPP-TT-T**). For the highest molecular weight samples, an extinction coefficient of 1.4 was observed, higher than that of the lower molecular weight fractions (ε = 1). This observation was attributed to the increase in oscillator strength (*f*) as the number of π-electrons in the system (N_π) increased. Thus, this led to a higher extinction coefficient, as a result of a superlinear increase in polarizability with oligomer length.[128]

This result can be rationalized by the relationship between polarizability and the induced dipole moment (μ_{ind}) as shown in Equation 2.3.

Equation 2.3:

$$\mu_{ind} = \alpha E$$

In which α is the polarizability constant given in cm^2/V and *E* is the strength of the electric field.[127]

As the planarity and ECL increases in a conjugated system, so does the oscillator strength. This is due to an increase in the polarizability, thus a subsequent increase in the induced dipole moment (μ_{ind}) as shown in Equation 2.3. Consequently, this increases the probability of a photon being absorbed by the molecule (*f*), resulting in a higher extinction coefficient (ε).

Eventually, the oscillator strength was observed to decrease with N_π, once the maximum had been reached. This was due to oligomer curvature which caused the μ_{ind} to increase sub linearly with N_π. However the extent of this effect was dependent on chemical structure, for example while other polymers in the study such as **SiPCPDTBT** suffered a large loss of in ε due to its high chain curvature, **PDPP-TT-T** suffered the least as a result of its high chain linearity (Figure 2.2). This effect can be

described by the concept of persistence length, a basic mechanical property that quantifies the flexibility of the chain and is directly related to the μ_{ind}. In general, a higher persistence length is often associated with a higher extinction coefficient.[128]

*Figure 2.2- Structures of **DPP-TT-T** and **SiPCPDTBT**.*[128]

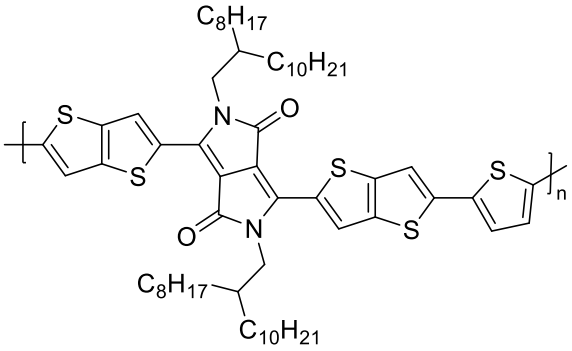

DPP-TT-T

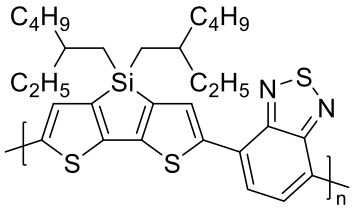

SiPCPDTBT

2.1.3 Chapter Objectives

As previously discussed, the relationship between chain length, absorption and chemical structure of conjugated systems, has not yet been widely studied in previous literature. In particular, its effect on the fundamental optical properties (i.e. the extinction coefficient), has gone largely ignored. In addition, it has not been fully established as to whether conjugated polymers or small molecules perform higher in OPV devices, or what design rules to follow in order to increase their magnitude of absorption.

In order to begin to unravel these complex structure-property relationships, it is important to base the study on a widely investigated conjugated motif such as DPP, which has been incorporated into both conjugated polymers and small molecules. Additionally, DPP-based materials have demonstrated great potential for application in various optoelectronic devices due to their high charge-carrier mobilities, high fluorescence and excellent stability, as discussed in *Chapter I, Sub-section 1.7*. In general, many studies have investigated the effect of chain length in regard to the optical band gap in oligomers, however fewer studies on narrow band-gap materials have been reported. While there have been a few notable studies based upon DPP oligomers,[131–133] limited investigation has gone into the effect of chain length on the strength of absorbance (ε).

Previously, another member of our research group (Dr Anastasia Leventis, University of Cambridge) sought to 'unravel the effect of chain length and hence molecular weight on the wavelength and strength of absorption through the synthesis of a series of thienyl-DPP-based conjugated small molecules (n =

1-5) and their polymeric counterpart (**PDPPTPT**).'[127] The polymer **PDPPTPT** consisting of a phenyl co-monomer, was chosen as the model system of the study due to its high performance and ease of synthesis (Figure 2.3). It was first reported as having a reasonable PCE of 5.5% however, Janssen *et al*[117] later reported an improved PCE of 7.4% as a result of a higher molecular weight polymer, highlighting the importance of molecular weight on the performance of conjugated polymers. As the polymer was based upon the same monomer unit as the oligomers, it was possible to compare their optical and morphological properties. While previous oligomeric studies[125] have reported longer repeat units such as the 20-mer and 27-mer, each repeat unit often consists of a *single* aryl unit (such as for oligo(α-thiophene)s). In contrast, in Leventis's study, each repeat unit consists of three *individual* aryl units (i.e. two thienyl units and one DPP core unit), which are linked together by a phenyl unit for oligomers n = 2-5. Thus, the pentamer consists of 19 individual aryl units, comparable to previous oligomeric studies.

*Figure 2.3- Structure of **PDPPTPT**.*

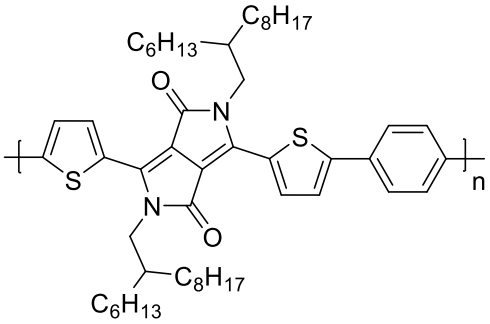

PDPPTPT
PCE 7.4 %

The study resulted in the successful synthesis of **PDPPTPT** as well as the DPP monomer, dimer, trimer and pentamer. While the tetramer was also made, after analysis *via* MALDI, it was observed that the tetramer contained a significant amount of hexamer impurities (Figure 2.4). It was believed that these impurities originated during the synthesis of a precursor, the bis-borylated dimer. Due to poor solubility in most common organic solvents, the tetramer could not be purified *via* column chromatography. As a result of time constraints, the materials could not be re-synthesised.

Therefore, in *this* work, here we intend to re-synthesise the tetramer *via* alternative reaction conditions and purification methods to ensure a higher purity. In addition, new samples of the monomer, dimer and reference polymer **PDPPTPT** to be used in *this* study, are also to be prepared.

Figure 2.4- Structure of the DPP tetramer.

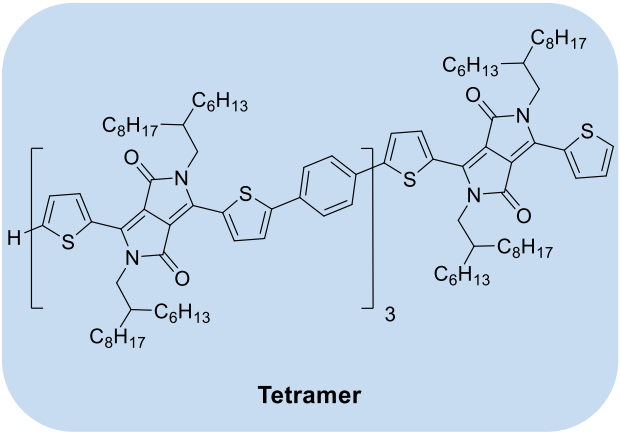

The proposed synthetic route towards the oligomers, begins with a Suzuki cross-coupling between mono-brominated DPP (**a**) with 1,4-benzenediboronic acid bis(pinacol)ester to give the dimer (**b**) (Scheme 2.1).

*Scheme 2.1- Proposed synthetic route to bis-borylated dimer (**d**) from (**a**).*

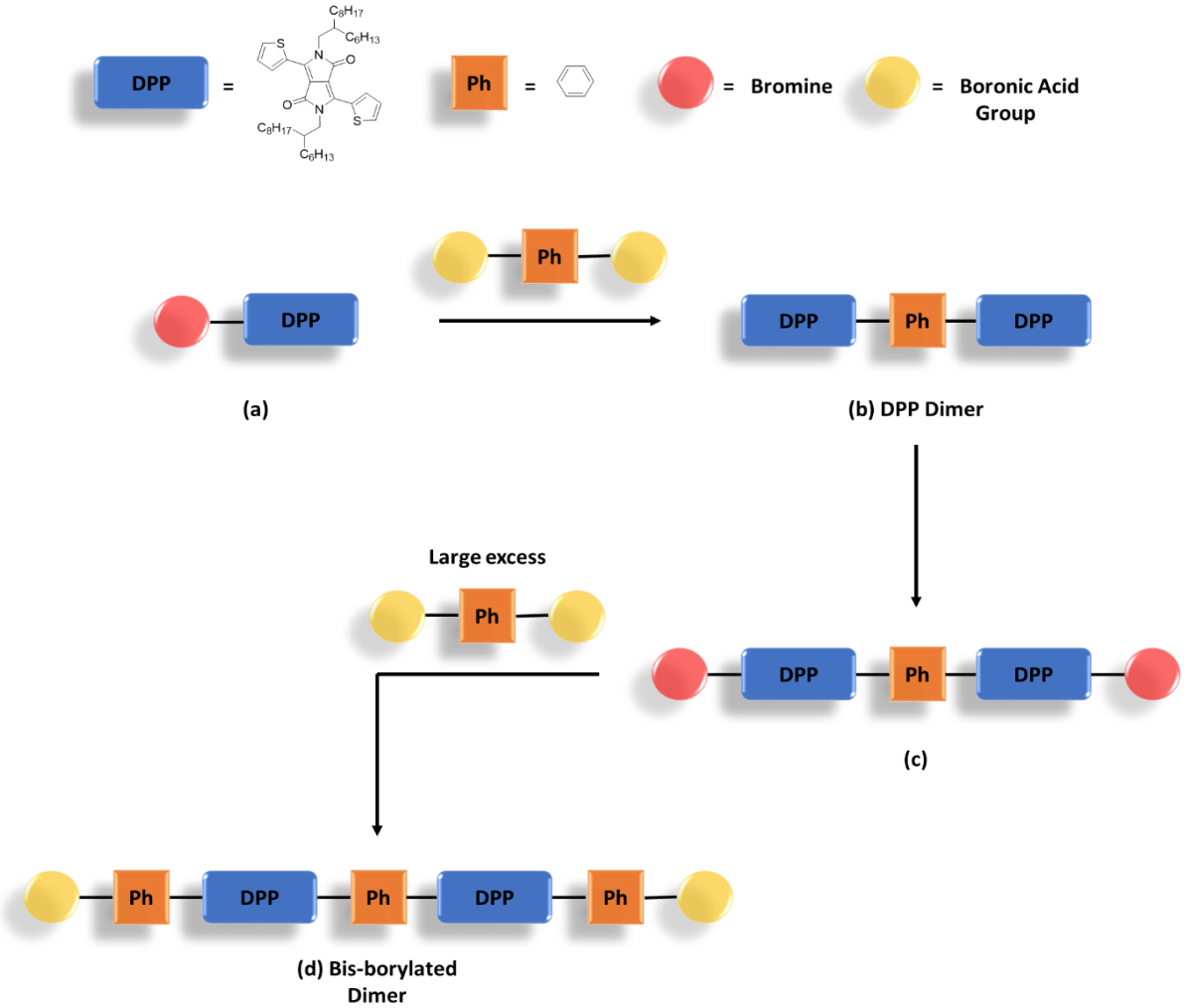

The next step of the synthesis will involve the di-bromination of (**b**) to give (**c**), followed by a second Suzuki cross-coupling with 1,4-benzenediboronic acid bis(pinacol)ester to give the bis-borylated dimer (**d**).

It is believed that the hexamer impurity found within the tetramer as synthesised by Leventis, originated during this step *via* unwanted polymerisation between (**c)** and 1,4-benzenediboronic acid bis(pinacol)ester. Thus, in *this* study we intend to prevent this by using a larger equivalent of 1,4-benzenediboronic acid bis(pinacol)ester (20 equiv.) than in the previous study (10 equiv.).

Finally, in the last step, the bis-borylated dimer (**d**) will undergo a final Suzuki cross-coupling with (**a**) to give the tetramer (**e**) (Scheme 2.2).

*Scheme 2.2- Synthetic route towards the tetramer (**e**) from the bis-borylated dimer (**d**).*

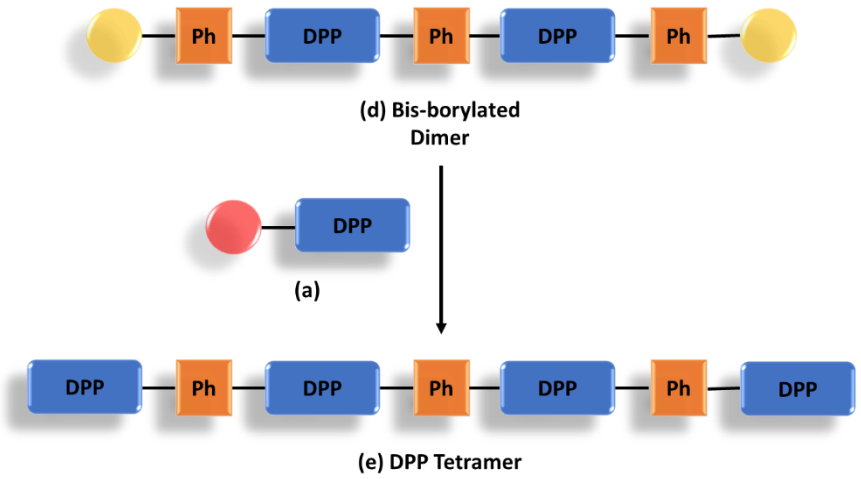

2.2 Synthesis

2.2.1 Synthesis of the Mono-Brominated DPP Monomer

*Scheme 2.3- Synthesis of the DPP core **1**.*

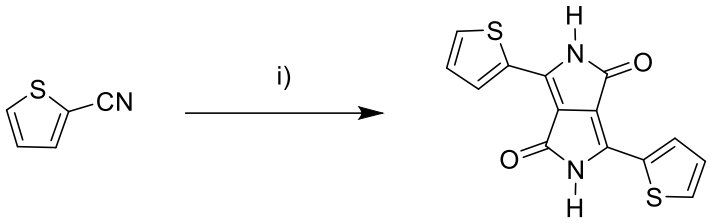

1

57 %

i) Diethyl succinate, Na, $FeCl_3$, 2-Methyl-2-butanol, 90 °C, 2 h.

The first step in the synthetic route towards the tetramer was the synthesis of DPP **1** (Scheme 2.3). The synthesis of DPP, involves the condensation of diethylsuccinate with 2-cyanothiophene, using a sodium alkoxide base in a one-step reaction.[60] To begin, an enamine ester is formed, which then undergoes self-condensation to give a pyrrolinone ester. This is followed by further condensation with another molecule of the nitrile and subsequent cyclisation, to yield the DPP core **1** as a dark magenta/purple solid (57%).

A common problem faced with unsubstituted DPP (**1**), is the lack of solubility in many organic solvents. This is due to the formation of strong hydrogen bonds between the N-H and oxygen atoms on the DPP core, as well as π-π stacking in the solid state.[56] This is undesirable, as in order for DPP based materials to be used in electronic devices solubility is essential, as organic thin films are synthesised from solution through spin coating and inkjet printing.[134] Therefore, this issue was overcome through the alkylation of the lactam N-H groups on **1** to give **2**. (Scheme 2.4).[135]

*Scheme 2.4- Synthesis of **2** via the alkylation of **1**.*

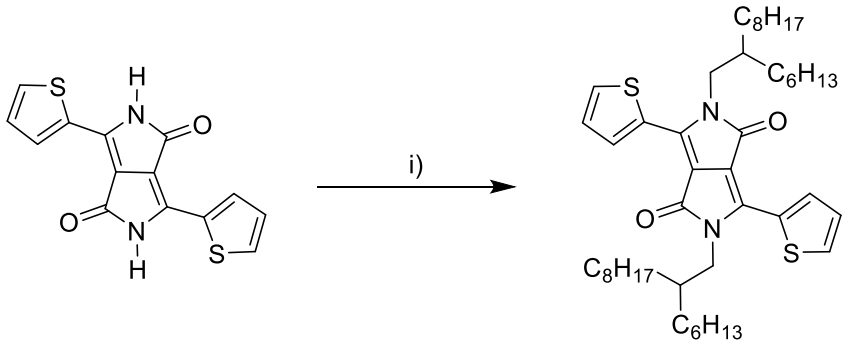

1 **2**

26 %

i) 7-(Bromomethyl)pentadecane, K_2CO_3,18-crown-6, DMF, 120 °C, 18 h.

To deprotonate the lactam amide groups, K_2CO_3 was chosen as a mild base, while stronger bases may lead to unwanted side products.[136] The reaction solvent DMF, was chosen as a polar and aprotic solvent, therefore capable of partially dissolving the largely insoluble unsubstituted DPP **1**.[137] Deprotonation was then followed by nucleophilic substitution with the alkyl bromide chain, 7-(bromomethyl)pentadecane (branched chain). This resulted in the successful formation of the alkylated DPP derivative **2**.

Although branched alkyl chains have the advantage of giving DPP compounds a higher solubility in comparison to linear chains, they are often reported to produce low yields.[137] The low yields are attributed to the multiple side reactions that compete directly with the nucleophilic substitution of the alkyl bromide, by the nitrogen atoms on the deprotonated DPP.[137] In this case, alongside the *N,N*-alkylated product **2**, a reoccurring side product, the *N,O*-alkylated DPP derivative **3** was also observed (Figure 2.5). It was possible to isolate **2** *via* flash-column chromatography, followed by recrystallisation in ethanol, which yielded **2** as a deep pink solid (26%). However, only a small amount of product could be obtained due to the similar polarities of the structural isomers **2** and **3**, on silica.

*Figure 2.5- Structures of the N,N-alkylated product **2** and the unwanted N,O-alkylated side product **3**.*

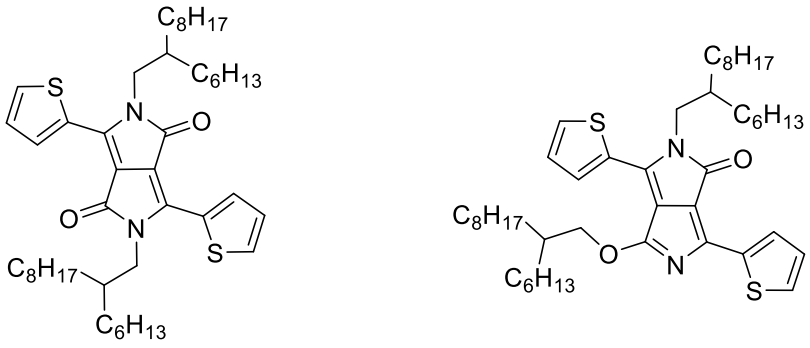

2 **3**

Finally, compound **2** underwent mono-bromination *via* electrophilic addition with NBS, based on a procedure by Bronstein (Scheme 2.5).[60] Upon workup, the product was isolated *via* flash column chromatography to yield **4** as a deep pink solid (39%). Again, the yield was limited by the similar polarities of the mono (**4**) and di-brominated (**5**) DPP compounds on silica, which were both present in the crude mixture, thus making purification difficult and time consuming. In the future, mono-brominated DPP derivatives may be more conveniently prepared *via* an asymmetric selective synthesis.

*Scheme 2.5- Synthetic route to **4**.*

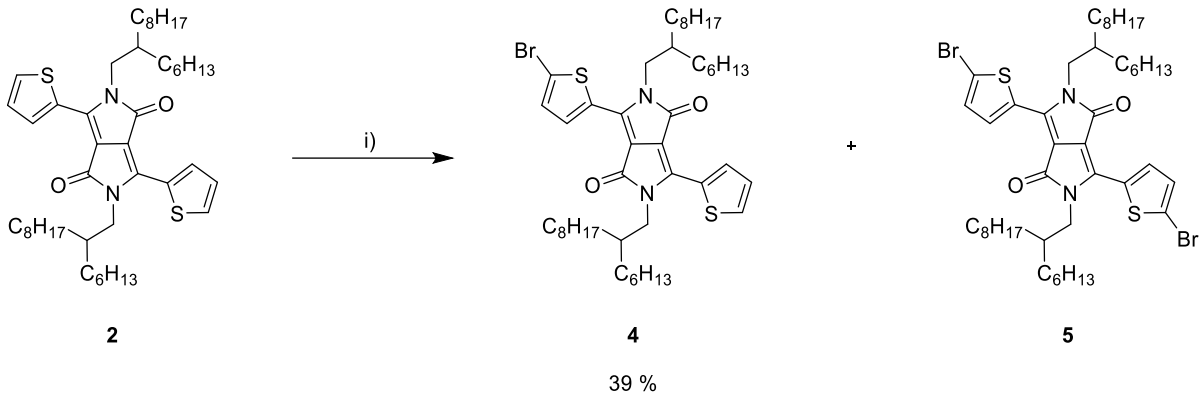

i) NBS, $CHCl_3$, 0 °C- RT, Overnight.

Compound **5** can be made selectively, *via* bromination of **2** using 2.2 equivalents of NBS, under the same reaction conditions as making **4**. The product was isolated *via* flash column chromatography to yield **5** as a shiny purple solid (68%) (Scheme 2.6).

*Scheme 2.6- Selective synthetic route to **5**.*

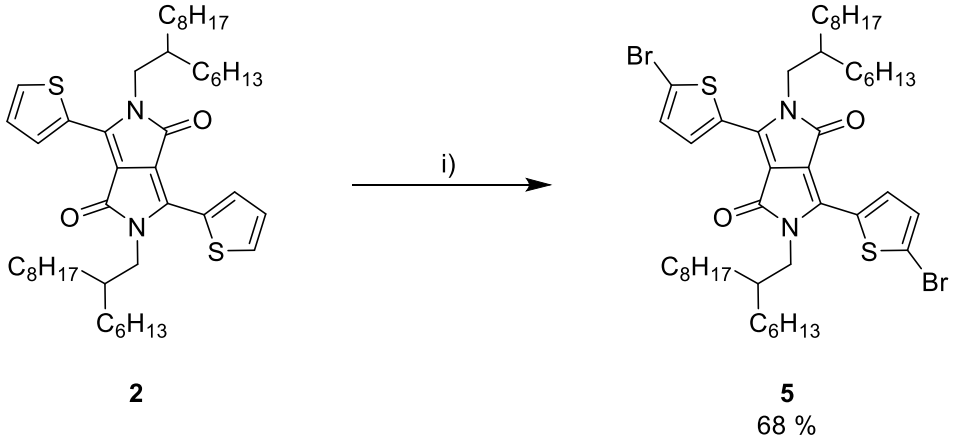

i) NBS, $CHCl_3$, 0 °C- RT, Overnight.

2.2.2 Synthesis of PDPPTPT

Following the synthesis of compound **5** was the preparation of polymer **PDPPTPT**, which involved the Suzuki cross-coupling of monomer **5** with 1,4-benzenediboronic acid bis(pinacol) ester, based on a procedure by Janssen *et al* (Scheme 2.7).[117] Aliquat 336 (*N*-Methyl-*N*,*N*,*N*-trioctylammonium chloride) is a quaternary ammonium salt, which was used in the reaction as a phase transfer catalyst.[138] The crude polymer underwent Soxhlet-extraction using acetone, hexane, and chloroform to afford **PDPPTPT** at a 77% yield.

*Scheme 2.7- Synthesis of literature polymer **PDPPTPT**.*

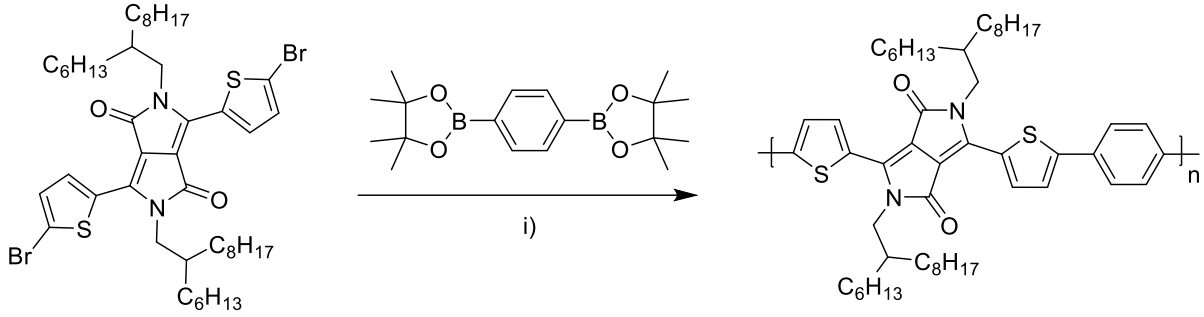

5 **PDPPT-P**

i) $Pd_2(dba)_3$, PPh_3, K_3PO_4, Aliquat 336, Toluene, H_2O, 115 °C, 3 days.

As the original literature polymer was reported to exhibit a large amount of aggregation in solution,[117] the molecular weight was determined by hot GPC (1,2,4-trichlorobenzene) at 160 °C (M_w= 72700 and M_n= 25100).[†]

2.2.3 Synthesis of the Bis-borylated Dimer

Following the preparation of the mono-brominated DPP derivative **4**, it was possible to synthesise the bis-borylated dimer (Scheme 2.8). The synthetic route began with the synthesis of the DPP dimer **6**, which was synthesised *via* a Suzuki-Miyaura cross-coupling between mono-brominated DPP **4** (2 equiv.) and 1,4-benzenediboronic acid bis(pinacol) ester, based on a procedure by Hendriks.[117]

Upon workup, the crude ^{1}H NMR showed that the reaction had been successful and that compound **4** had reacted on both sides of 1,4-benzenediboronic acid bis(pinacol) ester. This was observed *via* the characteristic peaks at 4.06 ppm (doublet) that integrated to eight protons, corresponding to the four NCH_2 groups on the DPP cores and 7.73 ppm (singlet), that integrated to four protons corresponding to the central phenyl unit protons. The crude product was purified *via* column chromatography to remove excess mono-brominated DPP **4**, followed by recrystallisation in ethanol, to yield **6** as a blue solid (66%). This was then followed by bromination of **6** to give the di-brominated DPP dimer **7** using the same procedure as when making di-brominated DPP **5**.[60] Compound **7** was obtained in good yield, as a shiny copper/blue solid (74%).

Finally, the bis-borylated dimer **8**, was synthesised from the di-brominated dimer **7**, via another Suzuki-Miyaura cross-coupling with 1,4-benzenediboronic acid bis(pinacol) ester, based on a procedure by Zou.[139] To prevent polymerisation, 20 equivalents of 1,4-benzenediboronic acid bis(pinacol) ester were used in contrast to the 10 equivalents used by Leventis in the same step.[127] It was believed that the hexamer impurity found in the tetramer as synthesised by Leventis, originated from undesired

[†]Molecular weight determined by Dr. Samuel Lawton, University of Warwick.

polymerisation during the synthesis of the bis-borylated dimer. Therefore, to prevent this from reoccurring in *this* synthesis, a higher equivalent of 1,4-benzenediboronic acid bis(pinacol) ester was used.

*Scheme 2.8- Synthetic route to the bis-borylated dimer **8**.*

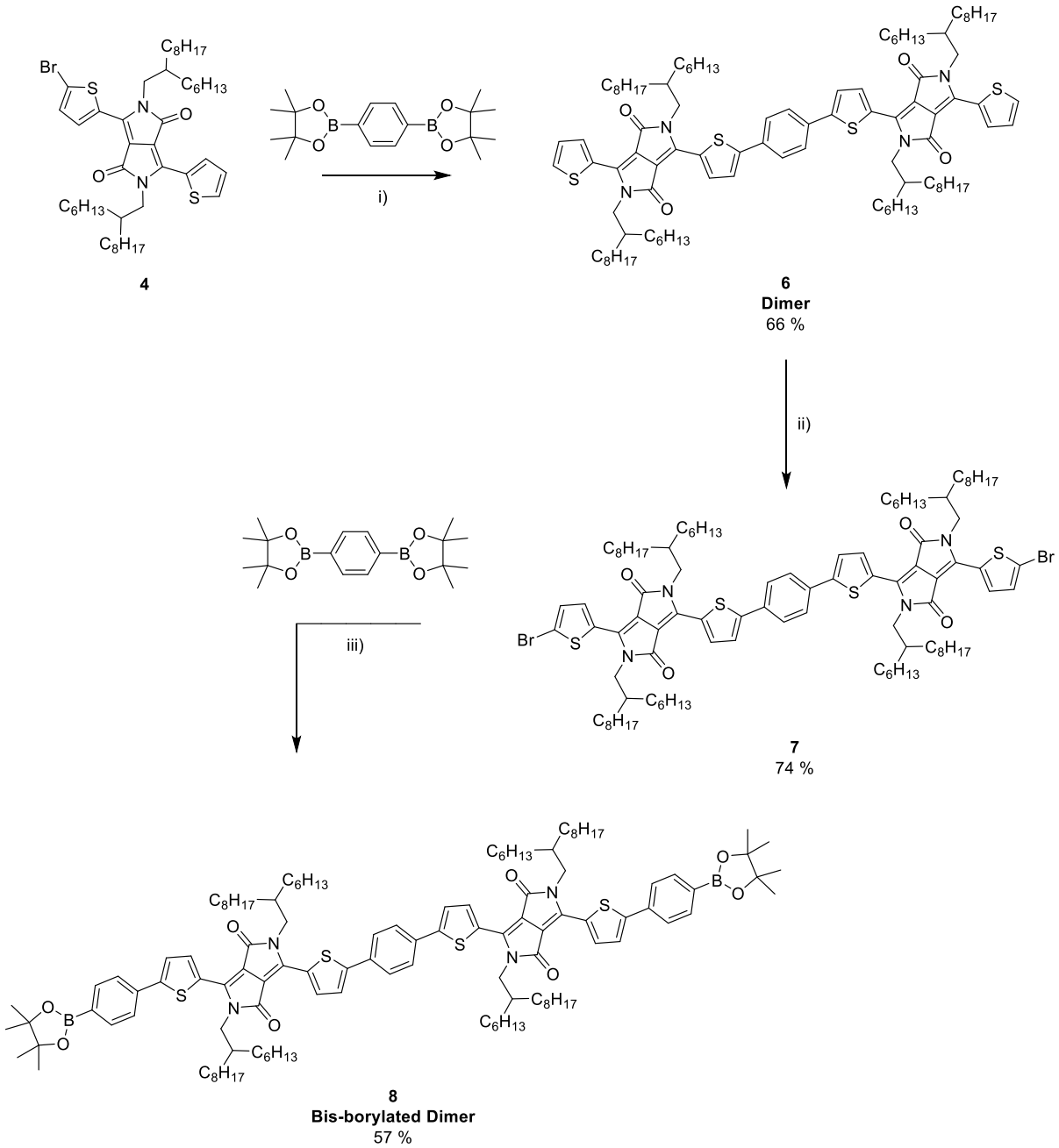

i) $Pd_2(dba)_3$, PPh_3, Aliquat 336, K_3PO_4, Toluene, H_2O, 115 °C, 20 h; ii) NBS, $CHCl_3$, 0 °C- RT, Overnight; iii) $Pd(Ph_3)_4$, K_2CO_3, THF, H_2O, 85 °C, 20 h.

Upon workup, the crude ^{1}H NMR showed that the reaction had been successful and that 1,4-benzenediboronic acid bis(pinacol) ester had reacted on both sides of compound **7**. This was observed

via the characteristic peaks at 4.08 ppm (doublet) that integrated to eight protons, corresponding to the four NCH_2 groups on the DPP cores and 1.36 ppm (singlet), that integrated to twenty-four protons corresponding to $BO_2C(CH_3)_2$. In addition, new peaks at 7.85 ppm (doublet) and 7.67 ppm (doublet) that integrated to four protons each were also observed, corresponding to the two outer phenyl units' protons. However, excess 1,4-benzenediboronic acid bis(pinacol) ester was also observed.

Previously, Leventis attempted to purify **8** *via* column chromatography which resulted in a large loss of product and possible compound degradation. This was due to the high polarity of compound **8**, causing it to stick to the silica in the column. Thus, in *this* study the product was purified *via* Soxhlet extraction in ethanol overnight. The remaining solid in the thimble was washed with methanol and collected *via* filtration, to afford **8** as a dark blue solid (57%). By ^{1}H NMR, while it was possible to fully characterise the bis-borylated dimer, baseline broadness was visible in the spectrum. It was not certain whether this was simply from aggregation of the compound or a hexamer/polymeric side impurity. A heated ^{1}H NMR (60 °C) sample in $CDCl_3$ was also run, however no change was observed, suggesting aggregation was not the issue. Due to the low solubility and high polarity of compound **8**, it was not possible to use column chromatography for further purification. However, after analysis by MALDI-TOF MS, we were confident **8** had been successfully made as the major product with no hexamer impurity (*m/z* 4861) observed (MALDI-TOF-(LD+): calculated for $C_{122}H_{176}B_2N_4O_8S_4$: 1975 found *m/z* 1976) (Figure 2.6). In addition, the isotopic (1:4,^{10}B:^{11}B) splitting pattern observed for the two boron atoms was as expected (three peaks at *m/z* 1976, 1975 and 1974 at a ~ 20:10:1 ratio, respectively). The additional peak at ~ *m/z* 1998 likely corresponds to the sodium adduct $C_{122}H_{176}B_2N_4O_8S_4Na^+$, commonly observed for DPP compounds.

*Figure 2.6- MALDI-TOF mass spectra of the bis-borylated dimer **8** (MALDI-TOF-(LD+): calculated for $C_{122}H_{176}B_2N_4O_8S_4$: 1975 found m/z 1976).*

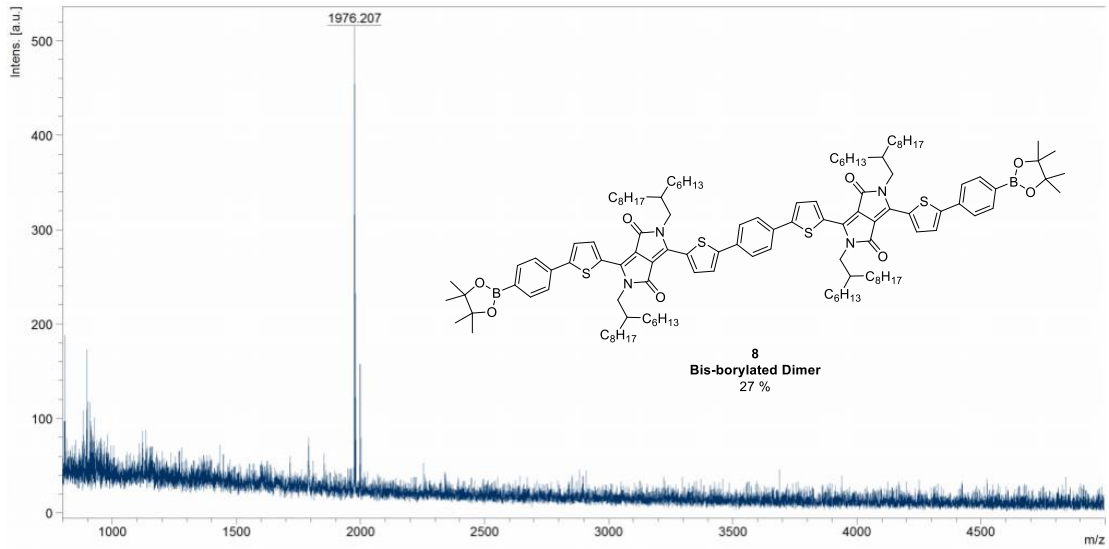

2.2.4 Synthesis of the DPP Tetramer

Following the preparation of the bis-borylated dimer **8**, was the synthesis of the DPP tetramer **9** *via* a Suzuki-Miyaura cross-coupling with mono-brominated DPP **4** (2.5 equiv.), based on a procedure by Zou (Scheme 2.9).[139]

Scheme 2.9- Synthesis of the DPP tetramer **9**.

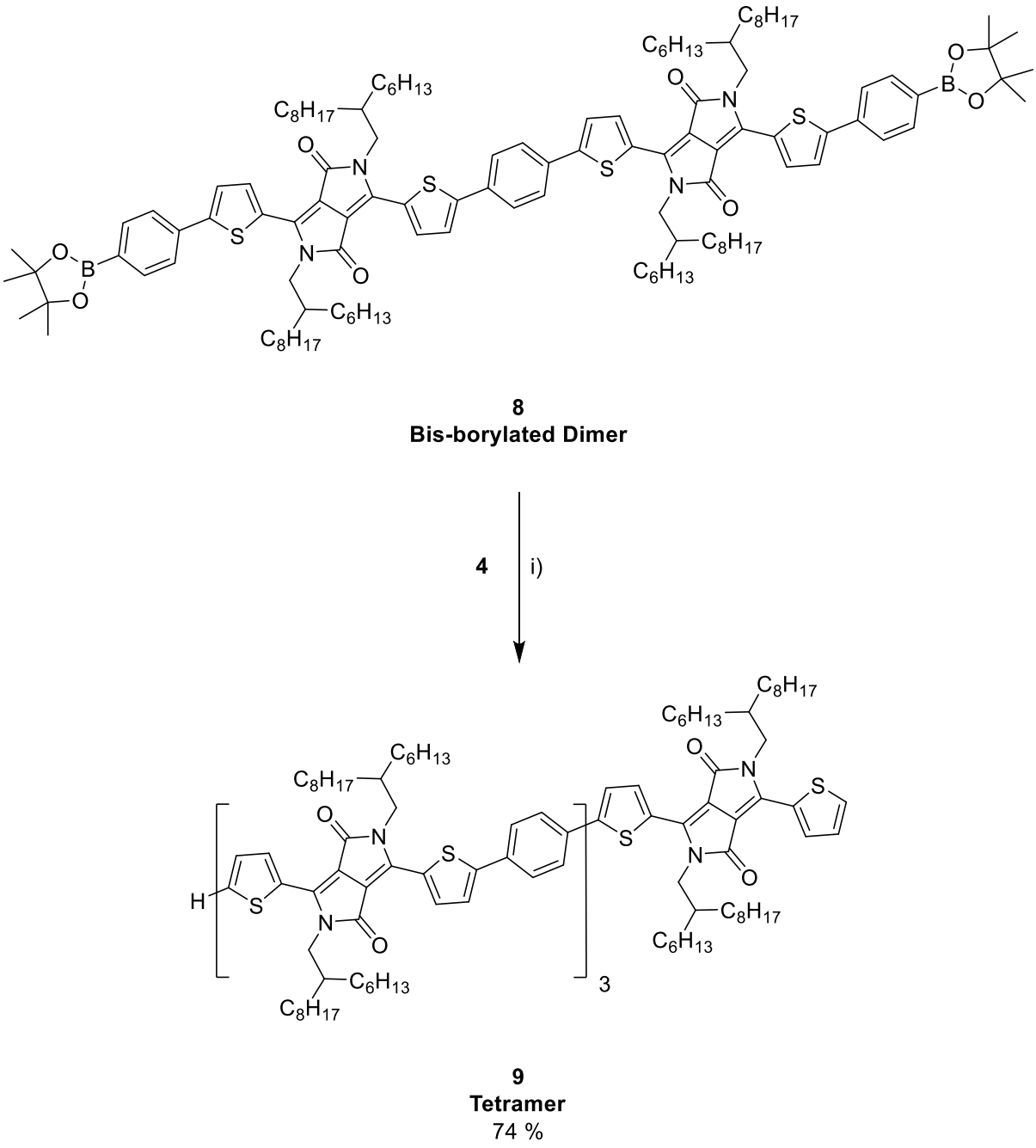

i) $Pd(Ph_3)_4$, K_2CO_3, THF, H_2O, 85 °C, 20 h.

Upon workup, crude ^{1}H NMR of tetramer **9** showed broader peaks in comparison to the defined spectrum of dimer **6** (Figure 2.7). This was to be expected, as the chain length of the oligomer doubles, solution aggregation increases. In addition, compound **9** had a lower solubility in $CDCl_3$, than that of compound **6**.

*Figure 2.7- Crude ^{1}H NMR in $CDCl_3$ of the tetramer **9** compared to that of the dimer **6** in the aromatic region. Aggregation can be seen in the tetramer as the oligomer chain increases in length.*

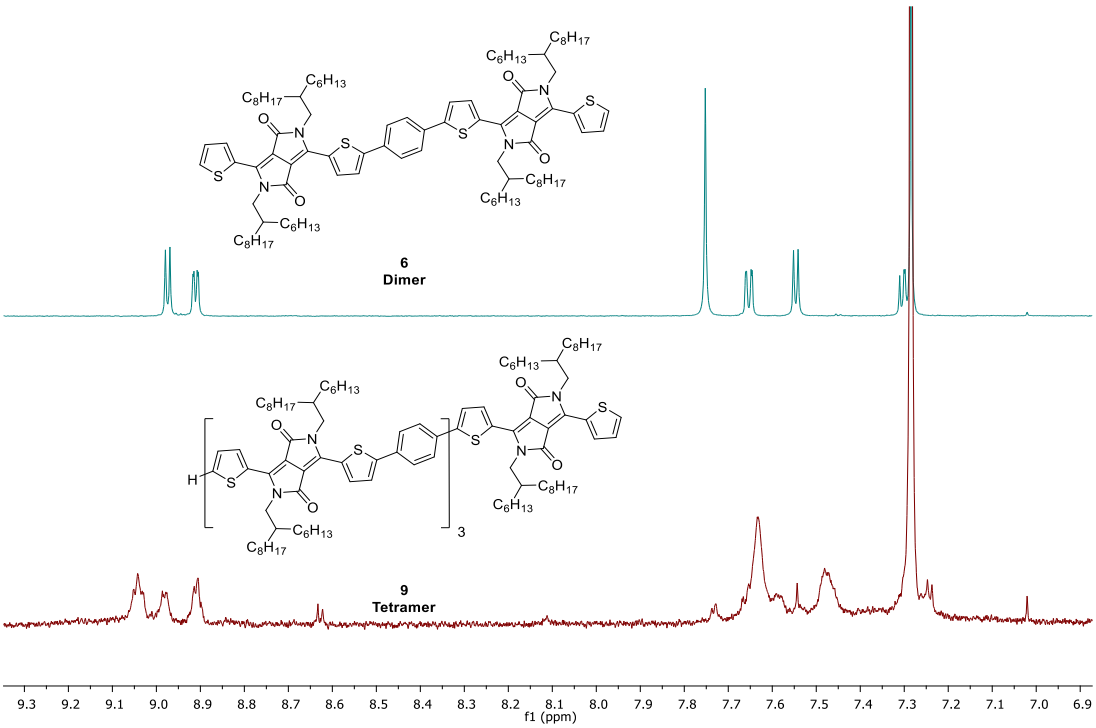

The compound was purified *via* Soxhlet extraction in methanol to remove any excess mono-brominated DPP **4**. After multiple washing cycles, when no more colour was visible in the extraction solvent, the solid remaining in the thimble was washed with methanol and collected *via* filtration, to yield **9** as a blue film-like solid (74%). While the ^{1}H NMR was largely broad thus difficult to interpret, MALDI mass spectra confirmed the successful synthesis of the tetramer (MALDI-TOF-(LD+): calculated for $C_{202}H_{294}N_8O_8S_8$: 3216 found *m/z* 3218), with no hexamer impurity observed (*m/z* 4861) (Figure 2.8). A small peak near the product at ~ *m/z* 3240 was also observed. This likely corresponds to the sodium adduct $C_{202}H_{294}N_8O_8S_8Na^+$.

Figure 2.8- MALDI-TOF mass spectra of the tetramer ***9*** *(MALDI-TOF-(LD+): calculated for* $C_{202}H_{294}N_8O_8S_8$*: 3216 found m/z 3218 (circled in green). Minor impurities observed at ~ m/z 2500 and ~ m/z 3500 (circled in red).*

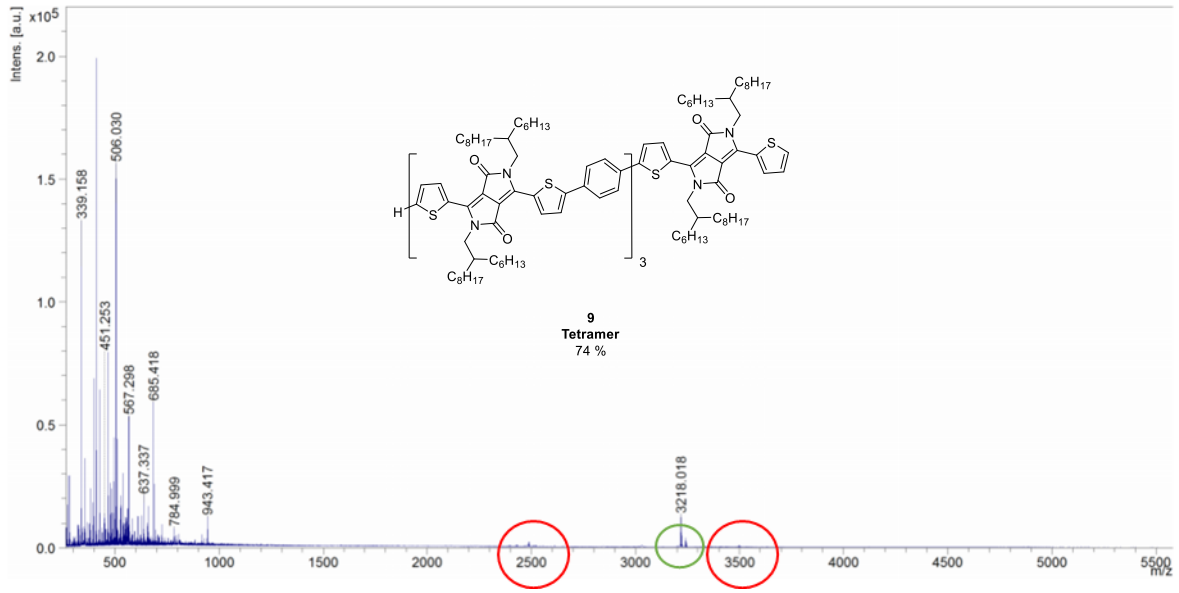

However, it was observed that a small impurity was present in the sample at ~ *m/z* 2500. This was most likely to be compound **10** (*m/z* 2596) formed *via* partial reactivity when synthesising tetramer **9**, in which mono-brominated DPP **4** reacted with only one side of the bis-borylated dimer **8** (Figure 2.9). There was also an additional impurity at ~ *m/z* 3500, however it was uncertain as to which compound this may be. It is possible that a small amount of mono-brominated DPP dimer was formed *via* partial reactivity during the synthesis of the di-brominated DPP dimer **7**. This may have then reacted with the bis-borylated DPP dimer **8** in order to produce a trace amount of compound **11** (*m/z* 3418).

*Figure 2.9- Structures of the possible impurities **10** and **11** observed in the MALDI spectra of tetramer **9**.*

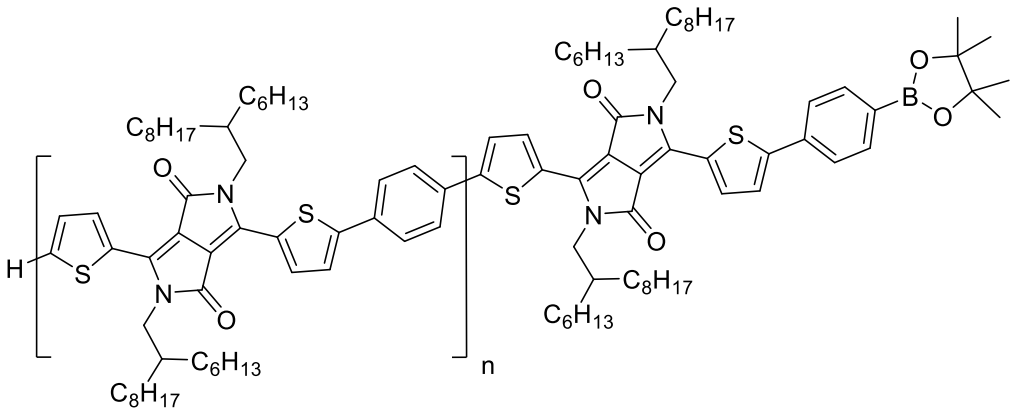

n = 2 **10** *m/z* 2596
3 **11** *m/z* 3418

While the presence of such impurities is undesirable, it seems that they are only present in small amounts and tetramer **9** appears to be the major product. As tetramer **9** was of poor solubility and low quantity, no further purification could be attempted. Thus, the synthesis of the tetramer concluded this project, however some uncertainties regarding purity remained.

2.3 Characterisation

2.3.1 Optical Properties

2.3.1.1 UV-vis Absorption Spectra

The solution UV-vis absorption spectra in chlorobenzene (CB) (100 μg/mL, path length 10 mm, RT) of the DPP monomer (**2**), dimer (**6**), trimer,[†] tetramer (**9**), pentamer,[†] and polymer (**PDPPPDT**) are presented in Figure 2.10.[††] All compounds displayed good solubility in the chosen solvent, chlorobenzene (CB).

*Figure 2.10- Normalised solution (CB, 100 μg/mL, path length 10 mm, RT) UV-vis absorption for the DPP monomer (**2**), dimer (**6**), trimer[†], tetramer (**9**), pentamer[†] and polymer (**PDPPPDT**).*

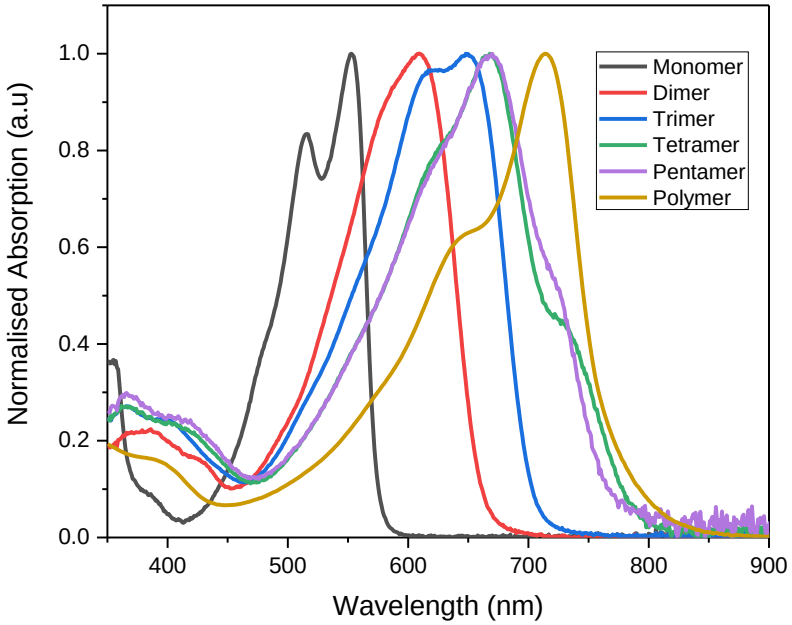

[†]The DPP trimer and pentamer used within this study were synthesised by Dr Anastasia Leventis, University of Cambridge. [††]Solution UV-vis absorption of the DPP oligomers were measured by Dr Elham Rezasolatani, Imperial College London.

In general, as the chain length increases from monomer through to polymer, a red shift in the absorption can be observed. This is to be expected, as the effective conjugation length (ECL) increases, this leads to narrowing of the band gap as discussed in *Chapter I*, and thus, a red-shifted absorption. In addition, an increase in aggregation (arising from an increase in the number of chromophores) may also lead to a red-shifted spectrum. While there are distinct differences in absorption between most of the DPP oligomers within the study, it appears that the UV-vis spectra of the tetramer (**9**) and pentamer are very

similar. It is possible that at this chain length, the band gap begins to slowly converge, however this is challenged by the largely red-shifted absorption of the polymer, compared to that of the DPP oligomers. In order for the ECL to be determined, extended chain lengths (i.e. hexamer) must be synthesised and measured.

2.3.1.2 Extinction Coefficient

The extinction coefficients in CB (100 µg/mL, path length 10 mm, RT) of the DPP monomer (**2**), dimer (**6**), trimer,[†] tetramer (**9**) and pentamer,[†] are presented in Figure 2.11.[††]

Figure 2.11- The extinction coefficients of the DPP oligomers (CB, 100 µg/mL, path length 10 mm, RT). The molecular molar extinction coefficient (ε) was calculated according to the Beer Lambert Law $A = \varepsilon \cdot l \cdot c$.

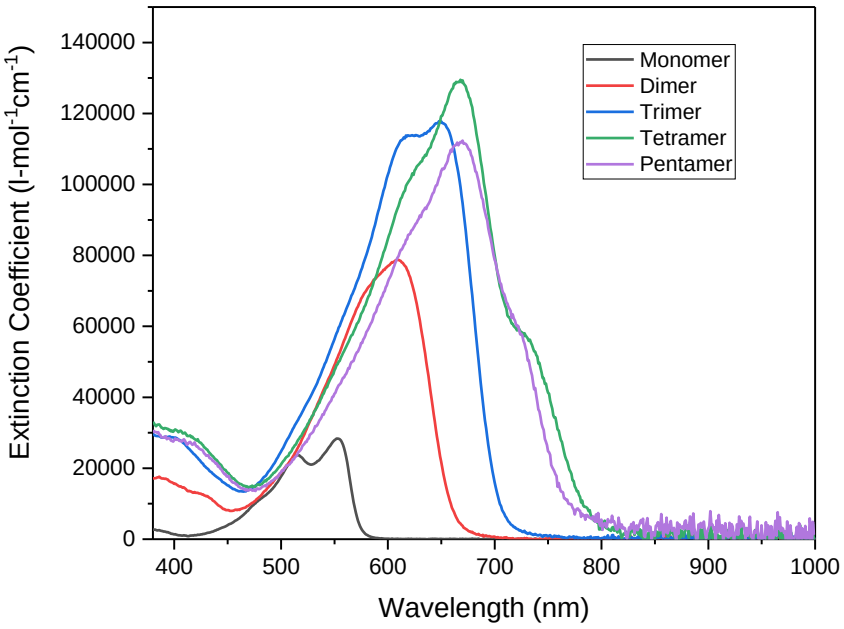

[†]The DPP trimer and pentamer used within this study were synthesised by Dr Anastasia Leventis, University of Cambridge. [††]Extinction coefficients of the DPP oligomers were measured by Dr Elham Rezasolatani, Imperial College London.

It was observed that as the chain length increases from monomer to tetramer, a general increase in the extinction coefficient can be seen. Again, this is to be expected as the chain length increases, the number of co-planar monomer units and thus the effective conjugation length, also increase. This leads to an increase in the polarizability of the oligomer, and subsequently its oscillator strength. As a result, absorption ability is enhanced. It was also observed that the extinction coefficient of the pentamer was

lower than that off the tetramer and trimer. This suggests that a saturation limit has been reached, which may be due to chain curvature in the pentamer, thus a decrease in co-planarity between the monomer units and a lowered extinction coefficient.

It is to be noted however, that this data does not take into account the total number of π-electrons in each of the oligomeric systems that contribute to the absorption strengths of the conjugated materials. Therefore, as previously reported by Vezie *et al*,[128] the extinction coefficient must be normalised. Thus, the extinction coefficients were then normalised by dividing the values by the total number of estimated π-electrons (N_π) in each of the conjugated systems. Previously, Leventis calculated that the DPP core contributes 8 π-electrons (4 π-electrons from the two double bonds adjacent to the thienyl units and 4 π-electrons from the lone pair on the two nitrogen atoms), thiophene 6 π-electrons and the phenyl unit 6 π-electrons, based on DFT models and resonance effects.[127] Therefore, the total number of π-electrons in each oligomeric system was calculated as monomer: 20 π-electrons, dimer: 46 π-electrons, trimer: 72 π-electrons, tetramer: 98 π-electrons and pentamer: 124 π-electrons.[127] The oscillator strength in the visible region, mainly resides in this first electronic transition.[128]

The normalised extinction coefficients in CB (100 µg/mL, path length 10 mm, RT) of the DPP monomer (**2**), dimer (**6**), trimer, tetramer (**9**) and pentamer are presented in Figure 2.12.

Figure 2.12- The normalised extinction coefficients of the DPP oligomers (CB, 100 µg/mL, path length 10 mm, RT). The molecular molar extinction coefficient (ε) was calculated according to the Beer Lambert Law $A = \varepsilon \cdot l \cdot c$.

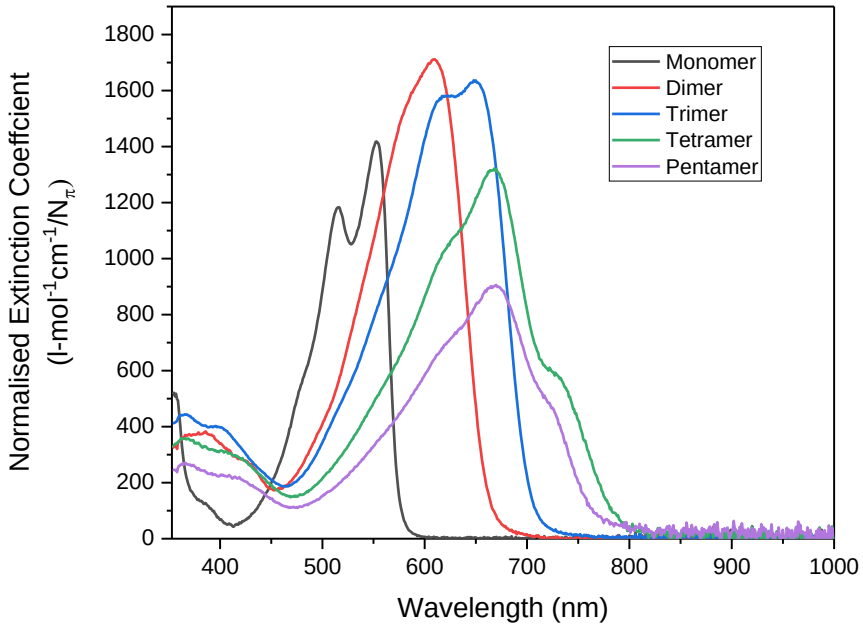

It was observed that as the chain length increased from the monomer to the dimer, the extinction coefficient also increased and as expected, a significant red shift in absorption was seen. While the absorption band of the monomer showed two distinct vibronic progressions, the dimer was instead broad and featureless. However, from the dimer to the pentamer, the extinction coefficient largely decreases. This may suggest that as the chain length increases from the dimer to the trimer, chain curvature begins to occur, thus resulting in torsional disorder between monomer units. Therefore, this loss in co-planarity would result in decreased conjugation and thus, a lower extinction coefficient. This may also explain why no red shift in absorption was observed between the tetramer and pentamer and therefore, it appears that a saturation limit has been reached.

On the other hand, while the trimer is observed to have a higher extinction coefficient, an unexpected significant red shift in absorption between the trimer and pentamer can be seen. In addition, while measurements of the extinction coefficient of the polymer are still currently ongoing, from Figure 2.10, it can be seen that the polymer's absorption is largely red-shifted compared to all other chain lengths. This is somewhat unusual, as the expected size of the red shift should decrease with extending conjugation length, as saturation of the band gap begins to approach. Thus, it appears that the ECL is not the sole contributor towards the absorption of the DPP oligomers.

One possible explanation may be due to increased intermolecular aggregation between longer oligomer chains in the π-π stacking direction (H-aggregate behaviour), thus resulting in extended conjugation and therefore, a red-shifted absorption. However, when studying the peaks of the spectrum, it is observed that the intensity of the 0-0 transition with respect to the 0-1 transition, generally increases from the dimer to the polymer. Typically, when the absorption is dominated by the 0-0 peak, it is characteristic of intra-molecular self-aggregation (J-aggregate behaviour), in which the oligomer chains fold upon themselves, leading to a red-shifted absorption.[140] To determine which type of aggregation is more prevalent within the DPP oligomers, further UV-vis measurements (i.e. heat cycles) are required.

Literature polymer **PDPPTPT**, has previously been reported to exhibit large amounts of aggregation of the polymer chains in solution,[117] thus, this extended conjugation may also lead to the largely red-shifted absorption of the polymer, which in part is likely due to increased intermolecular aggregation. It was also observed that the onset of the absorption of the tetramer, was fairly similar to that of the polymer. This may suggest that for oligomers with a chain length of four repeating units and above, the conjugated system begins to display some polymeric behaviour.

2.4 Conclusions

In conclusion, in Leventis's original study, a series of thienyl-DPP-based conjugated small molecules (n = 1-5) and their polymeric counterpart (**PDPPTPT**) were synthesised in order to study the effect of chain length, on the optical properties of conjugated materials based on DPP. However, the tetramer was found to contain a significant quantity of hexamer impurities and could not be included in the optical study. Thus, continuing from this previous work, we re-synthesised the tetramer. In addition, we also re-synthesised new samples of the DPP monomer, dimer and **PDPPTPT**, to be used in *this* study. The monomer and dimer were determined to be of high purity *via* ^{1}H NMR and MALDI mass spectrometry.

In attempt to improve the purity of the tetramer from the previous study, the compound was re-synthesised *via* alternative reaction conditions. While MALDI mass spectrometry suggested that the tetramer was made, some impurities were observed in the spectra. However, these impurities were present in only trace amounts within the sample and it appeared that the tetramer was the major product.

The UV-vis absorption of the DPP oligomers (n = 1-5) were measured, alongside polymer **PDPPTPT**. It was generally observed, that as the chain length of the oligomer increased, the further red-shifted the absorption. The absorption of the tetramer and pentamer appeared to be the same and thus, it is possible that at this chain length, the band gap begins to slowly converge. However, this was challenged by the largely red-shifted absorption of the polymer, compared to that of the DPP oligomers.

The extinction coefficients were also measured, and it was observed that as the chain length increased from the monomer to the dimer, as expected the extinction coefficient also increased. However, it was also observed that as the chain length then increased from dimer to pentamer, the extinction coefficient largely decreased. This may suggest that as the chain length increases from the dimer to the trimer, chain curvature begins to occur and thus a saturation limit is reached.

On the other hand, a significant red shift in absorption between the trimer and pentamer was observed. In addition, the polymer's absorption is largely red-shifted compared to all other chain lengths in the study. Thus, it appears that the ECL may not be the sole contributor towards the absorption of the DPP oligomers. While this result was unexpected, it is possible that this may have been due to increased aggregation in longer oligomer chains, resulting in extended conjugation and therefore, a red-shifted absorption. In order to fully understand the trends observed in this study, extended chain lengths such as the DPP hexamer would be desirable. In addition, control of aggregation effects would help us better understand the trends observed in this study. Due to shortage of material and time constraints, optoelectronic studies could not be conducted. Future work may also include re-synthesis of these materials on a larger scale, to allow investigation of their structure-property relationships in optoelectronics.

III

Encapsulated Polymers Based on Thienyl-Diketopyrrolopyrrole

3.1 Encapsulated Polymers Based on DPP to Increase the V_{oc}

3.1.1 Introduction

As discussed previously in *Chapter I*, organic photovoltaic (OPV) devices have demonstrated to be a promising low-cost technology to meet the ever-growing need for renewable energy sources. The active layer in OPVs, consists of an organic electron donor (D) and an electron acceptor (A) that are assembled into a bulk-heterojunction (BHJ) architecture. The performance of the device is measured by the power conversion efficiency (PCE) and the three important parameters that determine this value include the short-circuit current density (J_{sc}), the fill factor (*FF*) and the maximum open circuit voltage (V_{oc}). High performing organic solar cells can achieve internal and external quantum efficiencies approaching 100% and 80% respectively, thus all photons absorbed by the organic active layer can be converted into collected electrons at the short current circuit. As a result, experimental J_{sc} is often within close range of its predicted maximum. On the other hand, the V_{oc} is often low compared to the value of the optical band gap (E_g) as a result of energetic loss, consequently limiting the PCE. Thus, in order to improve efficiencies of OPV devices, it is critical to understand the factors that affect the V_{oc}.[141] The donor-acceptor (D-A) interface plays a key role in determining the V_{oc} (Figure 3.1) thus, molecular level control of the D-A interface is crucial in order to improve the performance of organic solar cell devices.

Figure 3.1- Schematic of a typical bulk-heterojunction (BHJ) solar cell depicting charge separation at the donor-acceptor interface. Figure reproduced from J. Zhang et al.[142]

A schematic of a typical bulk-heterojunction (BHJ) removed for copyright reasons. Copyright holder is Springer Nature Limited.

3.1.1.1 Parameters Influencing the V_{oc}

In an OPV device, absorption of a photon leads to the formation of a singlet-exciton (a neutral electron-hole pair) on the donor material (S_0-S_1 transition) (Figure 3.2).[143] The exciton can then diffuse to the D-A interface, where it may undergo fast electron transfer to the acceptor material, resulting in either immediate long-range charge separation or the formation of interfacial charge transfer (CT) states, that vibrationally relax to the lowest CT_1 state. This transition may only occur, providing the singlet-exciton energy which is given by the optical absorption gap (E_{abs}), exceeds the energy of the charge-transfer state (E_{CT}). The CT state is populated by the electrostatically bound polaron pair and is coupled to the ground state (GS). Thus, the CT state can either recombine to the GS (*via* radiative or non-radiative processes) or *via* a triplet state (through electron back-transfer), or instead dissociate to produce the charge separated (CS) state. In the CS state, the charge-carriers have overcome the Coulomb binding energy of the polaron pair and are able to migrate freely in the active layer to their respective electrodes.[143,144]

Figure 3.2- Energy levels found in a donor-acceptor system depicting; (i) light absorption of a photon leading to the generation of a singlet-exciton on the donor (S_0-S_1 transition), (ii) diffusion of the exciton to the D-A interface where it may (iii) undergo electron transfer to the acceptor resulting in the formation of the charge transfer (CT) state, which may either decay to the ground state or (iv) form the charge separated state (CS) in which the bound polaron pair can be separated to generate free charges. Figure amended from C. Deibe, T. Strobe and V. Dyakonov.[143]

A diagram depicting the energy levels found in a donor-acceptor system removed for copyright reasons. Copyright holder is John Wiley & Sons, Inc.

Many studies have shown that the V_{oc} has a linear dependence on the E_{CT} and can be represented by the formula:

Equation 3.1:

$$qV_{oc} = E(CT_1) - (0.6 \pm 0.1\ eV)$$

Where q is the elementary charge and the 0.6 eV energetic loss, arises from radiative and non-radiative recombination. As the E_{CT} sets the maximum for the V_{oc}, one strategy to obtain efficient free charge generation, is *via* delocalized, higher energy CT states.[144,145]

During electroluminescence studies carried out on polymer-fullerene complexes, low electroluminescent external quantum efficiencies were observed, suggesting that CT non-radiative recombination represents the majority of this voltage loss.[141,145] In general, voltage loss arising from non-radiative recombination is low for inorganic solar cells (0.04 - 0.21 V), while for organic solar cells is much larger, with values of 0.34 - 0.44 V observed in a range of devices.[146] Thus, in order for OPVs to compete with inorganic technology, methods of preventing non-radiative energy loss mechanisms are crucial.

The non-radiative voltage loss in an OPV, can be expressed by the following equation:

Equation 3.2:

$$q\Delta V_{oc,nr} = qV_{oc,rad} - qV_{oc} = -k_B T \ln[Q_{LED}(V_{oc})]$$

Where Q_{LED} (V_{oc}) is the external quantum efficiency of the electroluminescence (EL) emission, at an applied internal voltage equal to the V_{oc} of the cell.[147] Thus, based on this model, several design rules have been proposed in order to increase the V_{oc}, such as using materials with a high luminescence efficiency for the CT state. This requires high luminescence from both the donor *and* the acceptor.[148] Therefore, these factors should be carefully considered when designing next generation materials for OPV devices. In order to control the V_{oc}, careful modification of the D-A interface is required.

In general, the interaction between the D-A interface can play a large role in determining the PCE of OPV devices. For example, Yao *et al*[149] reported an OPV device based on an NFA **PTO2:IT-4F** system, that achieved an impressive PCE of 14.7%. In comparison, the reference blend **PTO2:PC$_{71}$BM** only achieved a 5% efficiency (Figure 3.3a). These results were attributed to the large difference in molecular electrostatic potential (ESP) across the **PTO2**:**IT-4F** interface and thus, the induced intermolecular electric field (IEF) may have assisted with exciton separation. In contrast, due to the smaller difference

in ESP across the **PTO2-PC$_{71}$BM** interface, an additional electric field was required to drive charge-transfer, which may be related to the energy loss of the device. In both systems, it was observed that application of an additional electric field led to enhanced charge separation. However, while for the **PTO2**:**PC$_{71}$BM** system, an electric field of 0.0025 au was required to observe complete hole/electron separation, only 0.0005 au was needed for the **PTO2**:**IT-4F** blend (Figure 3.3b).[149] Thus, the results from this study demonstrate a way in which factors affecting the D-A interface, play a key role in determining the performance of OPV devices.

*Figure 3.3- a) Structures of **PTO2** and **IT-4F**; b) The electron/hole density distributions of the lowest excited states without/with the additional electric field between **PTO2:PC$_{71}$BM** and **PTO2:IT-4F**; red and blue represent hole and electron densities, respectively. Adapted with permission from Huifeng Yao, Yong Cui, Deping Qian, et al., J. Am. Chem. Soc., 2019, **141**, 7743–7750. Copyright 2021 American Chemical Society.*[149]

a)

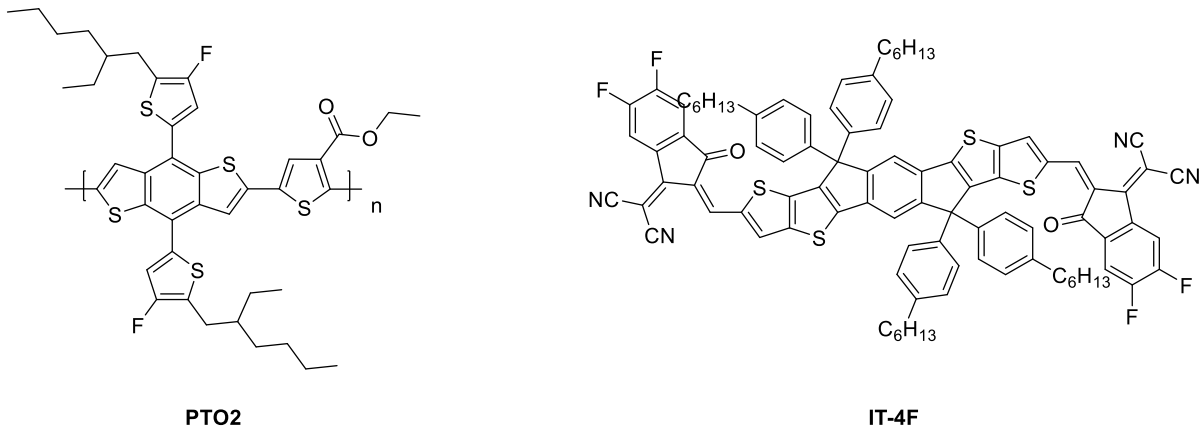

PTO2 **IT-4F**

b)

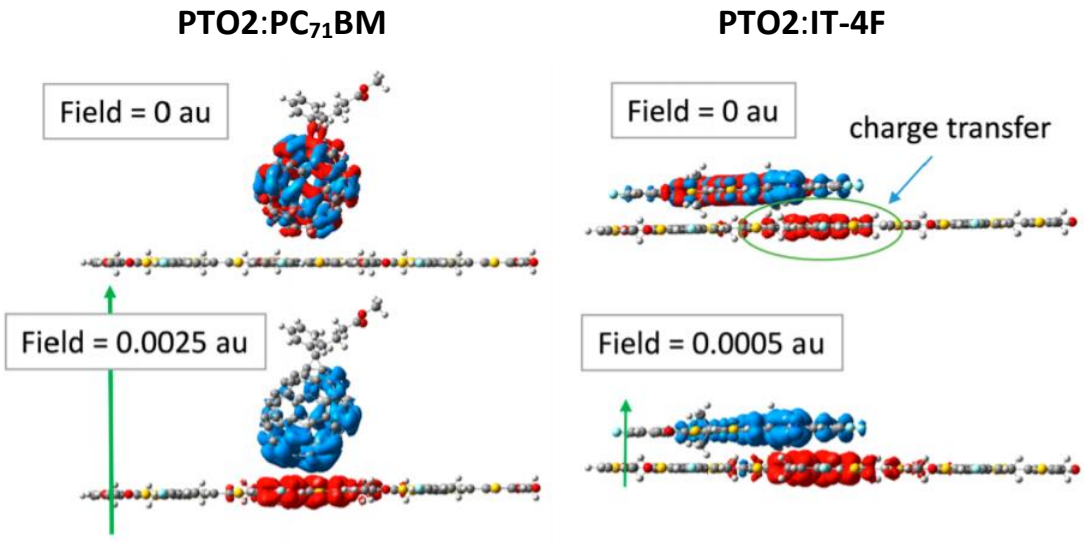

3.1.1.2 Modification of the D-A Interface

It has been previously demonstrated that it is possible to raise the E_{CT} and therefore the V_{oc}, *via* modification of the D-A interface. Zhong *et al*[150] reported a study in which the D-A interface of a PCBM:**P3HT** system was modified by increasing the distance between the donor and acceptor layers (Figure 3.4). This was achieved through the introduction of a thin insulating transparent layer made from a fluorinated polymer **CYTOP®**, between the D and A layers in the bilayer OPV device. The CYTOP polymer was doped with a silicon phthalocyanine dye molecule with axial semi fluoroalkyl chains (**F-SiPc**), due to its intermediate HOMO-LUMO structure. This allowed energy transfer from **P3HT** to the insulating layer, preventing a reduction of the J_{sc}.

*Figure 3.4- Structures of **P3HT**, **CYTOP**, **F-SiPc** and schematic diagram of bilayer organic solar cells; a) without spacer PBCM/**P3HT** and b) with spacer PBCM/**CYTOP**:**F-SiPc**/**P3HT**. Figure amended from Zhong et al.*[150]

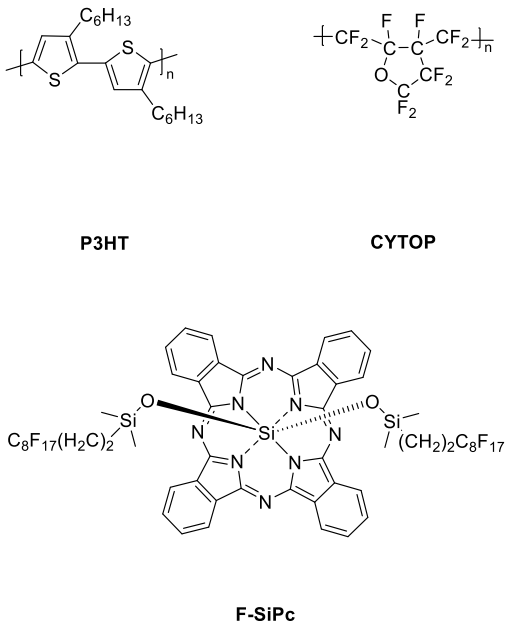

Schematic diagrams of bilayer organic solar cells with and without a spacer removed for copyright reasons. Copyright holder is WILEY-VCH Verlag GmbH & Co. KGaA, Weinheim.

It was observed that in the reference PCBM/**P3HT** device (Figure 3.4a), a V_{oc} of 0.49 V and a PCE of 0.397% was achieved. In contrast, when the 0.95 nm **CYTOP**:**F-SiPc** layer was inserted between the D-A interface (Figure 3.4b), the V_{oc} and PCE increased to 0.60 V and 0.531%, respectively. This increase in efficiency was attributed to the increased distance between the D and A, thus weakening the Coulomb interaction between the polaron pair. This led to an increase in the E_{CT} and suppression of charge recombination, resulting in an increase of the V_{oc}.

Thus, these results demonstrate it is possible to increase the efficiencies of OPV devices *via* careful modification of the D/A interface.[150] If it were possible to manipulate the D-A interface without the requirement for an additional layer, this would be ideal.

3.1.1.3 Encapsulation of Conjugated Polymers

As discussed earlier, non-radiative decay is responsible for majority of the voltage loss between the V_{oc} and the E_{CT}, thus strategies of prevention are highly sought after. Highly emissive conjugated polymers are vastly desirable and have application in a wide range of devices including organic light-emitting diodes (OLEDs) and biomedical imaging. Emission generally arises from the radiative decay of singlet-excitons, however competing non-radiative pathways such as energy migration/transfer, charge separation and interchain processes, often result in low fluorescence quantum yields (ΦF). This is particularly the case in the solid state, in which π–π stacking and aggregation of the conjugated polymer, results in the formation of non-emissive CT states.[151]

A method reported by Leventis *et al*[151] to overcome this problem, was demonstrated *via* double encapsulation of the π-conjugated backbone, thereby isolating individual polymer chains and constructing rigid insulated molecular wires (IMW). They reported the synthesis of a novel phenyl-DPP polymer (**E-DPPT**) **(**Figure 3.5), encapsulated by alkyl chains in the π–π stacking direction. While the linear chained reference polymer (**N-DPPT**) showed poor ΦFs of 18.2% and 5.6% for solution and thin film respectively, in contrast **E-DPPT** exhibited remarkably high ΦFs of 73.6% and 27.8%. It was also observed that **E-DPPT** displayed sharper emissive spectral features in comparison to **N-DPPT**, suggesting the suppression of intra- and intermolecular aggregation. Furthermore, it was found that the encapsulating steric shield promoted enhanced backbone colinearity, due to an increase in rigidity. For example, STM imaging of the encapsulated material revealed linear conformationally defect-free polymer domains, while in comparison **N-DPPT** showed a coiled nanostructure with numerous conformational defects.[151]

*Figure 3.5- Structures of **N-DPPT** and **E-DPPT**.*[151]

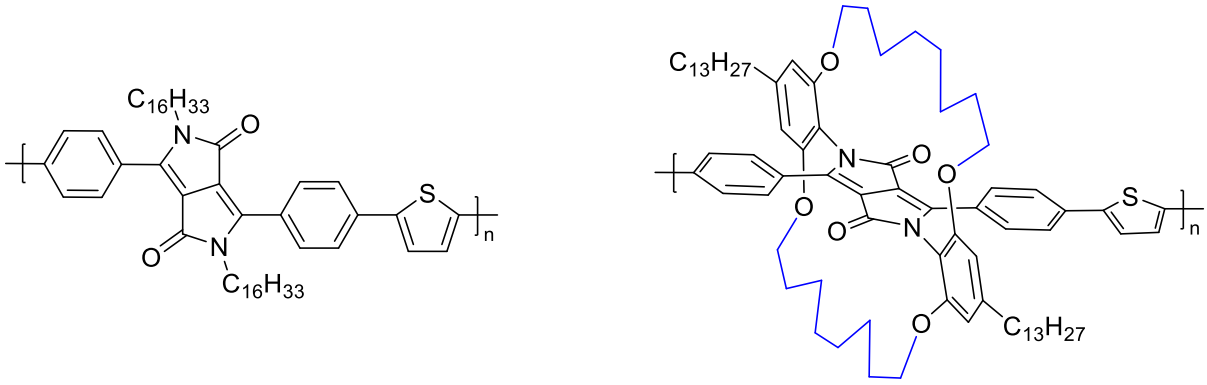

N-DPPT **E-DPPT**

In addition to double encapsulation of conjugated polymers, examples of half encapsulation have also been reported. McDearmon *et al*[152] reported the synthesis of a series of BDT co-polymers, in which the BDT monomer consisted of a macrocyclic side chain, therefore blocking one side of the conjugated backbone (Figure 3.6). As a result, the half-encapsulated polymers showed restricted π–π stacking, in comparison to their linear chained acyclic counterparts.

Figure 3.6- Schematic of side view a) close π- π stacking in a linear side-chained BDT polymer and b) restricted π–π stacking in a macrocyclic side-chained BDT polymer. Figure amended from McDearmon et al.[152]

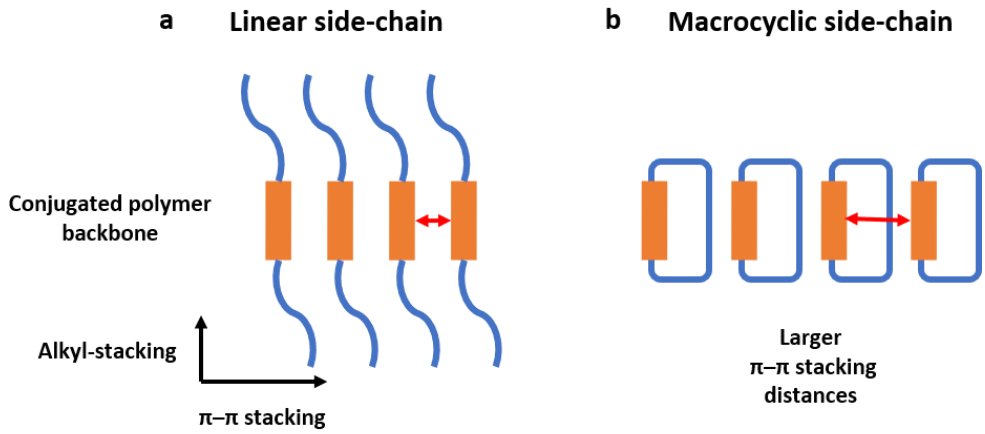

Due to supressed aggregation, the encapsulated BDT polymers displayed higher photoluminescence yields compared to their linear chained derivatives. Additionally, grazing incidence wide-angle X-ray scattering (GIWAX), revealed that the encapsulated polymers remain more ordered in the solid state. These promising results indicate that even partial encapsulation can greatly influence the properties and performance of conjugated polymers.

3.1.1.4 Sub-Chapter Objectives

It has been demonstrated that encapsulation is an effective method of exploring interchain interactions, reducing aggregation and non-radiative pathways, thereby improving the ΦF in conjugated polymers. However, investigation of how encapsulation can affect the performance in OPV devices, has yet to be explored. Encapsulation can also have an impact on the microscale morphology, due to the increased distances between polymer chains in the π–π stacking direction. Additionally, encapsulation has been shown to improve the colinearity and rigidity of the polymer system.

Building on previous literature, here we intend to investigate the effect of encapsulated DPP polymers, on the D-A interface and the $V_{oc,}$ in OPV devices. In this sub-chapter, we synthesised two series of branched thienyl-DPP co-polymers, doped with increasing amounts (0%, 5%, 10%, 20% and 30%) of a novel partially encapsulated thienyl-DPP monomer **EC10DPPT** (Figure 3.7). In order to prevent large

disruption of the crystalline packing within the polymer (which may occur in fully encapsulated polymers), doping was restricted to a maximum of 30%.

Figure 3.7- Structures of -Ph and -TT DPP polymer series, and novel encapsulated thienyl-DPP monomer ***EC10DPPT****.*

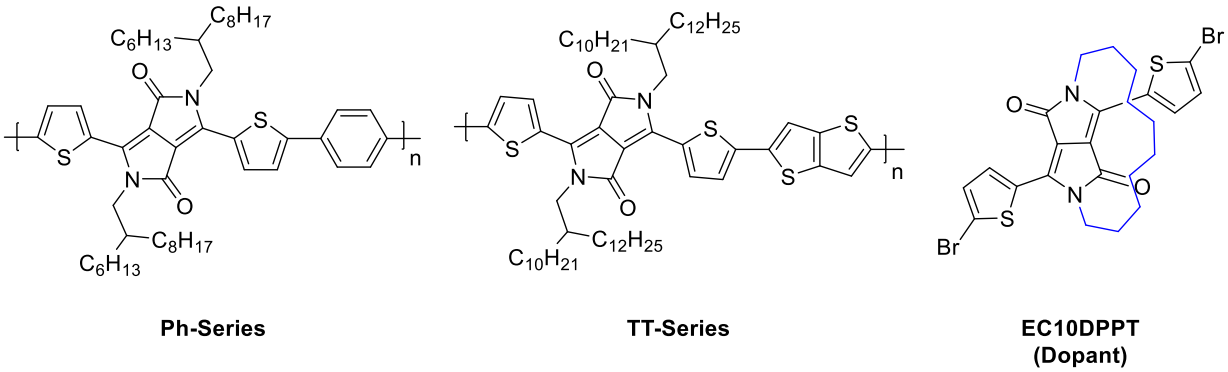

This allowed elucidation on how the ratio of the encapsulation, can affect the structure-property relationship of DPP polymers. The polymers chosen for the study consisted of phenyl (Ph-series) and thienothiophene (TT-series) co-monomers, based on high performing DPP polymers in literature.[28,117]

It is proposed that within the doped DPP polymers, a proportion of the encapsulated polymer chains will be located at the D-A interface, leading to a greater difference in the static dipole moment. (Figure 3.8). As a result, this will weaken the electronic coupling between the charge pairs, thereby suppressing charge recombination. Thus, this will result in an increase of the V_{oc} compared to that of the naked (non-encapsulated) polymer.

Figure 3.8- Schematic representation of the naked and encapsulated polymers at the D-A interface. In the encapsulated polymer, it is proposed that a larger difference in the static dipole moment at the D-A interface will result in an increase of the $V_{oc,}$ *compared to that of the naked polymer.*

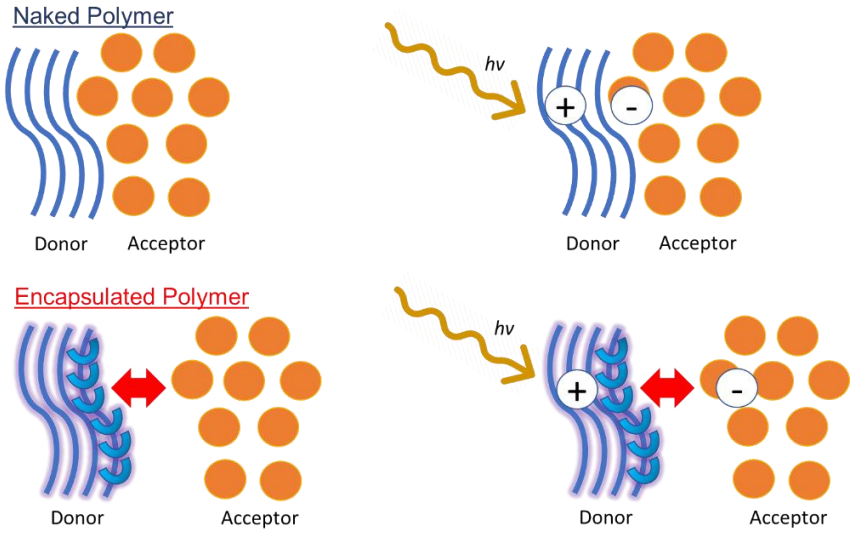

3.1.2 Synthesis

3.1.2.1 Synthesis of EC10DPPT

The preparation of the encapsulated dopant **EC10DPPT**, began with the synthesis of the thienyl-DPP core *via* the condensation of diethylsuccinate with 2-cyanothiophene in the presence of a sodium alkoxide base, to yield **1** as a magenta solid (57%) (Scheme 3.1).

*Scheme 3.1- Synthetic route to **2**.*

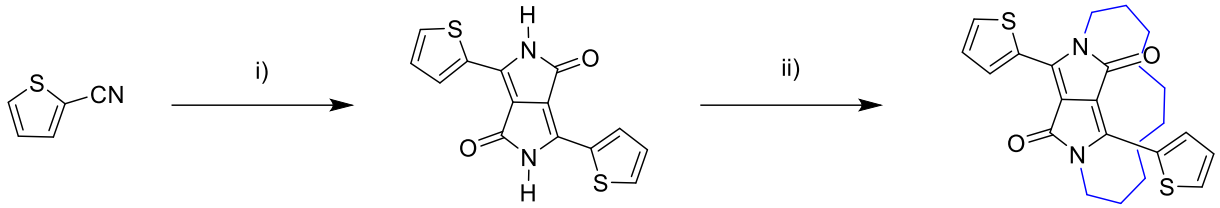

1
57 %

2
16 %

i) Diethyl succinate, Na, $FeCl_3$, 2-Methyl-2-butanol, 90 °C, 2 h; ii) 1,10-dibromodecane, K_2CO_3, 18-crown-6, DMF, 120 °C, 18 h.

This was followed by the encapsulation of the DPP core, using 1,10-dibromodecane in DMF and K_2CO_3 as the base. In order to minimise the production of the competing side products, including mono- and di-alkylated DPP, a solution of the alkyl chain in DMF underwent slow dropwise addition to a largely diluted basic solution of **1** (~ 800 mL of DMF per 0.58 g of **1**). Upon work up, the crude material was purified *via* column chromatography, followed by sonication in hexane. The pure product was then collected *via* filtration, to give **2** as a bright pink solid (16%). Finally, **2** underwent di-bromination with a quantitative amount of NBS at 50 °C, to afford **3** as a dark purple solid (79%) (Scheme 3.2).

*Scheme 3.2- Synthetic route to **3**.*

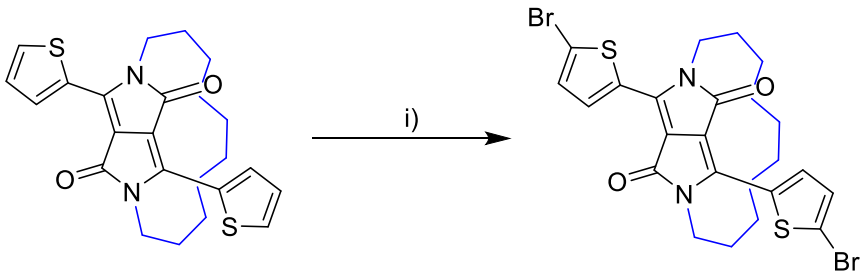

2

3
EC10DPPT
79 %

i) NBS, $CHCl_3$, 50 °C, 5 h.

The structure of compound **3**, was determined by X-ray crystallographic analysis[†] (single crystals grown from $CHCl_3$: MeOH, Figure 3.9), confirming the successful encapsulation of the DPP core. However, it was noted that the nitrogen atoms on the DPP ring (shown in green), were bent slightly out of plane in comparison to the rest of the DPP core, indicating the presence of ring strain. It should be noted that the crystal structure of **3** was not obtained until after the synthesis of the doped polymers.

*Figure 3.9- Crystal structure of encapsulated DPP compound **3**. Crystals grown from $CHCl_3$: MeOH.*

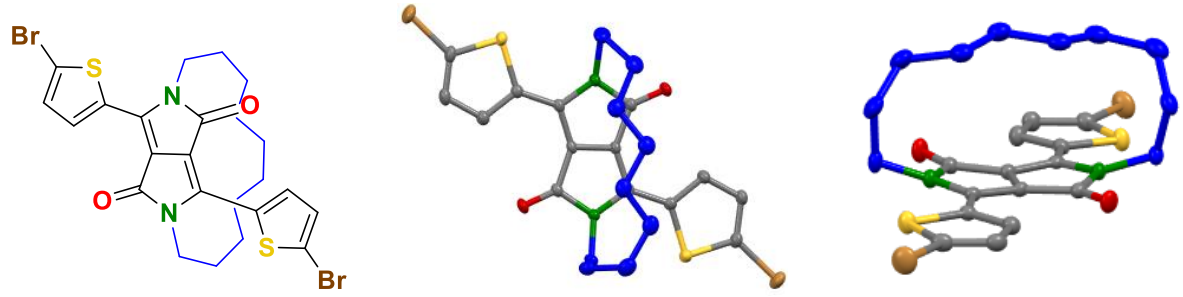

[†]X-ray structure determined by Dr Andrew Bond, University of Cambridge.

In order to gain an estimation as to how the encapsulating ring may affect distances at the D-A interface when incorporated into a DPP polymer, the interplanar distances between the DPP cores of **3** were also measured. Generally, most common DPP compounds (i.e. alkylated with either linear or branched chains) tend to have one interplanar distance, often ranging between 3-4 Å. For example, hexyl-DPP (**4**) has been observed to have an interplanar distance of 3.5 Å,[153] as measured by X-ray crystallographic analysis (Figure 3.10).

*Figure 3.10- Interplanar distance of hexyl-DPP **4** as measured by X-ray crystallographic analysis. Figure amended from F. Pop, W. Lewis and D. B. Amabilino. Published by the RSC.*[153]

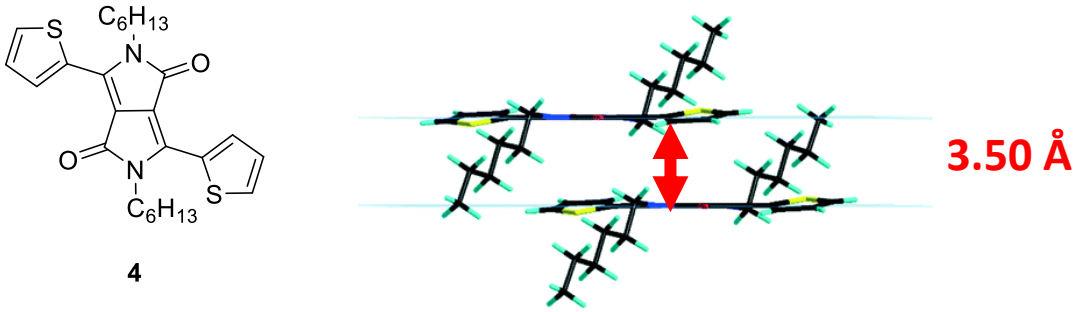

4

In contrast, **3** was observed to have two interplanar distances, one unusually short distance of 2.98 Å (between two non-encapsulated faces) and a much larger distance of 6.63 Å (between two encapsulated faces) (Figure 3.11). Thus, in some areas of the crystalline region within compound **3**, it appeared that

the interchromophore distance had increased. It was noted that the shorter distance of 2.98 Å, was smaller than generally observed in DPP monomers (~3-4 Å). While the cause for this is unknown, it is thought to be related to the ring strain observed in compound **3**, allowing the non-encapsulated faces to come into closer contact.

*Figure 3.11- Interplanar distances of **3** (**EC10DPPT**) as measured by X-ray crystallographic analysis.*

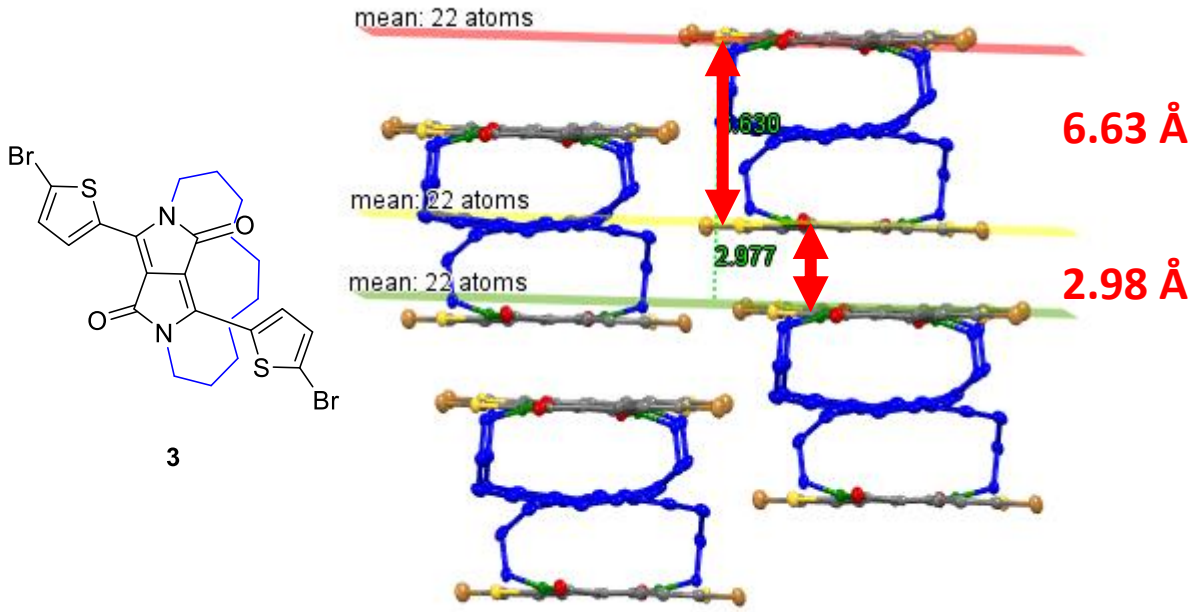

3.1.2.2 Synthesis of the DPP Monomers

Following the synthesis of the encapsulated dopant **3**, was the preparation of the DPP monomers **5** and **6**, for the Ph- and TT- polymer series respectively (Figure 3.12).

*Figure 3.12- Structures of DPP monomers **5** and **6**.*

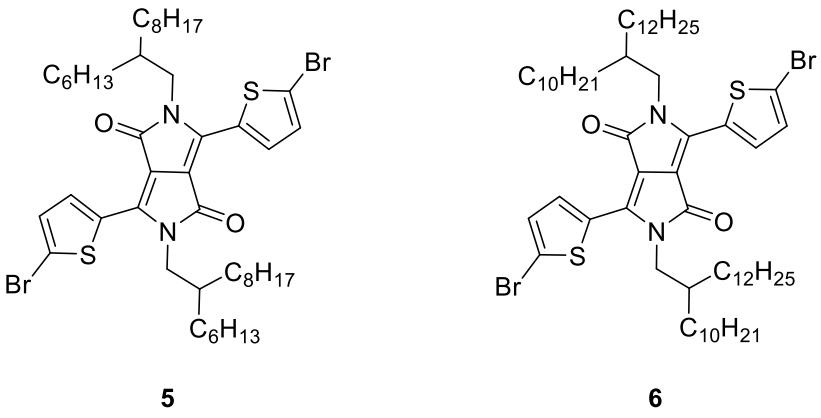

Compound **5** was prepared as previously discussed in *Chapter II*, while the synthesis of compound **6** followed a similar route (Scheme 3.3). To begin, the DPP core **1** was alkylated using 7-(bromomethyl)pentadecane, to obtain **7** as a magenta solid (23%). This was followed by quantitative di-bromination of **7** using NBS and upon workup, the crude product was purified *via* column chromatography and subsequent recrystallisation in isopropanol, to afford **6** as a waxy dark purple solid (79%).

*Scheme 3.3- Synthetic route to **6**.*

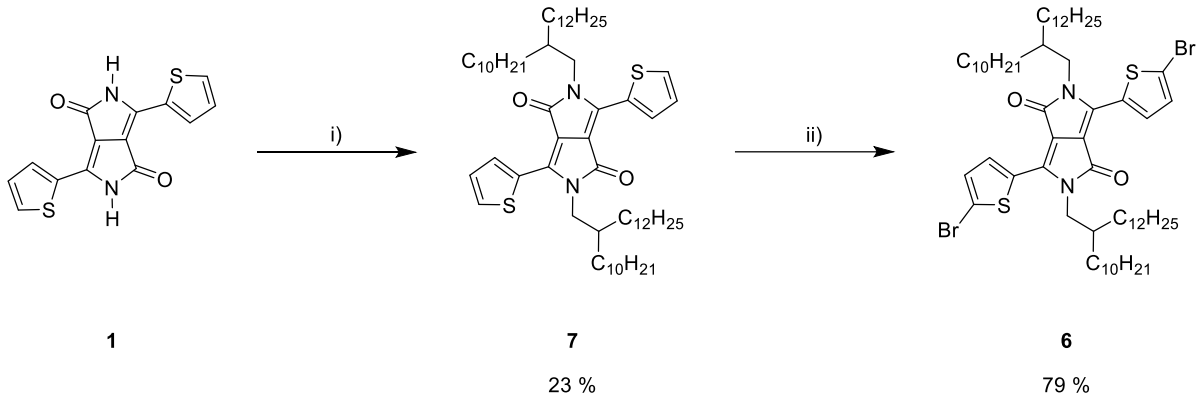

i) 7-(Bromomethyl)pentadecane , K_2CO_3, 18-crown-6, DMF, 120 °C, 18 h; ii) NBS, $CHCl_3$, 0 °C- RT, Overnight.

3.1.2.3 Synthesis of the Doped DPP Polymers

Following the preparation of the chosen DPP monomers **5** and **6**, was the synthesis of the DPP polymer series Ph- and TT-, doped with increasing amounts of the encapsulated DPP monomer **3**. The first set of polymers to be synthesised were the Ph-series, which involved the Suzuki cross-coupling of monomer **5** with 1,4-benzenediboronic acid bis(pinacol) ester, based on a procedure by Janssen *et al* (Scheme 3.4).[117] The reference polymer (absent of monomer **3**), underwent Soxhlet-extraction using acetone, hexane, and chloroform to afford **PDPPT-P** at a 77% yield.

*Scheme 3.4- Synthesis of reference polymer **PDPPT-P**.*

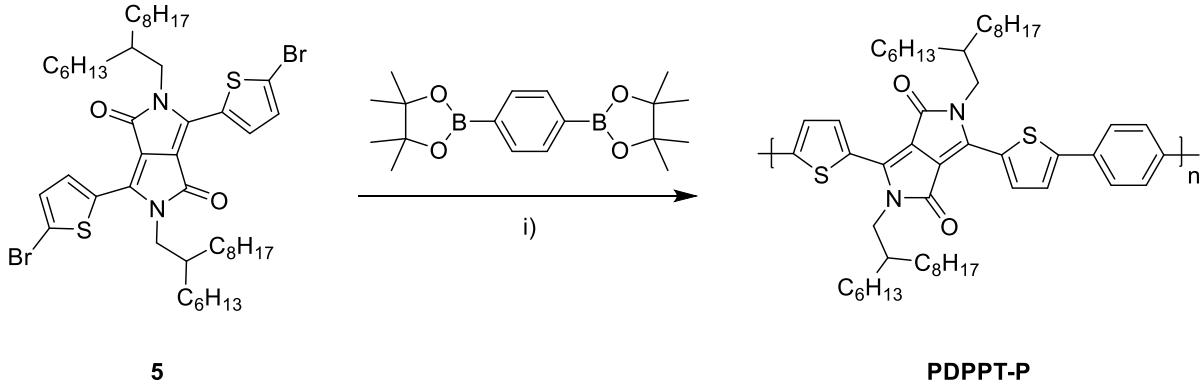

i) $Pd_2(dba)_3$, PPh_3, K_3PO_4, Aliquat 336, Toluene, H_2O, 115 °C, 3 days.

The remaining polymers were then synthesised by incorporating an increasing ratio of the dopant monomer **3** in place of monomer **5**, using the same procedure to synthesise **PDPPT-P**. Thus, the following DPP polymers were prepared, doped with increasing amounts of **3**: **PE5DPPT-P** (5%), **PE10DPPT-P** (10%), **PE20DPPT-P** (20%) and **PE30DPPT-P** (30%). The polymers were then purified *via* Soxhlet extraction as before, and isolated in chlorobenzene. The monomer ratios, yields, molecular weights† and extraction solvents used to isolate the polymers in the Ph-series, are summarised below in Table 3.1.

Table 3.1- A summary of the monomer ratios, yields, molecular weights and extraction solvents used to isolate the doped DPP polymers of the Ph-series.

Ph-Series

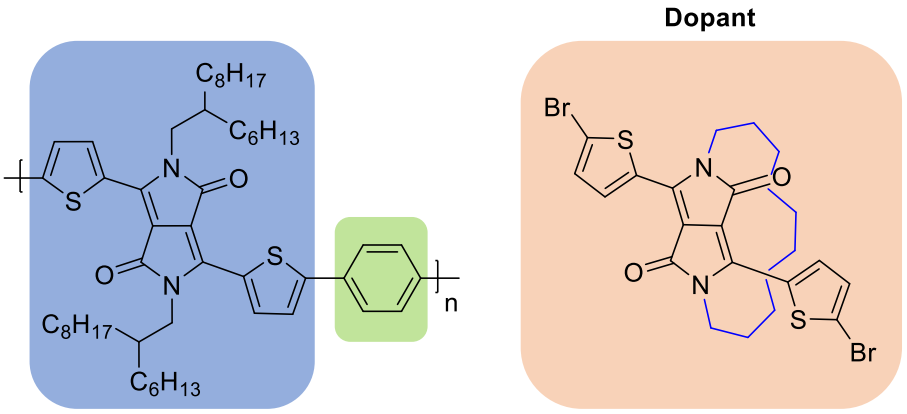

5 **P** **3**

	Monomer Ratio			Extraction Solvent	Yield (%)	Molecular Weight (KDa)†	
Polymer	**5**	**3**	**P**			M_n[a]	M_w[a]
PDPPT-P	1	0	1	$CHCl_3$	77	25.1	72.7
PE5DPPT-P	0.95	0.05	1	CB	54	28.4	86.1
PE10DPPT-P	0.90	0.1	1	CB	64	25.1	79.5
PE20DPPT-P	0.80	0.2	1	CB	36	40.7	210.7
PE30DPPT-P	0.70	0.3	1	CB	25	24.4	100.5

[a]*Determined by GPC (1,2,4-trichlorobenzene) against PS standard.*

†Molecular weights determined by Dr Samuel Lawton, University of Warwick

As the literature polymer was reported to exhibit a large amount of aggregation in solution,[117] the molecular weights were determined by hot GPC (1,2,4-trichlorobenzene) at 160 °C. While most of the

polymers in the series were within a similar range, it was observed that **PE20DPPT-P** was of a much higher molecular weight, which was reflected in its poor solubility in chlorobenzene (CB). In general, as the ratio of monomer **3** increased, the solubility of the polymers decreased. This was likely due to the decrease in percentage of solubilising alkyl chain density within the polymer.

The second stage of the project was the synthesis of the TT- polymer series. The reference polymer **PDPPT-TT**, was synthesised *via* a Stille cross-coupling between monomer **6** and 2,5-bis(trimethylstannyl)-thieno[3,2-*b*]thiophene, based on a procedure by Heeger *et al* (Scheme 3.5).[28] The polymer then underwent Soxhlet extraction using acetone, hexane and dichloromethane to afford **PDPPT-TT** at a 74% yield.

*Scheme 3.5- Synthesis of reference polymer **PDPPT-TT**.*

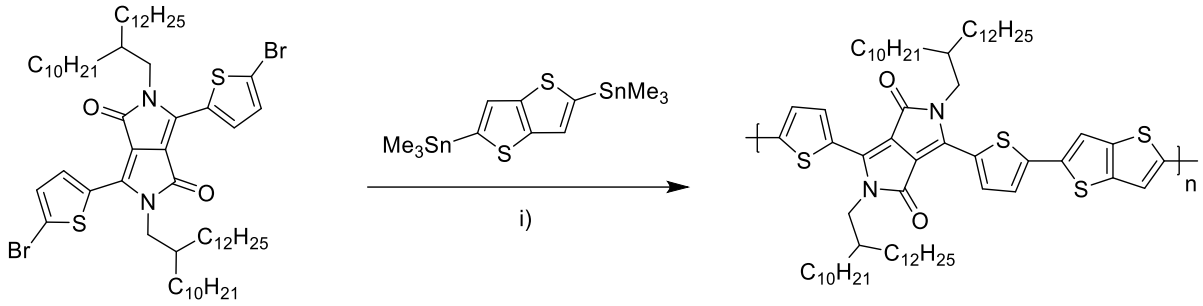

6 **PDPPT-TT**

i) Pd(dba)$_3$, P(o-tol)$_3$, Toluene, DMF, 115 °C, 18 h.

As before, the remaining polymers were synthesised *via* the same procedure, with increasing amounts of monomer **3**. However, due to the anticipated low solubility at higher ratios of the encapsulated monomer, the dopant was maximised at 20%. Additionally, due to the high planarity of the thienothiophene units within the polymer, this often results in efficient π–π stacking and poor solubility.

Thus, the following polymers were prepared: **PE5DPPT-TT** (5%), **PE10DPPT-TT** (10%) and **PE20DPPT-TT** (20%). The polymers were then purified *via* Soxhlet extraction as before, and isolated in either dichloromethane (DCM), chlorobenzene (CB) or chloroform. The monomer ratios, yields, molecular weights and extraction solvents used to isolate the polymers in the TT-series, are summarised below in Table 3.2.

Table 3.2- A summary of the monomer ratios, yields, molecular weights and extraction solvents used to isolate the doped DPP polymers of the TT-series.

TT-Series

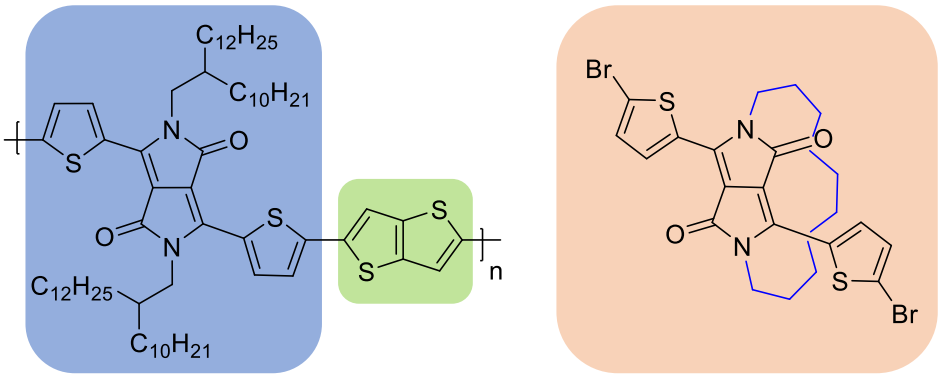

6 **TT** **3**

	Monomer Ratio			Extraction Solvent	Yield (%)	Molecular Weight (KDa)	
Polymer	**6**	**3**	**TT**			M_n[a]	M_w[a]
PDPPT-TT	1	0	1	DCM	77	26.3	102.7
PE5DPPT-TT	0.95	0.05	1	$CHCl_3$	83	24.4	79.1
PE10DPPT-TT	0.90	0.1	1	CB	71	78.4	221.2
PE20DPPT-TT	0.80	0.2	1	$CHCl_3$	39	14.0	76.4

[a]*Determined by GPC (CB) against PS standard.*

The molecular weights were determined by GPC (CB) and in general were within a similar range however, it was observed that for **PE10DPPT-TT**, the molecular weight was significantly higher, and the polymer had to be extracted using CB. In contrast, it was noted **PE20DPPT-TT** had a much lower M_n in comparison to the rest of the polymers, which may suggest that the polymerisation did not go to completion or human error regarding the reactant stoichiometry, when weighing the material. Overall, the polymers within the TT-series showed higher solubility in common chlorinated solvents than anticipated, in comparison to that of the Ph-series. This may be due to the longer branched alkyl chains present on monomer **6,** compared to that of monomer **5**.

It is to be noted, that in both the Ph- and TT- polymer series, little is known about dopant distribution within the encapsulated polymers. As dopant monomer **3** contains the same bi-functional reactive end groups as monomers **5** and **6**, it is expected that the reactivity of the dopant during polymerisation should be similar to that of the non-encapsulated DPP monomers. On the other hand, it may also be

possible that the encapsulating ring on dopant **3** affects the rate of reactivity due to steric hinderance, in turn affecting distribution of the dopant along the polymer chain, however this is still unknown.

3.1.3 Characterisation

3.1.3.1 Optical Properties of the Ph-Series

The optical properties of the polymers within the Ph-series are tabulated below in Table 3.3.

Table 3.3- Optical properties of the polymers within the Ph-series.

Polymer	λ_{max}^{soln} (nm)[a]	λ_{max}^{film} (nm)[b]
PDPPT-P	756	760
PE5DPPT-P	752	757
PE10DPPT-P	749	750
PE20DPPT-P	741	737
PE30DPPT-P	741	739

[a]CB solution. [b]Spin coated from CB (5 mg/mL).

The solution (in CB) (a) and thin film (spin coated from CB 5 mg/mL) (b) UV-vis absorption spectra of the polymers within the Ph-series are presented in Figure 3.13.

Figure 3.13- Normalised solution (in CB) (a) and thin film (spin coated from CB 5 mg/mL) (b) UV-vis absorption for the polymers within the Ph-series.

a) Solution

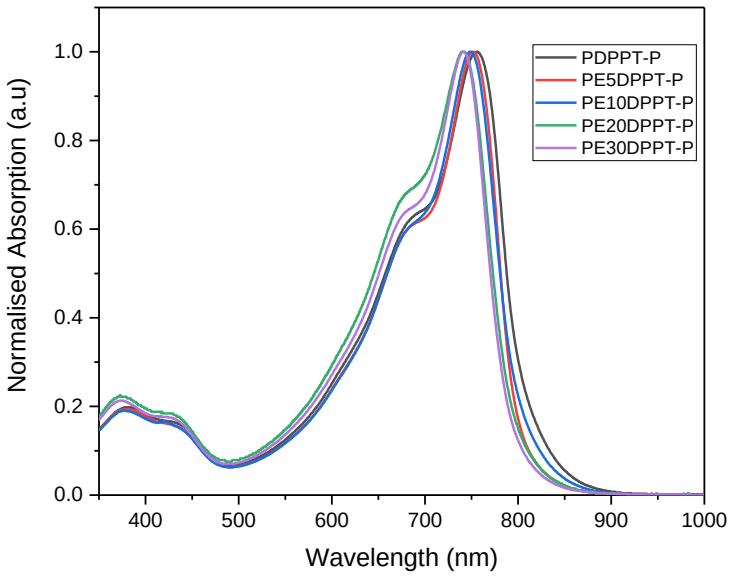

b) Thin Film

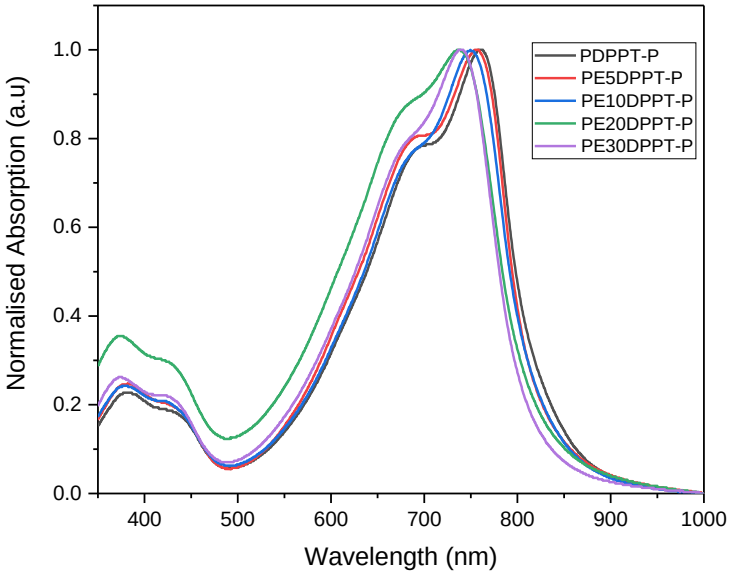

The general trend observed in the solution spectra, was that as the ratio of encapsulated monomer **3** increased within the doped polymers, the further blue-shifted the absorption. For example, the solution absorption maxima (λ_{max}^{soln}) for reference polymer **PDPPT-P** was 756 nm, while for **PE30DPPT-P** the λ_{max}^{soln} was at 741 nm. This trend may have been attributed to the increase of encapsulated monomer, thus leading to a decrease in π–π stacking and aggregation, resulting in a blue-shifted absorption. However as previously mentioned, it was observed that encapsulated monomer **3** exhibited ring strain. This can lead to torsional disorder within regions of the conjugated backbone, which also results in a blue-shifted absorption.

This trend was also observed in the thin-film spectra, which appeared broader than solution due to solid-state packing effects, such as aggregation. Additionally, π–π stacking/aggregation and planarization in the solid state, often leads to red-shifted absorption from solution to thin film, as observed in polymers **PDPPT-P** and **PE5DPPT-P**.[153] However, the remaining polymers doped with higher ratios of monomer **3** did not exhibit red-shifted absorption in the solid state, which may suggest suppression of aggregation. It was noted, that in both the solution and thin-film spectra, **PE20DPPT-P** did not fit the general trend and was blue-shifted in comparison to **PE30DPPT-P**. This was most likely due to the large difference in molecular weight of **PE20DPPT-P**, compared to the rest of the series.

3.1.3.2 Optical Properties of the TT-Series

The optical properties of the polymers within the TT-series are tabulated below in Table 3.4.

Table 3.4- Optical properties of the polymers within the TT-series.

Polymer	λ_{max}^{soln} (nm)[a]	λ_{max}^{film} (nm)[b]
PDPPT-TT	821	821
PE5DPPT-TT	810	812
PE10DPPT-TT	812	813
PE20DPPT-TT	804	802

[a]CB solution. [b]Spin coated from CB (5 mg/mL).

The solution (in CB) (a) and thin film (spin coated from CB 5 mg/mL) (b) UV-vis absorption spectra of the polymers within the TT-series are presented in Figure 3.14.

Figure 3.14- Normalised solution (in CB) (a) and thin film (spin coated from CB 5 mg/mL) (b) UV-vis absorption for the polymers within the TT-series.

a) Solution

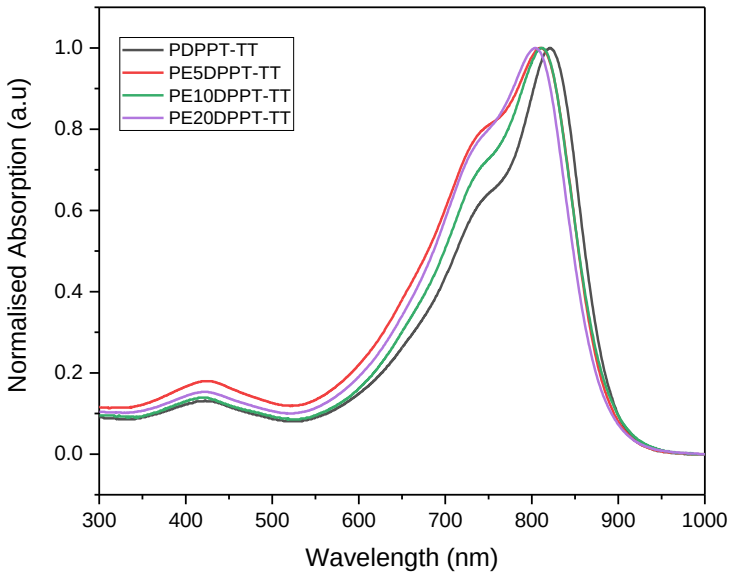

b)

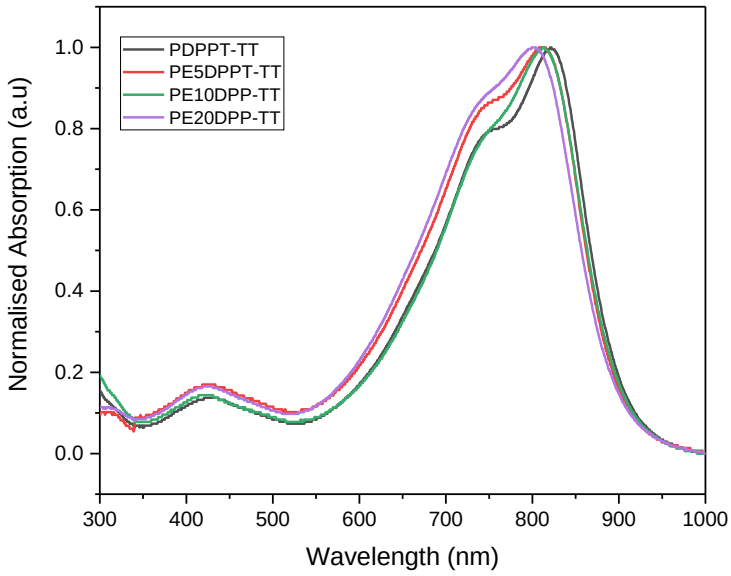

Overall, the absorption spectra for the TT-series was largely red-shifted in comparison to the Ph-series, as a result of the thienothiophene unit, which is a stronger electron donor than the phenyl unit, thus resulting in a narrower band gap and a red-shifted absorption.[103] As with the Ph-series, the polymers within the TT-series followed the same trend in both solution and thin film absorption spectra, with the increase in dopant **3** resulting in a blue-shifted absorption. While again, the thin-film spectra appeared broader than in solution, a significant red-shift was not observed in the solid state for any of the polymers, including the reference polymer **PDPPT-TT**. It was observed that **PE10DPPT-TT** did not fit the general trend, and as before with **PE20DPPT-P**, this was likely due to the large difference in molecular weight, compared to the rest of the polymers in the series.

3.1.4 Organic Photovoltaic Devices (OPVs)

Preliminary bulk heterojunction OPV devices, were constructed for both the Ph- and TT polymer series, in order to examine how the ratio of encapsulation affected the V_{oc}. The devices were fabricated in a conventional architecture, consisting of ITO/PEDOT/Polymer:$PC_{71}BM$/DPO/Ag and were tested under a 100 mW/cm^2 white light, under AM 1.5G conditions.[†] Additionally, diphenyl ether (DPE) was used as an additive to optimise the devices.

The current-voltage characteristics of the Ph-series are shown below in Figure 3.15 and the data from the devices are summarised in Table 3.5. As the devices were processed from $CHCl_3$, of which **PE20DPPT-P** and **PE30DPPT-P** showed poor solubility, it was not possible to fabricate devices from these polymers.

Figure 3.15- Current-voltage characteristics of Polymer:$PC_{71}BM$ (1:2) + 2% DPE Ph-series OPV devices.

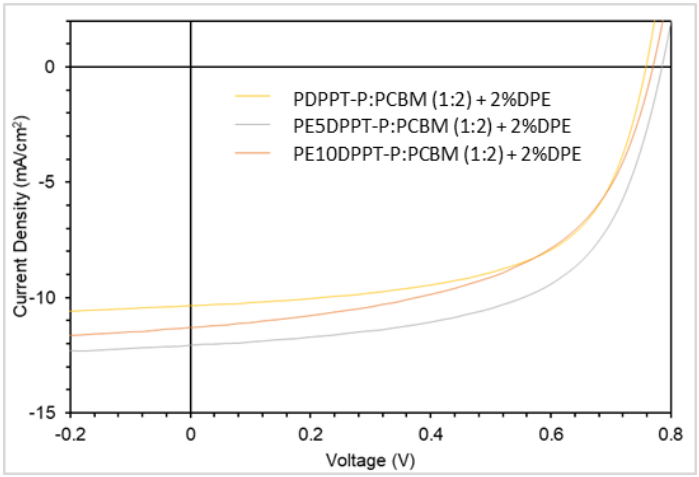

Table 3.5- Properties of the Ph-series based OPV devices spun from $CHCl_3$ solution with a 1:2 ratio of Polymer:$PC_{71}BM$ + 2% DPE.

Polymer	J_{sc} (mA/cm^2)[a]	V_{oc} (Max) (V)	V_{oc} (Avg.) (V)	*FF* (Max) (%)	*FF* (Avg.) (%)	PCE (Max) (%)
PDPPT-P	10.3	0.76	0.76	61	60	4.8 (4.7)[b]
PE5DPPT-P	12.1	0.79	0.78	60	59	5.7 (5.6)[b]
PE10DPPT-P	11.3	0.77	0.76	55	51	4.8 (4.4)[b]

[a]The J_{scs} were calculated, by integrating the EQE (The external quantum efficiency) spectrum by the AM 1.5G spectrum. [b]Average PCE value.

[†]All OPV devices within this study were fabricated by Anirudh Sharma, Jules Bertrandie and Dr Derya Baran, KAUST Solar Centre.

It was observed, that compared to the reference polymer **PDPPT-P**, encapsulation led to an increase in both the J_{sc} and V_{oc}. In particular, **PE5DPPT-P** showed a maximum V_{oc} of 0.79 V, which was over 20 mV more than that of **PDPPT-P**. Although encapsulation also led to a slight decrease in the *FF*, overall the best performing polymer was **PE5DPPT-P**, which achieved an improved maximum PCE of 5.7% in comparison to the reference (4.8%). While **PE10DPPT-P** showed an increase of the J_{sc} and maximum V_{oc}, it also had a reduced maximum *FF* of 55%, thus showing no improvement of the PCE. This may suggest that for this particular polymer system, doping beyond 5% leads to detrimental effects on the working order of the OPV device.

While the literature reference polymer, achieved a higher PCE of 7.4%, it is important to note the large difference in molecular weight between the polymers of the two studies.[117]

As the TT-series were found to be far more soluble in $CHCl_3$, all polymers were fabricated into devices identical to the architecture of the Ph-series. However, due to small pixel, the PCE obtained for **PE20DPPT-TT** was inaccurate as the J_{sc} could not be calculated by integrating the EQE, thus the device was not included in the study. The current-voltage characteristics of the TT-series are shown below in Figure 3.16 and the data from the devices are summarised in Table 3.6.

Figure 3.16- Current-voltage characteristics of Polymer:$PC_{71}BM$ (1:3) + 3% DPE TT-series OPV devices.

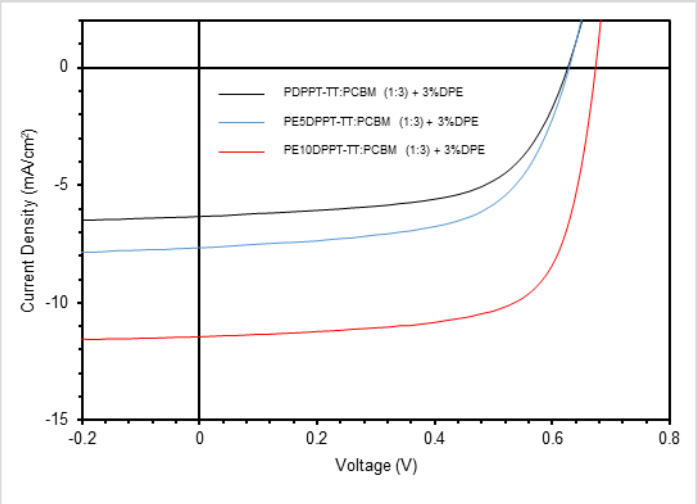

Table 3.6- Properties of the TT-series based OPV devices spun from $CHCl_3$ solution with a 1:3 ratio of Polymer:$PC_{71}BM$ + 3% DPE.

Polymer	J_{sc} (mA/cm^2)[a]	V_{oc} (Max) (V)	V_{oc} (Avg.) (V)	*FF* (Max) (%)	*FF* (Avg.) (%)	PCE (Max.) (%)
PDPPT-TT	6.3	0.63	0.62	61	61	2.4 (2.4)[b]
PE5DPPT-TT	7.7	0.63	0.62	61	60	2.9 (2.9)[b]
PE10DPPT-TT	11.4	0.67	0.66	70	69	5.3 (5.2)[b]

[a]*The J_{scs} were calculated, by integrating the EQE (The external quantum efficiency) spectrum by the AM 1.5G spectrum.* [b]*Average PCE value.*

When the polymer was doped with 10% of the encapsulated monomer, improvements in the J_{sc}, V_{oc}, and *FF* were observed compared to the reference **PDPPT-TT**. In particular, **PE10DPPT-TT** showed a maximum V_{oc} of 0.67 V, 50 mV more than **PDPPT-TT**, achieving the highest maximum PCE of 5.3%. In comparison, **PE5DPPT-TT** showed little change in performance compared to **PDPPT-TT**, although a slight increase in the J_{sc} was observed. The difference in performance between **PE10DPPT-TT** and **PE5DPPT-TT**, may have been related to large differences in molecular weight. While again, the reference polymer achieved a higher PCE of 9.4% in literature, it is noteworthy that there were very

large differences in molecular weight, between the two studies. For example, in this study the M_w= 103 KDa and M_n= 26.3 KDa, while Heeger *et al*[28] reported higher molecular weights of M_w= 449 KDa and M_n= 209 KDa.

Overall, in both the TT and Ph-series, encapsulation generally led to an increase in the V_{oc} and it is possible that these results are attributed to several different factors. For example, a known effective strategy to increase the V_{oc}, is by raising the difference of the static dipole moment at the D-A interface, which has a direct relationship with the electronic coupling in the CT state, as expressed in the following equation:

Equation 3.3:

$$V = \frac{ME_{CT}}{\sqrt{|\Delta\vec{\mu}|^2 + 4M^2}}$$

Where V is the electronic coupling, M is the transition dipole moment and $|\Delta\vec{\mu}|$ is the difference in the static dipole moment between the CT state and GS respectively.[147] Thus, by raising the interfacial static dipole moment, this leads to decreased electronic coupling in the CT state. As a result, charge recombination is supressed, thereby increasing the V_{oc}. Various other parameters affecting the V_{oc} have been widely studied and are summarised by Nelson *et al*[147] in Table 3.7, with the parameters of interest to the study highlighted in blue.

Table 3.7- Potential V_{oc} increase when changing different parameters in the range shown below as presented by Nelson et al,[147] with the parameters of interest to the study highlighted in blue.

Parameter improvement strategy	V_{oc} increase
Reduce the ratio of CT-state density from 1% to 0.01%	40 mV
Reduce the low-frequency reorganization energy (λ_0) from 0.2 to 0.1 eV	55 mV
Reduce the high-frequency reorganization energy (λ_i) from 0.2 to 0.1 eV	130 mV
Increasing the energy of the CT state by 100 meV (from 1.45 to 1.55 eV)	130 mV
Reducing $E_g - E_{CT}$ from 300 to 100 meV (E_g is decreased)	140 mV
Increasing the oscillator strength of the transition from 1 X 10^{-2} to 1	10 mV
Increasing the difference in the static dipole moment $\|\Delta\vec{\mu}\|$ from 10 to 30 D	45 mV

From these results, another effective strategy is *via* the reduction of the reorganization energy. By reducing the conformational change of the molecule following charge-transfer transition and its impact on the surrounding environment, the V_{oc} can be improved by ~ 0.2 V. The reorganization energy in an OPV, is largely dependent on the chemical structure of the D/A materials, thus rigidified systems

preventing large conformational changes would be ideal. It was also observed, that the $|\Delta\vec{\mu}|$ has a significant effect on the V_{oc}. For example, just a 20 D increase can raise the V_{oc} by over 40 mV.[147]

Statistically, a proportion of the encapsulated polymer chains in the doped DPP polymers, were located at the D-A interface. Therefore, this modification may have influenced several different parameters affecting the V_{oc} as described in Table 3.7.

Firstly, the encapsulating rings may have increased the difference in the static dipole moment between the CT state and GS, thus decreasing electronic coupling. Therefore, by suppressing charge recombination, the V_{oc} was increased. Encapsulation may have also increased the distance between the D and A at the interface. As a result, this would weaken the Coulombic interactions between the polaron charge pairs, thereby raising the E_{CT}. Alternatively, this increased distance if large enough, may have prevented the formation of CT states at the encapsulated sites, thus reducing the ratio of the CT-state density. In both cases, this would lead to an increase of the V_{oc}. Finally, as discussed previously, encapsulated materials generally show an increased rigidity, brought about by the macrocyclic steric shield. Thus, following charge-transfer transition, it is likely that the doped polymers exhibit a lower conformational change compared to that of the reference. This results in a lower reorganization energy thereby, increasing the $V_{oc.}$

While the specific factor responsible for this trend is unknown, it is possible that different ratios of encapsulation influenced various parameters at different extents. As the maximum increase of the V_{oc} was ~ 50 mV, from the results reported by Nelson *et al* in Table 3.7,[147] this may suggest that either a reduced ratio of the CT-state density, a reduced reorganization energy or an increase of the difference in the static dipole moment were responsible for the results of this study, either individually or as a combination of these factors.

3.1.5 Conclusions

In conclusion, the novel encapsulated monomer **EC10DPPT** was synthesised and showed larger interplanar distances in the solid state, compared to most standard DPP compounds in literature. The encapsulated monomer was doped in increasing ratios (0%, 5%, 10%, 20% and 30%), into two novel series of DPP polymers (Ph and TT-series).

Overall, the general trend observed in the UV-vis spectra, was that as the ratio of **EC10DPPT** increased within the doped polymers, the further blue-shifted the absorption. As observed previously in *Chapter II*, intermolecular interactions between polymer chains can lead to red-shifted absorption. This may suggest that the increase in ratio of **EC10DPPT** led to suppression of aggregation, thus resulting in a blue-shifted absorption. However, as **EC10DPPT** exhibited ring strain, this may have also led to torsional disorder within regions of the conjugated backbone, which also results in a blue-shifted absorption.

It was discovered, that *via* the introduction of the encapsulated dopant, it was possible to raise the V_{oc} in some of the fabricated OPV devices. This may suggest that there was an increase in the $|\Delta\vec{\mu}|$, resulting in a raise of the $V_{oc.}$ Various other parameters influencing the V_{oc} such as the E_{CT} and the reorganization energy, may have also been altered by encapsulation and contributed to these results.

It was also observed that encapsulation generally resulted in a higher J_{sc}. In the Ph-series, encapsulation led to small decreases of the *FF*, while interestingly led to an increase in the TT-series. Overall, the encapsulated polymers generally showed higher device efficiencies in comparison to the reference, with **PE5DPPT-P** and **PE10DPPT-TT** achieving the highest maximum PCEs of 5.7% and 5.3% in the Ph- and TT-series respectively. While this suggests that the optimum amount of encapsulation can vary in different polymer systems, it is possible that differences in molecular weight of the polymers, also contributed to these results.

These results demonstrate the possibility of monomer **EC10DPPT**, to be incorporated into various other polymers systems, in order to modify the D-A interface and raise the V_{oc} in OPV devices.

3.2 Encapsulated Polymers based on DPP-BDT

3.2.1 Introduction

3.2.1.1 The Effect of Ring Size

Following the previous study, it was concluded that by doping known DPP polymer systems with certain amounts of the encapsulated DPP monomer **EC10DPPT**, this led to an increase in the V_{oc} and PCE. However, when studying the X-ray crystal structure of **3** (**EC10DPPT**), significant ring strain could be observed, which may have contributed to the blue-shifted UV-vis spectra of the encapsulated polymers. Additionally, ring strain can also lead to torsional disorder within the conjugated backbone of the polymer, resulting in decreased device efficiency. As the encapsulated DPP monomer is a highly novel and unique structure, investigation of appropriate ring size and basic structure-property relationship is largely important.

It has been previously shown that the ring size of encapsulated organic materials, can affect their physical properties and performance. Fujiwara *et al,*[154] reported the synthesis of a double-encapsulated anthracene compound, strapped with three different ring sizes (**C6**, **C7** and **C8**) (Figure 3.17). Compared to the non-encapsulated reference compound **DPA**, the encapsulated materials showed higher photostability. However, among the three encapsulated anthracenes, it appeared that the **C7** chain was the most effective, resulting in the highest ΦFs of 0.87 and 0.93, in both cast film and powder state respectively. These results were attributed to the nature of the encapsulating rings, for example, the **C6** ring size was thought to be too tight, resulting in strain of the excited state. In contrast, the **C8** ring was too loose, leading to thermal vibrational deactivation of the excited state. Thus, the optimum ring size **C7**, effectively blocked aggregation and fluorescence self-quenching, resulting in a higher ΦF.

*Figure 3.17- Structures of **DPA**, **C6** (m= 1), **C7** (m= 2) and **C8** (m= 3). Adapted with permission from Y. Fujiwara et al, J. Org. Chem., 2013, **78**, 2206–2212. Copyright 2021 American Chemical Society.*[154]

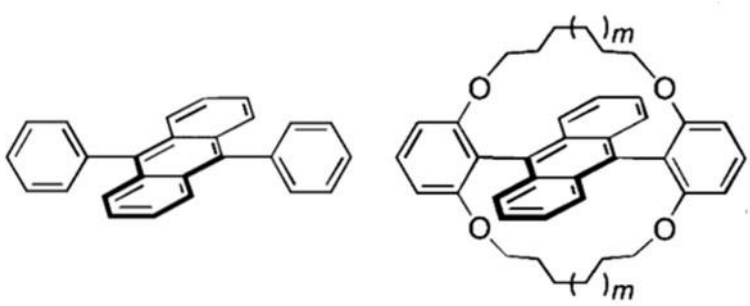

Therefore, these results demonstrate the importance of choosing the correct ring size, when encapsulating organic materials. While the effect of different ring sizes has been explored in small molecules, they have yet to be investigated in a polymer system. Such a study would be ideal, allowing elucidation on how subtle structural changes, can impact the properties and performance of conjugated polymers.

3.2.1.2 Non-Fullerene Acceptors (NFAs)

While high performing DPP polymers have achieved large mobilities and J_{scs}, the PCEs are often hindered by relatively low V_{ocs}. In the previous sub-chapter, we established that the structural modification of DPP based polymers can result in an increased $V_{oc,}$ however another strategy is to increase the electron affinity of the acceptor material. As previously discussed in *Chapter I*, until recently, fullerene derivatives were the most commonly used acceptors in OPV devices however they are limited by their fixed absorption and electron affinities. Thus, more recently non-fullerene acceptors (NFAs) have emerged, providing tuneable optical band gaps, adjustable energy levels and controllable crystallinity through molecular design, superior to that of fullerene derivatives.[155] Commonly used NFA materials include dithieno-indacenodithiophene derivatives (**ITIC**) and rylene diimides.

While the introduction of NFAs, have led to remarkably impressive PCEs of over 15%,[80] less success has been found when used in combination with thienyl-DPP based polymers. Various NFAs such as N2200 polymers[156] and ITIC[157] have been tested, resulting in low PCEs of under 5% due to poor *FFs* and $J_{scs.}$ However, in 2019 Baran *et al*[155] reported a highly efficient DPP:NFA BHJ solar cell, consisting of a DPP-BDT co-polymer (**PBDTT-DPP**) which was used in combination with the low band-gap NFA **IEICO-4F**, to achieve a remarkably high PCE of 9.66% (Figure 3.18). In comparison, the reference device which featured the more commonly known NFA ITIC, achieved a PCE of only 3.70%. These results were attributed to the stronger intramolecular effect and crystallinity of **IEICO-4F**, than that of ITIC, resulting in a higher efficiency of charge generation and lower charge recombination.

The BDT unit was chosen as the co-monomer due to its stronger intermolecular π–π interaction than that of thiophene, thus extending the conjugation in the backbone and therefore, facilitating better charge transport. Additionally, as BDT is a weaker electron donor than thiophene, this then lowered the ionization potential of the donor, thus increasing the V_{oc}.[155] Therefore, these results demonstrate the potential of high efficiency DPP:NFA solar cell devices, particularly when using a BDT co-monomer and an NFA possessing a low band gap and high crystallinity, such as **IEICO-4F**.

*Figure 3.18- Structure of **PBDTT-DPP** and **IEICO-4F**.*[155]

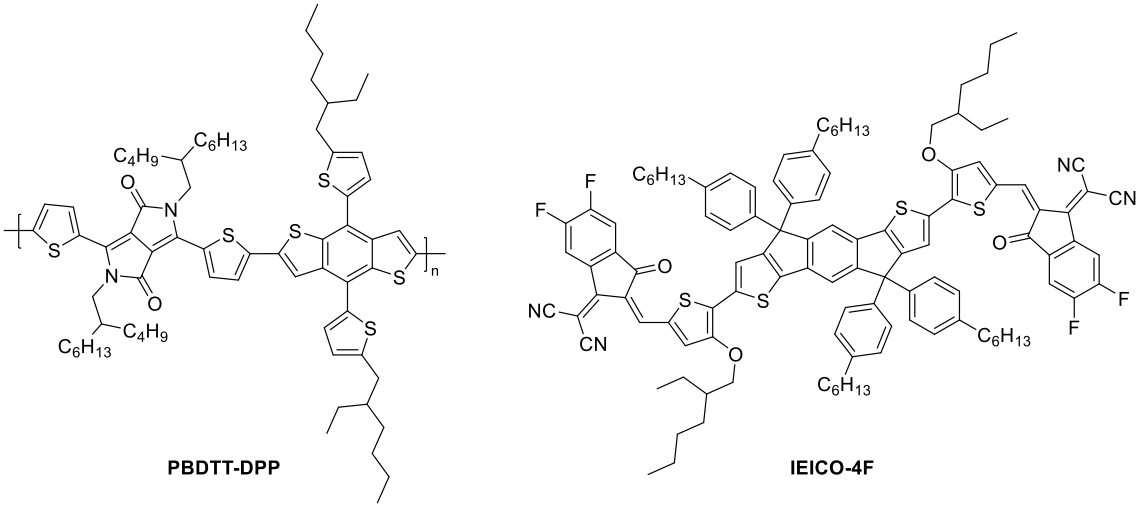

3.2.1.3 Sub-Chapter Objectives

As demonstrated by McDearmon *et al's*[152] previous research on encapsulated BDT polymers (discussed in *Chapter III, Sub-section 3.1.1.3*), full encapsulation along the conjugated backbone results in higher ΦFs and increased order in the solid state. However, the effect of such polymers in OPV devices, has yet to be explored.

Here we intend to study the effect of fully encapsulated DPP polymers on the performance of OPV devices. As the encapsulated DPP monomer **EC10DPPT** from the previous *Sub-Chapter 3.1* exhibited ring strain, here we investigated two additional ring sizes (C12 and C11) and an ethylene glycol ring (P11), *via* synthesis of the novel DPP monomers **EC12DPPT**, **EC11DPPT** and **EP11DPPT** (Figure 3.19).

*Figure 3.19- Structure of **EC12DPPT**, **EC11DPPT** and **EP11DPPT.***

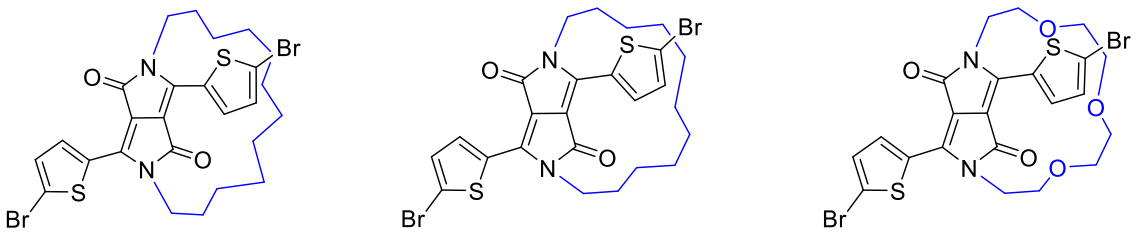

In order to investigate the effect of ring size on the properties of conjugated polymers, the encapsulated monomers were incorporated into a novel series of fully encapsulated DPP-BDT co-polymers (Figure 3.20), based on a high performing polymer in literature.[158] A non-encapsulated reference polymer (**PDPP-BDT**) was also synthesised in order to investigate the effect of encapsulation.

An alkylated BDT unit was chosen as the co-monomer, in order to provide the polymers with sufficient solubility and its demonstrated compatibility with NFAs, when co-polymerised with DPP units.[155] An encapsulated BDT polymer (**PDPP-E10BDT**) was also synthesised based upon a previously reported method by McDearmon *et al*,[152] to explore whether encapsulation of specific monomer units can influence the properties of the polymer. Inspired by Baran *et al's*[155] research, the polymers were then fabricated into OPV devices, in combination with both a fullerene (PCBM) and a non-fullerene (IEICO-4F) acceptor, to study which type of material is more compatible with this particular polymer system.

Figure 3.20- Structures of the fully encapsulated polymers ***PE12DPP-BDT***, ***PE11DPP-BDT***, ***PP11DPP-BDT***, ***PDPP-E10BDT*** *and the non-encapsulated reference polymer* ***PDPP-BDT***.

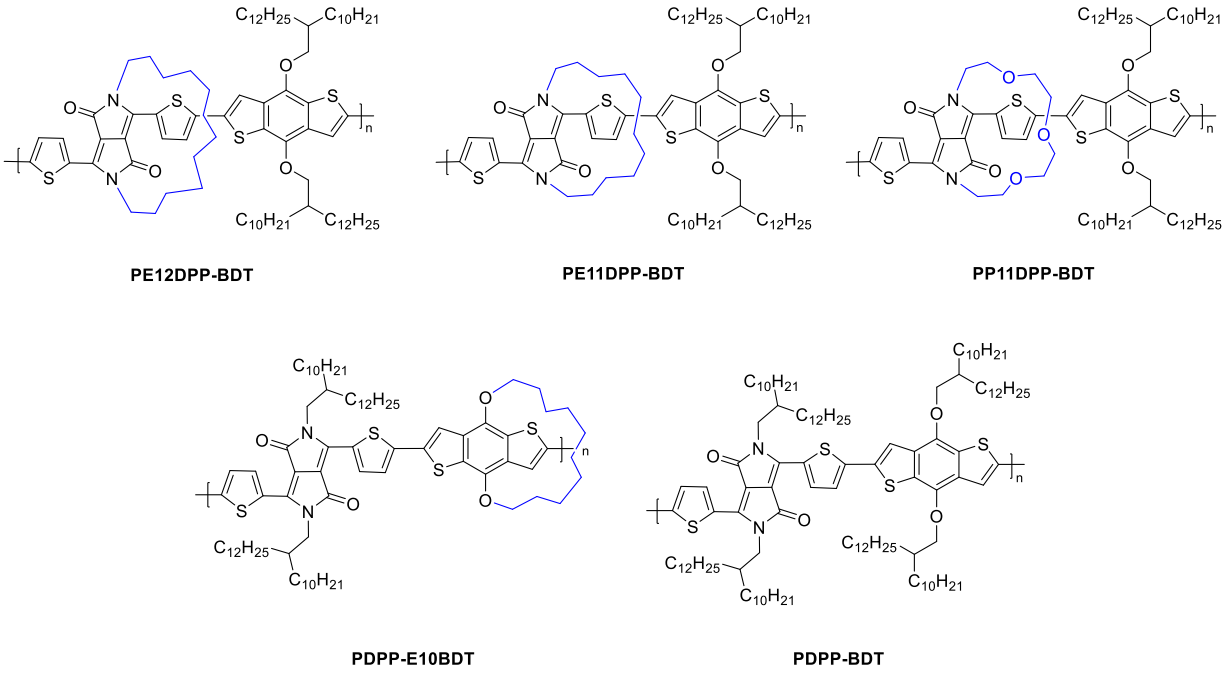

3.2.2 Synthesis

3.2.2.1 Synthesis of the Encapsulated DPP Monomers

*Scheme 3.6- Synthetic route to **8a** and **8b**.*

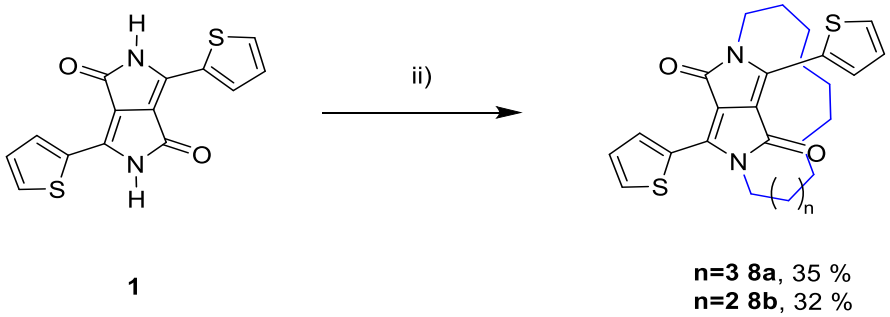

1

n=3 8a, 35 %
n=2 8b, 32 %

*i) 1,12 dibromododecane (**8a**) /1,12 dibromododecane (**8b**), K_2CO_3, 18-crown-6, DMF, 100 °C, 18 h.*

The preparation of the encapsulated DPP monomers, began with the alkylation of **1** (DPP) using a di-bromide alkyl chain, as previously when making compound **2**. In order to make **8a** and **8b**, 1,12 dibromododecane and 1,11-dibromoundecane were used respectively. The reactions were carried out using a similar procedure as before when making **2**. As a low yield was obtained for compound **2**, it was thought that the reaction may have been made too dilute, thus a more concentrated solution **(~** 182 mL of DMF per 0.5 g of **1**) was used instead (Scheme 3.6). A lower reaction temperature of 100 °C was also used, in attempt to decrease the amount of di-alkylated side-product.

Upon work up, the crude material was purified *via* column chromatography, followed by sonication in hexane. The pure products were then collected *via* filtration, to give **8a** (35%) and **8b** (32%) as dark purple solids. It was noted that the yields obtained for **8a** and **8b** were much higher, then that of **2**. While this may have been attributed to the change in dilution, the larger ring sizes may have also contributed to these results.

Compound **8c** was made *via* the same procedure, using tetraethylene glycol di(p-toluenesulfonate) in the place of a di-bromide alkyl chain (Scheme 3.7). This chain length was chosen, to allow a direct comparison to its alkyl counterpart, **8b**. Upon work up, the crude material was purified *via* column chromatography, followed by recrystallisation in methanol to afford **8c** as shiny champagne coloured crystals (12%).

*Scheme 3.7- Synthetic route to **8c**.*

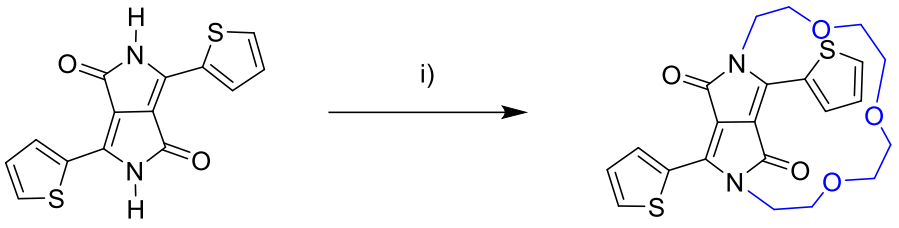

1 **8c**

12 %

i) Tetraethylene glycol di(p-toluenesulfonate), K_2CO_3, 18-crown-6, DMF, 100 °C, 18 h.

It was observed that **8c** had a low yield of just 12%. This was due to the multiple side reactions that compete directly with the nucleophilic substitution of the tetraethylene glycol di(p-toluenesulfonate), by the nitrogen atoms on the deprotonated DPP. In this case, a common side product observed was the *O,N*-encapsulated DPP **9** (Figure 3.21), a structural isomer of the *N,N*-encapsulated product **8c**. While the product could be isolated *via* column chromatography, only a small amount was obtained due to the similar polarities of the structural isomers on silica. While similar side products were observed during the synthesis of **8a** and **8b**, smaller amounts were made and could be removed *via* sonication in hexane. However, this purification technique did not work for **8c**, due to increased solubility in hexane.

*Figure 3.21- Chemical and crystal structure of the O,N-encapsulated DPP **9** obtained as a side product when synthesising **8c**. Crystals grown from $CHCl_3$: MeOH.*

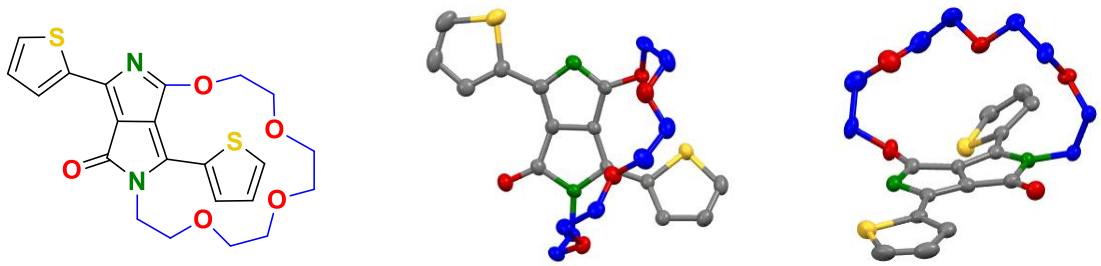

[†]X-ray structure determined by Dr Andrew Bond, University of Cambridge.

The structure of side product **9**, was determined by X-ray crystallographic analysis[†] (single crystals grown from $CHCl_3$: MeOH, Figure 3.21), which showed a highly distorted structure. Interestingly, it was observed that both thiophene units on either side of the DPP core faced the same direction, which

is highly unusual for any thienyl-DPP compound. This may have been due to a S-O interaction between the second thiophene unit and the ethylene glycol ring.

Finally, **8a** and **8b** underwent di-bromination with a quantitative amount of NBS. Initially, the reaction was carried out at 50 °C as when making **3**, however in both cases crude ^{1}H NMR showed the presence of both mono and di-brominated product. It was believed that this was due to a poor solubility in the reaction solvent, $CHCl_3$. Thus, the temperature of the reaction was raised to 90 °C and the reaction time increased to 18 h, to afford **10a** (48%) and **10b** (60%) as dark purple solids (Scheme 3.8).

*Scheme 3.8- Synthetic route to **10a** and **10b**.*

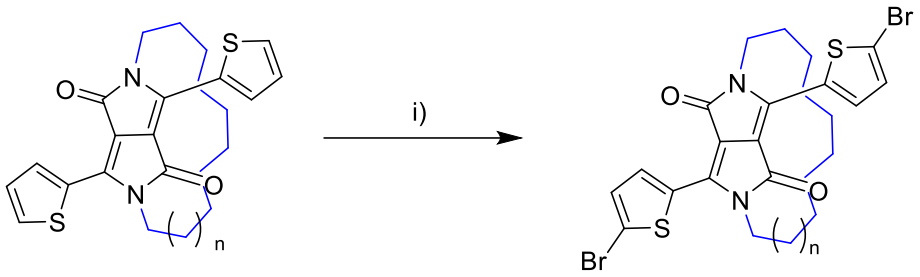

i) NBS, $CHCl_3$, 90 °C, 18 h.

Compound **8c** was observed to be far more soluble in $CHCl_3$ in comparison to **8a** and **8b**, as a result of the solubilising ethylene glycol chain. Therefore, **8c** underwent di-bromination with a quantitative amount of NBS at 0 °C - RT overnight, yielding **10c** as a gold flecked purple solid (21%) (Scheme 3.9).

*Scheme 3.9- Synthetic route to **10c**.*

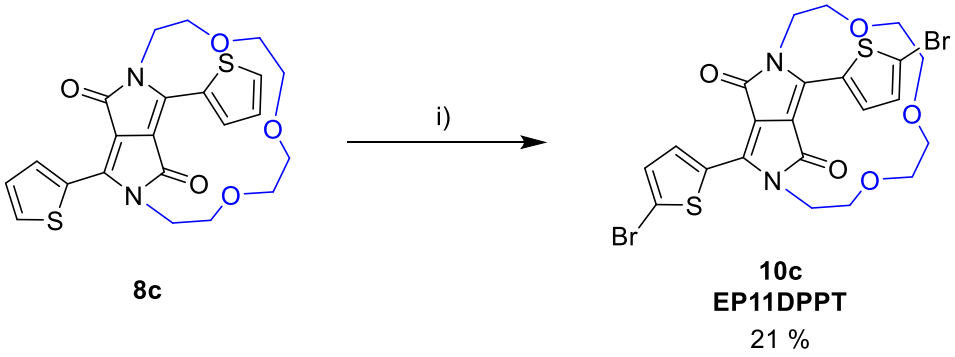

i) NBS, $CHCl_3$, 0 °C- RT, Overnight.

The structures of **10a**, **10b** and **10c**, were determined by X-ray crystallographic analysis[†] (single crystals grown from $CHCl_3$: MeOH, Figure 3.22), confirming the successful encapsulation of the DPP cores. The X-ray structures of **8a**, **8b** and **8c** were also obtained and can be found in the appendix.

It was observed that among the three monomers, **10a** (**EC12DPPT**) appeared to be the most ideal for polymerisation, exhibiting the least amount of ring strain and a relatively planar structure. The encapsulating alkyl ring appeared to be ordered, creating a well-defined steric shield of the DPP core. While **10b** (**EC11DPPT**) displayed less ring strain than **3** (**EC10DPPT**) (Figure 3.9), the encapsulating ring was observed to be rather disordered. However, **10b** showed greater planarity than its ethylene glycol counterpart **10c** (**EP11DPPT**), which was isolated as a pair of structural isomers. It was observed that **10c** showed a great amount of structural disorder and ring strain. The thiophene units were observed to twist out of plane, unusual for most thienyl-DPP compounds. This may have been due to S-O interactions between the sulfur atoms on the thiophene units and the oxygen atoms on the ethylene glycol ring.

Figure 3.22- Crystal structures of a) ***10a****, b)* ***10b*** *and c)* ***10c****. Crystals grown from $CHCl_3$: MeOH.*

*a)****10a*** *(****EC12DPPT****)*

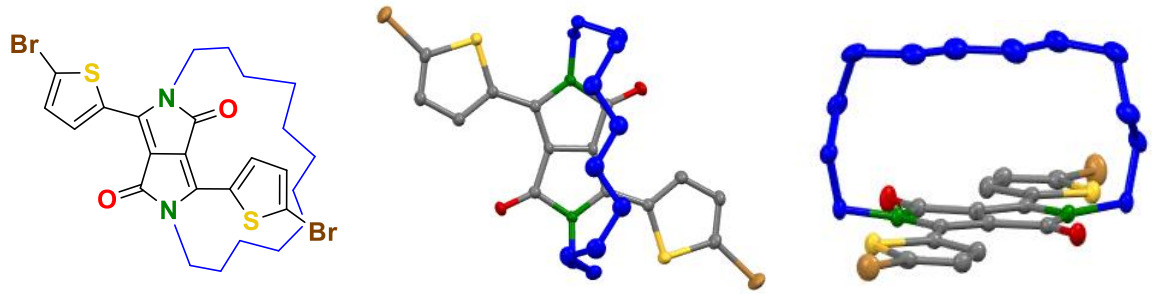

*b)****10b*** *(****EC11DPPT****)*

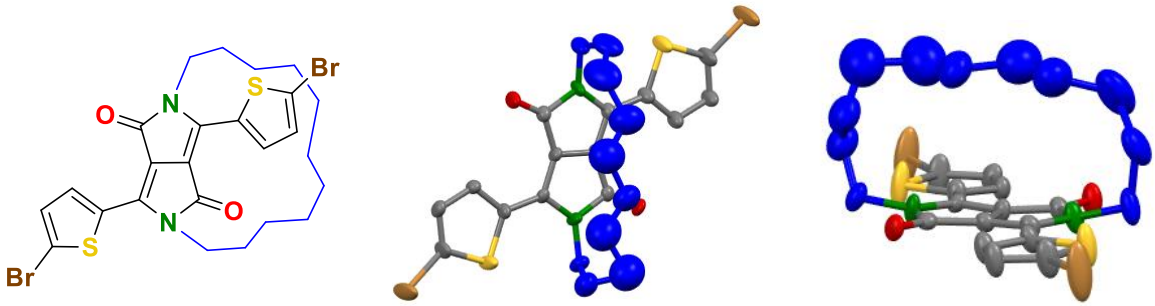

*c)****10c*** *(****EP11DPPT****)*

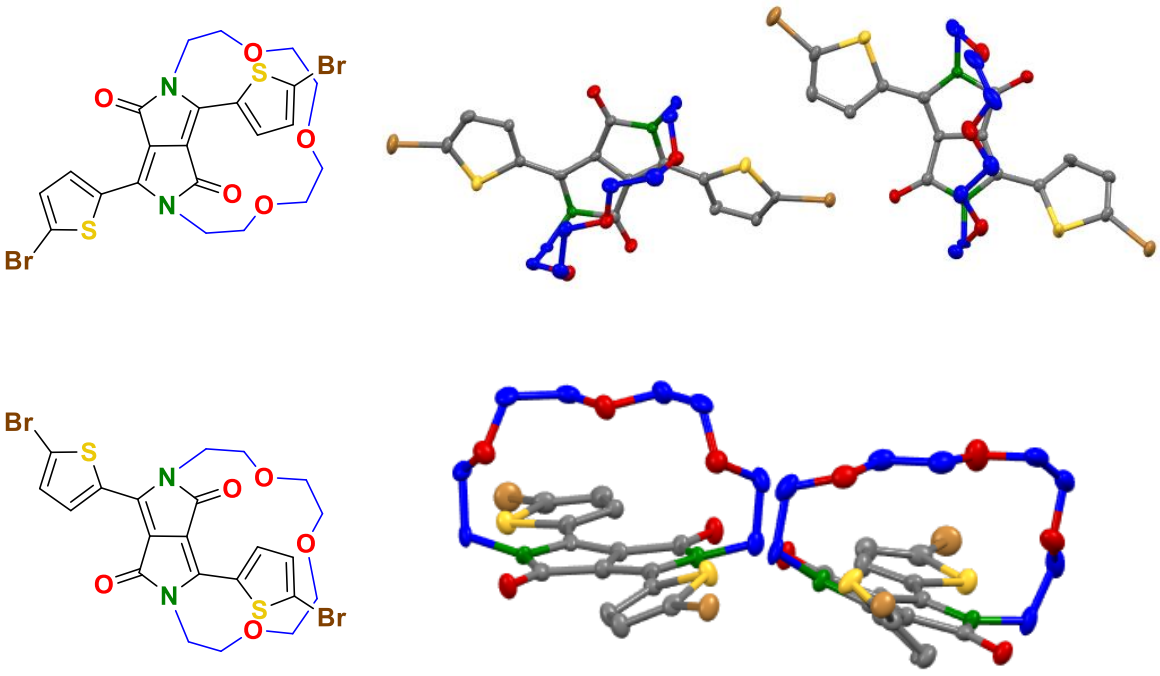

†X-ray structures determined by Dr Andrew Bond, University of Cambridge.

As before with compound **3**, to study how differing ring sizes may affect the π–π stacking distances when incorporated into conjugated polymers, the interplanar distances of **10a** and **10b** were also measured (Figure 3.23).

*Figure 3.23- Interplanar distances of **10a** and **10b** as measured by X-ray crystallographic analysis.*

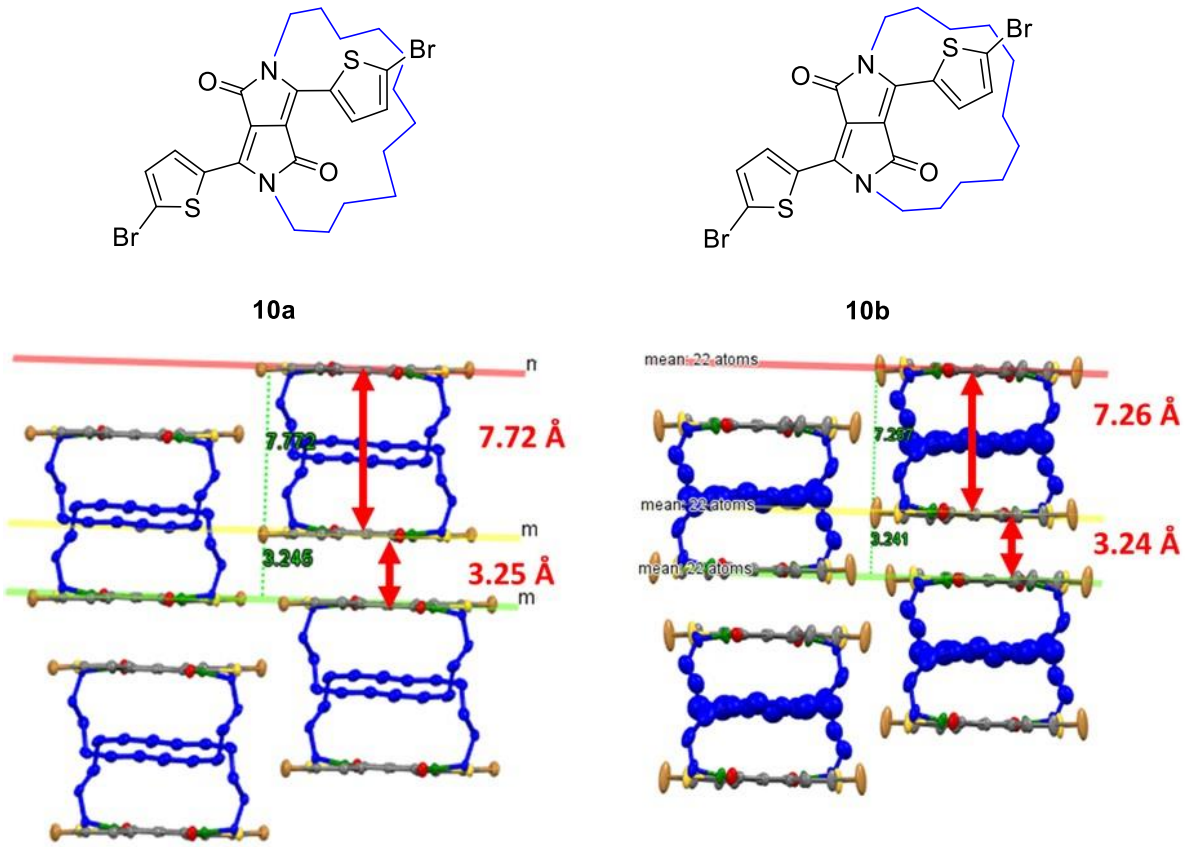

As with compound **3**, **10a** and **10b** were observed to have two interplanar distances, one larger distance between two encapsulated faces and a shorter one between two non-encapsulated faces. As expected, **10a** showed the largest distances of 7.72 Å and 3.25 Å, while **10b** was observed to have slightly shorter distances of 7.26 Å and 3.24 Å.

It was observed that the shorter interplanar distance for both compounds **10a** and **10b**, were significantly larger than that of compound **3** (2.98 Å) and within the range of most non-encapsulated DPP monomers. While the reason for this is unknown, it may suggest that **10a** and **10b** experience significantly less ring strain than **3**.

3.2.2.2 Synthesis of the DPP-BDT Polymers

Following the preparation of the encapsulated DPP monomers **10a**, **10b** and **10c**, was the synthesis of the encapsulated DPP-BDT polymers.

To begin, the non-encapsulated reference polymer **PDPP-BDT**, was synthesised *via* a Stille cross-coupling between **6** (as synthesised in *Sub-Section 3.1*) and the alkylated stannylated BDT monomer **11**† based on a similar procedure by Yang *et al* (Scheme 3.10).[159] The polymer underwent Soxhlet-extraction using acetone and hexane, to afford **PDPP-BDT** as a waxy blue solid (24%).

*Scheme 3.10- Synthesis of reference polymer **PDPP-BDT**.*

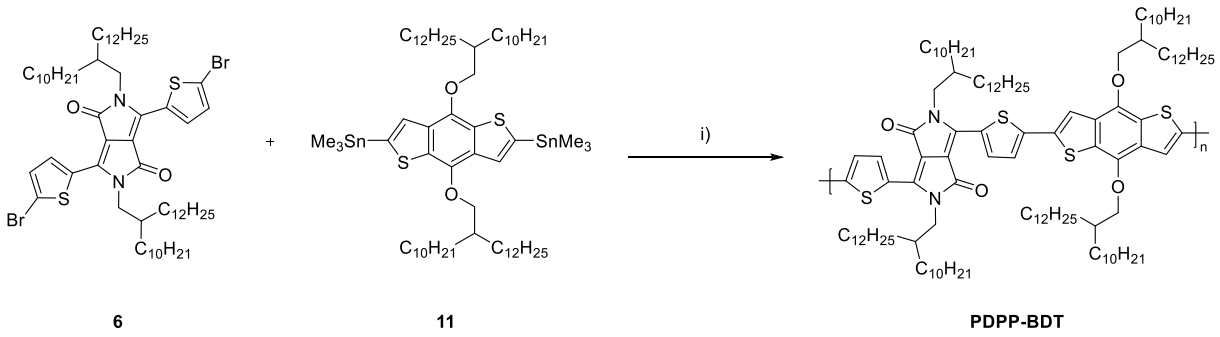

6 **11** **PDPP-BDT**

i) $Pd(PPh_3)_4$, Toluene, DMF, 110 °C, 18 h.

†Compound **11** was synthesised by Dr Anastasia Leventis, University of Cambridge.

Following the synthesis of the reference polymer **PDPP-BDT**, the encapsulated DPP-BDT polymers **PE12DPP-BDT**, **PE11DPP-BDT**, **PP11DPP-BDT** and **PDPP-E10BDT** were made *via* the same procedure (Scheme 3.11). Monomer **12**,† was synthesised *via* a previously published procedure by McDearmon *et al.*[152] The polymers were purified *via* Soxhlet-extraction as before and were isolated in chloroform as dark blue solids.

Scheme 3.11- Synthesis of encapsulated polymers ***PE12DPP-BDT***, ***PE11DPP-BDT***, ***PP11DPP-BDT*** *and* ***PDPP-E10BDT****.*

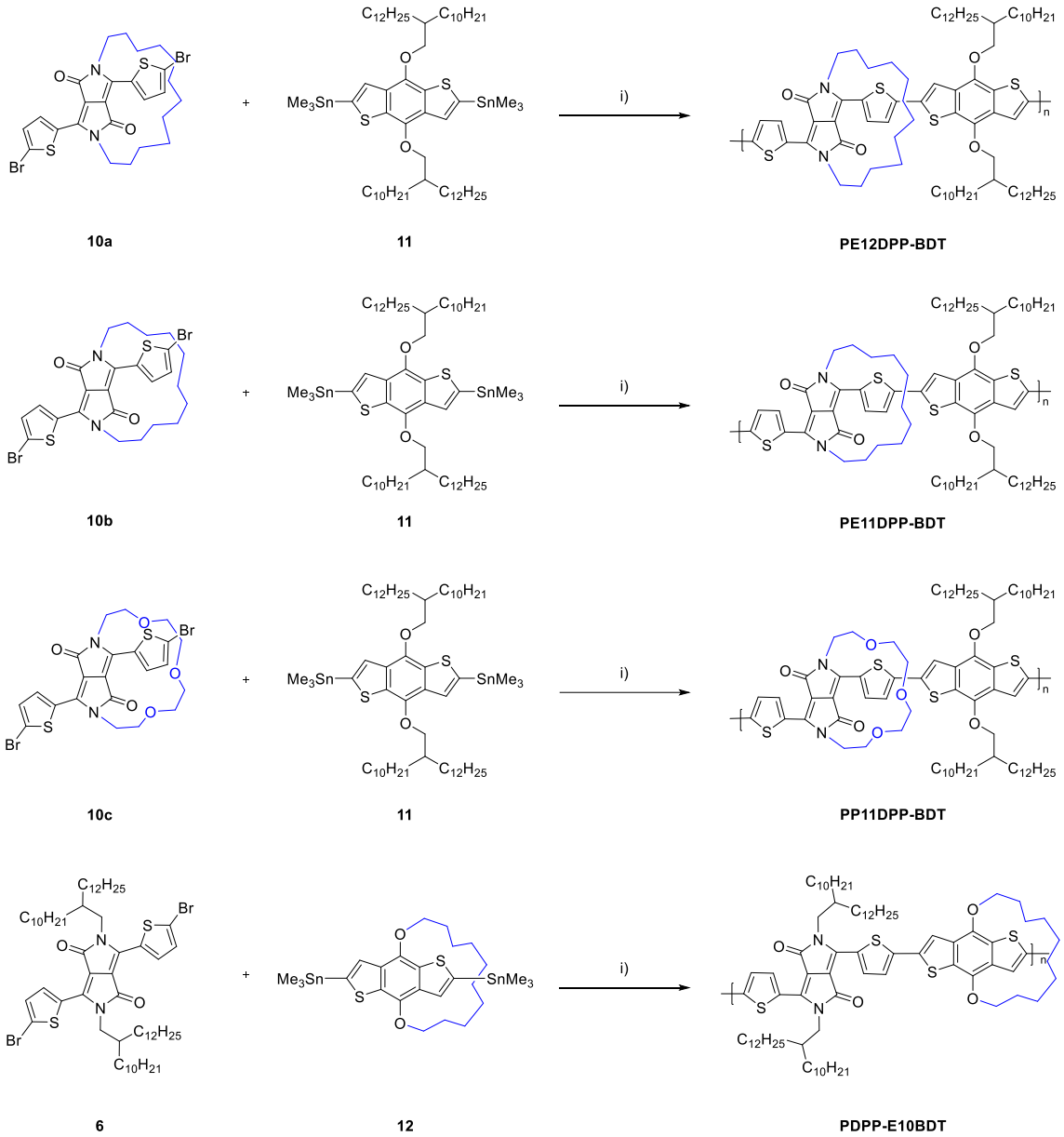

i) Pd(PPh₃)₄, Toluene, DMF, 110 °C, 18 h.

---

†Compounds **11** and **12**,[152] were synthesised by Dr Anastasia Leventis, University of Cambridge**.**

The yields, molecular weights and extraction solvents used to isolate the polymers in the encapsulated DPP-BDT series are summarised below in Table 3.8.

Table 3.8- A summary of the yields, molecular weights and extraction solvents used to isolate the encapsulated DPP-BDT polymers.

Polymer	Extraction Solvent	Yield (%)	Molecular Weight (KDa)	
			M_n[a]	M_w[a]
PDPP-BDT	Hexane	24	15.9	30.4
PE12DPP-BDT	$CHCl_3$	81	44.0	104.9
PE11DPP-BDT	$CHCl_3$	62	42.4	83.6
PP11DPP-BDT	$CHCl_3$	70	27.5	37.5
PDPP-E10BDT	$CHCl_3$	87	31.2	75.4

[a]*Determined by GPC (CB) against PS standard.*

In general, the encapsulated polymers **PE12DPP-BDT**, **PE11DPP-BDT** and **PDPP-E10BDT** were obtained in a good yield and were of relatively high molecular weights, all within a similar range. While **PP11DPP-BDT** was also obtained in a good yield of 70%, the molecular weight was significantly lower than that of the other encapsulated polymers. This may have either been due to poor solubility in the reaction solvent, as a result of the ethylene glycol chain or the fact that the reaction was carried out on a very small scale (i.e. 30 mg of **10c**), due to a shortage of monomer **10c**. Thus, this may have resulted in stoichiometric error when weighing out the reagents during synthesis. The reference polymer **PDPP-BDT** was obtained in a 24% yield, as a large quantity of material was isolated in the acetone fraction during Soxhlet extraction. This was due to the polymer's increased solubility as a result of its large density of solubilising alkyl chain.

A Stille cross-coupling between **10a** and **12** was also attempted, in order to synthesise **PEDPP-EBDT**, consisting of encapsulation along the entirety of the conjugated backbone (Scheme 3.12). However, upon work up no polymeric material could be isolated *via* Soxhlet-extraction, due to complete insolubility. Additionally, the molecular weight of the crude product could not be determined by GPC. This was likely due to a lack of solubilising alkyl chain density on either of the monomers. Thus, the polymer was discounted from the study.

*Scheme 3.12- Unsuccessful synthetic attempt towards **PEDPP-EBDT**.*

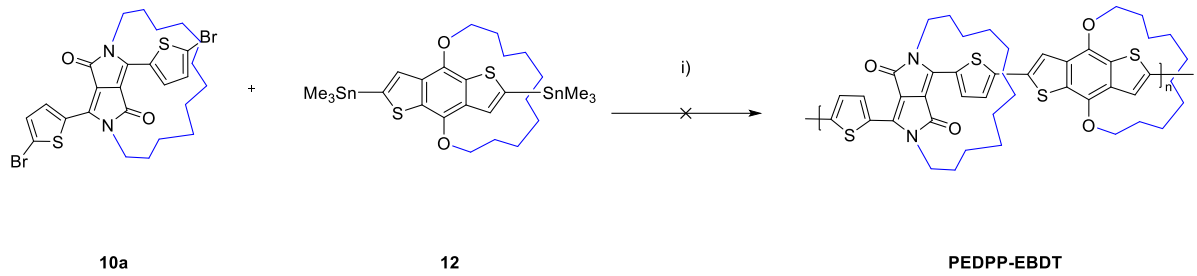

10a **12** **PEDPP-EBDT**

i) $Pd(PPh_3)_4$, Toluene, DMF, 110 °C, 18 h.

3.2.3 Characterisation

3.2.3.1 Optical Properties of the encapsulated DPP-BDT Polymers

The optical properties of the encapsulated DPP-BDT polymers are tabulated below in Table 3.9.

Table 3.9- Optical properties of the encapsulated DPP-BDT polymers.

Polymer	λ_{max}^{soln} (nm)[a]	λ_{max}^{film} (nm)[b]
PE12DPP-BDT	755	757
PE11DPP-BDT	755	757
PP11DPP-BDT	741	743
PDPP-E10BDT	759	759

[a]CB solution. [b]Spin coated from CB (5 mg/mL).

The solution (in CB) (a) and thin film (spin coated from CB 5 mg/mL) (b) UV-vis absorption spectra of the encapsulated DPP-BDT polymers are presented in Figure 3.24.

Figure 3.24- Normalised solution (in CB) (a) and thin film (spin coated from CB 5 mg/mL) (b) UV-vis absorption for the encapsulated DPP-BDT polymers.

a) Solution

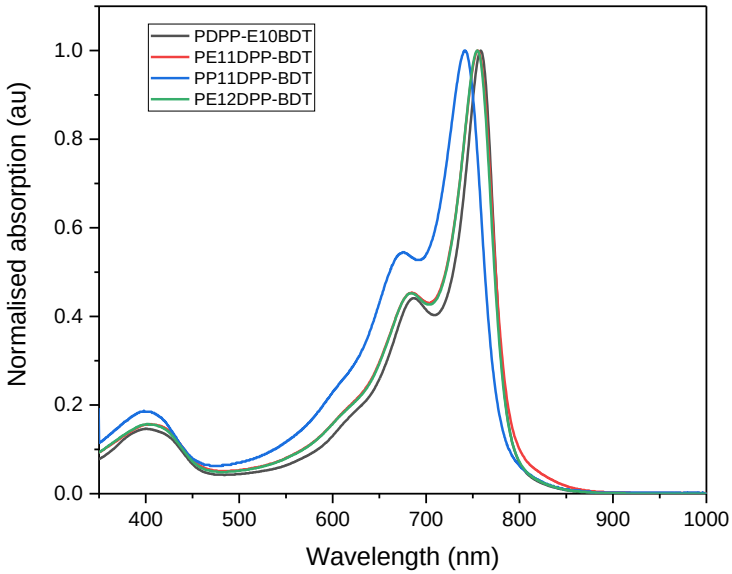

b) Thin Film

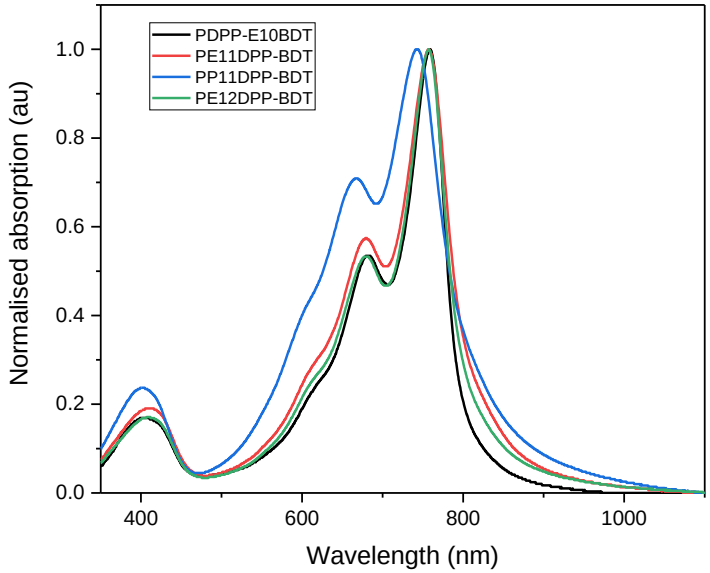

It was observed that the UV-vis spectra of **PDPP-E10BDT** was the most red-shifted of the encapsulated polymers. For example, **PDPP-E10BDT** had a λ_{max}^{soln} of 759 nm, while **PE12DPP-BDT** and **PE11DPP-BDT** had identical λ_{max}^{soln} of 755 nm. In contrast, **PP11DPP-BDT** showed a significantly blue-shifted spectra, with a λ_{max}^{soln} of 741 nm. As expected, the thin-film spectra appeared slightly broader, however

little to no red-shift was observed for any of the encapsulated polymers, going from solution to the solid state. This may suggest that aggregation had been supressed, as observed previously by Leventis *et al*[151] for their double-encapsulated phenyl-DPP polymers. When observing the onset in the solid state, distinct fine-tuning of the spectra could be seen. Polymer **PDPP-E10BDT** exhibited the steepest onset, followed by **PE12DPP-BDT**, **PE11DPP-BDT** and finally **PP11DPP-BDT**. This suggested that **PDPP-E10BDT** experienced the least amount of energetic disorder, out of all the polymers within the study.

While the crystal structures of the encapsulated DPP monomers, are not an accurate representation of how these materials may behave within the polymer, some insight may be gained from the trend observed. For example, among the *encapsulated DPP* polymers **PE12DPPT-BDT** exhibited the steepest onset. This can be related back to the highly ordered and planar structure of monomer **10a**. In contrast, **PP11DPP-BDT** exhibited both a broad onset and a blue-shifted absorption, suggesting it experienced the most amount of energetic disorder out of the encapsulated polymers. Once again, this can be related back to the crystal structure of **10c**, that was observed to display a high amount of torsional disorder. However, as the molecular weight of **PP11DPP-BDT** was significantly lower than that of the other encapsulated polymers, this may have also contributed to these results.

3.2.4 Organic Photovoltaic Devices (OPVs)

Preliminary bulk heterojunction OPV devices, were constructed for the reference polymer **PDPP-BDT** and the encapsulated DPP-BDT polymers, in order to examine how encapsulation and ring size can affect the PCE. The devices were fabricated in a conventional architecture, consisting of ITO/PEDOT/Polymer:$PC_{71}BM$/Ag and were tested under a 100 mW/cm^2 white light, under AM 1.5G conditions.[†]

The current-voltage characteristics of the reference polymer **PDPP-BDT** (a) and the encapsulated DPP-BDT polymers (b) are shown below in Figure 3.25. The data from the devices are summarised in Table 3.10.

*Figure 3.25- Current-voltage characteristics of Polymer:$PC_{71}BM$ (1:2) (a) reference **PDPP-BDT** and (b) encapsulated DPP-BDT polymer OPV devices.*

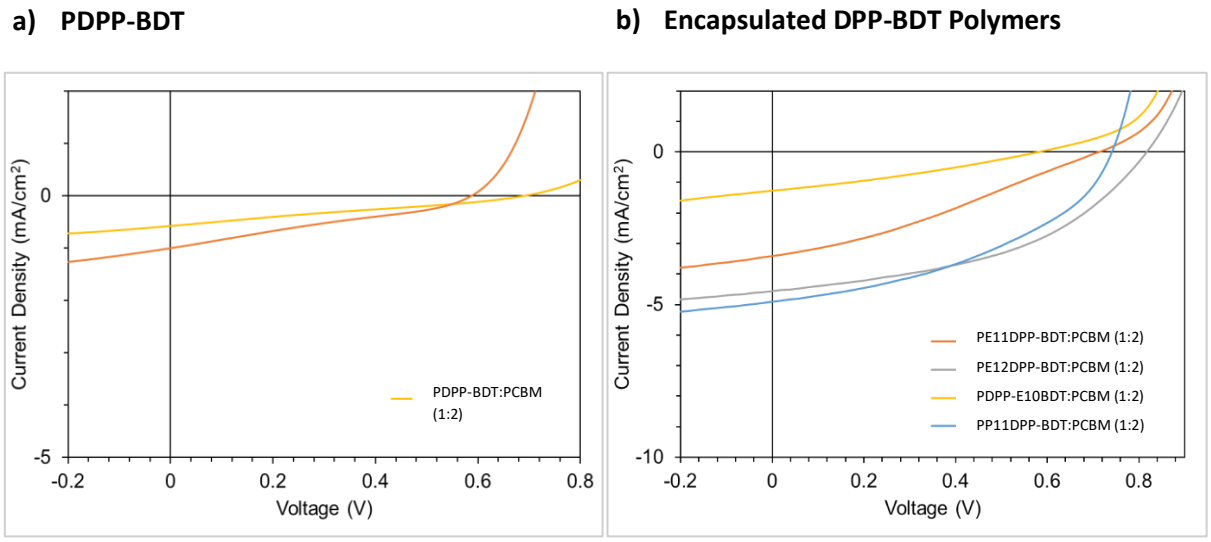

Table 3.10- Properties of the reference and encapsulated DPP-BDT polymer based OPV devices spun from $CHCl_3$ solution with a 1:2 ratio of Polymer:$PC_{71}BM$.

Polymer	J_{SC} (mA/cm^2)[a]	V_{oc} (V)	*FF* (%)	PCE (Max) (%)
PDPP-BDT	0.6	0.69	26	0.1
PE12DPP-BDT	4.6	0.82	45	1.7
PE11DPP-BDT	3.4	0.72	31	0.8
PP11DPP-BDT	4.9	0.74	42	1.5
PDPP-E10BDT	1.3	0.58	30	0.2

[a]*The J_{scs} were calculated by integrating the EQE spectrum by the AM 1.5G spectrum.*

[†]All OPV devices within this study were fabricated by Anirudh Sharma, Jules Bertrandie and Dr Derya Baran, KAUST Solar Centre.

While overall, the devices performed poorly, in general the encapsulated devices performed better than the reference **PDPP-BDT**, which obtained a very low PCE of just 0.1%. Among the encapsulated polymers, **PE12DPP-BDT** showed the best performance, achieving the highest V_{oc} (0.82 V), *FF* (45%) and PCE of 1.7%. This suggests that among those tested, the ideal ring size of the encapsulated DPP monomer was C12. Interestingly, despite the disordered crystal structure of monomer **10c** and its broad blue-shifted UV-vis spectra, **PP11DPP-BDT** was the second highest performing polymer, achieving the highest J_{sc} of 4.9 mA cm^{-2} and a PCE of 1.5%. In comparison, its alkyl-chained counterpart **PE11DPP-BDT** showed a poorer performance, obtaining a PCE of just 0.8%. The lowest performing

encapsulated polymer was **PDPP-E10BDT** (0.2%), which may suggest that for this particular system, encapsulation of the DPP unit is preferred. However, in general as all devices performed poorly, it is not possible to make any definite conclusions on the basis of these results.

In order to investigate whether non-fullerene acceptors (NFAs) could give a higher device performance, two additional OPV devices were constructed from **PDPP-BDT** and the highest performing encapsulated polymer **PE12DPP-BDT**, using **IEICO-4F** as the acceptor. As previously, the devices were fabricated in a conventional architecture, consisting of ITO/PEDOT/Polymer:IEICO-4F/Ag and were tested under a 100 mW/cm^2 white light, under AM 1.5G conditions.

The current-voltage characteristics of the reference polymer **PDPP-BDT** (a) and **PE12DPP-BDT** (b) are shown below in Figure 3.26. The data from the devices are summarised in Table 3.11.

Figure 3.26- Current-voltage characteristics of (a) ***PDPP-BDT*****:*****IEICO-4F*** *(1:1) and (b)* ***PE12DPP-BDT:IEICO-4F*** *(1:2) + 2% CN (1-chloronaphthalene) OPV devices.*

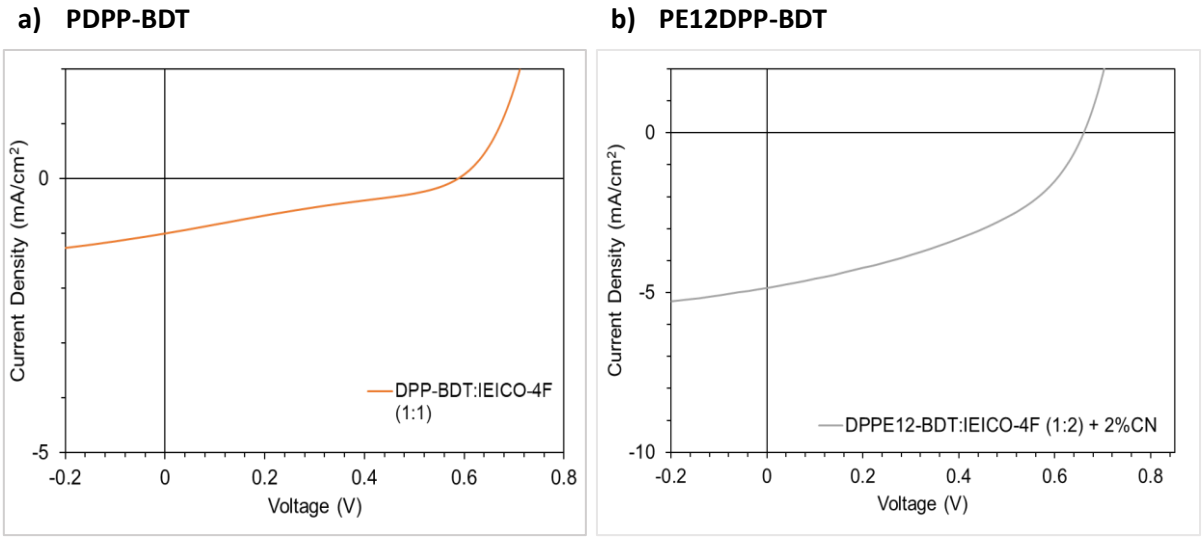

Table 3.11- Properties of the ***PDPP-BDT*****:*****IEICO-4F*** *(1:1) and* ***PE12DPP-BDT:IEICO-4F*** *(1:2) + 2% CN OPV devices spun from $CHCl_3$ solution.*

Polymer	J_{SC} (mA/cm^2)[a]	V_{oc} (V)	*FF* (%)	PCE (Max) (%)
PDPP-BDT	1.0	0.59	26	0.2
PE12DPP-BDT	4.9	0.66	42	1.4

[a]*The J_{scs} were calculated, by integrating the EQE spectrum by the AM 1.5G spectrum.*

While **PDPP-BDT** showed little change in efficiency (0.2%), **PE12DPP-BDT** showed a decrease in performance (1.4%). Additionally, compared to when using PCBM, a significant reduction in the V_{oc}

was observed (i.e. 820 mV compared to 660 mV), suggesting large voltage losses with the NFA. A reduction of over 100 mV was also observed in **PDPP-BDT**, suggesting that for this DPP-BDT polymer system, better performances can be obtained with fullerene acceptors.

3.2.5 Conclusions

In conclusion, following on from the study in *Sub-Section 3.1*, the novel encapsulated DPP monomers **EC12DPPT**, **EC11DPPT** and **EP11DPPT** were synthesised, in order to investigate the effect of different ring sizes. Through X-ray crystallographic analysis, it was observed that a C12 ring gave the most ordered structure, while the ethylene glycol ring introduced the largest amount of strain and disorder. These monomers were then used to synthesise a series of novel encapsulated DPP-BDT polymers *via* co-polymerisation with an alkylated BDT unit (**11**). In addition, **PDPP-E10BDT** was also synthesised, in which the BDT unit was encapsulated instead of the DPP core. These polymers were then fabricated into OPV devices using PCBM as an acceptor.

It was discovered, that while all the devices generally performed poorly, the encapsulated polymers achieved higher efficiencies than that of the reference **PDPP-BDT** (0.1%). Among them, **PE12DPP-BDT** achieved the highest efficiency of 1.7%, which may be attributed to the highly ordered structure of **EC12DPPT**. Surprisingly, despite the large torsional disorder observed in monomer **EP11DPPT** and a broad blue-shifted UV-vis spectra, **PP11DPP-BDT** was the second highest performing polymer (1.5%) followed by **PE11DPP-BDT** (0.8%). As observed with the doped TT- and Ph-series in *Sub-section 3.1*, encapsulation generally led to an increase in the V_{oc}, likely due to the same parameters discussed in the previous sub-chapter. The lowest performing encapsulated polymer was **PDPP-E10BDT** (0.2%), suggesting that for this polymer system, encapsulation is preferred on the DPP unit. However ultimately, as all devices performed poorly, it is not possible to make any firm conclusions based on the trends observed in these results.

Polymers **PDPP-BDT** and **PE12DPP-BDT** were also fabricated into additional OPV devices, using the NFA, **IEICO-4F**. However, lower efficiencies and large voltage losses in comparison to PCBM were observed, suggesting that for this DPP-BDT polymer system, fullerene acceptors are preferred.

Overall, these results demonstrate that the difference in ring size, can have a great effect on the performance of encapsulated conjugated polymers. We have also shown that it may be possible to control the distances in the π–π stacking direction *via* difference in chain length. While device performance was generally poor, the encapsulated polymers displayed higher V_{oc}s than the reference device. While the results obtained from the devices are not fully conclusive, this may demonstrate the potential of **EC12DPPT** to be incorporated into alternative polymer systems, as a potential strategy to raise the V_{oc}.

3.3 Encapsulated Polymers Based on Thienyl-DPP Containing Ethylene Glycol Side Chains

3.3.1 Introduction

Continuing from the previous study in *Chapter III, subsection 3.2*, it was observed that the encapsulated monomer **EC11DPPT** showed relatively less ring strain than its ethylene glycol counterpart, **EP11DPPT**. In addition, **PP11DPP-BDT** exhibited a largely blue-shifted absorption in comparison to **PE11DPP-BDT**, likely due to an increased torsional disorder as a result of the greater ring strain found in **EP11DPPT**. Thus, investigation of a larger ethylene glycol ring size was required.

In general, DPP polymers containing (oligio) ethylene glycol (OEG) chains have shown to possess extended absorption, smaller π-π stacking distances arising from increased flexibility of the OEG chain, higher dielectric constants and higher hole mobilities in comparison to their alkyl-chained counterparts, [114,115] as previously discussed in *Chapter I subsection 1.7.* In addition, certain DPP polymers containing OEG side chains have been shown to offer advantageous properties, that can be utilized in various applications such as bioelectronic devices and sensors.[116]

3.3.1.1 Conjugated Polymers for Application in Organic Electrochemical Transistors (OECTs)

An example of such application includes organic electrochemical transistors (OECT), in which ions injected from an electrolyte penetrate the organic film, resulting in modulation of its doping state and conductivity. Therefore, OECTs can transduce ionic signals into chemical ones, allowing application as biosensing elements. In general, OECTs operate in an aqueous environment and doping changes occur along the whole volume of the active material, rather than a thin interfacial region as seen in OFET-based sensors. This results in various advantages such as a lower impedance and a higher transconductance. Additionally, the characteristic tunability of the active organic material, enables further optimisation of ion and electron transport and facile biofunctionalization.[121,160] As a result, the uses of OECTs have been widely explored, including clinical neuroscience applications such as electrocardiography,[161] electroencephalography[162] and neural stimulation.[163]

Currently, the most commonly used active material in OECTs, is the conducting polymer poly(3,4-ethylenedioxythiophene) doped with poly(styrene sulfonate) (PEDOT:PSS), a p-type material.[160] As such, OECTs based on PEDOT:PSS operate in depletion mode. In contrast, OECTs can also operate in accumulation mode, which often results in lower power consumption devices with higher ON/OFF ratios.[121] For example, Inal *et al*[164] reported a polythiophene based polyelectrolyte operating as an accumulation mode OECT device, achieving transconductances of up to 2.0 mS.[164]

However, while several p-type (hole transport) OECTs have been reported, in contrast n-type (electron transporting) and ambipolar OECT devices have not yet been widely investigated. While such devices would allow many advantages such as development of complimentary circuits and more versatile bioelectronic devices, large challenges remain in developing appropriate semiconducting materials requiring both stability in aqueous media and the ability to be reversely reduced and oxidized within the electrochemical window, given by the electrolyte. In order to achieve this, the design of the material must allow for a high electron affinity (EA), a low ionization potential, the capacity for facile ion penetration and high electron and hole mobilities.[121] While a few examples of air-stable n-type OECTs have been reported, they often face degradation when exposed to water.

In 2016, McCulloch *et al*[121] reported the first n-type and ambipolar accumulation mode OECT, based on an NDI-bithiophene co-polymer (**p(gNDI-gT2**) consisting of long linear ethylene glycol side chains (Figure 3.27). The polymer supported both hole and electron transport along the conjugated backbone when doped through an aqueous electrolyte and in the presence of oxygen. In addition, stability measurements in water showed there was no degradation when tested for 2 h under continuous cycling. When comparing **p(gNDI-gT2)** to **p(gNDI-T2)** (which consisted of lower glycol side chain density)**,** it was observed that the former showed an improved performance. This was thought to be likely due to an enhanced ion injection, as a result of the increased glycol side chain density. In general, glycol side chains show a strong tendency to interact with hydrated ions and water, thus facilitating electrochemical switching between the reduced, neutral and oxidized states in aqueous solution.[121] The results from this study thereby demonstrate the potential of semiconducting materials consisting of ethylene glycol side chains and should be considered when designing next generation polymers for application in high performing OECTs.

*Figure 3.27- Structure of **p(gNDI-gT2)** and **p(gNDI-T2)**.*[121]

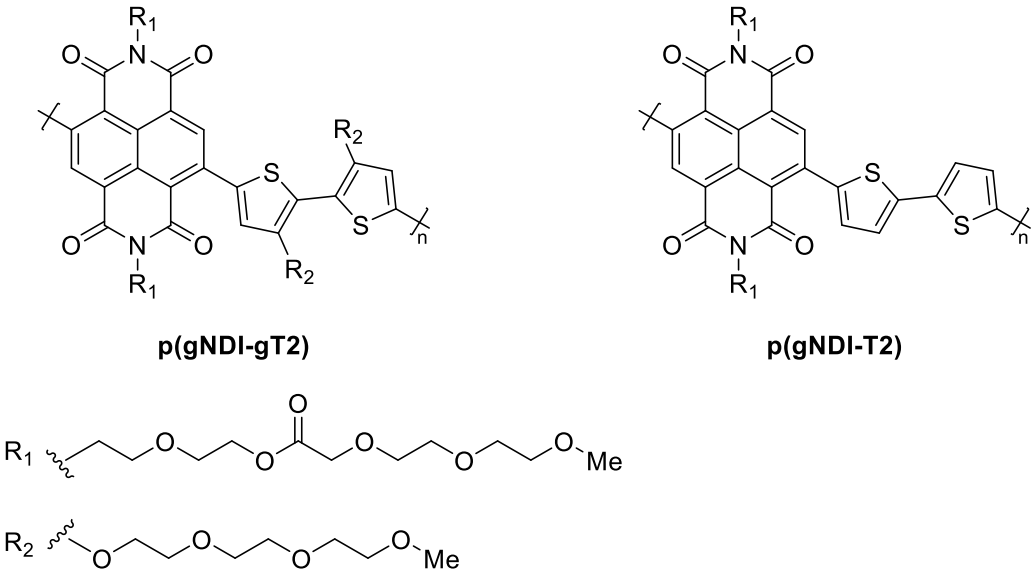

3.3.1.2 Sub-Chapter Objectives

As demonstrated by McCulloch *et al*,[121] incorporation of ethylene glycol side-chains onto conjugated materials, allows for new functionalities and effective application in OECTs for bioelectronic devices. However, conjugated polymers consisting of only ethylene glycol side chains have yet to be investigated in DPP-based systems. Similarly to NDI, DPP-based polymers have demonstrated excellent charge mobilities in OFETs as well as ambipolar properties,[100] making them a promising candidate for application in OECTs.

Building upon McCulloch *et al's*[121] research, here we intend to investigate both encapsulated and linear ethylene glycol chained thienyl DPP-based polymers, for potential application in OECTs and bioelectronics. Therefore, we also aim to investigate how interlayer separation can affect the performance of an OECT device. It is possible that increased distances in the π–π stacking direction of the polymer chains *via* backbone encapsulation, may allow better ion penetration and thus, enhance device performance. In addition, polar glycol chains in both the alkyl stacking and π–π stacking direction may further enhance reversible electrochemical switching. As the encapsulated DPP monomer **EP11DPPT** from the previous *Sub-Chapter 3.2* exhibited significant ring strain and torsional disorder, here we investigated a larger ring size *via* the synthesis of **EP14DPPT** (Figure 3.28).

*Figure 3.28- Structure of **EP14DPPT**.*

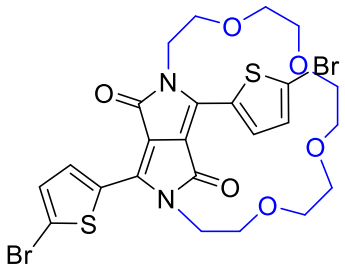

EP14DPPT

In this sub-chapter we aimed to synthesise two novel DPP-bithiophene co-polymers, the encapsulated **PE14DPP-T2** and the linear chained **PDPP-T2**, in order to investigate the effect of encapsulation on their fundamental properties and performance (Figure 3.29). The novel bithiophene co-monomer consisting of linear ethylene glycol side chains, was synthesised based on a previously reported procedure in literature.[165]

*Figure 3.29- Structures of the encapsulated **PE14DPP-T2** and the linear chained **PDPP-T2**.*

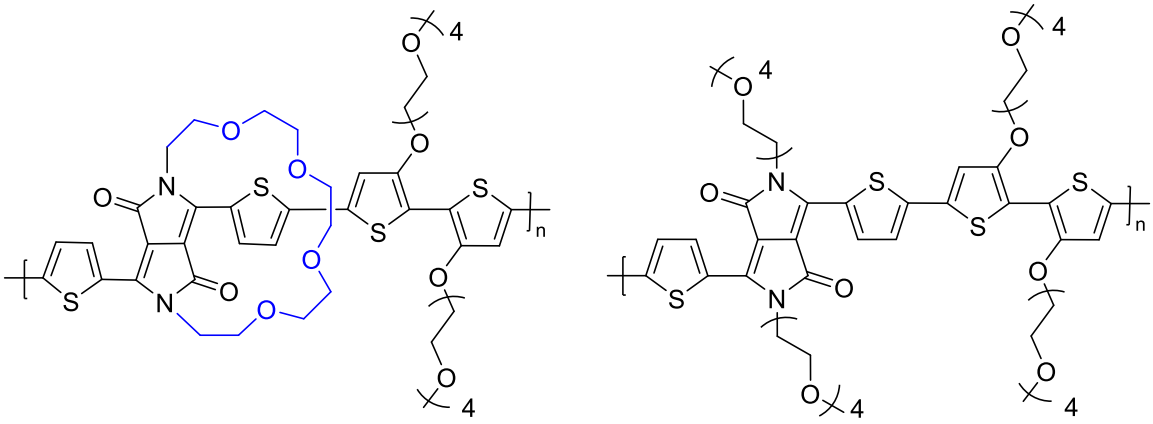

PE14DPP-T2 **PDPP-T2**

3.3.2 Synthesis

3.3.2.1 Synthesis of EP14DPPT

*Scheme 3.13- Synthetic route to **13**.*

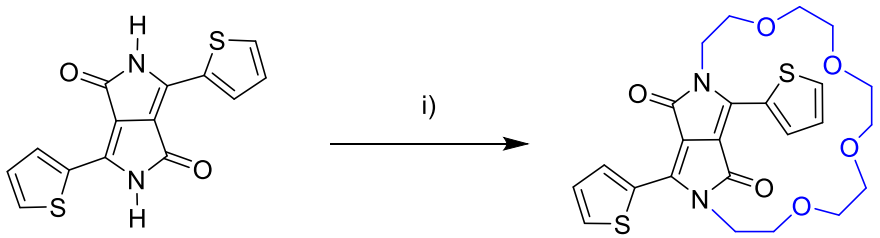

1 **13**

18 %

i) Pentaethylene glycol di(p-toluenesulfonate), K_2CO_3, 18-crown-6, DMF, 120 °C, 18 h.

The preparation of **EP14DPPT** began with the alkylation of **1** using pentaethylene glycol di(p-toluenesulfonate). A longer ethylene glycol chain was chosen, in order to reduce the ring strain observed in **EP11DPPT**. The reaction was carried out under the same conditions as when synthesising **8c** and upon work up, the crude material was purified *via* column chromatography, followed by recrystallisation in isopropanol to afford **13** as bronze coloured crystals (18%). As before with **8c**, the low yield obtained was partly due to the formation of the *O,N*-encapsulated DPP side product, a structural isomer of the *N,N*-encapsulated product **13**. While the product could be isolated *via* column

chromatography, only a small amount was obtained due to the similar polarities of the structural isomers on silica.

As with the synthesis of **10c**, **13** then underwent subsequent di-bromination with a quantitative amount of NBS at 0 °C - RT overnight, yielding **14** as a dark purple solid (26%) (Scheme 3.14).

*Scheme 3.14- Synthetic route to **14**.*

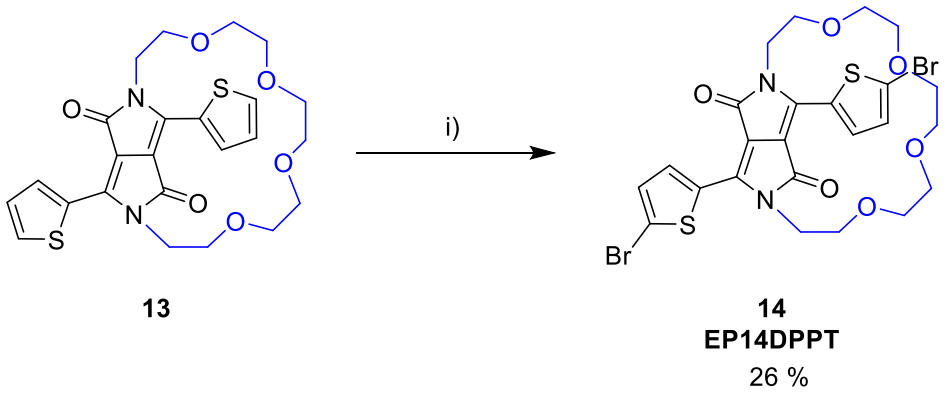

NBS, $CHCl_3$, 0 °C- RT, Overnight.

The structure of **14** was determined by X-ray crystallographic analysis† (single crystals grown from $CHCl_3$: MeOH, Figure 3.30), confirming the successful encapsulation of the DPP core. The X-ray structure of **13** was also obtained and can be found in the appendix.

*Figure 3.30- Crystal structure of **14**. Crystals grown from $CHCl_3$: MeOH.*

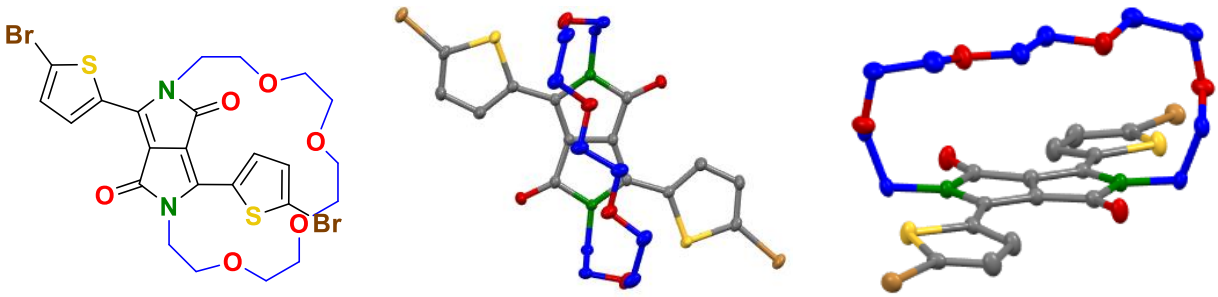

---

†X-ray structure determined by Dr Andrew Bond, University of Cambridge.

It was observed that compared to compound **10c** (Figure 3.22), **14** showed significantly less ring strain. Additionally, compound **14** showed far less torsional disorder making it largely preferred for polymerisation. It was observed however, that the encapsulating chain of **14** took on a slightly 'floppy' nature. As there are no intermediate ethylene glycol chain lengths between compounds **10c** and **14**, we proceeded with **14** as the chosen encapsulated monomer due to its increased planarity.

3.3.2.2 Synthesis of the Linear Chained DPP Monomer

Following the synthesis of the encapsulated DPP monomer **14**, was the preparation of the linear chained DPP monomer **15**. This began with the alkylation of **1,** using triethylene glycol 2-bromoethyl methyl ether, to obtain **16** as a waxy purple solid (18%). This was followed by quantitative di-bromination of **16** using NBS and upon workup, the crude product was purified *via* column chromatography and subsequent recrystallisation in isopropanol, to afford **15** as a waxy dark purple solid (48%) (Scheme 3.15).

*Scheme 3.15- Synthetic route to **15**.*

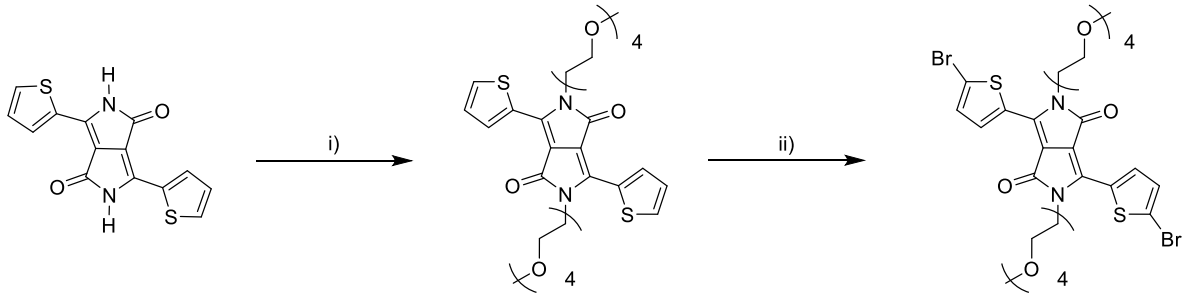

i) Triethylene glycol 2-bromoethyl methyl ether, K_2CO_3, 18-crown-6, DMF, 120 °C, 18 h; ii) NBS, $CHCl_3$, 0 °C - RT, Overnight.

3.3.2.3 Synthesis of the Bithiophene Monomer

Following the synthesis of the DPP monomers, was the preparation of the novel bithiophene co-monomer (Scheme 3.16) based on a similar procedure by Song *et al*.[165] A longer ethylene glycol chain was chosen to ensure sufficient solubility of the DPP polymers. This began with the coupling of tetraethylene glycol monomethyl ether with 3-bromothiophene (**17**) in the presence of potassium *t*-butoxide, Copper (I) iodide and pyridine. The reaction was heated at 100 °C for 24 h and upon work up, the crude product was purified *via* column chromatography to afford **18** as a dark yellow oil (28%). This was then followed by oxidative coupling of **18**, which first underwent lithiation at the 2-position using n-BuLi, followed by the addition of iron (III) acetylacetonate ($Fe(acac)_3$). The reaction was then heated under reflux for 2 h to give the dimer **19**. The crude product was purified *via* column chromatography to afford **19** as a pale-yellow oil (20%).

*Scheme 3.16- Synthetic route to **19**.*

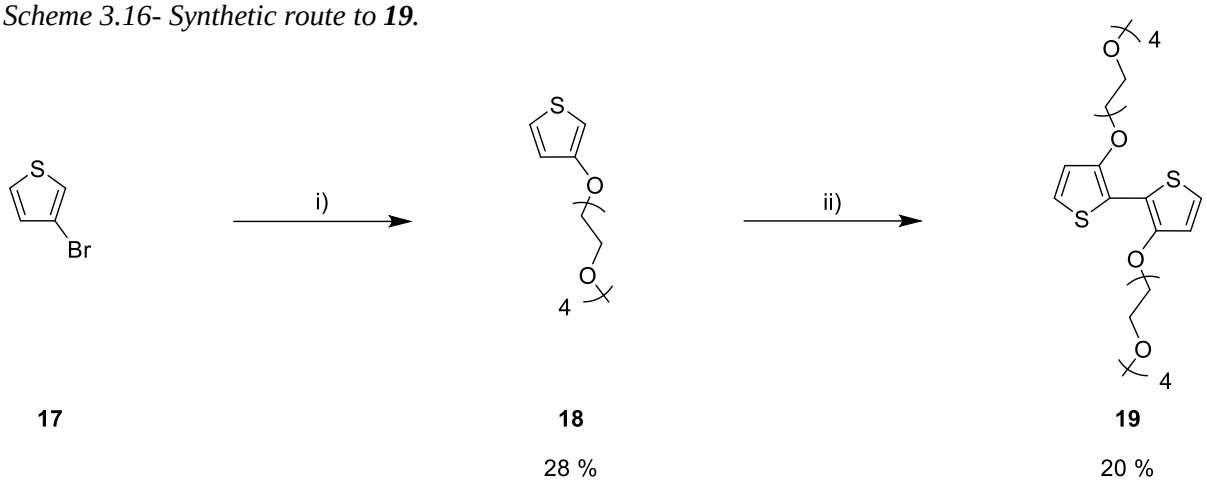

17 **18** **19**

28 % 20 %

i) Tetraethylene glycol monomethyl ether, ^{t}BuOK, CuI, Pyridine, 100 °C, 24 h; ii) n-BuLi, Fe(acac)$_3$, THF, Reflux, 2 h.

Finally, the last step of the synthesis was the stannylation of compound **19**, to give the final monomer **20** (Scheme 3.17). Compound **19** was dissolved in THF and cooled to -78 °C, which was followed by the dropwise addition of n-BuLi. The reaction was then allowed to stir for 2 h before warming to RT. After 15 minutes, the reaction was then cooled back down to -78 °C, before the addition of trimethyltin chloride. The reaction was then allowed to warm to RT overnight.

*Scheme 3.17- Synthetic route to **20**.*

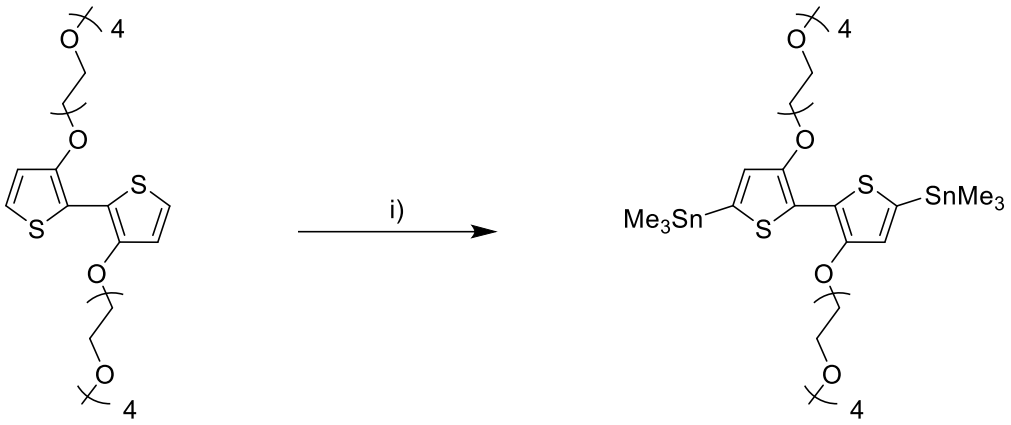

19 **20**

64 %

i) n-BuLi, SnMe$_3$Cl, THF, -78 °C, 2 h.

Upon work up, crude ^{1}H NMR showed the reaction had not gone to completion. Several recrystallisations in various solvents were attempted, including methanol, ethanol and isopropanol, however all were unsuccessful. Due to the toxicity and sensitivity of stannylated materials, it was not possible to purify the compound *via* column chromatography. The reaction was then repeated, this time

allowing the reaction to stir for longer (1 h) at RT before the addition of trimethyltin chloride. Upon work up, crude ^{1}H NMR showed that the reaction had mostly gone to completion, however small baseline impurities remained. Thus, **20** was obtained as a crude brown oil (64%). As further purification was not possible (either *via* recrystallisation or column chromatography), monomer **20** was used in the subsequent polymerisation as crude. Due to a shortage of compound **19** and time constraints, the reaction could not be repeated.

3.3.2.4 Synthesis of PDPP-T2

Following the preparation of the bithiophene monomer **20**, was the synthesis of the linear chained polymer **PDPP-T2**.

A microwave assisted Stille cross-coupling between monomers **15** and **20** was attempted, based on a similar procedure by McCulloch *et al*[121] (Scheme 3.18). As monomer **20** was slightly crude, in order to compensate, the stoichiometry of the reaction was altered to 1:1.1 equiv. (**15**:**20**) rather than the 1:1 ratio used in the literature procedure. The polymer underwent Soxhlet-extraction using hexane, MeOH, acetone and THF, to afford **PDPP-T2** as a waxy blue solid**.**

*Scheme 3.18- Unsuccessful attempt at synthesising **PDPP-T2**.*

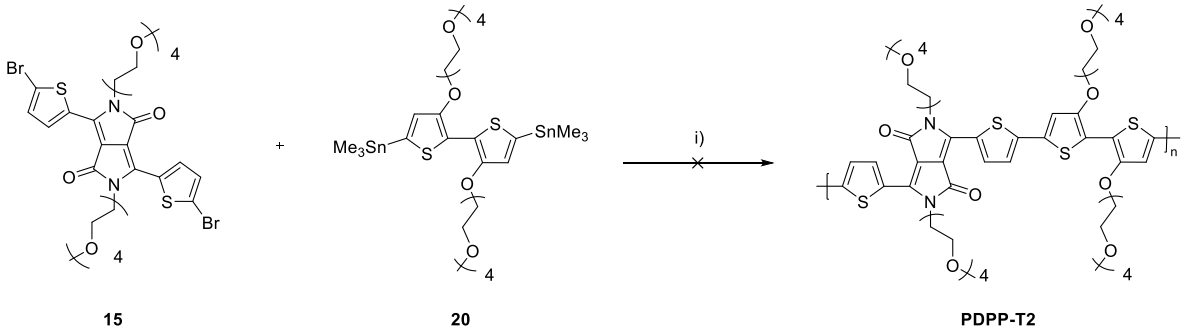

15 **20** **PDPP-T2**

i)Pd(dba)$_3$, P(o-tol)$_3$, CB, µW; 100 °C 5 min, 120 °C 5 min, 140 °C 5 min, 160 °C 5 min, 180 °C 5 min, 200 °C 25 min.

As seen in literature by McCulloch *et al,*[121] the highly polar nature of the polymer meant it was not possible to determine its molecular weight by GPC in chlorobenzene. Thus, the molecular weight of **PDPP-T2** was determined by GPC in THF, against polystyrene standards.[†] It was observed that **PDPP-T2** was of very low molecular weight, with an M_n of 5128 and M_w of 7701, therefore the polymerisation had been unsuccessful. This was likely due to the impure nature of monomer **20**, thereby creating large errors in the reaction's stoichiometry. As mentioned previously, due to time constraints and a shortage of monomer, it was not possible to repeat or optimise the polymerisation attempt. As a result, it was also not possible to synthesise **PE14DPP-T2**.

[†]Molecular weight determined by Dr Patrick de Jongh, University of Oxford.

3.3.3 Conclusions

In conclusion, following on from the study in *Sub-Section 3.2*, the novel encapsulated DPP monomer **EP14DPPT** was synthesised, in order to compare different ethylene glycol ring sizes. Through X-ray crystallographic analysis, it was observed that **EP14DPPT** showed far less ring strain than **EP11DPPT**. Additionally, the increased planarity observed in **EP14DPPT** made it the preferred choice for polymerisation.

DPP monomer **15** and bithiophene monomer **20** were also synthesised, each consisting of linear ethylene glycol-based side chains. However, it was observed that monomer **20** contained impurities that could not be removed *via* recrystallisation or column chromatography. Due to time constraints and shortage of compound **19**, it was not possible to remake monomer **20**. Thus, **20** was used as crude in an attempted Stille cross-coupling with **15** to synthesise the linear chained DPP polymer **PDPP-T2**. However, the polymerisation attempt was unsuccessful as a very low molecular weight was determined for **PDPP-T2**. This was likely due to the impure nature of monomer **20**, thereby creating large errors in the reaction's stoichiometry. Due to a lack of monomer **20**, it was not possible to synthesise **PP14DPP-T2**.

Future work would include re-synthesising monomer **20** in a high purity, ensuring the lithiation and stannylation of **19** goes to completion, *via* frequent D_2O quenching and monitoring by ^1H NMR. Alternatively, a shorter ethylene glycol chain should be implemented onto the bithiophene as seen in the literature, in which the final compound is a crystalline solid. Thus, purification is then possible *via* recrystallisation, allowing the stannylated monomer to be obtained in a high purity. This would likely improve the key polymerisation step, allowing **PDPP-T2** and **PP14DPP-T2** to be obtained at reasonable molecular weights. Based on the promising results by McCulloch *et al*,[121] it is possible that these novel ethylene glycol side chained DPP polymers, could have great potential in OECTs and bioelectronic devices.

IV

DPP Polymers that Show Tolerance to Disorder

4.1 Introduction

When the planarity of a polymer increases, aggregation can arise as a result of increased π–π stacking of the chromophores. Thus, as we saw in *Chapter II*, these strong interactions can lead to significant changes in the optical properties of the polymer. This was also seen in *Chapter III*, in which the higher the planarity of the encapsulated DPP monomer (as observed by X-ray crystallographic analysis), the sharper the onset of the absorption UV-vis spectra for the corresponding polymer, suggesting that these materials experience a lower amount of energetic disorder. Energetic disorder can be found in most conjugated polymers in varying degrees, which can cause localization of the orbitals that in turn, leads to charge traps. This can have a significantly detrimental effect on charge transport and device performance. Thus, in order to develop higher performing optoelectronic devices, it is important that we begin to understand how energetic disorder arises within conjugated polymers, how it can be limited or possibly, even tolerated.

4.1.1 Charge Transport in Conjugated Polymers

Until 2010, it was long believed that the impressive charge-carrier mobilities of high performing polymers, were the result of highly ordered compounds with domains of optimal orientation. As a result, conjugated polymers were designed with long range order in mind, such as the regio-regular **P3HT**[14,11] and in particular, PBTTT (poly(2,5-bis(thiophene-2-yl)thieno[3,2-*b*]thiophene)) which was often considered the benchmark for charge-carrier mobility ($\mu \approx 1$ cm^2 V^{-1} s^{-1}).[136] The high charge-carrier mobilities found in ordered crystalline and semi-crystalline polymers, were believed to arise from a 2D in plane packing motif composed of lamellae of π-stacked conjugated backbones edge on, spaced by lamellae of alkyl side chains stacking along the substrate (Figure 4.1).[56] At the time, it was widely believed that the active charge transport pathway along the π-π stacking direction, was highly critical in achieving high charge-carrier mobility.[136]

However more recently, several donor-acceptor co-polymers with high field-effect mobilities of >1 cm^2 V^{-1} s^{-1} have been reported to perform significantly better than **P3HT**,[59,60] and interestingly

their microstructures revealed significantly less long-range order than observed in semi-crystalline polymers.

*Figure 4.1- A schematic illustration of the charge transport in a semi-crystalline polymer film such as **P3HT**. Figure reproduced from A. Salleo.*[56]

A schematic illustration of the charge transport in a semi-crystalline polymer film such as P3HT removed for copyright reasons. Copyright holder is Elsevier Ltd.

To gain some insight on the charge-transport mechanism within high charge-carrier mobility polymers, Zhang *et al*[136] reported a study on the orientational order of an indacenodithiophene-benzothiadiazole (C_{16}IDT-BT) co-polymer, in order to decipher its structure-property relationship. While the X-ray diffraction pattern of C_{16}IDT-BT was observed to show weak and broad peaks that stemmed from defective π- and lamellar- stacking, it exhibited a high charge-carrier mobility of $\mu \approx 3.6\ cm^2\ V^{-1}\ s^{-1}$. A quantitative comparison with the 2D diffraction of the ordered regions, revealed that between the crystalline and non-crystalline regions, there was a consistency of π-conjugated plane orientation. Thus, this suggested that there was local molecular order (co-planarity). It was concluded that a rigid and planar backbone was essential in achieving high charge-carrier mobility and in fact, only occasional π-stacking is required to relay charge carriers between the polymer chains.[136]

Another report,[61] also investigating the origin of high charge-carrier mobility in conjugated polymers with low crystallinity, conducted a study in which the energetic disorder in several different polymer systems were investigated. Among the polymers described were **IDTBT** and **PBTTT** (which was used as a semi-crystalline reference system) (Figure 4.2).

*Figure 4.2- Structures of **IDTBT** and **PBTTT**.*[61]

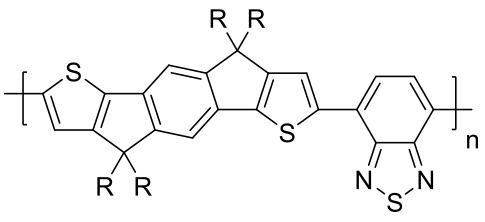

IDTBT

R = $-C_{16}H_{33}$

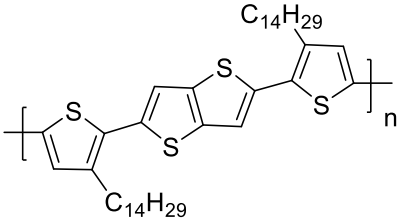

PBTTT

It was observed that not only did **IDTBT** have one of the highest mobilities among the polymers studied, but also exhibited a lower degree of energetic disorder than **PBTTT**. This result arose from the fact that while **IDTBT** possesses a largely torsion-free backbone, **PBTTT** though linear, experiences a wider range of torsion angles between its thiophene and thienothiophene units (torsional/energetic disorder). Thus, it was concluded that **IDTBT'**s high mobility was the result of its low degree of energetic disorder, due to a resilience of the backbone conformation to side-chain disorder. This disorder is generally unavoidable because of solution deposition of thin films by rapid drying techniques. Based on this discovery, suggested guidelines in designing disorder free and high mobility polymers were put forward. This included minimising the conjugated units present in the polymer's backbone that are susceptible to torsion, which hinders close π-π contacts and consequently, lowers the charge-carrier mobility.[61]

Thus, these results demonstrate, that in order to achieve high charge-carrier mobility in conjugated polymers, efforts towards designing a planar torsion-free backbone, is critical. As a result, much research has gone into synthesising polymers that show co-planarity between monomer units along the polymer backbone, *via* various structural strategies such as fused ring systems and conformational locks, as discussed previously in *Chapter I*.

4.1.2 Designing Monomers with Tolerance to Disorder

In the solid-state structure of most conjugated polymers, including high charge-carrier mobility polymers, there are usually always regions of disordered, non-crystalline phases. As a result, regions of the polymer are non-planar, and what is observed, is a distribution of torsional angles (twisting) between the monomer units along the conjugated backbone of the polymer. Consequently, this causes localization of the orbitals, that in turn leads to charge traps and therefore, decreased charge-carrier mobility. However, since some polymers *do* exhibit high charge-carrier mobility, several studies have suggested they exhibit resilience to disorder due to various structural and electronic reasons such as conformational locks, as previously discussed.[43,61]

When it comes to designing next-generation high performing polymers, various guidelines have been previously put forward. Some designs have proven more successful for example, inclusion of monomers that appear more often in high charge-carrier mobility polymers such as thiophene units, due to their highly planar structure. While designing a polymer of high co-planarity is desirable, energetic disorder is often hard to avoid. In addition, there can only be a limit to the rigidity of the polymer backbone, before poor solubility begins to take effect. Thus, it would be ideal to design a polymer, such that the electronic coupling between the conjugated monomers, is not affected by the torsional angle between them. In other words, designing a conjugated polymer that is tolerant to energetic disorder.

It has been reported by Troisi *et al*,[43] that this may be the case for certain motifs. Following electronic structure calculations (Figure 4.3),[43] it was observed that as expected for a typical conjugated structure (in black), such as a fluorene dimer (in green), when the dihedral angle between the two monomers is at zero (co-planarity), the electronic coupling between the two monomers is at a maximum. However, as the angle is increased, the electronic coupling decreases, resulting in a reduction of charge-carrier mobility within the system. This situation would apply to energetic disorder present between monomer units within a conjugated polymer. However, it has been proposed that for a DPP dimer (in red), the electronic coupling between the HOMOs localized on each monomer, is insensitive to a torsional angle of up to 60°.[43]

Figure 4.3- Dependence of intermonomer coupling on the torsional angle connecting two monomer units, for the fluorene dimer in green (cos(1)) and the DPP dimer in red (cos(2)). The expected cosine dependence is shown in black (cos(θ)). Adapted with permission from A. Troisi and A. Shaw, J. Phys. Chem. Lett., 2016, 7, 4689–4694. Copyright 2021 American Chemical Society.[43]

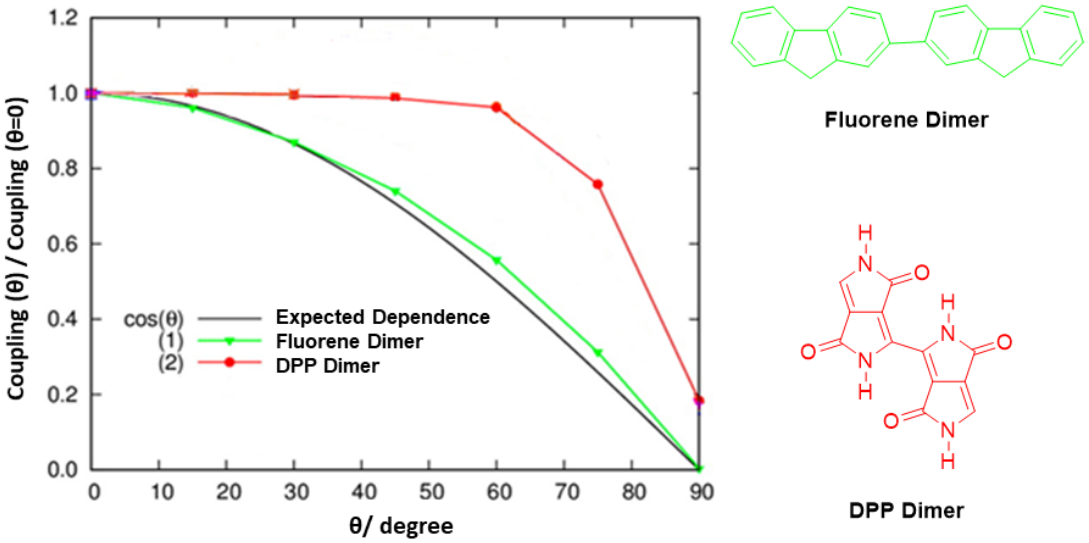

While hydrogen bonding within the DPP dimer has influence over the structure, it was discovered that this conformational lock was not responsible for the unusual inter-monomer coupling but instead, related to first-order orbital overlap interaction. The overlap between the DPP units, can be deconstructed into pairwise atomic components **ABC** and $\mathbf{A^1B^1C^1}$, as seen in Figure 4.4.[43]

Figure 4.4- Pairwise atomic components present in the DPP dimer.[43]

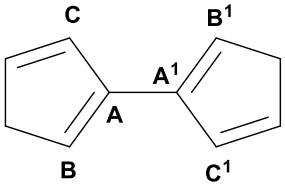

While the **AA**^{1} overlap follows a cos(θ) dependence, the other contributions deviate from this trend. In particular, the **BC**^{1} **+ C**^{1}**B** contribution becomes less negative as θ increases and thus, compensates for the decrease of the **AA**^{1} overlap, in the θ = 0−60° interval. These calculations were then repeated for a DPP-thienothiophene oligomer (Figure 4.5).[43]

Figure 4.5- DPP-thienothiophene oligomer highlighting the two torsional angles (θ_1 and θ_2) present in the structure. Adapted with permission from A. Troisi and A. Shaw, J. Phys. Chem. Lett., 2016, 7, 4689–4694. Copyright 2021 American Chemical Society.[43]

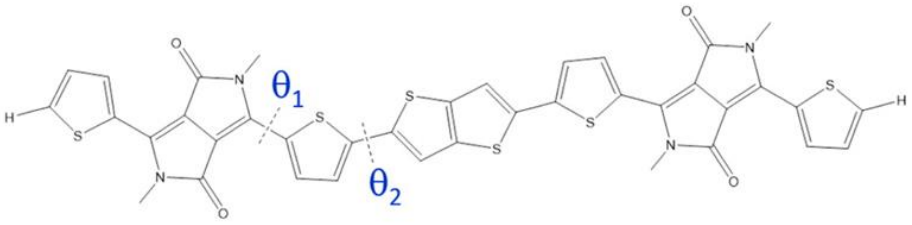

It was observed that when considering the torsion around angle θ_1, in which the thiophene unit is adjacent to the DPP unit, the intrachain coupling does not follow the typical cos(θ) dependence, similarly to the DPP dimer. However, for angle θ_2, in which the thiophene unit is adjacent to the thienothiophene unit, the expected decrease in electronic coupling was observed.

Thus, these results suggest, that by synthesising DPP polymers that incorporate the DPP dimer motif or contain a higher DPP to thiophene unit ratio, should show more tolerance to disorder than those currently reported in the literature.[43]

4.1.3 Chapter Objectives

Inspired by Troisi's results,[43] here we intend to synthesise a new thienyl-DPP based polymer with a higher DPP to thiophene unit ratio, than previously reported in literature, **P(a)** (Figure 4.6). It is theorised, that due to secondary overlap contribution between the thiophene/DPP units that do not follow a cos(θ) dependence, this novel polymer will show a higher tolerance to energetic/torsional disorder than previously reported in DPP polymers.

*Figure 4.6- Structure of target polymer **P(a)**.*

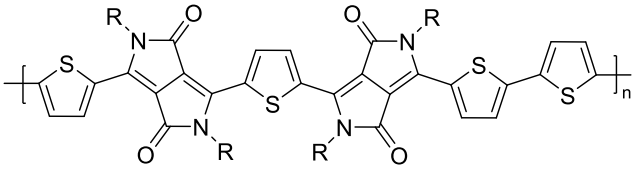

P(a)

R= Alkyl Chain

The first proposed synthetic route towards **P(a)** involves the condensation between 2 equiv. of thienyl pyrrolinone ester and 1 equiv. of 2,5-dicyanothiophene under basic conditions, to give the DPP dimer (Scheme 4.1).

Scheme 4.1- Proposed synthesis of the DPP dimer via condensation between thienyl pyrrolinone ester and 2,5-dicyanothiophene.

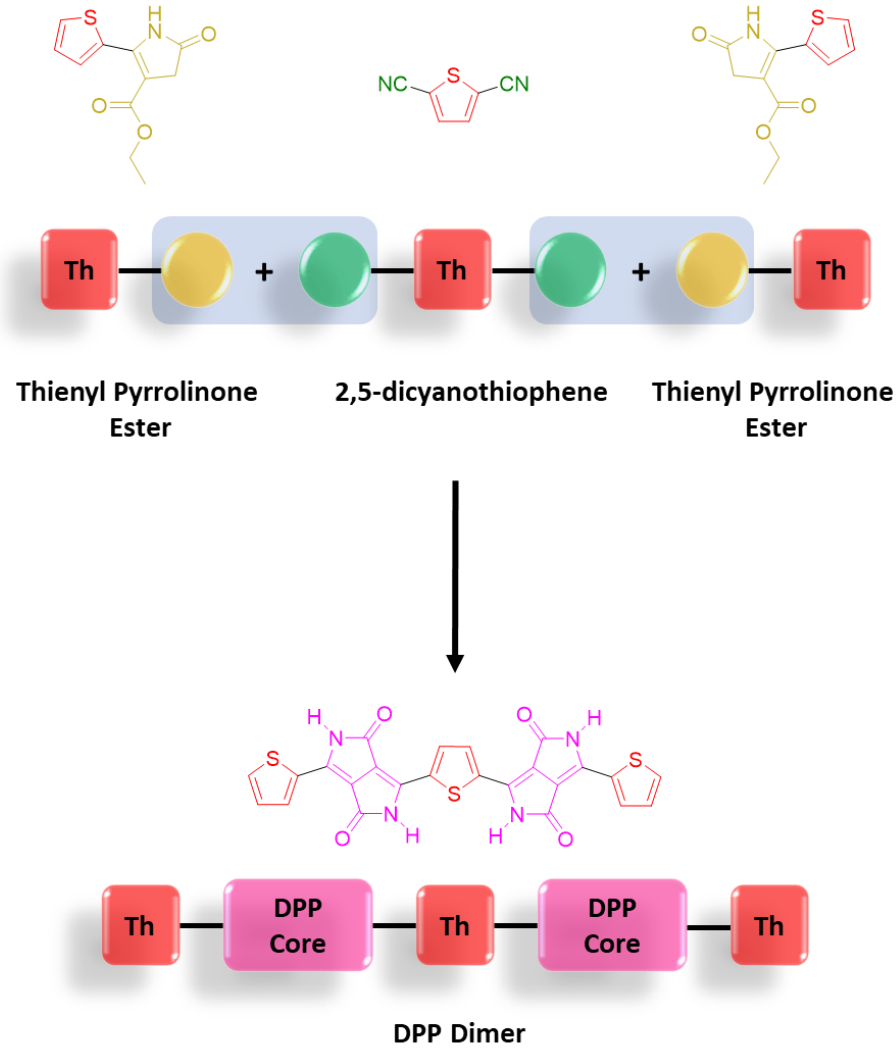

The DPP dimer can then undergo alkylation, bromination and subsequent polymerisation with 2,5-bis(trimethylstannyl)thiophene to give **P(a)** (Scheme 4.2).

*Scheme 4.2- Proposed synthesis to **P(a)** from DPP dimer.*

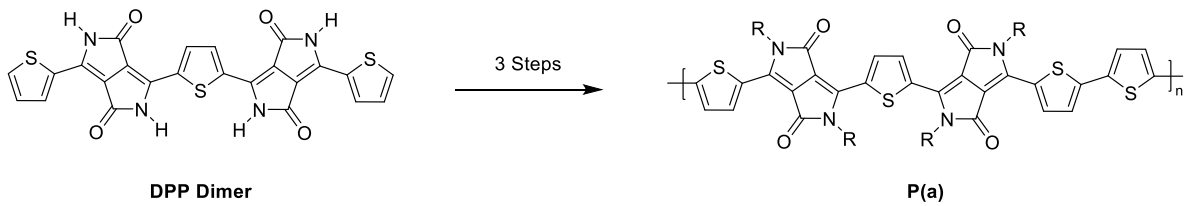

4.2 Synthesis

4.2.1 Thienyl Pyrrolinone Ester Strategy

4.2.1.1 Synthesis of Thienyl Pyrrolinone ester

The first synthetic strategy attempted towards the target DPP polymer, began with the synthesis of a thienyl pyrrolinone ester, as previously reported in literature.[166]

The three-step synthesis began with a Claisen condensation between compound **1** and diethyl carbonate under basic conditions, based on a procedure by Jiang *et al* (Scheme 4.3),[167] to give the beta-keto ester. The crude product was purified *via* column chromatography to afford **2** as an orange oil (95%).

*Scheme 4.3- Synthetic route to **4**.*

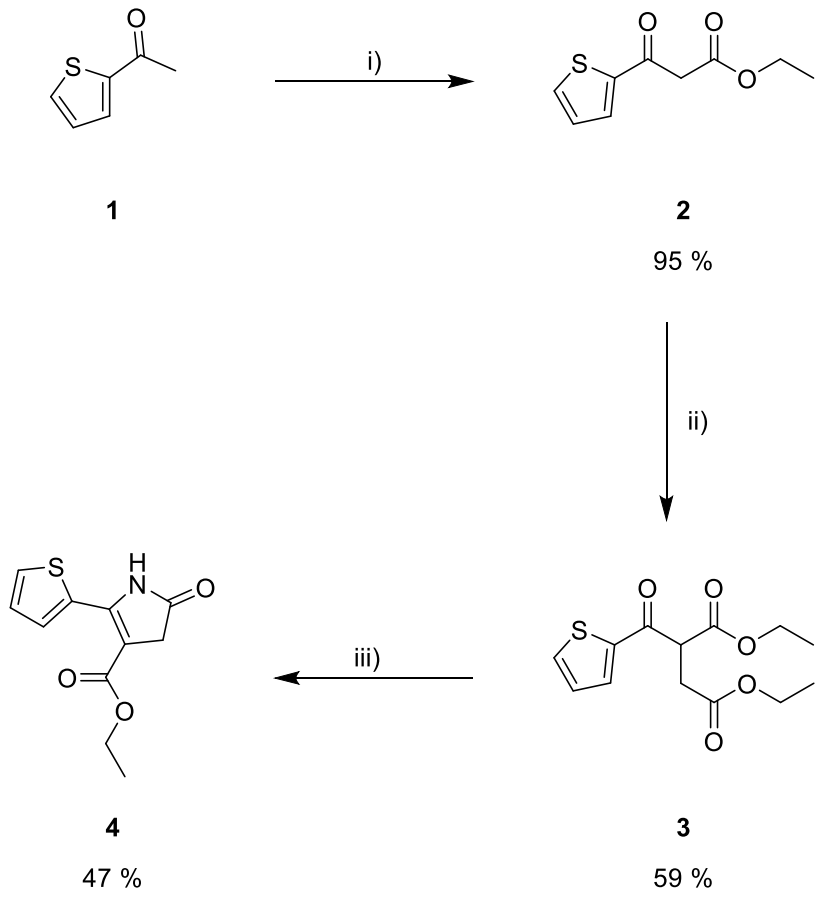

i) Diethyl carbonate, NaH, Toluene, Reflux, 1.5 h; ii) Ethyl bromoacetate, Na_2CO_3, Acetone, DME, Reflux, 20 h; iii) Ammonium acetate, Acetic acid, Reflux, 4 h.

This was then followed by alkylation reaction between **2** and ethyl bromoacetate under basic conditions, based on a previously reported procedure,[166] to give the product as a crude brown oil. The crude product

was partially purified *via* column chromatography to yield **3** (59%), which was used in the next step without further purification.

Finally, compound **3** underwent an amidation/cyclization with ammonium acetate in acetic acid, to give the thienyl pyrrolinone ester. The product was isolated *via* filtration and washed with MeOH to give **4** as a yellow solid (47%).

4.2.1.2 Synthesis of 2,5-Dicyanothiophene

Following the synthesis of **4**, was the synthesis of the second synthetic building block, 2,5-dicyanothiophene.

The synthesis began with the halogen exchange of compound **5** using n-BuLi, followed by the addition of DMF (Scheme 4.4), based on a procedure by Mitsumori *et al.*[168] The product was purified *via* column chromatography to afford **6** as yellow crystals (38%).

*Scheme 4.4- Synthesis of **6**.*

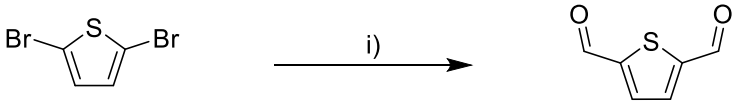

5 **6**

38 %

i) n-BuLi, DMF, Ether, -78 °C, Overnight.

This was then followed by the conversion of di-aldehyde **6** to di-nitrile **7**, using iodine in ammonia water, based on a procedure by Talukdar (Scheme 4.5).[169]

*Scheme 4.5- Synthesis of **7**.*

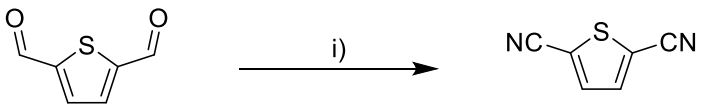

6 **7**

95 %

i) Iodine, Ammonia water, THF, MeCN, RT, Overnight.

Upon work up, compound **7** was isolated *via* filtration as a crude yellow solid (95%). Due to low solubility in most common organic solvents, compound **7** could not be purified *via* column

chromatography. Recrystallisation was attempted in several different solvents including MeCN and MeOH however all were unsuccessful. Therefore, compound **7** was used in the next reaction without further purification.

4.2.1.3 Synthetic attempts towards the DPP dimer

Following the synthesis of compounds **4** and **7**, it was then possible to attempt to synthesise the DPP dimer **8** (Scheme 4.6).

A condensation between **4** (2.5 equiv.) and **7** (1 equiv.) was attempted under the same conditions used to synthesise the thienyl-DPP core, as discussed in *Chapter II.* Compound **4** was initially added to the basic solution, Na dissolved in 2-methyl-2-butanol/*tert*-amyl alcohol (TAA), followed by **7**, and the reaction was heated for 2 h at 90 °C.

*Scheme 4.6- Unsuccessful synthetic attempt towards **8** via condensation between **4** and **7**.*

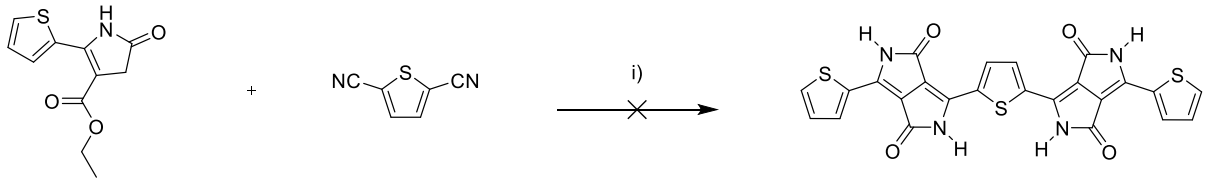

4 **7** **8**

i) Na, $FeCl_3$, 2-Methyl-2-butanol, 90 °C, 2 h.

While the isolated product had a distinct DPP-like purple colour, the ^{1}H NMR spectrum obtained was unclear as to what had been made. It is also to be noted that the compound only showed partial solubility in the ^{1}H NMR solvent (DMSO-d_6), thus it would have been preferred if precursor **4** contained alkyl chains in order to increase the solubility of the product. Due to the appearance of 7 peaks in the aromatic region, rather than the expected 4, it seemed as though a single asymmetric DPP unit had been made, as a result of partial reactivity on one side of compound **7**. (Figure 4.7). This was supported by the presence of two singlet peaks (**B**) at 11.35 ppm and 11.29 ppm, likely arising from asymmetric N-H protons (as observed for un-alkylated asymmetric DPP units in literature),[170] that integrate to one proton each. Although the sample was analysed by MALDI mass spectrometry, no clear outcome could be observed. Thus, based upon the ^{1}H NMR, we believe that a single DPP unit consisting of a nitrile group was formed during the reaction. However, as the spectrum does not integrate correctly for this compound, it is then possible that the nitrile underwent hydrolysis during work up, to give the DPP amide **9**. While **9** can then undergo further hydrolysis to form the DPP carboxylic acid, the integration of the spectrum did not match this compound.

The formation of compound **9** was supported by the integration of the spectrum as seen in Figure 4.7. It is believed that the three peaks at 8.25 ppm (doublet), 8.01 ppm (doublet) and 7.32 ppm (triplet) that integrate to one proton each, correspond to the three thienyl protons labelled (**A**), while the two doublets at 8.11 ppm and 7.83 ppm that also integrate to one proton each, correspond to the two thienyl protons labelled (**C**). It is then possible that the broad peaks visible at 8.18 ppm and 7.63 ppm that integrate to one proton each, correspond to the amide N-H protons labelled (**D**) (as similarly seen for 2-thiophenecarboxamide).[171]

*Figure 4.7- ^{1}H NMR in DMSO-d_6 of the aromatic region of the isolated solid when attempting to make **8**, likely to possess the structure of **9**.*

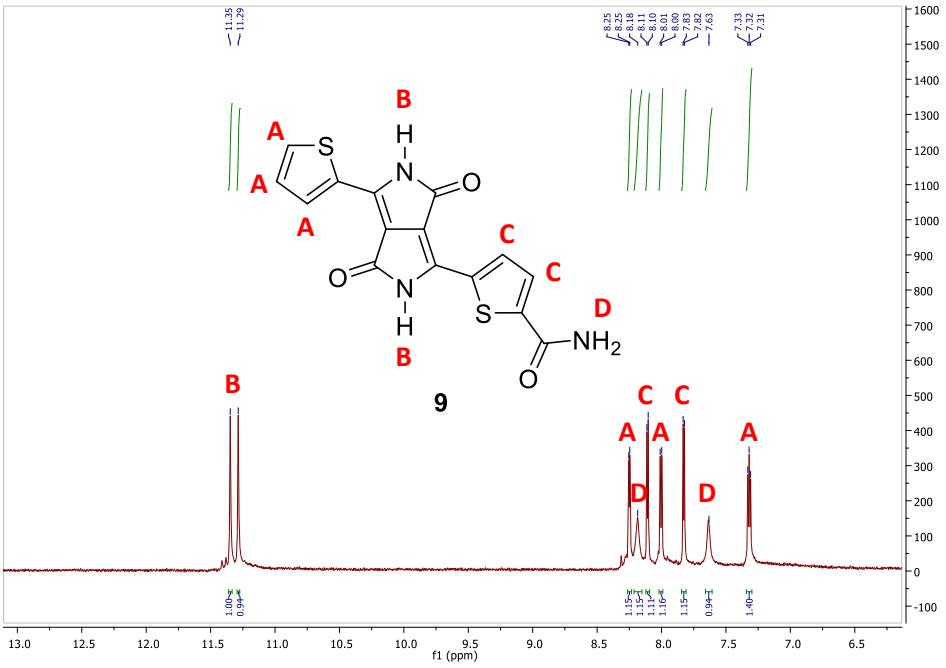

The condensation was then repeated with a longer reaction time of 18 h, in an attempt to drive the reaction to completion. However, the result remained the same and it appeared that only **9** had been made. Various other unsuccessful attempts were made under different reaction conditions, which are summarised in Table 4.1. In one attempt, an alternative base of NaH was implemented, based on a procedure by Metten,[172] however no reaction was observed by ^{1}H NMR. Additionally, in a further attempt, the order of addition was reversed in which **7** was added to the basic reaction mixture first. However, this led to the formation of an unidentifiable black insoluble product.

*Table 4.1- Summary of synthetic attempts towards the synthesis of **8** via condensation between **4** and **7**. Reactions were conducted in the presence of 2.5 equiv. of **4**, 1 equiv. of **7** and 9.4 equiv. of Na.*

Entry	Initial Reagent	Reaction Time (h)	Reaction Conditions	Reaction Temperature (°C)	Outcome
1	**4**	2	Na, TAA	90	Formation of **9**
2	**4**	18	Na, TAA	90	Formation of **9**
3	**4**	18	NaH, DMSO	RT	Starting material
4	**7**	18	Na, TAA	90	Unidentifiable insoluble black product

Further attempts to optimise this route were made using 1,4-dicyanobenzene (**10**) in the place of **7**, due to its similar reactivity and commercial availability. Thus, the desired product **8**, was modified to compound **11**. (Scheme 4.7). It was rationalised that if optimised conditions were obtained for the synthesis of compound **11**, these conditions could then be applied to the synthesis of compound **8**. The reaction conditions attempted are summarised below in Table 4.2.

*Scheme 4.7- Unsuccessful synthetic attempt towards **11** via condensation between **4** and **10**.*

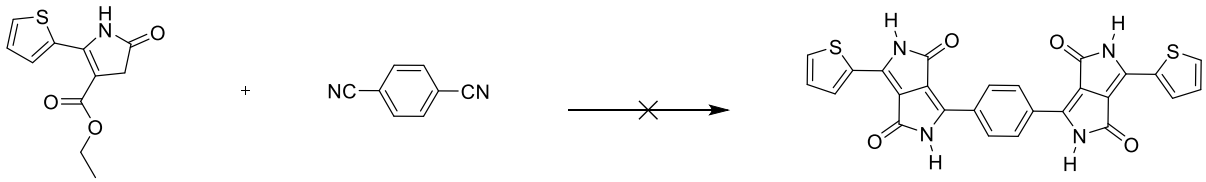

4 **10** **11**

*Table 4.2- Summary of synthetic attempts towards the synthesis of **11** via condensation between **4** and **10**. Reactions were conducted in the presence of 1 equiv. of **10** at 90 °C in 2-methyl-2-butanol (TAA).*

Entry	Initial Reagent	Equiv. of 4	Reaction Time (h)	Reaction Conditions	Equiv. of Na	Outcome
1	**4**	2.5	18	Na, TAA	3	Formation of **12**
2	**4**	2.5	2	Na, TAA	9.4	Formation of **12**
3	**4**	2.5	18	Na, TAA	9.4	Formation of **12**
4	**4**	2.5	18	Na, TAA	18.8	Unidentifiable insoluble black product
5	**4**	10	18	Na, TAA	37	Formation of **12**
6	**4**	10	48	Na, TAA	37	Formation of **12**

Due to fears of degradation of compound **4** *in situ*, the reaction was carried out using a lower equivalent of Na (3 equiv.). However, as similarly seen in Scheme 4.6, the reaction did not go to completion and ^{1}H NMR suggested that compound **4** had only reacted with one of the nitrile groups on compound **10**. Following this attempt, standard conditions used to synthesise thienyl-DPP were applied, first for a reaction time of 2 h and then a longer time of 18 h, however the same result was observed. In contrast, it was later thought that a large excess of Na (18.8 equiv.) may be required to fully deprotonate **4** and drive the reaction to completion. It was observed however, that an uncharacterizable insoluble black product had formed and thus, it was concluded that these conditions may have been too harsh due to the base sensitivity of compound **4**. Following this, a final attempt using a large excess of **4** and a corresponding amount of Na was carried out. Upon work up, a crude solid was isolated. The excess compound **4** was removed *via* washing with MeOH to obtain a purple DPP-like solid. The ^{1}H NMR obtained for the sample was identical to earlier attempts, and the integration of the spectra suggested that compound **4** had only reacted with one of the nitrile groups on compound **10**, to give the DPP nitrile **12**. While **12** can then undergo hydrolysis to form the DPP amide, integration of the spectrum did not match this compound. Following analysis by mass spectrometry, it was confirmed that compound **12** was observed as the major product; TOF MS ASAP+ *m/z* 320.0485 $[M+H]^{+}$ (Figure 4.8).

*Figure 4.8- TOF MS ASAP+ analysis of the undesired compound **12**; m/z 320.0485.*

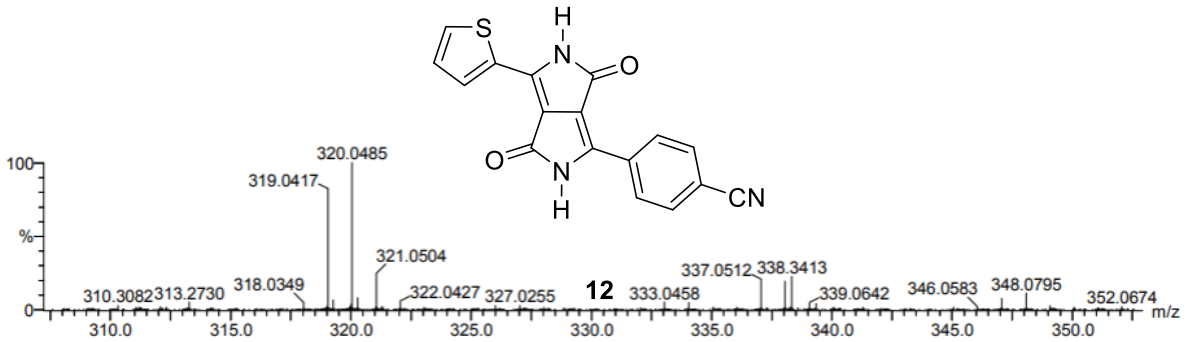

Analysis *via* MALDI-TOF was also carried out in order to check for any trace of dimer **11**, however no peak at *m/z* 510 was observed. These conditions were also repeated for a longer reaction time of 48 h; however, the same result was obtained. Thus, it was concluded that an alternative synthetic strategy should be investigated.

4.2.2 Di-Thienyl Pyrrolinone Ester Strategy

Following the unsuccessful synthetic strategy towards DPP dimer **8** *via* condensation between thienyl pyrrolinone ester **4** and nitrile **7**, an alternative route was sought. Recently, Ahner *et al*[173] reported a novel synthetic route towards the phenyl variant of the target monomer (**11**), through a reversed

synthesis in which a di-phenyl pyrrolinone ester (**13**) was built, starting from a neutral phenyl core. This was then reacted with 2-cyanothiophene (**14**) to give **11** (Scheme 4.8).

*Scheme 4.8- Synthesis of **11** via condensation between **13** and **14** as reported by Ahner et al.*[173]

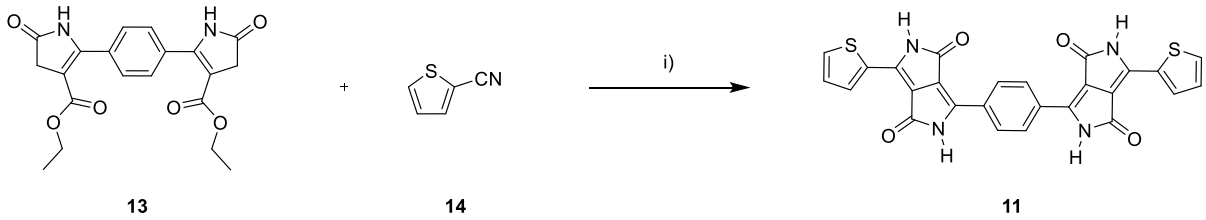

13 **14** **11**

i) Na, 2-methyl-2-butanol, 18 h, 80 °C.

Thus, based on this synthetic strategy, the revised proposed synthetic route towards the DPP dimer **8** involved the condensation between a novel di-thienyl pyrrolinone ester and 2 equiv. of 2-cyanothiophene under basic conditions (Scheme 4.9).

Scheme 4.9- Proposed synthesis of the DPP dimer via condensation between di-thienyl pyrrolinone ester and 2-cyanothiophene.

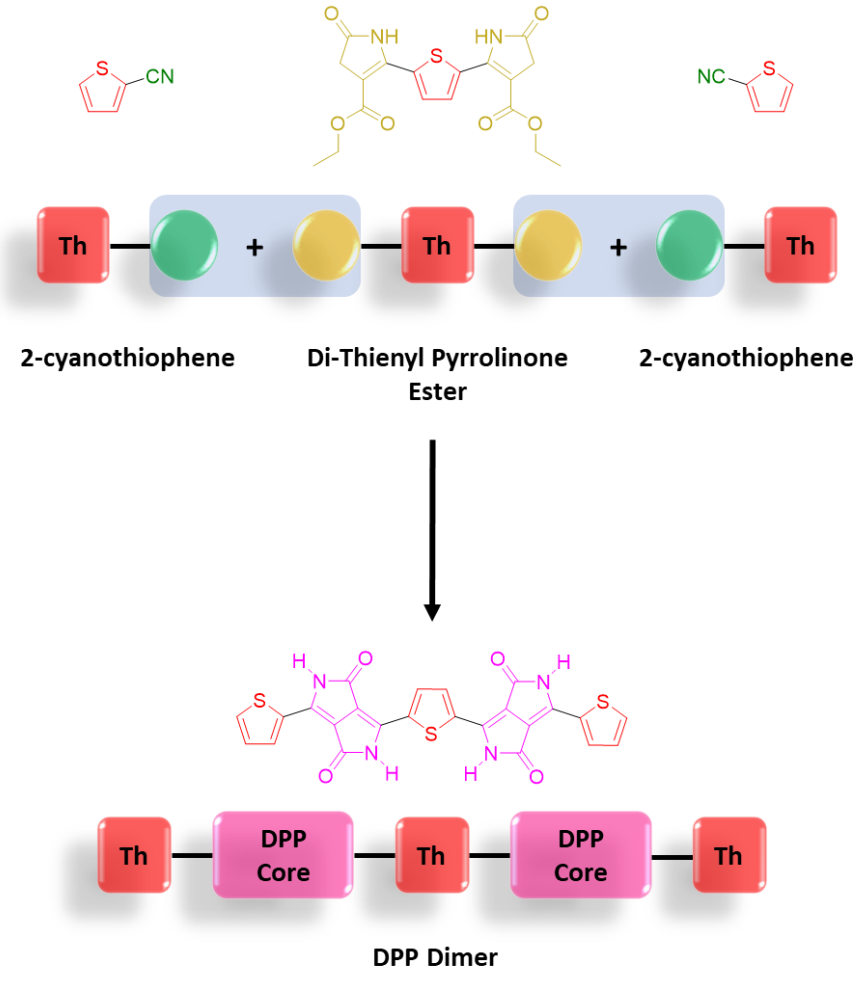

4.2.2.1 Synthesis of the Di-Thienyl Pyrrolinone Ester

To begin, it was required to synthesise a novel di-thienyl pyrrolinone ester *via* a similar synthetic route used to synthesise **4**, this time reacting on both the 2- and 5- positions of the core thiophene unit. The synthesis began with 2,5-dibromothiophene (**5**), which underwent halogen exchange using n-BuLi, followed by the addition of *N,N*-dimethylacetamide, to give **15** (34%) (Scheme 4.10).

*Scheme 4.10- Synthetic route to the di-thienyl pyrrolinone ester **18** from **5**.*

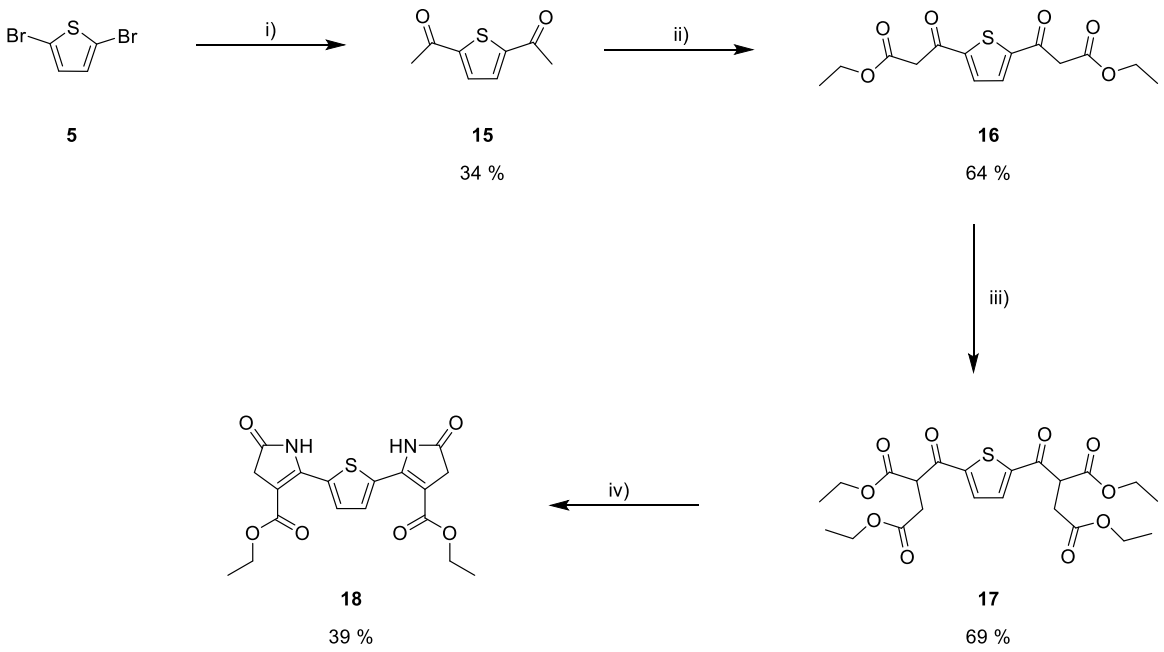

i) n-BuLi, N,N-Dimethylacetamide, Diethyl ether, -78 °C, Overnight; ii) Diethyl carbonate, NaH, DME, Reflux, 1.5 h; iii) Ethyl bromoacetate, Na_2CO_3, Acetone, DME, Reflux, 20 h; iii) Ammonium acetate, Acetic acid, Reflux, 4 h.

Compound **15** then underwent a double Claisen condensation with diethyl carbonate to give compound **16**. Initially, as with the synthesis of compound **2**, toluene was chosen as the reaction solvent. However, it was observed that **15** showed poor solubility in toluene and upon workup, ^{1}H NMR revealed that no reaction had taken place. Thus, an alternative method reported by Li *et al*[174] was implemented instead, in which DME replaced toluene as the reaction solvent. Upon work up, while partial purification was possible *via* column chromatography, it was not possible to separate the undesired mono-carbonate impurity from the di-carbonate product, due to their highly similar polarities on silica. Thus, **16** was obtained in a 64% yield and used in the next step with no further purification. This was followed by a di-alkylation reaction between compound **16** and ethyl bromoacetate to give **17** (69%). As before, while partial purification was carried out *via* column chromatography, due to the highly similar polarities of

the mono-aldol and di-aldol products, it was not possible to separate the two compounds. As a result, **17** was used in the next step with no further purification. Finally, **17** underwent a double amidation/cyclization with ammonium acetate in acetic acid, to give the di-thienyl pyrrolinone ester. The product was isolated *via* filtration and washed with water to give **18** as a green/blue solid (39%). It was noted that the ^{1}H NMR for **18** was slightly broad, due to poor solubility and increased aggregation.

4.2.2.2 Synthetic attempts towards the DPP dimer

Following the synthesis of **18**, it was then possible to attempt to synthesise the DPP dimer **8** *via* condensation between **14** and **18**. (Scheme 4.11).

*Scheme 4.11- Unsuccessful synthetic attempt towards **8** via condensation between **14** and **18**.*

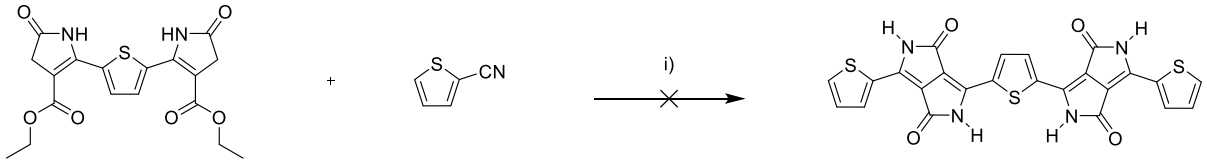

18 **14** **8**

i) Na, 2-methyl-2-butanol, 18 h, 85 °C.

Following the formation of the NaO^{t}Am base (5 equiv.), compounds **18** (1 equiv.) and **14** (3 equiv.) were added in one portion, and the reaction was stirred at 85 °C for 18 h, based on a procedure by Ahner *et al*.[173] Upon workup, a blue solid was isolated *via* filtration and washed with water, acetone, hexane and MeOH. Analysis *via* ^{1}H NMR proved to be difficult due to the broadness of the spectrum, likely arising from aggregation (Figure 4.9). While largely broad peaks were observed around the expected regions for compound **8** (i.e. 11.00 ppm for N-H), no definite conclusions could be made. In addition, due to low solubility in most organic solvents, it was not possible to analyse the product *via* mass spectrometry (MALDI). Thus, the formation of compound **8** could not be confirmed. As mentioned for the previous synthetic strategy, it would have been more ideal if precursor **18** consisted of alkyl chains in order to increase the solubility of the product. This would then allow sufficient solubility for characterisation by ^{1}H NMR and MALDI.

*Figure 4.9- ^{1}H NMR in DMSO-d_6 of the aromatic region of the isolated solid, when attempting to make **8** via condensation between **18** and **14**. The spectrum is largely broad which was likely due to aggregation in solution.*

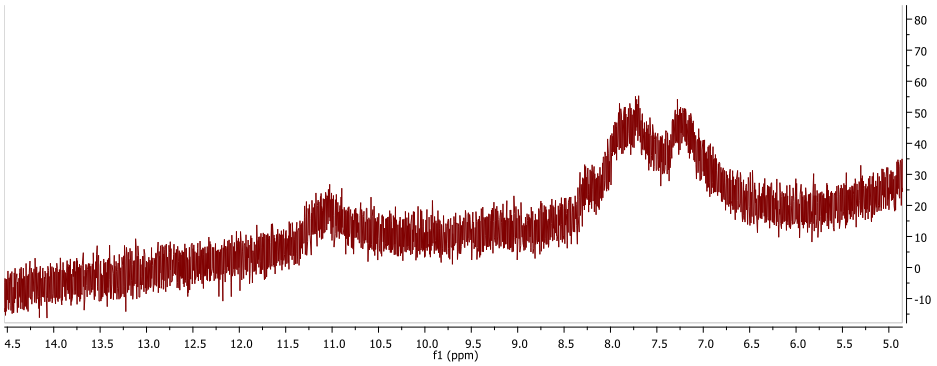

It was noted that Ahner's[173] phenyl variant **11** could not be analysed *via* mass spec or ^{1}H NMR and instead, the compound was characterised following alkylation. The addition of alkyl chains allowed suitable solubility for analysis. Therefore, in order to identify the unknown product and see whether compound **8** had in fact been made, an alkylation was attempted (Scheme 4.12).

*Scheme 4.12- Unsuccessful attempt at alkylation of the unknown isolated solid '**8**'.*

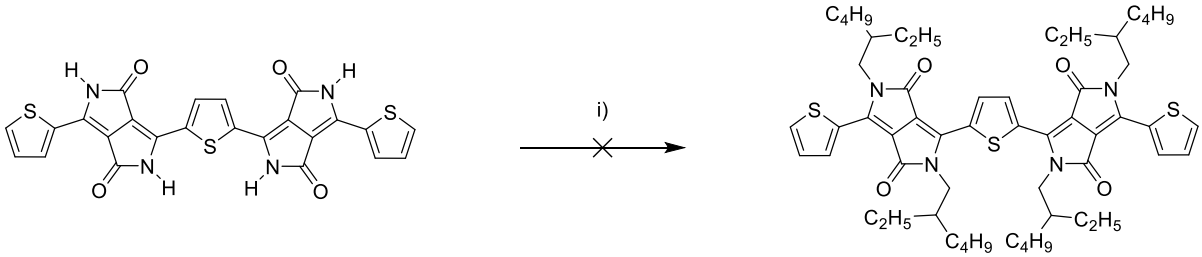

i) 2-Ethylhexyl bromide, K_2CO_3, 18-crown-6, DMF, 120 °C, 48 h.

The alkylation was carried out using 2-ethylhexyl bromide in DMF and K_2CO_3 as the base, based on a procedure by Bronstein.[60] Upon workup, an uncharacterizable insoluble black solid was isolated, which suggested that dimer **8** had not been made in the previous step. Thus, several other attempts of condensation and subsequent alkylation, under alternative reaction conditions were tested.

Following this initial attempt, the condensation was repeated under the same conditions, and two further alkylation conditions were tested. Firstly, a longer alkyl chain was used (9-(bromomethyl)nonadecane) in an attempt to provide the product with increased solubility. However, this again resulted with the formation of an insoluble black solid, suggesting that the previous condensation step did not work. As the unknown blue condensation product only showed a partial solubility in DMF, an alternative solvent

was also tested. Therefore, an alkylation was carried out in DMSO and stirred for 19 h at 100 °C, based on Ahner's procedure.[173] However, the same result was obtained. As no alkylation took place in any of the attempts, it appeared that under these reaction conditions, the condensation step did not work and dimer **8** had not been made.

Thus, alternative condensation conditions were also tested, following these initial attempts. It was thought that perhaps an alternative base was required. It was reported by Metten *et al,*[172] that NaH was observed to fully deprotonate aryl pyrrolinone esters. Thus, the condensation was also carried out using NaH (4 equiv.) in DMSO. As with previous attempts, upon workup the ^{1}H NMR obtained for the unknown blue compound, was broad and inconclusive. In addition, trace of starting material **18** was observed in the NMR, suggesting that the reaction did not go to completion. An alkylation was attempted in DMSO, however once again, this led to the isolation of an insoluble black solid. In two final attempts, the initial condensation conditions were repeated, this time using a larger excess of Na (7.6 equiv.). As with all other attempts, the ^{1}H NMR spectrum was broad, therefore the product was unknown. Subsequent alkylation was attempted using 9-(bromomethyl)nonadecane in DMF for 48 h at 120 °C and upon work up, an unidentifiable black solid was isolated. As all alkylation attempts resulted in no product, it was thought that perhaps the conditions were too harsh. Therefore, the reaction was repeated at a lower temperature of 80 °C however the same result was obtained. It was noted that starting material **18** showed poor/partial solubility in most solvents, thus this may have prevented the condensation reaction from occurring.

Following this unfortunate result, it was concluded than another route towards the DPP dimer should be investigated. In particular, one that incorporated solubilising alkyl chains on the thienyl pyrrolinone ester precursor, prior to the key coupling step. Therefore, what was required was a synthetic methodology towards alkylated thienyl pyrrolinone esters. This would ensure sufficient solubility for analysis *via* ^{1}H NMR.

4.2.3 Fully Asymmetric DPP Derivatives

Following the unsuccessful results of the previous two strategies, it was observed that the thienyl pyrrolinone esters **4** and **18** were largely insoluble in most common organic solvents, therefore most reaction attempts resulted in either partial reaction, or an insoluble crude material that could not be characterised *via* NMR or mass spectrometry.

Therefore, it would be desirable to synthesise an *alkylated* thienyl pyrrolinone ester (Figure 4.10), to undergo condensation with **7**, which would not only increase solubility in the chosen reaction solvent, but also allow characterisation of the reaction products.

Figure 4.10- Alkylated thienyl pyrrolinone ester.

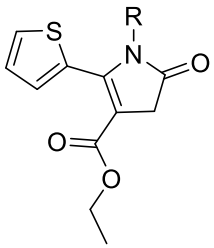

R= Alkyl Chain

As well as providing a new route towards the DPP dimer, it is possible that the successful synthesis of alkylated thienyl pyrrolinone esters, could also allow the synthesis of fully asymmetric DPP derivatives (Figure 4.11). Thus, to begin, the synthesis of these novel compounds was explored.

Figure 4.11- Fully asymmetric DPP.

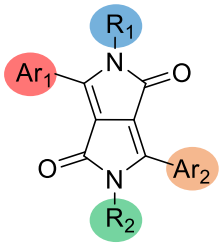

4.2.3.1 Introduction

While in previous chapters we have discussed symmetrical diketopyrrolopyrrole (DPP) compounds, in this sub-section, we now investigate asymmetric DPP derivatives, which have shown a growing interest within the field in recent years. Most conventional DPP compounds are synthesised *via* a one-pot procedure involving the condensation of 1 equiv. of diethyl succinate with 2 equiv. of an aromatic nitrile, using a sodium alkoxide base.[90] This then results in DPP with symmetrical aromatic flanking

groups on either side. Subsequently, these materials are then often alkylated at the N-H position with two identical alkyl chains, giving the unit a C2 symmetry (Scheme 4.13).

Scheme 4.13- One-pot synthesis of symmetrical DPP derivatives followed by alkylation.[90]

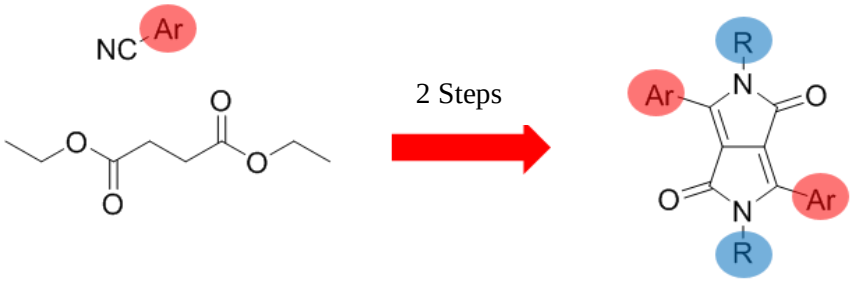

As well as these commonly known symmetrical DPP materials, in recent years there has been a growing interest in partially asymmetric DPP derivatives, in which the DPP cores are flanked with different aryl groups. There have been various reported examples of partially asymmetric DPP polymers (Figure 4.12) incorporating a wide variety of a secondary aryl group including pyridine (**PPyTDPP-TT**),[175] thienothiophene (**PDPPTT-2T**),[176] benzothiophene (**PBTTDPP-TT**)[177] and furan (**PTTFDPP-TT**).[178]

Figure 4.12- Structures of partially asymmetric DPP polymers.[175–178]

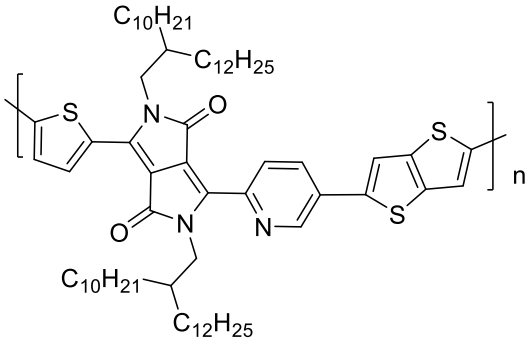

PPyTDPP-TT

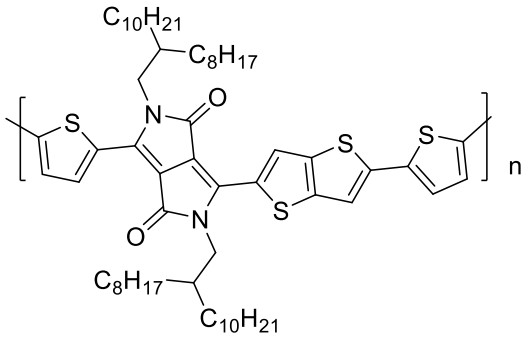

PDPPTT-2T

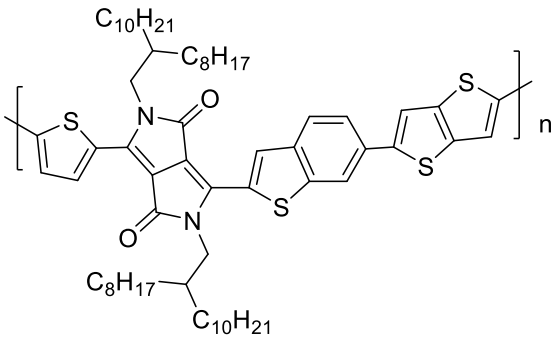

PBTTDPP-TT

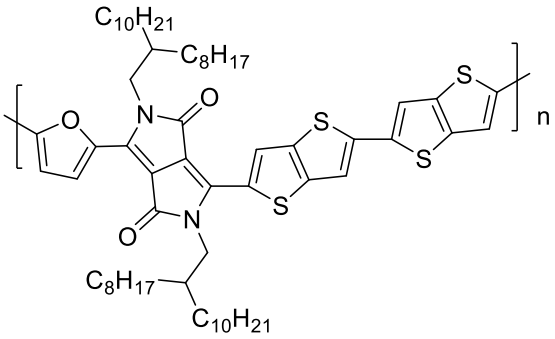

PTTFDPP-TT

These asymmetric DPP units are made *via* a two-step route, through the condensation of an aryl-pyrrolinone ester with an aromatic nitrile under basic conditions, followed by alkylation at the N-H positions with two identical alkyl chains.[176] (Scheme 4.14).

Scheme 4.14- Synthesis of partially asymmetric DPP derivatives via condensation of aryl-pyrrolinone esters with an aromatic nitrile, followed by alkylation.[176]

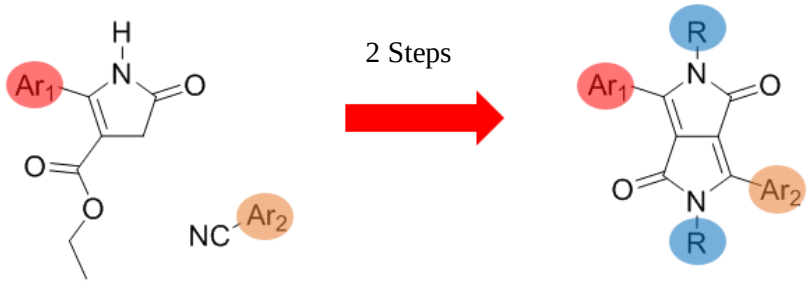

A key difference in the properties of such materials compared to its symmetrical counterpart when incorporated into conjugated polymers, are its solubility in common organic solvents. An issue found with many symmetrical conjugated DPP polymers are that they are often only soluble in chlorinated solvents such as chloroform, chlorobenzene and ortho-dichlorobenzene, which are required during thin film synthesis. This is undesirable, as the use of chlorinated solvents have a negative effect on the environment.

In 2016, Ji *et al*[176] reported the synthesis of two new asymmetric DPP polymers (**PDPPTT-2T** and **PDPPMT-2T**) containing two different aryl groups on either side of the DPP core (Figure 4.13). It was observed that due to the lack of translational symmetry along the backbone, the polymers were also soluble in non-chlorinated solvents such as THF and toluene, while still maintaining high crystallinity in films and achieved hole mobilities as high as 12.5 $cm^2 V^{-1} s^{-1}$.[176]

*Figure 4.13- Structures of asymmetric DPP Polymers **PDPPTT-2T** and **PDPPMT-2T**.*[176]

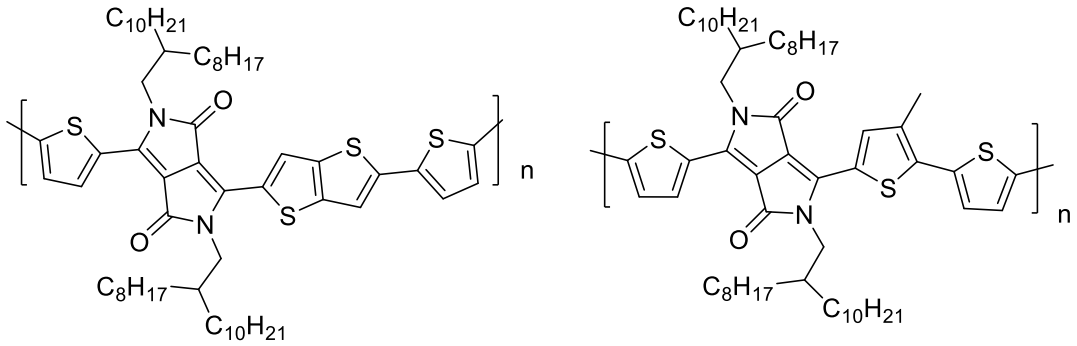

PDPPTT-2T **PDPPMT-2T**

As well as translational asymmetry along the conjugated backbone, there have also been examples of dissymmetry of the two solubilising alkyl chains on the DPP unit. It has been shown that the variation of alkyl chain groups can have a large effect on the charge mobility of the polymer. Commonly, long branched alkyl chains are used on DPP such as seen in Figure 4.13, as they largely improve the solubility of the polymer compared to linear alkyl chains.

There are however disadvantages, for example the bulky nature of the branched chains prevents intermolecular interactions and causes steric hinderance, which in turn reduces the planarity of the polymers conjugated backbone. In 2018 it was reported by Wang *et al,*[179] that for selenophene based DPP polymers (**PDPPSe** and **PDPPSe-12**) (Figure 4.14), by simply replacing two branched alkyl chains for one linear and one branched, reduced steric hindrance was observed as well as a higher planarity of the backbone. Improved inter-chain packing and thin-film crystallinity was also observed. This in turn, enhanced the charge mobility of the polymer.[179]

*Figure 4.14- Structures of **PDPPSe** and **PDPPSe-12**.*[179]

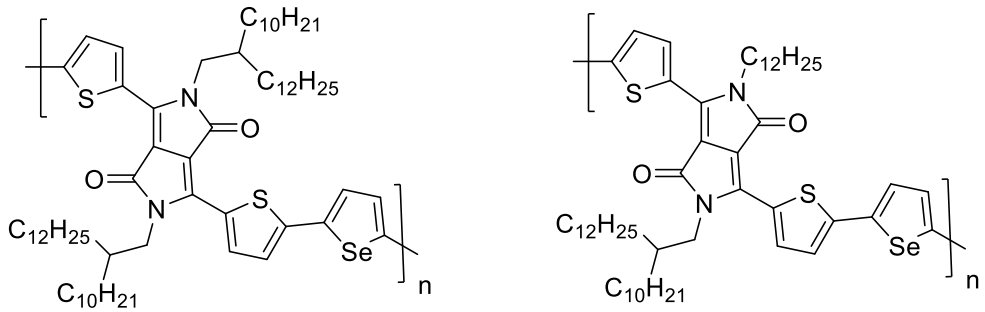

PDPPSe **PDPPSe-12**

Another interesting example is by Yang *et al,*[116] in which they reported a DPP polymer (**PDPP3T1**) incorporating both a hydrophobic alkyl chain and a hydrophilic tetraethylene glycol (TEEG) chain on a single DPP unit (Figure 4.15), that could form a stable monolayer at the air-water interface. This was then made into a monolayer FET device that showed a highly sensitive and selective response to ethanol vapor, demonstrating the potential of such compounds in future sensor applications.

Figure 4.15- Structure of ***PDPP3T1****.*

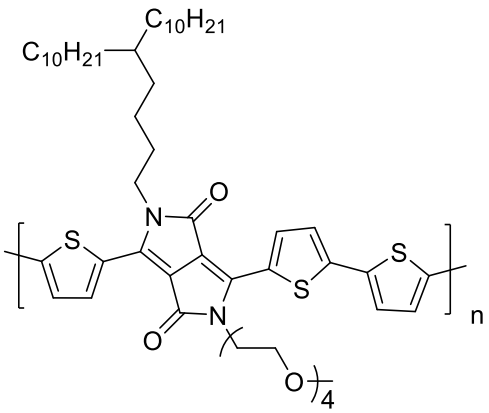

PDPP3T1

There have been other examples in literature such as by Morten *et al,*[170] reporting partially asymmetric DPP units flanked with both an aromatic and non-aromatic group (Figure 4.16). These were synthesised *via* the condensation of a phenyl pyrrolinone ester with a non-aromatic nitrile under basic conditions. Although of unique structure, these compounds are often unsuitable for subsequent synthesis of conjugated polymers.

Figure 4.16- Examples of asymmetric DPP units consisting of an aryl and non-aromatic group.[170]

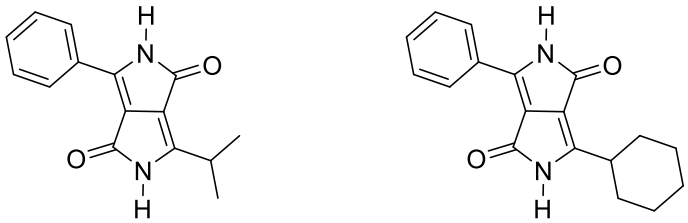

In summary, there has been a growing interest in asymmetric DPP polymers, due to their superior solubility, enhancement in charge mobility, greater fine tunability and their potential in various applications such as sensors.

While various asymmetric DPP units consisting of either different aromatic flanking units or dissimilar alkyl chains, a fully asymmetric DPP unit has not yet been reported, due to the prohibitively difficult purifications that would be required. If this were possible, it would allow the ability to fine tune both the optical and solid-state properties of DPP units, such that their performance across all relevant devices could be improved.

4.2.3.2 Sub-Chapter Objectives

Inspired by previous literature on *partially* asymmetric DPP derivatives, which have shown advantageous properties compared to that of its commonly known symmetrical counterpart, here we intend to establish a novel methodology towards fully asymmetric DPP compounds, which to our best knowledge has not yet been reported (Figure 4.17).

In this sub-chapter, we report a novel methodology towards fully asymmetric DPP units, in which we were able to systematically vary the positioning of the individual solubilising alkyl chains relative to the asymmetric aromatic units. We demonstrate this by synthesising a pair of fully asymmetric DPP structural isomers (**T-DPP-P** and **P-DPP-T**) (Figure 4.17) and investigate their optical and theoretical properties. We also expand the scope of this methodology to two further fully asymmetric DPP units incorporating different aromatic groups such as furan, as well as incorporating an ethylene glycol chain.

*Figure 4.17- Structures of asymmetric DPP structural isomers **T-DPP-P** and **P-DPP-T**.*

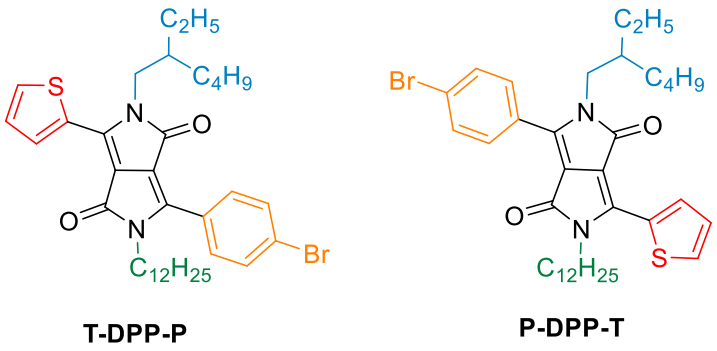

The proposed synthetic route towards the asymmetric DPP derivatives begins with the synthesis of *alkylated* thienyl pyrrolinone esters, followed by condensation with a secondary aryl nitrile and subsequent alkylation (Scheme 4.15).

Scheme 4.15- Proposed synthetic route towards fully asymmetric DPP derivatives.

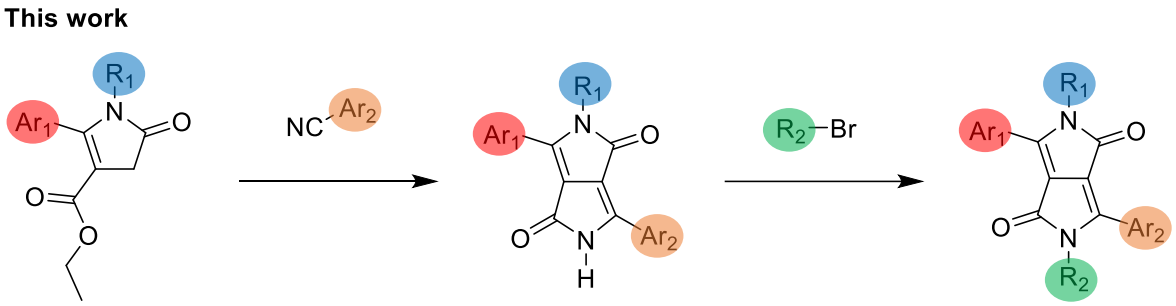

4.2.3.3 Synthesis of alkylated thienyl pyrrolinone esters

The synthesis towards fully asymmetric DPP derivatives began with the preparation of alkyl-thienyl pyrrolinone esters, which were the building blocks towards the synthesis of the fully asymmetric DPP compounds. In order to synthesise the pair of DPP structural isomers (**T-DPP-P** and **P-DPP-T**), two different alkyl-thienyl pyrrolinone esters were required, one consisting of a linear chain and one a branched chain. An interesting paper by Metten,[180] reported the synthesis of a series of 5-aryl-2-oxopyrrole derivatives *via* a three-component cyclization of sodium ethyl oxalacetate, aromatic aldehydes and primary amines. This was then followed by a zinc reduction to give the enol, which was subsequently mesylated and treated with TEA to the give the desired pyrrolinone esters.[180] Thus, we attempted to synthesise the novel alkyl thienyl pyrrolinone esters based on these conditions (Scheme 4.16).[180]

Scheme 4.16- Synthetic route towards novel alkylated thienyl pyrrolinone esters based on Metten's[180] procedure.

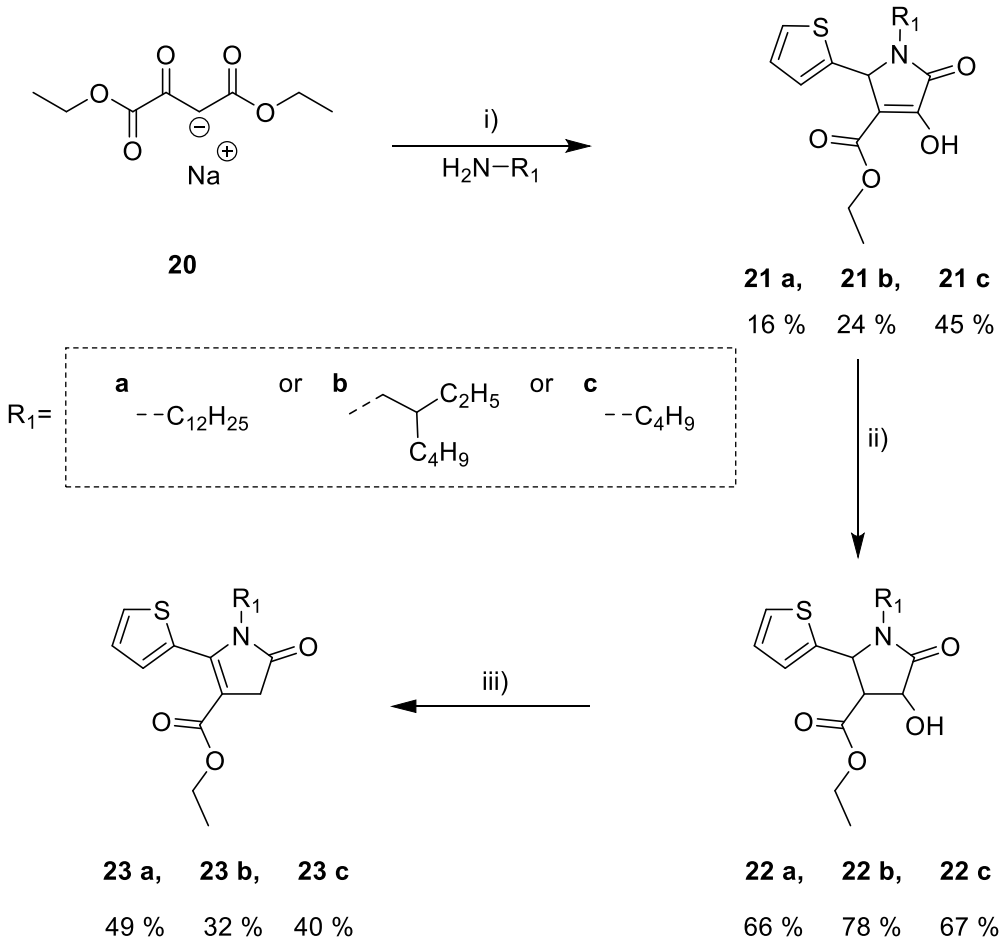

i) 2-Thiophenecarboxyaldehyde, EtOH, Reflux, 20 h; ii) Zn Powder, H_2SO_4, AcOH, 100 °C, 3 h; iii) Mesyl Chloride, TEA, $CHCl_3$, Reflux, 30 min.[180]

The synthesis began with a cyclization between sodium ethyl oxalacetate **20** (1 equiv.), 2-thiophenecarboxyaldehyde (1 equiv.) and dodecylamine (1 equiv.) based on Metten's procedure.[180] Dodecylamine was used, as its length was sufficient in increasing the solubility of the target compound. The reaction was heated under reflux for 20 h, before pouring the reaction mixture into water and acidifying with sulfuric acid. The crude product then precipitated out of solution and was collected *via* filtration, before washing with hexane to remove any excess aldehyde, which afforded **21a** as a pure white solid (16%).

The next step of the synthesis was a zinc reduction of **21a** to give the alcohol **22a**. The enol **21a** was dissolved in acetic acid mixed with a few drops of sulfuric acid, followed by the addition of zinc and the mixture was heated at 100 °C for 2 h. This was then followed by a second addition of zinc and the reaction was stirred for a further hour. Upon workup, compound **22a** was obtained in a crude yield of 66%. This was then used directly in the next step without further purification.

Compound **22a** was then used in the final step to make the alkylated thienyl pyrrolinone ester *via* elimination of the alcohol group through mesylation and treatment with triethylamine (TEA), followed by isomerisation of the double bond**.** The crude residue obtained was purified *via* dissolving in a minimum amount of MeOH followed by freezing overnight. The product was then isolated *via* filtration to afford **23a** as pure mink coloured crystals (49%).

Following the successful synthesis of **23a**, it was required to synthesise a secondary alkyl variant of the pyrrolinone ester, in order to synthesise the pair of DPP isomers. The second thienyl pyrrolinone ester **23b** was made in a similar manner to **23a**, beginning with the three-component cyclization under the same conditions, this time using the branched chained 2-ethylhexylamine. The product was isolated *via* column chromatography to give an off-white solid, which was then collected *via* filtration and washed with hexane, to afford **21b** in a 24% yield.

This was then followed by zinc reduction as before and the crude product **22b** was isolated in a 78% yield, used in the next reaction without further purification. Finally, the last step of the synthesis was mesylation of **22b** followed by treatment with TEA. The crude oil underwent purification *via* column chromatography to afford **23b** as a yellow/brown oil (32%).

The final butyl thienyl pyrrolinone ester **23c**, was made *via* a similar route. The three-component cyclization using butylamine, gave **21c** at a 45% yield, which was significantly higher than either **21a** or **21b**. This may have been due to its shorter linear alkyl chain, allowing the product to more readily precipitate from solution. This was then followed by zinc reduction, which afforded **22c** at a 67% yield. Finally, **22c** underwent mesylation and treatment with TEA, to give **23c** as a red oil (40%). While demonstrating the scope of this methodology, **23c** was not used in any further steps, as it was believed

that the short butyl chain was insufficient at providing suitable solubility, for the following asymmetric DPP derivatives.

4.2.3.4 Synthesis of fully asymmetric DPP derivatives

While most of the aromatic nitriles to be used were commercially available, the synthesis of 2-furanitrile was required. Based on a procedure by Talukdar,[169] **24** was converted into 2-furanitrile using ammonia water and iodine as an oxidant (Scheme 4.17). The reaction was stirred at RT for 1 h and upon work up, compound **25** was isolated at a 44% yield of sufficient purity and was used in the next reaction without further purification.

*Scheme 4.17- Synthetic route to **25**.*[169]

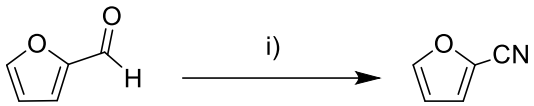

24 **25**

44 %

i) I_2, aq NH_3, MeCN, THF, RT, 1 h.

Following the synthesis of the alkyl-pyrrolinone ester building blocks, was condensation with either benzonitrile (**c**), 4-bromobenzonitrile (**d**) or 2-furanitrile (**e**) to give the asymmetric DPP cores. To begin, **23a** underwent condensation with 4-bromobenzonitrile based on a similar procedure by Aoshima *et al* (Scheme 4.18).[181] The synthesis began with the formation of sodium *tert*-butoxide, before addition of **23a** and 4-bromobenzonitrile. The reaction was heated for 2 h at 95 °C. However, upon work up only a trace amount of product **26ad** could be detected *via* TLC and ^{1}H NMR.

*Scheme 4.18- Unsuccessful attempt at synthesising **26ad**.*

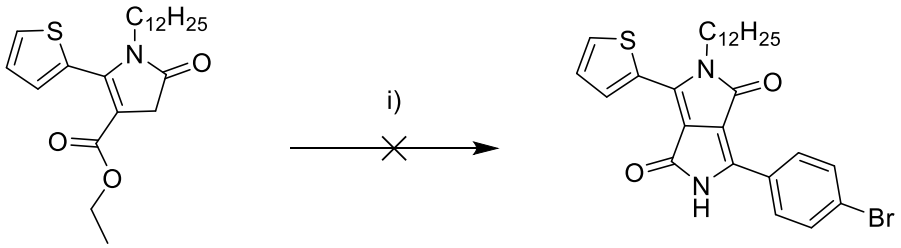

23a **26ad**

Trace

i) 4-Bromobenzonitrile, Na, 2-methyl-2-butanol, 95 °C, 2 h.

Following this, optimised reaction conditions for the synthesis of **26ad** were investigated and are summarised in Table 4.3.

*Table 4.3- Summary of optimisation attempts for the synthesis of **26ad**. Reactions were conducted in the presence of 1 equiv. of **23a**, 1.2 equiv. of nitrile **(d)** (4-bromobenzonitrile) and 3.1 equiv. of Na. Yields have been calculated on isolated and purified compounds.*

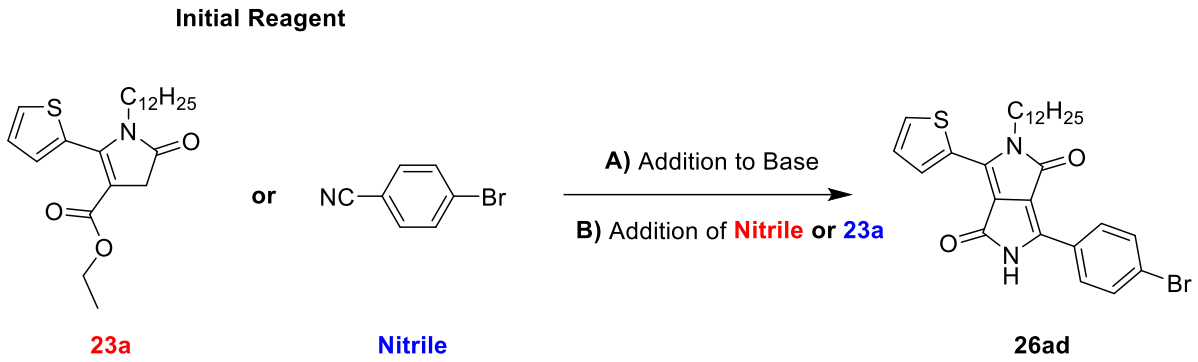

Entry	Initial Reagent	Step A (min)	Step B (h)	Reaction Conditions	Reaction Temperature (°C)	Yield (%)
1	**23a**	1	2	Na, TAA	95	Trace
2	**23a**	1	4	Na, TAA	95	3
3	**23a**	1	18	Na, TAA	95	28
4	**23a**	1	18	Na, TAA	120	8
5	**23a**	10	18	Na, TAA	95	16
6	**23a**	30	18	Na, TAA	95	Trace
7	**23a**	60	18	Na, TAA	95	Trace
8	**23a**	1	18	Pyrrolidine, DCM	50	Trace
9	**23a**	15	18	NaH, DMSO	RT	Trace
10	**23a**	15	18	NaH, DMSO	95	Trace
11	**Nitrile**	1	18	Na, TAA	95	9
12	**Nitrile**	10	18	Na, TAA	95	0.4
13	**Nitrile**	60	18	Na, TAA	95	Trace

The 'Initial Reagent' refers to the order of addition of the coupling reagents **23a** and 4-bromobenzonitrile, following the formation of the base. In an attempt to improve the yield, it was thought that a longer deprotonation time may be required (**Step A**), before addition of the second coupling reagent (**Step B**) in order to drive the reaction to completion. However, upon investigation, a shorter deprotonation time was found to be the most effective. In order to investigate the stability of the pyrrolinone ester in base, compound **23a** was added to a solution of NaO^{t}Am at 95 °C and samples were taken at 10-,30- and 60-minute intervals following addition, for analysis *via* ^{1}H NMR. It was observed

that at 30 minutes and beyond, degradation of **23a** had begun to occur (Figure 4.18). Thus, this may have affected the yield.

*Figure 4.18- ^{1}H NMR of the aromatic region of **23a** in $CDCl_3$, following 0, 10, 30 and 60 minutes of exposure to NaO^{t}Am (i.e. **Step A** in Table 4.3). Signs of degradation can be observed from 30 minutes onwards.*

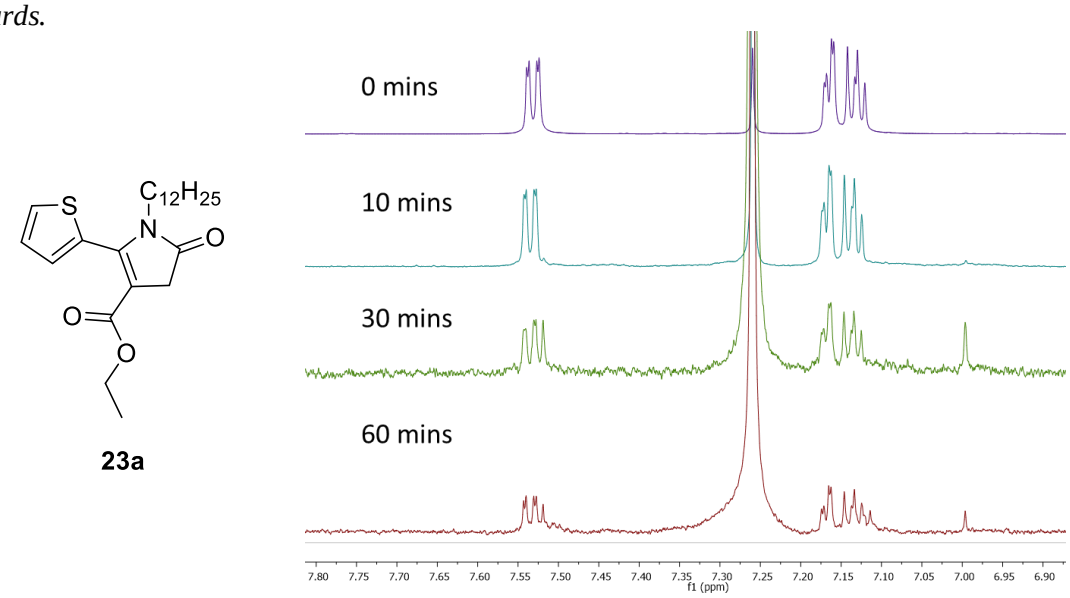

Alternative base/solvent systems, such as NaH/DMSO and pyrrolidine/DCM were also tested, however only a trace amount of product was detected. After several test reactions, it appeared that an initial addition of **23a** into NaO^{t}Am, followed by 4-bromobenzonitrile after 1 minute was most effective. Additionally, an increased reaction time of 18 h at 95 °C, was found to be the highest yielding (28%).

The optimised conditions were then applied to the synthesis of **26bc** and **26bd** (Scheme 4.19). However, it was observed that the condensation step gave a poor yield particularly when using the branched thienyl pyrrolinone ester **23b**. While condensation with benzonitrile gave **26bc** at a reasonable yield of 17%, it was noted that the brominated variant 4-bromobenzonitrile, gave **26bd** at a much lower yield (3%). However, regardless of this result, **26bd** was chosen for subsequent alkylation, as it had the potential for further bromination and therefore, could demonstrate the potential of these materials as monomers for subsequent polymerisation.

In order to expand the scope of the methodology, **26be** was also synthesised *via* condensation of **23b** and **25 (e)** based on previously reported conditions for the synthesis of an unsubstituted thieno[3,2-*b*]thiophene/furan asymmetric DPP derivative.[178] Following the formation of NaO^{t}Am, **23b** and **25** were heated at 120 °C for 2 h. Upon partial purification *via* column chromatography, **26be** was isolated as a pink oil at yield of 5%. In order to try and improve this yield, the reaction was repeated for a longer reaction time of 4 h, increasing the yield to 10%, which although still low, was sufficient to proceed.

Scheme 4.19- Synthetic route to fully asymmetric DPP derivatives.

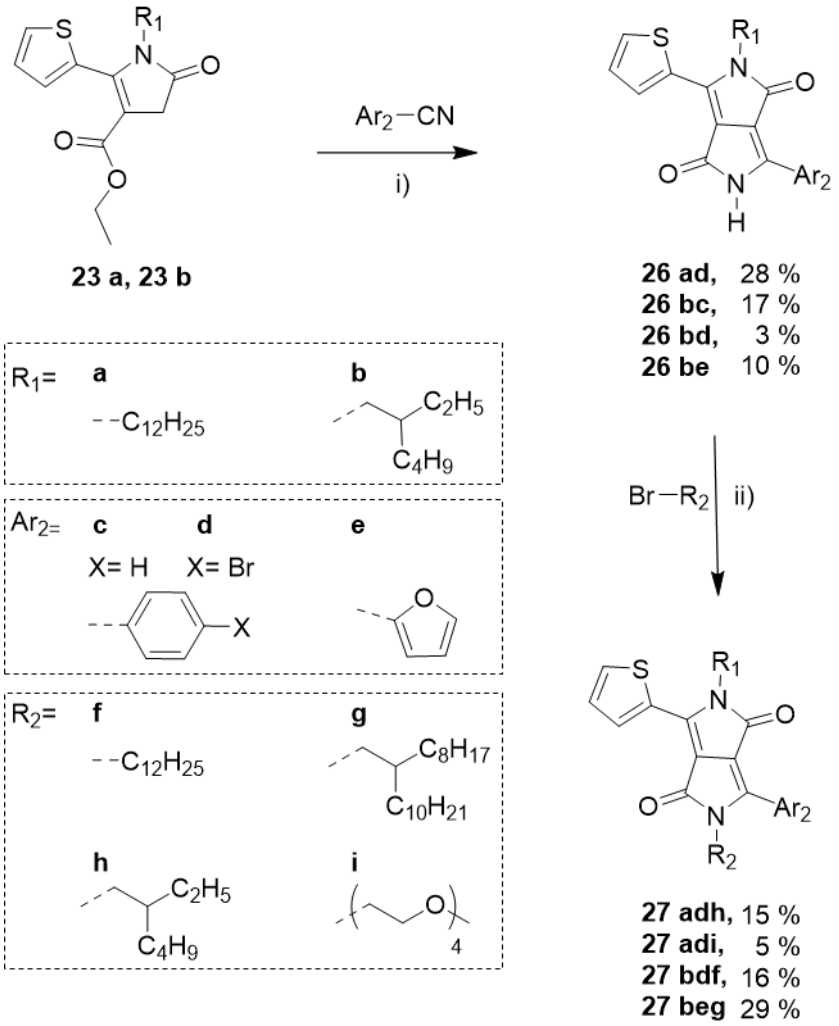

i) Na, 2-methyl-2-butanol, 95-120 °C, 2-18 h; ii) K_2CO_3, 18-crown-6, DMF, 120 °C, 18 h.

Derivatives **26ad**, **26bc** and **26bd** were purified *via* washing with MeOH. While **26ad** and **26bc** were obtained in high purity, some impurities remained in **26bd**. Derivative **26be** underwent partial purification *via* column chromatography however due to insufficient solubility and a high polarity (as a result of the short alkyl chain and the unsubstituted amide group), this led to large product loss on silica. Thus, **26bd** and **26be** were used in the next step with no further purification. In general, as previously reported for the synthesis of symmetric and asymmetric DPP cores, purification *via* column chromatography does not occur until subsequent di-alkylation, to ensure sufficient solubility.[60,176]

In general, condensation yields when using the linear chained **23a**, gave a higher yield compared to its branched counterpart **23b**. This may be due to the more crystalline nature of the linear chained compound, which allowed the product to precipitate out of solution more readily. One possible explanation for the poor yields observed may have been due to base sensitivity of **23a** and **23b**, as

observed in Figure 4.18. It is possible that through future investigation of alternative weaker bases such as LiO^{t}Bu, degradation of the pyrrolinone esters may be prevented and the yield can be improved. Due to time constraints, we were unable to investigate this in our study.

Following the synthesis of the asymmetric mono alkylated DPP cores, the final step was alkylation at the N-H position with an alternative chain. All alkylations were carried out under the same conditions based on a procedure by Bronstein.[60] The fully asymmetric structural DPP isomers were synthesised *via* alkylation of **26bd** with a dodecyl bromide chain, to afford **27bdf (T-DPP-P)** at a 16% yield. Likewise, **26ad** was then alkylated with 2-ethylhexyl bromide, to afford **27adh (P-DPP-T)** at a 15% yield. To demonstrate the scope of this new methodology, **26ad** was also alkylated with triethylene glycol 2-bromoethyl methyl ether, to afford **27adi** at a modest yield of 5%. Finally **26be** was alkylated with 9-(bromomethyl)nonadecane, to afford **27beg** at a 29% yield (Figure 4.19). However, it was observed that **27beg** showed poor stability upon contact to silica during purification and exposure to light in solution, leading to product degradation. The low yields following alkylation were in part due to obtaining the undesired *N*, *O*-alkylated side product, as well as the *N*, *N*-alkylated product. While it was possible to isolate the desired products *via* column chromatography, only small amounts could be obtained due to the similar polarities of the two compounds on silica. In general, it is often reported that the alkylation of DPP compounds are of low yield.[182]

Figure 4.19- Structures of the synthesised fully asymmetric DPP derivatives.

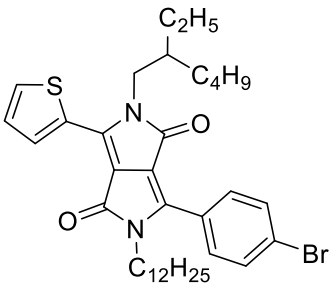

27bdf (T-DPP-P)

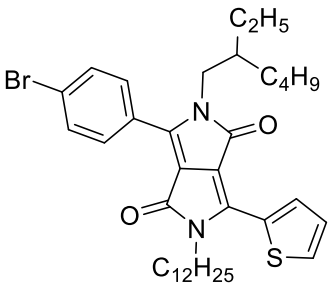

27adh (P-DPP-T)

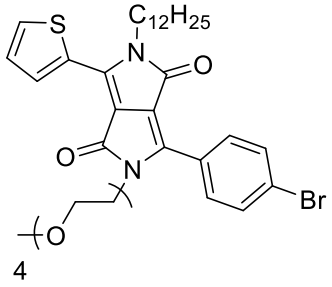

27adi

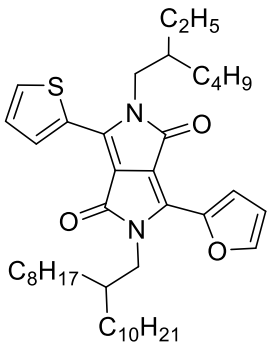

27beg

4.2.3.5 Synthesis of reference compounds

In order to study the effects of asymmetry on the optical properties of **T-DPP-P** and **P-DPP-T**, two symmetrical reference compounds **28 (P-DPP)** and **29 (T-DPP)** were also synthesised (Figure 4.20).

*Figure 4.20- Structures of reference compounds **P-DPP** and **T-DPP**.*

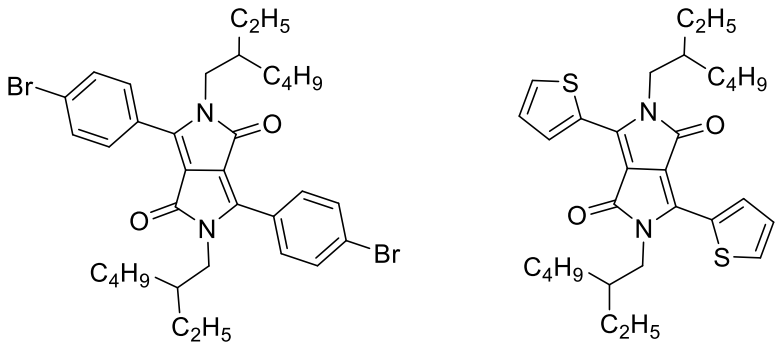

28 (P-DPP) **29 (T-DPP)**

While another member of our research group, Hayden Francis, prepared a sample of **P-DPP**, **T-DPP** was synthesised *via* the alkylation of thienyl DPP (Scheme 4.20) based on a procedure by Bronstein.[60]

*Scheme 4.20- Synthesis of reference compound **29 (T-DPP)**.*

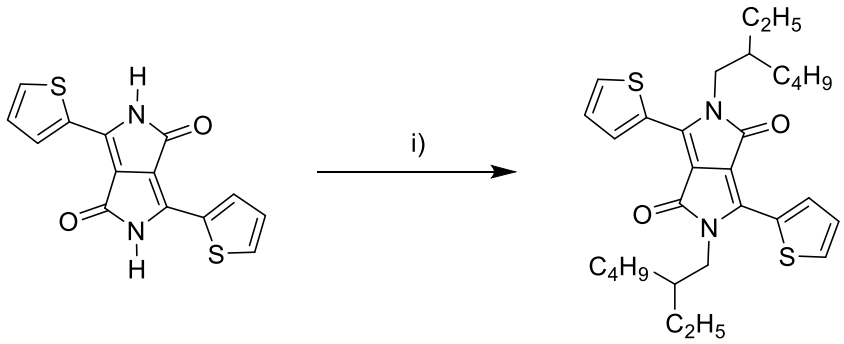

Thienyl DPP **29 (T-DPP)**

26 %

i) 2-Ethylhexyl bromide, K_2CO_3, 18-crown-6, DMF, 120 °C, 48 h.

Thienyl DPP underwent alkylation using 2-ethylhexyl bromide in DMF. The crude purple solid was purified *via* column chromatography followed by recrystallisation in EtOH, to afford the product **29** as dark shiny purple crystals (26%).

4.2.3.6 Optical and theoretical properties

The optical properties of **P-DPP**, **T-DPP**, **T-DPP-P** and **P-DPP-T** are shown below in the UV-vis spectra in chlorobenzene (~4 μg/mL*)* (Figure 4.21).

Figure 4.21- Normalised solution (chlorobenzene ~4 μg/mL) absorption spectra for ***P-DPP***, ***T-DPP,*** ***T-DPP-P*** *and* ***P-DPP-T.*** *Path length 10 mm. The molecular molar extinction coefficients (ε) were 110637 cm^{-1} L mol^{-1}, 115389 cm^{-1} L mol^{-1} and 90525 cm^{-1} L mol^{-1} for* ***P-DPP***, ***T-DPP/T-DPP-P*** *and* ***T-DPP*** *respectively.*

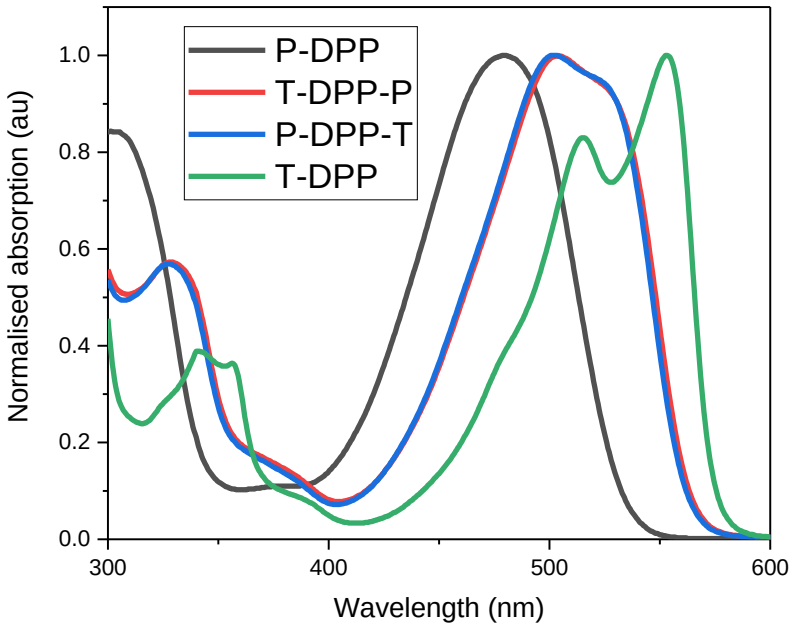

The absorption spectra of **T-DPP-P** and **P-DPP-T** were observed to be almost identical, as a result of the compounds being structural isomers. In comparison the **P-DPP** absorption was blue shifted and broad, which was likely as a result of the greater torsional angle between the DPP core and phenyl moieties. On the other hand, **T-DPP** absorption was the most red-shifted and sharpest of the structures, likely due to the enhanced conjugation as a result of the smaller torsional angle between the thiophene units and DPP core. Isomers **T-DPP-P** and **P-DPP-T** absorptions lied between that of **P-DPP** and **T-DPP**, as the compounds contain one thiophene and one phenyl moiety each.

Theoretical DFT calculations[183] were performed to give the geometry optimised molecular energy levels (the alkyl chains were replaced with methyl groups for simplicity). The HOMO and LUMO levels calculated for the structural isomers **T-DPP-P**/**P-DPP-T** were -5.32 eV and -2.78 eV. In comparison **P-DPP** and **T-DPP** calculated HOMO and LUMO levels were observed at -5.51 eV, -2.86 eV and -5.13 eV, -2.68 eV respectively. Again, the HOMO/LUMO levels of the asymmetric isomers were

observed to lie in-between that of the two symmetric DPP reference compounds, demonstrating the ability to fine tune the absorption and band gap *via* synthesis of asymmetric DPP derivatives.

4.2.3.7 Conclusion

In conclusion, a novel methodology towards fully asymmetric DPP derivatives was established and the first reported pair of asymmetric structural DPP isomers (**T-DPP-P** and **P-DPP-T**) were synthesised. We have demonstrated it is possible to systematically design and synthesise structural isomers of asymmetric DPP units. We have also shown that the scope of this methodology extends to further aromatic groups such as furan, and the possibility to introduce new functionalities to these compounds *via* incorporation of alternating OEG and alkyl chains.

It was observed that for **T-DPP-P**/**P-DPP-T**, their UV-vis solution absorptions as well as HOMO and LUMO levels, lie in-between that of their symmetrical counterparts, **P-DPP** and **T-DPP**. This shows it is possible to fine tune properties such as absorption and optical band gap *via* such design strategies.

As yields of the key condensation step between the alkylated thienyl pyrrolinone esters (**23a** and **23b**) and aryl nitriles could often be low, future work should focus on the optimisation of this step. This would allow future investigation on the effect of alkyl-aryl positioning, on the properties and performance of DPP based conjugated polymers and small molecules, in optoelectronic devices. Regardless of low yields, this new method allows the synthesis of previously unavailable DPP derivatives, allowing the possibility to greatly broaden the library of existing DPP compounds. Therefore, this opens new horizons towards novel and unique DPP structures and their application in optoelectronics.

4.2.4 Alkylated Thienyl Pyrrolinone Ester Strategy

Following the successful synthesis of the alkylated thienyl pyrrolinone esters **23a**, **23b** and **23c**, it was possible to attempt to synthesise the DPP dimer *via* a new proposed synthetic strategy (Scheme 4.21). While this strategy was similar to those outlined previously in *Subsection 4.2.1* and *Subsection 4.2.2*, here with the addition of a solubilising alkyl chain on the pyrrolinone ester, should allow characterisation of the reaction products *via* NMR.

This new route towards the dimer involves the condensation between 2 equiv. of an alkylated thienyl pyrrolinone ester and 1 equiv. of 2,5-dicyanothiophene under basic conditions, to give the partially alkylated DPP dimer.

Scheme 4.21- Proposed synthesis of the partially alkylated DPP dimer via condensation between an alkylated thienyl pyrrolinone ester and 2,5-dicyanothiophene.

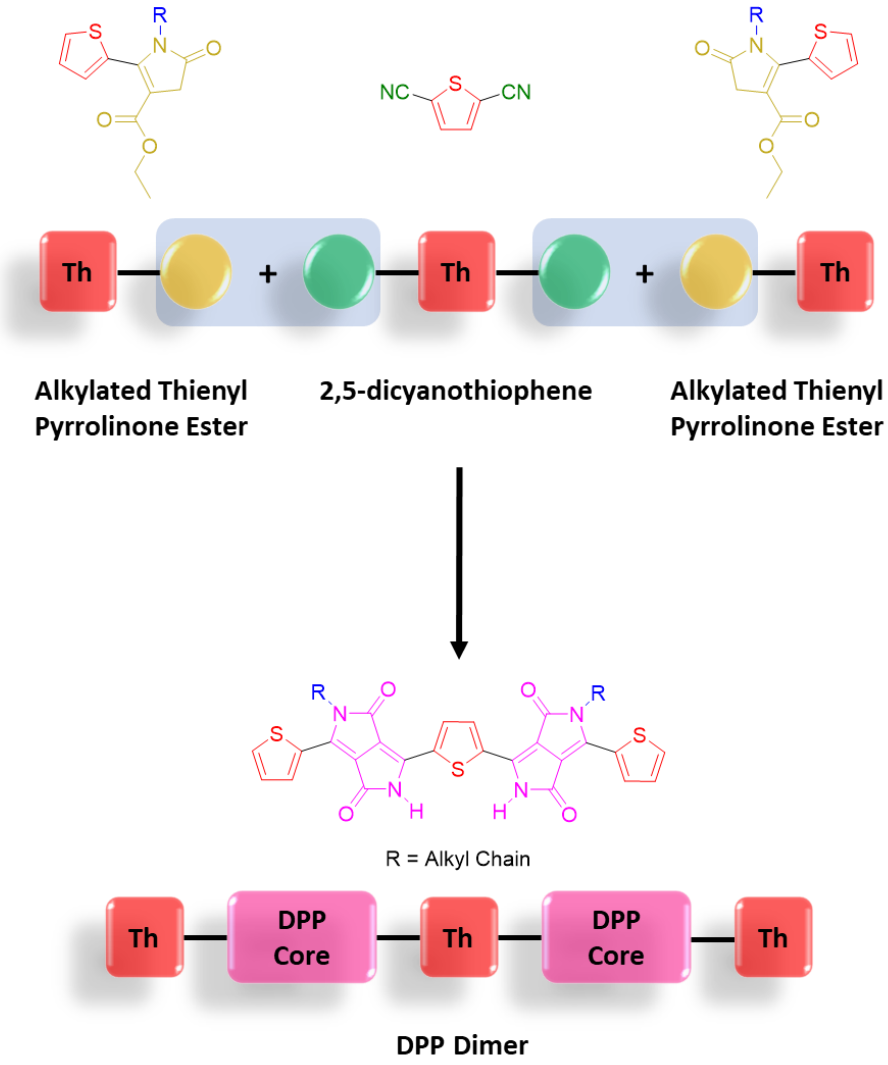

The initial test reactions were conducted using di-nitrile **10**, due to its commercial availability and low cost. If optimised reaction conditions were obtained, the reaction could then be later repeated with **7**, to give the target thienyl-based DPP dimer.

4.2.4.1 Synthetic attempts towards the DPP dimer

To begin, 2.5 equiv. of **23b** underwent condensation with 1 equiv. of **10** using an alkoxide base, in an attempt to synthesise the partially alkylated DPP dimer **30** (Scheme 4.22). Thienyl pyrrolinone ester **23b** was chosen due to its superior solubility, as a result of its branched alkyl chain. Following the formation of the base, **23b** was added to the reaction mixture followed by compound **10** after 1 minute. The reaction was then heated for 2 h at 95 °C, however upon work up ^{1}H NMR revealed that no reaction had taken place. The reaction was then repeated for a longer reaction time of 18 h (Table 4.4). Upon work up, crude ^{1}H NMR revealed the presence of starting material, as well as several new broad uncharacterizable peaks. It was observed *via* TLC, that as well as excess **23b**, there was a trace amount of unknown product. The product spot was pink, which is characteristic of alkylated DPP derivatives. The crude material then underwent column chromatography and while the product was isolated, the fraction was of such small quantity that the obtained ^{1}H NMR, was too weak to determine the structure.

*Scheme 4.22- Unsuccessful synthetic attempt towards **30** via condensation between **23b** and **10**.*

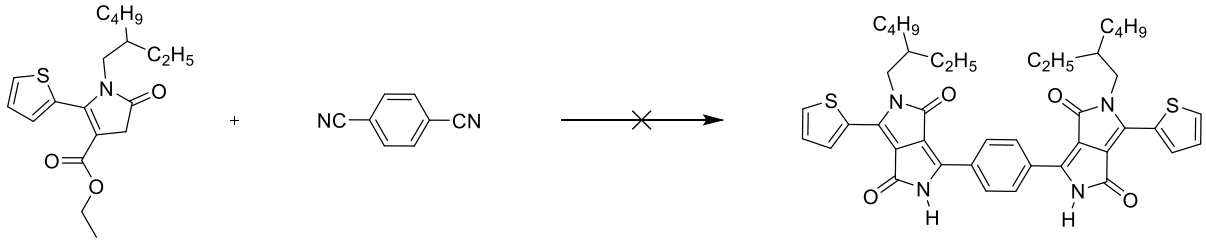

23b **10** **30**

*Table 4.4- Summary of synthetic attempts towards the synthesis of **30** via condensation between **23b** and **10**. Reactions were conducted in the presence of 1 equiv. of **10** at 95 °C.*

Entry	Equiv. of 10	Equiv. of 23b	Reaction Time (h)	Reaction Conditions	Equiv. of Na	Outcome
1	1	2.5	2	Na, TAA	9.4	Starting material
2	1	2.5	18	Na, TAA	9.4	Starting material and trace amount of unidentifiable pink product

As discussed previously in *Subsection 4.2.3*, the branched chained pyrrolinone ester **23b**, generally showed poor reactivity towards aromatic nitriles compared to the linear chained **23a**. Thus, the condensation was also repeated using 2.5 equiv. of **23a** and 1 equiv. of **10**, in an attempt to synthesise the DPP dimer **31** (Scheme 4.23).

*Scheme 4.23- Unsuccessful synthetic attempt towards **31** via condensation between **23a** and **10**. The reaction was conducted in the presence of 9.4 equiv. of Na.*

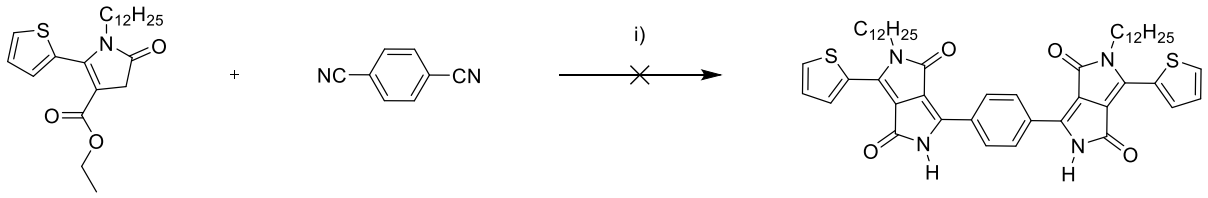

23a **10** **31**

i) Na, 2-methyl-2-butanol, 95 °C, 18 h.

The reaction was carried out based on the optimised reaction conditions for the synthesis of **26ad**, as discussed in *Subsection 4.2.3, Table 4.3*. The reaction was heated for 18 h at 95 °C, and upon work up, a dark purple DPP-like solid was isolated *via* filtration. Crude ^{1}H NMR in $CDCl_3$ revealed the presence of starting material **23a**, as well as several broad uncharacterizable peaks (Figure 4.22).

*Figure 4.22- ^{1}H NMR in $CDCl_3$ of the aromatic region of the crude mixture when attempting to synthesise **31**. The 3 peaks indicate the presence of starting material **23a**. There are also several unidentifiable broad peaks visible.*

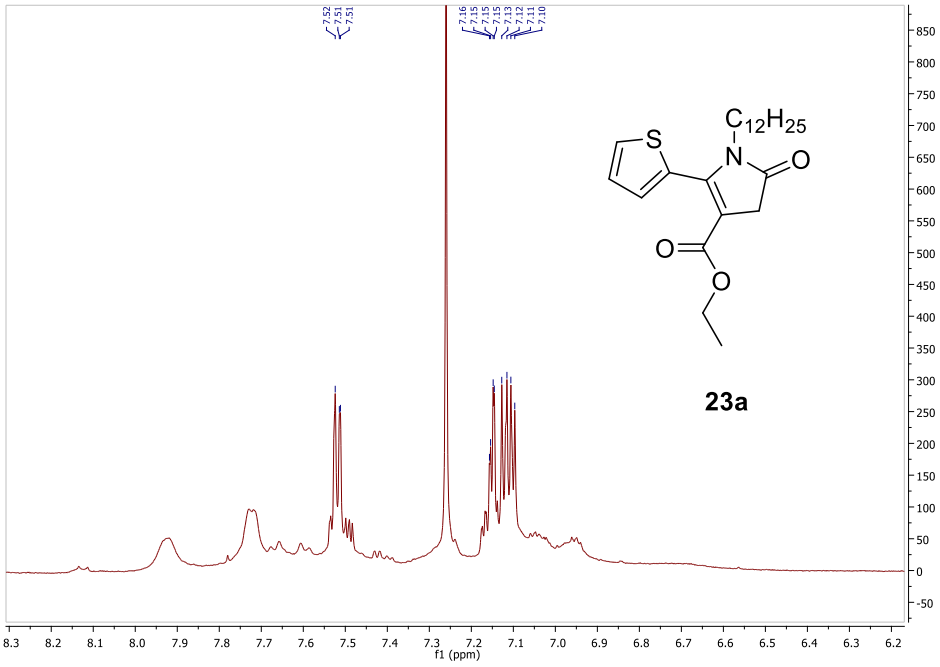

As observed *via* TLC, as well as excess **23a**, an unknown product was also present in the crude mixture. This fraction was isolated *via* column chromatography to give a trace amount of a dark purple/pink solid. While we were unable to obtain a mass spec for the sample, by ^{1}H NMR in DMSO-d_6 (Figure 4.23), it became apparent that this was not dimer **31**. Instead, it was likely that a single asymmetric DPP compound with a nitrile group on the phenyl unit (**32**) had been made, in which **23a** had only reacted on one side of di-nitrile **10**. In addition, some broad baseline impurities were also observed.

The formation of **32** was supported by the integration of the spectrum as seen in Figure 4.23. We believe that the two doublets and one triplet present in the spectrum (8.94 ppm, 8.17 ppm and 7.45 ppm, respectively) that integrate to one proton each, most likely correspond to the thienyl protons labelled (**A**), while the two doublets (8.59 ppm and 8.06 ppm) that integrate to two protons each, correspond to the four protons on the phenyl ring labelled (**C**). Finally, the singlet at 11.53 ppm, integrated to one and is characteristic of N-H (**B**) (as observed for the asymmetric mono-alkylated DPP cores synthesised in *Subsection 4.2.3*).

While DPP nitrile **32** can undergo hydrolysis to form the DPP amide, integration of the spectrum did not match this compound. The DPP amide can then undergo further hydrolysis to give the DPP carboxylic acid, however based upon the mass spec obtained for the similar reaction in Scheme 4.7, we believe it is more likely that the nitrile was made. In any case, all possible outcomes indicate that the reaction did not go to completion, thus we ceased to investigate this route.

*Figure 4.23- ^{1}H NMR in DMSO-d_6 of the aromatic region of the isolated product fraction when attempting to synthesise **31**, likely to possess the structure of **32**.*

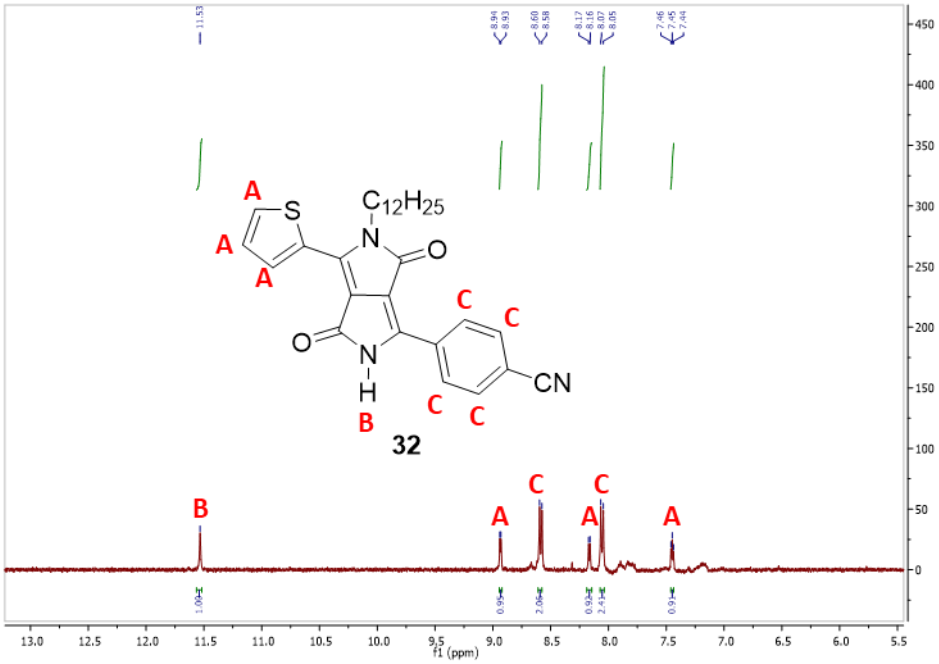

It was thought that perhaps the thienyl pyrrolinone ester may be degrading in the NaO^{t}Am base as observed previously in Figure 4.18, before the reaction could reach completion. Thus, it was decided to test an alternative base of LiO^{t}Bu, which is of weaker strength. Due to a lack of compound **23a** and **23b** as well as time constraints, thienyl pyrrolinone ester **23c** was used in the test reaction. However, as nitrile **7** had been recently re-synthesised, it was used in the place of the test nitrile **10** (Scheme 4.24).

Compound **23c** (2.5 equiv.) followed by di-nitrile **7 (**1 equiv.) were added to LiO^{t}Bu in 2-methyl-2-butanol, and the reaction mixture was heated to 95 °C for 18 h. Upon work up, a purple solid was isolated *via* filtration and similarly to the previous attempt, crude ^{1}H NMR in $CDCl_3$ revealed the presence of excess starting material **23c**, as well as several broad uncharacterizable peaks.

*Scheme 4.24- Unsuccessful synthetic attempt towards **33** via condensation between **23c** and **7**. The reaction was conducted in the presence of 9.4 equiv. of LiO^{t}Bu.*

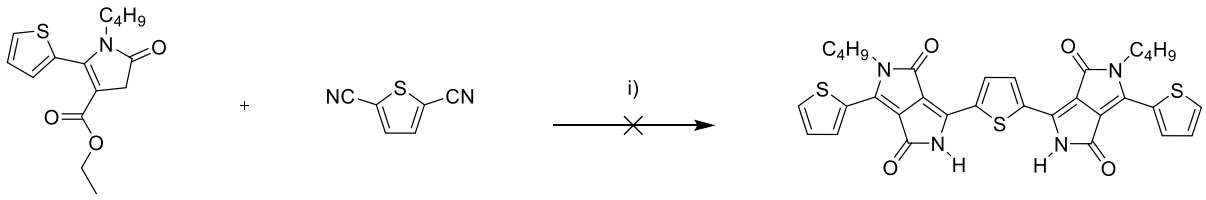

23c **7** **33**

i) LiO^{t}Bu, 2-methyl-2-butanol, 95 °C, 18 h.

As before, a trace amount of an unknown pink product was observed by TLC and isolated *via* column chromatography. However, much like the previous attempts, ^{1}H NMR in DMSO-d_6 suggested that **23c** had only reacted on one side of di-nitrile **7**, to give DPP nitrile **34** (Figure 4.24). In addition, several broad baseline impurities were observed. Once again, while **34** can then undergo hydrolysis to give the DPP amide, integration of the NMR spectrum did not match this compound.

As previously, while we were unable to obtain a mass spec for the sample, the formation of DPP nitrile **34** was supported by integration of the spectrum as seen in Figure 4.24. We believe that the two doublets and one triplet (8.81 ppm, 8.09 ppm and 7.40 ppm, respectively) that integrate to one proton each, most likely correspond to the thienyl protons labelled (**A**), while the two doublets (8.17 ppm and 7.84 ppm) that integrate to one proton each, correspond to the two thienyl protons labelled (**C**). The singlet at 11.43 ppm that integrates to one proton, most likely corresponds to the N-H labelled (**B**).

*Figure 4.24- ^{1}H NMR in DMSO-d_6 of the aromatic region of the isolated product fraction when attempting to synthesise **33**, likely to possess the structure of **34**.*

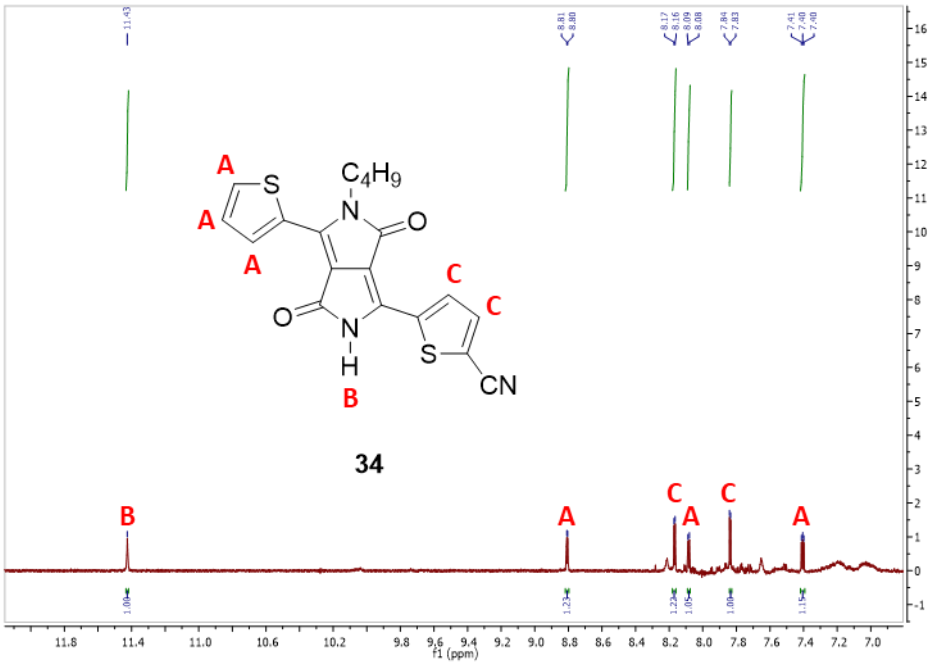

As before, while the integration of the spectrum may also indicate that the DPP carboxylic acid was made instead, ultimately either of these outcomes suggested that once again the reaction did not go to completion. Therefore, following this unsuccessful result, it was concluded that an alternative synthetic strategy should be explored.

It is to be noted, that compared to the previous synthetic strategies explored in *Subsection 4.2.1* and *Subsection 4.2.2*, all compounds within this current strategy showed good solubility in both the reaction and NMR solvents. While previously, the reaction outcomes were often ambiguous, we are now aware that only partial reaction is occurring. Thus, moving forward, any further strategies towards the dimer should also include solubilising chains prior to the key coupling step.

4.2.5 DPP-Nitrile Strategy

It was noted, that for both the previous strategy and the strategy outlined in *Subsection 4.2.1*, a frequent possible outcome of the condensation attempts was partial reaction, in which the thienyl pyrrolinone ester only reacted on one side of the chosen di-nitrile, to give a DPP-nitrile product. Thus, moving forward it may be possible, that if a di-alkylated DPP-nitrile could be synthesised, it can then undergo condensation with a thienyl pyrrolinone ester to give the partially alkylated DPP dimer (Scheme 4.25).

Scheme 4.25- Proposed synthesis of the partially alkylated DPP dimer via condensation between DPP nitrile and thienyl pyrrolinone ester.

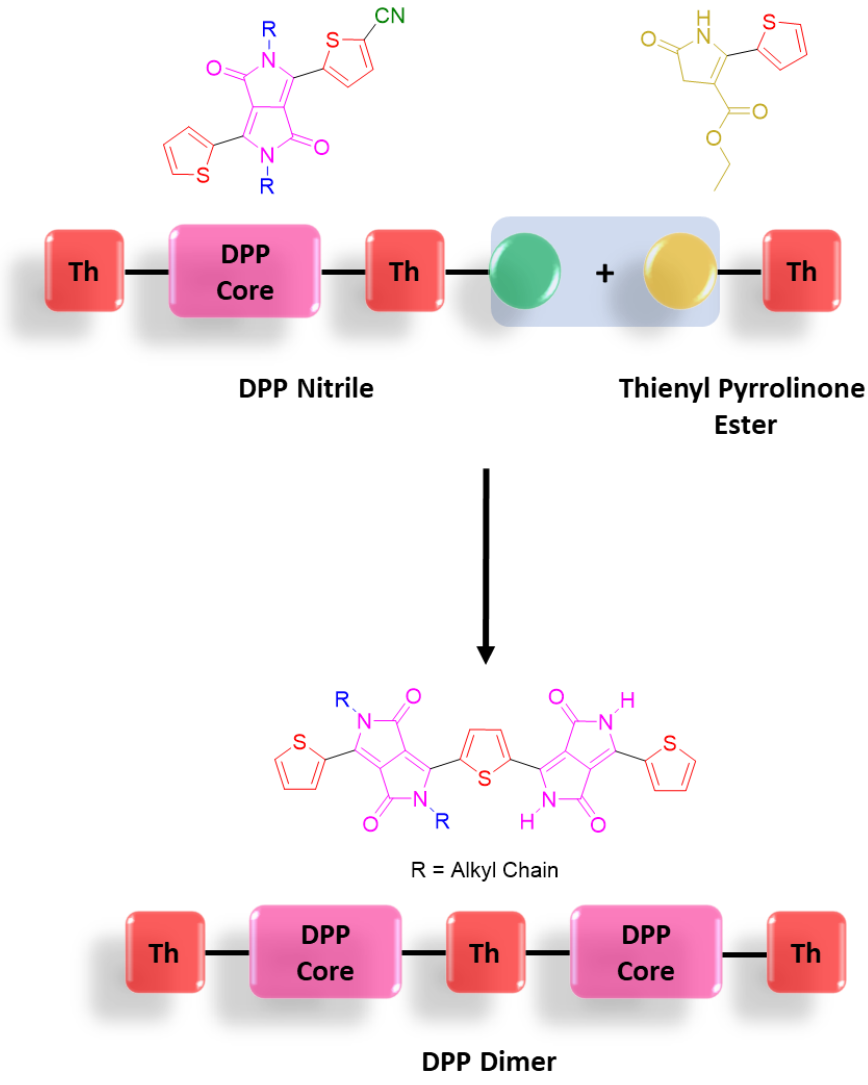

Thus, such a strategy relies on only one condensation to occur to give the desired product. In addition, as one of the DPP cores will already be di-alkylated, solubility of the dimer will be improved, making subsequent alkylation more likely to succeed.

4.2.5.1 Synthesis of the DPP-nitrile

To begin, it was required to synthesise the DPP-nitrile. This was done *via* direct cyanation of mono-brominated DPP (**35**) using Cu(I)CN in DMF, based on a procedure by Wang *et al* (Scheme 4.26).[184] Compound **35** was previously synthesised in *Chapter II.*

*Scheme 4.26- Synthesis of **36**.*

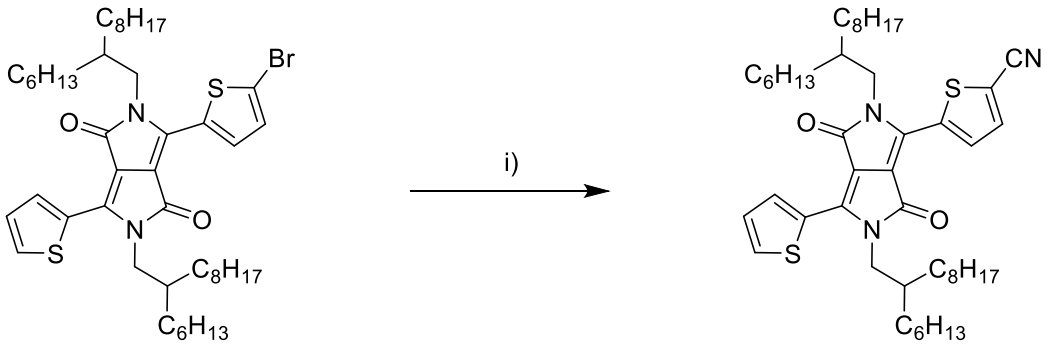

35 **36**

66 %

i) Cu(I)CN, DMF, 130 °C, 18 h.

The reaction was heated at 130 °C for 18 h. Once the reaction had cooled to RT, the inorganic salts were removed *via* silica plug. The crude product was then purified *via* column chromatography to yield **36** as a shiny purple/green solid (66%).

4.2.5.2 Synthetic attempt towards the DPP dimer

Following the synthesis of the di-alkylated DPP-nitrile **36**, it was possible to attempt to synthesise the DPP dimer.

Compound **36** underwent condensation with compound **4** under basic conditions using NaO^{t}Am as the base, in an attempt to synthesise DPP dimer **37**. To try and drive the reaction to completion, a large excess of compound **4** (20 equiv.) to **36** (1 equiv.) was used (Scheme 4.27). The reaction was heated to 95 °C and stirred for 2 h.

*Scheme 4.27- Unsuccessful synthetic attempt towards **37** via condensation between **36** and **4**. The reaction was conducted in the presence of 20 equiv. of Na.*

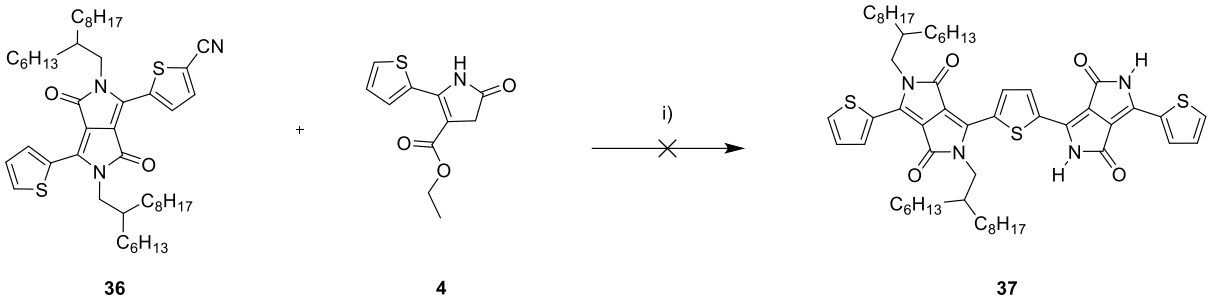

36 **4** **37**

i) Na, 2-methyl-2-butanol, 95 °C, 4 h.

The reaction was monitored *via* TLC however no new product could be detected after 2 h. The reaction was then left to stir for an additional 2 h. Upon workup, ^{1}H NMR revealed that no reaction had occurred and only starting material was observed.

While other reaction conditions were yet to be tested, due to a lack of compound **36** and the considerable effort towards synthesising the nitrile, it was decided that an alternative method should be sought. In general, it appeared that all strategies involving condensation between thienyl pyrrolinone esters (i.e. **4**, **18**, **23a**, **23b** and **23c**) and aromatic nitriles (i.e. **7**, **10** and **36**) had failed to produce the dimer in the key coupling step. Therefore, moving forward alternative coupling methods (i.e. cross-coupling) should be explored.

4.2.6 SDPP Strategy

Following the previous unsuccessful synthetic strategies towards the DPP dimer, involving condensation between a mono/di-thienyl pyrrolinone ester and an aromatic mono/di-nitrile, alternative coupling methods were sought.

As traditional methods such as Stille and Suzuki cross-couplings were not synthetically viable, a more unconventional approach was to be taken. A unique class of asymmetric DPP compounds are thioether DPP derivatives (SDPP), as reported by Metten,[172] which are synthesised *via* the cyclization of pyrrolinone esters with isothiocyanates under basic conditions. These compounds can subsequently undergo cross-coupling with various arylboronic acids *via* the Liebeskind-Srogl reaction.[185] This is a palladium catalysed cross-coupling (similar to Suzuki) between a heteroaromatic thioether and a boronic acid, under neutral reaction conditions, mediated by copper(I) thiophene-2-carboxylate. Thus, in a new proposed synthetic strategy, if a mono-alkylated thienyl SDPP could be synthesised, it can then undergo a double Liebeskind-Srogl cross-coupling with 2,5-thiophenediboronic acid, to give the partially alkylated DPP dimer (Scheme 4.28).

*Scheme 4.28- Proposed synthetic route to the target DPP dimer via a Liebeskind-Srogl cross-coupling between **SDPP** and 2,5-thiophenediboronic acid.*

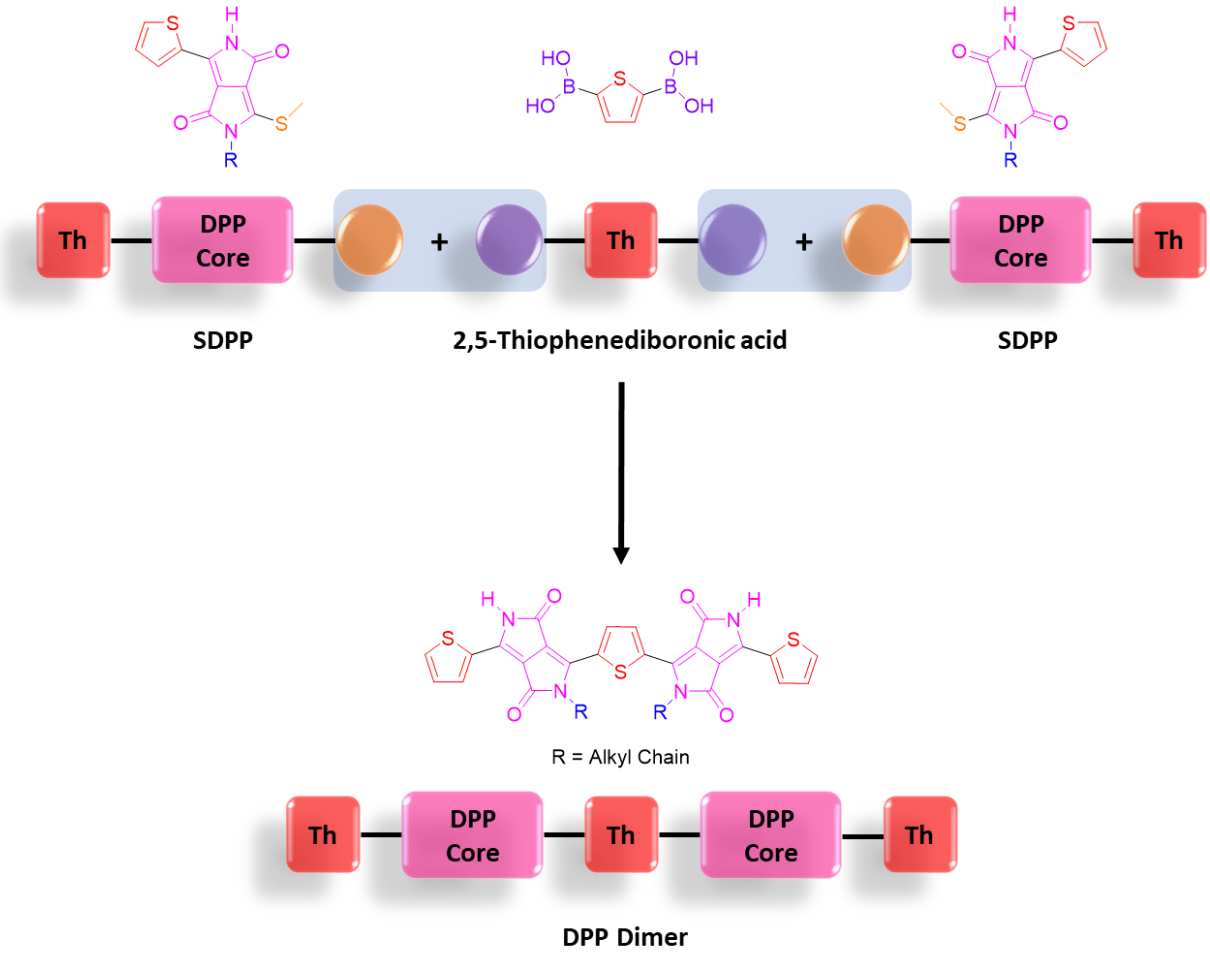

4.2.6.1 Synthesis of SDPP

The proposed synthetic strategy began with the synthesis of a novel thienyl-SDPP derivative, based on Metten's procedure (Scheme 4.29).[172] Compound **4** (1 equiv.) was added to a mixture of NaH (2 equiv.) in DMSO and was stirred for 15 minutes at RT. After deprotonation, this was followed by the addition of hexyl isothiocyanate and the reaction was left to stir for 6 h, to give an intermediate thioanimal. After cooling the reaction mixture down to 0 °C, MeI was added in one portion. The reaction was then allowed to warm to RT overnight.

*Scheme 4.29- Unsuccessful synthetic attempt towards **38**.*

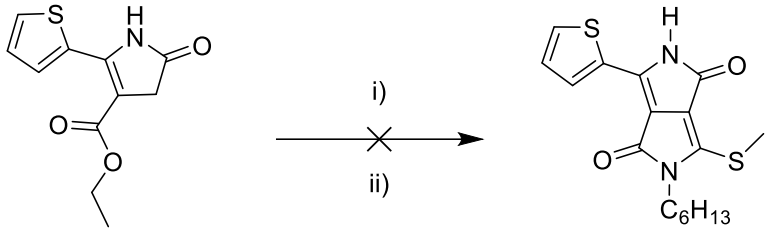

4 **38**

i) NaH (2 equiv.), hexyl isothiocyanate, DMSO, RT, 6 h; ii) MeI, 0 °C- RT, 12 h.

Upon work up, a golden crystalline product was isolated *via* column chromatography however after analysis by ^{1}H NMR, it appeared that the compound was not **38** as desired (Figure 4.25). Instead, it was suspected that only partial reaction had occurred to give the intermediate *S-alkylated* thioanimal **39**.

*Figure 4.25- ^{1}H NMR in CD_2Cl_2 of the isolated product fraction when attempting to synthesise **38**, likely to possess the structure of **39**. Full assignment of the spectra can be found in the experimental.*

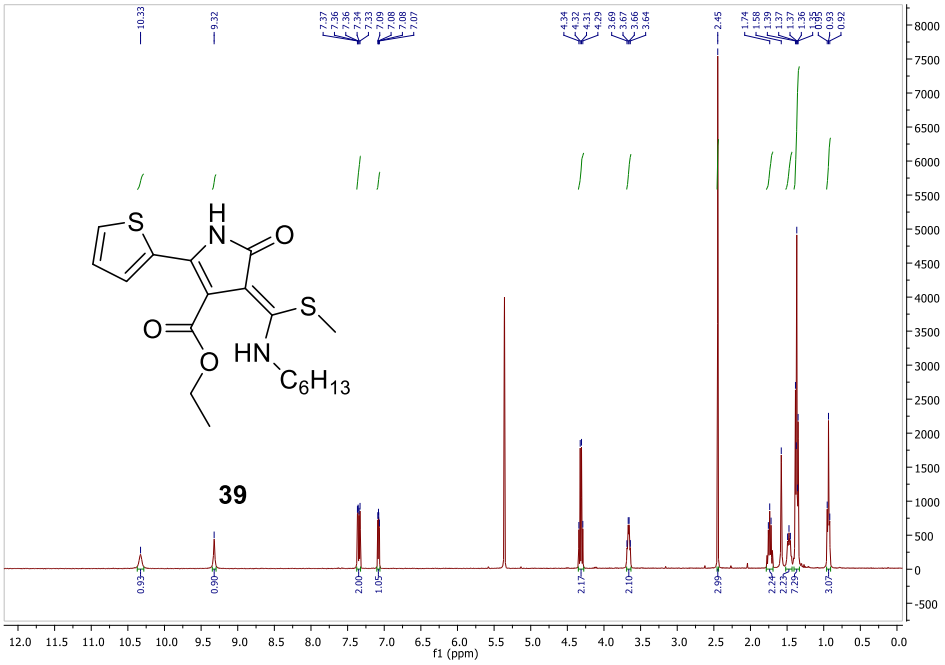

This was further supported by analysis *via* mass spectrometry and compound **39** was observed as the major product (TOF MS ASAP+ *m/z* 395.1459 $[M+H]^+$) (Figure 4.26).

*Figure 4.26- TOF MS ASAP+ analysis of the undesired compound **39**; m/z 395.1459.*

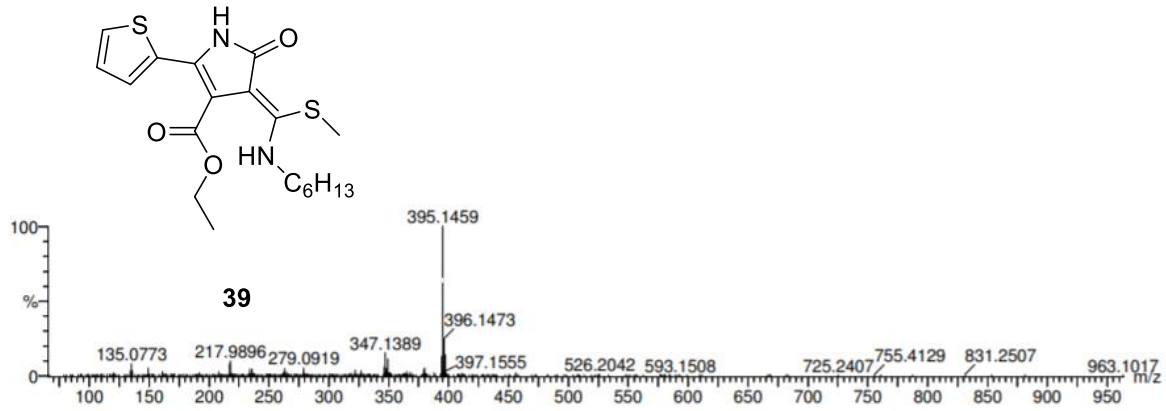

In an attempt to drive the reaction to completion, the synthesis was repeated with an excess of amount of NaH (4 equiv.). This was to ensure full deprotonation and subsequent cyclization of the intermediate thioanimal **39** (Scheme 4.30).

*Scheme 4.30- Synthesis of mono-alkylated **38** and di-alkylated **40** SDPP derivatives.*

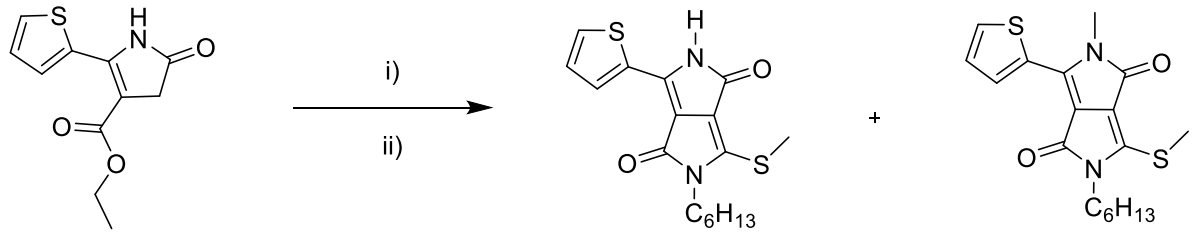

i) NaH (4 equiv.), Hexyl isothiocyanate, DMSO, RT, 6 h; ii) MeI, 0 °C- RT, 12 h.

Upon work up, TLC revealed that the crude mixture consisted of starting material, as well as two fluorescent yellow products which were isolated *via* column chromatography. The first product to elute from the column was an orange solid. After analysis *via* ^{1}H NMR, it appeared that the excess NaH used in the reaction, had resulted in some di-alkylation of the SDPP derivative to give compound **40** (7%). This was further supported *via* mass spec (TOF MS ASAP+ *m/z* 363.1202 $[M+H]^+$) (Figure 4.27).

Figure 4.27- TOF MS ASAP+ analysis of the di-alkylated compound ***40****; m/z 363.1202.*

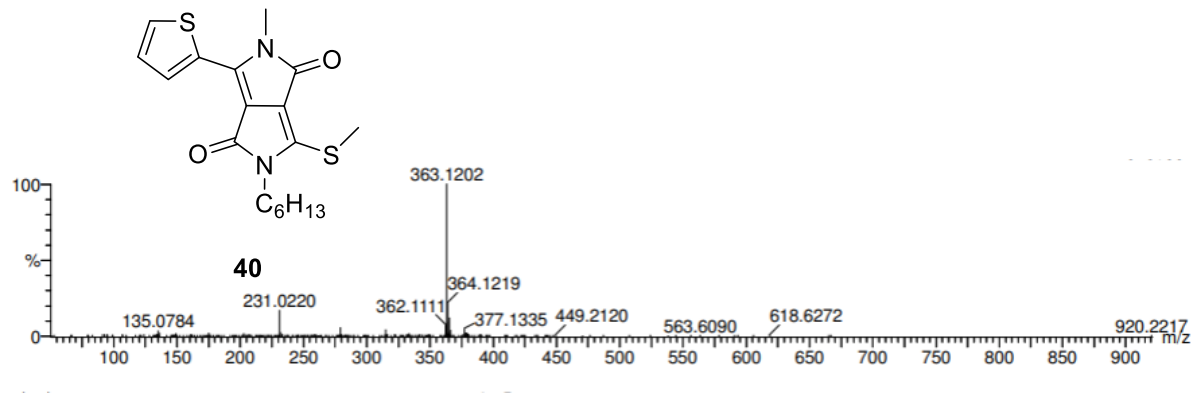

The second product to elute from the column was a shiny dark green, crystalline solid. Analysis *via* ^{1}H NMR suggested that the structure of the compound was of the desired SDPP **38** (21%). This was further supported by *via* mass spec (TOF MS ASAP+ *m/z* 349.1032 $[M+H]^{+}$) and in addition, X-ray crystallographic analysis† (single crystals grown from $CHCl_3$: MeOH, Figure 4.28).

Figure 4.28- Chemical and crystal structure of **38**. *Crystals grown from $CHCl_3$: MeOH.*

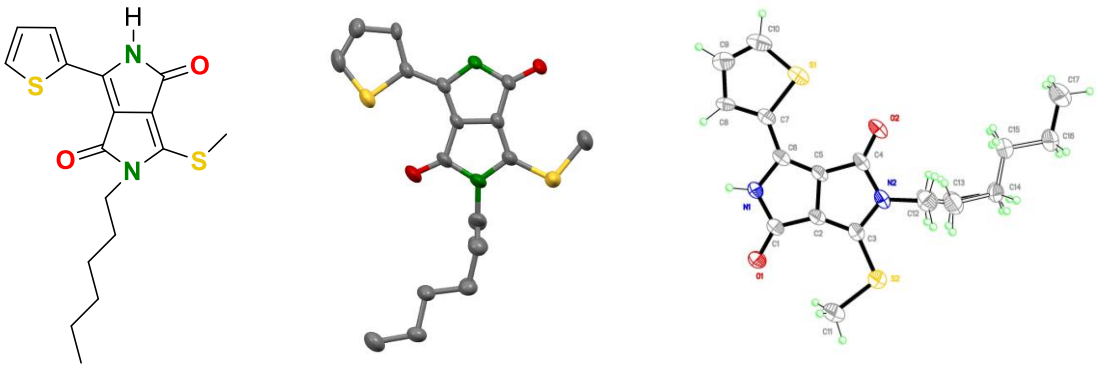

†X-ray structure determined by Dr Andrew Bond, University of Cambridge.

4.2.6.2 Synthetic attempt towards the DPP dimer

Following the synthesis of the SDPP derivatives, it was possible to attempt to synthesise the DPP dimer *via* the Liebeskind-Srogl reaction. We decided to use the di-alkylated SDPP derivative **40** in the initial test reaction instead of **38**, as the additional methyl group would provide increased solubility, decreased polarity and therefore, easier purification of the product.

Thus, a palladium-catalysed Liebeskind-Srogl cross-coupling between **40** (2.5 equiv.) and 2,5-thiophenediboronic acid (**41**) (1 equiv.) was attempted to give the DPP dimer **42**, based on a procedure by Metten (Scheme 4.31).[172]

*Scheme 4.31- Unsuccessful synthetic attempt towards **42** via a Liebeskind-Srogl cross-coupling between **40** and **41**.*

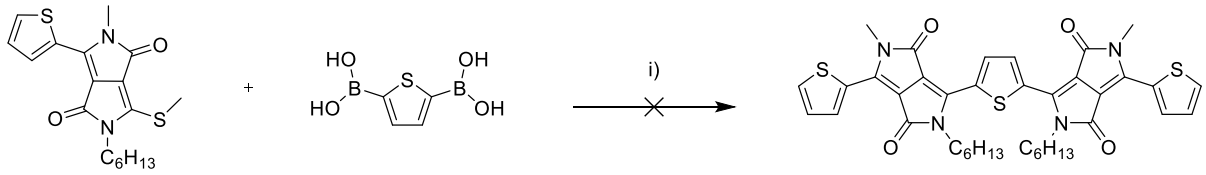

40 **41** **42**

i) Copper(I) thiophene-2-carboxylate, $Pd(PPh_3)_4$, THF, 50 °C, 18 h.

Upon work up, crude ^{1}H NMR revealed the presence of excess **40** in addition to an unknown product, which was isolated *via* column chromatography, to give a pink solid. Analysis of the product *via* ^{1}H NMR, suggested that compound **40** had only reacted on one side of **41**, to give the single DPP unit **43**, in which deborylation had occurred on the remaining boronic acid group. (Figure 4.29). Some trace of starting material was also visible in the spectrum.

*Figure 4.29- ^{1}H NMR in $CDCl_3$ of the isolated product fraction when attempting to synthesise **42**, likely to possess the structure of **43**.*

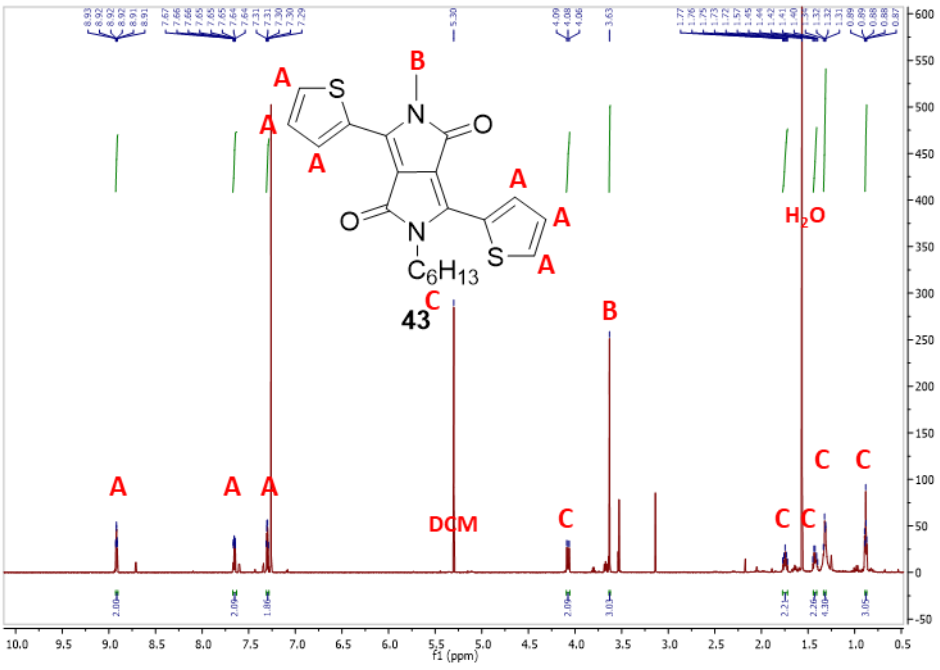

In the aromatic region of the spectrum, the three peaks observed at 8.92, 7.66 and 7.30 ppm that integrate to two protons each, likely correspond to the thienyl protons labelled **(A)**. Thus, this suggested that only a single DPP unit had been made, as the protons of the central thiophene unit on dimer **42**, were not present. In addition, the singlet at 3.63 ppm that integrates to three protons, most likely corresponds to the methyl group labelled **(B)**. Finally, the multiplets at 4.08 (two protons), 1.75 (two protons), 1.42 (two protons), 1.32 (four protons) and 0.88 (three protons) ppm, correspond to the thirteen protons on the hexyl chain labelled **(C)**. The peaks at 5.30 ppm and 1.57 ppm were residue solvents DCM and H_2O, respectively. This theory was further confirmed *via* mass spectrometry, in which **43** was found to be the major product (MS-TOF (ES+) *m/z* 399.1191 $[M+H]^+$) (Figure 4.30).

*Figure 4.30- MS-TOF analysis of the undesired compound **43**; m/z 399.1191.*

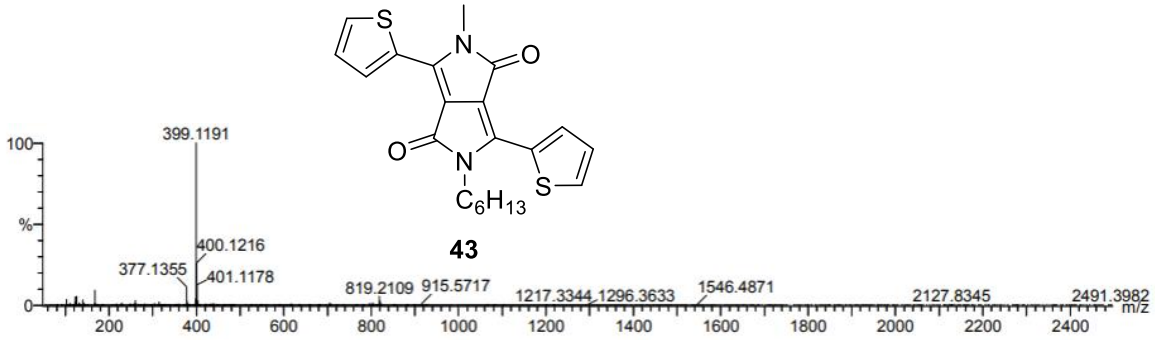

While alternative reaction conditions were yet to be tested, due to time constraints and a lack of starting material, no further tests could be attempted.

4.3 Conclusions

In conclusion, several different synthetic strategies towards the DPP dimer were explored. In particular, the key coupling step proved to be highly problematic.

The first strategy attempted, involved the synthesis of a previously reported thienyl pyrrolinone ester (**4**), which underwent condensation with 2,5-dicyanothiophene (**7**) or test di-nitrile (**10**). While several reaction conditions were tested, most of the outcomes consisted of only partial reactivity, in which compound **4** reacted on only one side of the di-nitrile. It was also noted that the reaction products were of poor solubility, resulting in difficult characterisation.

This was then followed by a reversed strategy, in which a novel di-thienyl pyrrolinone ester (**18**) was synthesised and underwent condensation with 2-cyanothiophene (**14**), based on a similar synthesis by Ahner *et al.*[173] However due to the poor solubility of compound **18**, all reaction attempts resulted in the formation of a highly insoluble product, unable to be characterised *via* NMR or mass spectrometry.

In an attempt to solve the solubility issues that the previous two strategies faced, three novel alkylated thienyl pyrrolinone esters (**23a, 23b,** and **23c**) were synthesised. Due to their solubilising alkyl chains, the pyrrolinone esters showed good solubility in most organic solvents. These compounds were also used to develop a novel methodology towards four fully asymmetric DPP derivatives, in which we were able to systematically vary the positioning of the individual solubilising alkyl chains relative to the asymmetric aromatic units. We demonstrated this by synthesising a pair of fully asymmetric DPP structural isomers (**T-DPP-P** and **P-DPP-T**), consisting of both a branched and linear alkyl chain and investigated their optical and theoretical properties, which were found to lie in-between that of their symmetrical counterparts. Thus, demonstrating the ability to fine tune the absorption and band gap *via* synthesis of asymmetric DPP derivatives.

These alkylated thienyl pyrrolinone esters then underwent condensation with either **7** or **10**, in a third synthetic strategy towards the DPP dimer. However as previously seen, only partial reactivity was observed, leading to the formation of a single asymmetric DPP unit, with the possible structure of a DPP nitrile. It was thought that if this intermediate could be isolated, it may then undergo further condensation to give the desired product. Thus, di-alkylated DPP-nitrile **36** was synthesised, which underwent condensation with thienyl pyrrolinone ester **4** in a further attempt to synthesise the dimer. However, no reaction was observed.

In a final attempt, a novel di-alkylated SDPP derivative (**40**) was synthesised and underwent a palladium catalysed Liebeskind-Srogl cross-coupling with 2,5-thiophenediboronic acid (**41**) however, once again only a single DPP unit was formed.

Ultimately, we were unable to synthesise the target compounds and partial reactivity was often a reoccurring outcome, among most of the synthetic strategies attempted. Although it is not fully understood as to why this may be, it is possible that the core thiophene unit is too electron rich, thus preventing the second condensation from occurring. However, it is also possible that optimised reaction conditions are yet to be found. In general, the target compound is of unique structure that cannot be synthesised *via* conventional cross-coupling methods (i.e. Stille/Suzuki) often used to synthesise DPP oligomers in literature (i.e. as discussed in *Chapter II*), and thus a creative synthesis is required.

Due to time constraints, further reaction conditions could not be tested for the Liebeskind-Srogl strategy. Future work should involve systematic optimisation of the cross-coupling reaction, in which it may then be possible to synthesise the DPP dimer. If this can be achieved, based on Troisi's study,[43] the resulting polymer may show a higher tolerance to energetic/torsional disorder than previously reported in DPP polymers. Such a result will pave the way for effective new design rules when designing high performance, next generation DPP polymers. Thus, these materials may demonstrate a significant improvement on the performance of current DPP-based optoelectronic devices.

V

Conclusions and Future Work

5.1 Aims of Thesis

The general aim at the beginning of this thesis was to '*gain a better understanding of the structure-property relationships within DPP-based materials, so we can begin to overcome the general limitations faced by conjugated polymers in this field.*'

To try and achieve this, we studied the effects of chain length, encapsulation and asymmetry of conjugated DPP-based polymers and small molecules, on their fundamental properties and performance. Here, we summarise the results from Chapters II - IV and thus, the overall conclusions, followed by an outlook and some closing remarks.

5.2 Chapter Summaries

5.2.1 Chapter II

In Chapter II, I continued the previous work of Dr Anastasia Leventis and investigated how chain length, polydispersity and defects can affect the wavelength and strength of absorption, of conjugated materials. Previously, Leventis synthesised a series of thienyl-DPP oligomers (n = 1-5) and their polymeric counterpart (**PDPPTPT**), a well-studied polymer previously reported in literature. However, among the oligomers, the tetramer was found to be impure (Figure 5.1). Thus, in this study we re-synthesised the tetramer *via* alternative reaction conditions. In addition, the monomer, dimer and polymer (**PDPPTPT**) were also re-synthesised for this study.

Figure 5.1- Structures of the DPP tetramer.

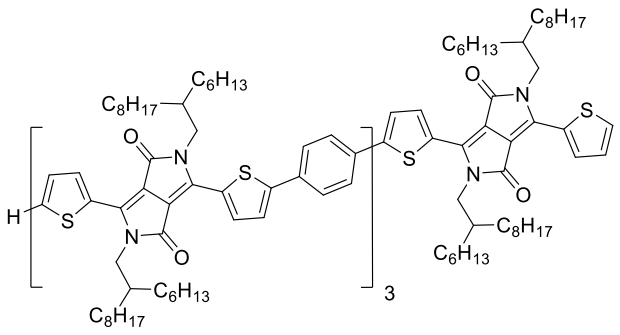

Tetramer

We then studied the optical properties of the DPP oligomers and the corresponding polymer.

The main findings from this chapter were:

- While MALDI mass spectrometry suggested that the tetramer was made, some impurities were observed in the spectra. However, these impurities were present in only trace amounts within the sample and it appeared that the tetramer was the major product.
- The UV-vis absorption of the DPP oligomers (n = 1-5) were measured, alongside polymer **PDPPTPT**. It was generally observed, that as the chain length of the oligomer increased, the further red-shifted the absorption.
- The absorption of the tetramer and pentamer were observed to be the same and thus, it is possible that at this chain length, the band gap begins to slowly converge. However, this was challenged by the largely red-shifted absorption of the polymer, compared to the oligomers in the study.
- The normalised extinction coefficients of the oligomers were also measured. It was observed that as the chain length increased from the monomer to the dimer, as expected, the extinction coefficient also increased. However, it was then observed that as the chain length then increased from dimer to pentamer, the extinction coefficient largely decreased instead. This may suggest that as the chain length increases from the dimer to the trimer, chain curvature begins to occur and thus, a saturation limit is reached.
- On the other hand, a significant red shift in absorption between the trimer and pentamer was observed. In addition, the polymer's absorption is largely red-shifted compared to all other chain lengths in the study. This was unusual, as the expected size of the red shift should decrease with extending conjugation length, as the saturation limit begins to approach. However, it is possible that this may have been due to increased aggregation with extended chain length. Thus, it appears that the ECL is not the only contributor towards the absorption of the DPP oligomers.

5.2.2 Chapter III

In Chapter III, we studied the effect of partial encapsulation on the performance of DPP-based polymers. In our first study, we aimed to alter the donor-acceptor interface in order to understand how this may affect the $V_{oc.}$ We did this by synthesising a novel encapsulated DPP monomer (**EC10DPPT**), followed by the synthesis of two series (Ph- and TT-) of novel DPP based polymers, doped with an increasing amount of **EC10DPPT** (Figure 5.2). It was proposed that within the doped polymers, a proportion of the encapsulated polymer chains will be located at the D-A interface, leading to a greater difference in the static dipole moment. Literature reference polymers were also synthesised for comparison. The polymers optical properties were measured and the corresponding OPV devices were fabricated.

*Figure 5.2- Structures of -Ph and -TT DPP polymer series, and novel encapsulated thienyl-DPP monomer **EC10DPPT**.*

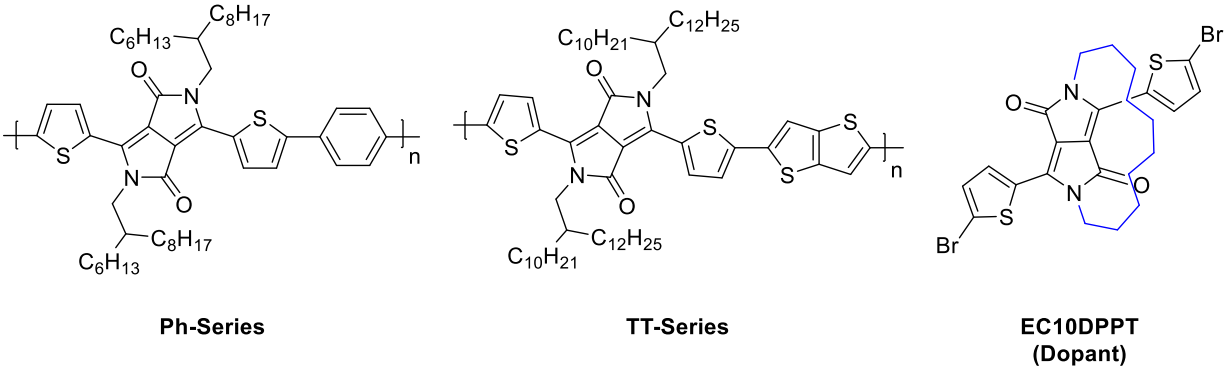

The main findings from this study were:

- It was observed *via* X-ray crystallographic analysis, that monomer **EC10DPPT** showed larger interplanar distances in the solid state, compared to most standard DPP compounds in literature.
- In general, as the ratio of **EC10DPPT** increased within the doped polymers, the further blue-shifted the absorption. While there were some exceptions to this trend, they were likely due to large differences in molecular weight.
- It was observed that *via* the introduction of the encapsulated dopant, it was possible to raise the V_{oc} in some of the OPV devices. This may suggest that there was an increase in the difference of the static dipole moment at the donor-acceptor interface, resulting in a raise of the $V_{oc.}$ Various other parameters influencing the V_{oc} such the E_{CT} and the reorganization energy, may have also been altered by encapsulation and contributed to these results.
- The encapsulated polymers showed higher device efficiencies in comparison to the reference, with **PE5DPPT-P** and **PE10DPPT-TT** achieving the highest maximum PCEs of 5.7% and 5.3% in the Ph- and TT-series respectively. While this suggests that the optimum amount of

encapsulation can vary in different polymer systems, it is possible that differences in the molecular weight also contributed to these results.

In our second study we investigated the effect of ring size, on the properties of encapsulated DPP polymers. To achieve this, we synthesised three additional encapsulated DPP monomers of different ring size, and their interplanar distances were compared *via* X-ray crystallographic analysis. These monomers were then polymerised into a novel series of encapsulated DPP-BDT based polymers (Figure 5.3). A reference polymer was also synthesised for comparison. The polymers optical properties were measured and corresponding OPV devices were fabricated.

Figure 5.3- Structures of the encapsulated DPP-BDT polymers.

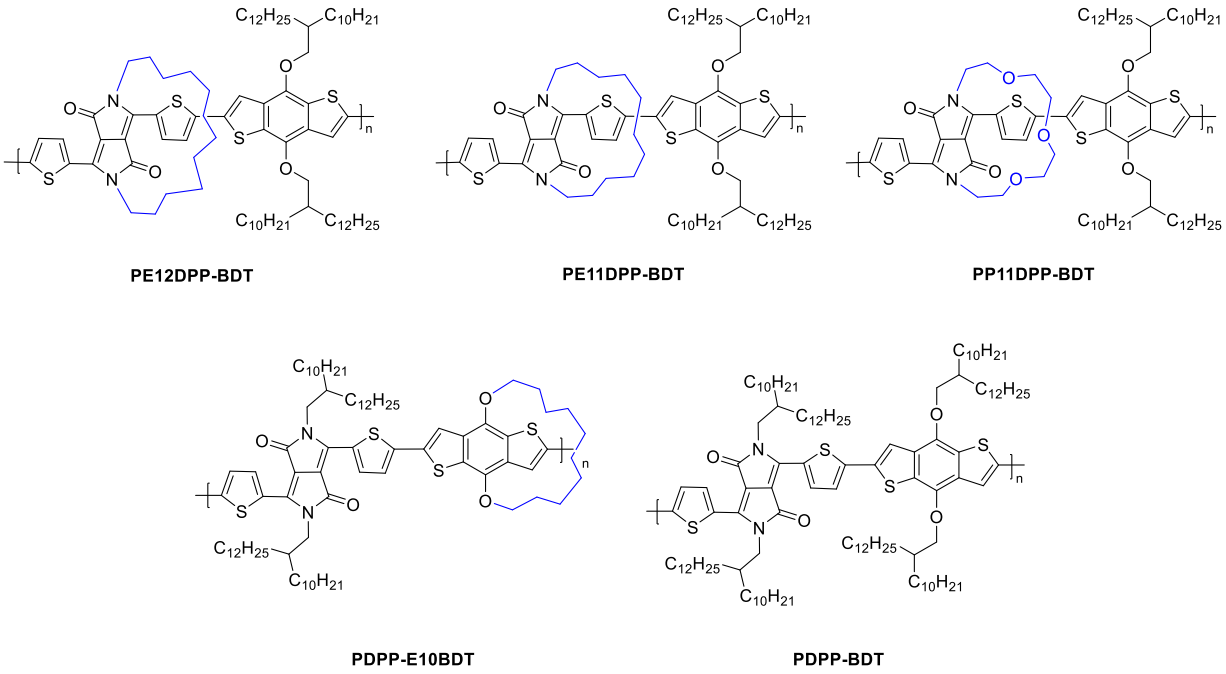

The main findings from this study were:

- It was observed *via* X-ray crystallographic analysis, that among the encapsulated DPP monomers, a C12 ring gave the most ordered structure, while the ethylene glycol ring introduced the largest amount of strain and torsional disorder.
- As expected, increased interplanar distances were observed for larger ring sizes. This suggests that it may be possible to control the distance in the π–π stacking direction *via* ring size.
- In the thin film UV-vis absorption, it was observed that among the encapsulated DPP polymers, **PE12DPP-BDT** exhibited the steepest onset. This may be related to the highly ordered and planar crystal structure observed for **EC12DPPT**. On the other hand, **PP11DPP-BDT** exhibited

both a broad onset and a blue-shifted absorption, suggesting it experienced the most amount of energetic disorder. Again, this may be related to the torsional disorder observed in the crystal structure of **EP11DPPT**.

- It was observed that the encapsulated polymers achieved higher efficiencies than that of the reference **PDPP-BDT**. **PE12DPP-BDT** showed the highest performance with a PCE of 1.7%. However, in general as all devices performed poorly, it is not possible to make any definite conclusions on any trends that were observed, based on these results.
- Polymers **PDPP-BDT** and **PE12DPP-BDT** were also fabricated into additional NFA devices, using **IEICO-4F**. However, lower efficiencies and large voltage losses in comparison to PCBM were observed.

Finally, building upon McCulloch *et al's*[121] research, we attempted to investigate the effect of encapsulation on the properties of ethylene glycol chained DPP-based polymers, for potential application in bioelectronics (Figure 5.4). Following the strained crystal structure observed for **EP11DPPT** in the previous study, we synthesised **EP14DPPT**, consisting of a larger ring. We also synthesised a linear chained DPP monomer and a bithiophene co-monomer, also consisting of ethylene glycol chains. However, due to the toxic and unstable nature of the stannylated bithiophene, purification was not possible. Consequently, the following polymerisation attempt was unsuccessful.

*Figure 5.4- Structures of the proposed encapsulated **PE14DPP-T2** and the linear chained **PDPP-T2**.*

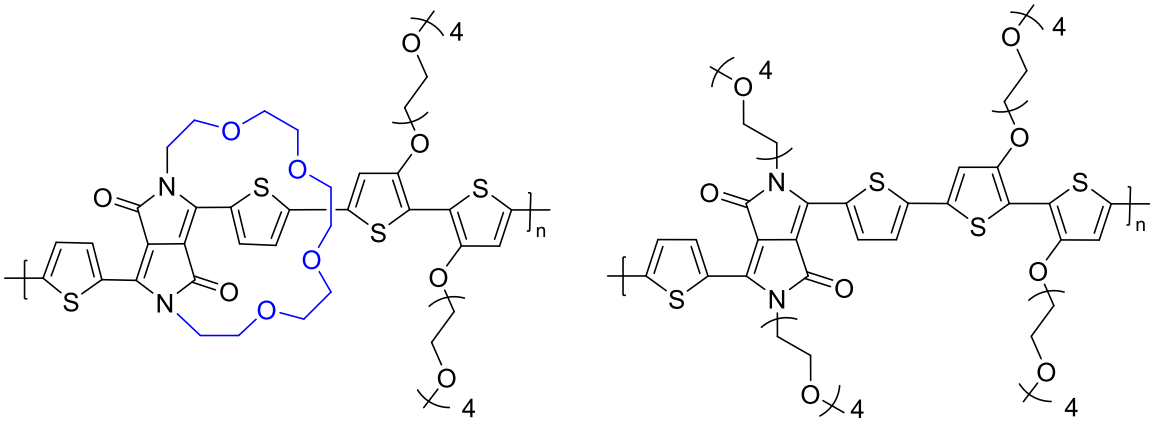

The main outcomes of this study were:

- It was observed *via* X-ray crystallographic analysis, that **EP14DPPT** showed far less ring strain than **EP11DPPT**. In addition, the increased planarity observed in **EP14DPPT** made it the preferred choice for polymerisation.

- While all other monomers were obtained in high purity, the stannylated bithiophene contained impurities that could not be removed *via* recrystallisation or column chromatography.
- Consequently, the monomer was used as crude in the Stille cross-coupling, in an attempt to synthesise **PDPP-T2**.
- However, the polymerisation attempt was unsuccessful as a very low molecular weight was determined for **PDPP-T2**. This was likely due to the impure nature of the bithiophene co-monomer, thereby creating large errors in the reaction stoichiometry.

5.2.3 Chapter IV

As seen in previous chapters, energetic disorder within conjugated polymers can largely affect its optical properties. In Chapter IV, we aimed to investigate the effect of torsional disorder on charge transport within DPP polymers, and how this problem can be overcome. Inspired by Troisi's work,[43] we attempted to synthesise a novel DPP polymer **P(a)**, which consists of a higher DPP to thiophene ratio than previously reported in literature (Figure 5.5). Based on Troisi's results, it is theorised that due to secondary overlap contribution between the thiophene/DPP units, this novel polymer will show a higher tolerance to energetic/torsional disorder, than previously reported for DPP polymers. However, all synthetic attempts towards the desired monomer were unsuccessful. In particular, the key coupling step in all synthetic strategies attempted, proved to be challenging.

*Figure 5.5- Structure of the proposed target polymer **P(a)**.*

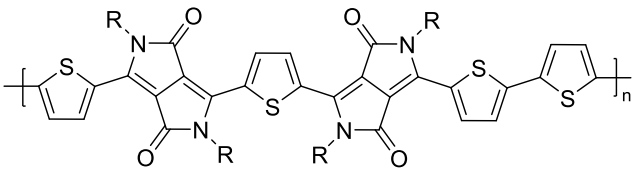

P(a)

R= Alkyl Chain

The main outcomes of this chapter were:

- The first strategy attempted, involved the synthesis of a previously reported thienyl pyrrolinone ester, which underwent condensation with a di-nitrile. While several reaction conditions were tested, most of the outcomes consisted of only partial reactivity. It was also noted that the reaction products were of poor solubility, resulting in difficult characterisation.
- This was then followed by a reversed strategy, in which a novel di-thienyl pyrrolinone ester was synthesised and underwent condensation with 2-cyanothiophene. However, due to a lack

of solubilising alkyl chains, all reaction attempts resulted in the formation of a highly insoluble product, unable to be characterised.

- In an attempt to solve the solubility issues of the previous two strategies, three novel alkylated thienyl pyrrolinone esters were synthesised. These compounds were also used to develop a novel methodology towards four fully asymmetric DPP derivatives, in which we were able to systematically vary the positioning of the individual solubilising alkyl chains relative, to the asymmetric aromatic units. We demonstrated this by synthesising a pair of fully asymmetric DPP structural isomers (**T-DPP-P** and **P-DPP-T**), and investigated their optical and theoretical properties, which were found to lie in-between that of their symmetrical counterparts (Figure 5.6). Thus, demonstrating the ability to fine tune the absorption and optical band gap *via* synthesis of asymmetric DPP derivatives.

Figure 5.6- Structures of the fully asymmetric DPP isomers.

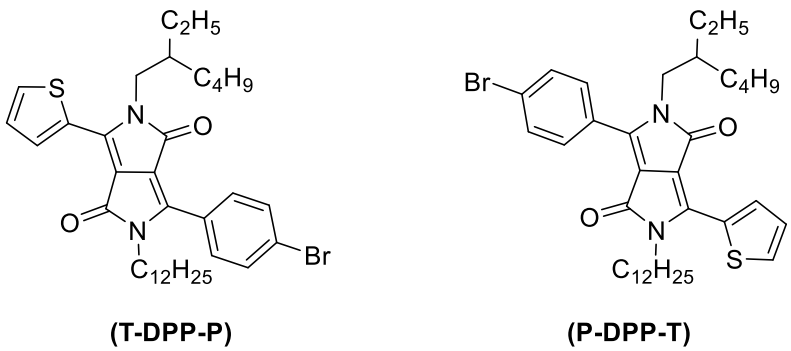

- The alkylated thienyl pyrrolinone esters then underwent condensation with a di-nitrile**,** in a third synthetic strategy towards the DPP dimer. However as previously seen, only partial reactivity was observed leading to the formation of a single asymmetric DPP unit.
- A di-alkylated DPP-nitrile was also synthesised, which underwent condensation with thienyl pyrrolinone ester, however, no reaction was observed.
- In a final attempt, a novel di-alkylated SDPP derivative was synthesised and underwent a palladium catalysed Liebeskind-Srogl cross-coupling with 2,5-thiophenediboronic acid however, once again only a single DPP unit was formed.
- Ultimately, we were unable to synthesise the target compound and partial reactivity was often a reoccurring outcome. Although it is not fully understood as to why this may be, it is possible that the core thiophene unit is too electron rich, thus preventing the second condensation from occurring.

5.3 Overall Conclusions

In this thesis, the structure-property relationships in DPP-based materials were investigated. We studied the effect of chain length, encapsulation and asymmetry on the properties and performance of DPP-based materials. It was observed that as the chain length increased from monomer to dimer, the normalised extinction coefficient did also, at which it reached a maximum. Then, as the chain length increased from the dimer to the pentamer, the value largely decreased. It is possible that this may have been due to chain curvature/torsional disorder as the chain length increases. However, in contrast, the polymer was observed to have a largely red-shifted absorption compared to any other compound in the study. This was likely related to intermolecular aggregation of the polymer chains, suggesting that the ECL is not the only contributor towards the absorption, in the DPP oligomers.

In addition to torsional disorder, another common problem faced within the field are the low V_{oc} values obtained for OPV devices as a result of energetic loss, consequently limiting the PCE. We found that by introducing an encapsulated DPP dopant into known DPP-polymer systems, we were able to modify the donor-acceptor interface and thus, increase the V_{oc}. It was also discovered that different degrees of encapsulation were preferred for different DPP polymer systems, however differences in molecular weight may have also influenced these results. While the specific factor responsible for this trend is unknown, it is likely that either a reduced ratio of the CT-state density, a reduced reorganization energy or an increase of the difference in the static dipole moment were responsible for the results of this study, either individually or as a combination of these factors. We also investigated different ring sizes of the encapsulated DPP monomer and found that this had an influence over the optical properties of the corresponding polymers, thus demonstrating the importance of choosing the correct ring size.

We developed a novel methodology towards fully asymmetric DPP derivatives including two structural isomers, *via* condensation between an alkylated thienyl pyrrolinone ester with an aromatic nitrile. When studying the optical and theoretical properties of the fully asymmetric DPP isomers, they were found to lie in-between that of their symmetrical counterparts. This shows it is possible to fine tune properties such as absorption and optical band gap *via* such design strategies. While yields were often low and further optimisation is required, this new method allows the synthesis of previously unavailable DPP derivatives, allowing the possibility to greatly broaden the library of existing DPP compounds and their application in optoelectronics.

5.4 Future Work

In Chapter II, we saw that as the chain length increased from monomer to dimer, the extinction coefficient did also, at which it reached a maximum. Then, as the chain length increased from dimer to pentamer, the value largely decreased, suggesting that a saturation limit had been reached. However, an unexpected red-shift in absorption between the trimer and polymer was also observed.

In order to fully understand the trends observed in this study, extended chain lengths beyond the pentamer are required. Thus, it would be desirable to also synthesise the DPP hexamer. This may be possible *via* a Suzuki cross-coupling between bis-borylated DPP dimer **(a)** (as previously synthesised in Chapter II) and mono-brominated DPP dimer **(b)**, which should give the hexamer **(c)** in a rapid synthesis (Scheme 5.1).

*Scheme 5.1- Proposed synthesis towards the DPP hexamer **(c)** via Suzuki cross-coupling between bis-borylated DPP dimer **(a)** and mono-brominated DPP dimer **(b)**.*

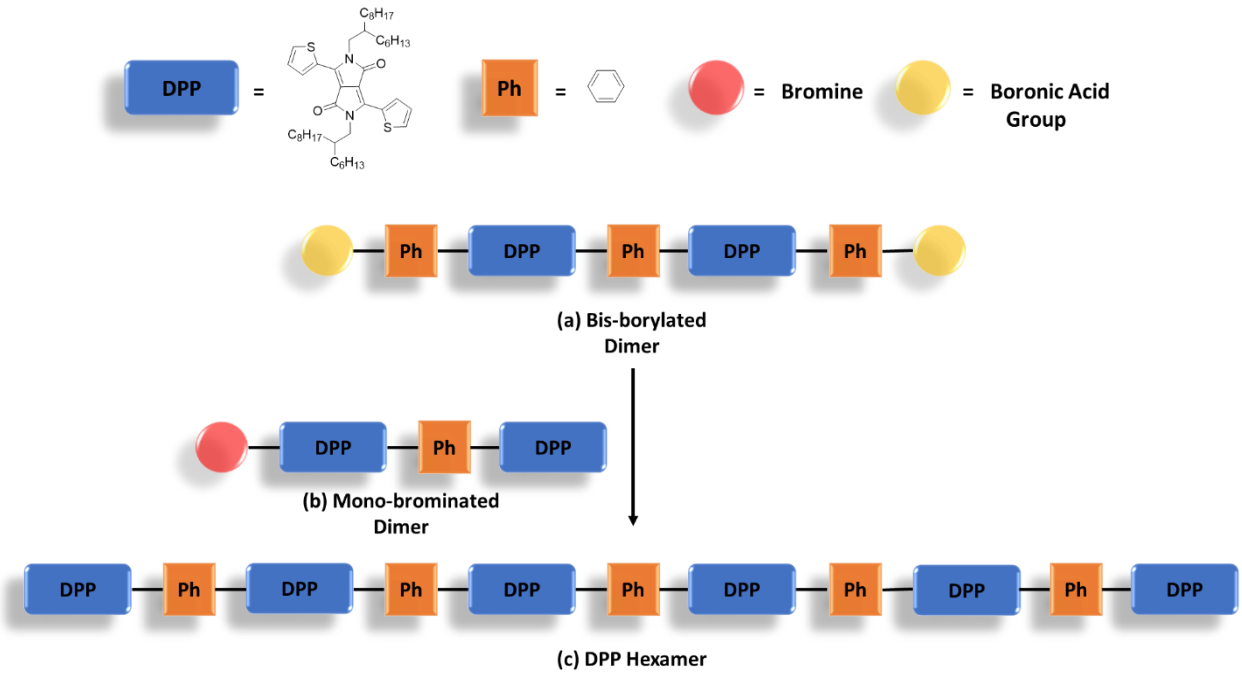

Thus, if obtained in high purity, the synthesis of the DPP hexamer will allow us to have a better estimation as to the value of the ECL, for the conjugated system. Future work should also include comparing the extinction coefficient of the polymer, to the other oligomers within the study, to see whether its value increases alongside its largely red-shifted absorption.

In Chapter III, we were unable to synthesise the ethylene glycol chained polymers (encapsulated) **PE14DPP-T2** and (linear) **PDPP-T2**, due to difficulty in purifying the stannylated bithiophene co-

monomer. Thus, to complete this project the bithiophene co-monomer should be re-synthesised and obtained in a high purity, to allow successful polymerisation. While a longer ethylene glycol chain (tetraethylene glycol monomethyl ether) was chosen to aid with polymer solubility, it may be beneficial to instead synthesise the literature bithiophene of which the synthesis was based upon, consisting of a slightly shorter chain (triethylene glycol monomethyl ether).[165] As the literature monomer was reported to be a solid, of which purification was possible *via* recrystallisation in isopropanol, this would allow a higher chance of successful polymerisation. Thus, we will be able to investigate the effect of encapsulation on the fundamental properties and performance of these polymers. In addition, due to their high glycol side chain density, it is possible that these DPP polymers will show great potential in OECTs and bioelectronic devices.

In Chapter IV, while we were able to synthesise the fully asymmetric DPP isomers **T-DPP-P** and **P-DPP-T**, due to a shortage of material, time constraints and low yields, we were unable to incorporate these monomers into polymers. Future work should include further optimisation of the key condensation step, and thus, allow a sufficient quantity of the monomers to be produced, for subsequent polymerisation. Such a study will allow us to investigate the effect of alkyl-aryl positioning on the properties and performance of DPP based polymers, particularly in the solid state. As *partially* asymmetric polymers have been previously reported, it would be ideal to compare their fundamental properties with those of *fully* asymmetric polymers, in order to further establish the effect of asymmetry on the performance of DPP-based materials.

Finally, the main objective of Chapter IV was to synthesise DPP polymer **P(a)**, consisting of a higher DPP to thiophene ratio than previously reported in literature. While various different synthetic strategies were explored, ultimately all were unsuccessful and in particular, the key coupling step towards the dimer proved to be highly problematic, with either partial or no coupling occurring. While condensation between thienyl pyrrolinone esters and aromatic nitriles were well explored, the final synthetic strategy attempted involving a palladium catalysed Liebeskind-Srogl cross-coupling between SDPP and 2,5-thiophenediboronic acid, was not fully investigated. Thus, future attempts towards **P(a)** should involve systematic optimisation of the catalysed Liebeskind-Srogl cross-coupling. Further investigation of reaction conditions is required and the optimum quantity of SDPP, catalyst, solvent, reaction temperature and reaction time, should be explored.

If the synthesis of **P(a)** can be achieved, based on the results of Troisi's study,[43] the resulting polymer may show a higher tolerance to energetic/torsional disorder, than previously reported in DPP polymers. Such a result will pave the way for effective new design rules when designing high performance, next generation DPP polymers. Thus, these materials may demonstrate a significant improvement on the performance of current DPP-based optoelectronic devices.

5.5 Closing Remarks

Overall, this thesis has shown that the structure-property relationships within DPP materials are often complex and therefore, not easily deciphered. Over the years, DPP-based materials have demonstrated to be excellent candidates for application in optoelectronic devices, however like most other conjugated materials, their performance can be severely limited by various factors such as energetic/torsional disorder leading to charge traps and thus, poor charge transport. In addition, with OPVs, poor PCE values are often the result of low V_{ocs}, due to energetic loss. Therefore, in order to continue to break benchmark efficiencies of DPP-based devices, it is vital that we investigate the factors that give rise to these limitations and how we can begin to control them through polymer structure and design. Careful modification of the donor-acceptor interface, is often crucial in controlling the $V_{oc.}$ It has been discovered that we are able to alter the D-A interface, *via* the introduction of an encapsulated DPP dopant into known DPP-polymer systems. As a proportion of the encapsulated polymer chains were located at the D-A interface, this likely led to either a reduced ratio of the CT-state density, a reduced reorganization energy or an increase of the difference in the static dipole moment. As a result, the V_{ocs} in some of the doped polymers were found to be higher than that of the reference, and thus the PCE was improved. However, it is to be noted that differences in molecular weight may have affected some of these results. Following the encouraging preliminary results from this study, we hope that we have met the general aim of this thesis and have begun to understand the structure-property relationship in DPP materials, in order to improve their performance in OPV devices. While this thesis has solely focused on DPP-based materials, we believe that this strategy may be applied to other conjugated systems in the future, as a potential method to improve the V_{oc}.

Overall, through the continuous investigation of the structural factors affecting the fundamental properties of conjugated materials, a more innovative and impressive range of next-generation optoelectronic devices can be developed, within this ever-advancing field.

VI

Experimental Procedures

6.1 General Information

General Experimental

All moisture and air sensitive reactions were carried out in oven dried flasks under an inert argon atmosphere. RT refers to 25 °C maintained by the use of a heating mantle. All reactions were covered with foil unless otherwise stated and were magnetically stirred. Merck Geduran® Si 60 silica gel or Biotage® Isolera™ Four with either Biotage® SNAP or SNAP Ultra cartridges (10 g, 20 g, 50 g or 100 g) were used for column chromatography during purification. Alternatively, a 'silica plug' was used which refers to a variable height of Geduran silica gel 60 (40-63 µm) of variable width, that was not pre-wetted into a gel prior to loading. DC Fertigfolien ALUGRAM aluminium sheets coated with silica gel, were used for carrying out analytical thin layer chromatography (TLC). Compounds were visualised by ultra-violet light. Chemicals were used as supplied.

Solvents

Anhydrous solvents were supplied commercially and used under an inert argon atmosphere. All other solvents and reagents used were supplied commercially and used as received.

Characterisation

^{1}H NMR were carried out at 600 MHz on a Bruker Avance III 600 Cryoprobe Spectrometer or at 400 MHz on a BRUKER Avance III 400 HD Spectrometer at the Department of Chemistry, University College London; or at 400 MHz on a Avance III 400 HD Spectrometer or at 600 MHz on a Avance 600 BBI Spectrometer at the Department of Chemistry, University of Cambridge. The internal standards used were $CDCl_3$ (δ = 7.26 ppm, s), $(CD_3)_2SO$ (δ = 2.50 ppm, s), CD_3COCD_3 (δ = 2.05, qn) and CD_2Cl_2 (δ = 5.32, t).^{1}H NMR shifts were reported to the nearest 0.01 ppm and the following abbreviations were used: s, singlet; d, doublet; t, triplet; q, quartet; qn, quintet; sxt, sextet; m, multiplet; br, broad; Ar, aromatic; Th, thienyl; Ph, phenyl. The coupling constants (*J*) are measured in Hertz. ^{13}C NMR spectra were recorded at 125 MHz on a BRUKER DCH Cryoprobe Spectrometer in the stated solvent. The internal standards used were $CDCl_3$ (δ = 77.2 ppm, t) and $(CD_3)_2SO$ (δ = 39.52 ppm, s). ^{13}C NMR chemical shifts are reported to the nearest 0.1 ppm. Mass spectra were obtained using a Waters LCT, Finnigan MAT 900XP or Waters MALDI micro MX spectrometer at the Department of Chemistry, University College London and University of Cambridge. UV-vis spectra were recorded on a Shimadzu UV-1800 spectrophotometer using Hellma® absorption cuvettes, 200 - 2500 nm spectral range,

pathlength 10 mm, chamber volume 3500 µL at RT. GPC/SEC samples were run at 80 °C at 2 mL/min on a Shimadzu Prominence instrument equipped with a differential refractive index and a UV-Vis detector. The mobile phase was chlorobenzene, and polystyrene was used as a standard for calibration. The analyte samples were filtered through a PTFE frit with 0.45 µm pore size before injection. The experimental molar mass (Mn, Mw,) and PDI values of synthesised polymers were obtained by using Shimadzu GPC/SEC software.

6.2 Experimental for Chapter II

3,6-Di(thiophen-2-yl)-2,5-dihydropyrrolo[3,4-c]pyrrole-1,4-dione (1)

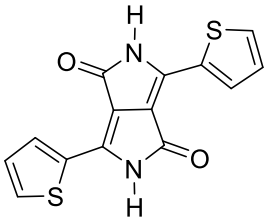

To an oven dried flask under argon set up for reflux, was added sodium chunks (1.62 g, 70.0 mmol) and 2-methyl-2-butanol (36 mL), followed by anhydrous iron (III) chloride (0.06 g, 0.370 mmol). The solution turned brown. The mixture was allowed to stir at reflux at 150 °C until all sodium had been consumed (30 min). After all the sodium was consumed, the reaction was allowed to cool to 85 °C. Thiophene-2-carbonitrile (4.3 mL, 45.8 mmol) was added to the mixture, followed by diethylsuccinate (3.1 mL, 18.3 mmol). The reaction turned magenta in colour and was left to stir at 90 °C for 2 h. The mixture was then allowed to cool to 50 °C, followed by the addition of methanol (60 mL). The reaction was quenched with glacial acetic acid (18 mL) and refluxed for 1 h. The mixture was then filtered, washed with water (10 mL), methanol (3 x 50 mL), acetone (2 x 25 mL) and hexane (50 mL) and dried under vacuum to afford the product as a magenta solid (3.12 g, 10.4 mmol, 57%) which was used without further purification.

^{1}H NMR (600 MHz, DMSO) δ (ppm): 11.26 (br, 2H, NH), 8.20 (br, 2H, ThH), 7.96 (br, 2H, ThH), 7.30 (br, 2H, ThH). **^{13}C NMR** (151 MHz, DMSO) δ 161.7, 136.2, 132.8, 131.3, 130.8, 128.8, 108.6. **LRMS** (EI+) *m/z* 300 $[M]^{+}$.

Spectroscopic data is supported by literature.[186]

2,5-bis(2-hexyldecyl)-3,6-di(thiophen-2-yl)-2,5-dihydropyrrolo[3,4-c]pyrrole-1,4-dione (2) (Monomer)

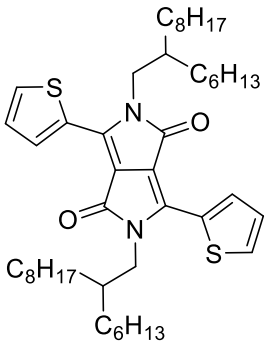

To an oven dried flask under argon was added compound **1** (3.79 g, 12.6 mmol), K_2CO_3 (5.80 g, 42.0 mmol), 18-crown-6 (0.05 g, 0.19 mmol), 7-(bromomethyl)pentadecane (12.8 g, 42.0 mmol), followed by anhydrous DMF (152 mL). The solution was then heated to 120 °C and was stirred for 18 h. The reaction mixture was then cooled to RT. Chloroform was then added to the flask and the solution was concentrated *in vacuo*. The crude product was then purified *via* column chromatography on silica gel (hexane: chloroform= 2:1) followed by recrystallisation in ethanol, to afford the product as a magenta solid (2.45 g, 3.27 mmol, 26%).

^{1}H NMR (400 MHz, $CDCl_3$) δ (ppm): 8.86 (dd, *J* = 3.9, 1.0 Hz, 2H, ThH), 7.62 (dd, *J* = 5.0, 1.0 Hz, 2H, ThH), 7.32 – 7.13 (m, 2H, ThH), 4.02 (d, *J* = 7.7 Hz, 4H, NCH_2), 1.90 (m, 2H, NCH_2CH), 1.35 – 1.04 (m, 48H, Alkyl Chain), 0.87-0.82 (m, 12H, Alkyl Chain). **^{13}C NMR** (101 MHz, $CDCl_3$) δ 161.8, 140.4, 135.2, 130.5, 129.8, 128.4, 107.9, 46.2, 37.7, 31.9, 31.8, 31.2, 30.0, 29.7, 29.5, 29.3, 26.2, 26.1, 22.7, 22.6, 14.1. **LRMS** (EI+) *m/z* 748 $[M-H]^+$.

Spectroscopic data is supported by literature.[187]

3-(5-bromothiophen-2-yl)-2,5-bis(2-hexyldecyl)-6-(thiophen-2-yl)-2,5-dihydropyrrolo[3,4-c]pyrrole-1,4-dione (4)

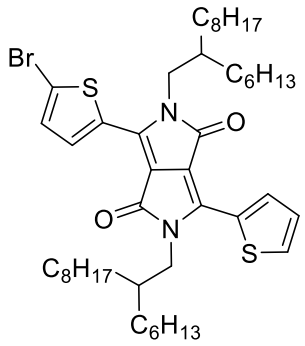

To a flask under argon was added **2** (2.46 g, 3.29 mmol) dissolved in chloroform (314 mL) and the reaction was cooled to 0 °C (30 min). N-bromosuccinimide (0.64 g, 3.60 mmol) was then added to the stirring solution and the reaction was covered with foil. The reaction was then stirred for a further 30 min at 0 °C before allowing to warm to RT and was left to stir for 12 h. The resulting solution was then diluted with chloroform and concentrated *in vacuo*. Methanol was then added to the flask and the resulting suspension was sonicated and collected *via* filtration. The crude product was then purified *via* column chromatography on silica gel (hexane: chloroform= 2:1), sonicated in methanol and collected by filtration to afford the product as a dark pink/purple solid (0.70 g, 0.85 mmol, 26%).

^{1}H NMR (400 MHz, $CDCl_3$) δ (ppm): 8.88 (dd, *J* = 3.9, 1.1 Hz, 1H, ThH), 8.60 (d, *J* = 4.2 Hz, 1H, ThH), 7.64 (dd, *J* = 5.0, 1.1 Hz, 1H, ThH), 7.27 (m, 1H, ThH), 7.22 (d, *J* = 4.2 Hz, 1H, ThH), 4.01 (d, J = 7.7 Hz, 2H, NCH_2), 3.93 (d, *J* = 7.7 Hz, 2H, NCH_2), 1.89 (s, 2H, NCH_2CH), 1.29-1.22 (m, 48H, Alkyl Chain), 0.88-0.82 (m, 12H, Alkyl Chain). **^{13}C NMR** (101 MHz, $CDCl_3$) δ 161.7, 161.5, 140.9, 138.9, 135.5, 135.0, 131.3, 130.8, 129.7, 128.5, 118.6, 108.2, 107.8, 46.3, 37.8, 37.7, 31.9, 31.8, 31.2, 29.9, 29.7, 29.5, 29.3, 26.2, 22.7, 22.6, 14.1. **LRMS** (EI+) *m/z* 827 $[M-H]^+$.

Spectroscopic data is supported by literature.[188]

3,6-bis(5-bromothiophen-2-yl)-2,5-bis(2-hexyldecyl)-2,5-dihydropyrrolo[3,4-c]pyrrole-1,4-dione (5)

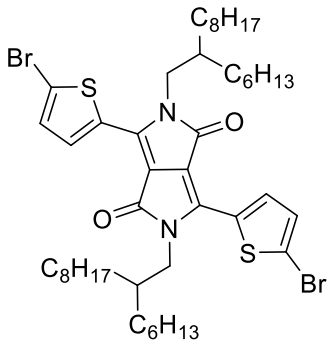

To a flask under argon was added **2** (0.65 g, 0.87 mmol) dissolved in chloroform (82 mL) and the reaction was cooled to 0 °C (30 min). N-bromosuccinimide (0.39 g, 2.19 mmol) was then added to the stirring solution and the reaction was covered with foil. The reaction was then stirred for a further 30 min at 0 °C before allowing to warm to RT and was left to stir for 12 h. The resulting solution was then diluted with chloroform and concentrated *in vacuo*. Methanol was then added to the flask and the resulting suspension was sonicated and collected *via* filtration. The crude product was then purified *via* column chromatography on silica gel (chloroform), sonicated in methanol and collected by filtration to afford the product as a purple solid (0.54 g, 0.60 mmol, 68%).

^{1}H NMR (600 MHz, $CDCl_3$) δ (ppm): 8.62 (d, *J* = 4.2 Hz, 2H, ThH), 7.22 (d, *J* = 4.2 Hz, 2H, ThH), 3.92 (d, *J* = 7.8 Hz, 4H, NCH_2), 1.95 – 1.75 (m, 2H, NCH_2CH), 1.37 – 1.11 (m, 48H, Alkyl Chain), 0.85 (m,12H, Alkyl Chain). **^{13}C NMR** (151 MHz, $CDCl_3$) δ 161.5, 139.5, 135.5, 131.6, 131.3, 119.1, 108.1, 46.4, 37.9, 32.0, 31.9, 31.2, 30.1, 29.8, 29.6, 29.4, 26.3, 26.2, 22.8, 14.3, 14.2. **LRMS** (ESI+) *m/z* 905 $[M+H]^+$.

Spectroscopic data is supported by literature.[188]

PDPPTPT

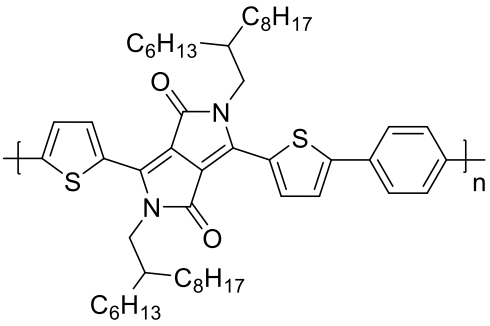

Same compound as **PDPPT-P** in *Chapter III*. Experimental and characterisation found on Page 195.

6,6'-(1,4-phenylenebis(thiophene-5,2-diyl))bis(2,5-bis(2-hexyldecyl)-3-(thiophen-2-yl)-2,5-dihydropyrrolo[3,4-c]pyrrole-1,4-dione) (6) (Dimer)

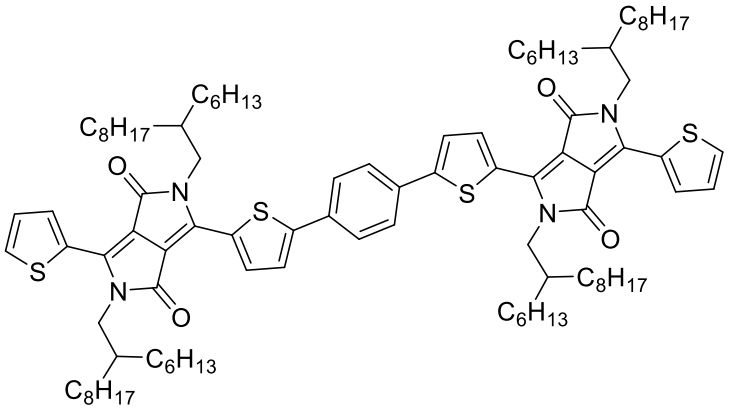

To an oven dried flask under argon equipped with a reflux condenser, was added **4** (0.50 g, 0.60 mmol), 1,4-benzenediboronic acid bis(pinacol) ester (0.097 g, 0.29 mmol), triphenylphosphine (7.60 mg, 0.030 mmol) and tris(dibenzylideneacetone)dipalladium (0) (6.70 mg, 0.0074 mmol). The reaction flask was then left to degas for 1 h. This was followed by the addition of degassed toluene (24 mL) containing a few drops of Aliquat 336 and degassed K_3PO_4 aq solution (0.73 mL) made from a stock solution (0.93 g of K_3PO_4 in 2.2 mL water). The reaction was then heated to 115 °C and allowed to stir for 20 h. The colour change observed was from magenta to blue. The reaction mixture was then allowed to cool to RT before precipitating into methanol (100 mL) and collected *via* filtration. The crude product was then purified *via* column chromatography on silica gel (hexane: chloroform= 1:1) to afford the product as a blue solid (0.30 g, 0.19 mmol, 66%).

^{1}H NMR (400 MHz, $CDCl_3$) δ (ppm): 8.95 (d, *J* = 4.1 Hz, 2H, ThH), 8.89 (dd, *J* = 3.9, 1.0 Hz, 2H, ThH), 7.73 (s, 4H, PhH), 7.63 (dd, *J* = 5.0, 1.0 Hz, 2H, ThH), 7.52 (d, *J* = 4.1 Hz, 2H, ThH), 7.29 – 7.24 (m, 2H, ThH), 4.06 (dd, *J* = 12.5, 7.8 Hz, 8H, NCH_2), 1.95 (m, 4H, NCH_2CH), 1.37 – 1.18 (m, 96H, Alkyl Chain), 0.88 – 0.81 (m, 24H, Alkyl Chain). **^{13}C NMR** (126 MHz, $CDCl_3$) δ 161.8, 161.7, 148.5, 140.2, 139.9, 136.8, 135.3, 133.4, 130.5, 129.9, 129.6, 128.4, 126.6, 124.8, 108.3, 108.1, 46.3, 37.9, 37.8, 31.9, 31.84, 31.8, 31.3, 31.2, 30.0, 29.7, 29.6, 29.5, 29.3, 26.4, 26.2, 22.7, 22.6, 14.1. **LRMS** MALDI-TOF-(LD+): Calculated for $C_{98}H_{146}N_4O_4S_4$: 1571 Found *m/z* 1576.

Spectroscopic data is supported by literature.[117]

6,6'-(1,4-phenylenebis(thiophene-5,2-diyl))bis(3-(5-bromothiophen-2-yl)-2,5-bis(2-hexyldecyl)-2,5-dihydropyrrolo[3,4-c]pyrrole-1,4-dione) (7)

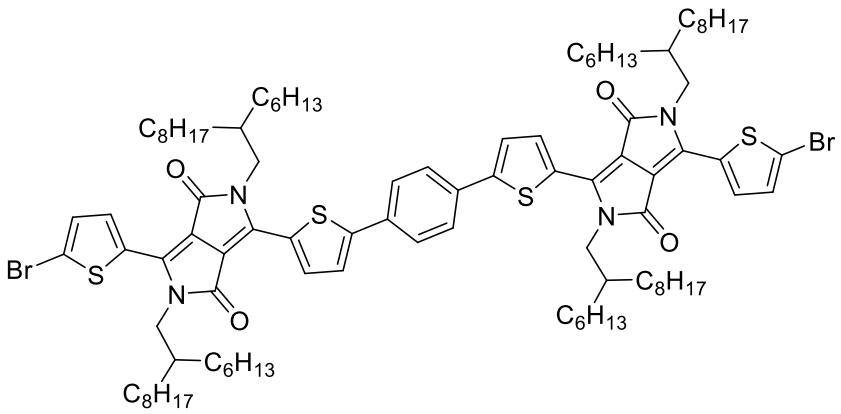

To a flask under argon was added **6** (0.28 g, 0.18 mmol) dissolved in chloroform (15 mL) and the reaction was cooled to 0 °C (30 min). N-bromosuccinimide (0.07 g, 0.39 mmol) was then added to the stirring solution and the reaction was covered with foil. The reaction was then stirred for a further 30 min at 0 °C before allowing to warm to RT and was left to stir for 12 h. The resulting solution was then precipitated into ethanol (100 mL) and collected *via* filtration to afford the pure product as a blue/copper solid (0.23 g, 0.13 mmol, 74%).

^{1}H NMR (400 MHz, $CDCl_3$) δ (ppm): 8.96 (d, *J* = 4.2 Hz, 2H, ThH), 8.62 (d, *J* = 4.2 Hz, 2H, ThH), 7.72 (s, 4H, PhH), 7.52 (d, *J* = 4.2 Hz, 2H, ThH), 7.22 (d, *J* = 4.2 Hz, 2H, ThH), 4.06 (d, *J* = 7.7 Hz, 4H, NC*H*$_2$), 3.95 (d, *J* = 7.7 Hz, 4H, NC*H*$_2$), 1.94 (br, 4H, Alkyl Chain), 1.36 – 1.18 (m, 96H, Alkyl Chain), 0.88 – 0.81 (m, 24H, Alkyl Chain).**^{13}C NMR** (126 MHz, $CDCl_3$) δ 161.7, 161.4, 148.8, 140.4, 138.8, 137.1, 135.1, 133.4, 131.4, 129.2, 126.7, 124.9, 118.7, 108.4, 108.2, 46.3, 37.9, 37.8, 31.9, 31.8, 31.3, 31.2, 30.0, 29.9, 29.7, 29.6, 29.5, 29.3, 26.3, 26.2, 22.7, 22.6, 14.1. **LRMS** MALDI-TOF-(LD+): Calculated for $C_{98}H_{144}Br_2N_4O_4S_4$: 1726 Found *m/z* 1728 $[M+2H]^+$.

Spectroscopic data is supported by literature.[117]

6,6'-(1,4-phenylenebis(thiophene-5,2-diyl))bis(2,5-bis(2-hexyldecyl)-3-(5-(4-(4,4,5,5-tetramethyl-1,3,2-dioxaborolan-2-yl)phenyl)thiophen-2-yl)-2,5-dihydropyrrolo[3,4-c]pyrrole-1,4-dione) (Bis-borylated Dimer) (8)

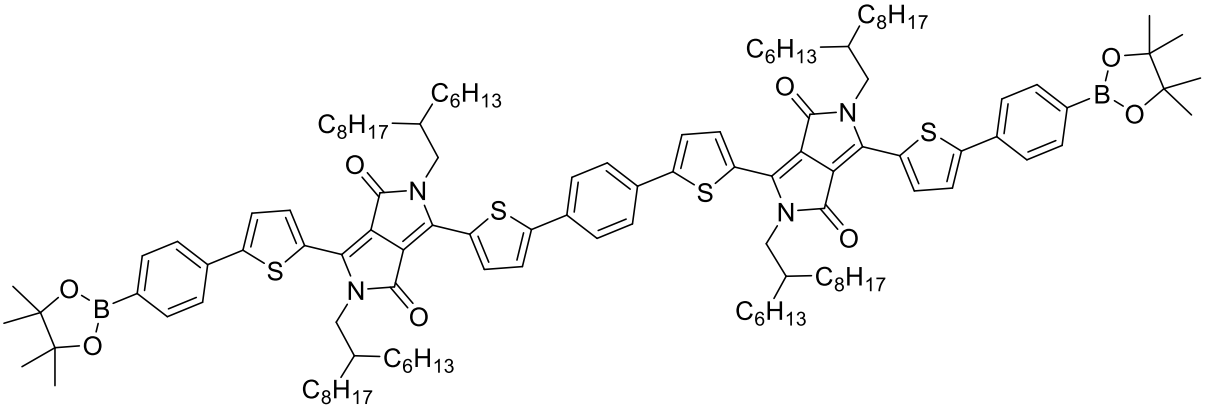

To an oven dried flask under argon equipped with a reflux condenser, was added **7** (0.23 g, 0.14 mmol), 1,4-benzenediboronic acid bis(pinacol) ester (0.92 g, 2.80 mmol, 20 equiv.) and tetrakis(triphenylphosphine)palladium(0) (3.00 mg, 0.0027 mmol). The reaction flask was then left to degas for 1 h. This was followed by the addition of degassed THF (6.6 mL) and degassed K_3CO_3 aq solution (2.2 mL) made from a stock solution (0.95 g of K_3CO_3 in 6.6 mL water). The reaction was then heated to 85 °C and allowed to stir for 20 h. After cooling to RT, the reaction mixture was then precipitated into methanol (100 mL) followed by collection *via* filtration. The crude product was then purified *via* Soxhlet extraction in ethanol for 12 h. The solid remaining in the thimble was then washed with methanol and collected *via* filtration to afford the product as a dark blue solid (0.15 g, 0.08 mmol, 57%).

^{1}H NMR (500 MHz, $CDCl_3$) δ (ppm): 8.95 (dd, *J* = 8.3, 4.1 Hz, 4H, ThH), 7.85 (d, *J* = 8.3 Hz, 4H, PhH), 7.73 (s, 4H, PhH), 7.67 (d, *J* = 8.3 Hz, 4H, PhH), 7.52 (d, *J* = 4.1 Hz, 4H, ThH), 4.08 (d, *J* = 7.4 Hz, 8H, NCH_2), 1.98 (br, 4H, Alkyl Chain), 1.36 (s, 24H, $BO_2C(CH_3)_2$), 1.36 – 1.16 (m, 96H, Alkyl Chain), 0.87 – 0.81 (m, 24H, Alkyl Chain).**^{13}C NMR** (126 MHz, $CDCl_3$) δ 161.8, 161.7, 149.6, 148.5, 139.9, 139.6, 136.8, 135.6, 133.4, 129.3, 129.2, 126.6, 125.2, 124.9, 124.8, 108.6, 108.4, 84.1, 46.3, 38.0, 31.9, 31.8, 31.3, 30.1, 29.7, 29.6, 29.3, 26.4, 24.9, 22.7, 22.6, 14.1. **LRMS** MALDI-TOF-(LD+): Calculated for $C_{122}H_{176}B_2N_4O_8S_4$: 1975 Found *m/z* 1976 $[M+H]^+$.

6,6'-(1,4-phenylenebis(thiophene-5,2-diyl))bis(3-(5-(4-(5-(2,5-bis(2-hexyldecyl)-3,6-dioxo-4-(thiophen-2-yl)-2,3,5,6-tetrahydropyrrolo[3,4-c]pyrrol-1-yl)thiophen-2-yl)phenyl)thiophen-2-yl)-2,5-bis(2-hexyldecyl)-2,5-dihydropyrrolo[3,4-c]pyrrole-1,4-dione) (9) (Tetramer)

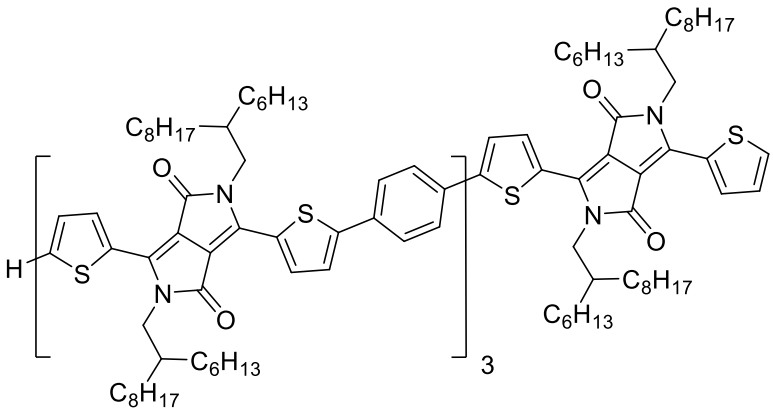

To a 10 mL oven dried microwave vial under argon was added **8** (0.05 g, 0.0253 mmol), **4** (0.0520 g, 0.0630 mmol) and tetrakis(triphenylphosphine)palladium(0) (2% mmol). The reaction vial was then allowed to degas for 1 h. This was followed by the addition of degassed THF (1.30 mL) and degassed K_3CO_3 aq solution (0.41 mL) made from a stock solution (0.24 g of K_3CO_3 in 1.64 mL water). The reaction was then heated to 85 °C and allowed to stir for 20 h. After cooling to RT, the reaction mixture was then precipitated into methanol (100 mL) followed by collection *via* filtration. The crude product was then purified *via* Soxhlet extraction in ethanol for 12 h. The solid remaining in the thimble was then washed with methanol and collected *via* filtration to afford the product as a dark blue solid (0.05 g, 0.0160 mmol, 64%).

^{1}H NMR (500 MHz, $CDCl_3$) Very broad spectra due to aggregation and poor solubility, thus hard to interpret. Integration of the broad peaks and MALDI mass spectrometry suggest that the target compound was made i.e. integration of NCH_2 and $NCH_2C\mathit{H}$ protons: 4.06 (m,16H, NCH_2) and ~30H in the aromatic region. **^{13}C NMR** (125 MHz, $CDCl_3$) δ 161.6, 148.5, 139.6, 137.0, 135.3, 133.3, 129.9, 129.2, 128.4, 126.4, 124.7, 108.5, 108.1, 46.3, 38.0, 37.8, 31.9, 31.8, 31.3, 31.2, 30.1, 29.8, 29.6, 29.5, 29.3, 26.4, 26.2, 22.7, 14.1. **LRMS** MALDI-TOF-(LD+): Calculated for $C_{202}H_{294}N_8O_8S_8$: 3216 Found *m/z* 3218 $[M+2H]^+$.

Trimer[†]

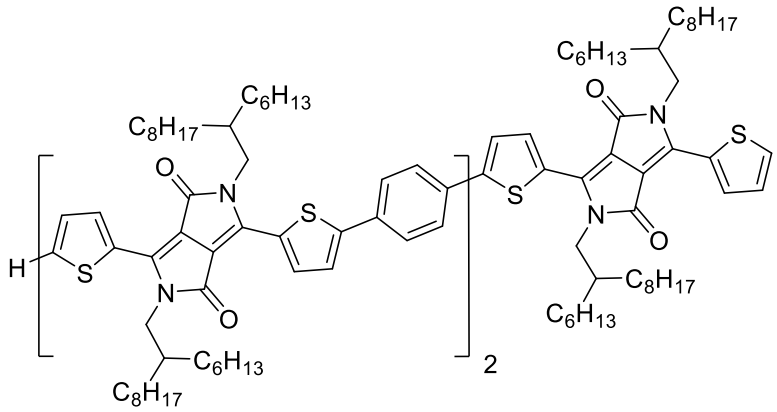

^{1}H NMR (600 MHz $CDCl_3$) δ (ppm): 8.99 (d, *J* = 4.1 Hz, 2H, ArH), 8.96 (d, *J* = 4.1 Hz, 2H, ArH), 8.90 (d, *J* = 3.2 Hz, 2H ArH), 7.74 (s, 8H, PhH), 7.64 (d, *J* = 4.8 Hz, 2H, ArH), 7.54 (t, *J* = 4.1 Hz, 4H, ArH) 7.29 (m, 2H, ArH), 4.08 (m, 8H, NCH_2), 4.05 (d, *J* = 7.6 Hz, 4H, NCH_2), 1.99 (m, 4H, NCH_2CH), 1.93 (m, 2H, NCH_2CH), 1.35- 1.22 (m, CH_2), 0.87-0.83 (m, CH_3). **^{13}C NMR** (151 MHz, $CDCl_3$): 161.8, 161.7, 148.6, 140.2, 140.0, 139.6, 137.1, 135.5, 133.3, 130.6, 130.0, 129.3, 128.5, 126.5, 124.8, 108.5, 108.3, 108.2, 46.4, 46.4, 38.1, 38.1, 37.9, 32.0, 32.0, 32.0, 32.0, 31.4, 31.3, 30.2, 30.2, 30.2, 29.9, 29.8, 29.7, 29.7, 29.7, 29.5, 26.5, 26.4, 26.3, 26.3, 22.8, 22.8, 14.3, 14.2. **LRMS** MALDI-TOF-(LD+): Calculated for $C_{150}H_{220}N_6O_6S_6$: 2396. Found *m/z* 2398 $[M+2H]^+$.

[†]The trimer was synthesised by Dr Anastasia Leventis, University of Cambridge. Characterisation reproduced directly from Leventis.[127]

Pentamer[†]

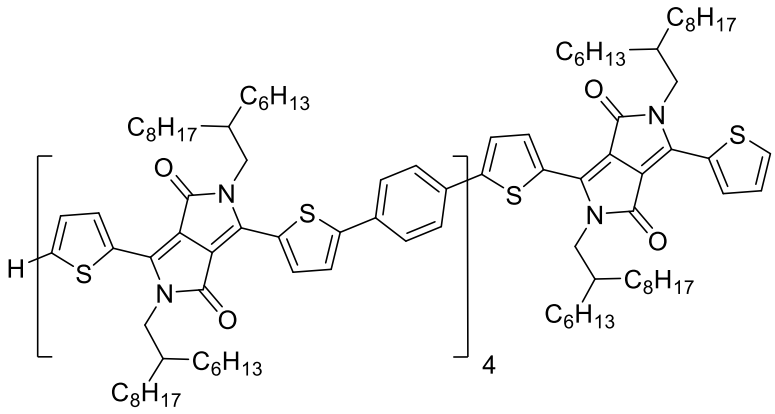

^{1}H NMR (500 MHz $CDCl_3$) δ (ppm): ns = 128. Individual peaks unable to be fully characterised however, integration tentatively suggests compound has been made. 9.20-8.80 (m, ~12 H), 7.76-6.85 (m, ~26 H), 4.21-3.86 (m, ~20 H), 1.97 (m, ~10 H), 1.45-1.0 (m, ~240 H), 0.81 (m, 60 H). ^{13}C NMR (126 MHz $CDCl_3$): UDEFT, ns = 12K, 14 hours. 161.2, 148.1, 139.7, 138.9, 137.3, 135.3, 132.7, 130.3, 130.0, 129.8, 129.7, 128.9, 128.3, 126.5, 125.6, 124.8, 124.2, 108.0, 46.3, 38.1, 38.0, 37.8, 31.9, 31.3, 31.2, 30.1, 29.7, 29.6, 29.3, 29.1, 27.2, 27.2, 26.4, 26.2, 22.7, 14.1. **LRMS** MALDI-TOF-(LD+): Calculated for $C_{254}H_{368}N_{10}O_{10}S_{10}$: 4047. Found: *m/z* 4046 $[M-H]^+$.

[†]The pentamer was synthesised by Dr Anastasia Leventis, University of Cambridge. Characterisation reproduced directly from Leventis.[127]

6.3 Experimental for Chapter III

(2)

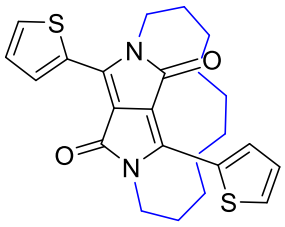

To an oven dried 3-necked flask, equipped with a dropping funnel and under argon, was added K_2CO_3 (0.58 g, 1.66 mmol), 18-crown-6 (6.0 mg, 0.022 mmol), and anhydrous DMF (800 mL). The reaction mixture was then stirred and heated to 120 °C. To a second oven dried flask under argon, was added DPP (**1**) (0.5 g, 1.66 mmol), 1,10-dibromodecane (0.54 g, 1.66 mmol) and DMF (626 mL) which was degassed for 30 min, before dropwise addition into the reaction flask. The reaction mixture was then allowed to stir overnight at 120 °C, before cooling to RT. The solvent was then removed *in vacuo* and the crude product was purified *via* column chromatography (hexane: chloroform= 2:1), sonicated in hexane and collected *via* filtration to give the title compound as a bright pink solid (0.12 g, 0.27 mmol, 16%).

^{1}H NMR (400 MHz, $CDCl_3$) δ (ppm): 8.84 (dd, *J* = 3.9, 1.1 Hz, 2H, ThH), 7.63 (dd, *J* = 5.0, 1.1 Hz, 2H, ThH), 7.28 – 7.25 (m, 2H, ThH), 4.53 (ddd, *J* = 15.0, 10.8, 4.2 Hz, 2H, Alkyl Chain), 4.04 (dt, *J* = 15.0, 4.2 Hz, 2H, Alkyl Chain), 1.85 – 1.74 (m, 2H, Alkyl Chain), 1.65 – 1.52 (m, 2H, Alkyl Chain), 1.36 – 0.77 (m, 12H, Alkyl Chain).**^{13}C NMR** (126 MHz, $CDCl_3$) δ 162.8, 141.1, 134.9, 130.7, 130.5, 128.5, 109.9, 42.8, 29.4, 28.9, 27.9, 26.0. **HRMS** (TOF MS ASAP+): Calculated for $C_{24}H_{26}N_2O_2S_2^+$: 439.1514. Found *m/z* 439.1502 $[M+H]^+$.

EC10DPPT (3)

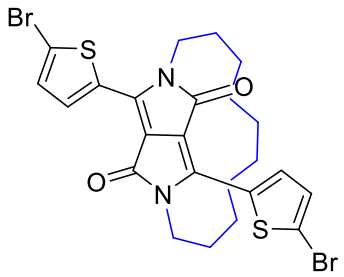

To a 3-necked flask under argon was added **2** (0.11 g, 0.25 mmol) dissolved in chloroform (25 mL) and the reaction was cooled to 0 °C (30 min). N-bromosuccinimide (0.98 g, 0.55 mmol) was then added to the stirring solution and the reaction was covered from light. After cooling, the reaction was heated to 50 °C and was left to stir for 5 h. The resulting solution was then diluted with chloroform and concentrated *in vacuo*. Methanol was then added to the flask and the resulting suspension was then sonicated. The product was purified *via* column chromatography (chloroform), sonicated in methanol and collected by filtration to afford the pure dark purple solid product (0.12 g, 0.20 mmol, 79%).

^{1}H NMR (400 MHz, $CDCl_3$) δ (ppm): 8.60 (d, *J* = 4.2 Hz, 2H, ThH), 7.23 (d, *J* = 4.2 Hz, 2H, ThH), 4.51 (ddd, *J* = 15.2, 11.0, 4.1 Hz, 2H, Alkyl Chain), 3.89 (dt, *J* = 15.2, 4.1 Hz, 2H, Alkyl Chain), 1.87 – 1.75 (m, 2H, Alkyl Chain), 1.66 – 1.50 (m, 2H, Alkyl Chain), 1.34 – 1.06 (m, 6H, Alkyl Chain), 1.02 – 0.76 (m, 6H, Alkyl Chain).**^{13}C NMR** (126 MHz, $CDCl_3$) δ 162.5, 140.0, 135.0, 131.9, 131.6, 119.3, 110.0, 42.9, 29.4, 28.9, 27.9, 25.9. **HRMS** (TOF MS ASAP+): Calculated for $C_{24}H_{25}Br_2N_2O_2S_2^+$: 594.9724. Found *m/z* 594.9714 $[M+H]^+$.

2,5-bis(2-decyltetradecyl)-3,6-di(thiophen-2-yl)-2,5-dihydropyrrolo[3,4-c]pyrrole-1,4-dione (7)

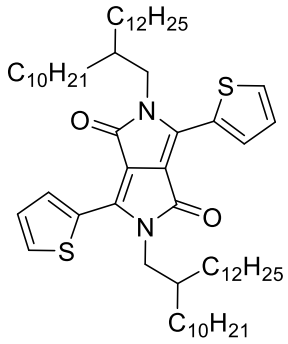

To an oven dried flask under argon was added DPP (**1)** (3.79 g, 12.6 mmol), K_2CO_3 (5.80 g, 42.0 mmol), 18-crown-6 (0.05 g, 0.19 mmol) and 7-(bromomethyl)pentadecane (12.8 g, 42.0 mmol), followed by anhydrous DMF (152 mL). The solution was then heated to 120 °C and was stirred for 18 h. The reaction mixture was then cooled to RT. Chloroform was then added to the flask and the solution was concentrated *in vacuo*. The crude product was then purified *via* column chromatography on silica gel (hexane: chloroform= 2:1) followed by recrystallisation in isopropanol to afford the product as a magenta solid (2.17 g, 2.9 mmol, 23%).

^{1}H NMR (400 MHz, $CDCl_3$) δ (ppm): 8.87 (dd, *J* = 3.9, 1.0 Hz, 2H, ThH), 7.62 (dd, *J* = 5.0, 1.0 Hz, 2H, ThH), 7.28 – 7.22 (m, 2H, ThH), 4.01 (d, *J* = 7.7 Hz, 4H, NCH_2), 1.90 (m, 2H, Alkyl Chain), 1.35 – 1.14 (m, 80H, Alkyl Chain), 0.87 (td, *J* = 6.8, 2.2 Hz, 12H, Alkyl Chain).**^{13}C NMR** (100 MHz, $CDCl_3$) δ 161.8, 140.4, 135.2, 130.4, 129.8, 128.4, 107.9, 46.2, 37.8, 31.9, 31.2, 30.0, 29.7, 29.7, 29.6, 29.4, 29.4, 26.2, 22.7, 14.1. **HRMS** (TOF MS ASAP+): Calculated for $C_{62}H_{105}N_2O_2S_2^+$: 973.7617. Found *m/z* 973.7609 $[M+H]^+$.

Spectroscopic data is supported by literature.[189]

3,6-bis(5-bromothiophen-2-yl)-2,5-bis(2-decyltetradecyl)-2,5-dihydropyrrolo[3,4-c]pyrrole-1,4-dione (6)

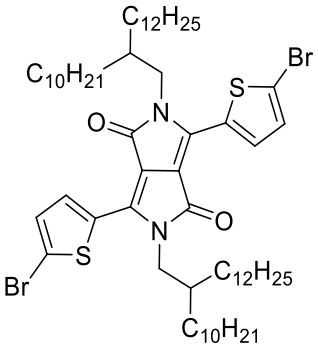

To a 3-necked flask under argon was added 2,5-bis(2-decyltetradecyl)-3,6-di(thiophen-2-yl)-2,5-dihydropyrrolo[3,4-c]pyrrole-1,4-dione (**7**) (1.20 g, 1.23 mmol) dissolved in chloroform (117 mL) and the reaction was cooled to 0 °C (30 min). *N*-bromosuccinimide (0.48 g, 2.71 mmol) was then added to the stirring solution and the reaction was covered from light. The reaction was then allowed to warm to RT and left to stir overnight. The resulting solution was then diluted with chloroform and concentrated *in vacuo*. The crude product was purified *via* column chromatography (hexane: chloroform= 1:2) followed by recrystallisation in isopropanol. The solid was then collected *via* filtration to give the title compound as a dark purple waxy solid (1.10 g, 0.97 mmol, 79%).

^{1}H NMR (400 MHz, $CDCl_3$) δ (ppm): 8.62 (d, *J* = 4.2 Hz, 2H, ThH), 7.22 (d, *J* = 4.2 Hz, 2H, ThH), 3.92 (d, *J* = 7.7 Hz, 4H, NCH_2), 1.87 (br s, 2H, NCH_2CH), 1.33 – 1.16 (m, 80H, Alkyl Chain), 0.87 (t, *J* = 6.8, 12H, CH_3). **^{13}C NMR** (100 MHz, $CDCl_3$) δ 161.4, 139.4, 135.3, 131.4, 131.2, 119.0, 108.0, 46.4, 37.8, 31.9, 31.2, 30.0, 29.7, 29.6, 29.4, 26.2, 22.7, 14.1. **HRMS** (TOF MS ASAP+): Calculated for $C_{62}H_{103}Br_2N_2O_2S_2^+$: 1129.5828. Found *m/z* 1129.5780 $[M+H]^+$.

Spectroscopic data is supported by literature.[189]

Doped DPP Polymers- Ph Series Synthesis

*Literature Polymer **PDPPT-P***

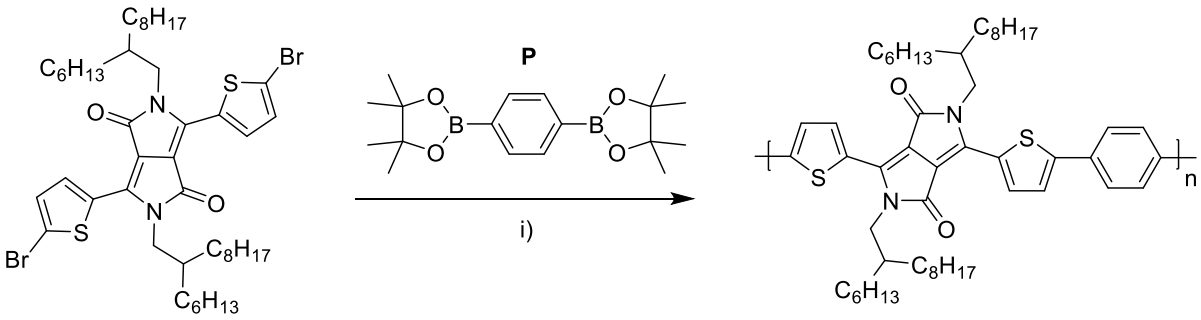

i)$Pd_2(dba)_3$, PPh_3, K_3PO_4, Aliquat 336, Toluene, H_2O, 115 °C, 3 days.

Procedure from literature.[117]

Doped Polymers- Monomer Ratios, Yields and Molecular Weights

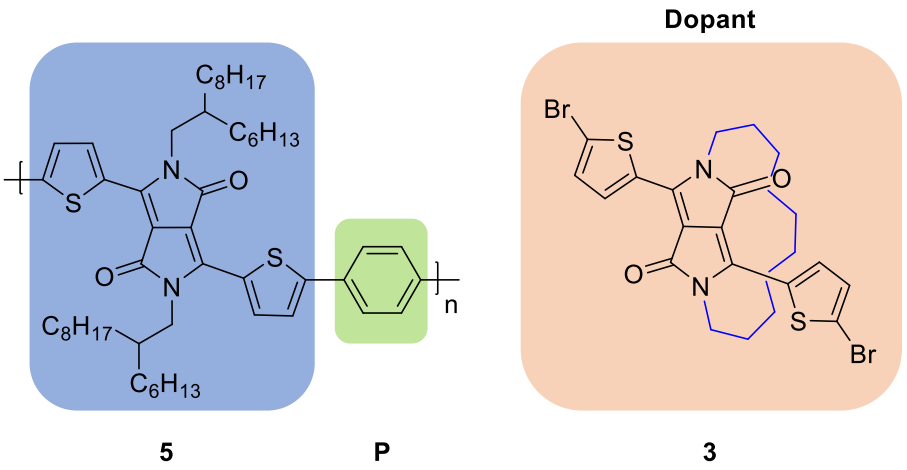

	Monomer Ratio			Yield (%)	Molecular Weight (KDa)	
Polymer	**5**	**3**	**P**		M_n^a	M_w^a
PDPPT-P	1	0	1	77	25.1	72.7
PE5DPPT-P	0.95	0.05	1	54	28.4	86.1
PE10DPPT-P	0.90	0.1	1	64	25.1	79.5
PE20DPPT-P	0.80	0.2	1	36	40.7	210.7
PE30DPPT-P	0.70	0.3	1	25	24.4	100.5

PDPPT-P

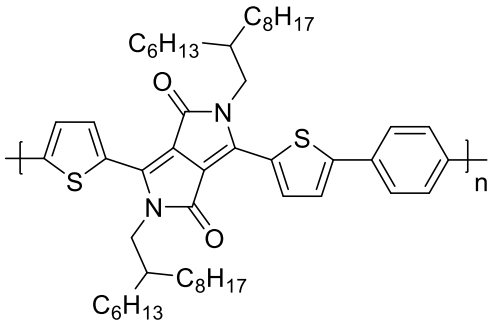

To a 10 mL oven dried microwave vial under argon was added **5** (0.10 g, 0.11 mmol), 1,4-benzenediboronic acid bis(pinacol) ester (0.036 g, 0.11 mmol), triphenylphosphine (3.10 mg, 0.0117 mmol) and tris(dibenzylideneacetone)dipalladium (0) (4.55 mg, 0.0050 mmol). The reaction vial was then sealed and left to degas for 1 h. This was followed by the addition of degassed toluene (1.81 mL) containing a few drops of Aliquat 336 and degassed K_3PO_4 aq solution (0.23 mL) made from a stock solution (0.99 g of K_3PO_4 in 2.3 mL water). The reaction was then heated to 115 °C and allowed to stir for 3 days. The vial was then left to cool to RT and the reaction mixture was then added dropwise into a flask of stirring methanol. Precipitate (blue stringy flakes) began to form and was filtered into a cellulose thimble under reduced pressure, which was then washed with acetone and methanol. The polymer was then purified *via* Soxhlet extraction in the following solvents: acetone (12 h), hexane (12 h) and chloroform (12 h). The chloroform fraction was then concentrated *in vacuo* to give a deep blue plastic-like film. The solid was dissolved in minimum chlorobenzene and added dropwise slowly into a flask of rapidly stirring methanol. Once the addition was completed, the mixture was allowed to stir for a further 30 min before the dark blue solid was collected *via* filtration and washed with methanol and acetone, to afford the dark blue polymer **PDPPT-P** (0.07 g, 77%); M_n: 25.1 KDa; M_w: 72.7 KDa; PDI: 2.9.

PE5DPPT-P

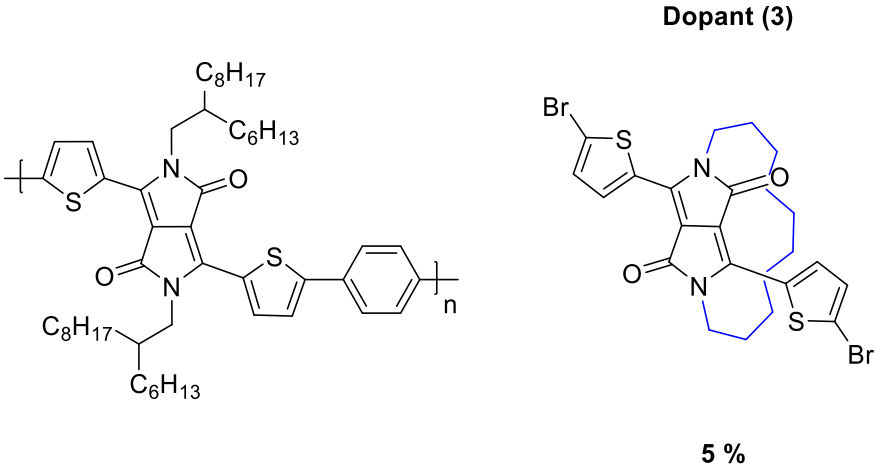

PE5DPPT-P was made *via* the same procedure as **PDPPT-P**, with the following amounts of reagents; **5** (0.10 g, 0.110 mmol), **3** (3.5 mg, 0.006 mmol), 1,4-benzenediboronic acid bis(pinacol) ester (0.038 g, 0.116 mmol). The polymer was then purified *via* Soxhlet extraction in the following solvents: acetone (12 h), hexane (12 h), chloroform (12 h) and chlorobenzene (12 h). The chlorobenzene fraction was then concentrated *in vacuo* to give a deep blue plastic-like film. The solid was dissolved in minimum chlorobenzene and added dropwise slowly into a flask of rapidly stirring methanol. Once the addition was completed, the mixture was allowed to stir for a further 30 min before the dark blue solid was collected *via* filtration and washed with methanol and acetone, to afford the dark blue polymer **PE5DPPT-P** (0.05 g, 54%); M_n: 28.4 KDa; M_w: 86.1 KDa; PDI: 3.0.

PE10DPPT-P

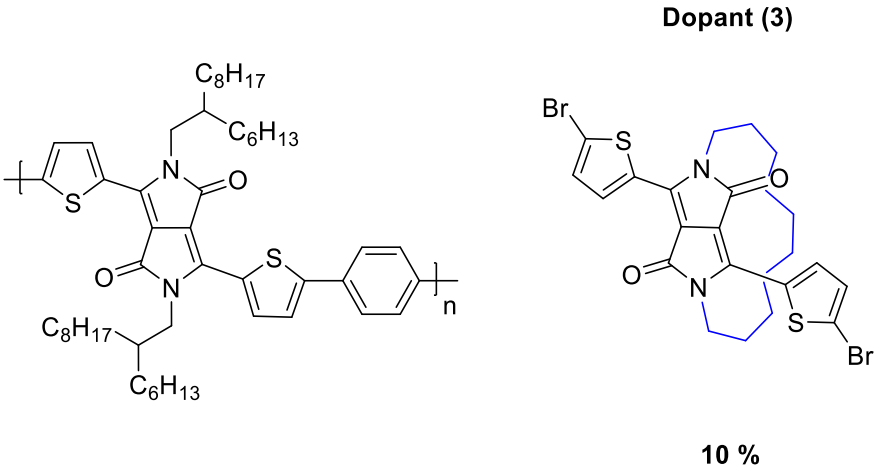

PE10DPPT-P was made *via* the same procedure as **PDPPT-P**, with the following amounts of reagents; **5** (0.09 g, 0.099 mmol), **3** (6.5 mg, 0.011 mmol), 1,4-benzenediboronic acid bis(pinacol) ester (0.036 g, 0.110 mmol). The polymer was then purified *via* Soxhlet extraction in the following solvents: acetone (12 h), hexane (12 h), chloroform (12 h) and chlorobenzene (12 h). The chlorobenzene fraction was then concentrated *in vacuo* to give a deep blue plastic-like film. The solid was dissolved in minimum chlorobenzene and added dropwise slowly into a flask of rapidly stirring methanol. Once the addition was completed, the mixture was allowed to stir for a further 30 min before the dark blue solid was collected *via* filtration and washed with methanol and acetone, to afford the dark blue polymer **PE10DPPT-P** (0.06 g, 64%); M_n: 25.1 KDa; M_w: 79.5 KDa; PDI: 3.2.

PE20DPPT-P

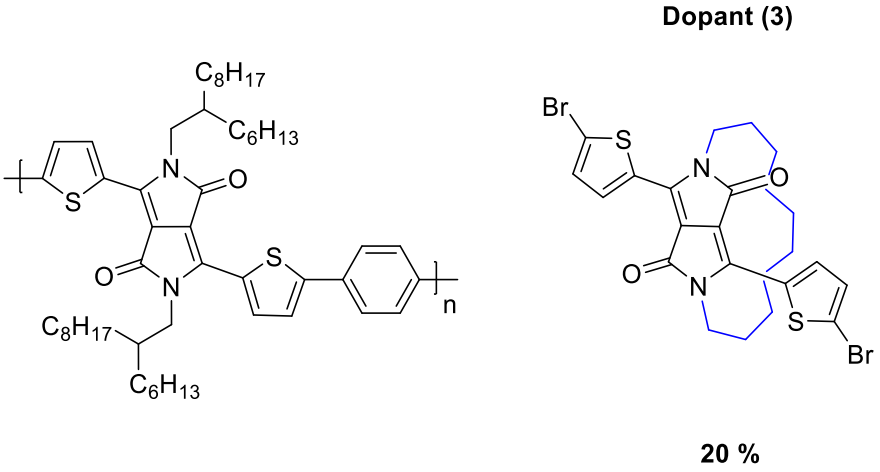

PE20DPPT-P was made *via* the same procedure as **PDPPT-P**, with the following amounts of reagents; **5** (0.094 g, 0.104 mmol), **3** (0.016 g, 0.026 mmol), 1,4-benzenediboronic acid bis(pinacol) ester (0.043 g, 0.130 mmol). The polymer was then purified *via* Soxhlet extraction in the following solvents: acetone (12 h), hexane (12 h), chloroform (12 h) and chlorobenzene (12 h). The chlorobenzene fraction was then concentrated *in vacuo* to give a deep blue plastic-like film. The solid was dissolved in minimum chlorobenzene and added dropwise slowly into a flask of rapidly stirring methanol. Once the addition was completed, the mixture was allowed to stir for a further 30 min before the dark blue solid was collected *via* filtration and washed with methanol and acetone, to afford the dark blue polymer **PE20DPPT-P** (0.04 g, 36%); M_n: 40.7 KDa; M_w: 210.7 KDa; PDI: 5.2.

PE30DPPT-P

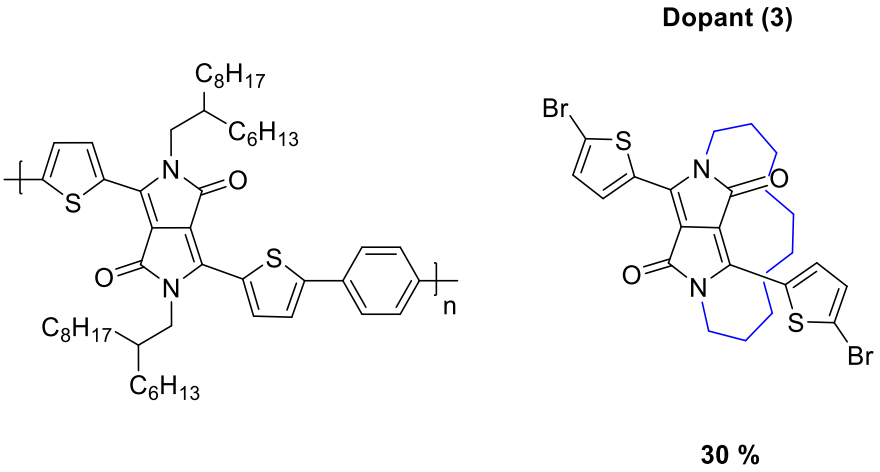

PE30DPPT-P was made *via* the same procedure as **PDPPT-P**, with the following amounts of reagents; **5** (0.083 g, 0.092 mmol), **3** (0.023 g, 0.039 mmol), 1,4-benzenediboronic acid bis(pinacol) ester (0.043 g, 0.131 mmol). The polymer was then purified *via* Soxhlet extraction in the following solvents: acetone (12 h), hexane (12 h), chloroform (12 h) and chlorobenzene (12 h). The chlorobenzene fraction was then concentrated *in vacuo* to give a deep blue plastic-like film. The solid was dissolved in minimum chlorobenzene and added dropwise slowly into a flask of rapidly stirring methanol. Once the addition was completed, the mixture was allowed to stir for a further 30 min before the dark blue solid was collected *via* filtration and washed with methanol and acetone, to afford the dark blue polymer **PE30DPPT-P** (0.03 g, 25%); M_n: 24.4 KDa; M_w: 100.5 KDa; PDI: 4.1.

Doped DPP Polymers-TT Series Synthesis

*Literature Polymer **PDPPT-TT***

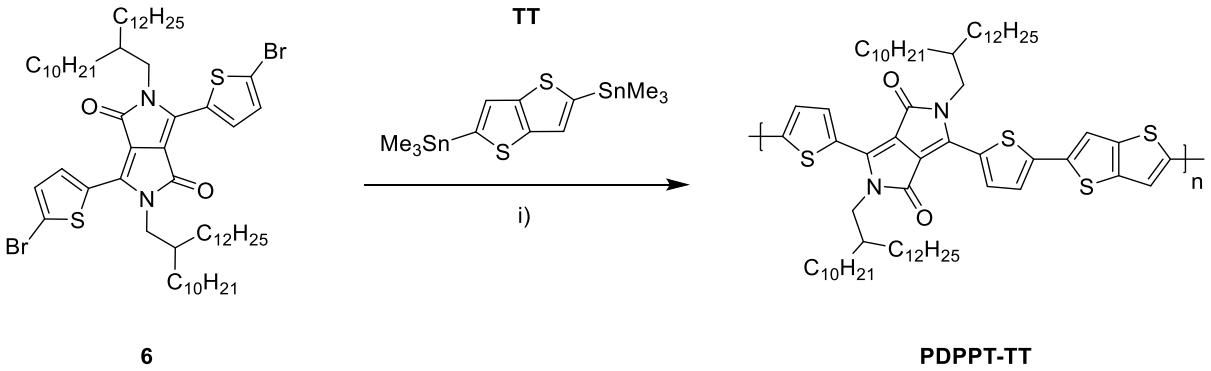

i) Pd(dba)$_3$, P(o-tol)$_3$, Toluene, DMF, 115 °C, 18 h.

Procedure from literature.[28]

Doped Polymers- Monomer Ratios, Yields and Molecular Weights

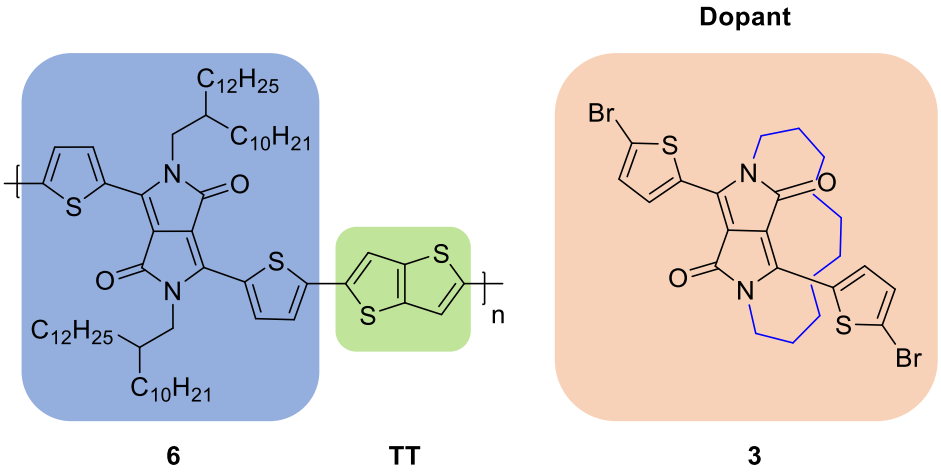

	Monomer Ratio			Yield (%)	Molecular Weight (KDa)	
Polymer	**6**	**3**	**TT**		M_n[a]	M_w[a]
PDPPT-TT	1	0	1	77	26.3	102.7
PE5DPPT-TT	0.95	0.05	1	83	24.4	79.1
PE10DPPT-TT	0.90	0.1	1	71	78.4	221.2
PE20DPPT-TT	0.80	0.2	1	39	14.0	76.4

PDPPT-TT

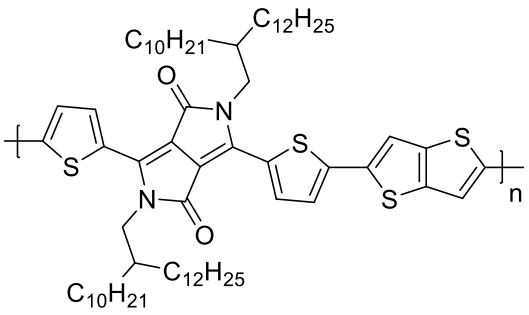

To an oven dried 10 mL microwave vial under argon was added **6** (0.10 g, 0.088 mmol), 2,5-bis(trimethylstannyl)-thieno[3,2-*b*]thiophene (0.041 g, 0.088 mmol), $Pd_2(dba)_3$ (0.003 g, 0.003 mmol) and P(*o*-tol)$_3$ (0.003 g, 0.011 mmol). The reaction vial was then sealed and left to degas for 1 h. This was followed by the addition of degassed toluene (4.70 mL) and degassed DMF (0.47 mL). The reaction was then heated to 115 °C and allowed to stir for 18 h. The vial was then left to cool to RT and the reaction mixture was then added dropwise into a flask of stirring methanol. Precipitate (blue stringy flakes) began to form and was filtered into a cellulose thimble under reduced pressure, which was then washed with acetone and methanol. The polymer was then purified *via* Soxhlet extraction in the following solvents: acetone (12 h), hexane (12 h) and dichloromethane (12 h). The dichloromethane fraction was then concentrated *in vacuo* to give a deep blue plastic-like film. The solid was dissolved in minimum chlorobenzene and added dropwise slowly into a flask of rapidly stirring methanol. Once the addition was completed, the mixture was allowed to stir for a further 30 min before the dark blue solid was collected *via* filtration and washed with methanol and acetone, to afford the dark blue polymer **PDPPT-TT** (0.07 g, 77%); M_n: 26.3 KDa; M_w: 102.7 KDa; PDI: 3.9.

PE5DPPT-TT

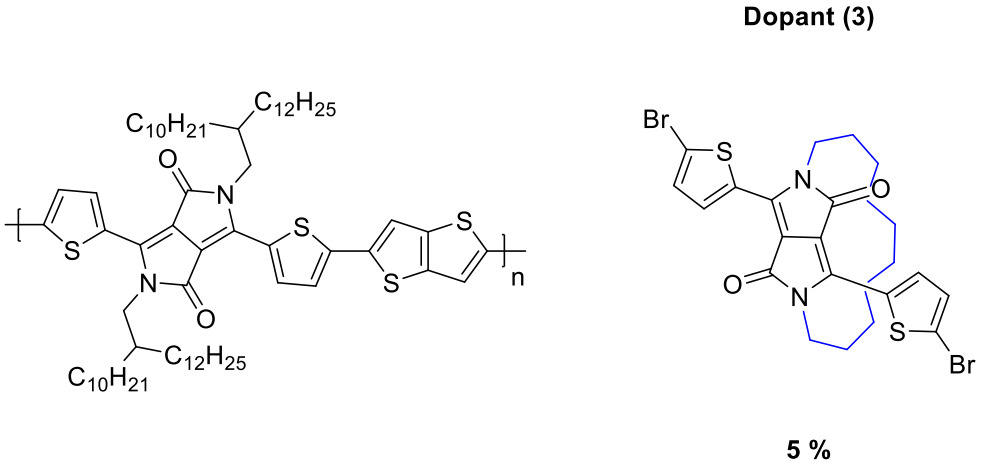

PE5DPPT-TT was made *via* the same procedure as **PDPPT-TT**, with the following amounts of reagents; **6** (0.10 g, 0.088 mmol), **3** (2.8 mg, 0.005 mmol) and 2,5-bis(trimethylstannyl)-thieno[3,2-*b*]thiophene (0.043 g, 0.093 mmol). The polymer was then purified *via* Soxhlet extraction in the following solvents: acetone (12 h), hexane (12 h), dichloromethane (12 h) and chloroform (12 h). The chloroform fraction was then concentrated *in vacuo* to give a deep blue plastic-like film. The solid was dissolved in minimum chlorobenzene and added dropwise slowly into a flask of rapidly stirring methanol. Once the addition was completed, the mixture was allowed to stir for a further 30 min before the dark blue solid was collected *via* filtration and washed with methanol and acetone, to afford the dark blue polymer **PE5DPPT-TT** (0.08 g, 83%); M_n: 24.4 KDa; M_w: 79.1 KDa; PDI: 3.2.

PE10DPPT-TT

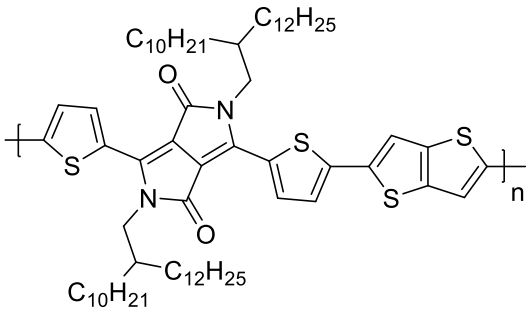

Dopant (3)

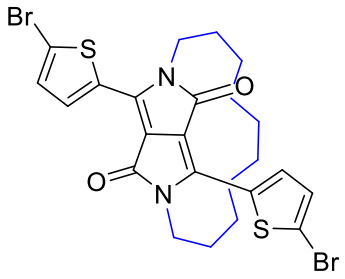

10 %

PE10DPPT-TT was made *via* the same procedure as **PDPPT-TT**, with the following amounts of reagents; **6** (0.10 g, 0.088 mmol), **3** (5.9 mg, 0.010 mmol) and 2,5-bis(trimethylstannyl)-thieno[3,2-*b*]thiophene (0.046 g, 0.098 mmol). The polymer was then purified *via* Soxhlet extraction in the following solvents: acetone (12 h), hexane (12 h), dichloromethane (12 h), chloroform (12 h) and chlorobenzene (12 h). The chlorobenzene fraction was then concentrated *in vacuo* to give a deep blue plastic-like film. The solid was dissolved in minimum chlorobenzene and added dropwise slowly into a flask of rapidly stirring methanol. Once the addition was completed, the mixture was allowed to stir for a further 30 min before the dark blue solid was collected *via* filtration and washed with methanol and acetone, to afford the dark blue polymer **PE10DPPT-TT** (0.07 g, 71%); M_n: 78.4 KDa; M_w: 221.2 KDa; PDI: 2.8.

PE20DPPT-TT

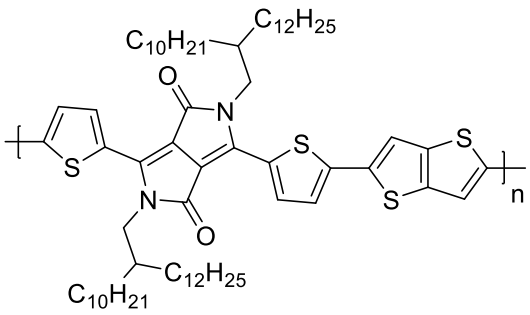

Dopant (3)

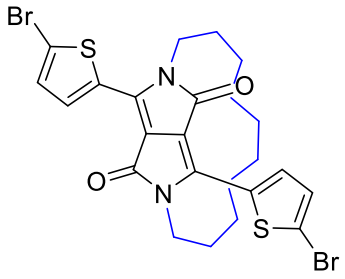

20 %

PE20DPPT-TT was made *via* the same procedure as **PDPPT-TT**, with the following amounts of reagents; **6** (0.10 g, 0.088 mmol), **3** (13.2 mg, 0.022 mmol) and 2,5-bis(trimethylstannyl)-thieno[3,2-*b*]thiophene (0.051 g, 0.110 mmol). The polymer was then purified *via* Soxhlet extraction in the following solvents: acetone (12 h), hexane (12 h), dichloromethane (12 h) and chloroform (12 h). The chloroform fraction was then concentrated *in vacuo* to give a deep blue plastic-like film. The solid was dissolved in minimum chlorobenzene and added dropwise slowly into a flask of rapidly stirring methanol. Once the addition was completed, the mixture was allowed to stir for a further 30 min before the dark blue solid was collected *via* filtration and washed with methanol and acetone, to afford the dark blue polymer **PE20DPPT-TT** (0.05 g, 39%); M_n: 14.0 KDa; M_w: 76.4 KDa; PDI: 5.5.

(8a)

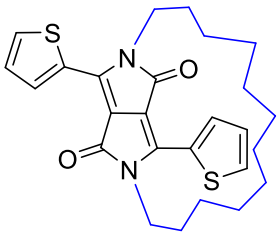

To an oven dried 3-necked flask, equipped with a dropping funnel and under argon, was added DPP (**1**) (0.50 g, 1.66 mmol), K_2CO_3 (0.77 g, 3.32 mmol), 18-crown-6 (6.0 mg, 0.022 mmol), and anhydrous DMF (182 mL). The reaction mixture was then stirred at 50 °C for 1 h. To a second oven dried flask under argon, was added 1,12-dibromododecane (0.50 g, 1.66 mmol) and DMF (182 mL) which was degassed for 30 min, before dropwise addition into the reaction flask. The reaction mixture was then allowed to stir overnight at 100 °C for two nights, before cooling to RT. The solvent was then removed *in vacuo* and the crude product was purified *via* column chromatography (hexane: chloroform= 2:1) followed by sonication in hexane. The solid was then collected *via* filtration to give the title compound as a dark purple solid (0.27 g, 0.58 mmol, 35%).

^{1}H NMR (400 MHz, $CDCl_3$) δ (ppm): 8.81 (d, *J* = 3.8 Hz, 2H, ThH), 7.62 (d, *J* = 5.0 Hz, 2H, ThH), 7.26 (m, 2H, ThH), 4.47 (ddd, *J* = 14.9, 11.3, 3.4 Hz, 2H, Alkyl Chain), 4.02 (dt, *J* = 14.9, 3.4 Hz, 2H, Alkyl Chain), 1.77 – 1.57 (m, 4H, Alkyl Chain), 1.31 – 0.96 (m, 16H, Alkyl Chain).**^{13}C NMR** (100 MHz, $CDCl_3$) δ 162.4, 140.3, 134.8, 130.6, 130.2, 128.4, 108.8, 41.9, 28.5, 28.3, 27.7, 27.6, 25.0. **HRMS** (TOF MS ASAP+): Calculated for $C_{26}H_{31}N_2O_2S_2^+$: 467.1827. Found *m/z* 467.1825 $[M+H]^+$.

(8b)

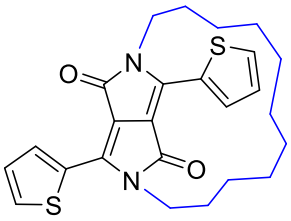

To an oven dried 3-necked flask, equipped with a dropping funnel and under argon, was added DPP (**1**) (0.50 g, 1.66 mmol), K_2CO_3 (0.77 g, 3.32 mmol), 18-crown-6 (6.0 mg, 0.022 mmol), and anhydrous DMF (182 mL). The reaction mixture was then stirred at 50 °C for 1 h. To a second oven dried flask under argon, was added 1,11-dibromoundecane (0.52 g, 1.66 mmol) and DMF (182 mL) which was degassed for 30 min, before dropwise addition into the reaction flask. The reaction mixture was then allowed to stir at 100 °C for two nights, before cooling to RT. The solvent was then removed *in vacuo* and the crude product was purified *via* column chromatography (hexane: chloroform= 2:1) followed by sonication in hexane. The solid was then collected *via* filtration to give the title compound as a dark purple solid (0.24 g, 0.53 mmol, 32%).

^{1}H NMR (400 MHz, $CDCl_3$) δ (ppm): 8.90 (dd, *J* = 4.0, 1.0 Hz, 2H, ThH), 7.63 (dd, *J* = 5.0, 1.0 Hz, 2H, ThH), 7.28 (dd, *J* = 5.0, 4.0 Hz, 2H, ThH), 4.49 (ddd, *J* = 15.0, 11.2, 3.9 Hz, 2H, Alkyl Chain), 4.05 (dt, *J* = 15.0, 3.9 Hz, 2H, Alkyl Chain), 1.86 – 1.75 (m, 2H, Alkyl Chain), 1.64 – 1.50 (m, 2H, Alkyl Chain), 1.46 – 1.36 (m, 2H, Alkyl Chain), 1.31 – 1.21 (m, 2H, Alkyl Chain), 1.08 – 0.92 (m, 10H, Alkyl Chain).**^{13}C NMR** (151 MHz, $CDCl_3$) δ 162.5, 140.5, 135.1, 130.6, 130.2, 128.5, 108.9, 42.4, 29.2, 28.8, 28.4, 28.1, 25.5. **HRMS** (TOF MS ASAP+): Calculated for $C_{25}H_{29}N_2O_2S_2^+$: 453.1670. Found *m/z* 453.1681 $[M+H]^+$.

(8c)

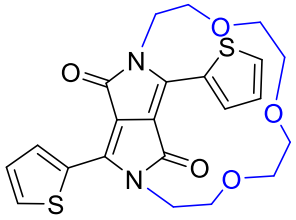

To an oven dried 3-necked flask, equipped with a dropping funnel and under argon, was added DPP (**1**) (0.50 g, 1.66 mmol), K_2CO_3 (0.77 g, 3.32 mmol), 18-crown-6 (6.0 mg, 0.022 mmol), and anhydrous DMF (182 mL). The reaction mixture was then stirred at 50 °C for 1 h. To a second oven dried flask under argon, was added tetraethylene glycol di(p-toluenesulfonate) (0.84 g, 1.66 mmol) and DMF (182 mL) which was degassed for 30 min, before dropwise addition into the reaction flask. The reaction mixture was then allowed to stir at 100 °C for two nights, before cooling to RT. The solvent was then removed *in vacuo* and the crude product was purified *via* column chromatography (DCM: ethyl acetate= 2:1) followed by recrystallisation in methanol. The solid was then collected *via* filtration to give the title compound as a shiny champagne coloured solid (0.09 g, 0.20 mmol, 12%).

^{1}H NMR (400 MHz, $CDCl_3$) δ (ppm): 8.67 (dd, *J* = 3.8, 0.7 Hz, 2H, ThH), 7.59 (dd, *J* = 5.0, 0.7 Hz, 2H, ThH), 7.28 – 7.22 (m, 2H, ThH), 4.56 (m, 2H, OCH_2), 4.20 – 4.10 (m, 2H, OCH_2), 3.71 (m, 2H, OCH_2), 3.54 – 3.41 (m, 2H, OCH_2), 3.38 – 3.23 (m, 6H, OCH_2). **^{13}C NMR** (100 MHz, $CDCl_3$) δ 163.4, 140.8, 134.2, 130.5, 129.9, 128.4, 110.5, 71.5, 70.4, 68.0, 42.7. **HRMS** (TOF MS ASAP+): Calculated for $C_{22}H_{23}N_2O_5S_2^+$: 459.1048. Found *m/z* 459.1048 $[M+H]^+$.

EC12DPPT (10a)

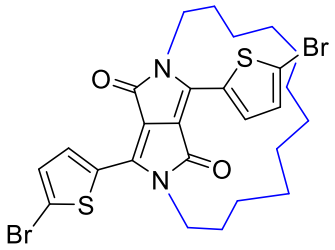

To a 3-necked flask under argon was added **8a** (0.092 g, 0.20 mmol) dissolved in chloroform (25 mL) and the reaction was cooled to 0 °C (30 min). *N*-bromosuccinimide (0.087 g, 0.49 mmol) was then added to the stirring solution and the reaction was covered from light. The reaction was heated to 90 °C and left to stir overnight. The resulting solution was then diluted with chloroform and concentrated *in vacuo*. The crude product was purified *via* column chromatography (hexane: chloroform= 1:2) followed by sonication in methanol. The solid was then collected *via* filtration to give the title compound as a dark purple solid (0.06 g, 0.10 mmol, 48%).

^{1}H NMR (400 MHz, $CDCl_3$) δ (ppm): 8.58 (d, *J* = 4.2 Hz, 2H, ThH), 7.22 (d, *J* = 4.2 Hz, 2H, ThH), 4.45 (ddd, *J* = 15.1, 11.4, 3.5 Hz, 2H, Alkyl Chain), 3.87 (dt, *J* = 15.1, 3.5 Hz, 2H, Alkyl Chain), 1.77 – 1.57 (m, 4H, Alkyl Chain), 1.35 – 0.91 (m, 16H, Alkyl Chain).**^{13}C NMR** (100 MHz, $CDCl_3$) δ 162.0, 139.2, 135.0, 131.5, 131.5, 119.1, 108.9, 42.0, 28.5, 28.3, 27.7, 27.6, 25.0. **HRMS** (TOF MS ASAP+): Calculated for $C_{26}H_{29}Br_2N_2O_2S_2^+$: 625.0037. Found *m/z* 625.0038 $[M+H]^+$.

EC11DPPT (10b)

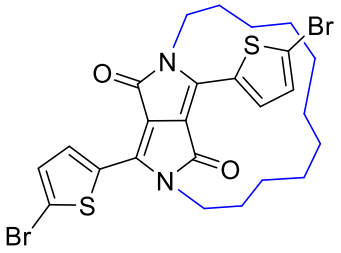

To a 3-necked flask under argon was added **8b** (0.130 g, 0.29 mmol) dissolved in chloroform (30 mL) and the reaction was cooled to 0 °C (30 min). *N*-bromosuccinimide (0.127 g, 0.71 mmol) was then added to the stirring solution and the reaction was covered from light. The reaction was then heated to 90 °C and was left to stir overnight. The resulting solution was then diluted with chloroform and concentrated *in vacuo*. The crude product was purified *via* column chromatography (hexane: chloroform= 1:2) followed by sonication in methanol. The solid was then collected *via* filtration to give the title compound as a dark purple solid (0.11 g, 0.17 mmol, 60%).

^{1}H NMR (400 MHz, $CDCl_3$) δ (ppm): 8.67 (d, *J* = 4.2 Hz, 2H, ThH), 7.23 (d, *J* = 4.2 Hz, 2H, ThH), 4.46 (ddd, *J* = 15.0, 11.5, 3.4 Hz, 2H, Alkyl Chain), 3.88 (dt, *J* = 15.0, 3.4 Hz, 2H, Alkyl Chain), 1.87 – 1.76 (m, 2H, Alkyl Chain), 1.62 – 1.49 (m, 2H, Alkyl Chain), 1.48 – 1.35 (m, 2H, Alkyl Chain), 1.27 – 1.14 (m, 2H, Alkyl Chain), 1.08 – 0.86 (m, 10H, Alkyl Chain).**^{13}C NMR** (151 MHz, $CDCl_3$) δ 162.1, 139.4, 135.2, 131.6, 131.5, 119.2, 109.0, 42.5, 29.1, 28.8, 28.4, 28.2, 25.5. **HRMS** (TOF MS ASAP+): Calculated for $C_{25}H_{28}Br_2N_2O_2S_2^+$: 608.9881. Found *m/z* 608.9862 $[M+H]^+$.

EP11DPPT (10c)

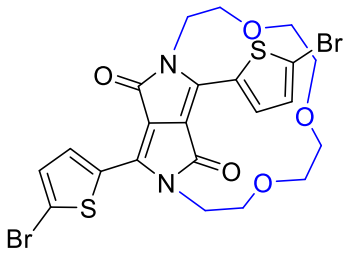

To a 3-necked flask under argon was added **8c** (0.14 g, 0.31 mmol) dissolved in chloroform (30 mL) and the reaction was cooled to 0 °C (30 min). *N*-bromosuccinimide (0.12 g, 0.69 mmol) was then added to the stirring solution and the reaction was covered from light. The reaction was then allowed to warm to RT and left to stir overnight. The resulting solution was then diluted with chloroform and concentrated *in vacuo*. The crude product was purified *via* column chromatography (chloroform: ethyl acetate= 2:1) followed by sonication in methanol. The solid was then collected *via* filtration to give the title compound as a dark purple gold flecked solid (0.04 g, 0.06 mmol, 21%).

^{1}H NMR (400 MHz, $CDCl_3$) δ (ppm): 8.39 (d, *J* = 4.1 Hz, 2H, ThH), 7.20 (d, *J* = 4.1 Hz, 2H, ThH), 4.51 (m, 2H, OCH_2), 4.00 (m, 2H, OCH_2), 3.74 – 3.63 (m, 2H, OCH_2), 3.56 – 3.22 (m, 10H, OCH_2).**^{13}C NMR** (126 MHz, $CDCl_3$) δ 163.1, 139.9, 134.3, 131.8, 131.4, 118.3, 110.5, 71.4, 70.4, 67.8, 42.7. **HRMS** (TOF MS ASAP+): Calculated for**:** $C_{22}H_{21}Br_2N_2O_5S_2^+$: 614.9259. Found *m/z* 614.9252 $[M+H]^+$.

DPP-BDT Polymer Synthesis[†]

*Reference Polymer **PDPP-BDT***

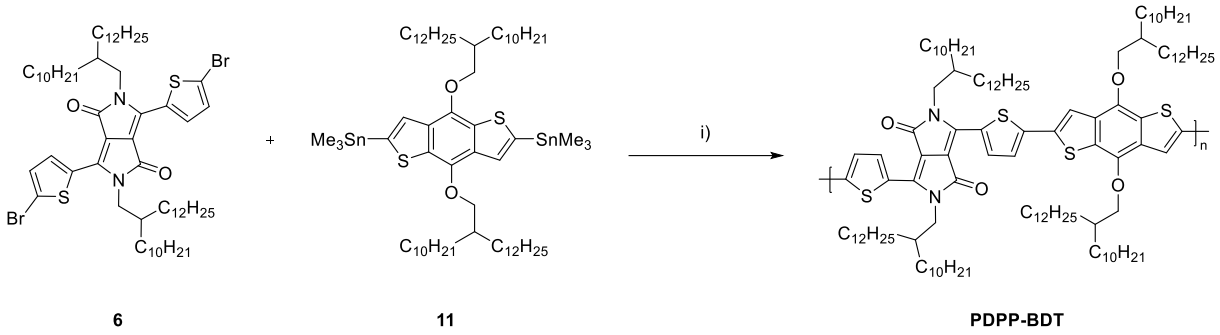

6 **11** **PDPP-BDT**

i) $Pd(PPh_3)_4$, Toluene, DMF, 110 °C, 18 h.

Procedure adapted from literature.[159]

[†]Compound **11** was synthesised by Dr Anastasia Leventis, University of Cambridge

Synthesis of encapsulated polymers ***PE12DPP-BDT, PE11DPP-BDT, PP11DPP-BDT*** *and* ***PDPP-E10BDT***[†]

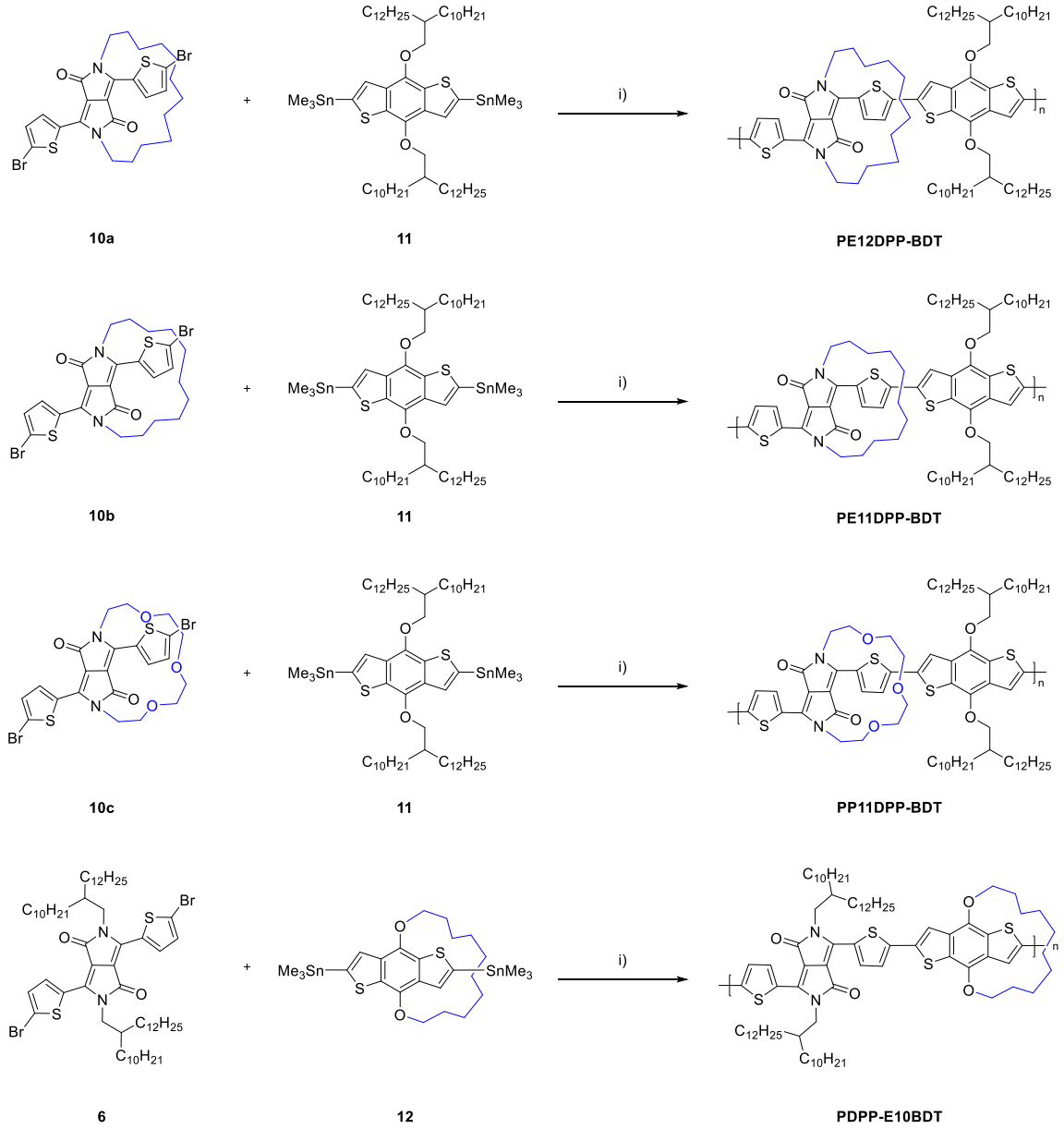

i) Pd(PPh₃)₄, Toluene, DMF, 110 °C, 18 h.

Procedure adapted from literature.[159]

[†]Compounds **11** and **12**,[152] were synthesised by Dr Anastasia Leventis, University of Cambridge.

PDPP-BDT

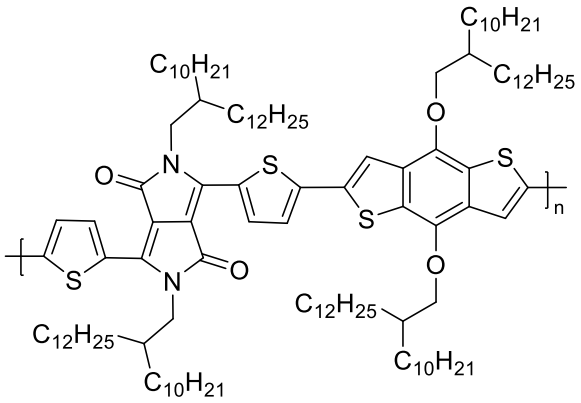

To an oven dried 10 mL microwave vial under argon was added **6** (0.056 g, 0.049 mmol), **11** (0.060 g, 0.049 mmol) and $Pd(PPh_3)_4$ (2.7 mg, 0.0023 mmol). The reaction vial was then sealed and left to degas for 1 h. This was followed by the addition of degassed toluene (1.99 mL) and degassed DMF (0.19 mL). The reaction was then heated to 110 °C and allowed to stir for 18 h. The vial was then left to cool to RT and the reaction mixture was then added dropwise into a flask of stirring methanol. Precipitate (blue stringy flakes) began to form and was filtered into a cellulose thimble under reduced pressure, which was then washed with acetone and methanol. The polymer was then purified *via* Soxhlet extraction in the following solvents: acetone (12 h) and hexane (12 h). The hexane fraction was then concentrated *in vacuo* to give a deep blue plastic-like film. The solid was dissolved in minimum hexane and added dropwise slowly into a flask of rapidly stirring methanol. Once the addition was completed, the mixture was allowed to stir for a further 30 min before the dark blue solid was collected *via* filtration and washed with methanol and acetone, to afford the waxy blue polymer **PDPP-BDT** (0.02 g, 24%); M_n: 15.9 KDa; M_w: 30.4 KDa; PDI: 1.9.

PE12DPP-BDT

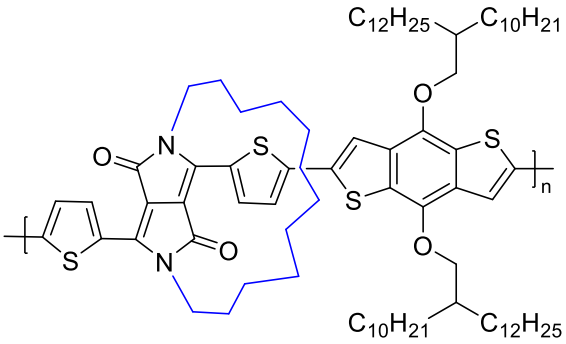

To an oven dried 10 mL microwave vial under argon was added **10a** (0.060 g, 0.096 mmol), **11** (0.118 g, 0.096 mmol) and $Pd(PPh_3)_4$ (4.8 mg, 0.0042 mmol). The reaction vial was then sealed and left to degas for 1 h. This was followed by the addition of degassed toluene (3.89 mL) and degassed DMF (0.389 mL). The reaction was then heated to 110 °C and allowed to stir for 18 h. The vial was then left to cool to RT and the reaction mixture was then added dropwise into a flask of stirring methanol. Precipitate (blue stringy flakes) began to form and was filtered into a cellulose thimble under reduced pressure, which was then washed with acetone and methanol. The polymer was then purified *via* Soxhlet extraction in the following solvents: acetone (12 h), hexane (12 h) and chloroform (12 h). The chloroform fraction was then concentrated *in vacuo* to give a deep blue plastic-like film. The solid was dissolved in minimum chloroform and added dropwise slowly into a flask of rapidly stirring methanol. Once the addition was completed, the mixture was allowed to stir for a further 30 min before the dark blue solid was collected *via* filtration and washed with methanol and acetone, to afford the dark blue polymer **PE12DPP-BDT** (0.11 g, 81%); M_n: 44.0 KDa; M_w: 104.9 KDa; PDI: 2.4.

PE11DPP-BDT

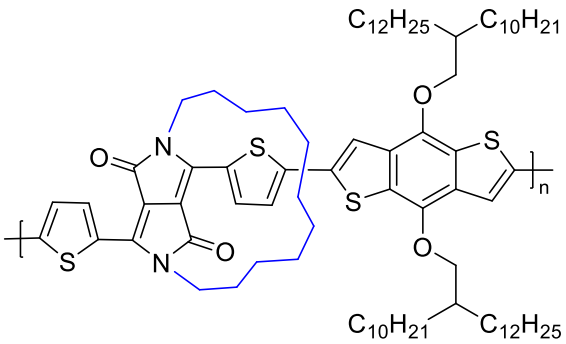

To an oven dried 10 mL microwave vial under argon was added **10b** (0.060 g, 0.098 mmol), **11** (0.120 g, 0.098 mmol) and $Pd(PPh_3)_4$ (5.2 mg, 0.0039 mmol). The reaction vial was then sealed and left to degas for 1 h. This was followed by the addition of degassed toluene (3.98 mL) and degassed DMF (0.398 mL). The reaction was then heated to 110 °C and allowed to stir for 18 h. The vial was then left to cool to RT and the reaction mixture was then added dropwise into a flask of stirring methanol. Precipitate (blue stringy flakes) began to form and was filtered into a cellulose thimble under reduced pressure, which was then washed with acetone and methanol. The polymer was then purified *via* Soxhlet extraction in the following solvents: acetone (12 h), hexane (12 h) and chloroform (12 h). The chloroform fraction was then concentrated *in vacuo* to give a deep blue plastic-like film. The solid was dissolved in minimum chloroform and added dropwise slowly into a flask of rapidly stirring methanol. Once the addition was completed, the mixture was allowed to stir for a further 30 min before the dark blue solid was collected *via* filtration and washed with methanol and acetone, to afford the dark blue polymer **PE11DPP-BDT** (0.08 g, 62%); M_n: 42.4 KDa; M_w: 83.6 KDa; PDI: 2.0.

PP11DPP-BDT

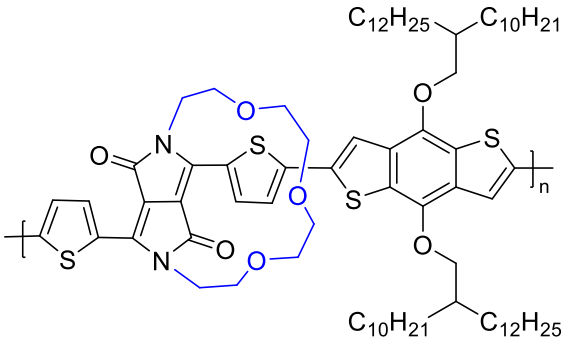

To an oven dried 10 mL microwave vial under argon was added **10c** (0.030 g, 0.049 mmol), **11** (0.059 g, 0.049 mmol) and $Pd(PPh_3)_4$ (2.5 mg, 0.0022 mmol). The reaction vial was then sealed and left to degas for 1 h. This was followed by the addition of degassed toluene (1.97 mL) and degassed DMF (0.197 mL). The reaction was then heated to 110 °C and allowed to stir for 18 h. The vial was then left to cool to RT and the reaction mixture was then added dropwise into a flask of stirring methanol. Precipitate (blue stringy flakes) began to form and was filtered into a cellulose thimble under reduced pressure, which was then washed with acetone and methanol. The polymer was then purified *via* Soxhlet extraction in the following solvents: acetone (12 h), hexane (12 h) and chloroform (12 h). The chloroform fraction was then concentrated *in vacuo* to give a deep blue plastic-like film. The solid was dissolved in minimum chloroform and added dropwise slowly into a flask of rapidly stirring methanol. Once the addition was completed, the mixture was allowed to stir for a further 30 min before the dark blue solid was collected *via* filtration and washed with methanol and acetone, to afford the dark blue polymer **PP11DPP-BDT** (0.05 g, 70%); M_n: 27.5 KDa; M_w: 37.5 KDa; PDI: 1.4.

PDPP-E10BDT

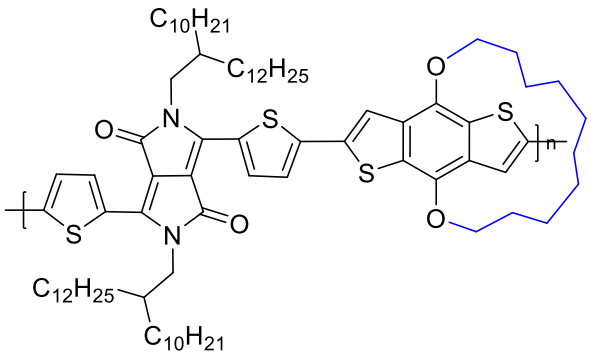

To an oven dried 10 mL microwave vial under argon was added **6** (0.148 g, 0.13 mmol), **12** (0.090 g, 0.13 mmol) and $Pd(PPh_3)_4$ (6.1 mg, 0.0052 mmol). The reaction vial was then sealed and left to degas for 1 h. This was followed by the addition of degassed toluene (5.30 mL) and degassed DMF (0.53 mL). The reaction was then heated to 110 °C and allowed to stir for 18 h. The vial was then left to cool to RT and the reaction mixture was then added dropwise into a flask of stirring methanol. Precipitate (blue stringy flakes) began to form and was filtered into a cellulose thimble under reduced pressure, which was then washed with acetone and methanol. The polymer was then purified *via* Soxhlet extraction in the following solvents: acetone (12 h), hexane (12 h) and chloroform (12 h). The chloroform fraction was then concentrated *in vacuo* to give a deep blue plastic-like film. The solid was dissolved in minimum chloroform and added dropwise slowly into a flask of rapidly stirring methanol. Once the addition was completed, the mixture was allowed to stir for a further 30 min before the dark blue solid was collected *via* filtration and washed with methanol and acetone, to afford the dark blue/purple polymer **PDPP-E10BDT** (0.15 g, 87%); M_n: 31.2 KDa; M_w: 75.4 KDa; PDI: 2.4.

(13)

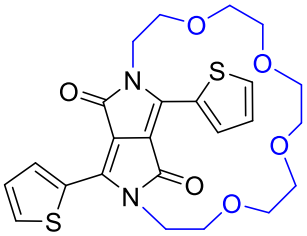

To an oven dried flask equipped with a dropping funnel under argon was added DPP (**1**) (1 g, 3.33 mmol), K_2CO_3 (1.52 g, 11.0 mmol), 18-crown-6 (12.0 mg, 0.044 mmol) and anhydrous DMF (364 mL).The reaction mixture was then stirred at 50 °C for 1 h. To a second oven dried flask under argon, was added pentaethylene glycol di(p-toluenesulfonate) (1.82 g, 3.33 mmol) in DMF (364 mL) which was degassed with argon for 30 min, before dropwise addition into the reaction flask. The reaction mixture was then allowed to stir at 100 °C for two nights, before cooling to RT. The solvent was then removed *in vacuo* and the crude product was purified *via* column chromatography (DCM: ethyl acetate= 2:1) followed by recrystallisation in isopropanol. The solid was then collected *via* filtration to give the title compound as a pink solid (0.30 g, 0.59 mmol, 18%).

^{1}H NMR (400 MHz, $CDCl_3$) δ (ppm): 8.77 (dd, *J* = 3.9, 1.0 Hz, 2H, ThH), 7.61 (dd, *J* = 5.0, 1.0 Hz, 2H, ThH), 7.30 – 7.22 (m, 2H, ThH), 4.48 (ddd, *J* = 15.2, 6.1, 3.3 Hz, 2H, OCH_2), 4.21 (ddd, *J* = 15.2, 7.1, 3.3 Hz, 2H, OCH_2), 3.79 (ddd, *J* = 10.2, 7.1, 3.3 Hz, 2H, OCH_2), 3.67 (ddd, *J* = 9.6, 6.1, 3.3 Hz, 2H, OCH_2), 3.60 – 3.52 (m, 6H, OCH_2), 3.45 (m, 2H, OCH_2), 3.34 (s, 4H, OCH_2).**^{13}C NMR** (126 MHz, $CDCl_3$) δ 161.9, 140.8, 135.1, 130.6, 130.1, 128.4, 108.5, 72.8, 71.6, 70.0, 68.5, 42.2. **HRMS** (TOF MS ASAP+): Calculated for $C_{24}H_{27}N_2O_6S_2^+$: 503.1311. Found *m/z* 503.1304 $[M+H]^+$.

EP14DPPT (14)

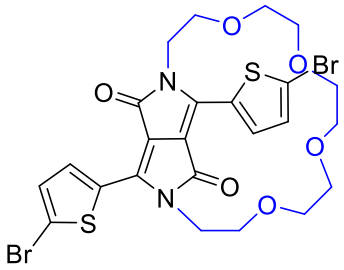

To a 3-necked flask under argon was added **13** (0.20 g, 0.40 mmol) dissolved in chloroform (40 mL) and the reaction was cooled to 0 °C (30 min). *N*-bromosuccinimide (0.16 g, 0.88 mmol) was then added to the stirring solution and the reaction was covered from light. The reaction was then allowed to warm to RT and left to stir overnight. The resulting solution was then diluted with chloroform and concentrated *in vacuo*. The crude product was purified *via* column chromatography (ethyl acetate: methanol= 9:1) followed by washing with isopropanol. The solid was then collected *via* filtration from isopropanol to give the title compound as a dark purple waxy solid (0.069 g, 0.10 mmol, 26%).

^{1}H NMR (400 MHz, $CDCl_3$) δ (ppm): 8.52 (d, *J* = 4.2 Hz, 2H, ThH), 7.21 (d, *J* = 4.2 Hz, 2H, ThH), 4.42 (ddd, *J* = 15.2, 5.5, 3.3 Hz, 2H, OCH_2), 4.06 (ddd, *J* = 15.2, 7.6, 3.3 Hz, 2H, OCH_2), 3.82 – 3.74 (m, 2H, OCH_2), 3.71 – 3.64 (m, 2H, OCH_2), 3.60 – 3.41 (m, 8H, OCH_2), 3.30 (s, 4H, OCH_2).**^{13}C NMR** (126 MHz, $CDCl_3$) δ 161.3, 139.7, 135.1, 131.3, 131.2, 119.0, 108.4, 72.5, 71.4, 69.8, 68.1, 42.1. **HRMS** (TOF MS ASAP+): Calculated for $C_{24}H_{25}N_2O_6S_2Br_2^+$: 658.9521. Found *m/z* 658.9493 $[M+H]^+$.

3,6-di(thiophen-2-yl)-2,5-di(2,5,8,11-tetraoxatridecan-13-yl)-2,5-dihydropyrrolo[3,4-c]pyrrole-1,4-dione (16)

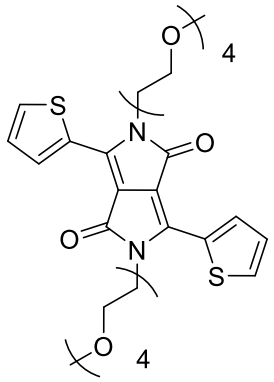

To an oven dried flask under argon was added DPP (**1**) (1 g, 3.33 mmol), K_2CO_3 (1.52 g, 11.0 mmol), 18-crown-6 (12.0 mg, 0.044 mmol), anhydrous DMF (40 mL) and triethylene glycol 2-bromoethyl methyl ether (2.98 g, 11.0 mmol). The solution was then heated to 120 °C and was stirred for 18 h. The reaction mixture was then cooled to RT. Chloroform was then added to the flask and the solution was concentrated *in vacuo.* The crude product was then purified *via* column chromatography (ethanol: methanol= 9:1) followed by recrystallisation in isopropanol to afford the product as a waxy purple solid (0.4 g, 0.59 mmol, 18%).

^{1}H NMR (400 MHz, $CDCl_3$) δ (ppm): 8.75 (dd, *J* = 3.9, 1.0 Hz, 2H, ThH), 7.64 (dd, *J* = 5.0, 1.0 Hz, 2H, ThH), 7.30 – 7.20 (m, 2H, ThH), 4.27 (t, *J* = 6.3 Hz, 4H, NCH_2), 3.79 (t, *J* = 6.3 Hz, 4H, OCH_2), 3.66 – 3.56 (m, 20H, OCH_2), 3.52 (dd, *J* = 5.7, 3.5 Hz, 2H, OCH_2), 3.36 (s, 6H, OCH_3).**^{13}C NMR** (126 MHz, $CDCl_3$) δ 161.5, 140.4, 134.8, 130.9, 129.7, 128.5, 107.9, 71.9, 70.7, 70.6, 70.5, 68.9, 59.0, 41.9. **HRMS** (TOF MS ASAP+): Calculated for $C_{32}H_{45}N_2O_{10}S_2^+$: 681.2516. Found *m/z* 681.2510 $[M+H]^+$.

3,6-bis(5-bromothiophen-2-yl)-2,5-bis(2-methoxyethyl)-2,5-dihydropyrrolo[3,4-c]pyrrole-1,4-dione (15)

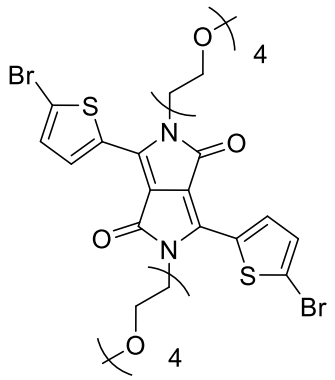

To a 3-necked flask under argon was added 3,6-di(thiophen-2-yl)-2,5-di(2,5,8,11-tetraoxatridecan-13-yl)-2,5-dihydropyrrolo[3,4-c]pyrrole-1,4-dione (**16**) (0.20 g, 0.29 mmol) dissolved in chloroform (30 mL) and the reaction was cooled to 0 °C (30 min). *N*-bromosuccinimide (0.12 g, 0.65 mmol) was then added to the stirring solution and the reaction was covered from light. The reaction was then allowed to warm to RT and left to stir overnight. The resulting solution was then diluted with chloroform and concentrated *in vacuo*. The crude product was purified *via* column chromatography (ethyl acetate: methanol= 9:1) followed by recrystallisation in isopropanol. The solid was then collected *via* filtration to give the title compound as a dark purple waxy solid (0.12 g, 0.14 mmol, 48%).

^{1}H NMR (500 MHz, $CDCl_3$) δ (ppm): 8.48 (d, *J* = 4.2 Hz, 2H, ThH), 7.21 (d, *J* = 4.2 Hz, 2H, ThH), 4.17 (t, *J* = 6.0 Hz, 4H, OCH_2), 3.77 (t, *J* = 6.0 Hz, 4H, OCH_2), 3.66 – 3.56 (m, 20H, OCH_2), 3.55 – 3.49 (m, 4H, OCH_2), 3.36 (s, 6H, OCH_3).**^{13}C NMR** (126 MHz, $CDCl_3$) δ 161.3, 139.5, 134.8, 131.4, 131.1, 119.4, 108.0, 71.9, 70.8, 70.6, 70.5, 70.5, 69.0, 59.0, 42.3. **HRMS** (TOF MS ASAP+): Calculated for $C_{32}H_{43}N_2O_{10}S_2Br_2^+$: 837.0726. Found *m/z* 837.0712 $[M+H]^+$.

13-(thiophen-3-yloxy)-2,5,8,11-tetraoxatridecane (18)

To an oven dried flask under argon was added ^{t}BuOK (9.00 g, 55.61 mmol), Cu(I)I (2.34 g, 12.28 mmol) and anhydrous pyridine (30 mL). This was then followed by tetraethyleneglycol monomethyl ether (13.5 mL, 67.74 mmol) which was added dropwise into the reaction mixture over 5 min. The reaction was then allowed to stir at RT for 30 min. 3-Bromothiophene (5.2 mL, 55.61 mmol) was then added in one portion and the reaction mixture was heated to 100 °C and left to stir overnight. The reaction was then cooled to RT and ethyl acetate was added to the solution. The inorganic solid was filtered off through celite and the resulting filtrate was added to water. The solution was washed with water, 5M HCL and the aqueous layers were extracted with ethyl acetate (3 x 100 mL). The combined organic layers were dried over $MgSO_4$ and concentrated *in vacuo*. The crude product was then purified *via* column chromatography (hexane: ethyl acetate= 1:1) to afford the product as a dark yellow oil (4.58 g, 15.77 mmol, 28%).

^{1}H NMR (400 MHz, $CDCl_3$) δ (ppm): 7.12 (dd, *J* = 5.2, 3.0 Hz, 1H, ThH), 6.74 (dd, *J* = 5.2, 1.3 Hz, 1H, ThH), 6.22 (dd, *J* = 3.0, 1.3 Hz, 1H, ThH), 4.10 – 4.05 (m, 2H, OCH_2), 3.83 – 3.77 (m, 2H, OCH_2), 3.71 – 3.58 (m, 10H, OCH_2), 3.51 (m, 2H, OCH_2), 3.34 (s, 3H, OCH_3).**^{13}C NMR** (151 MHz, $CDCl_3$) δ 157.6, 124.6, 119.6, 97.5, 71.9, 70.7, 70.6, 70.5, 70.5, 69.6, 59.0. **HRMS** (ESI+): Calculated for $C_{13}H_{23}O_5S^+$: 291.1266. Found *m/z* 291.1254 $[M+H]^+$.

3,3'-bis((2,5,8,11-tetraoxatridecan-13-yl)oxy)-2,2'-bithiophene (19)

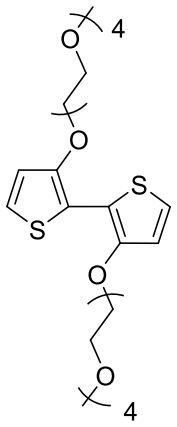

To an oven dried flask under argon was added 13-(thiophen-3-yloxy)-2,5,8,11-tetraoxatridecane **(18)** (4.50 g, 15.50 mmol) in anhydrous THF (32 mL). The reaction was then cooled to 0 °C in an ice bath over 15 min. 1.6 M n-BuLi in hexane (9.7 mL, 15.53 mmol) was then added dropwise to the solution over 10 min and the reaction was stirred for 2 h at 0 °C. The reaction mixture was then transferred to a flask charged with $Fe(acac)_3$ (1.88 g, 5.32 mmol) and anhydrous THF (38 mL). The reaction mixture was then heated at reflux and stirred for 2 h. After cooling to RT, the precipitate was filtered off and washed with ether. The filtrate was then washed with saturated $NH_4Cl_{(aq)}$ solution, dried over $MgSO_4$ and concentrated *in vacuo.* The crude product was then purified *via* column chromatography (hexane: ethyl acetate= 1:1) to afford the pure product as a yellow oil (1.76 g, 3.04 mmol, 20%).

^{1}H NMR (400 MHz, $CDCl_3$) δ (ppm): 7.07 (d, *J* = 5.5 Hz, 2H, ThH), 6.85 (d, *J* = 5.5 Hz, 2H, ThH), 4.27 – 4.21 (m, 4H, OCH_2), 3.92 – 3.87 (m, 4H, OCH_2), 3.74 (dd, *J* = 5.7, 3.5 Hz, 4H, OCH_2), 3.70 – 3.60 (m, 16H, OCH_2), 3.53 (dd, *J* = 5.7, 3.5 Hz, 4H, OCH_2), 3.36 (s, 6H, OCH_3).**^{13}C NMR** (100 MHz, $CDCl_3$) δ 151.7, 121.9, 116.6, 114.7, 71.9, 71.4, 70.9, 70.7, 70.6, 70.5, 70.0, 59.0. **HRMS** (ESI+): Calculated for $C_{26}H_{43}O_{10}S_2^+$: 579.2292. Found *m/z* 579.2285 $[M+H]^+$.

(Crude) (3,3'-bis((2,5,8,11-tetraoxatridecan-13-yl)oxy)-[2,2'-bithiophene]-5,5'-diyl)bis(trimethylstannane) (20)

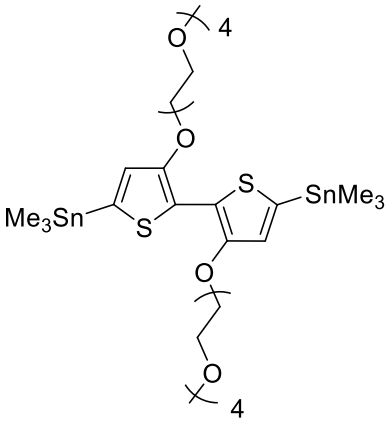

To an oven dried flask under argon was added 3,3'-bis((2,5,8,11-tetraoxatridecan-13-yl)oxy)-2,2'-bithiophene (**19**) (0.40 g, 0.69 mmol) in anhydrous THF (27 mL). The solution was cooled to -78 °C in an acetone/dry ice bath over 15 min. Following the dropwise addition of 1.6 M n-BuLi in hexane (0.92 mL, 1.47 mmol) over 10 min, the reaction was then allowed to stir for 2 h at -78 °C. The reaction was then warmed to RT for 1 h before cooling back down to -78 °C. Trimethyltin chloride 1 M in THF (2 mL) was then added in one portion and the reaction was stirred and allowed to warm to RT overnight. After quenching with water, the organic phase was washed with saturated brine solution and water, dried over $MgSO_4$ and concentrated *in vacuo* to afford the crude product as a light brown oil (0.40 g, 0.44 mmol, 64%).

^{1}H NMR (400 MHz, Acetone-D_6) δ (ppm): 7.09 (s, 2H, ThH), 4.27 (t, *J* = 4.8 Hz, 4H, OCH_2), 3.87 (t, *J* = 4.8 Hz, 4H, OCH_2), 3.73 – 3.68 (m, 4H, OCH_2), 3.64 – 3.60 (m, 4H, OCH_2), 3.56 (m, 12H, OCH_2), 3.49 – 3.41 (m, 4H, OCH_2), 3.27 (s, 6H, OCH_3), 0.37 (s, 18H, $SnMe_3$).**^{13}C NMR -Unable to obtain due to lack of material and degradation (compound had very low stability). HRMS** (ESI+) Calculated for $C_{32}H_{58}O_{10}S_2Sn_2$: 906.1510. Found *m/z* 906.1543 $[M]^+$.

6.4 Experimental for Chapter IV

Ethyl 3-oxo-3-(thiophen-2-yl)propanoate (2)

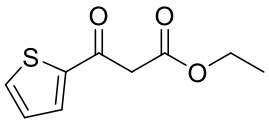

To an oven dried flask under argon equipped with a dropping funnel, reflux condenser and magnetic stirrer was added sodium hydride (16 g, 665.73 mmol), diethyl carbonate (58 mL, 475.51 mmol) and anhydrous toluene (240 mL). The mixture was then heated to reflux, which was followed by the dropwise addition of 2-acteyl thiophene (26 mL, 237.76 mmol) dissolved in anhydrous toluene (240 mL) *via* a dropping funnel. After addition was complete, the reaction mixture was left to stir at reflux for a further 1.5 h. The reaction was then cooled to RT before the addition of glacial acetic acid (360 mL) and ice water, to dissolve the orange solid formed. The organic layer was separated, and the aqueous layer was extracted with ethyl acetate (3 x 100 mL). The combined organic phases were washed with brine and dried over $MgSO_4$. The resulting solution was filtered and concentrated *in vacuo* to afford a brown oil product which was purified *via* silica plug (first hexane: chloroform= 1:1 then chloroform: ethyl acetate= 1:1) to afford the product as a dark amber oil (44.77 g, 225.84 mmol, 95%).

^{1}H NMR (400 MHz, $CDCl_3$) δ (ppm): 7.75 – 7.69 (m, 1H, ThH), 7.67 (d, *J* = 5.0 Hz, 1H, ThH), 7.11 (t, *J* = 4.4 Hz, 1H, ThH), 4.17 (q, *J* = 7.1 Hz, 2H, OCH_2), 3.89 (s, 2H, CH_2), 1.23 (t, *J* = 7.1 Hz, 3H, CH_3)**.** **^{13}C NMR** (150 MHz, $CDCl_3$): 185.1, 167.1, 143.4, 135.1, 133.4, 128.5, 61.8, 46.6, 14.2. **LRMS** (CI+) *m/z* 199.0 $[M+H]^+$.

Spectroscopic data is supported by literature.[166]

Diethyl 2-(thiophene-2-carbonyl)succinate (3)

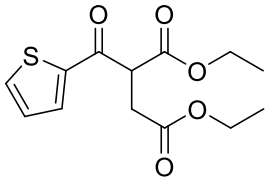

To an oven dried flask under argon equipped with a reflux condenser and magnetic stirrer was added **2** (13.08 g, 65.98 mmol), ethyl bromoacetate (7.31 mL, 65.98 mmol), Na_2CO_3 (9.73 g, 91.80 mmol), acetone (68.64 mL) and DME (16.5 mL). The reaction mixture was then heated under reflux and left to stir for 20 h. The reaction mixture was then left to cool to RT and filtered to remove the inorganic salts. The filtrate was then concentrated *in vacuo*. The crude product was partly purified *via* silica plug (chloroform: ethyl acetate= 1:1) to afford the product as a brown oil (11.15 g, 39.22 mmol, 59%), which was used in the next reaction without further purification.

^{1}H NMR (400 MHz, $CDCl_3$) δ (ppm): 7.89 (dd, *J* = 3.9, 1.0 Hz, 1H, ThH), 7.69 (dd, *J* = 4.9, 1.0 Hz, 1H, ThH), 7.15 (dd, *J* = 4.9, 3.9 Hz, 1H, ThH), 4.67 (t, *J* = 7.3 Hz, 1H, CH), 4.19 – 4.05 (m, 4H, OCH_2), 3.03 (dd, *J* = 7.3, 1.5 Hz, 2H, CH_2), 1.21 (m, 3H, CH_3), 1.17 (m, 3H, CH_3). **^{13}C NMR** (151 MHz, $CDCl_3$) δ 186.6, 171.1, 168.4, 143.0, 135.3, 133.9, 128.5, 62.0, 61.1, 50.9, 33.2, 14.1, 14.0. **LRMS** (CI+) *m/z* 283.1 $[M+H]^+$.

Spectroscopic data is supported by literature.[166]

Ethyl 5-oxo-2-(thiophen-2-yl)-4,5-dihydro-1H-pyrrole-3-carboxylate (4)

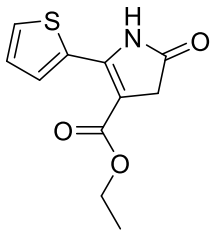

To an oven dried flask under argon equipped with a reflux condenser and magnetic stirrer, was added **3** (5.75 g, 20.2 mmol), ammonium acetate (8.56 g, 111 mmol) and acetic acid (15 mL). The reaction mixture was heated under reflux and allowed to stir for 4 h. The mixture was then cooled to RT and the solid that precipitated out of solution was collected by filtration and washed with water and MeOH, to afford the product as a sandy yellow solid (2.23 g, 9.40 mmol, 47%).

^{1}H NMR (400 MHz, DMSO) δ (ppm): 10.81 (s, 1H, NH), 7.88 (dd, *J* = 5.1, 1.1 Hz, 1H, ThH), 7.85 (dd, *J* = 3.8, 1.1 Hz, 1H, ThH), 7.19 (dd, *J* = 5.1, 3.8 Hz, 1H, ThH), 4.14 (q, *J* = 7.1 Hz, 2H, CH_2), 3.41 (s, 2H, CH_2), 1.22 (t, *J* = 7.1 Hz, 3H, CH_3).**^{13}C NMR** (151 MHz, DMSO) δ 176.2, 163.0, 145.1, 132.4, 131.8, 129.6, 126.8, 101.0, 59.5, 38.2, 14.3. **LRMS** (CI+): *m/z* 238 $[M+H]^+$.

Spectroscopic data is supported by literature.[166]

Thiophene-2,5-dicarbaldehyde (6)

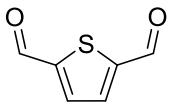

To an oven dried flask under argon equipped with a magnetic stirrer, was added a solution of 2,5-dibromothiophene (3 g, 12.4 mmol) in ether (60 mL). A solution of n-BuLi (17.05 mL, 27.8 mmol) was then added dropwise into the reaction mixture at -78 °C. The mixture was stirred for 30 min followed by the addition of DMF (9 mL). After stirring for 1 h at -78 °C, the reaction was allowed to warm up to RT overnight. The reaction was then quenched with ammonium chloride solution and the organic layers were extracted with ethyl acetate and washed with brine. The resulting solution was dried over $MgSO_4$ and concentrated *in vacuo*. The crude yellow oil was then purified *via* column chromatography on silica gel (hexane: DCM= 1:1) to afford the product as yellow crystals (0.67 g, 4.80 mmol, 38%).

^{1}H NMR (600 MHz, $CDCl_3$) δ (ppm): 10.04 (s, 2H, CHO), 7.84 (s, 2H, ThH). **^{13}C NMR** (151 MHz, $CDCl_3$) δ 183.6, 149.3, 135.2. **LRMS** (CI+) *m/z* 141.0 $[M+H]^+$.

Spectroscopic data is supported by literature.[168]

Thiophene-2,5-dicarbonitrile (7)

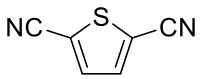

Ammonia hydroxide (28% solution) (27 mL) and iodine (3.56 g, 0.0140 mmol) were added to a solution of **6** (0.80 g, 4.65 mmol) in acetonitrile (120 mL) and THF (30 mL). The flask was then covered with foil and left to stir at RT for two nights. The reaction was then quenched with Na_2CO_3 solution (50 mL) and the organic layer was extracted with ether (2 x 50 mL). The resulting solution was dried over $MgSO_4$ and concentrated *in vacuo* to afford the product as a yellow/orange solid (0.59 g, 4.40 mmol, 95%).

^{1}H NMR (600 MHz, $CDCl_3$) δ (ppm): 7.63 (s, 2H, ThH). **^{13}C NMR** (151 MHz, $CDCl_3$) δ 137.0, 116.3, 112.0. **LRMS** (ESI+): *m/z* 135.2 $[M+H]^+$.

Spectroscopic data is supported by literature.[190]

1,1'-(thiophene-2,5-diyl)bis(ethan-1-one) (15)

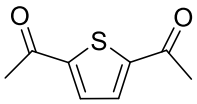

To an oven dried flask under argon equipped with a magnetic stirrer, was added a solution of 2,5-dibromothiophene (15.45 g, 63.9 mmol) in ether (600 mL). A solution of n-BuLi (100 mL, 160 mmol) was then added dropwise at -78 °C. The mixture was stirred for 30 min followed by the addition of *N*,*N*-dimethylacetamide (28 mL, 310 mmol). After stirring for 1 h at -78 °C, the reaction was allowed to warm up to RT overnight. The reaction was then quenched with 1 M HCL solution and the organic layer was extracted (3 x 100 mL) with ether. The organic layer was then washed with $NaHCO_3$ solution, brine, dried over Mg_2SO_4 and concentrated *in vacuo*. The crude yellow oil was then purified by recrystallisation from ethyl acetate to afford the product as shiny white crystals (3.65 g, 21.7 mmol, 34%).

^{1}H NMR (600 MHz, $CDCl_3$) δ (ppm): 7.67 (s, 2H, ThH), 2.60 (s, 6H, CH_3). **^{13}C NMR** (151 MHz, $CDCl_3$) δ 190.9, 149.1, 132.0, 27.2. **LSMS** (CI+): *m/z* 169.0 $[M+H]^+$.

Spectroscopic data is supported by literature.[168]

Diethyl 3,3'-(thiophene-2,5-diyl)bis(3-oxopropanoate) (16)

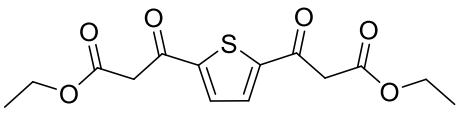

To an oven dried flask under argon equipped with a dropping funnel, reflux condenser and magnetic stirrer was added sodium hydride (2.9 g, 121 mmol), diethyl carbonate (10.5 mL, 86.8 mmol) and anhydrous DME (22 mL). The mixture was then heated to reflux. In a separate flask, **15** (3.65 g, 21.7 mmol) was dissolved in anhydrous DME (11 mL) which was added dropwise into the grey reaction mixture *via* dropping funnel. After addition was complete, the reaction mixture was left to stir at reflux for a further 1.5 h. The reaction was then cooled to RT before glacial acetic acid (32 mL) was added. This was followed by the addition of ice water to dissolve the orange solid formed. The organic layer was separated, and the aqueous layer was washed with ethyl acetate (3 x 100 mL). The combined organic phases were washed with brine and dried over $MgSO_4$. The resulting solution was filtered and concentrated *in vacuo* to afford the crude product, which was partially purified *via* silica plug (chloroform: ethyl acetate= 8:2 then chloroform: ethyl acetate= 1:1) to afford the product as a dark brown oil (4.33 g, 13.9 mmol, 64%), which was used in the next reaction without further purification. (Note: Mono- and di- products were inseparable by column chromatography).

^{1}H NMR (600 MHz, $CDCl_3$) δ (ppm): 7.68 (s, 2H, ThH), 4.16 (q, J = 7.1 Hz, 4H, OCH_2), 3.90 (s, 4H, CH_2), 1.23 – 1.17 (m, 6H, CH_3). **^{13}C NMR** (151 MHz, $CDCl_3$) δ 185.5, 166.6, 148.7, 133.0, 61.9, 46.6, 14.1. **LRMS** (CI+): *m/z* 313.0 $[M+H]^+$.

Tetraethyl 5,5'-(thiophene-2,5-dicarbonyl)bis(3-oxohexanedioate) (17)

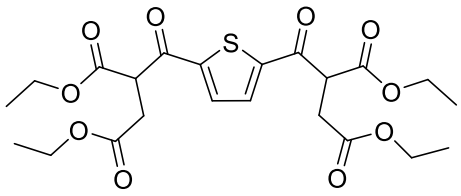

To an oven dried flask under argon equipped with a reflux condenser and magnetic stirrer was added **16** (4.33, 13.9 mmol), ethyl bromoacetate (3.17 mL, 28.4 mmol) and Na_2CO_3 (4.13 g, 38.9 mmol). This was followed by the addition of acetone (14.5 mL) and DME (5.6 mL). The reaction mixture was then heated under reflux and left to stir for 20 h. The reaction mixture was then left to cool to RT and filtered to remove the inorganic salts. The filtrate was then concentrated *in vacuo*. The crude product was partly purified *via* silica plug (chloroform: ethyl acetate= 1:1) to afford the product as a dark brown oil (4.65 g, 9.6 mmol, 69%), which was used in the next reaction without further purification.

^{1}H NMR (600 MHz, $CDCl_3$) δ (ppm): 7.88 (s, 2H, ThH), 4.67 (t, *J* = 4.2, 2.5 Hz, 2H, CH), 4.16 (m, 8H, OCH_2), 3.18 – 2.98 (m, 4H, CH_2), 1.26 – 1.17 (m, 12H, CH_3). **^{13}C NMR** (151 MHz, $CDCl_3$) δ 187.2, 171.1, 167.8, 148.7, 133.2, 62.4, 61.4, 51.1, 33.2, 14.2, 14.0. **HRMS** (ESI+): Calculated for $C_{22}H_{29}O_{10}S^+$: 485.1481. Found *m/z* 485.1488 $[M+H]^+$.

Diethyl 2,2'-(thiophene-2,5-diyl)bis(5-oxo-4,5-dihydro-1H-pyrrole-3-carboxylate (18)

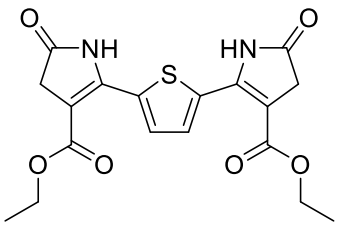

To an oven dried flask under argon equipped with a reflux condenser and magnetic stirrer, was added **17** (3.00 g, 6.57 mmol), ammonium acetate (9.56 g, 124 mmol) and acetic acid (38.1 mL). The reaction mixture was heated under reflux and allowed to stir for 20 h. The mixture was then cooled to RT and the dark solid that precipitated from solution was collected by filtration and washed with water, to afford the product as a dark green/blue solid (1.01 g, 2.59 mmol, 39%).

^{1}H NMR (400 MHz, DMSO) δ (ppm): 10.88 (s, 2H, NH), 7.78 (s, 2H, ThH), 4.23 – 4.11 (m, 4H, OCH_2), 3.45 (s, 4H, CH_2), 1.23 (t, *J* = 7.1 Hz, 6H, CH_3). **^{13}C NMR** (151 MHz, DMSO) δ 176.1, 162.9, 144.2, 134.1, 130.6, 103.2, 59.7, 22.6, 14.3. **HRMS** (ESI+): Calculated for $C_{18}H_{19}N_2O_6S^+$: 391.0964. Found *m/z* 391.0972 $[M+H]^+$.

Ethyl 1-dodecyl-4-hydroxy-5-oxo-2-(thiophen-2-yl)-2,5-dihydro-1H-pyrrole-3-carboxylate (21a)

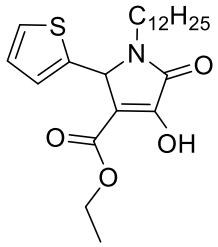

To an oven dried flask under argon equipped with a reflux condenser was added sodium alkyl oxalacetate (50 g, 238 mmol), dodecylamine (44 g, 238 mmol), EtOH (313 mL) and 2-thiophenecarboxaldehyde (26.68 g, 238 mmol). The reaction mixture was then heated under reflux and allowed to stir for 20 h. The reaction was allowed to cool to RT followed by the addition of water (400 mL) and acidified to pH 2 *via* dropwise addition of H_2SO_4. The white solid that precipitated out of solution was collected *via* filtration and was washed with hexane to afford the product as a white solid (16 g, 38.0 mmol, 16%).

^{1}H NMR (400 MHz, DMSO) δ (ppm): 7.49 (d, *J* = 5.0 Hz, 1H, ThH), 7.24 (d, *J* = 3.3 Hz, 1H, ThH), 7.00 (dd, *J* = 5.0, 3.3 Hz, 1H, ThH), 5.57 (s, 1H, C*H*N$C_{12}H_{25}$), 4.14 – 3.92 (m, 2H, OC*H*$_2$$CH_3$), 3.52 – 3.43 (m, 1H, Alkyl Chain), 2.75 (ddd, *J* = 13.5, 8.0, 5.3 Hz, 1H, Alkyl Chain), 1.53 – 1.10 (m, 20H, Alkyl Chain), 1.07 (t, *J* = 7.1 Hz, 3H, OCH_2CH_3), 0.86 (t, *J* = 6.7 Hz, 3H, Alkyl Chain). **^{13}C NMR** (101 MHz, DMSO) δ 164.5, 162.4, 154.9, 141.1, 128.6, 127.3, 126.5, 110.9, 59.8, 56.1, 31.8, 29.5, 29.4, 29.3, 29.2, 29.0 27.7, 26.6, 22.6, 14.5, 14.4. **HRMS** (TOF MS ASAP+): Calculated for $C_{23}H_{36}NO_4S^+$: 422.2365. Found *m/z* 422.2362 $[M+H]^+$.

Ethyl 1-(2-ethylhexyl)-4-hydroxy-5-oxo-2-(thiophen-2-yl)-2,5-dihydro-1H-pyrrole-3-carboxylate (21b)

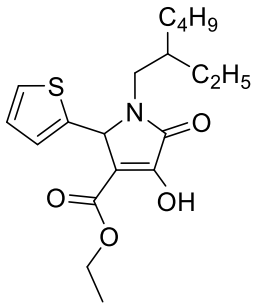

Compound **21b** was made using the same procedure as making **21a** with the following reagents: sodium alkyl oxalacetate (40.00 g, 190 mmol), 2-ethyl-1-hexylamine (24.60 g, 190 mmol), EtOH (250 mL) and 2-thiophenecarboxaldehyde (21.35 g, 190 mmol). The organic layer was then extracted with chloroform (3 x 100 mL) and dried over $MgSO_4$. The resulting solution was filtered and concentrated *in vacuo* to afford the dark brown oil crude product, which was partially purified *via* column chromatography on silica gel (hexane: chloroform= 1:1), (chloroform 100%) and finally (chloroform: ethyl acetate= 1:1) to give an off white solid which was collected *via* filtration. This was then washed with hexane to afford the pure product as a white solid (16.65 g, 44.5 mmol, 24%).

^{1}H NMR (400 MHz, DMSO) δ (ppm): 11.71 (br s, 1H, OH), 7.51 (d, *J* = 5.0 Hz, 1H, ThH), 7.24 – 7.21 (m, 1H, ThH), 7.04 – 6.99 (m, 1H, ThH), 5.55 (d, *J* = 5.2 Hz, 1H, C*H*NC_8H_{17}), 4.15 – 3.95 (m, 2H, O$C\mathit{H}_2CH_3$), 3.46 – 3.34 (m, 2H, N$C\mathit{H}_2$), 1.51 (s, 1H, Alkyl Chain), 1.31 – 1.11 (m, 8H, Alkyl Chain), 1.08 (t, *J* = 7.1 Hz, 3H, $OCH_2C\mathit{H}_3$), 0.79 (m, 6H, Alkyl Chain). **^{13}C NMR** (101 MHz, DMSO) δ 164.7, 162.4, 140.6, 128.9, 127.4, 126.8, 111.5, 60.0, 56.5, 44.0, 30.4, 28.6, 28.0, 24.0, 23.6, 22.9, 22.7, 14.5, 14.3. **HRMS** (TOF MS ASAP+): Calculated for $C_{19}H_{28}NO_4S^+$: 366.1739. Found *m/z* 366.1739 $[M+H]^+$.

Ethyl 1-butyl-4-hydroxy-5-oxo-2-(thiophen-2-yl)-2,5-dihydro-1H-pyrrole-3-carboxylate (21c)

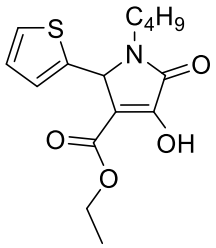

Compound **21c** was made using the same procedure as making **21a** with the following reagents: sodium alkyl oxalacetate (60.00 g, 285 mmol), butylamine (20.88 g, 285 mmol), EtOH (374 mL) and 2-thiophenecarboxaldehyde (31.96 g, 285 mmol). The reaction was allowed to cool to RT followed by the addition of water (400 mL) and acidified to pH 2 *via* dropwise addition of H_2SO_4. The white solid that precipitated out of solution was collected *via* filtration and was washed with hexane to afford the product as a white solid (40 g, 129 mmol, 45%).

^{1}H NMR (400 MHz, DMSO) δ (ppm): 11.68 (br s, 1H, OH), 7.50 (d, *J* = 5.0 Hz, 1H, ThH), 7.25 (d, *J* = 3.1 Hz, 1H, ThH), 7.01 (dd, *J* = 5.0, 3.1 Hz, 1H, ThH), 5.59 (s, 1H, C*H*NC_4H_9), 4.17 – 3.92 (m, 2H, O$C\mathit{H}_2CH_3$), 3.57 – 3.37 (m, 1H, Alkyl Chain), 2.76 (ddd, *J* = 13.6, 7.9, 5.3 Hz, 1H, Alkyl Chain), 1.51 – 1.29 (m, 2H, Alkyl Chain), 1.27 – 1.11 (m, 2H, Alkyl Chain), 1.08 (t, *J* = 7.1 Hz, 3H, $OCH_2C\mathit{H}_3$), 0.82 (t, *J* = 7.3 Hz, 3H, Alkyl Chain). **^{13}C NMR** (100 MHz, DMSO) δ 164.3, 162.3, 154.2, 140.8, 128.8, 127.4, 126.7, 111.5, 60.0, 56.1, 29.8, 19.9, 14.5, 13.9. **LRMS** (ESI+) *m/z* 310.11 $[M+H]^+$.

Ethyl 1-dodecyl-5-oxo-2-(thiophen-2-yl)-4,5-dihydro-1H-pyrrole-3-carboxylate (23a)

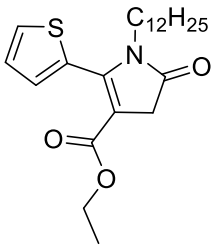

To an oven dried flask under argon equipped with a reflux condenser was added alcohol **22a**, (9.02 g, 20 mmol), mesyl chloride (2.68 g, 23 mmol), and TEA portion wise (8.61 g, 85 mmol). The reaction mixture was then heated under reflux and allowed to stir for 30 min. After cooling to RT, the mixture was diluted with 5% HCL solution (100 mL). The aqueous layers were extracted with dichloromethane and the combined organic layers were washed with 5% HCL solution followed by Sat Na_2HCO_3 until neutral, and finally water. The solution was dried over $MgSO_4$ and concentrated *in vacuo*, to give the crude brown residue which was purified *via* dissolving in minimum MeOH and freezing overnight. The solid was collected *via* filtration to afford the product as a mink coloured shiny solid (4.02 g, 9.9 mmol, 49%).

^{1}H NMR (400 MHz, $CDCl_3$) δ (ppm): 7.53 (dd, *J* = 5.0, 1.1 Hz, 1H, ThH), 7.16 (dd, *J* = 3.5, 1.1 Hz, 1H, ThH), 7.13 (dd, *J* = 5.0, 3.5 Hz, 1H, ThH), 4.05 (q, *J* = 7.1 Hz, 2H, OCH_2CH_3), 3.44 (s, 2H, $NCOCH_2$), 3.42 – 3.37 (m, 2H, NCH_2), 1.40 (m, 2H, Alkyl Chain), 1.32 – 1.12 (m, 18H, Alkyl Chain), 1.10 (t, *J* = 7.1 Hz, 3H, OCH_2CH_3), 0.87 (t, *J* = 6.9 Hz, 3H, Alkyl Chain). **^{13}C NMR** (101 MHz, $CDCl_3$) δ 175.4, 162.8, 147.9, 130.0, 128.8, 128.4, 127.0, 108.3, 59.9, 41.1, 37.5, 31.9, 29.6, 29.5, 29.4, 29.3, 29.0, 28.9, 26.6, 22.7, 14.1, 14.0. **HRMS** (TOF MS ASAP+): Calculated for $C_{23}H_{36}NO_3S^+$: 406.2416. Found *m/z* 406.2416 $[M+H]^+$.

Ethyl 1-(2-ethylhexyl)-5-oxo-2-(thiophen-2-yl)-4,5-dihydro-1H-pyrrole-3-carboxylate (23b)

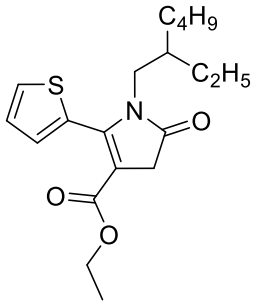

Compound **23b** was made using the same procedure as making **23a** with the following reagents, alcohol **22b** (1.16 g, 3.16 mmol) dissolved in anhydrous chloroform (20 mL), mesyl chloride (0.39 g, 3.50 mmol) and TEA (1.27 g, 12.6 mmol). After cooling to RT, the mixture was diluted with 5% HCL solution (100 mL). The aqueous layers were extracted with dichloromethane and the combined organic layers were washed with 5% HCL solution followed by Sat Na_2HCO_3 until neutral, and finally water. The solution was dried over $MgSO_4$ and concentrated *in vacuo*, to give the crude brown residue, which was purified *via* column chromatography on silica gel (chloroform: ethyl acetate= 95:5), to afford the pure product as a light brown/yellow oil (0.35 g, 1.00 mmol, 32%).

^{1}H NMR (400 MHz, $CDCl_3$) δ (ppm): 7.53 (dd, *J* = 4.9, 1.3 Hz, 1H, ThH), 7.15 (dd, *J* = 3.6, 1.3 Hz, 1H, ThH), 7.12 (dd, *J* = 4.9, 3.6 Hz, 1H, ThH), 4.06 (q, *J* = 7.1 Hz, 2H, OCH_2CH_3), 3.46 (s, 2H, $NCOCH_2$), 3.44 – 3.31 (m, 2H, NCH_2), 1.31 – 1.24 (m, 1H, Alkyl Chain), 1.11 (t, *J* = 7.1 Hz, 3H, OCH_2CH_3), 1.22 – 1.00 (m, 8H, Alkyl Chain), 0.82 (t, *J* = 7.2 Hz, 3H, Alkyl Chain), 0.69 (t, *J* = 7.4 Hz, 3H, Alkyl Chain). **^{13}C NMR** (101 MHz, $CDCl_3$) δ 175.7, 162.8, 148.0, 130.0, 128.9, 128.3, 126.9, 108.4, 60.0, 44.6, 38.6, 37.4, 30.4, 28.4, 23.8, 22.8, 14.0, 14.0, 10.5. **HRMS** (TOF MS ASAP+): Calculated for $C_{19}H_{28}NO_3S^+$: 350.1790. Found *m/z* 350.1793 $[M+H]^+$.

Ethyl 1-butyl-5-oxo-2-(thiophen-2-yl)-4,5-dihydro-1H-pyrrole-3-carboxylate (23c)

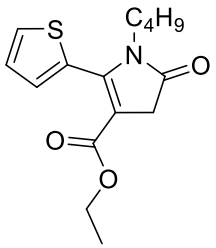

Compound **23c** was made using the same procedure as making **23a** with the following reagents, alcohol **22c** (13.72 g, 44.0 mmol) dissolved in anhydrous chloroform (186 mL), mesyl chloride (5.79 g, 50.0 mmol) and TEA (18.82 g, 186 mmol). After cooling to RT, the mixture was diluted with 5% HCL solution (100 mL). The aqueous layers were extracted with dichloromethane and the combined organic layers were washed with 5% HCL solution followed by Sat Na_2HCO_3 until neutral, and finally water. The solution was dried over $MgSO_4$ and concentrated *in vacuo*, to give the crude brown residue, which was purified *via* column chromatography on silica gel (chloroform: ethyl acetate= 95:5), to afford the pure product as a light brown/yellow oil (4.12 g, 17.8 mmol, 40%).

^{1}H NMR (400 MHz, $CDCl_3$) δ (ppm): 7.53 (dd, *J* = 4.9, 0.9 Hz, 1H, ThH), 7.17 (dd, *J* = 3.6, 0.9 Hz, 1H, ThH), 7.13 (dd, *J* = 4.9, 3.6 Hz, 1H), 4.05 (q, *J* = 7.1 Hz, 2H, OC*H*$_2$CH), 3.44 (s, 2H, NCOCH_2), 3.43 – 3.37 (m, 2H, NC*H*$_2$), 1.45 – 1.31 (m, 2H, Alkyl Chain), 1.24 – 1.13 (m, 2H, Alkyl Chain), 1.10 (t, *J* = 7.1 Hz, 3H, OCH$_2$C*H*$_3$), 0.79 (t, *J* = 7.4 Hz, 3H, Alkyl Chain). **^{13}C NMR** (126 MHz, $CDCl_3$) δ 175.4, 162.8, 147.9, 130.0, 128.8, 128.4, 127.0, 108.3, 59.9, 40.8, 37.5, 31.1, 19.8, 14.0, 13.5. **HRMS** (TOF MS ASAP+): Calculated for $C_{15}H_{20}NO_3S^+$: 294.1164. Found *m/z* 294.1156 $[M+H]^+$.

Furan-2-carbonitrile (25)

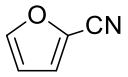

Ammonia hydroxide (28% solution) (220 mL) and iodine (10.91 g, 43.0 mmol) were added to a solution of furfural (4.00 g, 42.0 mmol) in THF (33 mL). The reaction mixture turned a dark black colour. The flask was then covered with foil and left to stir at RT for 1 h. The reaction was then quenched with Sat $Na_2S_2O_3$ solution (50 mL) and the organic layer was extracted with ether (3 x 100 mL). The resulting solution was dried over $MgSO_4$ and concentrated *in vacuo* to afford the product as a brown/yellow oil (1.72 g, 18.5 mmol, 44%).

^{1}H NMR (400 MHz, $CDCl_3$) δ (ppm): 7.56 (dd, *J* = 1.7, 0.5 Hz, 1H, ArH), 7.08 (dd, *J* = 3.6, 0.5 Hz, 1H, ArH), 6.51 (dd, *J* = 3.6, 1.7 Hz, 1H, ArH). **^{13}C NMR** (101 MHz, $CDCl_3$) δ 147.4, 126.3, 122.0, 111.5, 111.4. **LRMS** (ESI+) *m/z* 94.03 $[M+H]^+$.

Spectroscopic data is supported by literature.[191]

6-(4-bromophenyl)-2-dodecyl-3-(thiophen-2-yl)-2,5-dihydropyrrolo[3,4-c]pyrrole-1,4-dione (26ad)

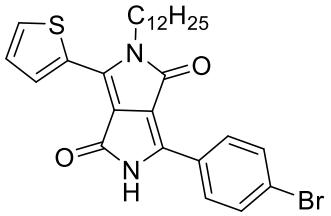

To an oven dried flask under argon set up for reflux, was added sodium chunks (0.46 g, 19.9 mmol) and 2-methyl-2-butanol (26.00 mL), followed by anhydrous iron (III) chloride (0.01 g). The mixture was allowed to stir at reflux until all sodium had been consumed. The reaction was then cooled to 95 °C and **23a** (2.60 g, 6.40 mmol) was added to the reaction mixture, followed by 4-bromobenzonitrile (1.40 g, 7.69 mmol) after 1 min. The reaction turned red in colour and was left to stir at 95 °C overnight. The mixture was then allowed to cool to 50 °C, followed by the addition of MeOH (35.00 mL). The reaction was quenched with glacial acetic acid (4.00 mL) and was cooled to RT. The solid that precipitated out of solution was washed with MeOH and collected *via* filtration to yield the product as a pink solid (1.01 g, 1.86 mmol, 28%).

^{1}H NMR (400 MHz, $CDCl_3$) δ (ppm): 9.85 (br s, 1H, NH), 8.95 (dd, *J* = 4.0, 1.1 Hz, 1H, ThH), 8.21 (d, *J* = 8.6 Hz, 2H, PhH), 7.71 (dd, *J* = 5.0, 1.1 Hz, 1H, ThH), 7.58 (d, *J* = 8.6 Hz, 2H, PhH), 7.29 (dd, *J* = 5.0, 4.0 Hz, 1H, ThH), 4.12 – 3.96 (m, 2H, NCH_2), 1.81 – 1.69 (m, 2H, Alkyl Chain), 1.48 – 1.21 (m, 20H, Alkyl Chain), 0.88 (t, *J* = 6.8 Hz, 3H, Alkyl Chain). **^{13}C NMR** (101 MHz, $CDCl_3$) δ 162.4, 161.8, 141.9, 141.6, 136.2, 132.3, 131.7, 129.5, 129.0, 128.6, 126.6, 126.1, 110.1, 108.7, 42.4, 31.9, 29.9, 29.6, 29.5, 29.4, 29.3, 26.9, 22.7, 14.1. **HRMS** (TOF MS ASAP+): Calculated for $C_{28}H_{34}BrN_2O_2S^+$: 541.1524. Found *m/z* 541.1534 $[M+H]^+$.

2-(2-ethylhexyl)-6-phenyl-3-(thiophen-2-yl)-2,5-dihydropyrrolo[3,4-c]pyrrole-1,4-dione (26bc)

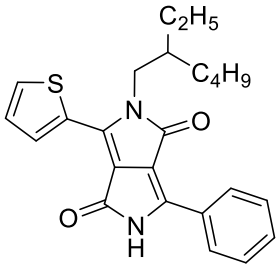

To an oven dried flask under argon set up for reflux, was added sodium chunks (0.46 g, 19.9 mmol) and 2-methyl-2-butanol (27.00 mL), followed by anhydrous iron (III) chloride (0.01 g). The mixture was allowed to stir at reflux until all sodium had been consumed (30 min). The reaction was then cooled to 95 °C and **23b** (2.00 g, 5.72 mmol) was added to the reaction mixture, followed by benzonitrile (0.71 g, 6.87 mmol) after 1 min. The reaction turned red in colour and was left to stir at 95 °C overnight. The mixture was then allowed to cool to 50 °C, followed by the addition of MeOH (27.00 mL). The reaction was quenched with glacial acetic acid (6.00 mL) and cooled to RT. The solid that precipitated out of solution was washed with MeOH and collected *via* filtration to yield the product as a pink solid (0.40 g, 0.98 mmol, 17%).

^{1}H NMR (600 MHz, $CDCl_3$) δ (ppm): 10.05 (s, 1H, NH), 8.97 (dd, *J* = 3.9, 0.8 Hz, 1H, ThH), 8.41 (d, *J* = 6.8 Hz, 2H, PhH), 7.69 (dd, *J* = 5.0, 0.8 Hz, 1H, ThH), 7.56 – 7.47 (m, 3H, PhH), 7.32 (dd, *J* = 5.0, 3.9 Hz, 1H, ThH), 4.08 – 4.00 (m, 2H, NCH_2), 1.92 – 1.84 (m, 1H, NCH_2CH), 1.43 – 1.18 (m, 8H, Alkyl Chain), 0.87 (m, 6H, Alkyl Chain). **^{13}C NMR** (151 MHz, $CDCl_3$) δ 162.8, 162.3, 143.3, 141.8, 135.9, 131.7, 131.2, 129.7, 129.1, 128.3, 127.9, 109.5, 109.3, 46.0, 39.1, 30.2, 28.4, 23.5, 23.1, 14.0, 10.5. **HRMS** (TOF MS ASAP+): Calculated for $C_{24}H_{27}N_2O_2S^+$: 407.1793. Found *m/z* 407.1775 $[M+H]^+$.

6-(4-bromophenyl)-2-(2-ethylhexyl)-3-(thiophen-2-yl)-2,5-dihydropyrrolo[3,4-c]pyrrole-1,4-dione (26bd)

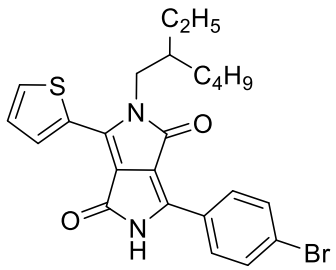

To an oven dried flask under argon set up for reflux, was added sodium chunks (0.736 g, 32.0 mmol) and 2-methyl-2-butanol (42.00 mL), followed by anhydrous iron (III) chloride (0.01 g). The mixture was allowed to stir at reflux until all sodium had been consumed (30 min). The reaction was then cooled to 95 °C and **23b** (3.60 g, 10.3 mmol) was added to the mixture, followed by 4-bromobenzonitrile (0.32 g, 3.43 mmol) after 1 min. The reaction turned red in colour and was left to stir at 95 °C overnight. The mixture was then allowed to cool to 50 °C, followed by the addition of MeOH (40.00 mL). The reaction was quenched with glacial acetic acid (4.00 mL). The reaction mixture was then cooled to RT followed by the addition of water (100 mL). The organic layer was then extracted with ethyl acetate (3 x 100 mL) and dried over $MgSO_4$. The resulting solution was filtered and concentrated *in vacuo* to afford a red solid, which was partially purified *via* washing with MeOH and collected *via* filtration to yield the product as a dark pink solid (0.142 g, 0.16 mmol, 3%) which was used in the next reaction without further purification.

^{1}H NMR (400 MHz, $CDCl_3$**)** δ (ppm): 10.02 (s, 1H, NH), 8.95 (dd, *J* = 3.9, 0.8 Hz, 1H, ThH), 8.26 (d, *J* = 8.7 Hz, 2H, PhH), 7.72 (dd, *J* = 5.0, 0.8 Hz, 1H, ThH), 7.61 (d, *J* = 8.7 Hz, 2H, PhH), 7.31 (dd, *J* = 5.0, 3.9 Hz, 1H, ThH), 4.07 – 3.97 (m, 2H, NCH_2), 1.86 (m, 1H, Alkyl Chain), 1.40 – 1.20 (m, 8H, Alkyl Chain), 0.87 (dt, *J* = 11.0, 7.3 Hz, 6H, Alkyl Chain). **^{13}C NMR** (101 MHz, $CDCl_3$) δ 162.5, 162.2, 142.3, 141.7, 136.2, 132.4, 131.7, 129.6, 129.1, 128.4, 126.7, 126.1, 110.0, 109.1, 46.0, 39.1, 30.2, 28.3, 23.5, 23.1, 14.0, 10.5. **HRMS** (TOF MS ASAP+): Calculated for $C_{24}H_{26}BrN_2O_2S^+$: 485.0898. Found *m/z* 485.0891 $[M+H]^+$.

2-(2-ethylhexyl)-6-(furan-2-yl)-3-(thiophen-2-yl)-2,5-dihydropyrrolo[3,4-c]pyrrole-1,4-dione (26be)

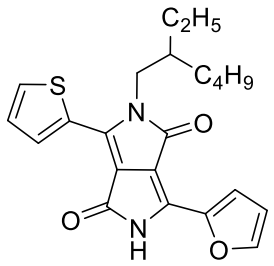

To an oven dried flask under argon set up for reflux, was added sodium chunks (0.46 g, 20.00 mmol) and 2-methyl-2-butanol (27.20 mL), followed by anhydrous iron (III) chloride (0.01 g). The mixture was allowed to stir at reflux until all sodium had been consumed. The reaction was then heated to 120 °C and **23b** (2.00 g, 5.72 mmol) was added to the reaction mixture, followed by **25** (0.60 g, 6.45 mmol). The reaction turned red in colour and was left to stir at 120 °C for 4 h. The mixture was then allowed to cool to 50 °C, followed by the addition of MeOH (27.20 mL). The reaction was quenched with glacial acetic acid (6.80 mL). The reaction mixture was then cooled to RT followed by the addition of water (200 mL). The organic layer was then extracted with ethyl acetate (x 3) and dried over $MgSO_4$. The resulting solution was filtered and concentrated *in vacuo* to afford a crude red oil, which was partially purified *via* column chromatography on silica gel (chloroform: ethyl acetate= 8:2), to give the product as a dark pink oil (0.240 g, 0.61 mmol, 10%) which was used in the next reaction without further purification.

^{1}H NMR (400 MHz, $CDCl_3$) δ (ppm): 8.80 (d, *J* = 3.5 Hz, 1H, ArH), 8.06 (br s, 1H, NH), 7.88 (d, *J* = 3.5 Hz, 1H, ArH), 7.64 (m, 1H, ArH), 7.60 (m, 1H, ArH), 7.31 – 7.24 (m, 1H, ArH), 6.68 (d, *J* = 2.1 Hz, 1H, ArH), 4.03 – 4.00 (m, 2H, NCH_2), 1.89 – 1.81 (m, 1H, Alkyl Chain), 1.43 – 1.16 (m, 8H, Alkyl Chain), 0.87 (m, 6H, Alkyl Chain). **^{13}C NMR** (101 MHz, $CDCl_3$) δ 161.3, 161.2, 145.4, 143.6, 140.9, 135.4, 130.8, 129.8, 128.5, 118.3, 113.9, 108.0, 107.3, 45.8, 39.1, 30.2, 28.3, 23.5, 23.1, 14.0, 10.5. **HRMS** (TOF MS ASAP+): Calculated for $C_{22}H_{25}N_2O_3S^+$: 397.1586. Found *m/z* 397.1596 $[M+H]^+$.

3-(4-bromophenyl)-5-dodecyl-2-(2-ethylhexyl)-6-(thiophen-2-yl)-2,5-dihydropyrrolo[3,4-c]pyrrole-1,4-dione (27adh) (P-DPP-T)

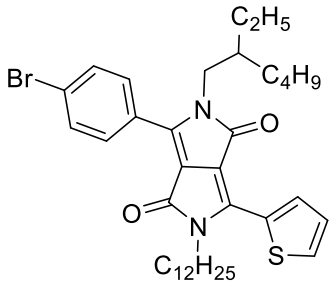

To an oven dried vial under argon was added **26ad** (0.20 g, 0.37 mmol), K_2CO_3 (0.086 g, 0.63 mmol), 18-crown-6 (5 mg), DMF (4.40 mL) and 2-ethylhexyl bromide (0.120 g, 0.63 mmol). The vial was sealed, and the reaction was stirred for 2 nights at 120 °C. The reaction mixture was then cooled to RT. Chloroform was then added to the flask and the solution was concentrated *in vacuo*. The crude product was then purified *via* column chromatography on silica gel (hexane: chloroform= 2:1) to afford the product as an orange/pink oil (0.036 g, 0.06 mmol, 15%).

^{1}H NMR (400 MHz, $CDCl_3$) δ (ppm): 8.97 (dd, *J* = 4.0, 1.0 Hz, 1H, ThH), 7.71 – 7.60 (m, 4H, 1H, PhH, ThH), 7.29 (dd, *J* = 4.9, 4.0 Hz, 1H, ThH), 4.03 – 3.95 (m, 2H, NCH_2), 3.85 – 3.72 (m, 2H, NCH_2), 1.71 (m, 2H, Alkyl Chain), 1.56 – 1.02 (m, 27H, Alkyl Chain), 0.87 (t, *J* = 6.8 Hz, 3H, CH_3), 0.80 (t, *J* = 6.8 Hz, 3H, CH_3), 0.72 (t, *J* = 7.4 Hz, 3H, CH_3). **^{13}C NMR** (100 MHz, $CDCl_3$) δ 162.0, 161.9, 145.2, 142.2, 136.0, 132.1, 131.3, 130.1, 129.6, 128.7, 127.5, 125.2, 110.1, 107.4, 45.1, 42.1, 38.6, 31.9, 30.3, 29.9, 29.6, 29.5, 29.3, 29.2, 28.2, 26.8, 23.7, 22.9, 22.7, 14.1, 14.0, 10.4. **HRMS** (TOF MS ASAP+): Calculated for $C_{36}H_{50}BrN_2O_2S^+$: 653.2776. Found *m/z* 653.2781 $[M+H]^+$.

3-(4-bromophenyl)-5-dodecyl-6-(thiophen-2-yl)-2-(2,5,8,11-tetraoxatridecan-13-yl)-2,5-dihydropyrrolo[3,4-c]pyrrole-1,4-dione (27adi)

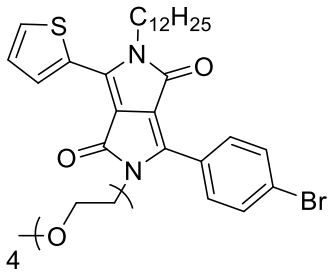

Compound **27adi** was made using the same procedure as making **27adh** with the following reagents; **26ad** (0.171 g, 0.32 mmol), K_2CO_3 (0.075 g, 0.54 mmol), 18-crown-6 (12 mg), DMF (3.80 mL) and triethylene glycol 2-bromoethyl methyl ether (0.14 g, 0.54 mmol). The crude product was then purified *via* column chromatography on silica gel (hexane: chloroform= 2:1) followed by (chloroform: ethyl acetate= 8:2) to afford the product as an orange oil (0.012 g, 0.016 mmol, 5%).

^{1}H NMR (400 MHz, $CDCl_3$) δ (ppm): 8.91 (d, *J* = 3.9 Hz, 1H, ThH), 7.91 (d, *J* = 8.5 Hz, 2H, PhH), 7.68 (d, *J* = 3.9 Hz, 1H, ThH), 7.64 (d, *J* = 8.5 Hz, 2H, PhH), 7.32 – 7.28 (m, 1H, ThH), 4.02 – 3.93 (m, 4H, NCH_2CH_2O), 3.79 (t, *J* = 5.3 Hz, 2H, NCH_2), 3.63 – 3.49 (m, 12H, OCH_2CH_2O), 3.35 (s, 3H, OCH_3), 1.70 (m, 2H, Alkyl Chain), 1.43 – 1.20 (m, 18H, Alkyl Chain), 0.87 (t, *J* = 6.8 Hz, 3H, Alkyl Chain). **^{13}C NMR** (100 MHz, $CDCl_3$) δ 162.2, 161.9, 145.9, 142.1, 135.8, 132.0, 131.4, 131.0, 129.6, 128.7, 126.9, 125.5, 109.9, 107.3, 71.9, 70.6, 70.5, 69.0, 59.0, 42.5, 42.1, 31.9, 29.9, 29.6, 29.5, 29.3, 29.2, 26.9, 22.7, 14.1. **HRMS** (TOF MS ASAP+): Calculated for $C_{37}H_{52}BrN_2O_6S^+$: 731.3729. Found *m/z* 731.3709 $[M+H]^+$.

3-(4-bromophenyl)-2-dodecyl-5-(2-ethylhexyl)-6-(thiophen-2-yl)-2,5-dihydropyrrolo[3,4-c]pyrrole-1,4-dione (27bdf) (T-DPP-P)

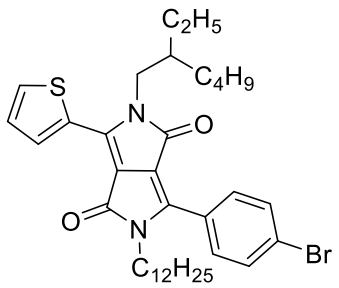

Compound **27bdf** was made using the same procedure as making **27adh** with the following reagents; **26bd** (0.14 g, 0.29 mmol), K_2CO_3 (0.073 g, 0.53 mmol), 18-crown-6 (5 mg), DMF (3.40 mL) and 1-bromododecane (0.13 g, 0.53 mmol). The crude product was then purified *via* column chromatography on silica gel (hexane: chloroform= 2:1) to afford the product as an orange/pink oil (0.030 g, 0.05 mmol, 16%).

^{1}H NMR (600 MHz, $CDCl_3$) δ (ppm): 8.91 (dd, *J* = 3.9, 1.1 Hz, 1H, ThH), 7.70 – 7.63 (m, 4H, 1H, PhH, ThH), 7.28 (dd, *J* = 5.0, 3.9 Hz, 1H, ThH), 3.95 (m, 2H, NCH_2), 3.81 – 3.75 (m, 2H, NCH_2), 1.85 – 1.78 (m, 1H, NCH_2CH), 1.65 – 1.58 (m, 2H, NCH_2CH_2), 1.38 – 1.18 (m, 26H, Alkyl Chain), 0.86 (m, 9H, CH_3). **^{13}C NMR** (100 MHz, $CDCl_3$) δ 162.3, 161.9, 145.2, 142.4, 135.8, 132.2, 131.2, 130.1, 129.6, 128.5, 127.2, 125.4, 109.7, 107.9, 45.7, 42.1, 39.1, 30.2, 29.6, 29.5, 29.3, 29.1, 28.4, 26.7, 23.5, 23.1, 22.7, 14.1, 14.0, 10.5. **HRMS** (TOF MS ASAP+): Calculated for $C_{36}H_{49}O_2N_2BrNaS^+$: 675.2590. Found *m/*z 675.2601 $[M+Na]^+$.

2-(2-ethylhexyl)-6-(furan-2-yl)-5-(2-octyldodecyl)-3-(thiophen-2-yl)-2,5-dihydropyrrolo[3,4-c]pyrrole-1,4-dione) (27beg)

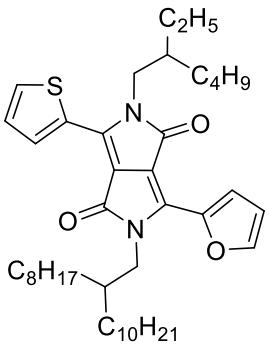

Compound **27beg** was made using the same procedure as making **27adh** with the following reagents; **26be** (0.17 g, 0.42 mmol), K_2CO_3 (0.98 g, 0.71 mmol), 18-crown-6 (0.012 g), DMF (12 mL) and 9-(bromomethyl)nonadecane (0.26 g, 0.71 mmol). The crude product was then purified *via* column chromatography on silica gel (hexane: chloroform= 2:1) to afford the product as a pink oil (0.082 g, 0.12 mmol, 29%).

^{1}H NMR (400 MHz, $CDCl_3$) δ (ppm): 8.89 (d, *J* = 3.8 Hz, 1H, ArH), 8.36 (d, *J* = 3.8 Hz, 1H, ArH), 7.61 (d, *J* = 1.9 Hz, 2H, ArH), 7.28 – 7.24 (m, 1H, ArH), 6.69 (dd, *J* = 3.8, 1.6 Hz, 1H, ArH), 4.03 (m, 4H, NCH_2), 1.75 – 1.71(m, 2H, Alkyl Chain), 1.42 – 1.05 (m, 40H, Alkyl Chain), 0.86 (m, 12H, Alkyl Chain). **^{13}C NMR** (101 MHz, $CDCl_3$) δ 161.7, 161.3, 144.9, 144.6, 140.2, 135.2, 134.2, 130.3, 129.9, 128.4, 120.3, 113.5, 108.0, 46.6, 45.8, 42.0, 39.1, 38.5, 31.9, 31.5, 30.2, 30.0, 29.6, 29.3, 28.3, 27.0, 26.5, 25.0, 23.5, 23.1, 22.7, 14.1, 14.0, 10.5. **HRMS** (TOF MS ASAP+): Calculated for $C_{42}H_{65}N_2O_3S^+$: 677.4716. Found *m/z* 677.4720 $[M+H]^+$.

2,5-bis(2-ethylhexyl)-3,6-di(thiophen-2-yl)-2,5-dihydropyrrolo[3,4-c]pyrrole-1,4-dione (29)

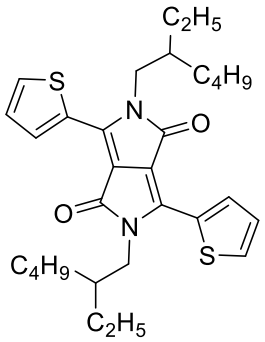

To an oven dried flask under argon was added Thienyl DPP (1.0 g, 3.32 mmol), K_2CO_3 (1.51 g, 10.93 mmol), 18-crown-6 (12.0 mg, 0.044 mmol), 2-ethylhexyl bromide (2.12 g, 10.93 mmol), followed by anhydrous DMF (40 mL). The solution was then heated to 120 °C and was stirred for 18 h. The reaction mixture was then cooled to RT. Chloroform was then added to the flask and the solution was concentrated *in vacuo*. The crude product was purified *via* column chromatography on silica gel (hexane: chloroform= 2:1) followed by recrystallisation in ethanol to afford the product as a dark purple shiny solid (0.46 g, 0.88 mmol, 26%).

^{1}H NMR (600 MHz, $CDCl_3$) δ (ppm): 8.89 (dd, *J* = 3.9, 1.1 Hz, 1H, ThH), 7.62 (dd, *J* = 5.0, 1.1 Hz, 1H, ThH), 7.27 (dd, *J* = 5.0, 3.9 Hz, 1H, ThH), 4.13 – 3.91 (m, 4H, NCH_2), 1.92 – 1.80 (m, 2H, Alkyl Chain), 1.45 – 1.13 (m, 16H, Alkyl Chain), 0.92 – 0.82 (m, 12H, Alkyl Chain). **^{13}C NMR** (126 MHz, $CDCl_3$) δ 161.8, 140.4, 135.3, 130.5, 129.8, 128.4, 107.9, 45.9, 39.1, 30.2, 28.4, 23.5, 23.1, 14.0, 10.5. **HRMS** (ESI+): Calculated for $C_{30}H_{41}N_2O_2S_2^+$: 525.2609. Found *m/z* 525.2587 $[M+H]^+$.

Spectroscopic data is supported by literature.[192]

5-(2,5-bis(2-hexyldecyl)-3,6-dioxo-4-(thiophen-2-yl)-2,3,5,6-tetrahydropyrrolo[3,4-c]pyrrol-1-yl)thiophene-2-carbonitrile (36)

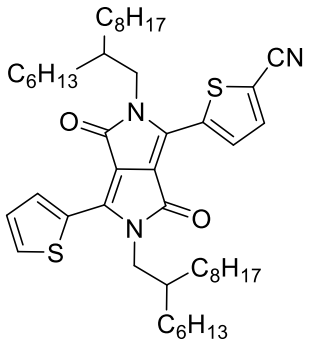

To a 25 mL oven dried microwave vial under argon, was added **35** (0.3 g, 0.36 mmol), Cu(I)CN (0.82 g, 9.16 mmol) and anhydrous DMF (15 mL). The vial was sealed, and the reaction was heated to 130 °C and stirred for 18 h. The reaction was then cooled to RT and the resulting mixture was passed through a silica: celite plug (chloroform) to remove any toxic inorganic salts. The solution was concentrated *in vacuo* and the crude product was purified *via* column chromatography on silica gel (hexane: chloroform= 2:1) to afford the product as a shiny purple/green solid (0.18 g, 0.24 mmol, 66%).

^{1}H NMR (500 MHz, $CDCl_3$) δ (ppm): 9.02 (dd, *J* = 4.1, 1.1 Hz, 1H, ThH), 8.74 (d, *J* = 4.2 Hz, 1H, ThH), 7.71 (dd, *J* = 5.0, 1.1 Hz, 1H, ThH), 7.70 (d, *J* = 4.2 Hz, 1H, ThH), 7.31 (dd, *J* = 5.0, 4.1 Hz, 1H, ThH), 4.00 (dd, *J* = 22.6, 7.8 Hz, 4H, NCH_2), 1.94 – 1.88 (m, 1H, Alkyl Chain), 1.87 – 1.78 (m, 1H, Alkyl Chain), 1.40 – 1.15 (m, 48H, Alkyl Chain), 0.85 (m, 12H, Alkyl Chain). **^{13}C NMR** (126 MHz, $CDCl_3$) δ 161.8, 161.1, 143.2, 137.7, 136.8, 136.6, 135.8, 133.3, 132.2, 129.4, 128.7, 113.6, 112.2, 110.7, 107.7, 46.4, 38.0, 37.7, 31.9, 31.7, 31.1, 30.0, 29.7, 29.6, 29.5, , 29.3, 26.1, 22.7, 22.6, 14.1. **HRMS** (ESI+): Calculated for $C_{47}H_{72}N_3O_2S_2^+$: 774.5066. Found *m/z* 774.5059 $[M+H]^+$.

2-hexyl-3-(methylthio)-6-(thiophen-2-yl)-2,5-dihydropyrrolo[3,4-c]pyrrole-1,4-dione (38)

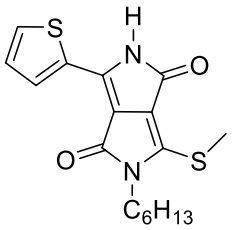

To an oven dried flask under argon was added **4** (1.0 g, 4.22 mmol), NaH (0.40 g, 16.83 mmol) and DMSO (11 mL). The mixture was stirred at RT for 15 min followed by the addition of hexyl isothiocyanate (0.67 g, 4.66 mmol). The mixture was then allowed to stir at RT for 6 h. After cooling the reaction to 0 °C, methyl iodide (0.66 g, 4.66 mmol) was then added to the mixture in one portion and the reaction was allowed to stir for a further 12 h at RT. The green/yellow solution was then poured into an ice/water mixture (60 mL) followed by the addition of acetic acid (0.5 mL). The resulting suspension was stirred for 15 min before the crude brown solid was collected by filtration and purified *via* column chromatography to afford the product as a dark shiny green/yellow solid (0.31 g, 0.88 mmol, 21%).

^{1}H NMR (400 MHz, $CDCl_3$) δ (ppm): 8.76 (br s, 1H, NH), 8.22 (d, *J* = 3.8 Hz, 1H, ThH), 7.60 – 7.51 (m, 1H, ThH), 7.22 – 7.12 (m, 1H, ThH), 3.74 – 3.58 (m, 2H, NCH_2), 3.14 (s, 3H, SCH_3), 1.66 (m, 2H, Alkyl Chain), 1.41 – 1.19 (m, 6H, Alkyl Chain), 0.89 (t, *J* = 6.8 Hz, 3H, Alkyl Chain). **^{13}C NMR** (100 MHz, $CDCl_3$) δ 162.5, 160.2, 152.2, 134.7, 131.1, 130.9, 130.3, 128.6, 108.9, 108.7, 41.9, 31.4, 29.1, 26.5, 22.5, 16.0, 14.0. **HRMS** (TOF MS ASAP+): Calculated for $C_{17}H_{21}N_2O_2S_2^+$: 349.1044. Found *m/z* 349.1032 $[M+H]^+$.

Ethyl (Z)-4-((hexylamino)(methylthio)methylene)-5-oxo-2-(thiophen-2-yl)-4,5-dihydro-1H-pyrrole-3-carboxylate (39)

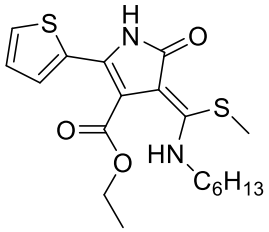

^{1}H NMR (400 MHz, CD_2Cl_2) δ (ppm): 10.29 (br s, 1H, NH), 9.28 (br s, 1H, NH), 7.35 – 7.31 (m, 1H, ThH), 7.30 (d, *J* = 5.1 Hz, 1H, ThH), 7.04 (dd, *J* = 5.1, 3.7 Hz, 1H, ThH), 4.28 (q, *J* = 7.2 Hz, 2H, OCH_2), 3.63 (m, NCH_2), 2.41 (s, 3H, SCH_3), 1.69 (m, 2H, Alkyl Chain), 1.49 – 1.38 (m, 2H, Alkyl Chain), 1.39 – 1.25 (m, 7H, Alkyl Chain, $OCH_2C\mathit{H_3}$), 0.90 (t, *J* = 7.0 Hz, 3H, Alkyl Chain). **^{13}C NMR** (151 MHz, $CDCl_3$) δ 166.6, 166.2, 132.8, 127.2, 125.8, 125.7, 107.4, 61.2, 45.6, 31.4, 30.3, 26.5, 22.5, 18.4, 14.1, 14.0. **HRMS** (TOF MS ASAP+): Calculated for $C_{19}H_{27}N_2O_3S_2^+$: 395.1463. Found *m/z* 395.1459 [M+H]+.

2-hexyl-5-methyl-3-(methylthio)-6-(thiophen-2-yl)-2,5-dihydropyrrolo[3,4-c]pyrrole-1,4-dione (40)

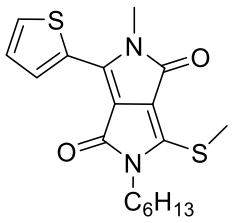

During the synthesis of **38**, compound **40** was also isolated from the crude mixture *via* column chromatography, to afford the product as a bright orange solid (0.10 g, 0.28 mmol, 7%).

^{1}H NMR (400 MHz, $CDCl_3$) δ (ppm): 8.70 (d, *J* = 3.2 Hz, 1H, ThH), 7.60 (d, *J* = 4.4 Hz, 1H, ThH), 7.32 – 7.21 (m, 1H, ThH), 3.71 – 3.63 (m, 2H, NCH_2), 3.52 (s, 3H, NCH_3), 3.13 (s, 3H, SCH_3), 1.64 (m, 2H, Alkyl Chain), 1.39 – 1.24 (m, 6H, Alkyl Chain), 0.88 (t, *J* = 6.6 Hz, 3H, Alkyl Chain). **^{13}C NMR** (100 MHz, $CDCl_3$) δ 160.7, 160.2, 151.6, 138.0, 134.0, 130.2, 130.1, 128.5, 108.0, 107.7, 41.8, 31.4, 29.2, 29.1, 26.5, 22.5, 16.0, 14.0. **HRMS** (TOF MS ASAP+): Calculated for $C_{18}H_{23}N_2O_2S_2^+$: 363.1201. Found *m/z* 363.1202 $[M+H]^+$.

VII

References

1 H. Spanggaard and F. C. Krebs, *Sol. Energy Mater. Sol. Cells*, 2004, **83**, 125–146.

2 B. A. Bolto, R. McNeill and D. E. Weiss, *Aust. J. Chem.*, 1963, **16**, 1090–1103.

3 J. H. Alan, *Adv. Mater.*, 2001, **40**, 2591–2611.

4 X. Guo, M. Baumgarten and K. Müllen, *Prog. Polym. Sci.*, 2013, **38**, 1832–1908.

5 B. Milián-Medina and J. Gierschner, *Wiley Interdiscip. Rev. Comput. Mol. Sci.*, 2012, **2**, 513–524.

6 G. Li, W. H. Chang and Y. Yang, *Nat. Rev. Mater.*, 2017, **2**, 1–13.

7 K. J.Fallon, *Synthesis of Naturally Inspired Conjugated Materials for Organic Electronics*, Univeristy College London, 2017.

8 H. A. M. Van Mullekom, J. A. J. M. Vekemans, E. E. Havinga and E. W. Meijer, *Mater. Sci. Eng. R Rep.*, 2001, **32**, 1–40.

9 J. L. Bredas, *Mater. Horizons*, 2014, **1**, 17–19.

10 A. Banerji, M. W. Tausch and U. Scherf, *Educ. Química*, 2013, **24**, 17–22.

11 Y. J. Cheng, S. H. Yang and C. S. Hsu, *Chem. Rev.*, 2009, **109**, 5868–5923.

12 T. Xu and L. Yu, *Mater. Today*, 2014, **17**, 11–15.

13 Fitch, K. & Kemke, C. Solar Radiation and Photosynethically Active Radiation. *Fundamentals of Environmental Measurements, Fondriest Environmental, Inc.* Available at: https://www.fondriest.com/environmental-measurements/parameters/weather/solar-radiation/. (Accessed: 20th December 2019).

14 A. Facchetti, *Chem. Mater.*, 2011, **23**, 733–758.

15 A. et al. Burroughes, J., Bradley, D., Brown, *Nature*, 1990, **347**, 539–541.

16 M. S. AlSalhi, J. Alam, L. A. Dass and M. Raja, *Int. J. Mol. Sci.*, 2011, **12**, 2036–2054.

17 B. D. Wohrle and D. Meissner, *Springer Ser. Mater. Sci.*, 2014, **208**, 67–214.

18 C. W. Tang, *Appl. Phys. Lett.*, 1986, **48**, 183–185.

19 Y. Lin, Y. Li and X. Zhan, *Chem. Soc. Rev.*, 2012, **41**, 4245.

20 S. Günes, H. Neugebauer and N. S. Sariciftci, *Chem. Rev.*, 2007, **107**, 1324–1338.

21 G. Yu, J. Gao, J. C. Hummelen, F. Wudl and A. J. Heeger, *Science.*, 1995, **270**, 1789–1791.

22 Y. Lin, Y. Li and X. Zhan, *Chem. Soc. Rev.*, 2012, **41**, 4245–4272.

23 C. Yan, S. Barlow, Z. Wang, H. Yan, A. K. Y. Jen, S. R. Marder and X. Zhan, *Nat. Rev. Mater.*, 2018, **3**, 1–19.

24 J. Hou, O. Inganas, R. H. Friend and F. Gao, *Nat. Mater.*, 2018, **17**, 119–128.

25 J. Liu, S. Chen, D. Qian, B. Gautam, G. Yang, J. Zhao, J. Bergqvist, F. Zhang, W. Ma, H. Ade, O. Inganäs, K. Gundogdu, F. Gao and H. Yan, *Nat. Energy*, 2016, **1**, 1–7.

26 C. B. Nielsen, S. Holliday, H. Y. Chen, S. J. Cryer and I. McCulloch, *Acc. Chem. Res.*, 2015, **48**, 2803–2812.

27 W. Zhao, S. Li, H. Yao, S. Zhang, Y. Zhang, B. Yang and J. Hou, *J. Am. Chem. Soc.*, 2017, **139**, 7148–7151.

28 H. Choi, S. J. Ko, T. Kim, P. O. Morin, B. Walker, B. H. Lee, M. Leclerc, J. Y. Kim and A. J. Heeger, *Adv. Mater.*, 2015, **27**, 3318–3324.

29 C. Y. Chang, C. E. Wu, S. Y. Chen, C. Cui, Y. J. Cheng, C. S. Hsu, Y. L. Wang and Y. Li, *Angew. Chemie - Int. Ed.*, 2011, **50**, 9386–9390.

30 S. H. Liao, H. J. Jhuo, Y. S. Cheng and S. A. Chen, *Adv. Mater.*, 2013, **25**, 4766–4771.

31 S. B. Darling and F. You, *RSC Adv.*, 2013, **3**, 17633.

32 D. Qian, Z. Zheng, H. Yao, W. Tress, T. R. Hopper, S. Chen, S. Li, J. Liu, S. Chen, J. Zhang, X. K. Liu, B. Gao, L. Ouyang, Y. Jin, G. Pozina, I. A. Buyanova, W. M. Chen, O. Inganäs, V. Coropceanu, J. L. Bredas, H. Yan, J. Hou, F. Zhang, A. A. Bakulin and F. Gao, *Nat. Mater.*, 2018, **17**, 703–709.

33 J. Xue, *Polym. Rev.*, 2010, **50**, 411–419.

34 Y. Cui, H. Yao, J. Zhang, T. Zhang, Y. Wang, L. Hong, K. Xian, B. Xu, S. Zhang, J. Peng, Z. Wei, F. Gao and J. Hou, *Nat. Commun.*, 2019, **10**, 1–8.

35 T. Yan, W. Song, J. Huang, R. Peng, L. Huang and Z. Ge, *Adv. Mater.*, 2019, **31**, 1–8.

36 L. Meng, Y. Zhang, X. Wan, C. Li, X. Zhang, Y. Wang, X. Ke, Z. Xiao, L. Ding, R. Xia, H. L. Yip, Y. Cao and Y. Chen, *Science.*, 2018, **361**, 1094–1098.

37 N. K. Elumalai and A. Uddin, *Energy Environ. Sci.*, 2016, **9**, 391–410.

38 N. Kaur, M. Singh, D. Pathak, T. Wagner and J. M. Nunzi, *Synth. Met.*, 2014, **190**, 20–26.

39 C. Liu, K. Wang, X. Gong and A. J. Heeger, *Chem. Soc. Rev.*, 2016, **45**, 4825–4846.

40 E. V. Canesi, D. Fazzi, L. Colella, C. Bertarelli and C. Castiglioni, *J. Am. Chem. Soc.*, 2012, **134**, 19070–19083.

41 S. Ray, S. Sharma, U. Salzner and S. Patil, *J. Phys. Chem. C*, 2017, **121**, 16088–16097.

42 J. L. Brédas, A. J. Heeger and F. Wudl, *J. Chem. Phys.*, 1986, **85**, 4673–4678.

43 A. Troisi and A. Shaw, *J. Phys. Chem. Lett.*, 2016, **7**, 4689–4694.

44 I. Osaka, M. Shimawaki, H. Mori, I. Doi, E. Miyazaki, T. Koganezawa and K. Takimiya, *J. Am. Chem. Soc.*, 2012, **134**, 3498–3507.

45 H. Brisset, C. Thobie-Gautier, A. Gorgues, M. Jubault and J. Roncali, *J. Chem. Soc. Chem. Commun.*, 1994, 1305–1306.

46 H. Zhou, L. Yang and W. You, *Macromolecules*, 2012, **45**, 607–632.

47 E. E. Havinga, W. ten Hoeve and H. Wynberg, *Synth. Met.*, 1993, **55**, 299–306.

48 J. L. Brédas and A. J. Heeger, *Chem. Phys. Lett.*, 1994, **217**, 507–512.

49 Y. Liang, D. Feng, Y. Wu, S. T. Tsai, G. Li, C. Ray and L. Yu, *J. Am. Chem. Soc.*, 2009, **131**, 7792–7799.

50 G. Conboy, H. J. Spencer, E. Angioni, A. L. Kanibolotsky, N. J. Findlay, S. J. Coles, C. Wilson, M. B. Pitak, C. Risko, V. Coropceanu, J. L. Brédas and P. J. Skabara, *Mater. Horizons*, 2016, **3**, 333–339.

51 S. Zhang, Y. Qin, M. A. Uddin, B. Jang, W. Zhao, D. Liu, H. Y. Woo and J. Hou,

Macromolecules, 2016, **49**, 2993–3000.

52 L. Bürgi, M. Turbiez, R. Pfeiffer, F. Bienewald, H. J. Kirner and C. Winnewisser, *Adv. Mater.*, 2008, **20**, 2217–2224.

53 H. Huang, L. Yang, A. Facchetti and T. J. Marks, *Chem. Rev.*, 2017, **117**, 10291–10318.

54 H. Bronstein, M. Hurhangee, E. C. Fregoso, D. Beatrup, Y. W. Soon, Z. Huang, A. Hadipour, P. S. Tuladhar, S. Rossbauer, E. H. Sohn, S. Shoaee, S. D. Dimitrov, J. M. Frost, R. S. Ashraf, T. Kirchartz, S. E. Watkins, K. Song, T. Anthopoulos, J. Nelson, B. P. Rand, J. R. Durrant and I. McCulloch, *Chem. Mater.*, 2013, **25**, 4239–4249.

55 Y. Yao, H. Dong and W. Hu, *Polym. Chem.*, 2013, **4**, 5197–5205.

56 A. Salleo, *Mater. Today*, 2007, **10**, 38–45.

57 R. Noriega, J. Rivnay, K. Vandewal, F. P. V. Koch, N. Stingelin, P. Smith, M. F. Toney and A. Salleo, *Nat. Mater.*, 2013, **12**, 1038–1044.

58 I. McCulloch, M. Heeney, C. Bailey, K. Genevicius, I. MacDonald, M. Shkunov, D. Sparrowe, S. Tierney, R. Wagner, W. Zhang, M. L. Chabinyc, R. J. Kline, M. D. McGehee and M. F. Toney, *Nat. Mater.*, 2006, **5**, 328–333.

59 H. N. Tsao, D. M. Cho, I. Park, M. R. Hansen, A. Mavrinskiy, D. Y. Yoon, R. Graf, W. Pisula, H. W. Spiess and K. Müllen, *J. Am. Chem. Soc.*, 2011, **133**, 2605–2612.

60 H. Bronstein, Z. Chen, R. S. Ashraf, W. Zhang, J. Du, J. R. Durrant, P. Shakya Tuladhar, K. Song, S. E. Watkins, Y. Geerts, M. M. Wienk, R. A. J. Janssen, T. Anthopoulos, H. Sirringhaus, M. Heeney and I. McCulloch, *J. Am. Chem. Soc.*, 2011, **133**, 3272–3275.

61 D. Venkateshvaran, M. Nikolka, A. Sadhanala, V. Lemaur, M. Zelazny, M. Kepa, M. Hurhangee, A. J. Kronemeijer, V. Pecunia, I. Nasrallah, I. Romanov, K. Broch, I. McCulloch, D. Emin, Y. Olivier, J. Cornil, D. Beljonne and H. Sirringhaus, *Nature*, 2014, **515**, 384–388.

62 K. Okamoto and C. K. Luscombe, *Polym. Chem.*, 2011, **2**, 2424–2434.

63 Z. Bao, W. K. Chan and L. Yu, *J. Am. Chem. Soc.*, 1995, **117**, 12426–12435.

64 T. Zheng, A. M. Schneider and L. Yu, *Synth. Methods Conjug. Polym. Carbon Mater.*, 2017, 1–58.

65 C. Cordovilla, C. Bartolomé, J. M. Martínez-Ilarduya and P. Espinet, *ACS Catal.*, 2015, **5**, 3040–

3053.

66 B. Carsten, F. He, H. J. Son, T. Xu and L. Yu, *Chem. Rev.*, 2011, **111**, 1493–1528.

67 Z. Wang, *Compr. Org. Name React. Reagents*, 2010, 2677–2685.

68 N. Miyaura, K. Yamada and A. Suzuki, *Tetrahedron Lett.*, 1979, **20**, 3437–3440.

69 A. Suzuki, *Chem. Commun.*, 2005, 4759–4763.

70 Z. Wang, *Compr. Org. Name React. Reagents*, 2010, 2733–2743.

71 J. E. Marcone and K. G. Moloy, *J. Am. Chem. Soc.*, 1998, **120**, 8527–8528.

72 A. T. T, *Agil. Technol. Tech. data*, 2011, **1**, 1–4.

73 A. Shrivastava, *Introd. to Plast. Eng.*, 2018, 1–16.

74 I. Yudhipratama, *Polymer Chemistry: Molecular Weight of Polymers*. Available at: https://chem-is-you.blogspot.com/2015/03/polymer-chemistry-molecular-weight-of.html, (Accessed 3rd December 2019).

75 WATERS, *Beginner's Guide to Size-Exclusion Chromatography*. Available at: https://www.waters.com/waters/de_DE/Size-exclusion-chromatography-%28SEC%29-Gel-Permeation-Chromatography-%28GPC%29-Guide/nav.htm?cid=10167568&locale=de_DE. (Accessed 3rd December 2019).

76 Cambridge Polymer Group, *GEL PERMEATION CHROMATOGRAPHY/SIZE EXCLUSION CHROMATOGRAPHY*. Available at: http://www.campoly.com/cpg-services/analytical-testing/chromatography/gpcsec/. (Accessed 3rd December 2019).

77 G. Klaerner and R. D. Miller, *Macromolecules*, 1998, **31**, 2007–2009.

78 S. C. Rasmussen, *Bull. Hist. Chem.*, 2014, **39**, 64–72.

79 M. D. McGehee and A. J. Heeger, *Adv. Mater.*, 2000, **12**, 1655–1668.

80 J. Yuan, Y. Zhang, L. Zhou, G. Zhang, H. L. Yip, T. K. Lau, X. Lu, C. Zhu, H. Peng, P. A. Johnson, M. Leclerc, Y. Cao, J. Ulanski, Y. Li and Y. Zou, *Joule*, 2019, **3**, 1140–1151.

81 Y. Sun, G. C. Welch, W. L. Leong, C. J. Takacs, G. C. Bazan and A. J. Heeger, *Nat. Mater.*, 2012, **11**, 44–48.

82 A. Menon, H. Dong, Z. I. Niazimbetova, L. J. Rothberg and M. E. Galvin, *Chem. Mater.*, 2002, **14**, 3668–3675.

83 F. Diederich and R. E. Martin, *Angew. Chem. Int. Ed.*, 1999, **38**, 1350–1377.

84 H. Bin, J. Yao, Y. Yang, I. Angunawela, C. Sun, L. Gao, L. Ye, B. Qiu, L. Xue, C. Zhu, C. Yang, Z. G. Zhang, H. Ade and Y. Li, *Adv. Mater.*, 2018, **30**, 1–8.

85 F. Garnier, A. Yassar, R. Hajlaoui, G. Horowitz, F. Deloffre, B. Servet, S. Ries and P. Alnot, *J. Am. Chem. Soc.*, 1993, **115**, 8716–8721.

86 J. Grimme, M. Kreyenschmidt, F. Uckert, K. Müllen and U. Scherf, *Adv. Mater.*, 1995, **7**, 292–295.

87 T. Maddux, W. Li and L. Yu, *J. Am. Chem. Soc.*, 1997, **119**, 844–845.

88 D. G. Farnum, G. Mehta, G. G. I. Moore and F. P. Siegal, *Tetrahedron Lett.*, 1974, **15**, 2549–2552.

89 S. Reformatsky, *Ber. Dtsch. Chem. Ges.*, 1887, **20**, 1210.

90 M. Grzybowski and D. T. Gryko, *Adv. Opt. Mater.*, 2015, **3**, 280–320.

91 A. Iqbal, M. Jost, R. Kirchmayr and A. Rochat, *Bull. SOC. Chim. Belg.*,1988, **97**, 615-644.

92 W. K. Chan, Y. Chen, Z. Peng and L. Yu, *J. Am. Chem. Soc.*, 1993, **115**, 11735–11743.

93 A. B. Tamayo, X. D. Dang, B. Walker, J. Seo, T. Kent and T. Q. Nguyen, *Appl. Phys. Lett.*, 2009, **94**, 11545–11551.

94 M. M. Wienk, M. Turbiez, J. Gilot and R. A. J. Janssen, *Adv. Mater.*, 2008, **20**, 2556–2560.

95 J. W. Jung, J. W. Jo, E. H. Jung and W. H. Jo, *Org. Electron. physics, Mater. Appl.*, 2016, **31**, 149–170.

96 Y. Qu, J. Hua and H. Tian, *Org. Lett.*, 2010, **12**, 3320–3323.

97 M. Fukuda, K. Kodama, H. Yamamoto and K. Mito, *Dye. Pigment.*, 2004, **63**, 115–125.

98 C. E. Creissen, J. Warnan, D. Antón-García, Y. Farré, F. Odobel and E. Reisner, *ACS Catal.*, 2019, **9**, 9530–9538.

99 S. Qu and H. Tian, *Chem. Commun.*, 2012, **48**, 3039–3051.

100 Q. Liu, S. E. Bottle and P. Sonar, *Adv. Mater.*, 2019, **32**, 1–46.

101 Z. Chen, M. J. Lee, R. Shahid Ashraf, Y. Gu, S. Albert-Seifried, M. Meedom Nielsen, B. Schroeder, T. D. Anthopoulos, M. Heeney, I. McCulloch and H. Sirringhaus, *Adv. Mater.*, 2012, **24**, 647–652.

102 X. Zhang, L. J. Richter, D. M. Delongchamp, R. J. Kline, M. R. Hammond, I. Mcculloch, M. Heeney, R. S. Ashraf, J. N. Smith, T. D. Anthopoulos, B. Schroeder, Y. H. Geerts, D. A. Fischer and M. F. Toney, *J. Am. Chem. Soc.*, 2011, **38**, 15073–15084.

103 W. Li, K. H. Hendriks, M. M. Wienk and R. A. J. Janssen, *Acc. Chem. Res.*, 2016, **49**, 78–85.

104 C. Kim, J. Liu, J. Lin, A. B. Tamayo, B. Walker, G. Wu and T. Q. Nguyen, *Chem. Mater.*, 2012, **24**, 1699–1709.

105 C. B. Nielsen, M. Turbiez and I. McCulloch, *Adv. Mater.*, 2013, **25**, 1859–1880.

106 B. Sun, W. Hong, H. Aziz and Y. Li, *Polym. Chem.*, 2015, **6**, 938–945.

107 Y. Li, P. Sonar, S. P. Singh, W. Zeng and M. S. Soh, *J. Mater. Chem.*, 2011, **21**, 10829–10835.

108 Q. Liu, H. Sun, S. P. Ponnappa, K. Feron, S. Manzhos, M. W. M. Jones, S. E. Bottle, J. Bell, Y. Y. Noh and P. Sonar, *Org. Electron.*, 2019, **74**, 290–298.

109 Z. Chen, D. Gao, J. Huang, Z. Mao, W. Zhang and G. Yu, *ACS Appl. Mater. Interfaces*, 2016, **8**, 34725–34734.

110 A. J. Kronemeijer, E. Gili, M. Shahid, J. Rivnay, A. Salleo, M. Heeney and H. Sirringhaus, *Adv. Mater.*, 2012, **24**, 1558–1565.

111 W. Li, K. H. Hendriks, A. Furlan, W. S. C. Roelofs, S. C. J. Meskers, M. M. Wienk and R. A. J. Janssen, *Adv. Mater.*, 2014, **26**, 1565–1570.

112 I. Meager, R. S. Ashraf, S. Rossbauer, H. Bronstein, J. E. Donaghey, J. Marshall, B. C. Schroeder, M. Heeney, T. D. Anthopoulos and I. Mcculloch, *Macromolecules*, 2013, **46**, 5961–5967.

113 I. Meager, R. S. Ashraf, S. Mollinger, B. C. Schroeder, H. Bronstein, D. Beatrup, M. S. Vezie, T. Kirchartz, A. Salleo, J. Nelson and I. McCulloch, *J. Am. Chem. Soc.*, 2013, **135**, 11537–11540.

114 C. Kanimozhi, N. Yaacobi-Gross, K. W. Chou, A. Amassian, T. D. Anthopoulos and S. Patil, *J.*

Am. Chem. Soc., 2012, **134**, 16532–16535.

115 X. Chen, Z. Zhang, Z. Ding, J. Liu and L. Wang, *Angew. Chemie - Int. Ed.*, 2016, **55**, 10376–10380.

116 S. F. Yang, X. Zhang, P. L. Chen, Z. T. Liu, J. W. Tian, G. X. Zhang and D. Q. Zhang, *Adv. Electron. Mater.*, 2017, **3**, 1–7.

117 K. H. Hendriks, G. H. L. Heintges, V. S. Gevaerts, M. M. Wienk and R. A. J. Janssen, *Angew. Chemie - Int. Ed.*, 2013, **52**, 8341–8344.

118 H. Zhang, S. Zhang, K. Gao, F. Liu, H. Yao, B. Yang, C. He, T. P. Russell and J. Hou, *J. Mater. Chem. A*, 2017, **5**, 10416–10423.

119 J. Li, Y. Zhao, H. S. Tan, Y. Guo, C. A. Di, G. Yu, Y. Liu, M. Lin, S. H. Lim, Y. Zhou, H. Su and B. S. Ong, *Sci. Rep.*, 2012, **2**, 1–9.

120 H. J. Yun, S. J. Kang, Y. Xu, S. O. Kim, Y. H. Kim, Y. Y. Noh and S. K. Kwon, *Adv. Mater.*, 2014, **26**, 7300–7307.

121 A. Giovannitti, C. B. Nielsen, D. T. Sbircea, S. Inal, M. Donahue, M. R. Niazi, D. A. Hanifi, A. Amassian, G. G. Malliaras, J. Rivnay and I. McCulloch, *Nat. Commun.*, 2016, **7**, 1–9.

122 S. S. Zade, N. Zamoshchik and M. Bendikov, *Acc. Chem. Res.*, 2011, **44**, 14–24.

123 L. Yuan, Y. Zhao, J. Zhang, Y. Zhang, L. Zhu, K. Lu, W. Yan and Z. Wei, *Adv. Mater.*, 2015, **27**, 4229–4233.

124 H. Meier, U. Stalmach and H. Kolshorn, *Acta Polym.*, 1997, **48**, 379–384.

125 H. Nakanishi, N. Sumi, Y. Aso and T. Otsubo, *J. Org. Chem.*, 1998, **63**, 8632–8633.

126 F. P. V Koch, P. Smith and M. Heeney, *J. Am. Chem. Soc*. 2013, **135**, 13695–13698 .

127 A. Leventis, *Understanding the Fundamental Properties of Conjugated Materials for Organic Electronics*, University College London, 2018.

128 M. S. Vezie, S. Few, I. Meager, G. Pieridou, B. Dörling, R. S. Ashraf, A. R. Goñi, H. Bronstein, I. McCulloch, S. C. Hayes, M. Campoy-Quiles and J. Nelson, *Nat. Mater.*, 2016, **15**, 746–753.

129 U. Zhokhavets, G. Gobsch, H. Hoppe and N. S. Sariciftci, *Thin Solid Films*, 2004, **451**–**452**, 69–73.

130 U. Zhokhavets, T. Erb, G. Gobsch, M. Al-Ibrahim and O. Ambacher, *Chem. Phys. Lett.*, 2006, **418**, 347–350.

131 S. Y. Liu, J. Z. Cheng, X. F. Zhang, H. Liu, Z. Q. Shen and H. R. Wen, *Polym. Chem.*, 2019, **10**, 325–330.

132 S. Y. Liu, D. G. Wang, A. G. Zhong and H. R. Wen, *Org. Chem. Front.*, 2018, **5**, 653–661.

133 M. Smet, B. Metten and W. Dehaen, *Tetrahedron Lett.*, 2001, **42**, 6527–6530.

134 M. A. Naik and S. Patil, *J. Polym. Sci. Part A Polym. Chem.*, 2013, **51**, 4241–4260.

135 Y. Zhu, A. R. Rabindranath, T. Beyerlein and B. Tieke, *Macromolecules*, 2007, **40**, 6981–6989.

136 X. Zhang, H. Bronstein, A. J. Kronemeijer, J. Smith, Y. Kim, R. J. Kline, L. J. Richter, T. D. Anthopoulos, H. Sirringhaus, K. Song, M. Heeney, W. Zhang, I. McCulloch and D. M. Delongchamp, *Nat. Commun.*, 2013, **4**, 1–9.

137 S. Stas, S. Sergeyev and Y. Geerts, *Tetrahedron*, 2010, **66**, 1837–1845.

138 C. M. Starks, *J. Am. Chem. Soc.*, 1971, **93**, 195–199.

139 Y. Zou, D. Gendron, A. Najari, Y. Tao and M. Leclerc, *Macromolecules*, 2009, **42**, 2891–2894.

140 H. Yamagata and F. C. Spano, *J. Chem. Phys.*, 2012, **136**, 184901-184914.

141 X. K. Chen, M. K. Ravva, H. Li, S. M. Ryno and J. L. Brédas, *Adv. Energy Mater.*, 2016, **6**, 1–10.

142 J. Zhang, H. S. Tan, X. Guo, A. Facchetti and H. Yan, *Nat. Energy*, 2018, **3**, 720–731.

143 C. Deibe, T. Strobe and V. Dyakonov, *Adv. Mater.*, 2010, **22**, 4097–4111.

144 K. Vandewal, S. Albrecht, E. T. Hoke, K. R. Graham, J. Widmer, J. D. Douglas, M. Schubert, W. R. Mateker, J. T. Bloking, G. F. Burkhard, A. Sellinger, J. M. J. Fréchet, A. Amassian, M. K. Riede, M. D. McGehee, D. Neher and A. Salleo, *Nat. Mater.*, 2014, **13**, 63–68.

145 D. Veldman, S. C. J. Meskers and R. A. J. Janssen, *Adv. Funct. Mater.*, 2009, **19**, 1939–1948.

146 J. Yao, T. Kirchartz, M. S. Vezie, M. A. Faist, W. Gong, Z. He, H. Wu, J. Troughton, T. Watson, D. Bryant and J. Nelson, *Phys. Rev. Appl.*, 2015, **4**, 1–10.

147 M. Azzouzi, J. Yan, T. Kirchartz, K. Liu, J. Wang, H. Wu and J. Nelson, *Phys. Rev. X*, 2018, **8**,

31055.

148 M. Azzouzi, T. Kirchartz and J. Nelson, *Trends Chem.*, 2019, **1**, 49–62.

149 H. Yao, Y. Cui, D. Qian, C. S. Ponseca, A. Honarfar, Y. Xu, J. Xin, Z. Chen, L. Hong, B. Gao, R. Yu, Y. Zu, W. Ma, P. Chabera, T. Pullerits, A. Yartsev, F. Gao and J. Hou, *J. Am. Chem. Soc.*, 2019, **141**, 7743–7750.

150 Y. Zhong, A. Tada, S. Izawa, K. Hashimoto and K. Tajima, *Adv. Energy Mater.*, 2014, **4**, 1–8.

151 A. Leventis, J. Royakkers, A. G. Rapidis, N. Goodeal, M. K. Corpinot, J. M. Frost, D. K. Bučar, M. O. Blunt, F. Cacialli and H. Bronstein, *J. Am. Chem. Soc.*, 2018, **140**, 1622–1626.

152 B. McDearmon, E. Lim, I. H. Lee, L. M. Kozycz, K. O'Hara, P. I. Robledo, N. R. Venkatesan, M. L. Chabinyc and C. J. Hawker, *Macromolecules*, 2018, **51**, 2580–2590.

153 F. Pop, W. Lewis and D. B. Amabilino, *CrystEngComm*, 2016, **18**, 8933–8943.

154 Y. Fujiwara, R. Ozawa, D. Onuma, K. Suzuki, K. Yoza and K. Kobayashi, *J. Org. Chem.*, 2013, **78**, 2206–2212.

155 X. Song, N. Gasparini, M. M. Nahid, S. H. K. Paleti, C. Li, W. Li, H. Ade and D. Baran, *Adv. Funct. Mater.*, 2019, **29**, 1–8.

156 C. Li, A. Zhang, Z. Wang, F. Liu, Y. Zhou, T. P. Russell, Y. Li and W. Li, *RSC Adv.*, 2016, **6**, 35677–35683.

157 X. Jiang, Y. Xu, X. Wang, Y. Wu, G. Feng, C. Li, W. Ma and W. Li, *Phys. Chem. Chem. Phys.*, 2017, **19**, 8069–8075.

158 W. Li, K. H. Hendriks, A. Furlan, W. S. C. Roelofs, M. M. Wienk and R. A. J. Janssen, *J. Am. Chem. Soc.*, 2013, **135**, 18942–18948.

159 L. Dou, J. Gao, E. Richard, J. You, C. C. Chen, K. C. Cha, Y. He, G. Li and Y. Yang, *J. Am. Chem. Soc.*, 2012, **134**, 10071–10079.

160 J. Rivnay, S. Inal, A. Salleo, R. M. Owens, M. Berggren and G. G. Malliaras, *Nat. Rev. Mater.*, 2018, **3**, 1-14.

161 A. Campana, T. Cramer, D. T. Simon, M. Berggren and F. Biscarini, *Adv. Mater.*, 2014, **26**, 3874–3878.

162 P. Leleux, J. Rivnay, T. Lonjaret, J. M. Badier, C. Bénar, T. Hervé, P. Chauvel and G. G. Malliaras, *Adv. Healthc. Mater.*, 2015, **4**, 142–147.

163 A. Williamson, M. Ferro, P. Leleux, E. Ismailova, A. Kaszas, T. Doublet, P. Quilichini, J. Rivnay, B. Rõzsa, G. Katona, C. Bernard and G. G. Malliaras, *Adv. Mater.*, 2015, **27**, 4405–4410.

164 S. Inal, J. Rivnay, P. Leleux, M. Ferro, M. Ramuz, J. C. Brendel, M. M. Schmidt, M. Thelakkat and G. G. Malliaras, *Adv. Mater.*, 2014, **26**, 7450–7455.

165 C. K. Song, B. J. Eckstein, T. L. D. Tam, L. Trahey and T. J. Marks, *ACS Appl. Mater. Interfaces*, 2014, **6**, 19347–19354.

166 T. Aysha, S. Luňák, A. Lyčka, J. Vyňuchal, Z. Eliáš, A. Růžička, Z. Padělková and R. Hrdina, *Dye. Pigment.*, 2013, **98**, 530–539.

167 Y. Jiang, X. Chen, Y. Zheng, Z. Xue, C. Shu, W. Yuan and X. Zhang, *Angew. Chemie - Int. Ed.*, 2011, **50**, 7304–7307.

168 T. Mitsumori, K. Inoue, N. Koga and H. Iwamura, *J. Am. Chem. Soc.*, 1995, **117**, 2467–2478.

169 S. Talukdar, J. L. Hsu, T. C. Chou and J. M. Fang, *Tetrahedron Lett.*, 2001, **42**, 1103–1105.

170 C. J. H. Morton, R. Gilmour, D. M. Smith, P. Lightfoot, A. M. Z. Slawin and E. J. MacLean, *Tetrahedron*, 2002, **58**, 5547–5565.

171 W. Xu, Y. Jiang and H. Fu, *Synlett*, 2012, **23**, 801–804.

172 B. Metten, K. Martinez, J. Thomas, W. Qin, M. Smet, N. Boens and W. Dehaen, *Org. Biomol. Chem.*, 2007, **5**, 2587–2591.

173 J. Ahner, J. Nowotny, U. S. Schubert and M. D. Hager, *Des. Monomers Polym.*, 2017, **20**, 210–220.

174 B. Li, H. Li, P. Chen, W. Sun, C. Wang, T. Gao and P. Yan, *Dalt. Trans.*, 2016, **45**, 11459–11470.

175 G. Qiu, Z. Jiang, Z. Ni, H. Wang, H. Dong, J. Zhang, X. Zhang, Z. Shu, K. Lu, Y. Zhen, Z. Wei and W. Hu, *J. Mater. Chem. C*, 2017, **5**, 566–572.

176 Y. Ji, C. Xiao, Q. Wang, J. Zhang, C. Li, Y. Wu, Z. Wei, X. Zhan, W. Hu, Z. Wang, R. A. J. Janssen and W. Li, *Adv. Mater.*, 2016, **28**, 943–950.

177 Z. Jiang, Z. Ni, H. Wang, Z. Wang, J. Zhang, G. Qiu, J. Fang, Y. Zhang, H. Dong, K. Lu, W. Hu and Z. Wei, *Polym. Chem.*, 2017, **8**, 5603–5610.

178 S. Ding, Z. Ni, M. Hu, G. Qiu, J. Li, J. Ye, X. Zhang, F. Liu, H. Dong and W. Hu, *Macromol. Rapid Commun.*, 2018, **39**, 1–8.

179 Z. Wang, Z. Liu, L. Ning, M. Xiao, Y. Yi, Z. Cai, A. Sadhanala, G. Zhang, W. Chen, H. Sirringhaus and D. Zhang, *Chem. Mater.*, 2018, **30**, 3090–3100.

180 B. Metten, M. Kostermans, G. Van Baelen, M. Smet and W. Dehaen, *Tetrahedron*, 2006, **62**, 6018–6028.

181 K. Aoshima, M. Ide and A. Saeki, *RSC Adv.*, 2018, **8**, 30201–30206.

182 Š. Frebort, Z. Eliáš, A. Lyčka, S. Luňák, J. Vyňuchal, L. Kubáč, R. Hrdina and L. Burgert, *Tetrahedron Lett.*, 2011, **52**, 5769–5773.

183 S. Grimme, J. Antony, S. Ehrlich and H. Krieg, *J. Chem. Phys.*, 2010, **132**, 154104.

184 L. Wang, X. Zhang, H. Tian, Y. Lu, Y. Geng and F. Wang, *Chem. Commun.*, 2013, **49**, 11272–11274.

185 L. S. Liebeskind and J. Srogl, *Org. Lett.*, 2002, **4**, 979–981.

186 R. Y. Mahale, S. S. Dharmapurikar and M. K. Chini, *Chem. Phys. Lett.*, 2018, **696**, 48–54.

187 M. Kirkus, L. Wang, S. Mothy, D. Beljonne, J. Cornil, R. A. J. Janssen and S. C. J. Meskers, *J. Phys. Chem. A*, 2012, **116**, 7927–7936.

188 A. Riaño, P. Mayorga Burrezo, M. J. Mancheño, A. Timalsina, J. Smith, A. Facchetti, T. J. Marks, J. T. López Navarrete, J. L. Segura, J. Casado and R. Ponce Ortiz, *J. Mater. Chem. C*, 2014, **2**, 6376.

189 S. Cho, J. Lee, M. Tong, J. H. Seo and C. Yang, *Adv. Funct. Mater.*, 2011, **21**, 1910–1916.

190 H. Bock and B. Roth, *Phosphorus Sulfur Relat. Elem.*, 1983, **14**, 211–223.

191 J. H. Noh and J. Kim, *J. Org. Chem.*, 2015, **80**, 11624–11628.

192 C. H. Woo, P. M. Beaujuge, T. W. Holcombe, O. P. Lee and J. M. J. Fréchet, *J. Am. Chem. Soc.*, 2010, **132**, 15547–15549.

VIII

Appendix

8.1 Chapter II

8.1.1 ^{1}H NMR and ^{13}C NMR

3,6-Di(thiophen-2-yl)-2,5-dihydropyrrolo[3,4-c]pyrrole-1,4-dione (1)

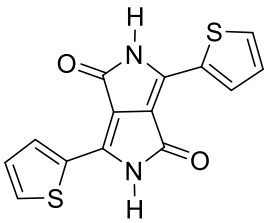

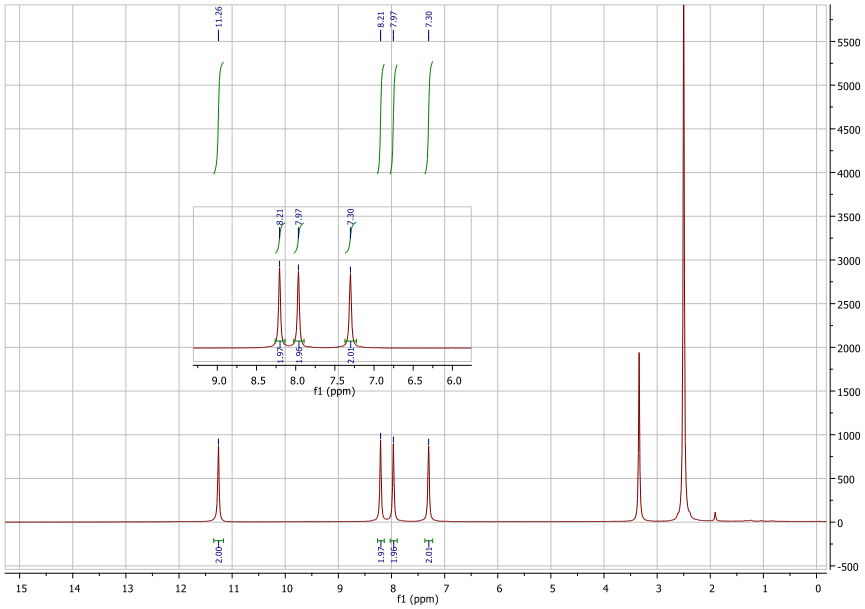

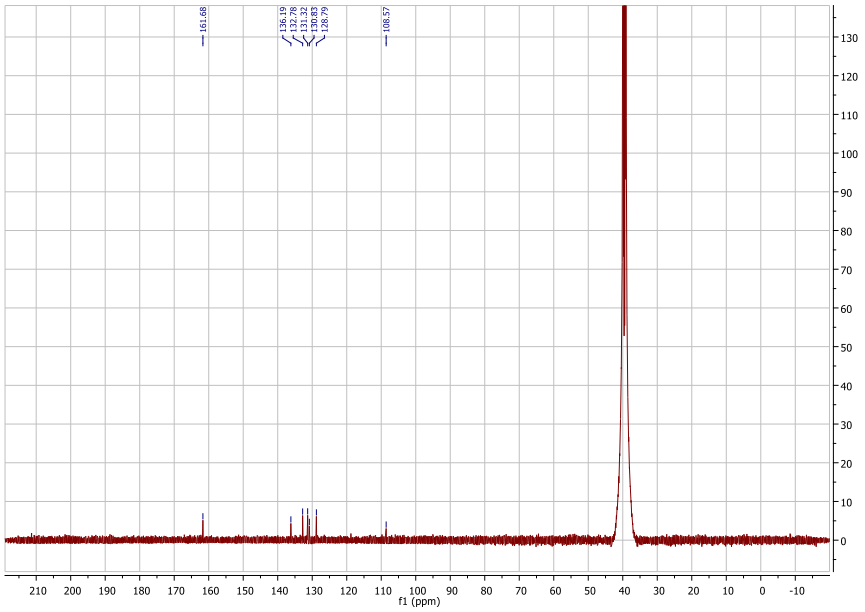

2,5-bis(2-hexyldecyl)-3,6-di(thiophen-2-yl)-2,5-dihydropyrrolo[3,4-c]pyrrole-1,4-dione (2)

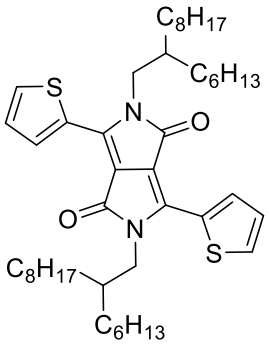

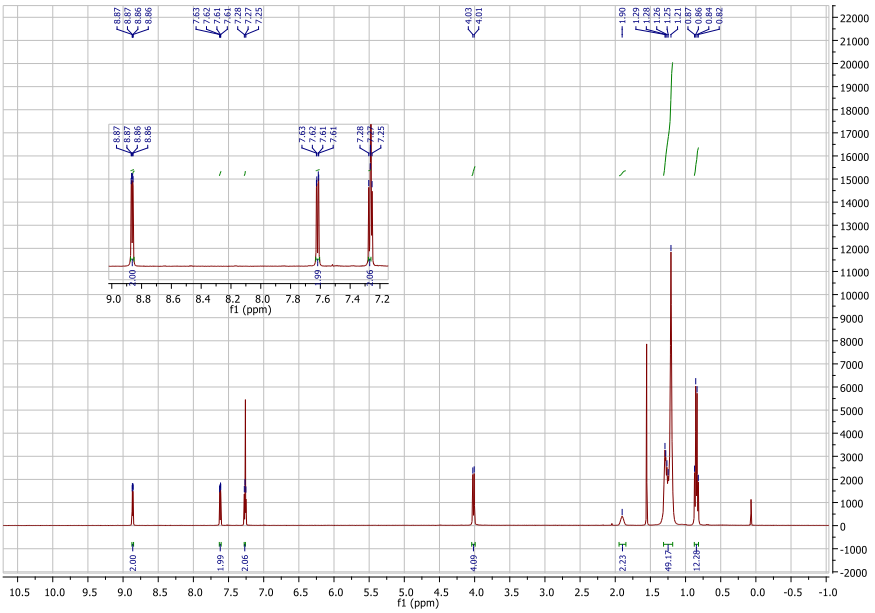

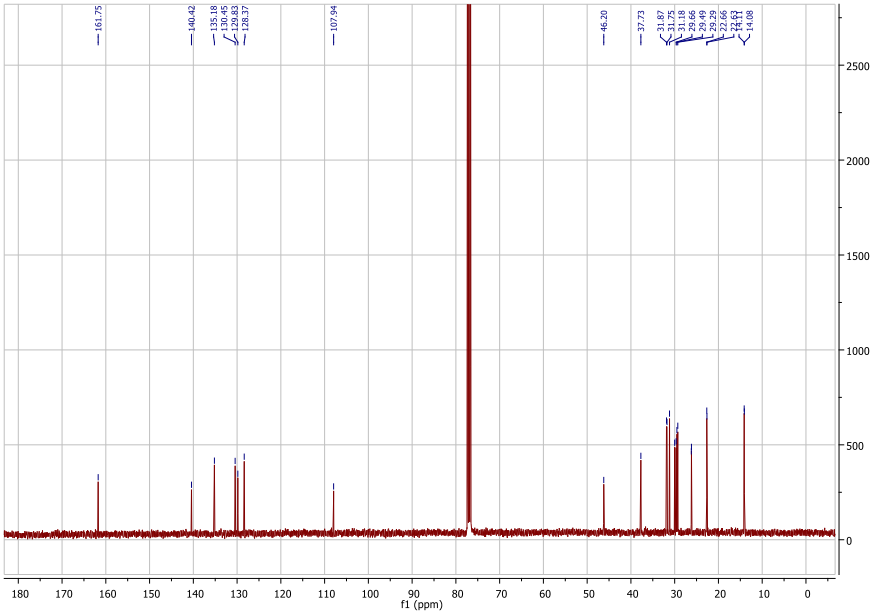

3-(5-bromothiophen-2-yl)-2,5-bis(2-hexyldecyl)-6-(thiophen-2-yl)-2,5-dihydropyrrolo[3,4-c]pyrrole-1,4-dione (4)

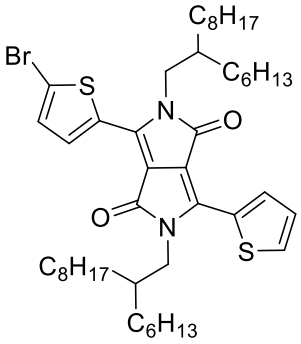

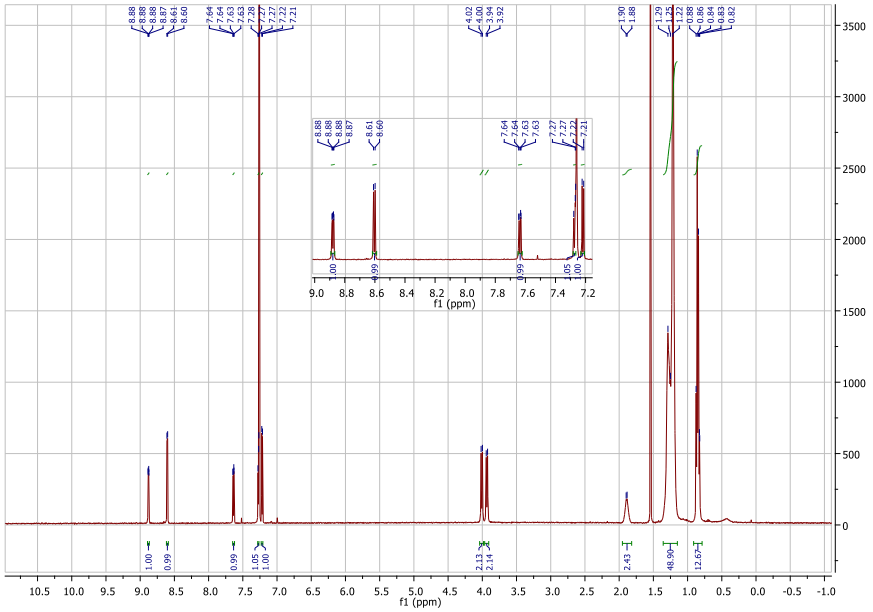

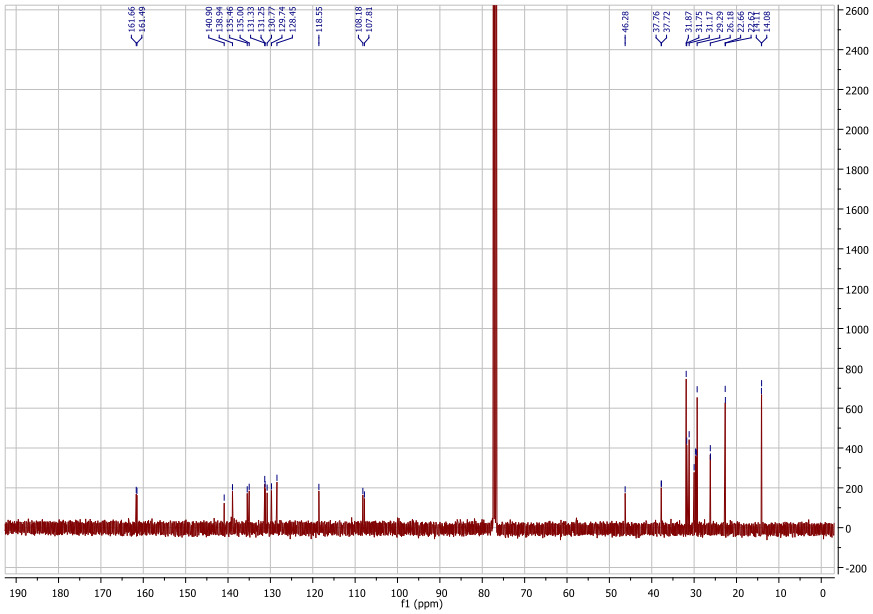

3,6-bis(5-bromothiophen-2-yl)-2,5-bis(2-hexyldecyl)-2,5-dihydropyrrolo[3,4-c]pyrrole-1,4-dione (5)

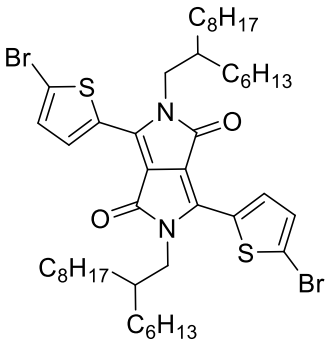

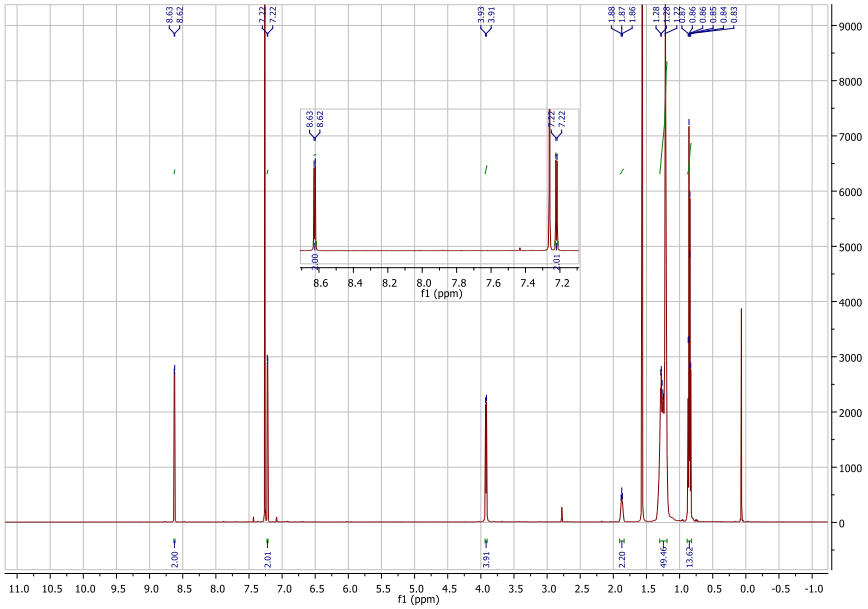

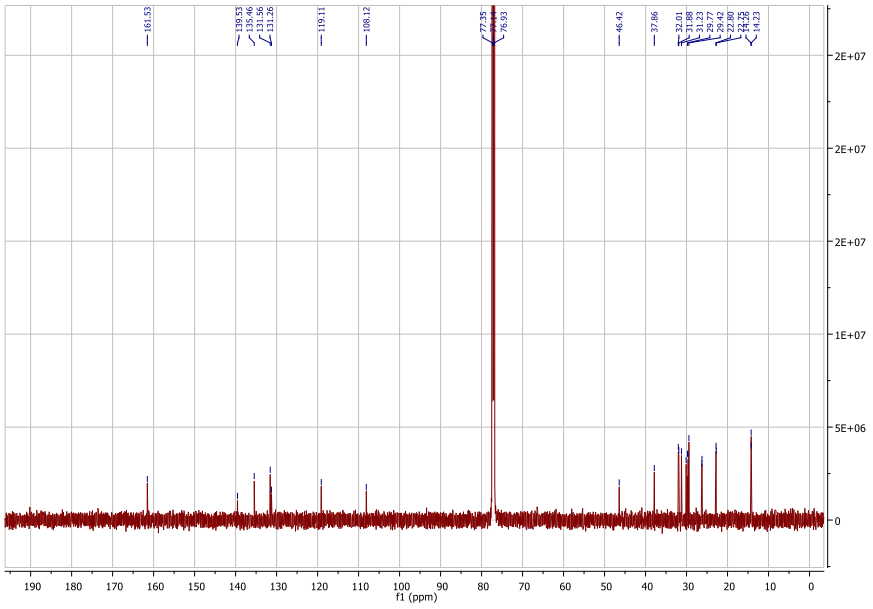

6,6'-(1,4-phenylenebis(thiophene-5,2-diyl))bis(2,5-bis(2-hexyldecyl)-3-(thiophen-2-yl)-2,5-dihydropyrrolo[3,4-c]pyrrole-1,4-dione) (6) (Dimer)

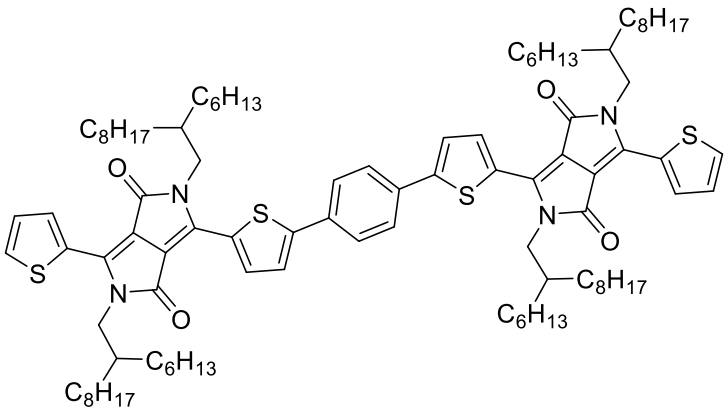

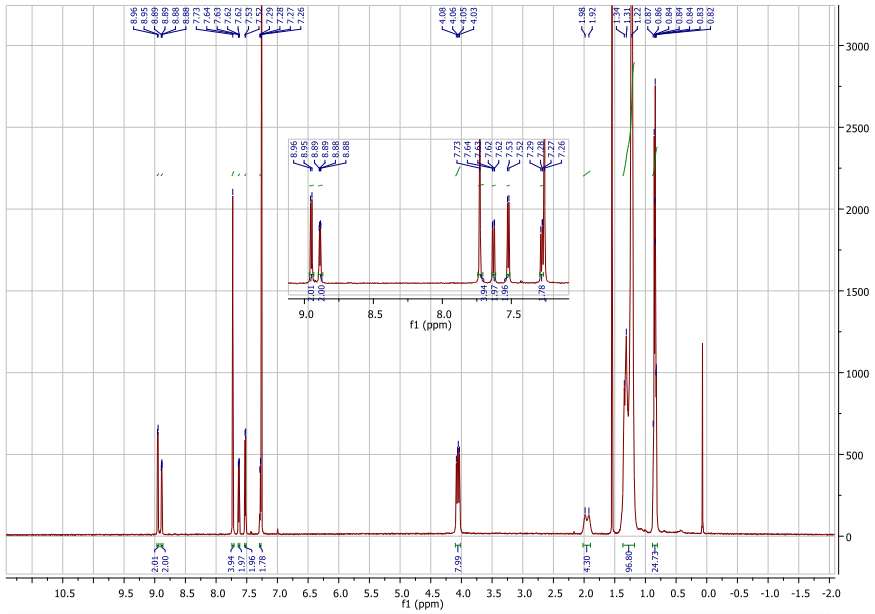

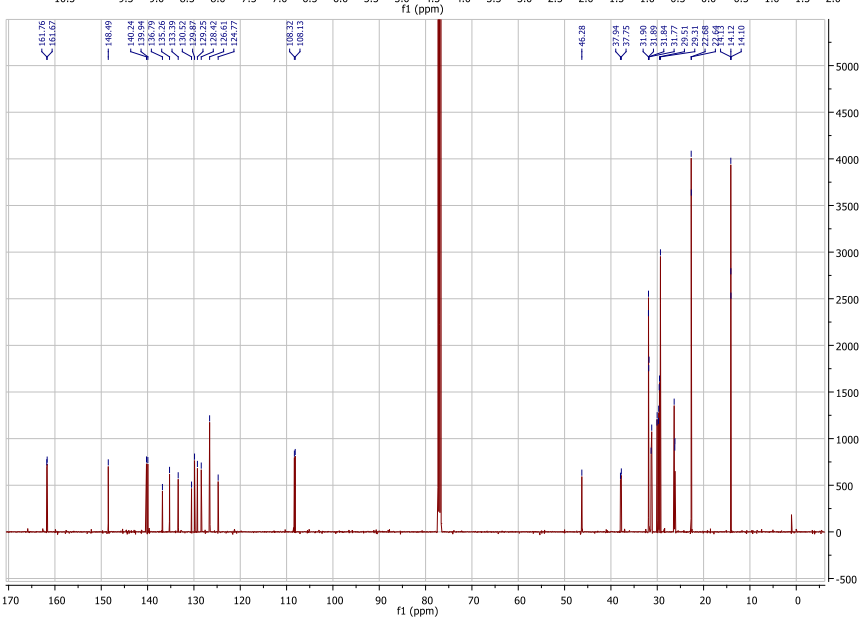

6,6'-(1,4-phenylenebis(thiophene-5,2-diyl))bis(3-(5-bromothiophen-2-yl)-2,5-bis(2-hexyldecyl)-2,5-dihydropyrrolo[3,4-c]pyrrole-1,4-dione) (7)

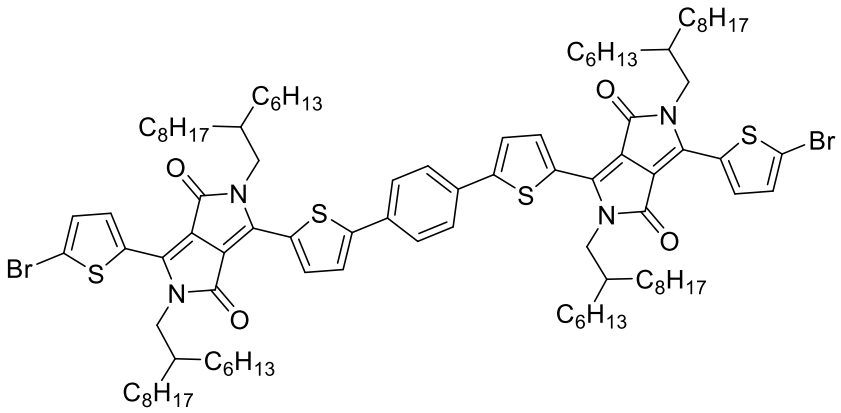

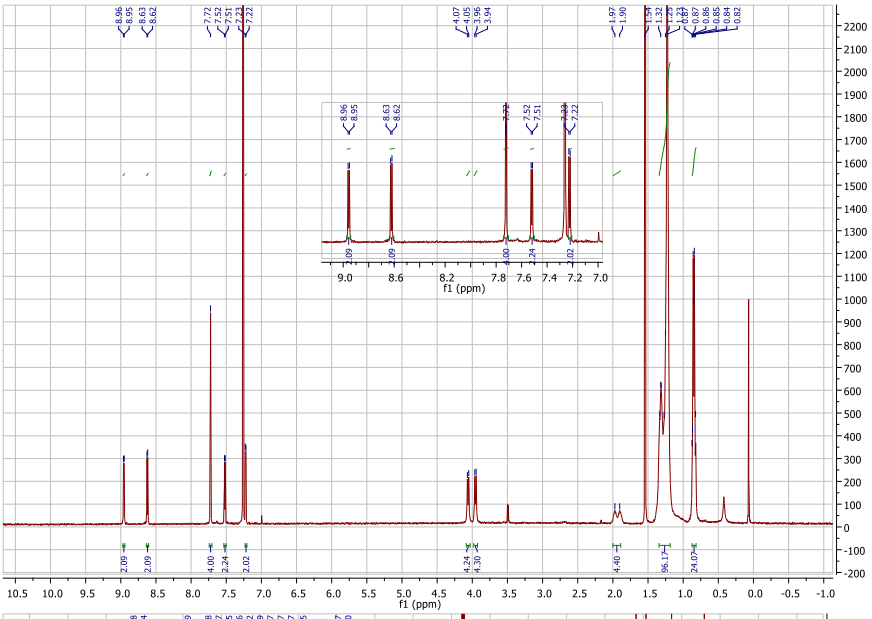

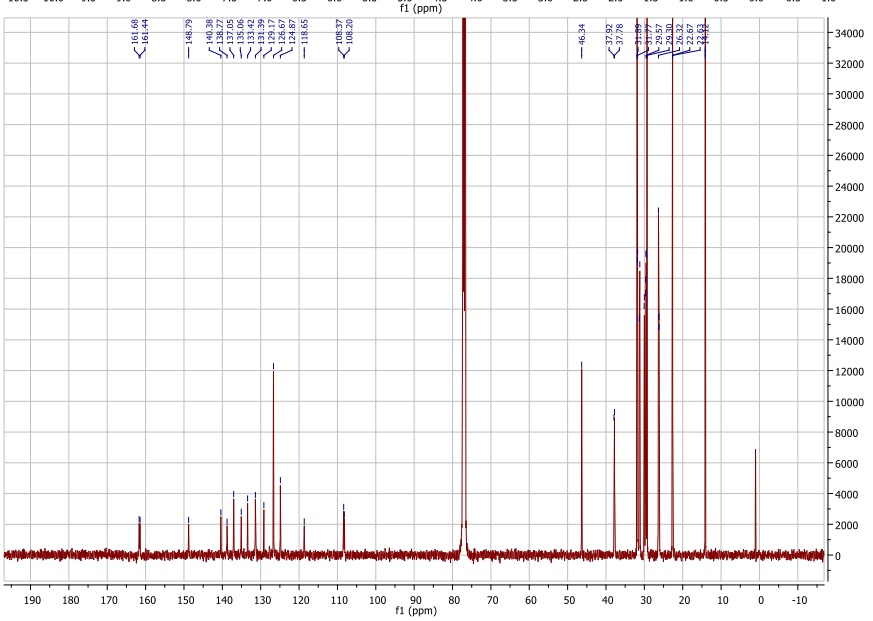

6,6'-(1,4-phenylenebis(thiophene-5,2-diyl))bis(2,5-bis(2-hexyldecyl)-3-(5-(4-(4,4,5,5-tetramethyl-1,3,2-dioxaborolan-2-yl)phenyl)thiophen-2-yl)-2,5-dihydropyrrolo[3,4-c]pyrrole-1,4-dione) (Bis-borylated Dimer) (8)

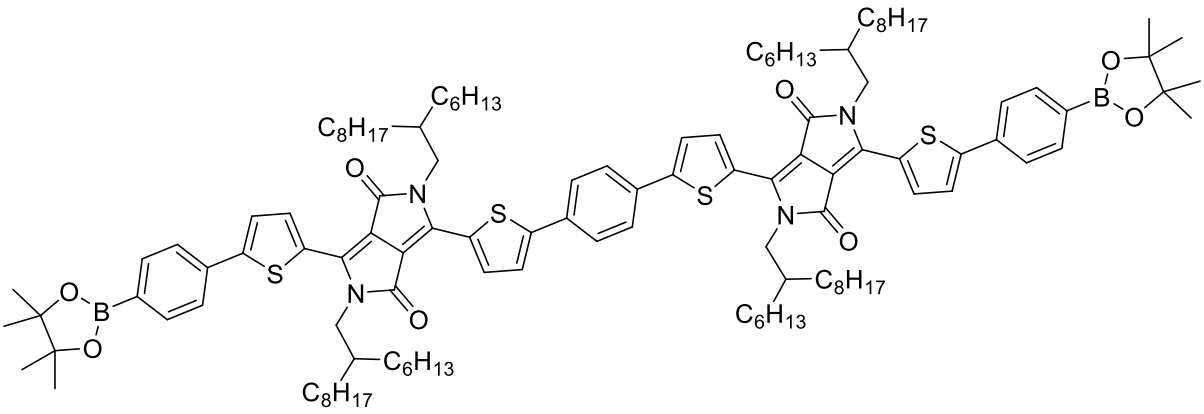

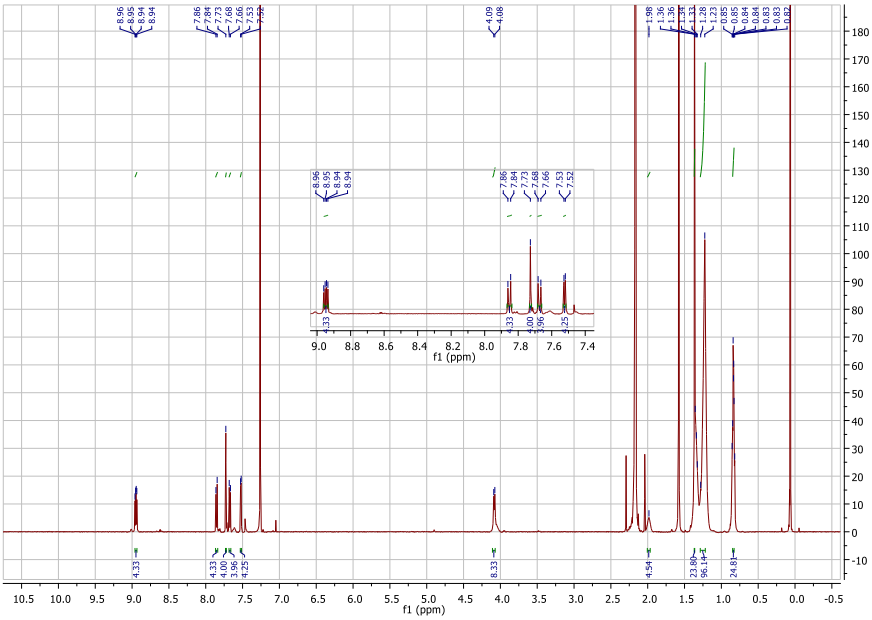

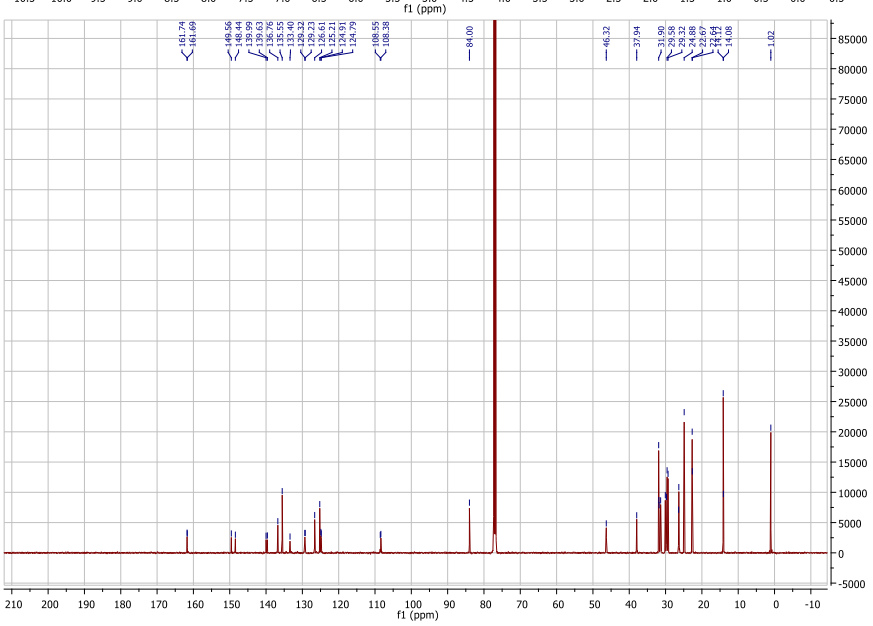

6,6'-(1,4-phenylenebis(thiophene-5,2-diyl))bis(3-(5-(4-(5-(2,5-bis(2-hexyldecyl)-3,6-dioxo-4-(thiophen-2-yl)-2,3,5,6-tetrahydropyrrolo[3,4-c]pyrrol-1-yl)thiophen-2-yl)phenyl)thiophen-2-yl)-2,5-bis(2-hexyldecyl)-2,5-dihydropyrrolo[3,4-c]pyrrole-1,4-dione)(9) (Tetramer)

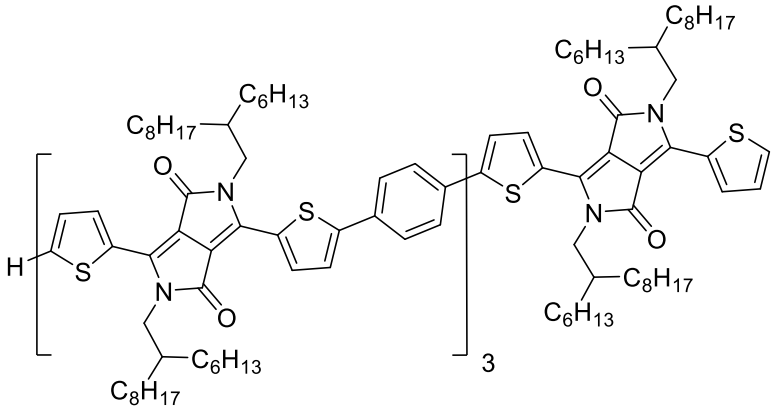

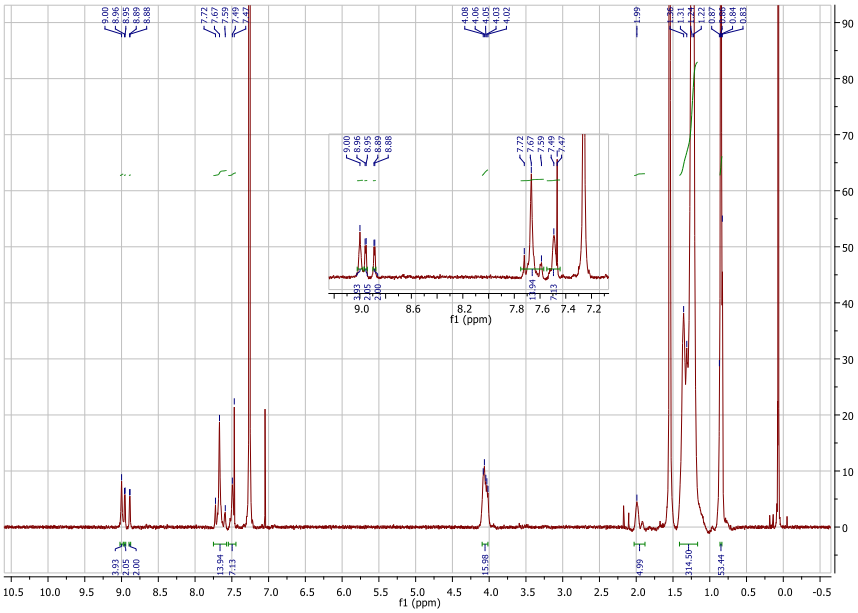

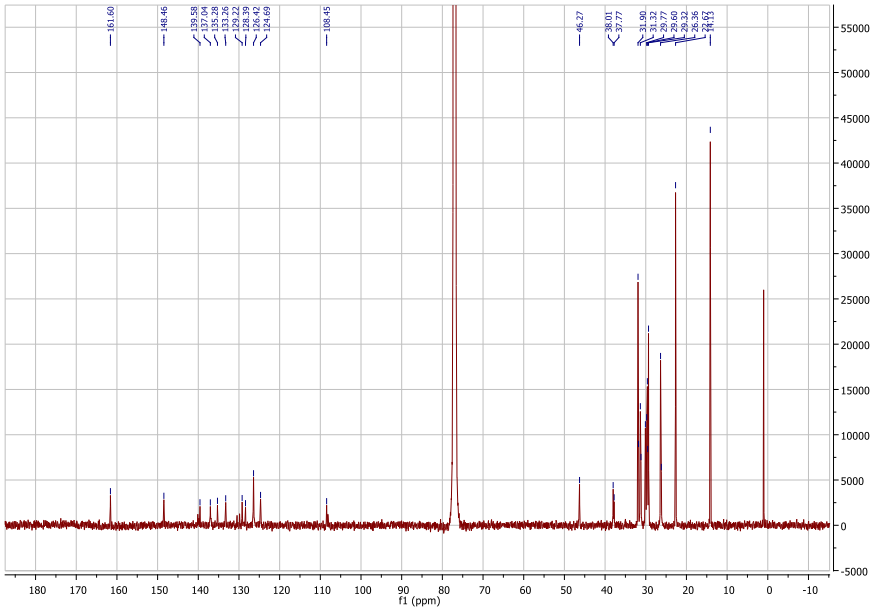

8.2 Chapter III

8.2.1 ^{1}H NMR and ^{13}C NMR

(2)

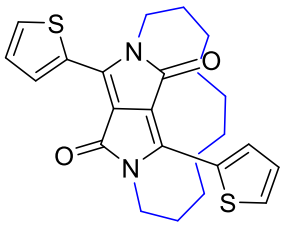

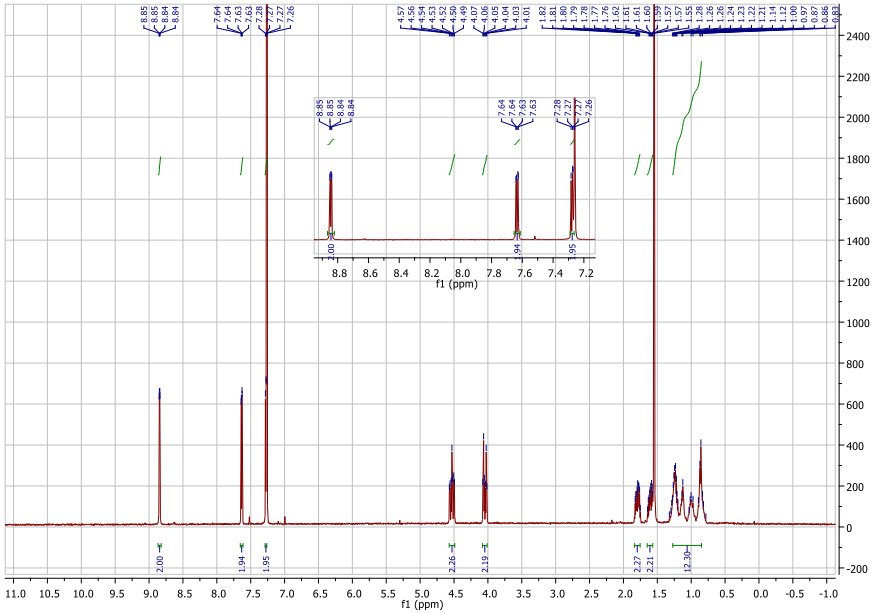

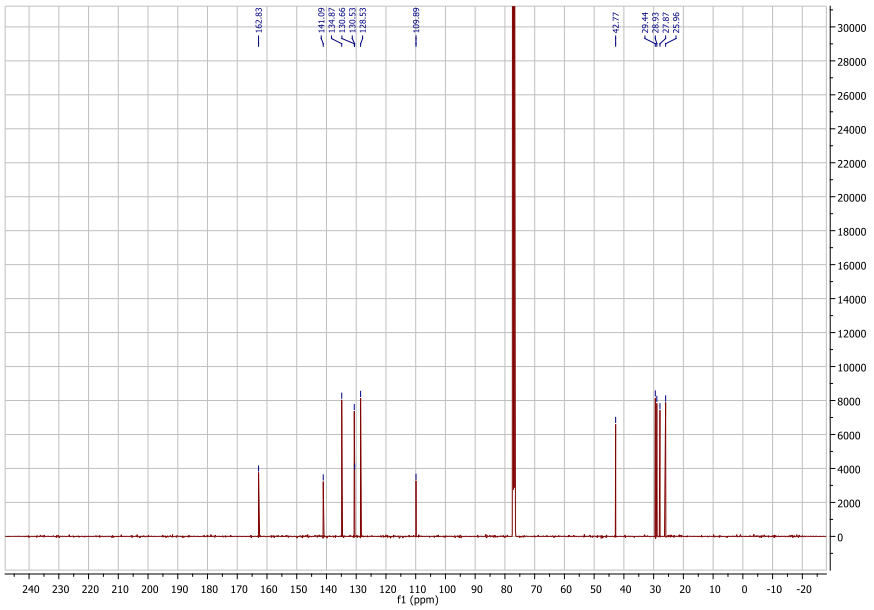

EC10DPPT (3)

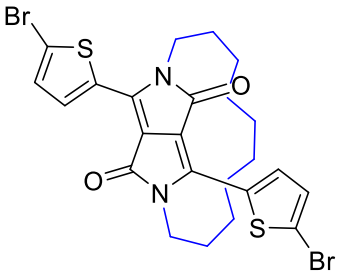

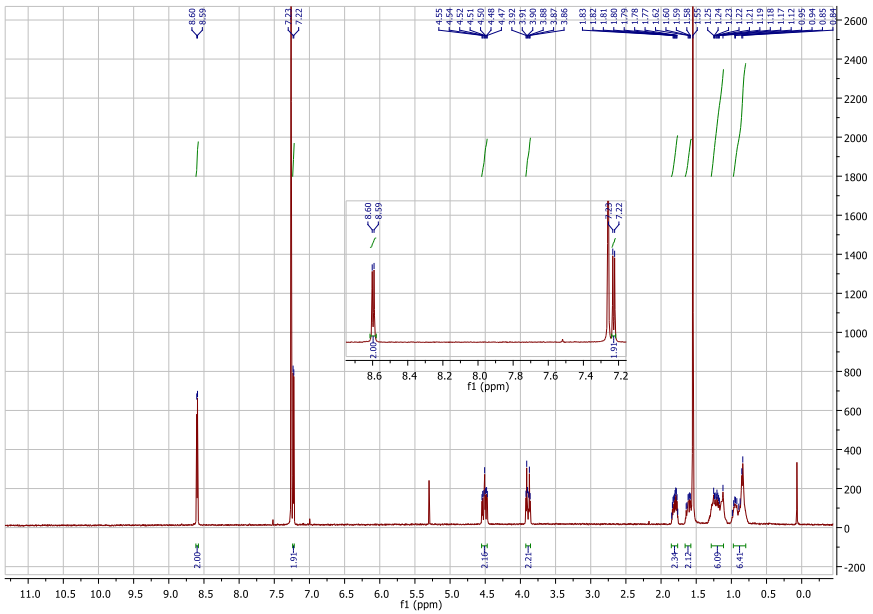

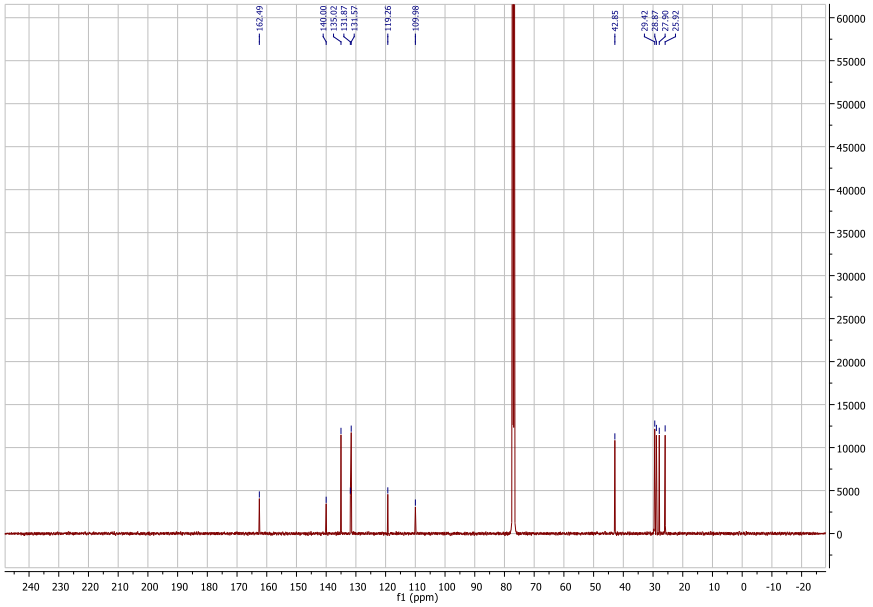

2,5-bis(2-decyltetradecyl)-3,6-di(thiophen-2-yl)-2,5-dihydropyrrolo[3,4-c]pyrrole-1,4-dione (7)

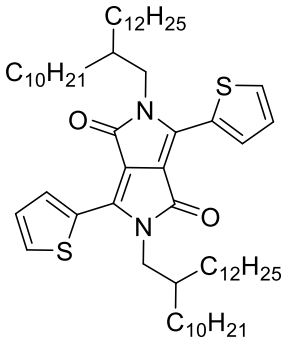

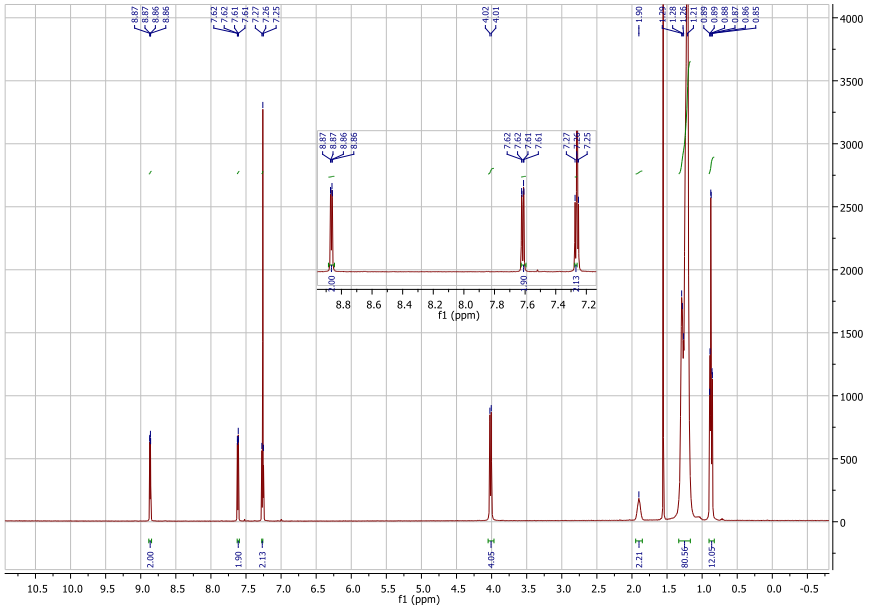

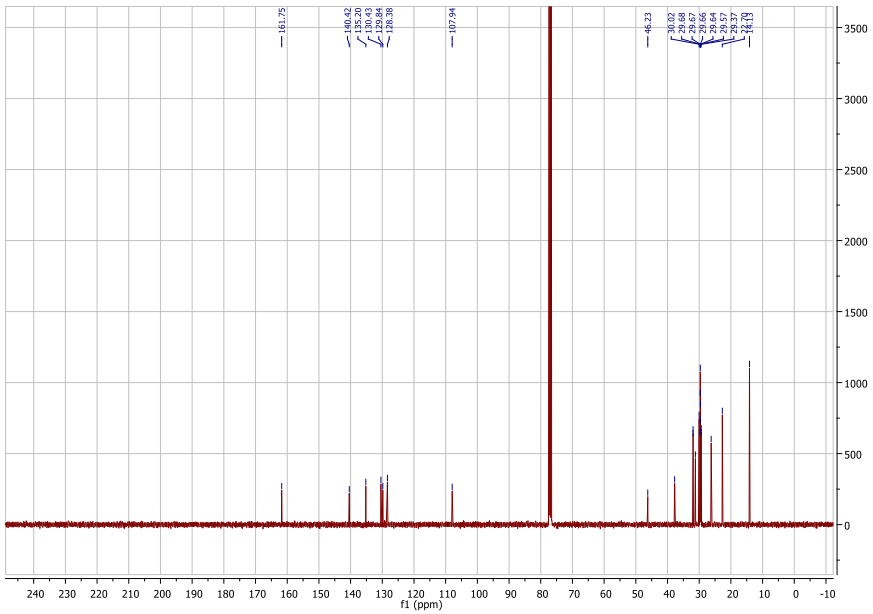

3,6-bis(5-bromothiophen-2-yl)-2,5-bis(2-decyltetradecyl)-2,5-dihydropyrrolo[3,4-c]pyrrole-1,4-dione (6)

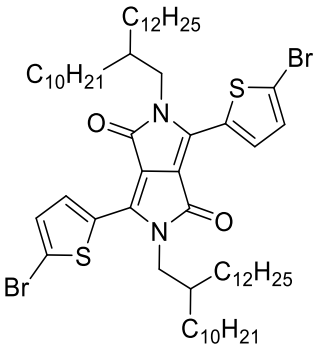

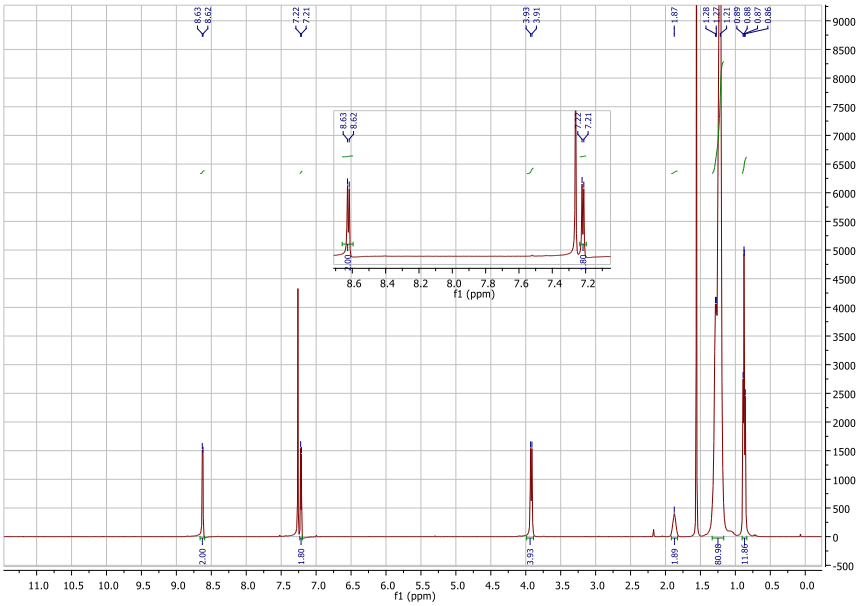

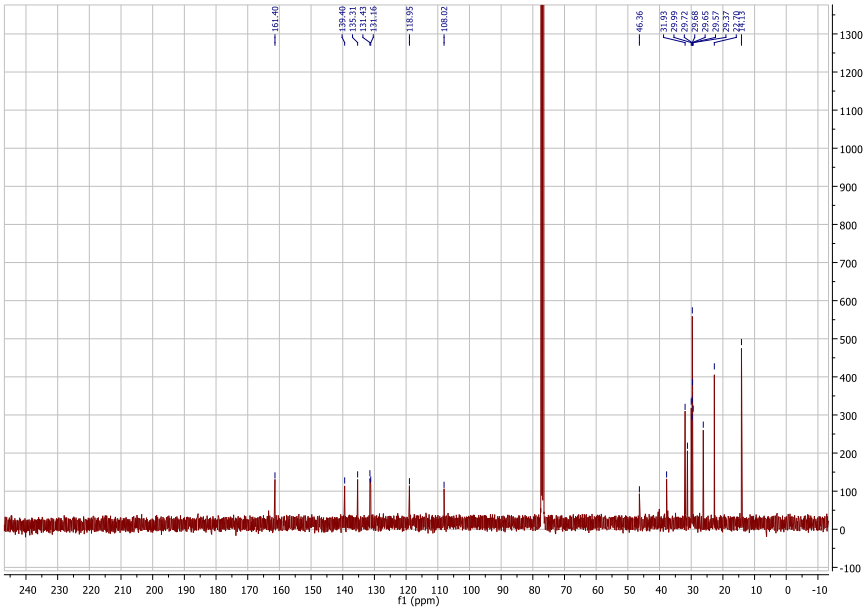

(8a)

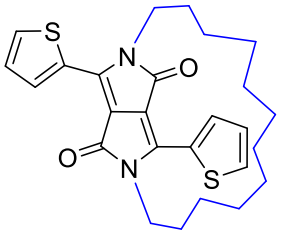

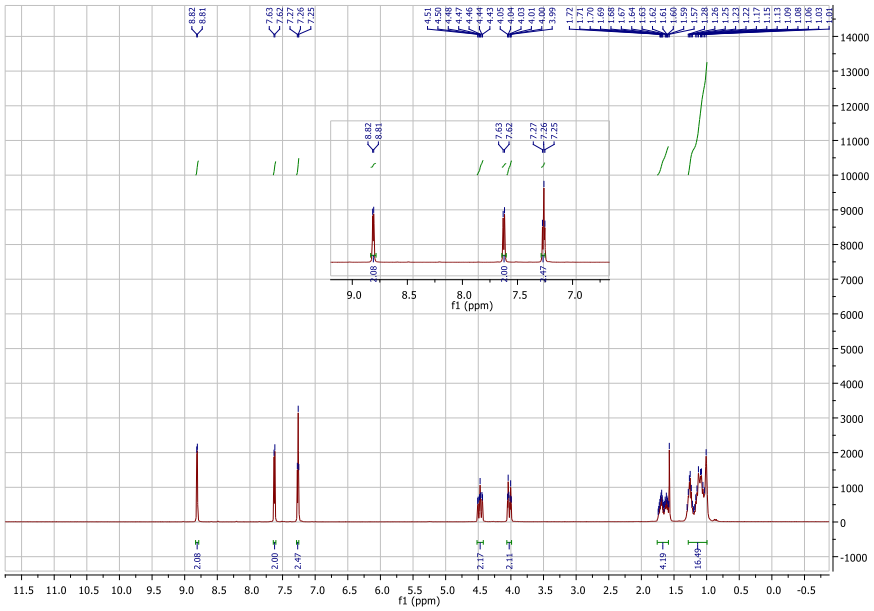

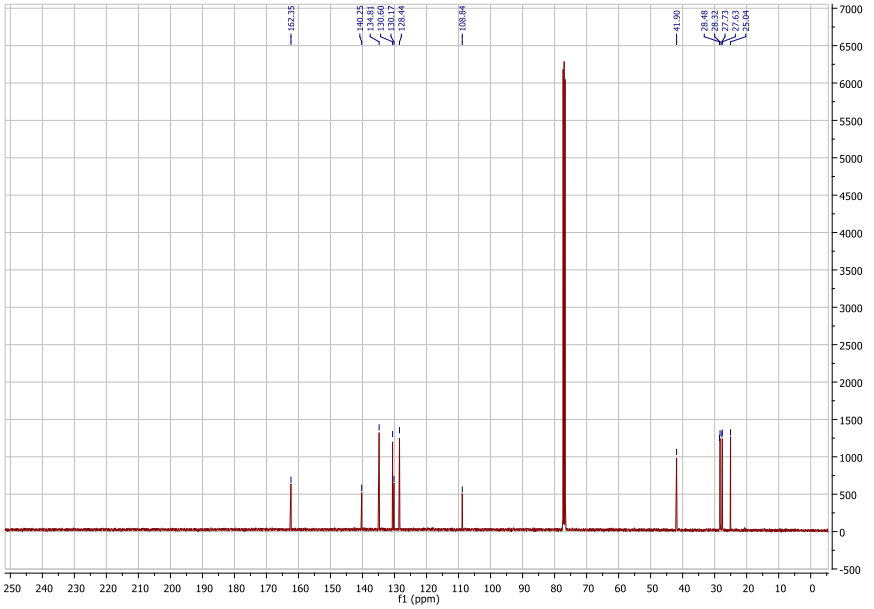

(8b)

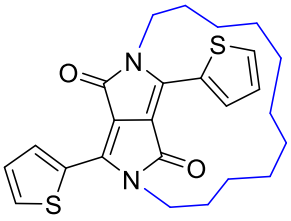

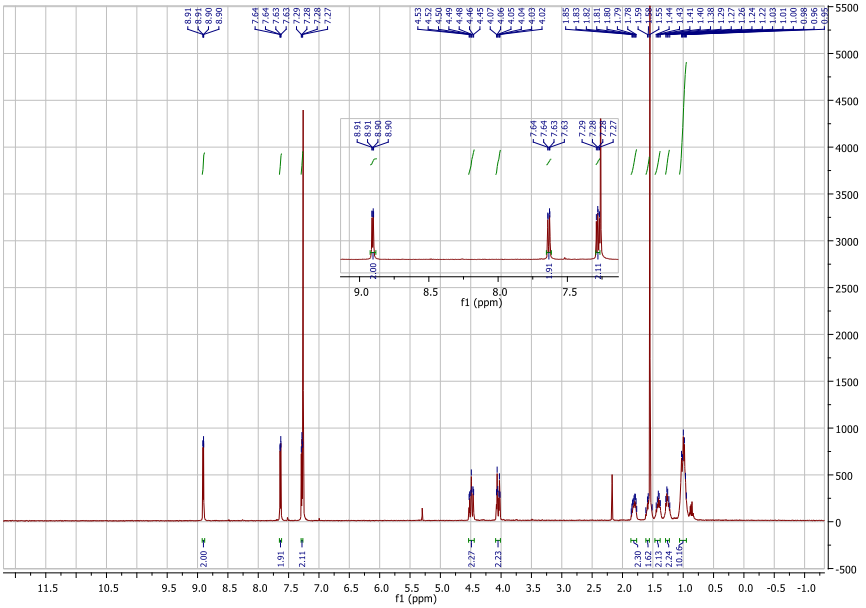

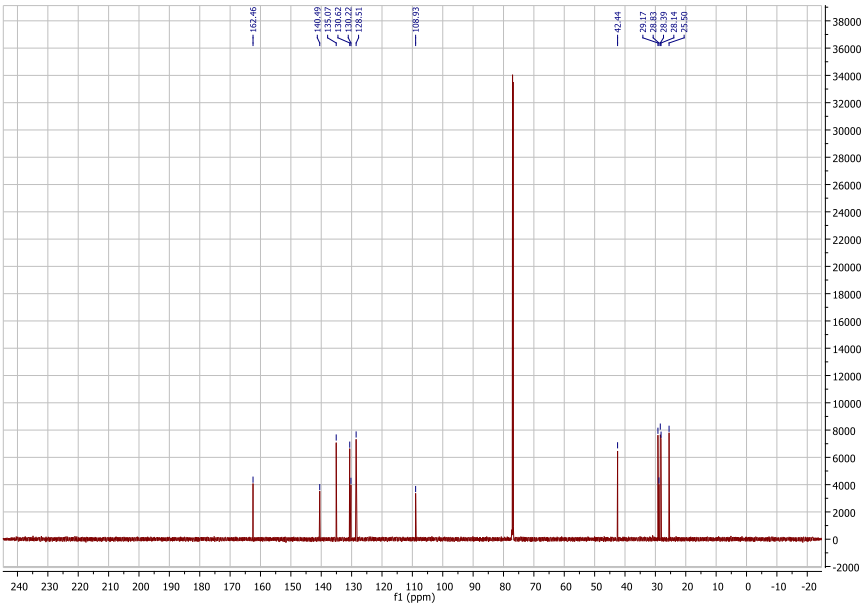

(8c)

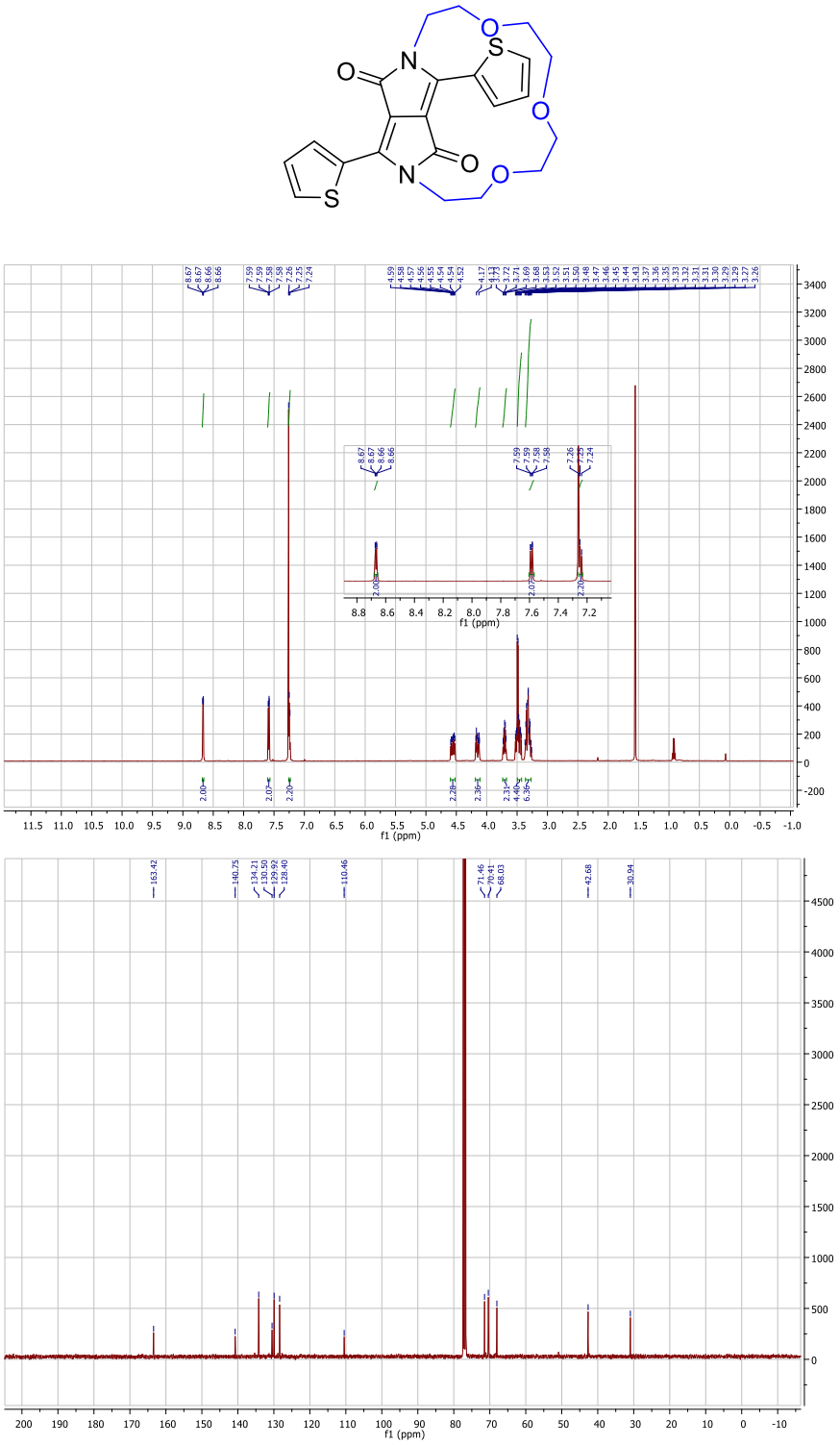

EC12DPPT (10a)

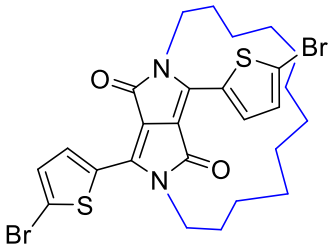

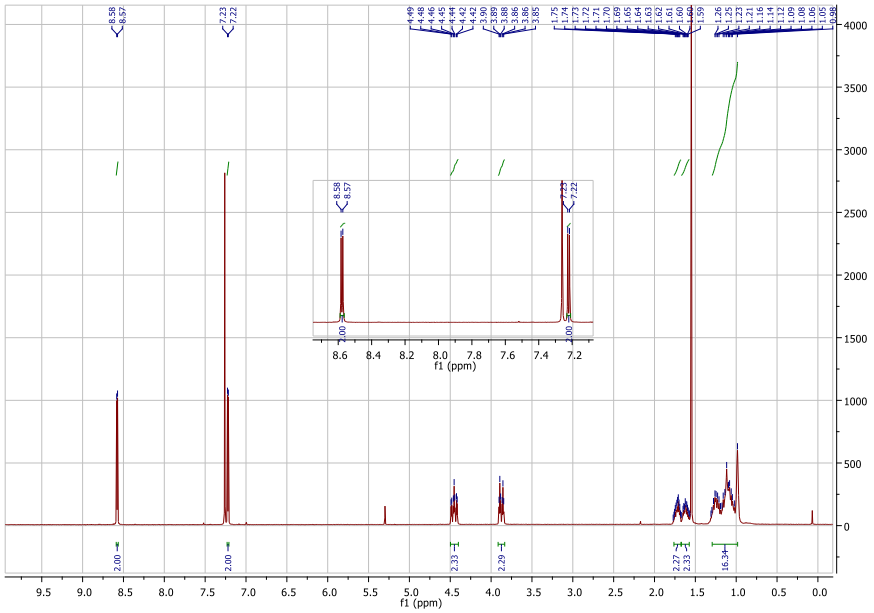

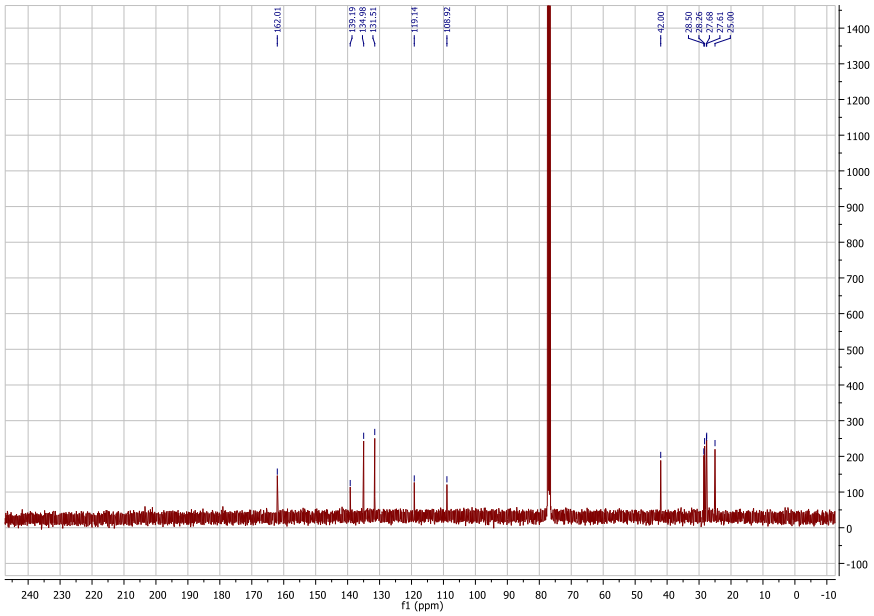

EC11DPPT (10b)

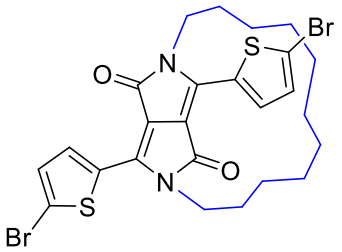

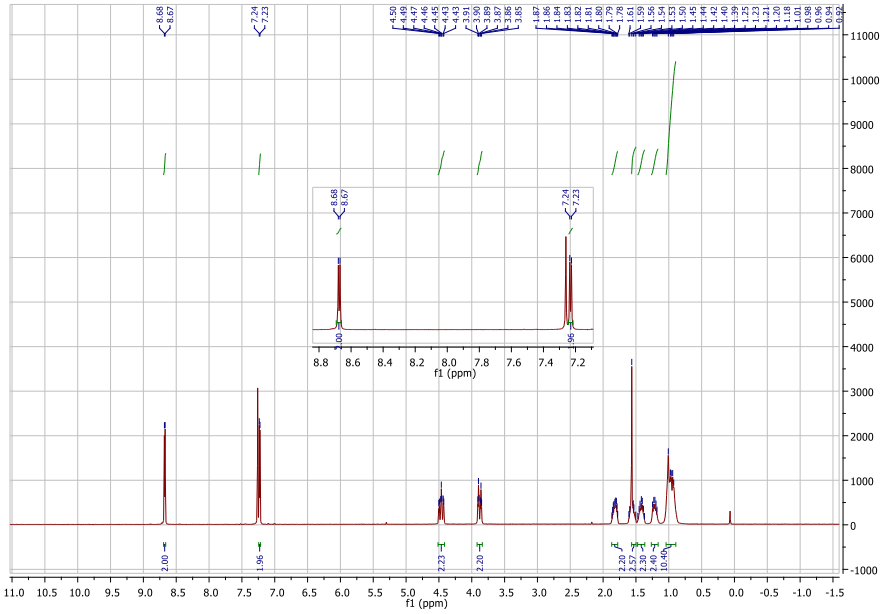

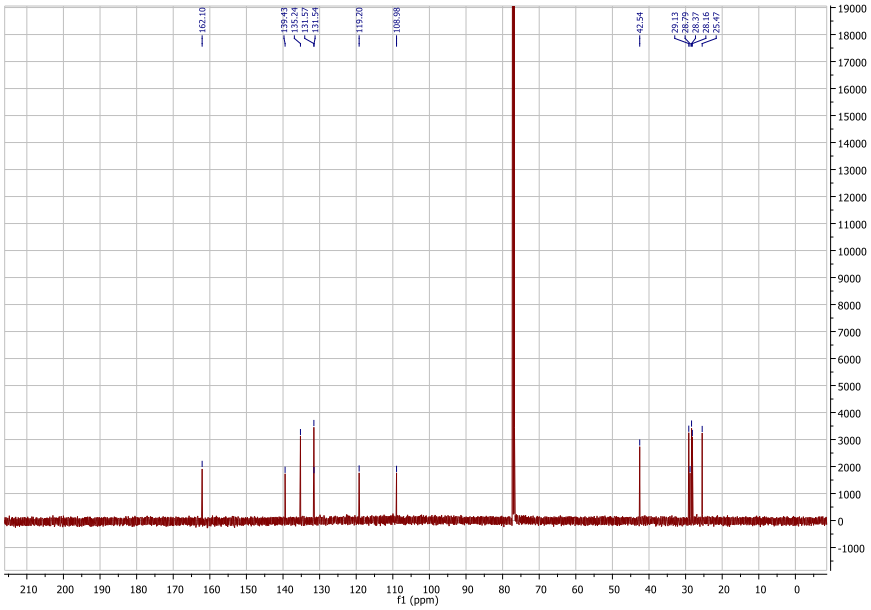

EP11DPPT (10c)

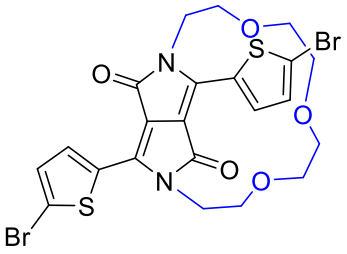

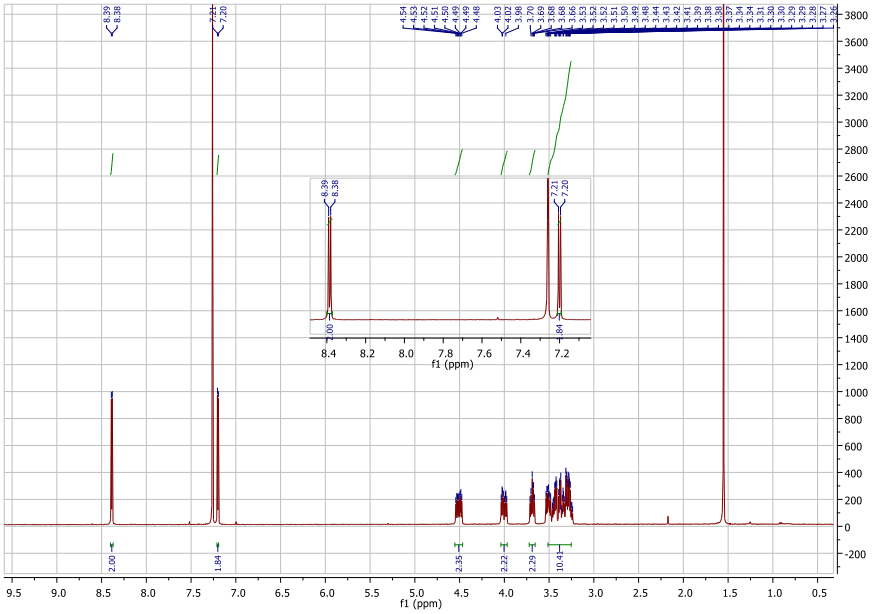

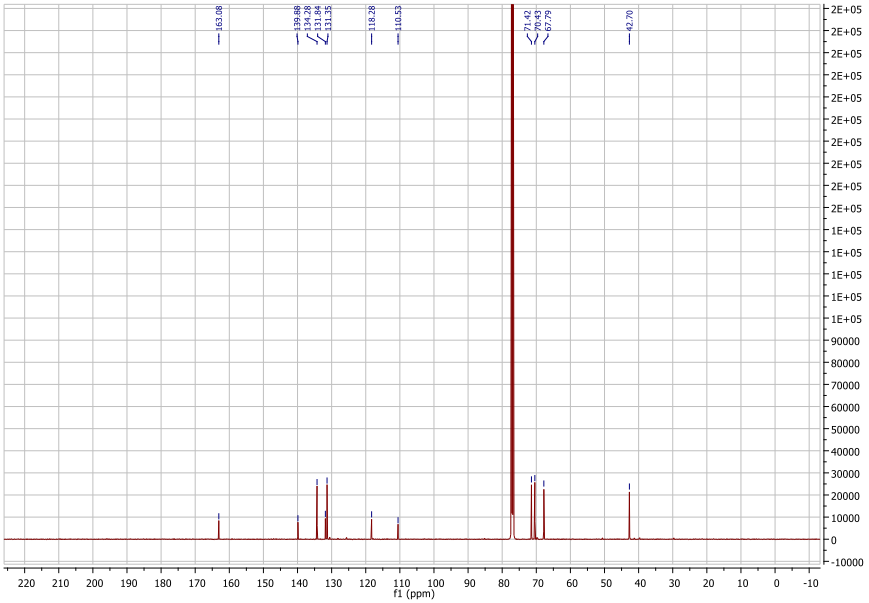

(13)

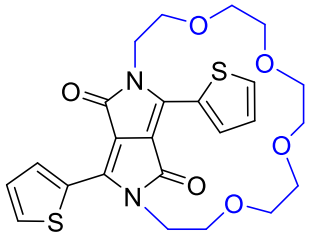

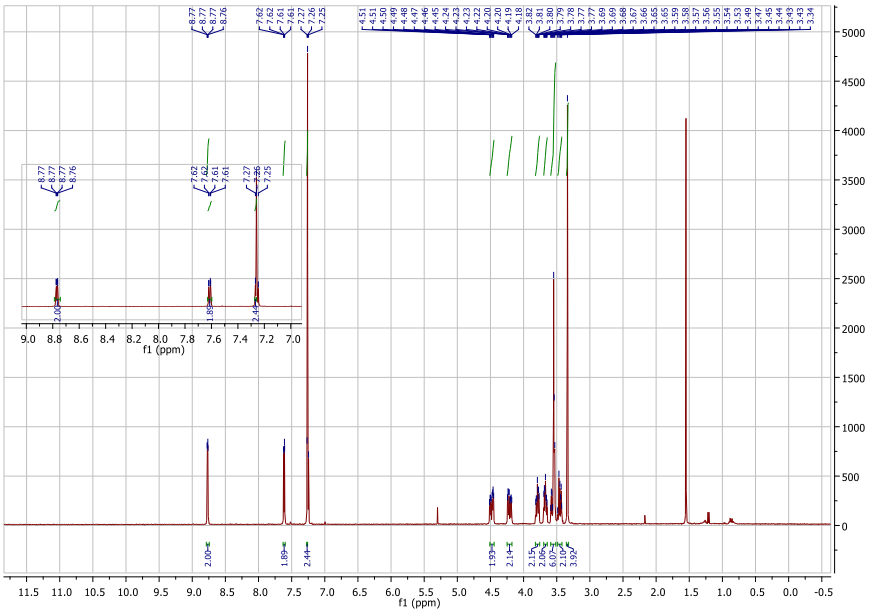

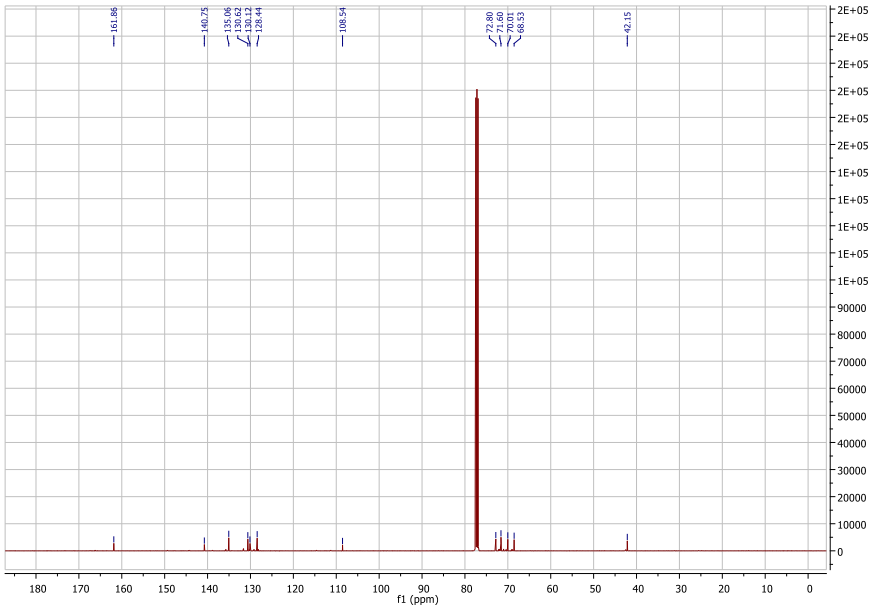

EP14DPPT (14)

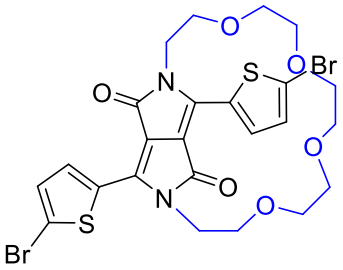
O
N
O
S
O
Br
O
O
N
O
S
Br
O

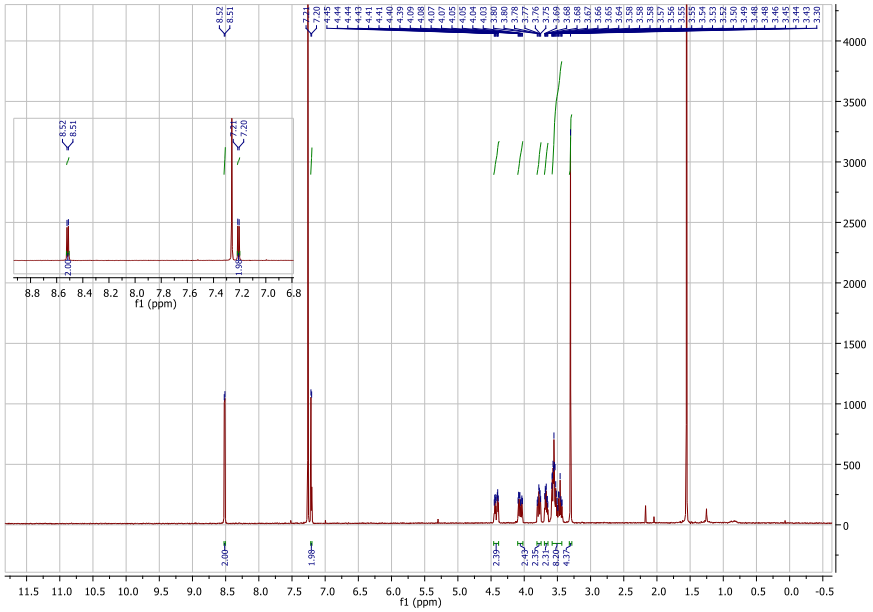
8.52
8.51
7.21
7.20
f1 (ppm)

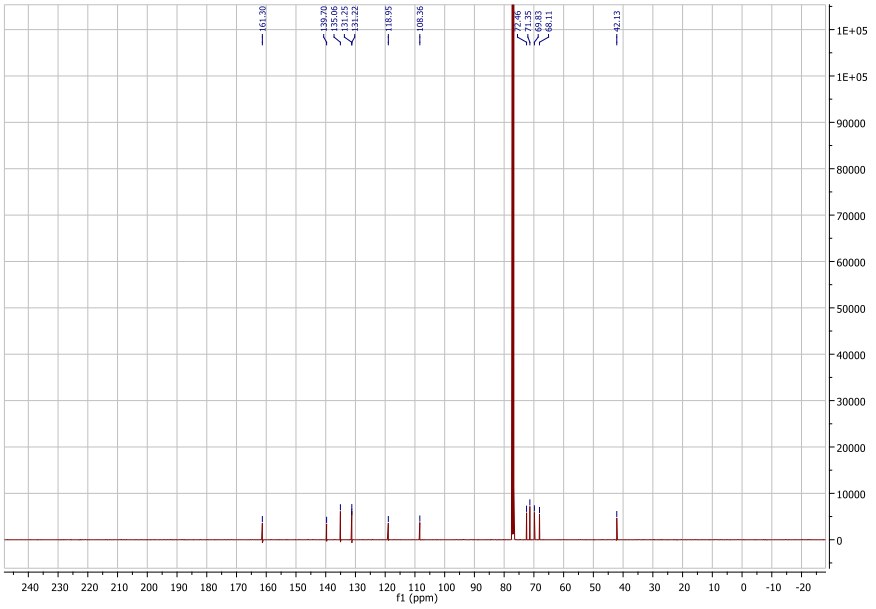
161.30
139.20
135.06
133.35
131.22
118.95
108.36
77.46
77.35
77.25
69.83
68.11
42.13
f1 (ppm)

3,6-di(thiophen-2-yl)-2,5-di(2,5,8,11-tetraoxatridecan-13-yl)-2,5-dihydropyrrolo[3,4-c]pyrrole-1,4-dione (16)

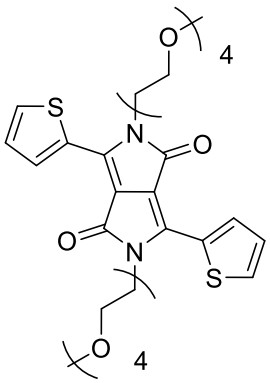

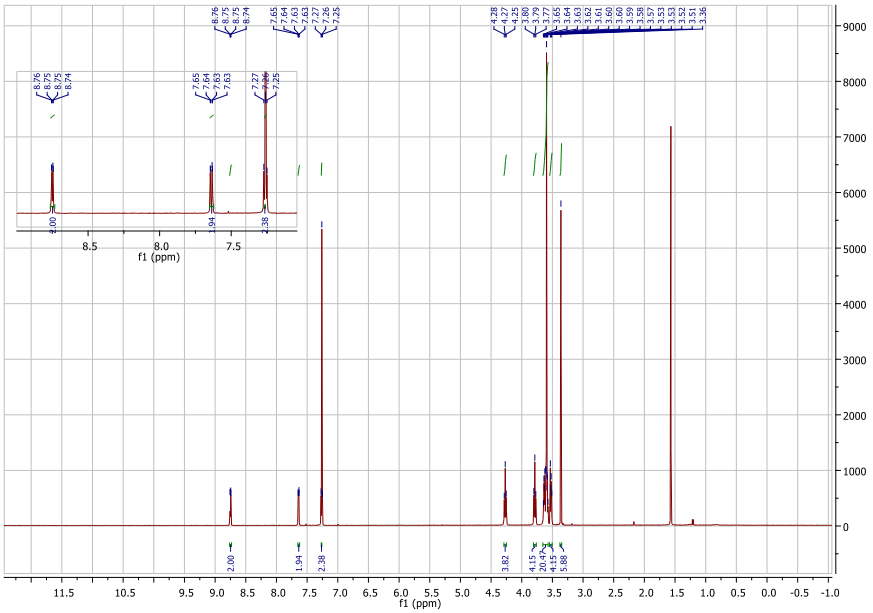

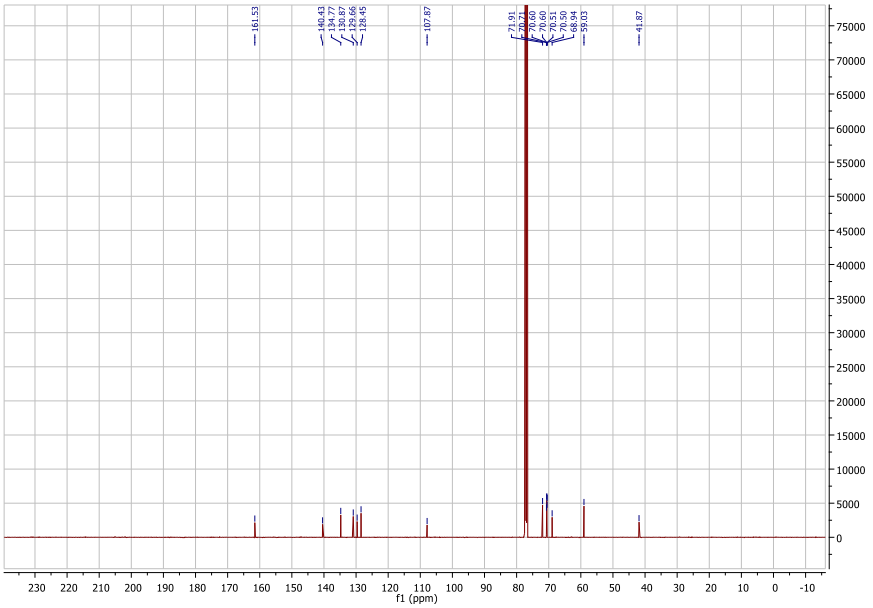

3,6-bis(5-bromothiophen-2-yl)-2,5-bis(2-methoxyethyl)-2,5-dihydropyrrolo[3,4-c]pyrrole-1,4-dione (15)

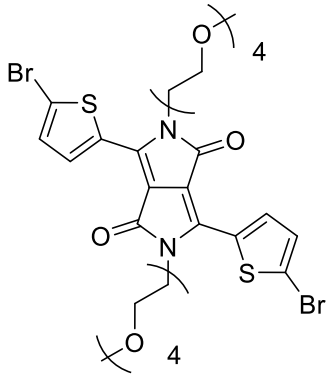

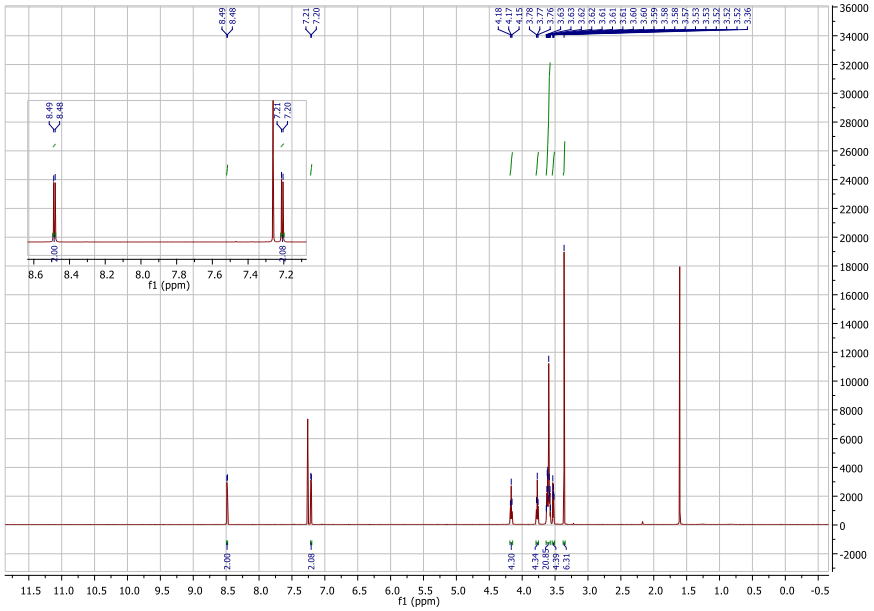

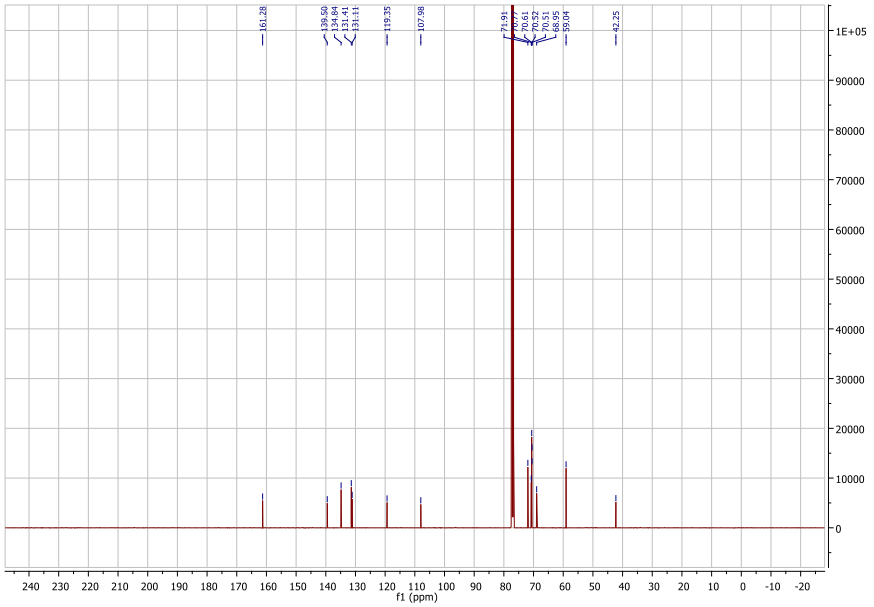

13-(thiophen-3-yloxy)-2,5,8,11-tetraoxatridecane (18)

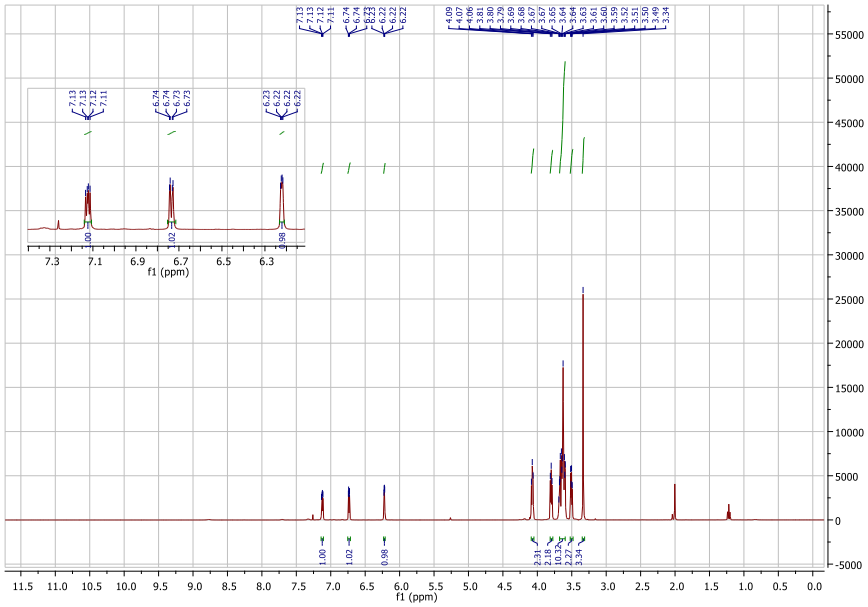

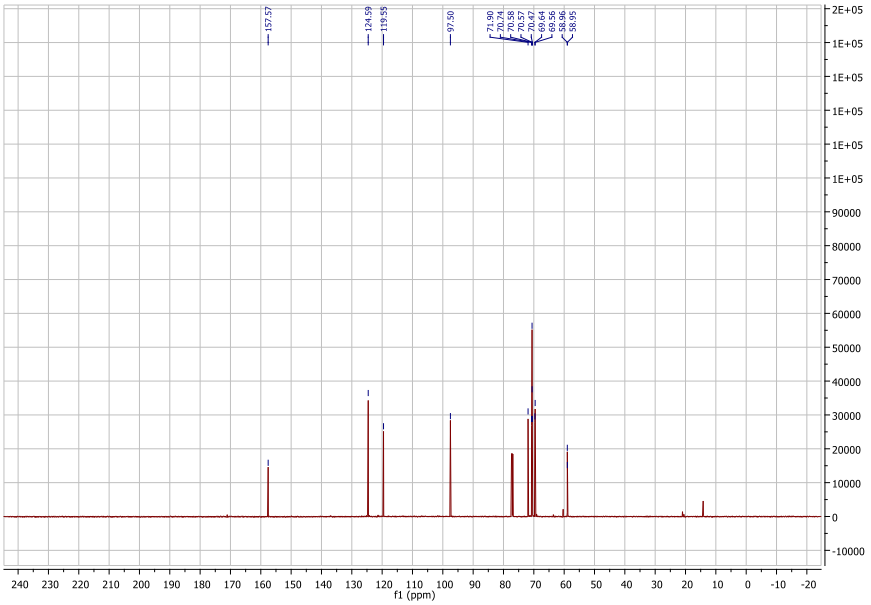

3,3'-bis((2,5,8,11-tetraoxatridecan-13-yl)oxy)-2,2'-bithiophene (19)

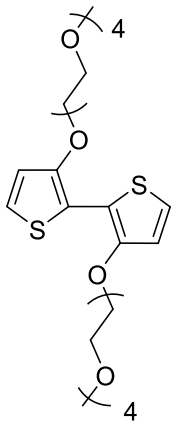

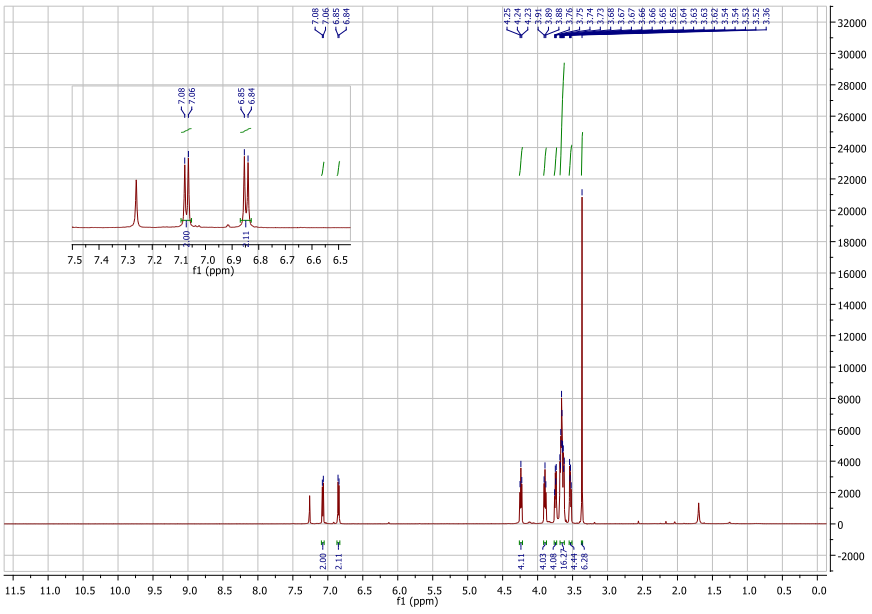

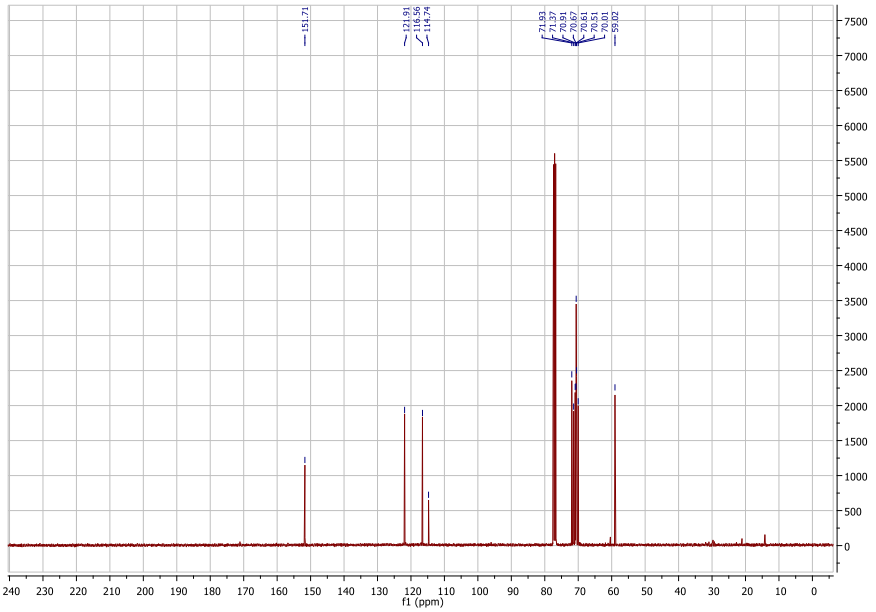

(Crude) (3,3'-bis((2,5,8,11-tetraoxatridecan-13-yl)oxy)-[2,2'-bithiophene]-5,5'-diyl)bis(trimethylstannane) (20)

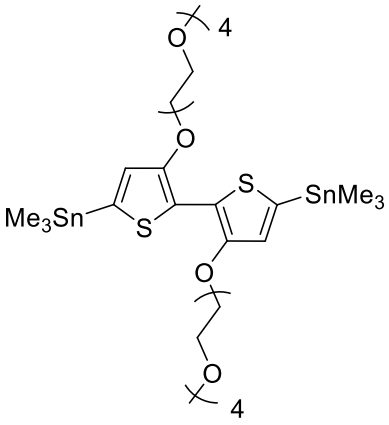

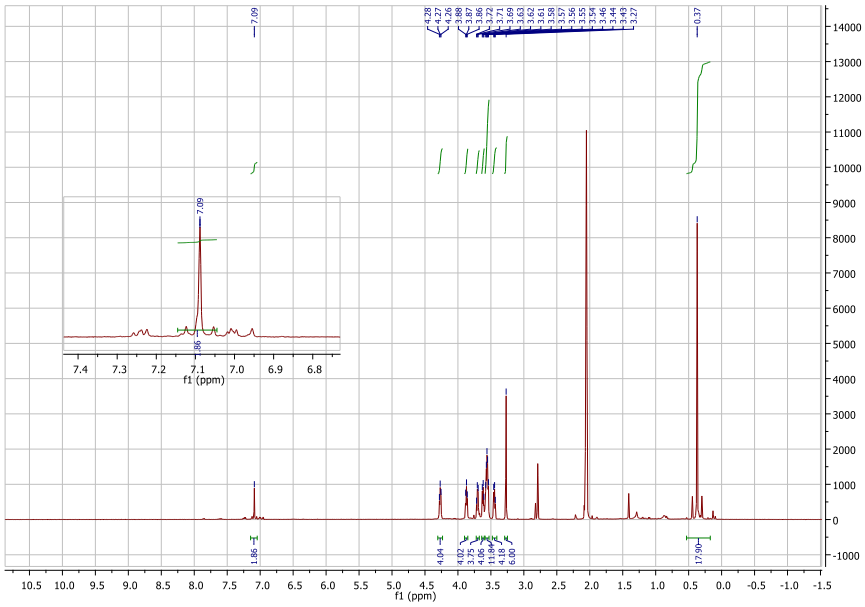

8.2.2 Single Crystal X-Ray Diffraction Studies[†]

Single X-ray diffraction data was collected using either a Bruker D8-QUEST PHOTON100 diffractometer (Cu radiation) or a Nonius KappaCCD diffractometer (Mo radiation). Mercury software was used to visualise and analyse the data obtained. Hydrogen atoms were omitted for simplicity.

[†]All X-ray structures determined by Dr Andrew Bond, University of Cambridge.

(2)

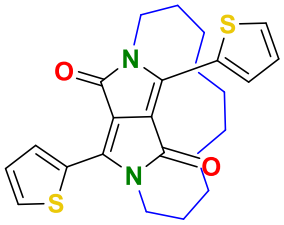

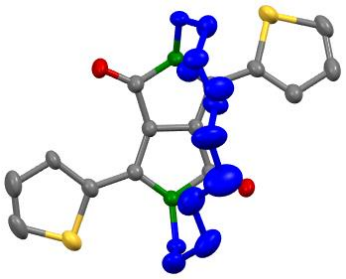

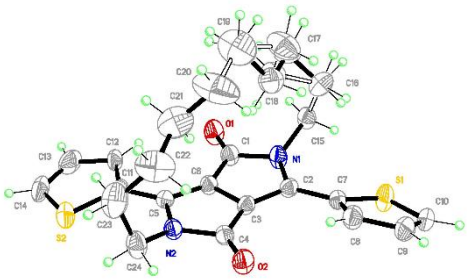

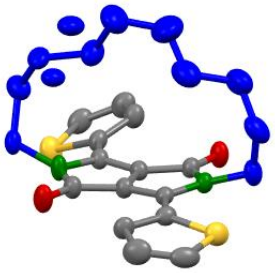

EC10DPPT (3)

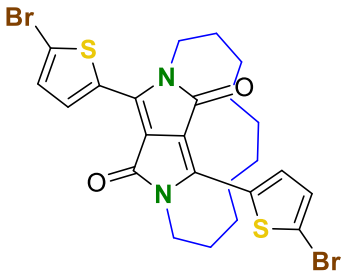

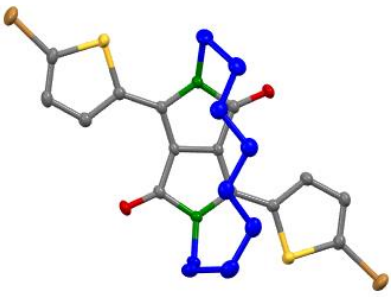

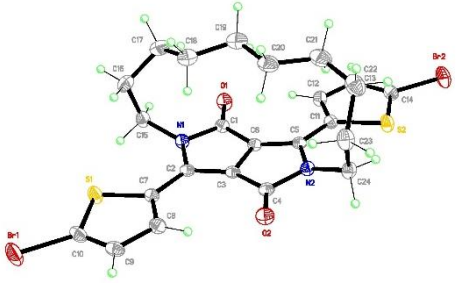

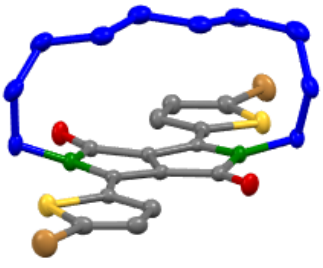

*Table S1- Crystallographic parameters for crystal structures **2** and **3**.*

Compound	**2**	**3**
Chemical formula	$C_{24}H_{26}N_2O_2S_2$	$C_{24}H_{24}Br_2N_2O_2S_2$
Formula weight	438.59	596.39
Temperature / *K*	180(2)	180(2)
Crystal system	monoclinic	triclinic
Space group	C 2/*c*	P -1
a / Å	28.3920(9)	10.0631(3)
b / Å	8.9830(3)	10.1990(4)
c / Å	19.2814(6)	11.4730(4)
alpha / degrees	90	95.6730(10)
beta / degrees	117.135(2)	98.5890(10)
gamma / degrees	90	92.6600(10)
Unit-cell volume / $Å^3$	4376.4(3)	1156.37(7)
Z	8	2
Calc. density / gcm^{-3}	1.331	1.713
F(000)	1856	600
Radiation type	CuK*a*	CuK*a*
Absorption coefficient / mm^{-1}	2.389	6.342
Crystal size / mm^3	0.220 x 0.150 x 0.060	0.150 x 0.080 x 0.040
2-Theta range / degrees	7.00-133.66	7.84-133.87
Completeness to max 2-theta	0.998	0.993
No. of reflections measured	19770	13431
No. of independent reflections	3887	4095
R_{int}	0.0429	0.0266
No. parameters / restraints	290 / 36	290 / 0
Final R_1 values ($I > 2s(I)$)	0.0547	0.0231
Final $wR(F^2)$ values (all data)	0.0694	0.0273
Goodness-of-fit on F^2	1.063	1.050
Largest difference peak & hole / $eÅ^{-3}$	0.761, -0.376	0.336, -0.295

(8a)

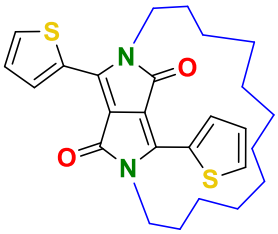

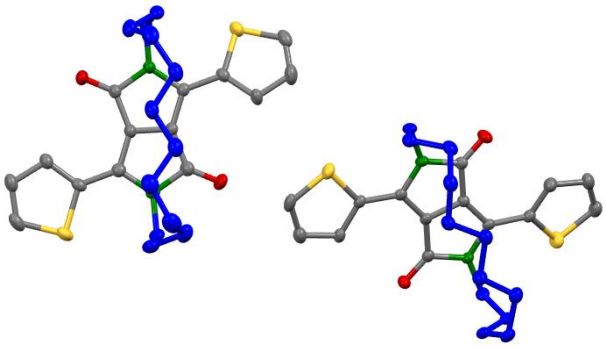

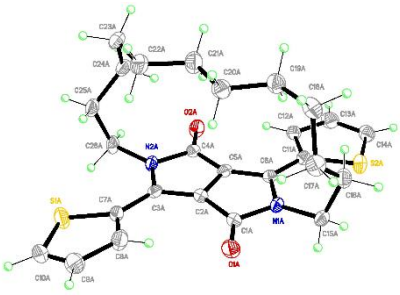

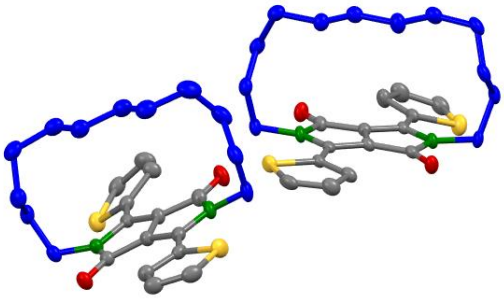

EC12DPPT (10a)

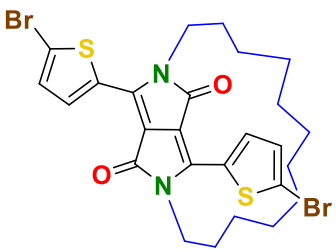

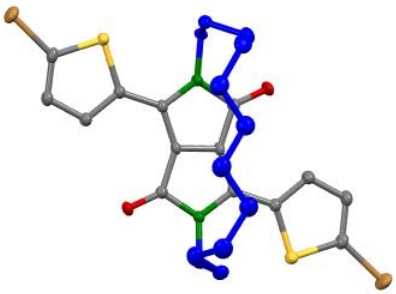

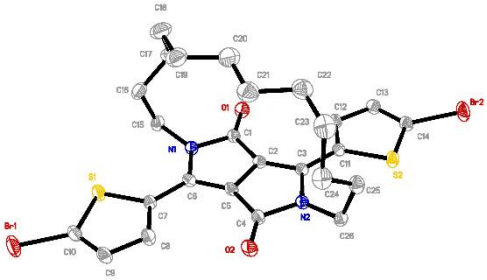

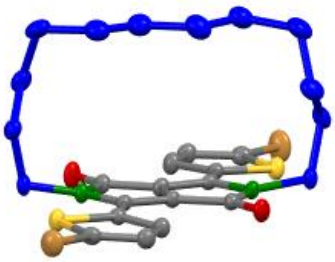

*Table S2- Crystallographic parameters for crystal structures **8a** and **10a**.*

Compound	**8a**	**10a**
Chemical formula	$C_{26}H_{30}N_2O_2S_2$	$C_{26}H_{28}Br_2N_2O_2S_2$
Formula weight	466.64	624.44
Temperature / *K*	180(2)	180(2)
Crystal system	triclinic	triclinic
Space group	P -1	P -1
a / Å	11.1422(4)	10.2157(6)
b / Å	11.5766(4)	11.1106(8)
c / Å	18.9226(7)	11.5586(8)
alpha / degrees	104.267(2)	79.926(3)
beta / degrees	90.925(2)	78.850(3)
gamma / degrees	97.996(2)	88.105(3)
Unit-cell volume / $Å^3$	2339.29(15)	1267.32(15)
Z	4	2
Calc. density / gcm^{-3}	1.325	1.636
F(000)	992	632
Radiation type	CuK*a*	CuK*a*
Absorption coefficient / mm^{-1}	2.266	5.815
Crystal size / mm^3	0.220 x 0.120 x 0.070	0.200 x 0.120 x 0.020
2-Theta range / degrees	4.83-134.09	7.91-133.69
Completeness to max 2-theta	0.983	0.984
No. of reflections measured	28465	12624
No. of independent reflections	8218	4437
R_{int}	0.0629	0.0273
No. parameters / restraints	577 / 0	307 / 0
Final R_1 values ($I > 2s(I)$)	0.0474	0.0264
Final $wR(F^2)$ values (all data)	0.0756	0.0328
Goodness-of-fit on F^2	1.014	1.038
Largest difference peak & hole / $eÅ^{-3}$	0.323, -0.303	0.271, -0.441

(8b)

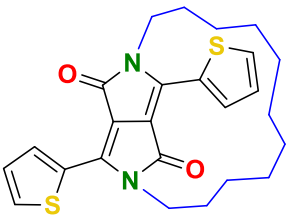

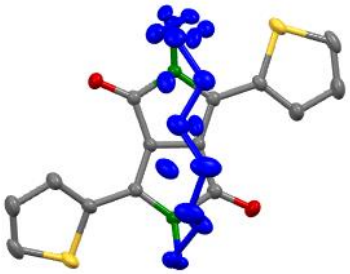

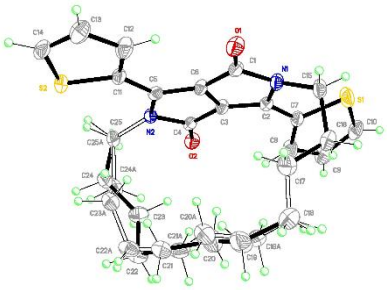

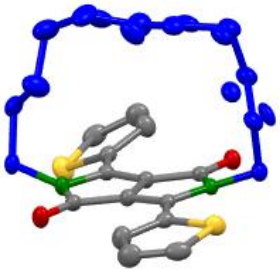

EC11DPPT (10b)

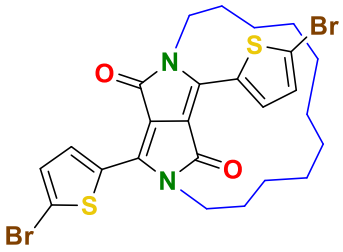

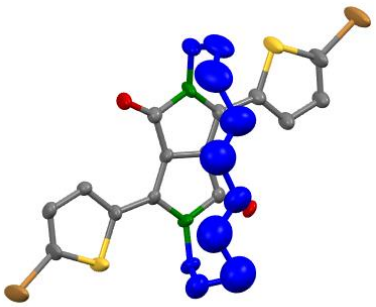

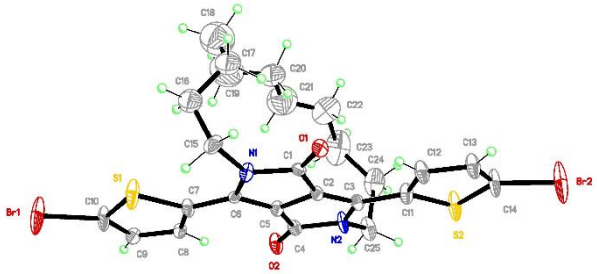

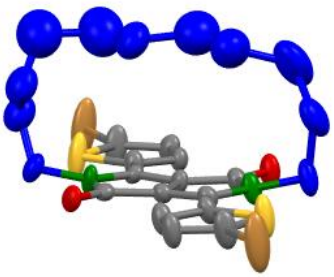

*Table S3- Crystallographic parameters for crystal structures **8b** and **10b**.*

Compound	**8b**	**10b**
Chemical formula	$C_{25}H_{28}N_2O_2S_2$	$C_{25}H_{26}Br_2N_2O_2S_2$
Formula weight	452.61	610.42
Temperature / *K*	180(2)	180(2)
Crystal system	monoclinic	triclinic
Space group	I 2/*a*	P -1
a / Å	18.9570(6)	10.2189(5)
b / Å	9.4634(3)	10.5300(8)
c / Å	25.4074(11)	11.6970(6)
alpha / degrees	90	78.821(4)
beta / degrees	98.2530(10)	79.243(3)
gamma / degrees	90	89.159(4)
Unit-cell volume / $Å^3$	4510.8(3)	1212.77(13)
Z	8	2
Calc. density / gcm^{-3}	1.333	1.672
F(000)	1920	616
Radiation type	CuK*a*	CuK*a*
Absorption coefficient / mm^{-1}	2.334	6.062
Crystal size / mm^3	0.180 x 0.180 x 0.180	0.200 x 0.040 x 0.010
2-Theta range / degrees	7.03-134.08	7.84-133.74
Completeness to max 2-theta	0.993	0.994
No. of reflections measured	20342	15845
No. of independent reflections	4010	4288
R_{int}	0.0327	0.0828
No. parameters / restraints	335 / 26	298 / 66
Final R_1 values ($I > 2s(I)$)	0.0346	0.1007
Final $wR(F^2)$ values (all data)	0.0398	0.1559
Goodness-of-fit on F^2	1.039	1.068
Largest difference peak & hole / $eÅ^{-3}$	0.189, -0.350	1.213, -1.763

(8c)

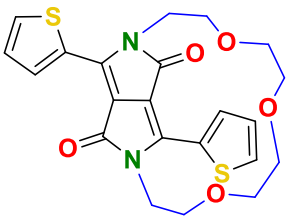

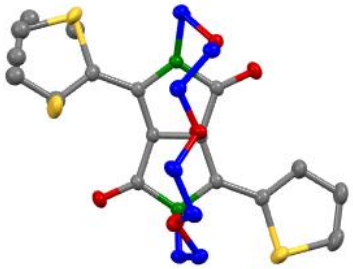

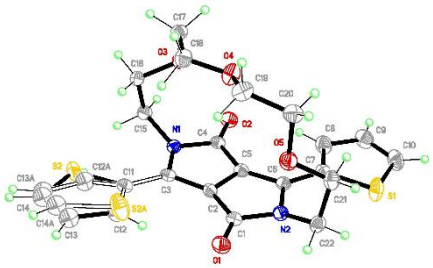

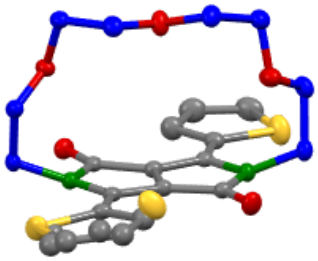

EP11DPPT (10c)

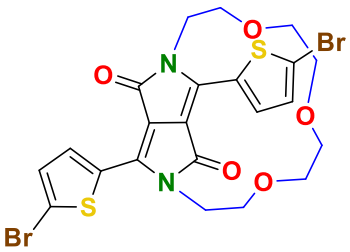

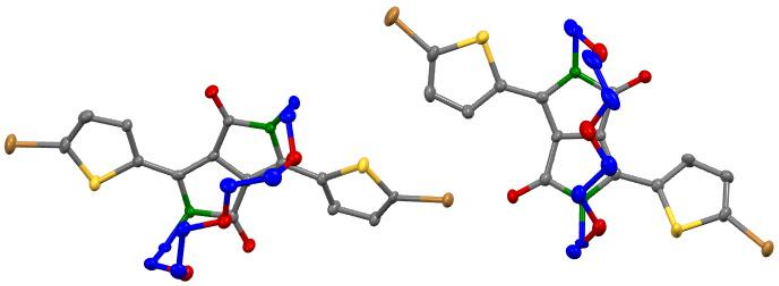

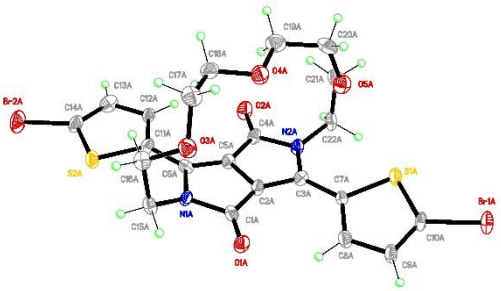

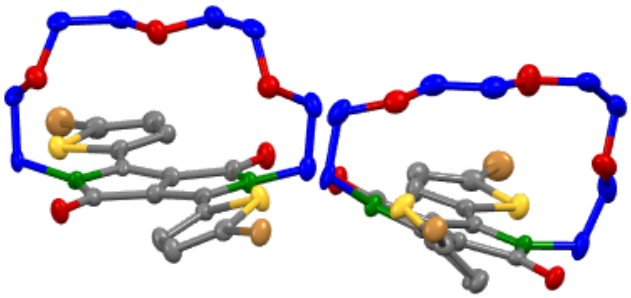

*Table S4- Crystallographic parameters for crystal structures **8c** and **10c**.*

Compound	**8c**	**10c**
Chemical formula	$C_{22}H_{22}N_2O_5S_2.CH_4O$	$C_{22}H_{20}Br_2N2O_5S_2$
Formula weight	490.58	616.34
Temperature / *K*	180(2)	180(2)
Crystal system	monoclinic	triclinic
Space group	P 21/*c*	P -1
a / Å	15.4072(5)	9.6003(4)
b / Å	17.3396(6)	11.4878(5)
c / Å	8.7356(3)	21.6545(7)
alpha / degrees	90	87.614(2)
beta / degrees	101.958(2)	87.863(2)
gamma / degrees	90	74.054(3)
Unit-cell volume / $Å^3$	2283.11(13)	2293.48(16)
Z	4	4
Calc. density / gcm^{-3}	1.427	1.785
F(000)	1032	1232
Radiation type	CuK*a*	CuK*a*
Absorption coefficient / mm^{-1}	2.487	6.522
Crystal size / mm^3	0.200 x 0.160 x 0.120	0.160 x 0.160 x 0.040
2-Theta range / degrees	5.86-133.78	8.01-133.94
Completeness to max 2-theta	0.999	0.990
No. of reflections measured	25068	24795
No. of independent reflections	4062	8116
R_{int}	0.0526	0.1056
No. parameters / restraints	305 / 0	595 / 0
Final R_1 values ($I > 2s(I)$)	0.0362	0.0506
Final $wR(F^2)$ values (all data)	0.0469	0.0873
Goodness-of-fit on F^2	1.065	1.022
Largest difference peak & hole / $eÅ^{-3}$	0.249, -0.376	1.435, -0.650

(13)

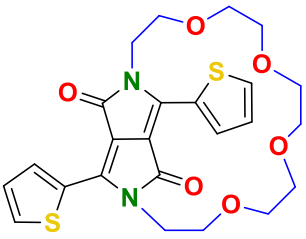

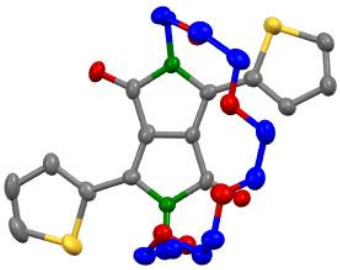

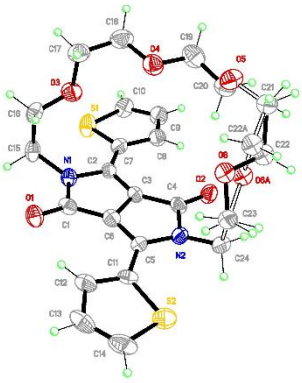

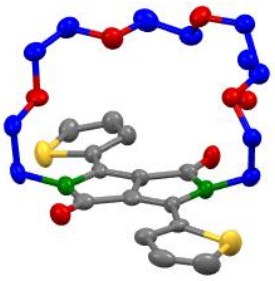

EP14DPPT (14)

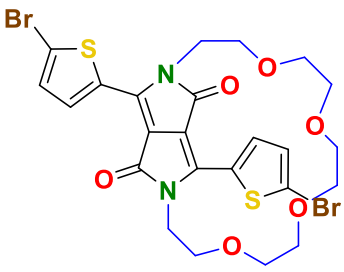

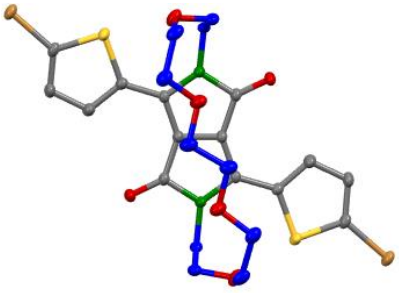

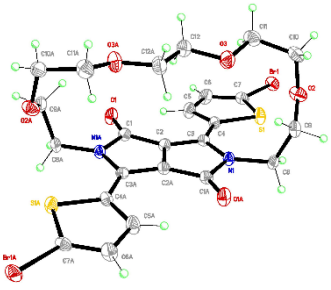

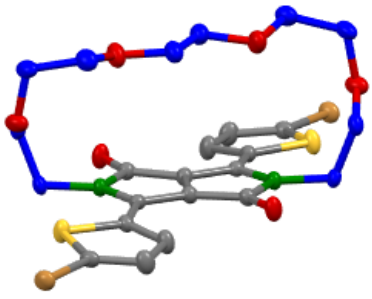

*Table S5- Crystallographic parameters for crystal structures **13** and **14**.*

Compound	**13**	**14**
Chemical formula	$C_{24}H_{26}N_2O_6S_2$	$C_{24}H_{24}Br_2N_2O_6S_2$
Formula weight	502.59	660.39
Temperature / *K*	180(2)	180(2)
Crystal system	monoclinic	monoclinic
Space group	P 21/*c*	C 2/*c*
a / Å	17.0689(11)	23.9709(8)
b / Å	9.5916(7)	10.4802(4)
c / Å	14.3768(9)	10.1917(3)
alpha / degrees	90	90
beta / degrees	98.185(4)	105.0330(10)
gamma / degrees	90	90
Unit-cell volume / $Å^3$	2329.8(3)	2472.73(15)
Z	4	4
Calc. density / gcm^{-3}	1.433	1.774
F(000)	1056	1328
Radiation type	CuK*a*	CuK*a*
Absorption coefficient / mm^{-1}	2.453	6.128
Crystal size / mm^3	0.100 x 0.100 x 0.020	0.150 x 0.070 x 0.030
2-Theta range / degrees	5.23-108.64	7.64-133.69
Completeness to max 2-theta	1.000	0.997
No. of reflections measured	26114	14742
No. of independent reflections	2844	2194
R_{int}	0.2597	0.0377
No. parameters / restraints	306 / 4	163 / 0
Final R_1 values ($I > 2s(I)$)	0.0592	0.0218
Final $wR(F^2)$ values (all data)	0.1105	0.0269
Goodness-of-fit on F^2	1.027	1.075
Largest difference peak & hole / $eÅ^{-3}$	0.222, -0.232	0.240, -0.323

8.3 Chapter IV

8.3.1 Additional Experimental

Ethyl 1-dodecyl-4-hydroxy-5-oxo-2-(thiophen-2-yl)pyrrolidine-3-carboxylate (22a)

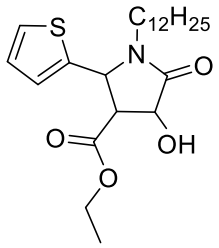

To an oven dried flask under argon was added enol **21a**, (15 g, 35.6 mmol), zinc powder (13.80 g, 212 mmol) and a few drops of H_2SO_4 into acetic acid (500 mL). The reaction was heated to 100 °C and allowed to stir for 2 h. This was then followed by the addition of a second portion of zinc (13.80 g, 212 mmol) and the reaction was stirred for a further 1 h. The reaction mixture was then cooled to RT and the excess zinc/inorganic salts were removed *via* filtration. The filtrate was diluted with 300 mL of water and the organic layer was extracted with dichloromethane. The combined organic layers were then washed with saturated $NaHCO_3$ solution until neutral and dried over $MgSO_4$. The solution was then concentrated *in vacuo* to give a crude oil. Hexane was added to the oil and the white precipitate that formed was collected *via* filtration and washed with hexane to afford the product as a crude white solid (9.02 g, 21.3 mmol, 66%), which was used directly in the next reaction without further purification.

HRMS (TOF MS ASAP+): Calculated for $C_{23}H_{38}NO_4S^+$: 424.2522. Found *m*/z 424.2511 $[M+H]^+$.

Ethyl 1-(2-ethylhexyl)-4-hydroxy-5-oxo-2-(thiophen-2-yl)pyrrolidine-3-carboxylate (22b)

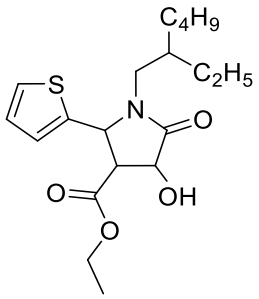

Compound **22b** was made using the same procedure as making **22a** with the following reagents: enol **21b** (16.65 g, 47.0 mmol), zinc powder (18.32 g, 280 mmol) and a few drops of H_2SO_4 in acetic acid (500 mL). The combined organic layers were then washed with saturated $NaHCO_3$ solution until neutral and dried over $MgSO_4$. The solution was then concentrated *in vacuo* to afford the product as a crude red oil (12.98 g, 35.0 mmol, 78%), which was used directly in the next reaction without further purification.

HRMS (TOF MS ASAP+): Calculated for $C_{19}H_{30}NO_4S^+$: 368.1896. Found *m/z* 368.1907 $[M+H]^+$.

Ethyl 1-butyl-4-hydroxy-5-oxo-2-(thiophen-2-yl)pyrrolidine-3-carboxylate (22c)

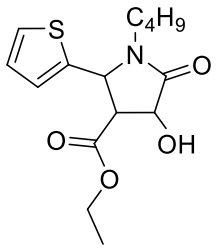

Compound **22c** was made using the same procedure as making **22a** with the following reagents: enol **21c** (20.00 g, 65.0 mmol), zinc powder (24.90 g, 381 mmol) and a few drops of H_2SO_4 in acetic acid (500 mL). The combined organic layers were then washed with saturated $NaHCO_3$ solution until neutral and dried over $MgSO_4$. The solution was then concentrated *in vacuo* to afford the product as a crude green oil (13.72 g, 44.0 mmol, 67%), which was used directly in the next reaction without further purification.

HRMS (TOF MS ASAP+): Calculated for $C_{15}H_{21}NO_4S^+$: 312.1270. Found *m/z* 312.1258 $[M+H]^+$.

8.3.2 ^{1}H NMR and ^{13}C NMR

Ethyl 3-oxo-3-(thiophen-2-yl)propanoate (2)

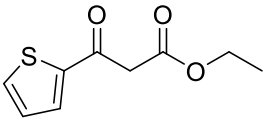

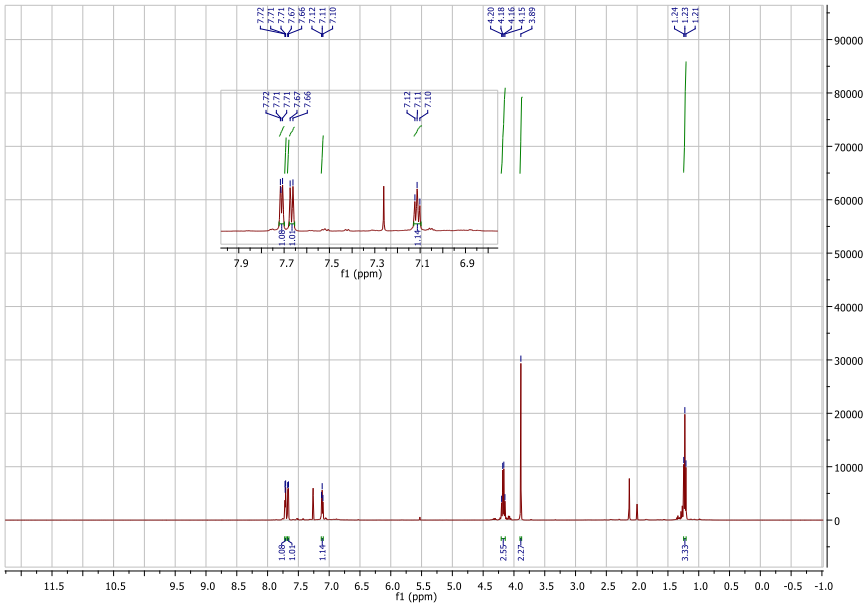

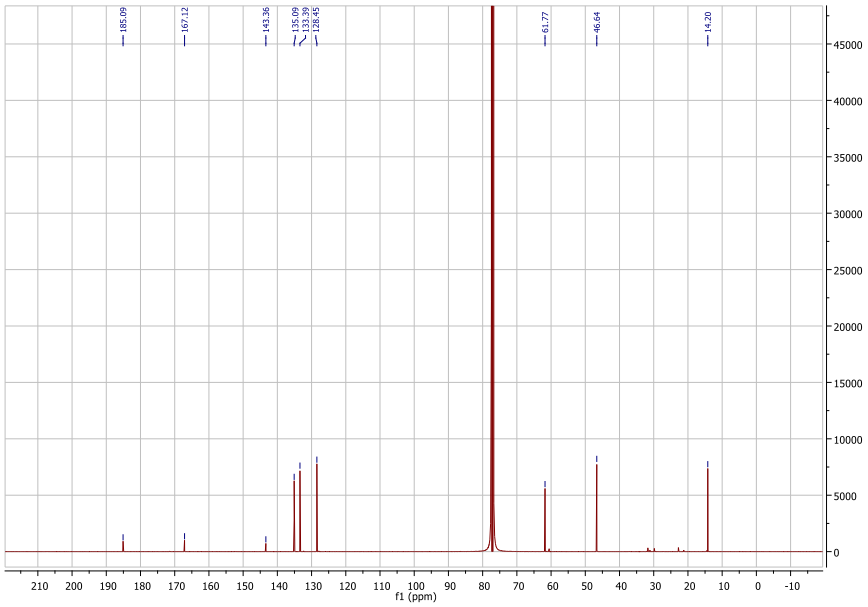

Diethyl 2-(thiophene-2-carbonyl)succinate (3)

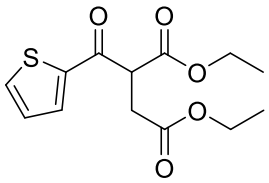

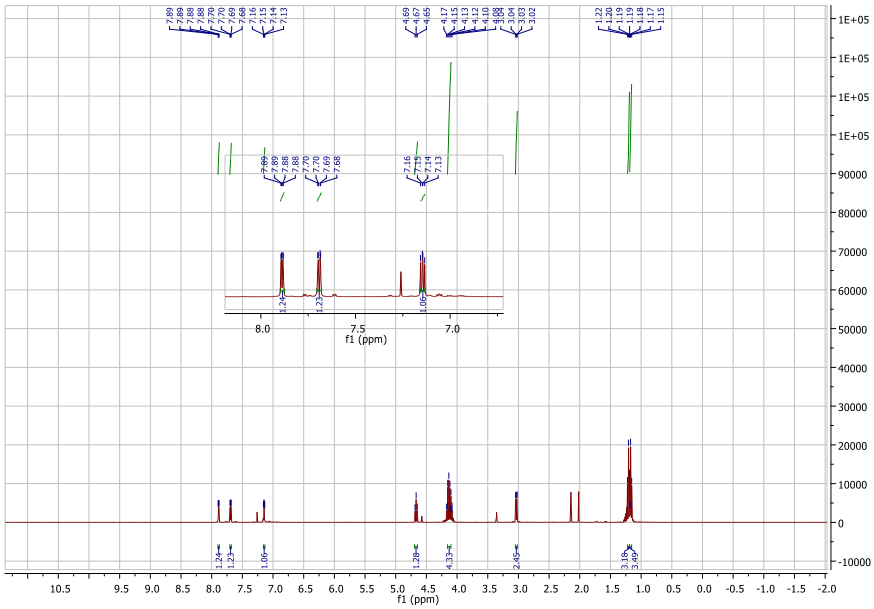

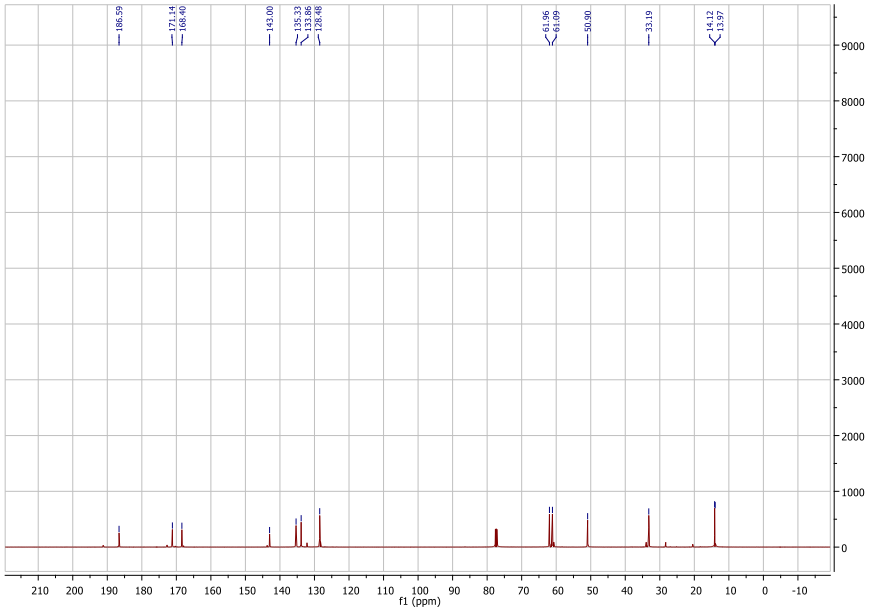

Ethyl 5-oxo-2-(thiophen-2-yl)-4,5-dihydro-1H-pyrrole-3-carboxylate (4)

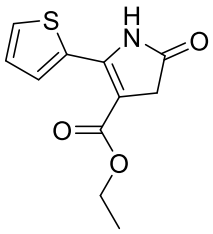

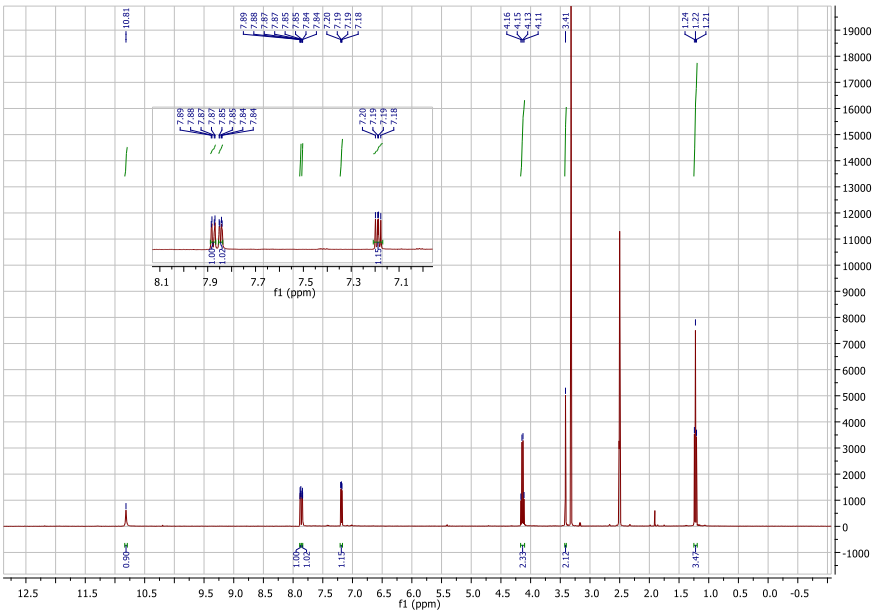

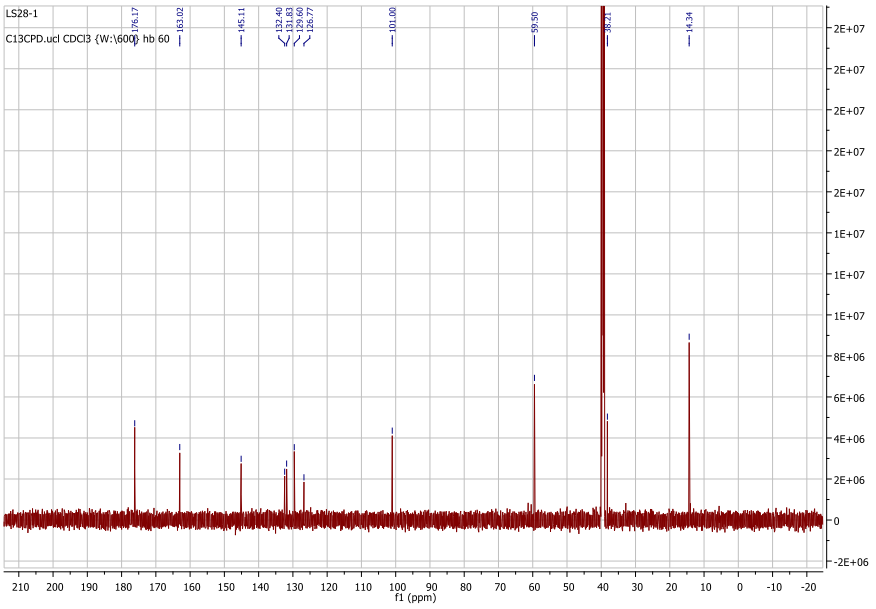

Thiophene-2,5-dicarbaldehyde (6)

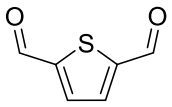

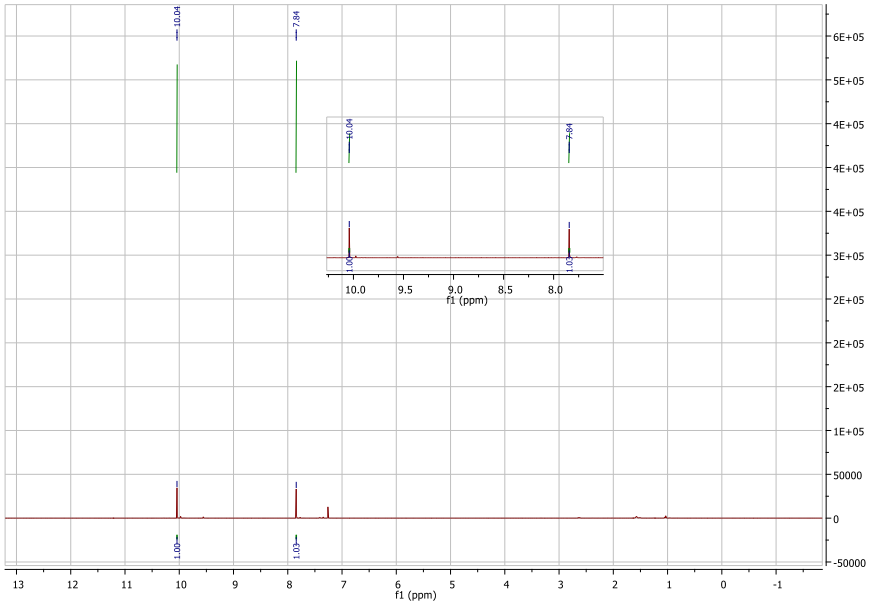

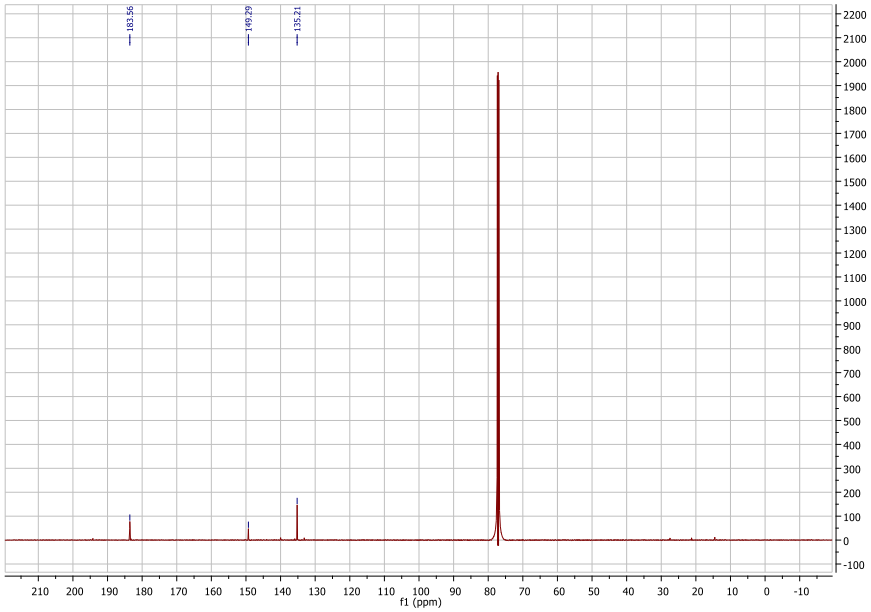

Thiophene-2,5-dicarbonitrile (7)

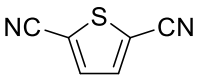

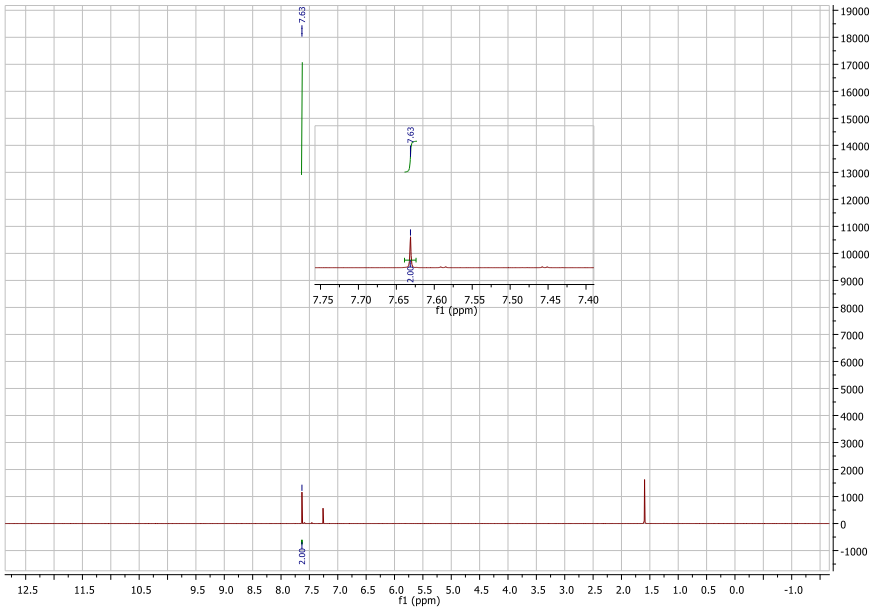

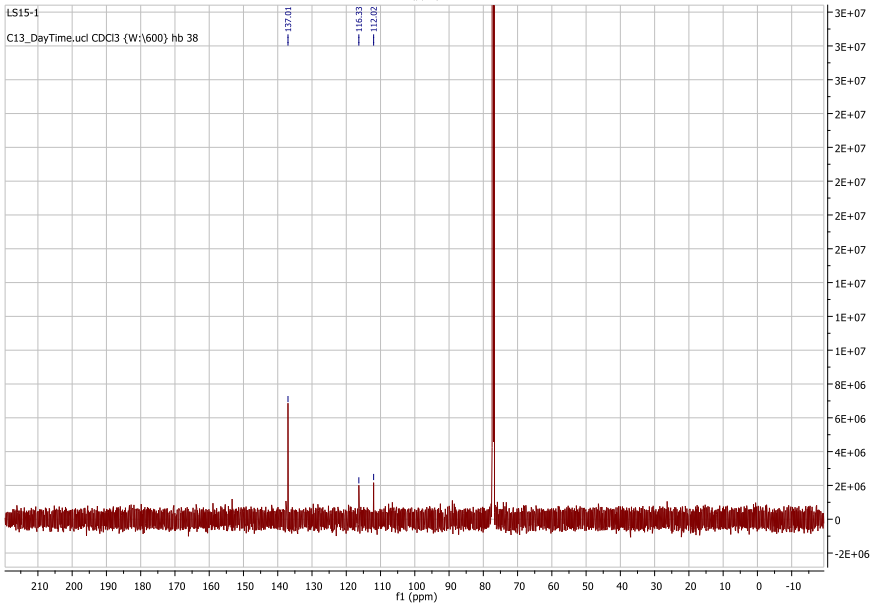

1,1'-(thiophene-2,5-diyl)bis(ethan-1-one) (15)

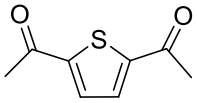

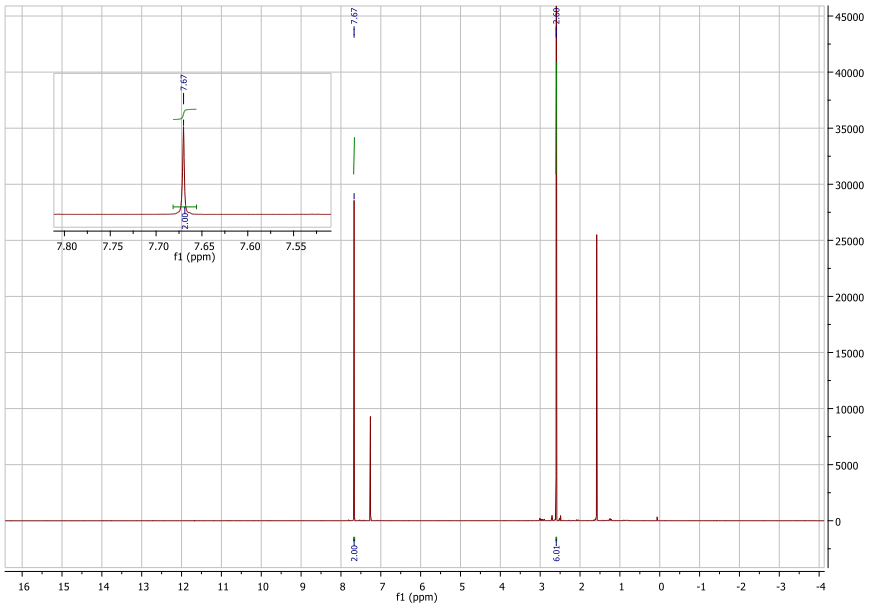

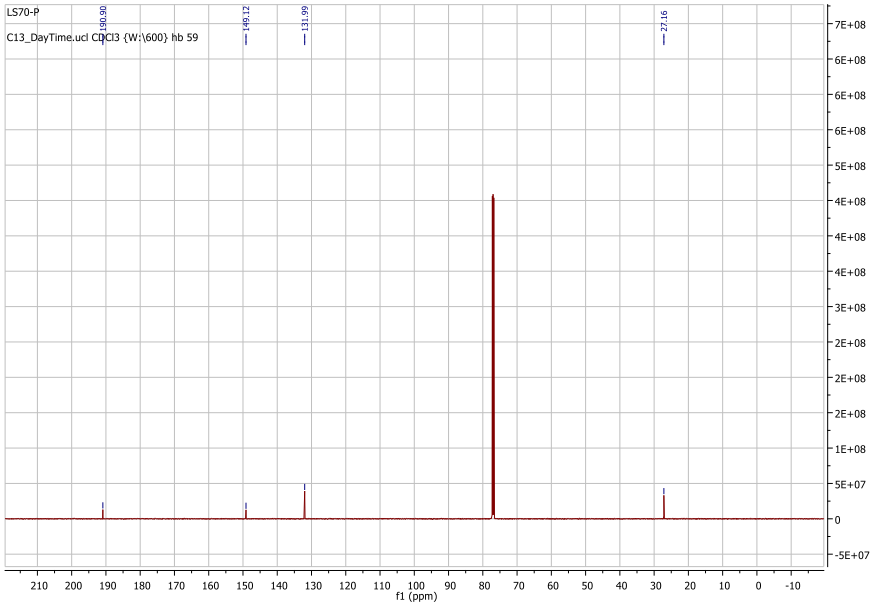

Diethyl 3,3'-(thiophene-2,5-diyl)bis(3-oxopropanoate) (16)

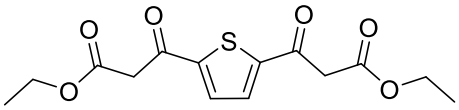

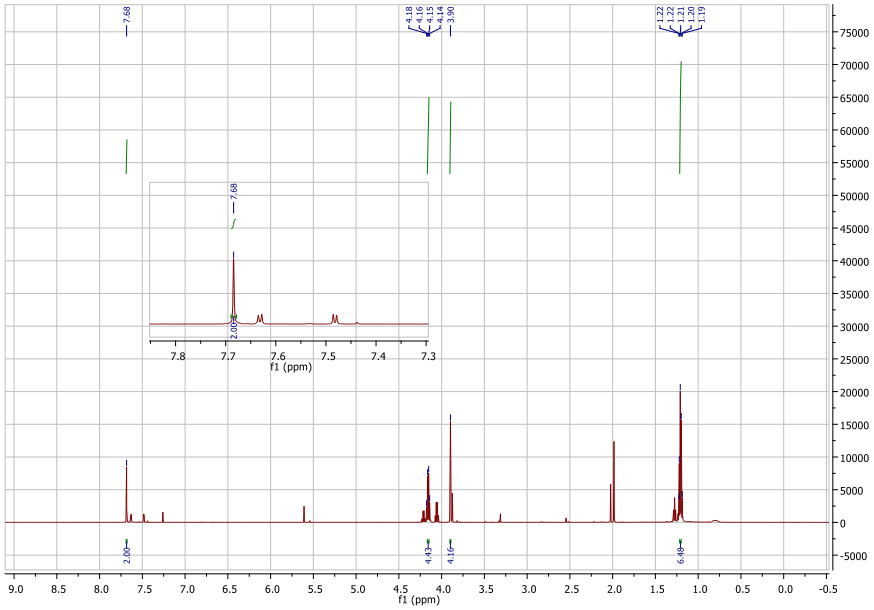

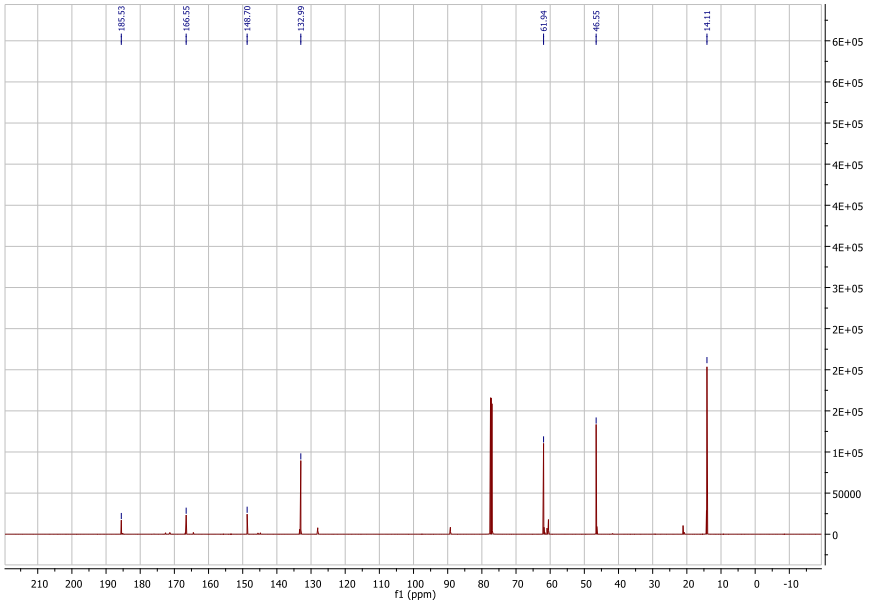

Tetraethyl 5,5'-(thiophene-2,5-dicarbonyl)bis(3-oxohexanedioate) (17)

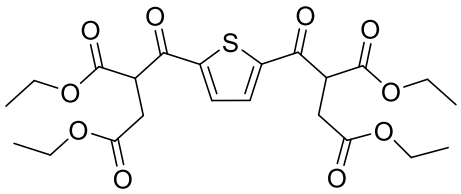

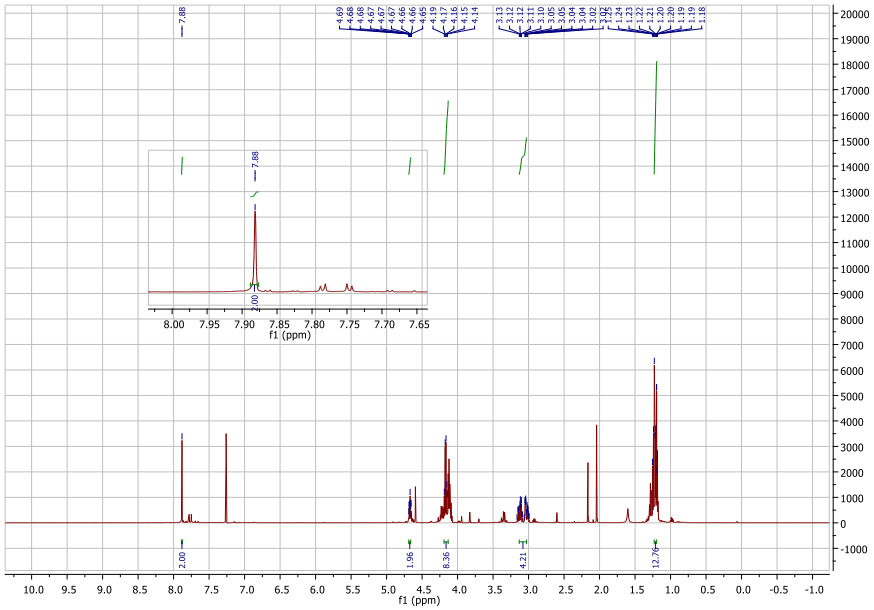

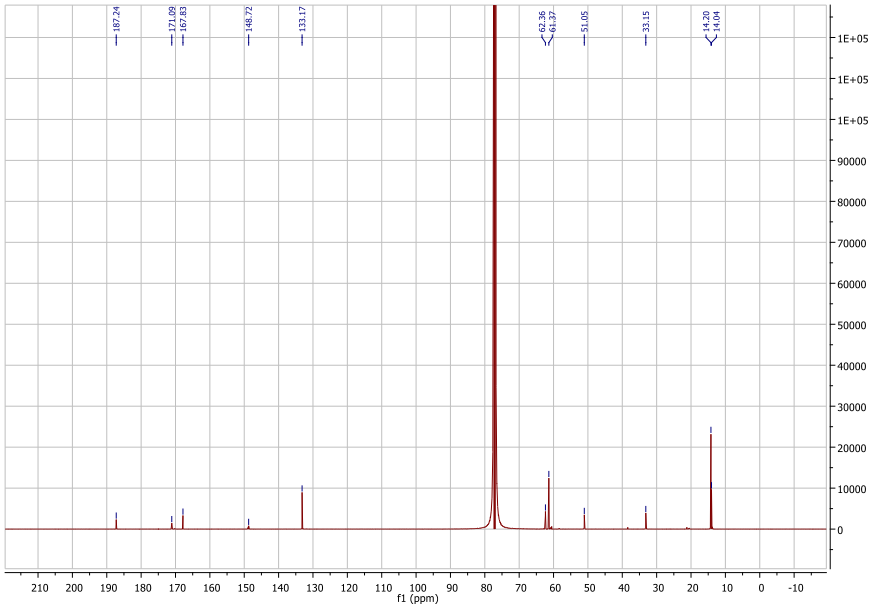

Diethyl 2,2'-(thiophene-2,5-diyl)bis(5-oxo-4,5-dihydro-1H-pyrrole-3-carboxylate (18)

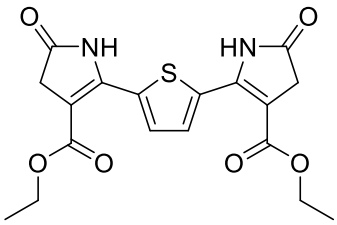

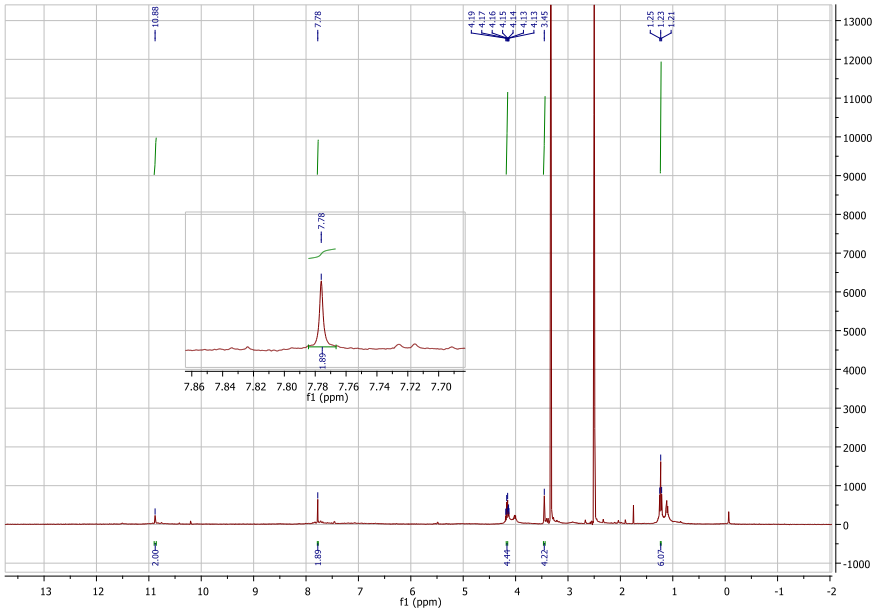

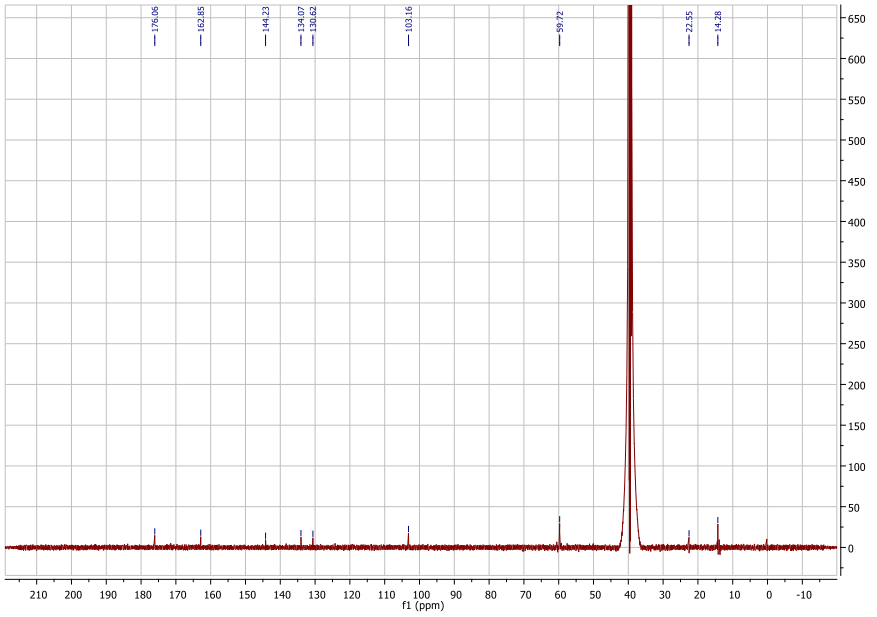

Ethyl 1-dodecyl-4-hydroxy-5-oxo-2-(thiophen-2-yl)-2,5-dihydro-1H-pyrrole-3-carboxylate (21a)

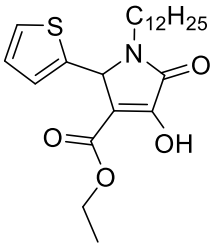

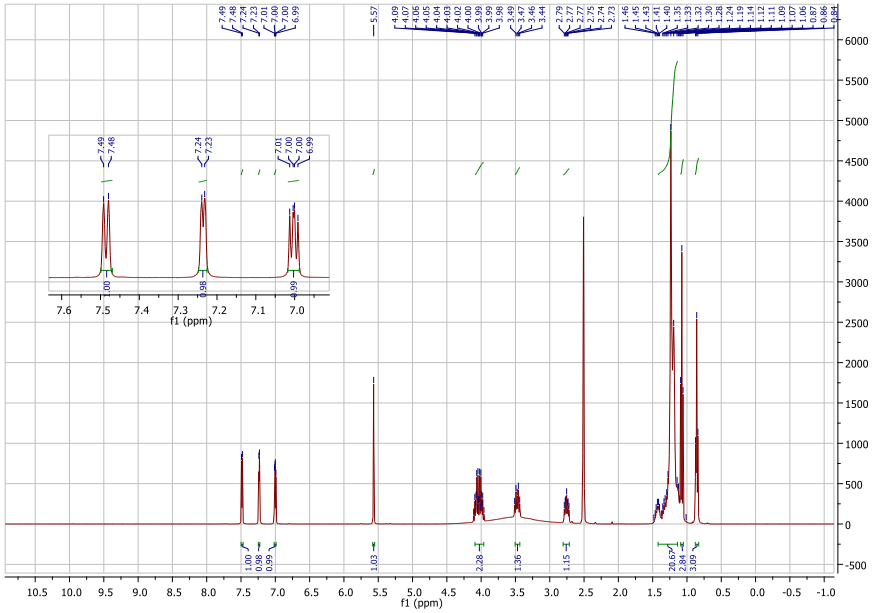

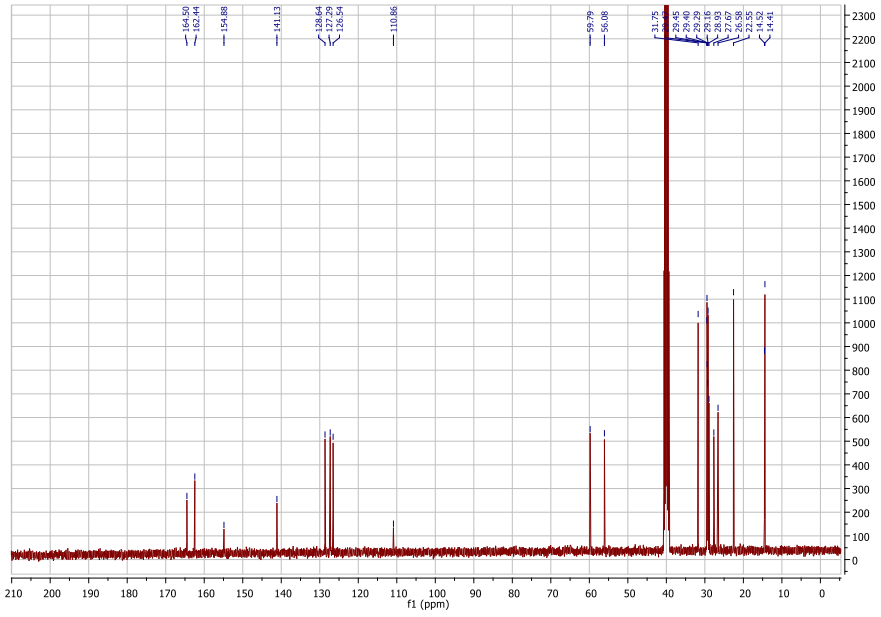

Ethyl 1-(2-ethylhexyl)-4-hydroxy-5-oxo-2-(thiophen-2-yl)-2,5-dihydro-1H-pyrrole-3-carboxylate (21b)

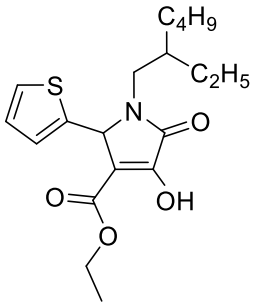

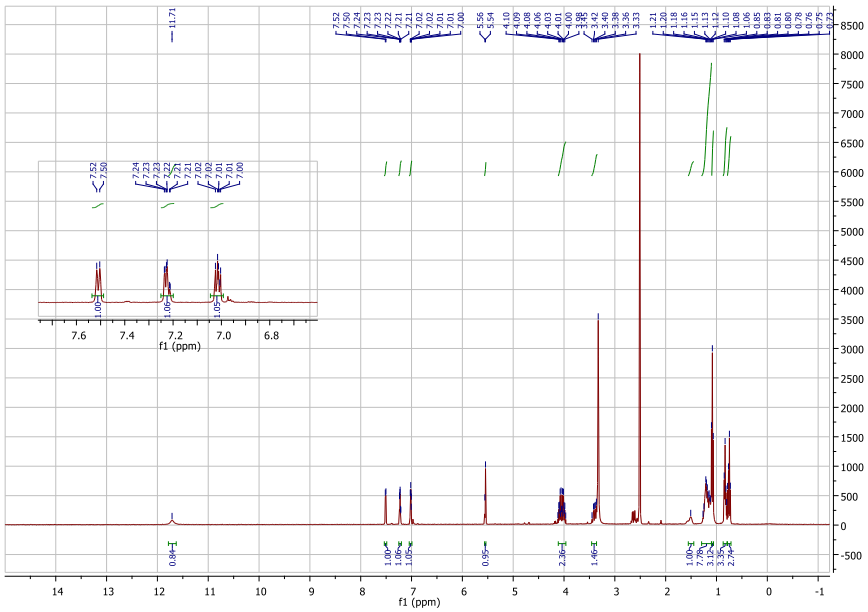

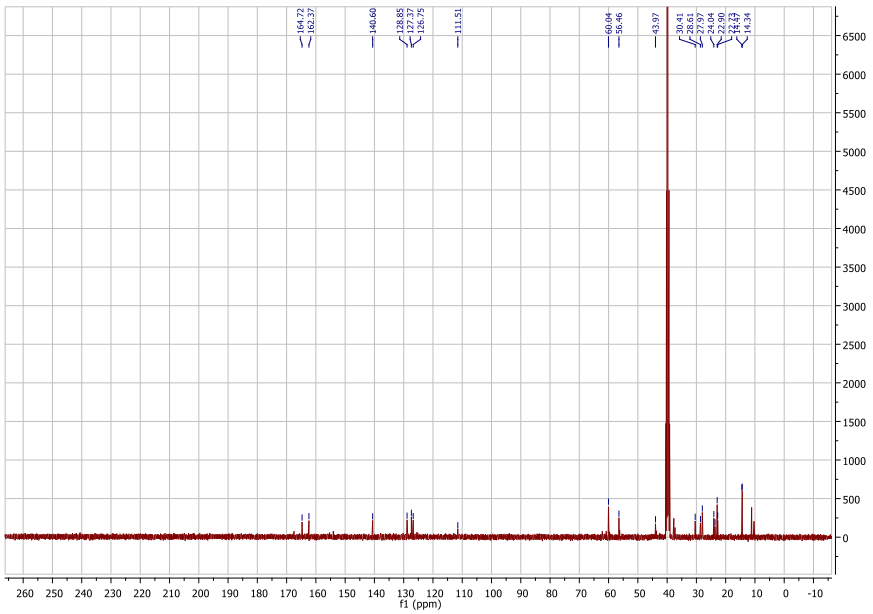

Ethyl 1-butyl-4-hydroxy-5-oxo-2-(thiophen-2-yl)-2,5-dihydro-1H-pyrrole-3-carboxylate (21c)

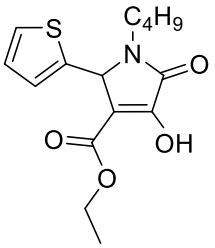

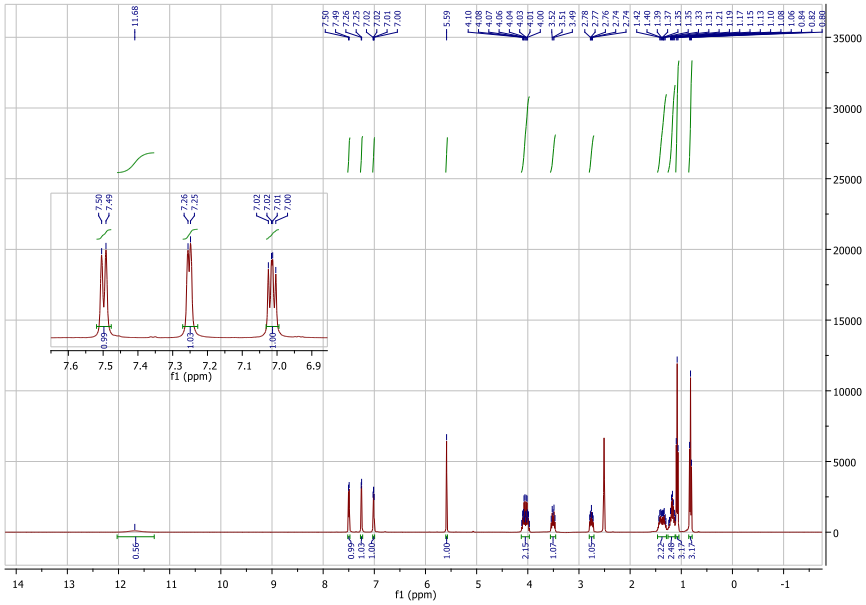

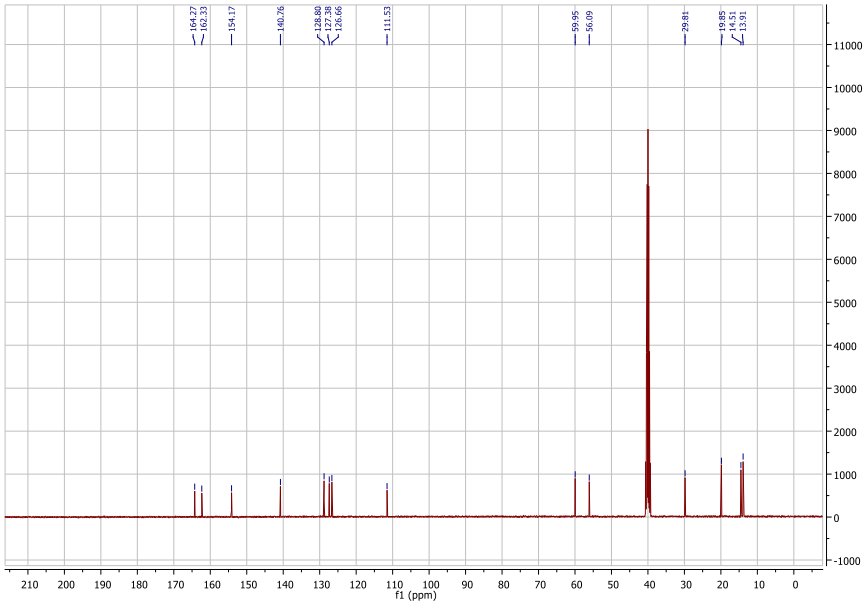

Ethyl 1-dodecyl-5-oxo-2-(thiophen-2-yl)-4,5-dihydro-1H-pyrrole-3-carboxylate (23a)

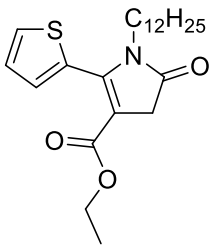

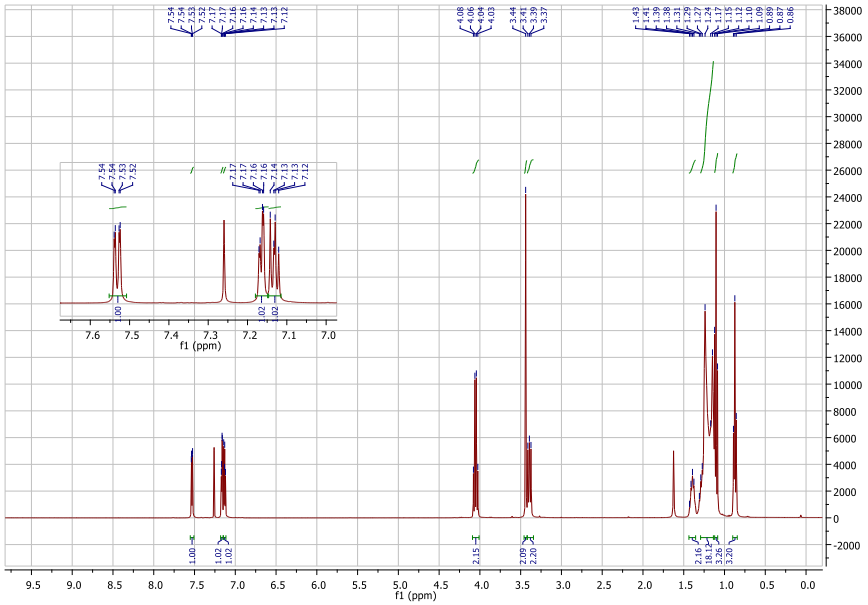

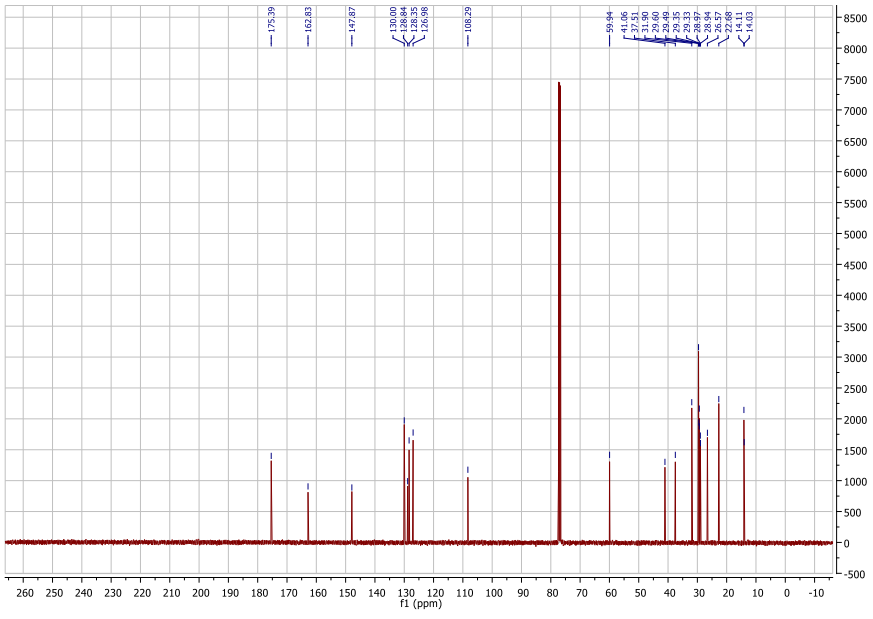

Ethyl 1-(2-ethylhexyl)-5-oxo-2-(thiophen-2-yl)-4,5-dihydro-1H-pyrrole-3-carboxylate (23b)

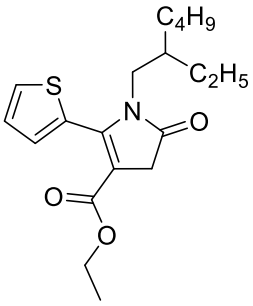

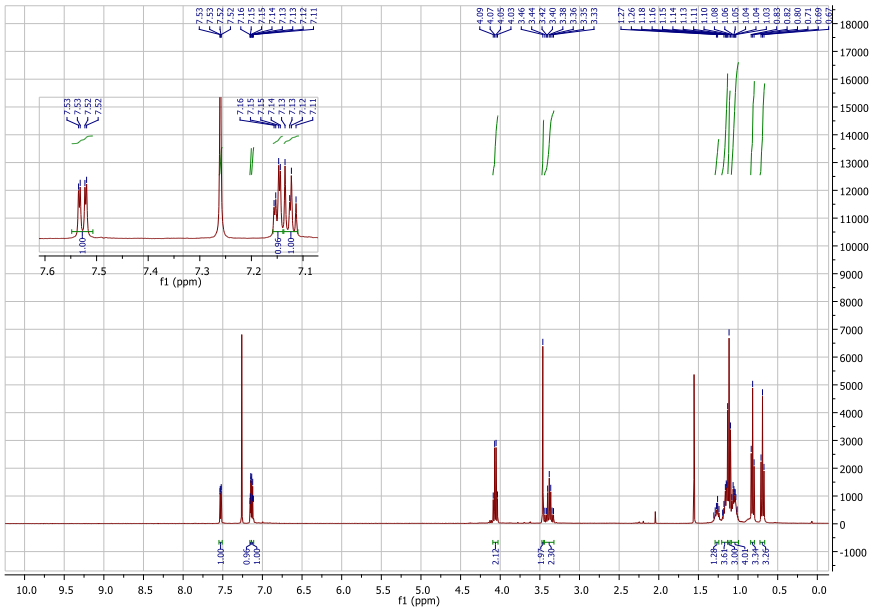

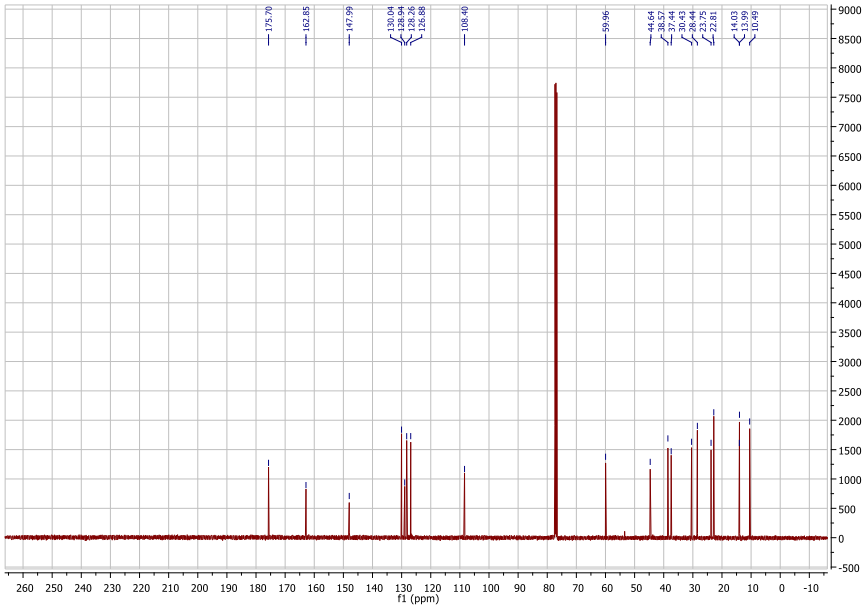

Ethyl 1-butyl-5-oxo-2-(thiophen-2-yl)-4,5-dihydro-1H-pyrrole-3-carboxylate (23c)

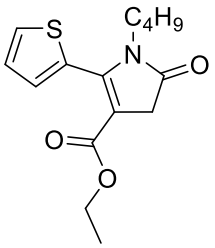

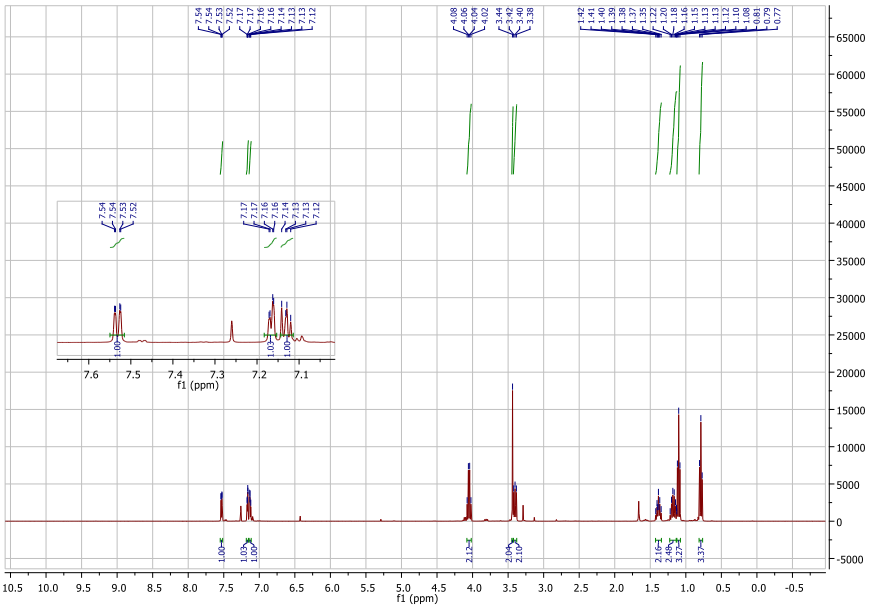

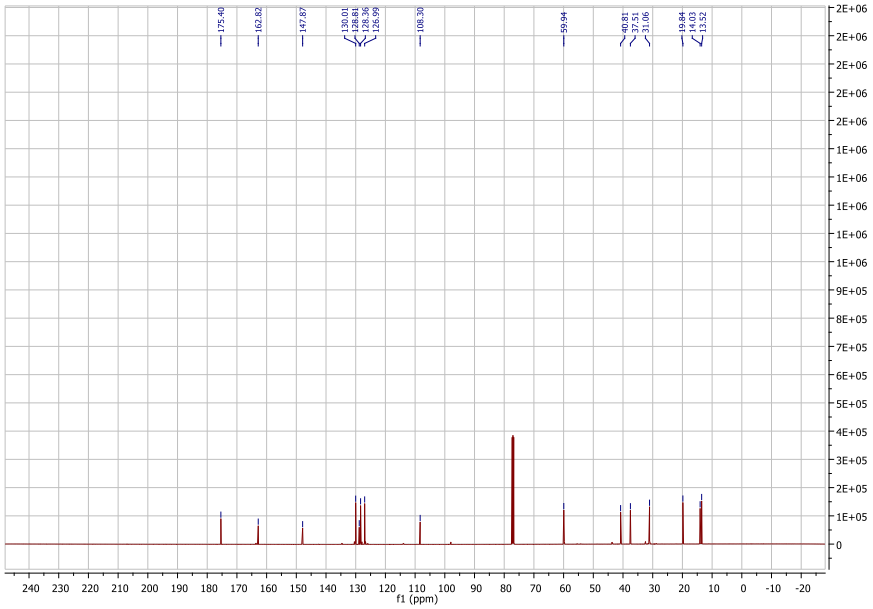

Furan-2-carbonitrile (25)

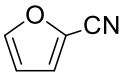

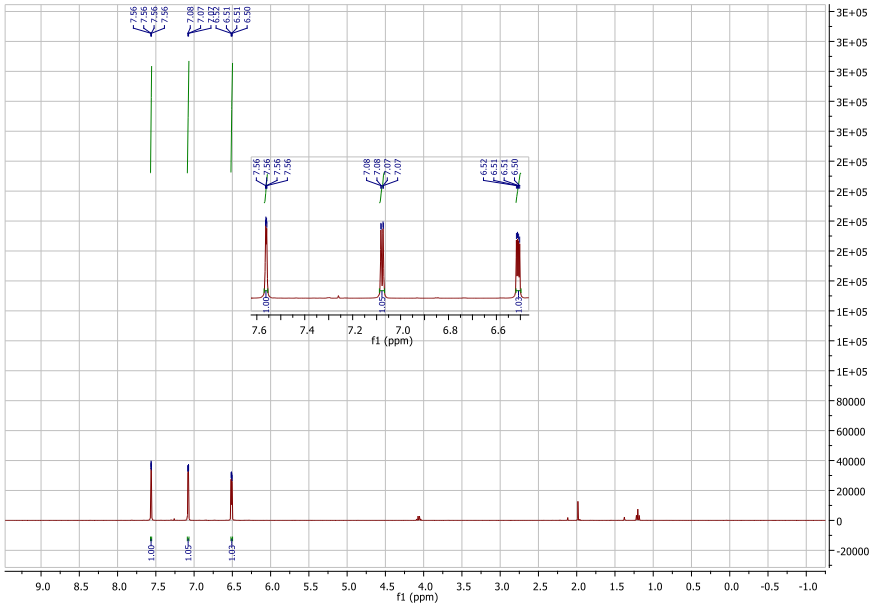

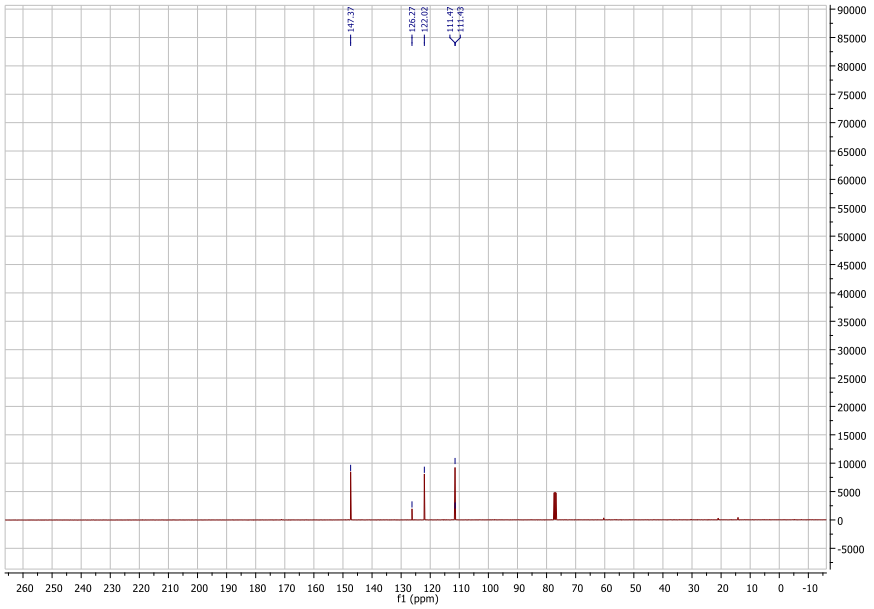

6-(4-bromophenyl)-2-dodecyl-3-(thiophen-2-yl)-2,5-dihydropyrrolo[3,4-c]pyrrole-1,4-dione (26ad)

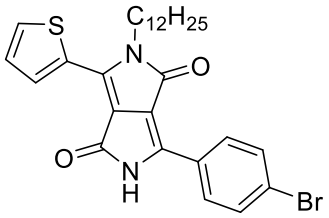

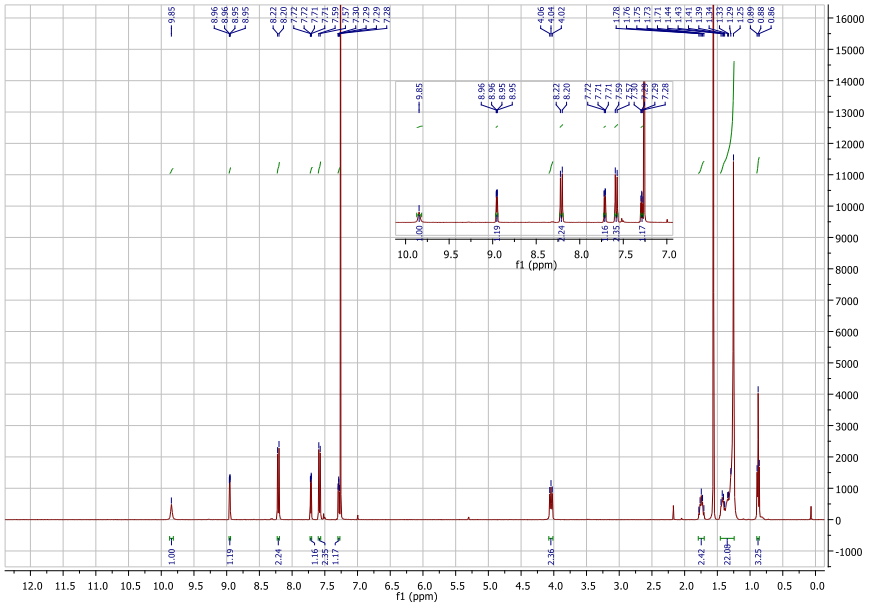

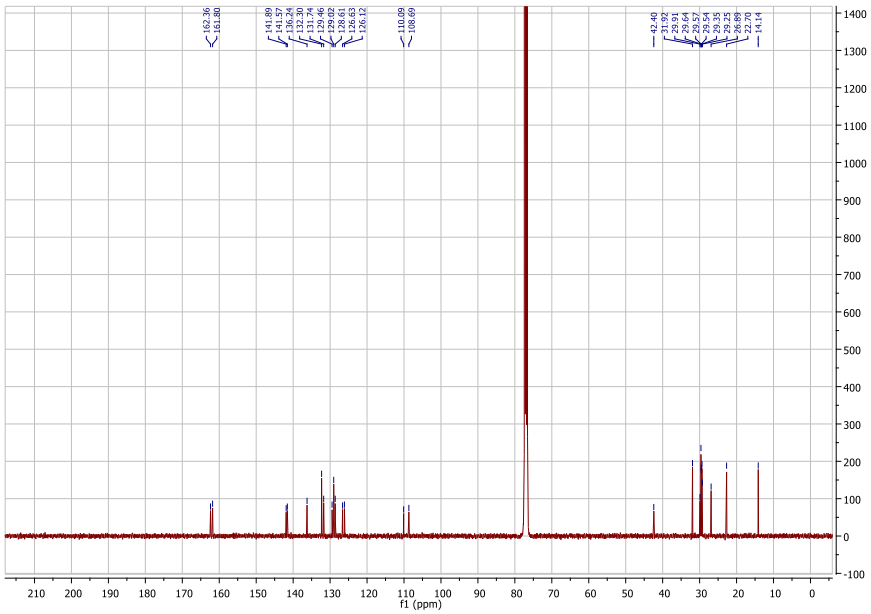

2-(2-ethylhexyl)-6-phenyl-3-(thiophen-2-yl)-2,5-dihydropyrrolo[3,4-c]pyrrole-1,4-dione (26bc)

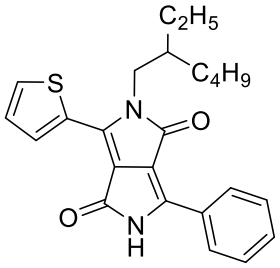

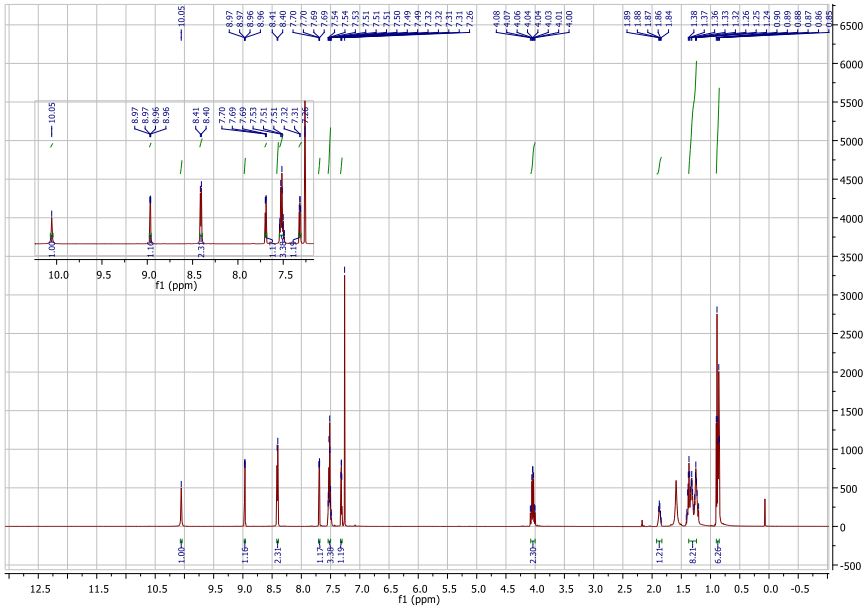

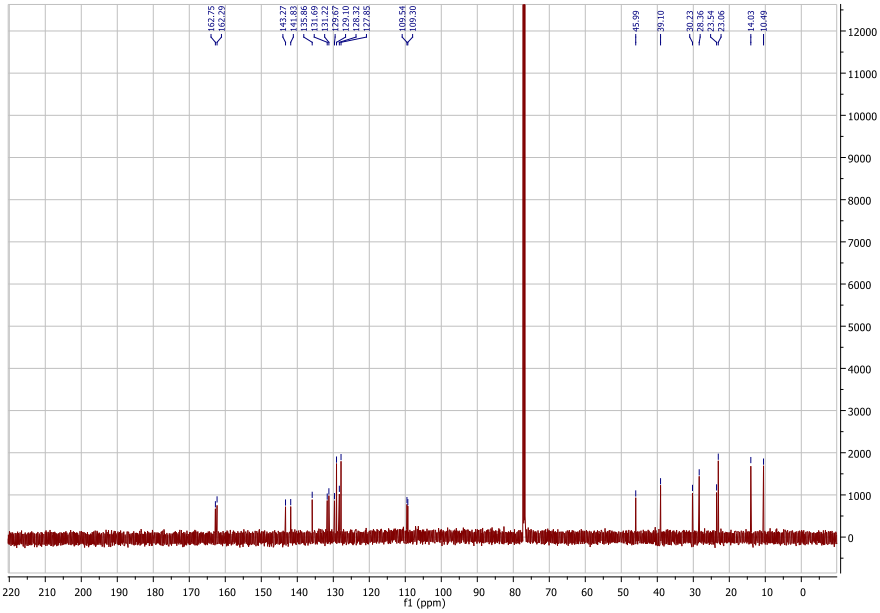

6-(4-bromophenyl)-2-(2-ethylhexyl)-3-(thiophen-2-yl)-2,5-dihydropyrrolo[3,4-c]pyrrole-1,4-dione (26bd)

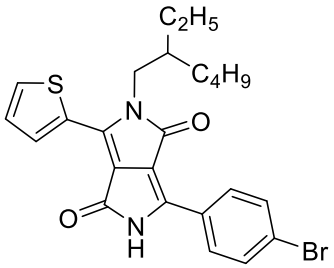

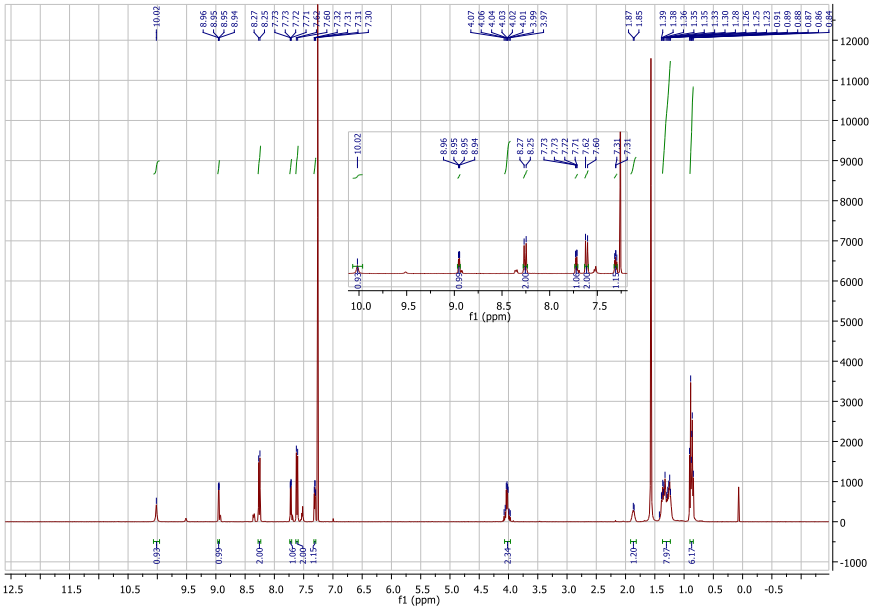

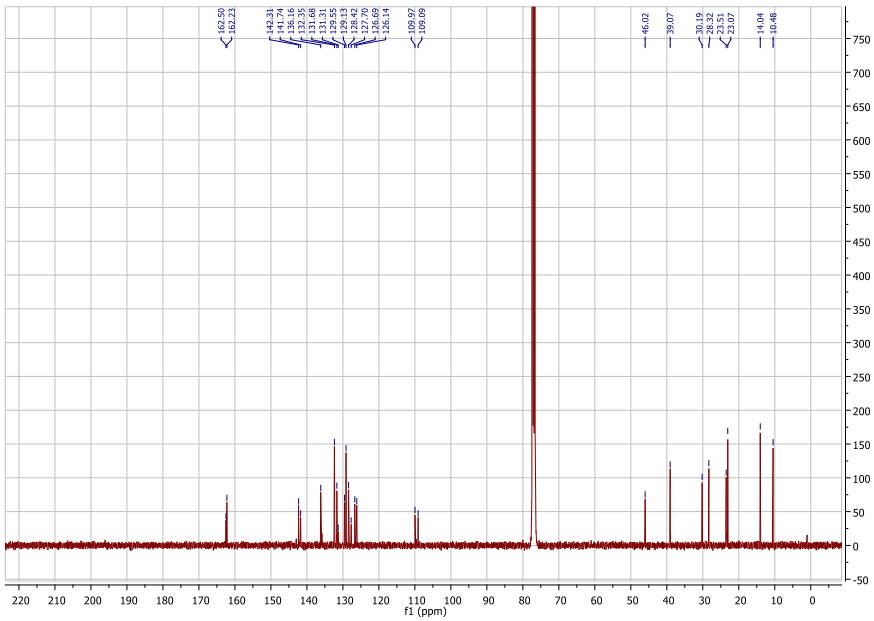

2-(2-ethylhexyl)-6-(furan-2-yl)-3-(thiophen-2-yl)-2,5-dihydropyrrolo[3,4-c]pyrrole-1,4-dione (26be)

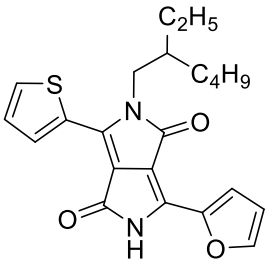

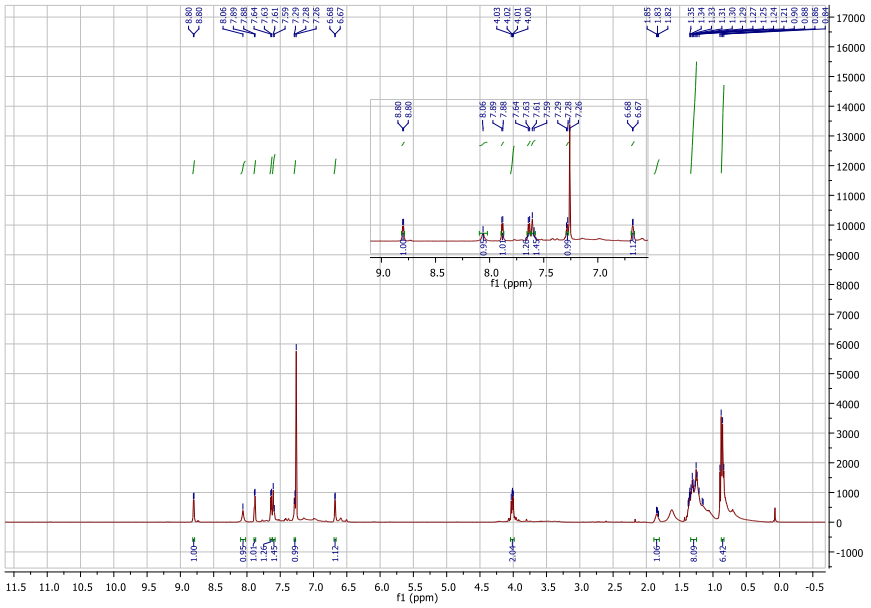

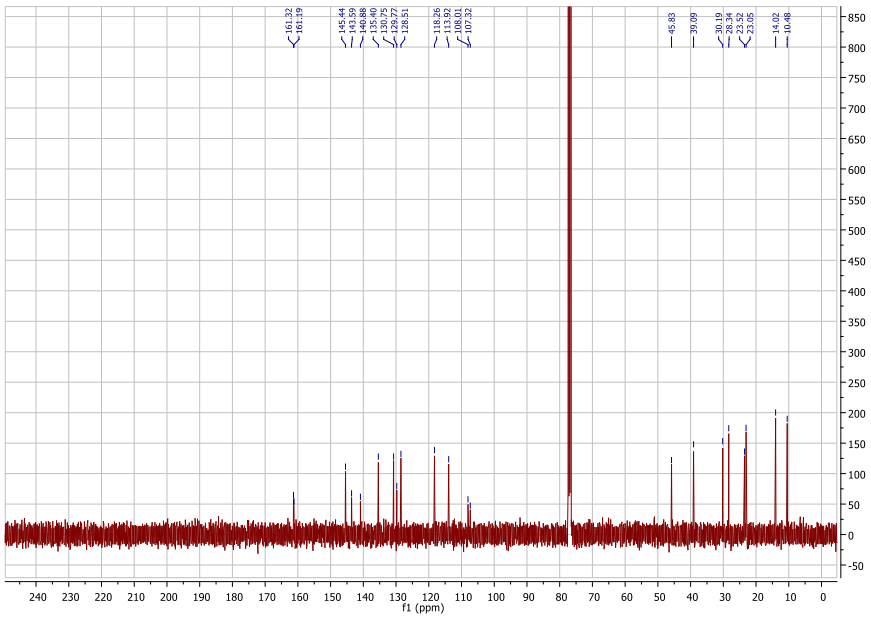

3-(4-bromophenyl)-5-dodecyl-2-(2-ethylhexyl)-6-(thiophen-2-yl)-2,5-dihydropyrrolo[3,4-c]pyrrole-1,4-dione (27adh) (P-DPP-T)

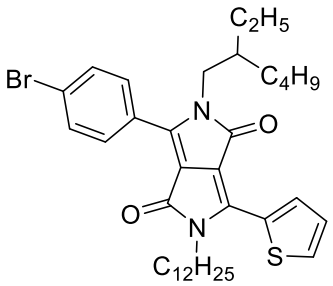

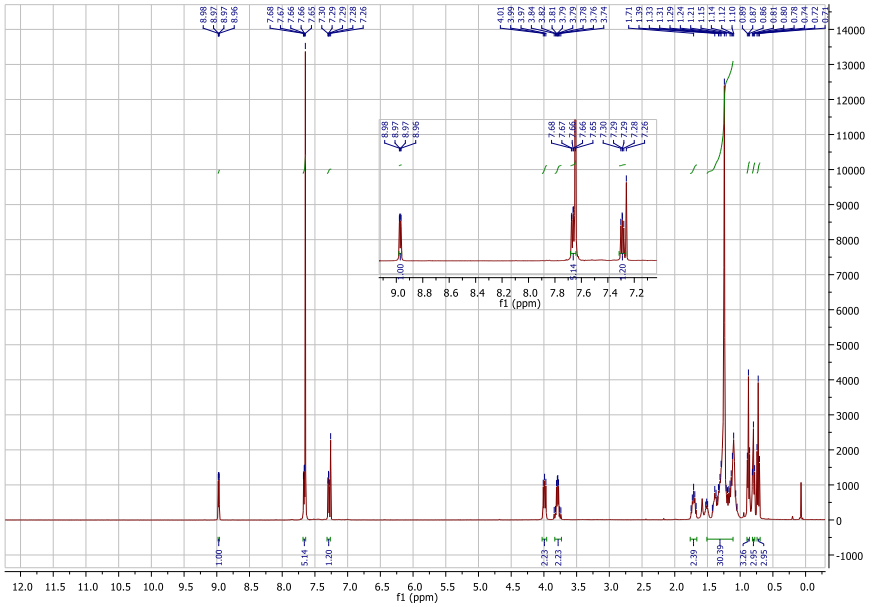

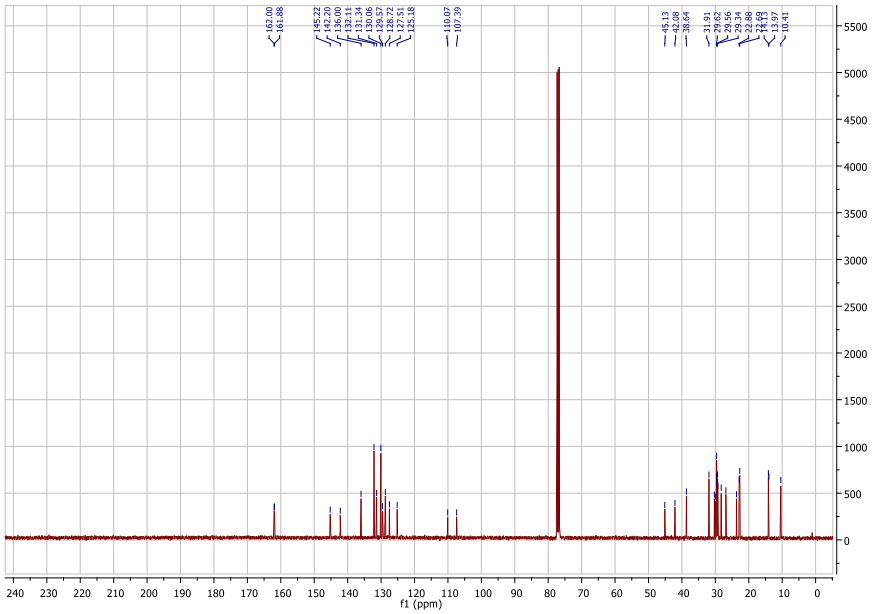

3-(4-bromophenyl)-5-dodecyl-6-(thiophen-2-yl)-2-(2,5,8,11-tetraoxatridecan-13-yl)-2,5-dihydropyrrolo[3,4-c]pyrrole-1,4-dione (27adi)

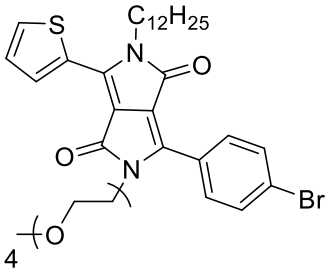

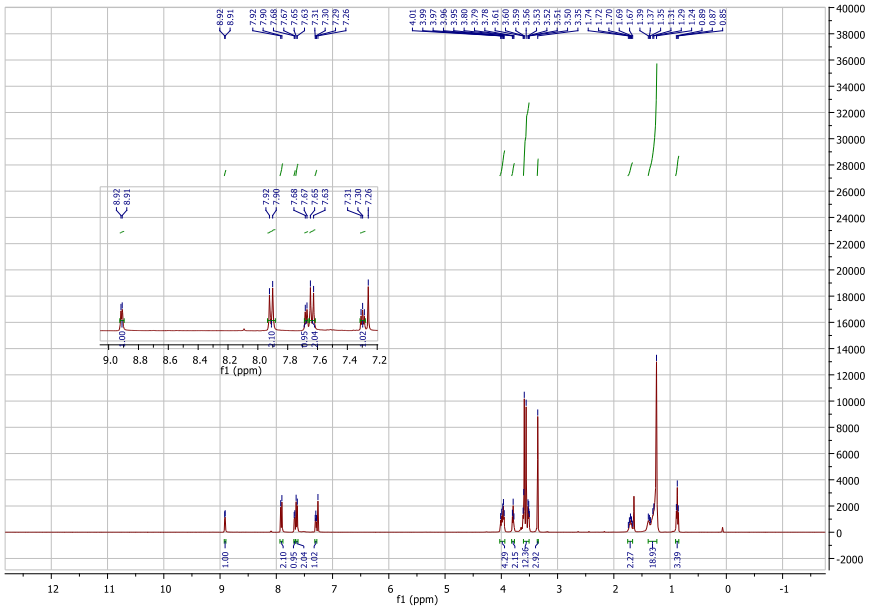

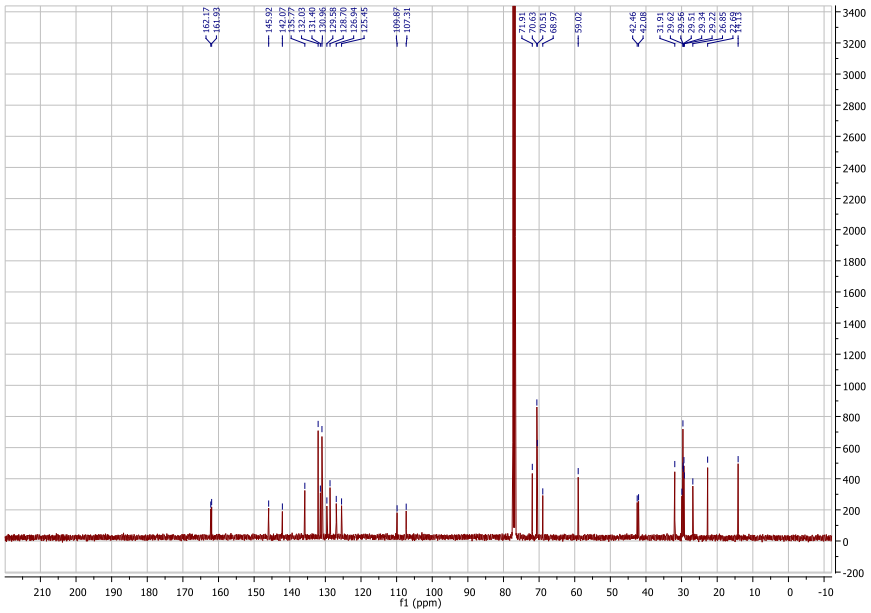

3-(4-bromophenyl)-2-dodecyl-5-(2-ethylhexyl)-6-(thiophen-2-yl)-2,5-dihydropyrrolo[3,4-c]pyrrole-1,4-dione (27bdf) (T-DPP-P)

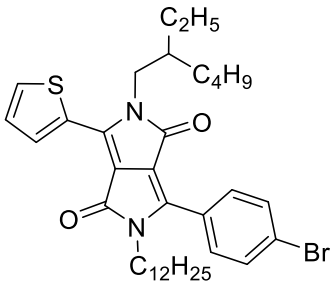

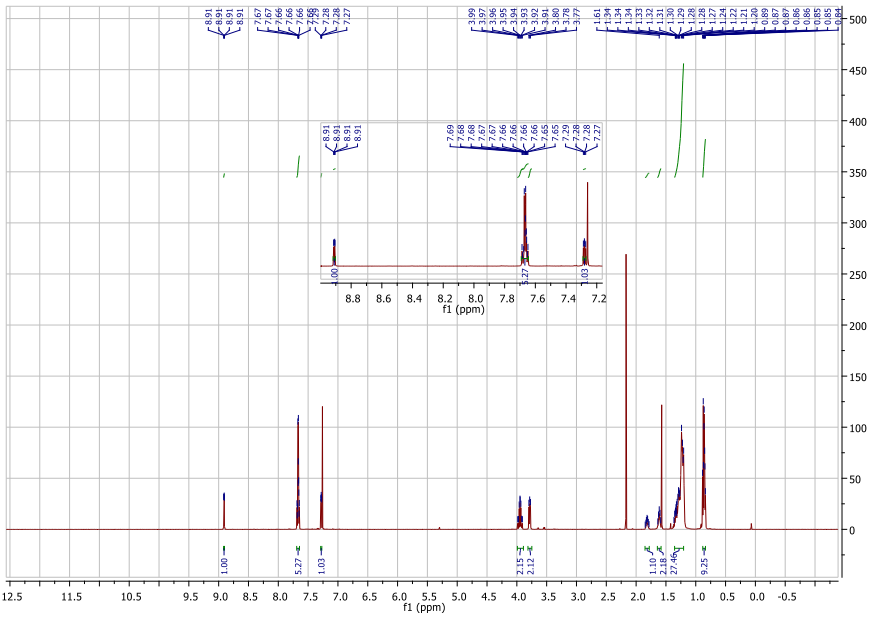

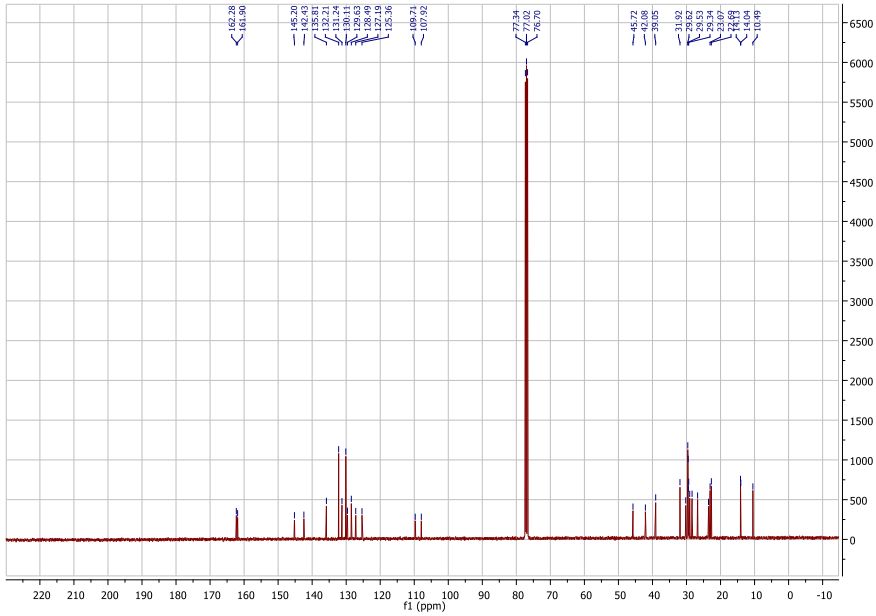

2-(2-ethylhexyl)-6-(furan-2-yl)-5-(2-octyldodecyl)-3-(thiophen-2-yl)-2,5-dihydropyrrolo[3,4-c]pyrrole-1,4-dione) (27beg)

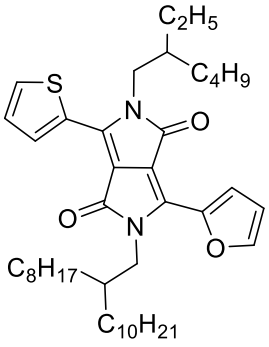

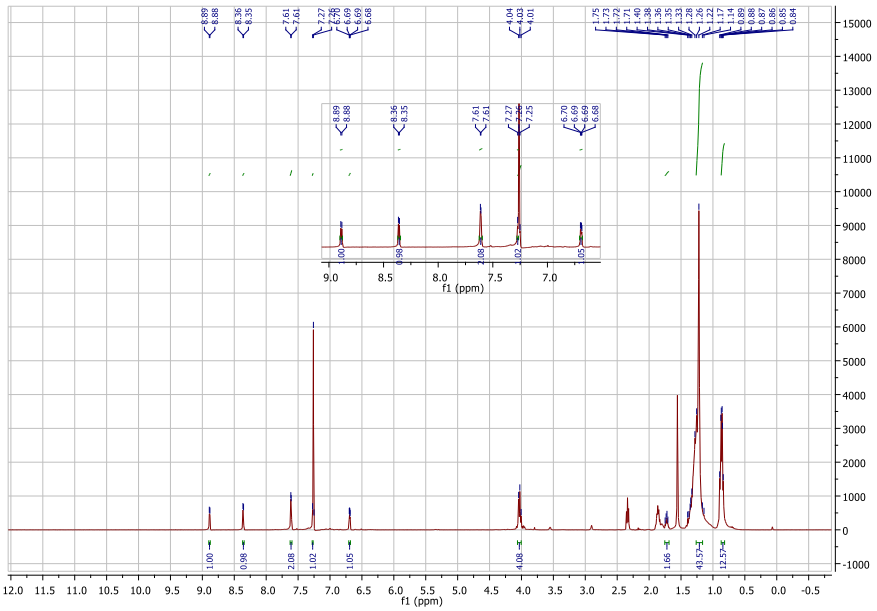

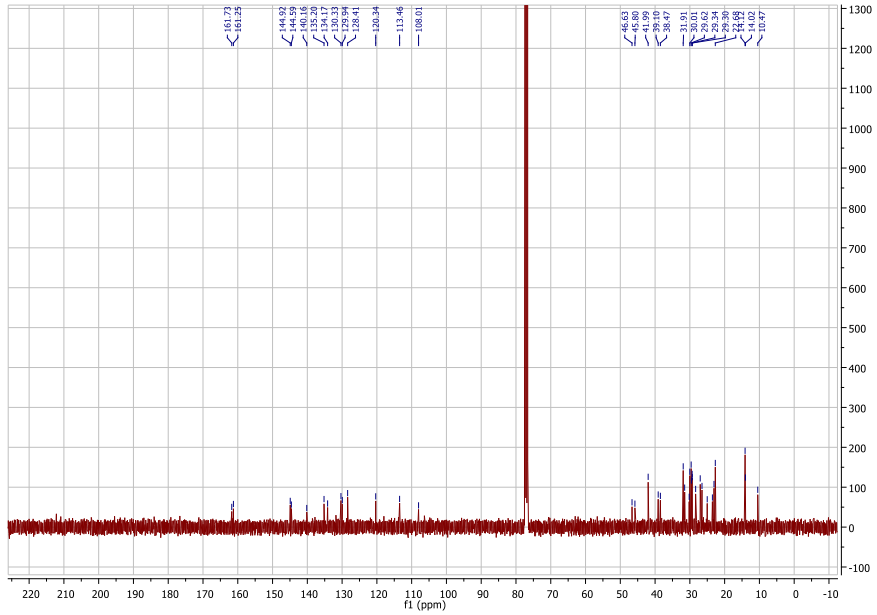

2,5-bis(2-ethylhexyl)-3,6-di(thiophen-2-yl)-2,5-dihydropyrrolo[3,4-c]pyrrole-1,4-dione (29)

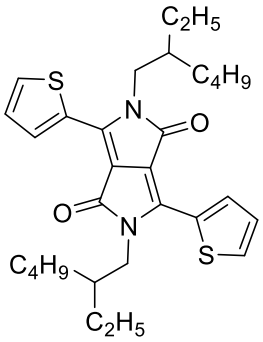

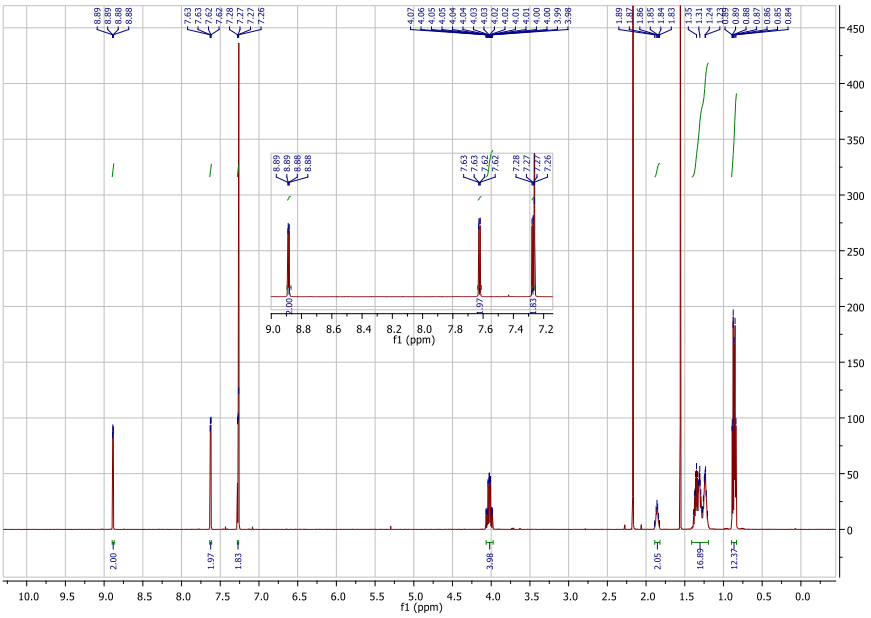

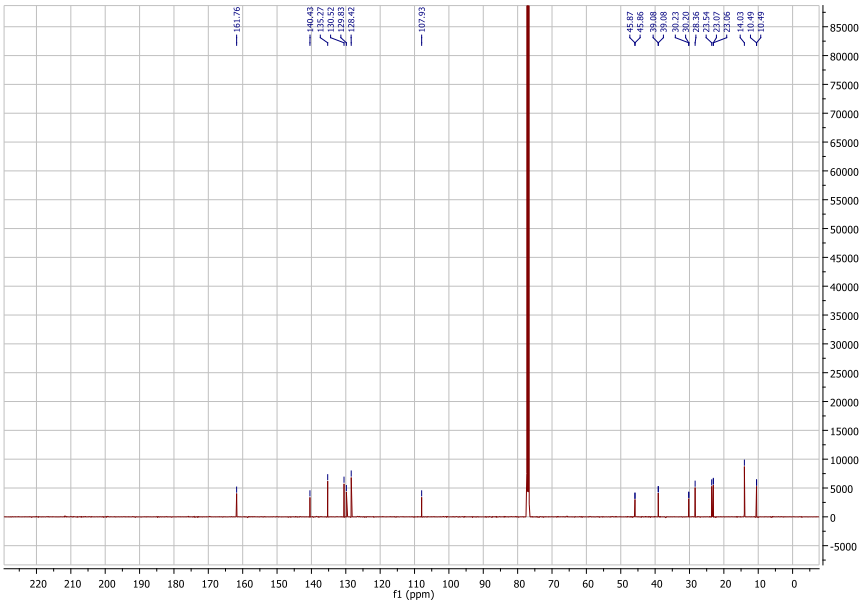

5-(2,5-bis(2-hexyldecyl)-3,6-dioxo-4-(thiophen-2-yl)-2,3,5,6-tetrahydropyrrolo[3,4-c]pyrrol-1-yl)thiophene-2-carbonitrile (36)

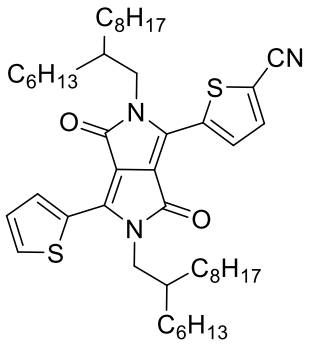

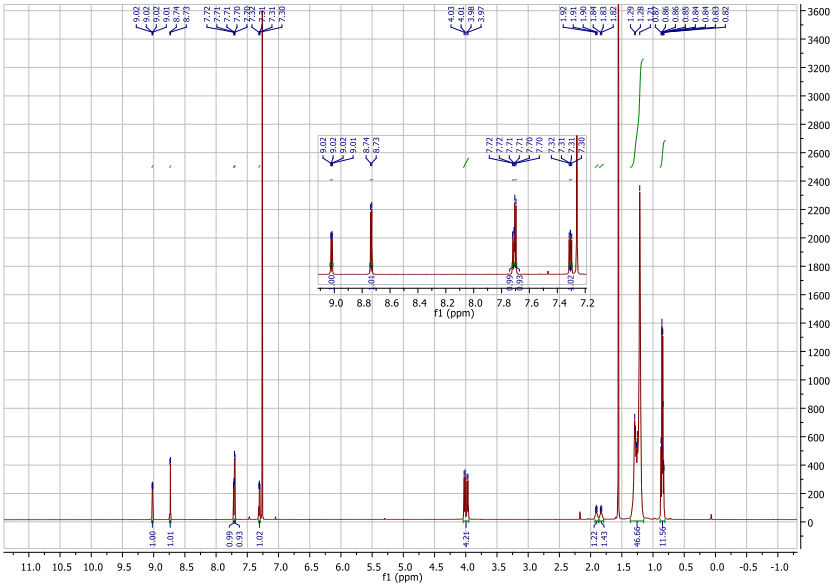

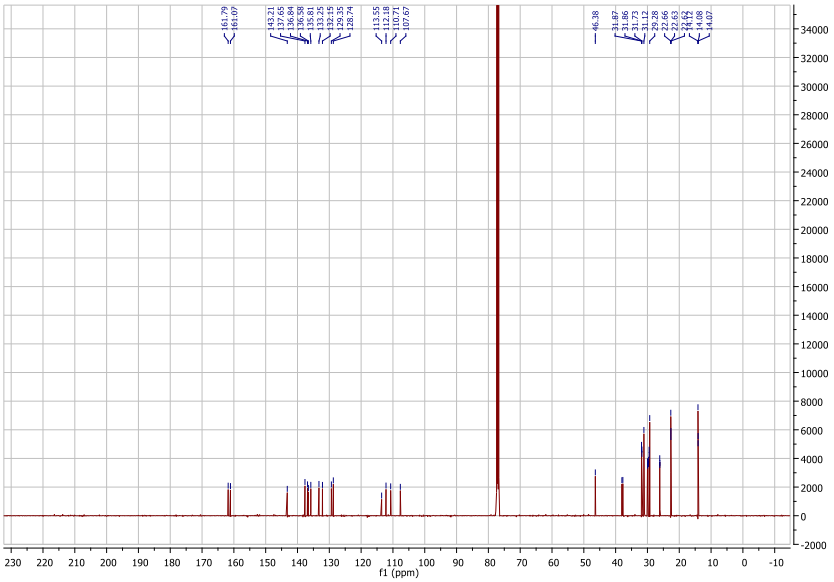

2-hexyl-3-(methylthio)-6-(thiophen-2-yl)-2,5-dihydropyrrolo[3,4-c]pyrrole-1,4-dione (38)

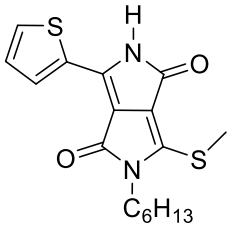

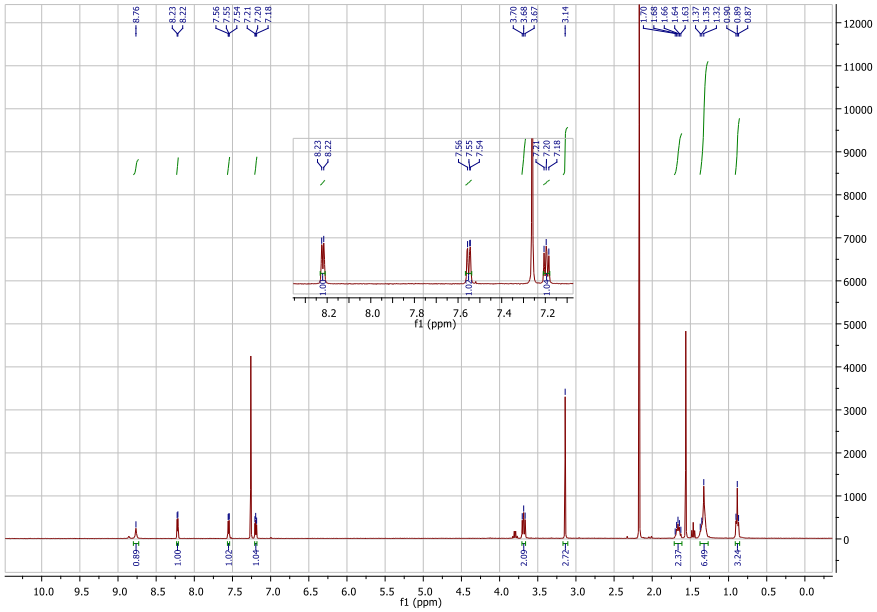

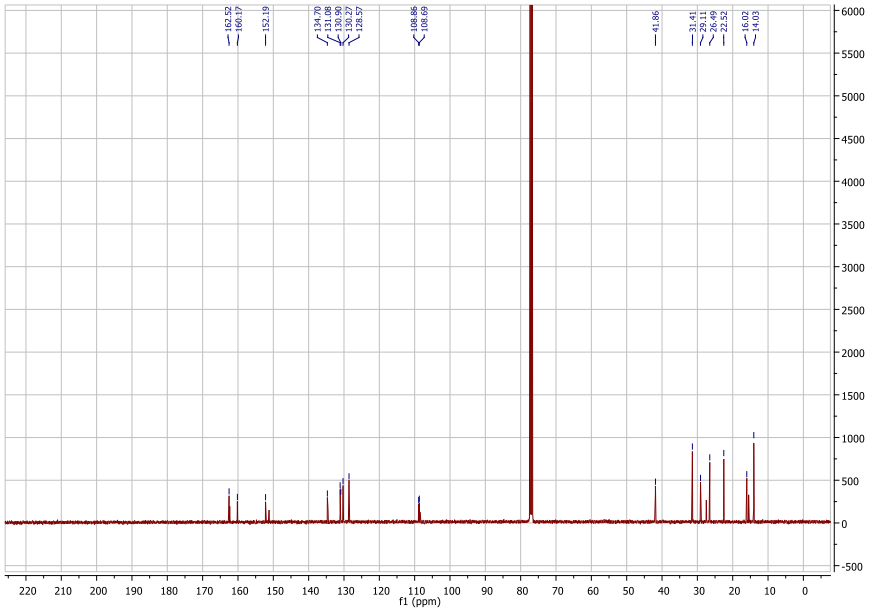

Ethyl (Z)-4-((hexylamino)(methylthio)methylene)-5-oxo-2-(thiophen-2-yl)-4,5-dihydro-1H-pyrrole-3-carboxylate (39)

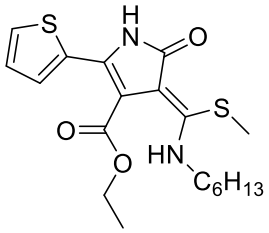

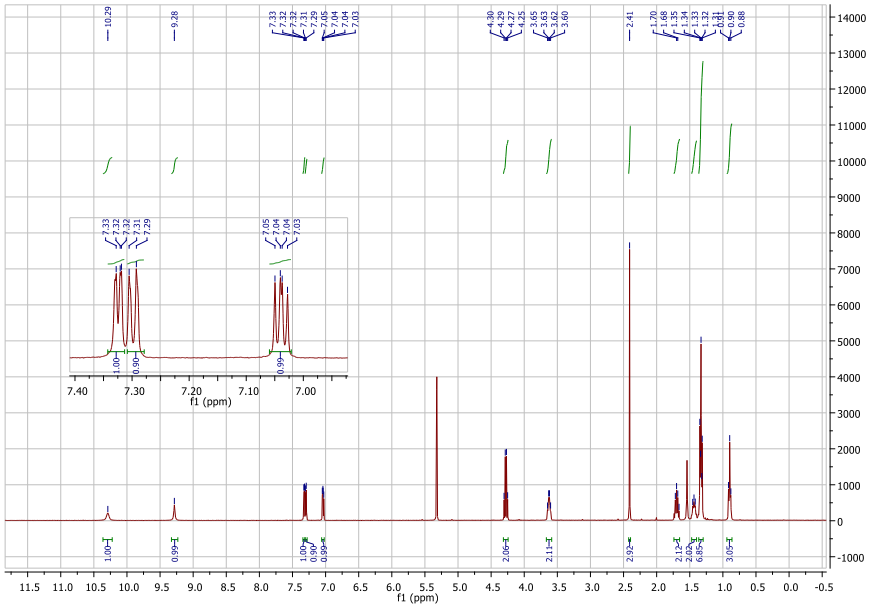

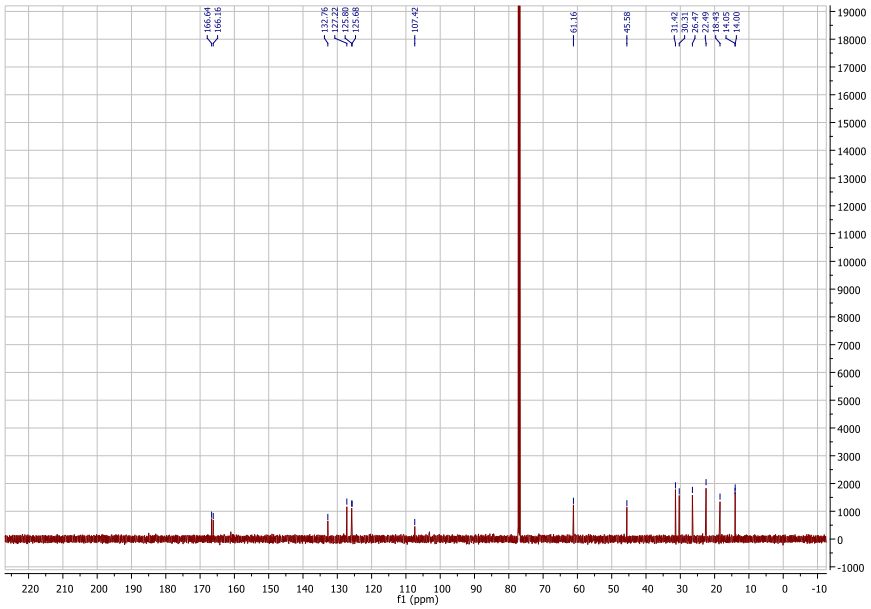

2-hexyl-5-methyl-3-(methylthio)-6-(thiophen-2-yl)-2,5-dihydropyrrolo[3,4-c]pyrrole-1,4-dione (40)

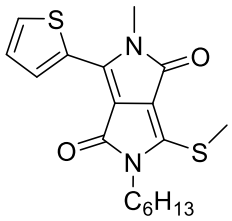

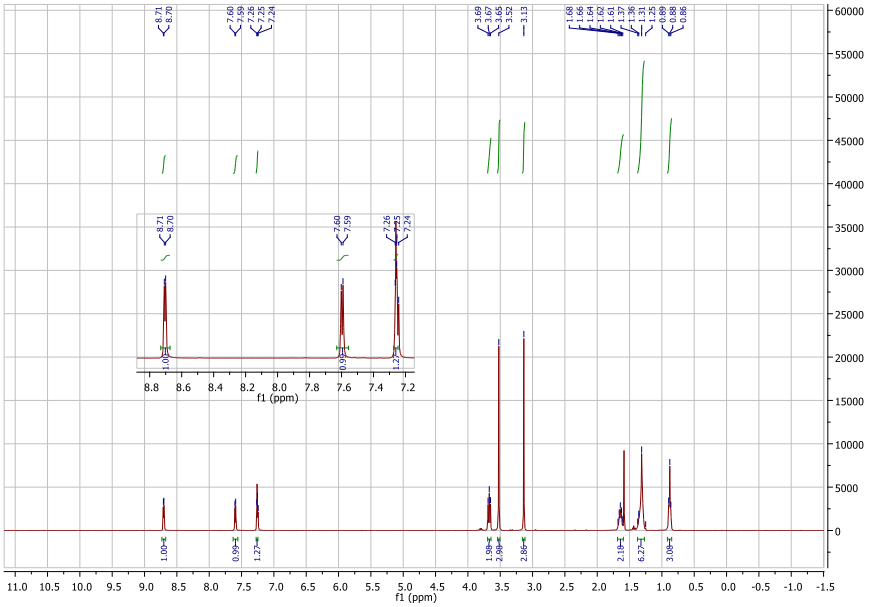

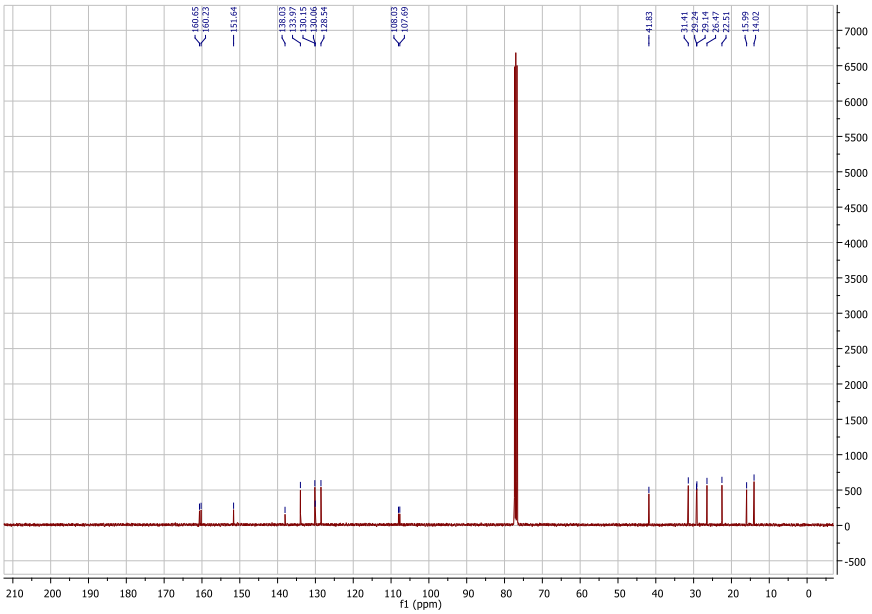

8.3.3 Single Crystal X-Ray Diffraction Studies[†]

Single X-ray diffraction data was collected using either a Bruker D8-QUEST PHOTON100 diffractometer (Cu radiation) or a Nonius KappaCCD diffractometer (Mo radiation). Mercury software was used to visualise and analyse the data obtained. Hydrogen atoms were omitted for simplicity.

[†]X-ray structure determined by Dr Andrew Bond, University of Cambridge.

2-hexyl-3-(methylthio)-6-(thiophen-2-yl)-2,5-dihydropyrrolo[3,4-c]pyrrole-1,4-dione (38)

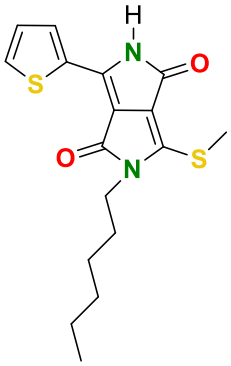

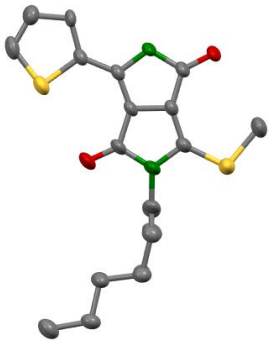

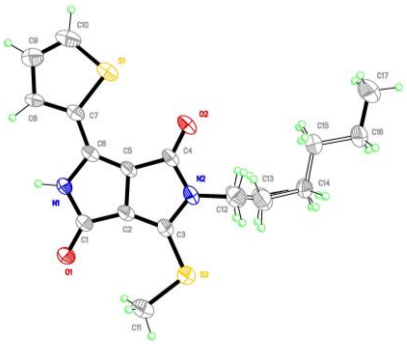

*Table S6- Crystallographic parameters for crystal structure **38**.*

Compound	**38**
Chemical formula	$C_{17}H_{20}N_2O_2S_2$
Formula weight	348.47
Temperature / *K*	180(2)
Crystal system	triclinic
Space group	P -1
a / Å	8.7286(4)
b / Å	10.1207(4)
c / Å	11.2092(5)
alpha / degrees	93.887(2)
beta / degrees	103.035(3)
gamma / degrees	113.046(3)
Unit-cell volume / $Å^3$	874.15(7)
Z	2
Calc. density / gcm^{-3}	1.324
F(000)	368
Radiation type	CuK*a*
Absorption coefficient / mm^{-1}	2.845
Crystal size / mm^3	0.160 x 0.120 x 0.050
2-Theta range / degrees	8.22-133.22
Completeness to max 2-theta	0.997
No. of reflections measured	9600
No. of independent reflections	3088
R_{int}	0.0466
No. parameters / restraints	238 / 16
Final R_1 values ($I > 2s(I)$)	0.0681
Final $wR(F^2)$ values (all data)	0.0936
Goodness-of-fit on F^2	1.046
Largest difference peak & hole / $eÅ^{-3}$	1.097, -0.382

8.3.4 Geometry Optimised Structures and Molecular Orbitals

Optimised ground state geometries of P-DPP, T-DPP-P/P-DPP-T and T-DPP at the B3LYP/def2-SVP level. The energy minimised structures have been obtained using a structurally modified model where both the alkyl chains have been replaced with methyl groups for simplicity.

HOMO

P-DPP

HOMO -5.51 eV

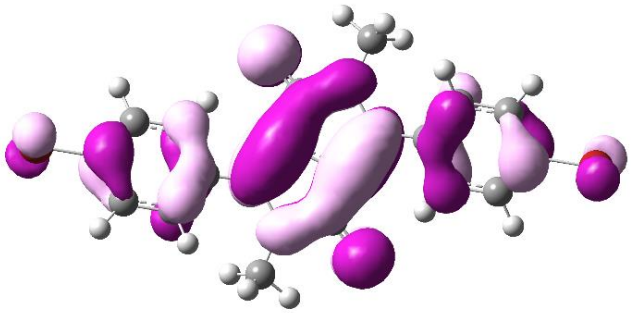

T-DPP-P/P-DPP-T

HOMO -5.32 eV

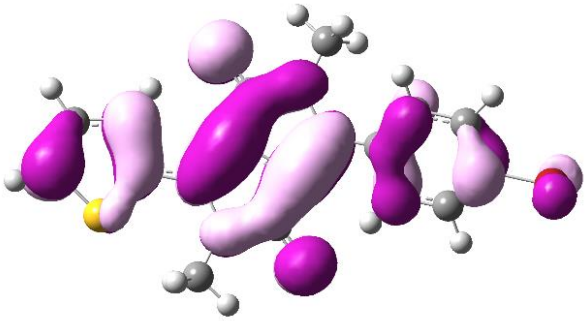

T-DPP

HOMO -5.13 eV

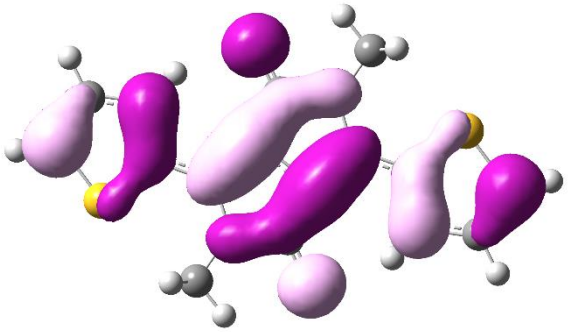

LUMO

P-DPP

LUMO -2.86 eV

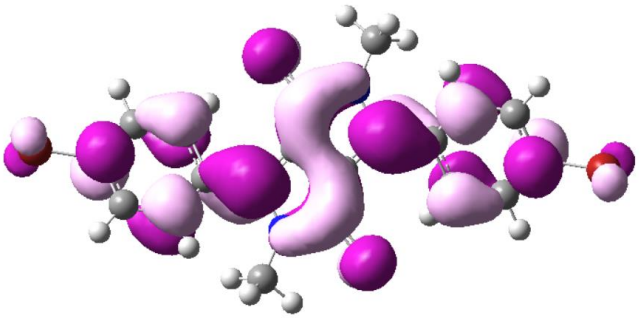

T-DPP-P/P-DPP-T

LUMO -2.78 eV

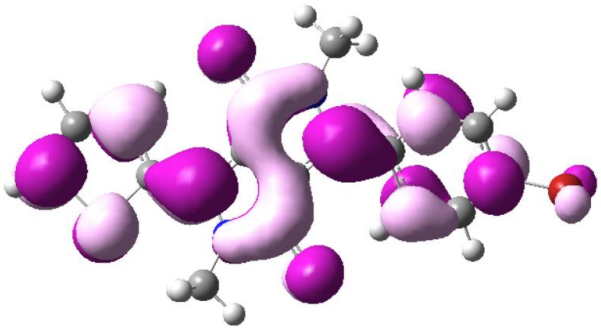

T-DPP

LUMO -2.68 eV